Mono- and Bi-functional Chelated Ruthenium(II) Arene Complexes as Potential Anticancer Agents

A Thesis Submitted for the Degree of

Doctor of Philosophy

by

Michael Melchart, *MEnvChem.*

School of Chemistry

College of Science and Engineering

University of Edinburgh

June 2006

Abstract

Ruthenium(II) arene complexes of the type [(η^6-arene)Ru(L)Cl], where arene = *p*-cymene (*p*-cym), biphenyl, indan, benzene and L = bidentate, monoanionic, *O,O*-chelating ligands including β-diketonates, hydroxy-ketonates and acetate were synthesised. Chelate ring sizes vary from four- to six-membered. X-ray crystal structures, confirming coordination of each class of ligand and the characteristic "piano stool" conformation, were determined. Some structures show H-bond interactions between arene protons and oxygen atoms of the chelate. Cytotoxicity towards the A2780 human ovarian cancer cell line (in a range of 11 to > 100 μM) was found to dependent strongly on both the nature of the chelate and the arene. Steric bulk around the metal centre appears to be important for activity. Hydrolysis of [(η^6-*p*-cym)Ru(acac)Cl], where acac = acetylacetonate, is rapid and the pK_a value of coordinated water (9.4) is ca. 1.2 units higher than that of the ethylenediamine (en) analogue. Thus the chelating ligand in Ru^{II} arene complexes can control the rate and extent of hydrolysis. The acetato complex readily decomposes in water to form the hydroxo-bridged dimer [((η^6-*p*-cym)Ru)$_2$(μ-OH)$_3$]$^+$. Binding to G-*N7* or A-*N7* and A-*N1* with displacement of Cl^- was observed for reactions of [(η^6-*p*-cym)Ru(acac)Cl] with guanine (G) and adenine (A) derivatives. This is in contrast to cytotoxic [(η^6-arene)Ru(en)Cl]$^+$ complexes, which have very little affinity for adenine. Formation of a strong H-bond (2.07 Å) between A-N6H···O(chelate) was observed in the X-ray crystal structure of [(η^6-*p*-cym)Ru(acac)9EtA]$^+$, where 9EtA = 9-ethyladenine, and could contribute to the observed change in base selectivity.

Six novel tethered Ru^{II} arene complexes of the type $[(\eta^6:\eta^1\text{-}C_6H_5(T\text{-}N)RuCl_2]$, where T is a linker of varying nature between the η^6-coordinated arene and a coordinating nitrogen atom, were synthesised and fully characterised, including four X-ray crystal structures. Tethered complexes can undergo partial or complete hydrolysis in water. Loss of one chloride appears to be strongly favoured, with anation complete only to ca. 40% at a total chloride concentration of ca. 275 mM for $[(\eta^6:\eta^1\text{-}C_6H_5(CH_2)_3NH_2)RuCl_2]$. Tethered complexes, such as $[(\eta^6:\eta^1\text{-}C_6H_5(CH_2)_nNH_2)RuCl_2]$, where n = 2 or 3, containing an NH_2 group react with guanine derivatives. Mono-adducts form rapidly and almost completely, and formation of di-adducts proceeds to ca. 35 – 50 % completion after ca. 10 h, depending on pH and concentration of chloride and substrate. Such bifunctional binding indicates potential for cross-linking of DNA, similar to cisplatin. Bifunctional coordination of 9EtG in an unusual *head-to-head* orientation, with formation of H-bonds (1.98 Å and 2.32 Å) between the tether NH_2 group and C6O(9EtG), was confirmed by X-ray crystallography for $[(\eta^6:\eta^1\text{-}C_6H_5(CH_2)_3NH_2)Ru(9EtG)_2](CF_3SO_3)_2$. Substitution of the chloride ligands by bidentate chelating ligands yields tethered complexes comparable to second generation platinum drugs (e.g. carboplatin, oxaliplatin).

The cytotoxic Ru^{II} arene complex $[(\eta^6\text{-hmb})Ru(en)Cl]PF_6$, where hmb = hexamethylbenzene, can catalyse the transfer hydrogenation of acetone by formate. The regioselective reduction of NAD^+ in water to form 1,4-NADH was complete after 3 h at biologically relevant conditions of 310 K and pD 7.2.

To the memory of my great-uncle Karl Bartl,

whose childhood dream it was to study chemistry.

His dream did not come true, but his support

over the years has helped me to come this far.

Acknowledgements

I would like to thank Professor Peter J. Sadler for his guidance, supervision and encouragement during this project. I particularly enjoyed the freedom to develop the project freely and his understanding of my idea of time-management. Being able to look over his shoulder frequently and learn directly from an expert in the field was a great help to develop new skills.

Every-day work would not have been the same, and especially not nearly as productive and enjoyable, without Dr. Abraha Habtemariam. It was fantastic to be able to profit from his wealth of synthetic experience, but more importantly to go beyond being just colleagues and to build up a very good understanding and appreciation of each other. These things count more than any written words could express. Abraha, you made it all worth-while! Ta!

The conferences in Zurich and Rimini were made all the more fun by the presence of Miss Anna Peacock, and in general her ability to bring in a little sunshine makes her a good friend. Thank you for being you.

A special olé goes out to the Spanish connection. Dr. Ana Pizarro is the dos in dos tontos muy tontos, for sure! Thanks for the smiles, the laughs, the excitement and friendship over the years. The relaxed attitude of Dr. Rafael Fernández greatly helped me settle into lab-work and his sevillano-outbursts are still inspiring to this very day.

A big thank you goes to the PJS group, past and present members, for being a good bunch of people and especially to Drs. Viv Alberts and Fuyi Wang for helpful discussions.

I was fortunate to be able to work together with two very gifted chemists and great people, namely Dr. Yaw Kai Yan and Mr. Erwin van der Geer. People like these make work seem like a hobby.

Thank you also to the very talented, first class, former MChem project students Sarah Dougan and Melanie Brown, with whom working was very enjoyable and enlightening.

A very special thank you goes out to Dr. Simon Parsons and his crew, notably Drs. Francesca Fabbiani and Stephen Moggach, for their interest in and solving of my crystal structures. Their helpfulness and service was outstanding at any time.

The help of Dr. Dusan Uhrin and in particular Mr Juraj Bella with NMR spectroscopy is highly appreciated and gratefully acknowledged.

Mr. Stuart Johnstone did a great job in producing the pressure vessel, which proved to be a bit of a mile-stone.

Thank you to Rhona Aird and Duncan Jodrell, Western General Hospital, Edinburgh as well as Emily Jones and Oncosense Ltd. for cytotoxicity studies.

I would like to thank Viktor Brabec and co-workers, Academy of Sciences of the Czech Republic in Brno for their interest in undertaking DNA binding studies with some of my complexes.

The discussions about aspects of organic synthesis with Drs. George Tennant and John Sharp as well as Prof. Hamish McNab were very useful.

The funding by the Departmental Watt Bursary was very much appreciated and welcome.

Thank you to everybody behind the scenes, like the secretaries and the technicians, who ensure smooth proceedings and are all good and nice people.

I would like to express my gratefulness towards all those special people, who have become good friends. At the end of the day, this is the real thing, so thank you very much Alejandro Sanchez-Perucha, Michele Melchionna, Jesus Perea-Buceta, Maria Kaisheva, Philip Tobias Robinson, Andrew Rutherford, Anestis Tsakiridis, Akunna Ezebuiro and Giai Petit to name but a few.

The whole of the international community in the School of Chemistry ("Los Vellendos") deserves a special mention, the parties were crazy.

Finally, a sincere thank you goes out to Miss Maria Manoli (η κορη μου) for her patience and understanding, her exceptional kindness and extraordinarily big heart. The support was excellent and it was greatly appreciated. Thank you very much!

And now really finally, maybe the biggest thank you to my parents and my sister. Their interest in my progress and their support have been invaluable. Looking forward to coming home soon, by the way!

Declaration

I hereby declare that except where specific reference is made to other sources, the work contained in this thesis is the original work of the author. It has been composed by the candidate and has not been submitted, in whole or in part, for any other degree, diploma, or other qualification.

Michael Melchart

June 6th 2006

(06/06/06)

Contents

Abbreviations

5'AMP	adenosine 5'-monophosphate
5'CMP	cytidine 5'-monophosphate
5'GMP	guanosine 5'-monophosphate
5'TMP	thymidine 5'-monophosphate
9EtA	9-ethyladenine
9EtG	9-ethylguanine
acac	acetylacetonate
AcO	acetate
Ado	adenosine
bap	2-benzylaminopyridine
bip	biphenyl
bpy	2,2'-bipyridine
bz	benzene
ca.	*circa* (about)
cisplatin	*cis*-$[PtCl_2(NH_3)_2]$
COSY	correlation spectroscopy
Cp	cyclopentadienyl
dcp	3,5-dichloropyridine
DHA	9,10-dihydroanthracene
DMSO	dimethyl sulfoxide
dppz	dipyrido[3,2-a:2',3'-c]phenazine
en	ethylenediamine
GSH	glutathione
Guo	guanosine
hmb	hexamethylbenzene
IC_{50}	50% inhibitory concentration
ind	indan
LC-ESI-MS	Liquid chromatography electrospray ionisation tandem mass spectrometry
L-Cys	*L*-cysteine
L-His	*L*-histidine
L-MetH	*L*-methionine

L-pal	*L*-phenylalanine
ma	maltolate
mes	1,3,5-trimethylbenzene
NMR	nuclear magnetic spectroscopy
NOESY	nuclear Overhauser effect spectroscopy
ox	oxalate
p-cym	*para*-cymene
ROESY	rotating frame nuclear Overhauser effect spectroscopy
THA	1,4,9,10-tetrahydroanthracene
THF	tetrahydrofuran
trop	tropolonate

Chapter 1
Introduction

This thesis describes studies of organometallic mono- and bifunctional ruthenium(II) arene complexes which have potential anticancer applications, focussing on aspects of their design and reactivity.

First a short introduction to classical coordination and organometallic anticancer complexes is given, highlighting work involving ruthenium and relevant aspects of its chemistry. A summary of the synthesis and structures of Ru^{II} arene complexes is followed by a more detailed discussion of research on their biological activity. Particular attention is paid to the aqueous chemistry of some cytotoxic Ru^{II} arene complexes containing ethylenediamine as a chelating ligand and their reactivity with biomolecules, with an emphasis on DNA bases.

1.1 Metallodrugs

Most new drugs are organic (carbon) compounds but there is an increasing realisation that many metal ions are involved in natural biological processes and that there is much scope for the design of therapeutic agents based on both biologically-essential and non-essential metal ions [1, 2]. Metal complexes with their wide spectrum of coordination numbers, coordination geometries, thermodynamic and kinetic preferences (which cover enormous scales of magnitude) for ligand atoms, and in some cases redox activity, offer novel mechanisms of action which are unavailable to organic compounds. In general, the nature of the metal ion, its oxidation state, and the types and number of bound ligands, can all exert a critical influence on the biological activity of a metal complex [3, 4]. An understanding of how these factors affect biological activity should enable the design of metal complexes with specific medicinal properties. The wide spectrum of contrasting

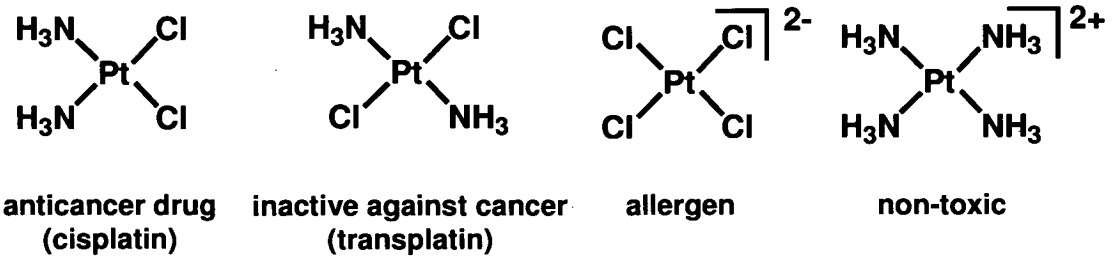

Figure 1.1: The contrasting biological activities of platinum complexes.

biological activity amongst platinum complexes (Figure 1.1) [1, 5, 6] and the clinical success of platinum(II) dia(m)mine complexes, *e.g.* cisplatin, as anticancer drugs provide a good illustration of this point. For example, not all platinum complexes are active anticancer agents. Some platinum complexes are inert and relatively non-toxic, some attack DNA, some do not. Although platinum complexes are now widely used for the treatment of cancer, the development of drug resistance, the toxic side-effects of cisplatin, and the lack of activity of platinum compounds against several types of cancer are problems which need to be overcome [7]. This provides the impetus for the search for anticancer activity amongst complexes of other metals.

Organometallic chemistry evolved rapidly during the second half of the 20th century [8, 9] and bioorganometallic chemistry is now establishing itself as an important branch of the subject [10]. In particular, organometallic complexes, *i.e.* complexes with at least one direct metal-carbon bond, offer much potential for exploration as anticancer agents due to the large diversity of structure and bonding modes (*e.g.* π-coordination, M-C multiple bonds) that are unique to them [11]. Despite this, few systematic attempts have been made to design organometallic complexes as therapeutic agents [12, 13]. This is perhaps due to the assumption that organometallic chemistry and biology are mutually incompatible, many organometallic compounds being sensitive to water and oxygen. However, research in the past decade or so, notably by Köpf [12], Alberto [14], Fish [15] and Jaouen [16], has demonstrated that these problems can be overcome, and that organometallic pharmaceuticals can be formulated.

1.2 Metal-based Anticancer Complexes

Current interest in the use of metal complexes for the treatment of cancer was triggered by the discovery of the anticancer activity of Pt^{II} amine complexes in 1969 by Rosenberg [17]. The primary target is DNA [18]. Since then at least four platinum complexes have been approved for clinical use (Figure 1.2) and they are the most widely-used anticancer drugs. Stimulation for the discovery of anticancer complexes of metals other than platinum arises from the cellular resistance to platinum which is sometimes encountered in the clinic, the toxic side-effects of cisplatin, which can be severe, and the limited spectrum of activity against different types of cancer [7].

The organometallic complex titanocene dichloride, Cp_2TiCl_2, where Cp = cyclopentadienyl (Figure 1.3), was originally investigated because it was believed that the *cis*-$TiCl_2$ motif would react with DNA to form bifunctional cross-links in a similar manner to cisplatin. However, Cp_2TiCl_2 binds only weakly to DNA bases, but more strongly to the phosphate backbone [19]. Cp_2TiCl_2 is difficult to formulate for administration because of its ease of chloride and Cp hydrolysis and formation of hydroxo- and oxo-bridged species. Responses to titanocene dichloride in the clinic were not encouraging and the trials have now been abandoned [20, 21]. Other

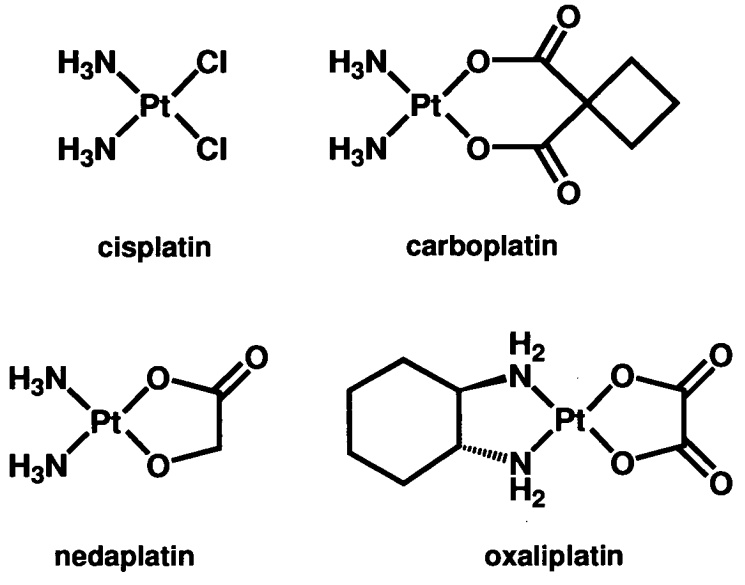

Figure 1.2: Platinum(II) complexes approved for clinical use as anticancer drugs.

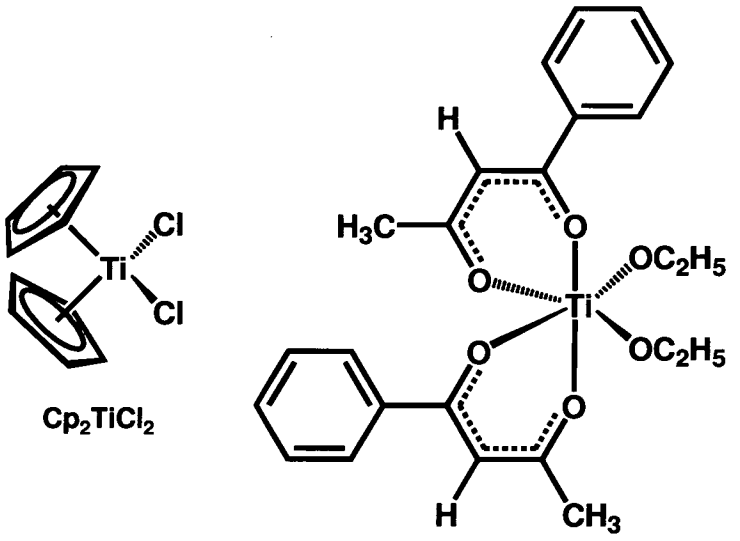

Figure 1.3: Titanium anticancer drugs which have been on clinical trials.

metallocenes are active *in vitro*, *e.g.* Cp_2VCl_2 and Cp_2NbCl_2 [12], but have not reached clinical trials.

Another Ti^{IV} complex, budotitane (Figure 1.3) was the first non-platinum complex to be approved for clinical trials, but poor solubility and hydrolysis made formulation difficult even in micelles, and the trials were abandoned [22].

More recently, Jaouen *et al.* prepared a series of ferrocenyl derivatives ("ferrocifens") of the breast cancer drug tamoxifen (Figure 1.4) [23, 24]. Several of these compounds are highly active against both estrogen-dependent and estrogen-independent breast cancer cells. Ferrocifens are thought to act against estrogen-independent breast cancer cells by causing oxidative damage to DNA, after the ferrocenyl group is oxidized in the cells [24].

1.3 Ruthenium

1.3.1 Chemistry and medicinal applications

Ruthenium (Ru, atomic number 44, atomic weight 101.07(2), [Kr] $4d^7\ 5s^1$) belongs to the so-called "platinum" metals group together with the elements Rh, Pd,

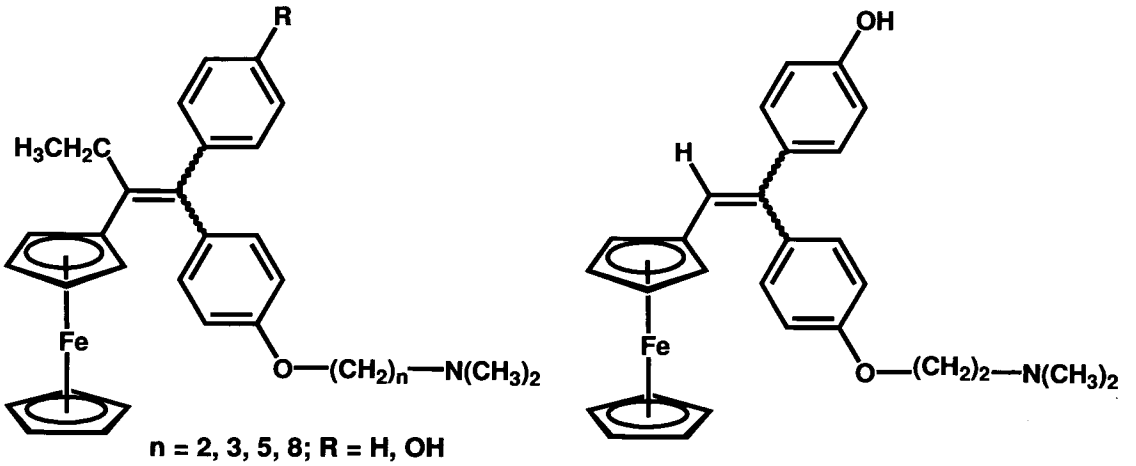

Figure 1.4: Ferrocifens: active against breast cancer cells.

Os, Ir and Pt. It has a rich redox chemistry with possible oxidation states ranging from –II to +VIII. Due to strong ligand-field stabilisation, ruthenium in its more common oxidation states Ru^{II}, Ru^{III} and Ru^{IV} in aqueous solution is usually low spin octahedral and nearly always six-coordinate.

Ruthenium compounds in general are well-suited for medicinal applications [25]. With seven naturally occurring isotopes, ruthenium can be used in radiopharmaceuticals (radioactive ruthenium γ-ray emitters ^{97}Ru, $t_{1/2}$ 2.9 d, 216 keV, and ^{103}Ru, $t_{1/2}$ 39 d, 497 keV) [2]. Other complexes have been investigated as immunosuppressants [26, 27], nitric oxide scavengers [28], antimicrobial agents [29] and antimalarials [30]. Ruthenium Red, $[(NH_3)_5Ru^{III}ORu^{IV}(NH_3)_4ORu^{III}(NH_3)_5]^{6+}$, is known to inhibit calcium ion uptake by the mitochondria [31].

In the context of anticancer research (*vide infra*) Clarke has proposed that the activity of Ru^{III} complexes, which are usually relatively inert towards ligand substitution, is dependent on *in vivo* reduction to more labile Ru^{II} complexes [32, 33]. As reduction of Ru^{III} to Ru^{II} fills the d_π (t_{2g}) orbitals, π-donor ligands that coordinate firmly to Ru^{III} are no longer able to do so with Ru^{II} and bind less strongly

[2]. In the case of Ru^{II} am(m)ine complexes, acido ligands are lost fairly rapidly (k = 1 – 10 s^{-1}) [34, 35].

In reactions with biomolecules, many am(m)ine complexes of Ru^{II} and Ru^{III} tend to selectively bind to imine sites, which have available nitrogen lone pairs of electrons, as opposed to amine sites, which tend to be protonated at neutral pH [2]. Consequently, nitrogens of imidazole rings on histidine (on proteins) and purines (on DNA) present the readiest binding targets to Ru^{II}. Thiolato complexes, which are very stable for platinum(II) complexes [36], are often kinetically unstable with ruthenium [37], particularly in air [38].

1.3.2 Anticancer complexes

Early interest in the anticancer activity of ruthenium complexes stemmed from the observations of Clarke [32] that Ru^{III} am(m)ines, *e.g.* $[RuCl_3(NH_3)_3]$, are active anticancer agents (Figure 1.5). However, these were too insoluble for use.

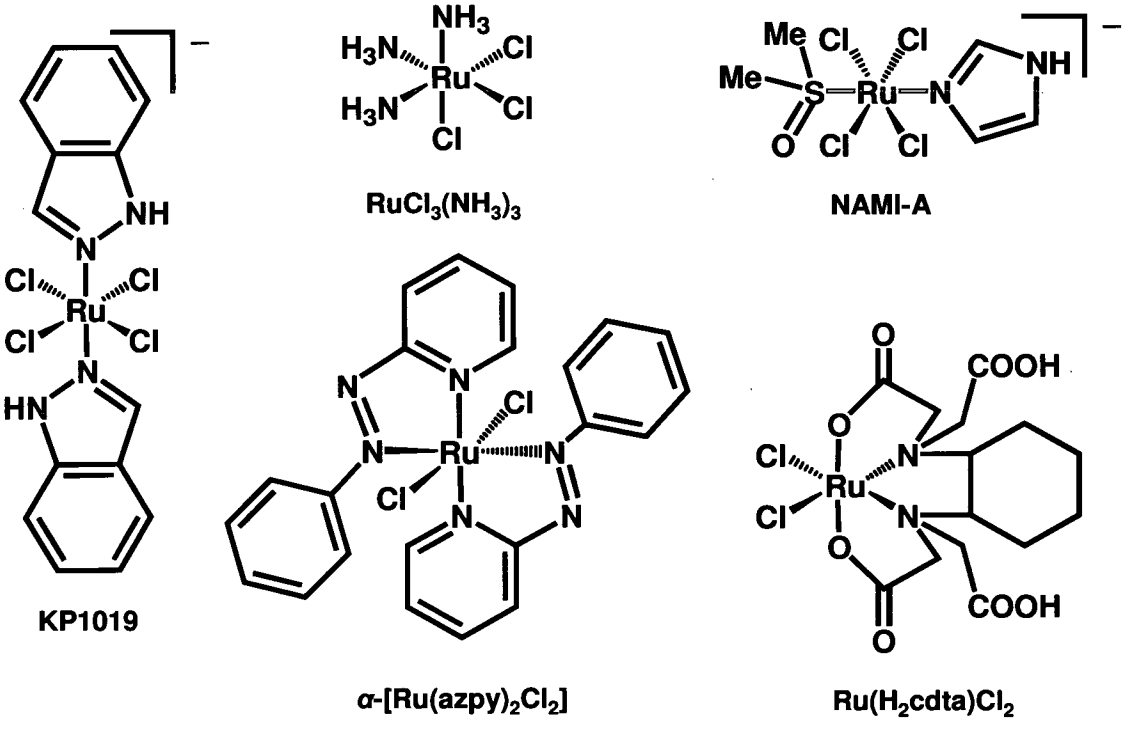

Figure 1.5: Ruthenium anticancer complexes.

Two other Ru^{III} complexes, *trans*-[$RuCl_4$(DMSO)(Im)]ImH, where Im = imidazole (NAMI-A) [39], and *trans*-[$RuCl_4(Ind)_2$]IndH, where Ind = indazole (KP1019) [40], have now entered trials. KP1019 is cytotoxic to cancer cells, whereas NAMI-A is relatively non-toxic but has antimetastatic activity and prevents the spread of cancer. Several other Ru complexes have shown promise recently [41, 42] as anticancer complexes, *e.g.* the Ru^{II} complex α-[$Ru(azpy)_2Cl_2$], where azpy = 2-phenylazopyridine) and the Ru^{IV} complex [$Ru(H_2cdta)Cl_2]\cdot 2H_2O$, where H_2cdta = 1,2-cyclohexanediaminotetraacetate (Figure 1.5).

The hypothesis of "activation by reduction" led to the exploration of the anticancer activity of Ru^{II} complexes, namely Ru^{II} aminophosphines, which were cytotoxic to cancer cells [43], but had poor aqueous solubility and were difficult to isolate and purify in large quantities. Arene ligands are known to stabilise ruthenium in its +II oxidation state and the suitability of ruthenium(II) arene complexes for biological applications was recognised by Sheldrick and co-workers. They studied the interactions of such complexes with α-amino acids [44] as well as purine nucleobases and nucleotides [45 – 49]. Investigations of the potential of Ru^{II} arene complexes as anticancer agents and their associated aqueous chemistry were carried out by Sadler *et al.* [50, 51]. It was found that "half-sandwich" Ru^{II} mono-arene complexes often possess good aqueous solubility (an advantage for clinical use) and that the arene ligand is relatively inert towards displacement under physiological conditions.

Initial interest in Ru^{II} mono-arene complexes was mainly dominated by catalytic properties [52] ranging from alkene- and aromatic-hydrogenation, to Diels-Alder reactions, alkene metathesis, and asymmetric hydrogen transfer reductions of ketones and imines [53]. Catalytic activity usually requires the presence of a labile coordination site on Ru^{II} and/or arene displacement [54, 55]. The pH-dependent transfer hydrogenation of ketones with formate as a hydride donor by {(η^6-

$C_6Me_6)Ru(bpy)\}^{2+}$, where bpy = 2,2'-bipyridine, in water was reported recently by Ogo *et al.* [56].

1.4 Ruthenium(II) Arene Complexes

1.4.1 Synthesis

The synthesis of Ru^{II} arene complexes cannot usually be achieved by simple reaction of Ru^{II} with an arene, but requires a redox reaction. The first arene complexes of Ru^{II} were synthesized as sandwich molecules in 1957 by Fischer and Böttcher (Figure 1.6) by stirring $RuCl_3$ with anhydrous $AlCl_3$, powdered Al, and the respective arene under N_2 at 130°C for 8-10 h [57]. In 1967 Fischer *et al.* [58] reported the synthesis of $[(\eta^6\text{-naphthalene})_2Ru](PF_6)_2$, and Winkhaus and Singer [59] synthesized the polymeric mono-arene complex $[(\eta^6\text{-benzene})RuCl_2]_x$ by reaction of $RuCl_3$ with 1,3-cyclohexadiene in ethanol. Subsequently Bennett *et al.* [60] reported piano-stool geometries for $[(\eta^6\text{-arene})RuCl_2(P(CH_3)Ph_2)]$ with arene = benzene or *p*-

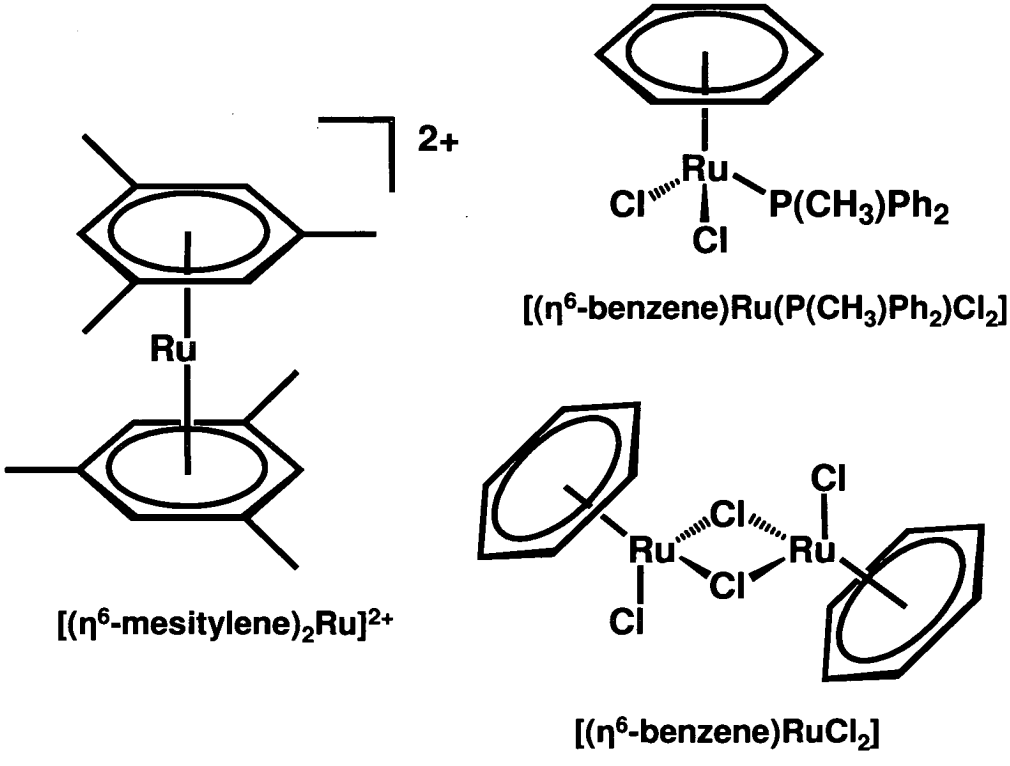

Figure 1.6: Early examples of sandwich and half-sandwich Ru^{II} arene complexes.

cymene (Figure 1.6), as determined by X-ray crystallography, and Zelonka and Baird [61] found that the dimer $[(\eta^6\text{-benzene})RuCl_2]_2$ (Figure 1.6) undergoes useful reactions with electrophilic as well as nucleophilic reagents such as phosphines with formation of monomeric complexes *e.g.* $[(\eta^6\text{-benzene})Ru(PR_3)Cl_2]$, where R = Ph, Bu, Et, OPh, OEt and OMe. In 'piano-stool' complexes, the arene forms the seat of the "piano stool" and the other three ligands the legs. Distortion of the bound arene ring was noted for $[(\eta^6\text{-benzene})Ru(P(CH_3)Ph_2)Cl_2]$ (Figure 1.6) (four Ru-C bonds of *ca.* 2.19 Å, two Ru-C bonds of 2.27 Å with the longer bonds *trans* to P). The slight bend (dihedral angle 5°) suggested some degree of localization of the ring π-electrons. Later work on other compounds has also suggested that localization of π-electron density can occur, and is accompanied by alternating long and short C-C bonds [62, 63]. The general structural, stereochemical and electronic features of metal-arene complexes have been discussed [64].

There are a number of very different routes towards the synthesis of Ru^{II} arene complexes and their starting dimers. Examples have been reviewed [51, 52].

It is possible to introduce a bound arene as part of a chelate ring in the form of a tethered complex [65, 66]. Such syntheses often require high pressures, and tethered complexes, such as that shown in Figure 1.7, have been of particular interest in the catalysis field [67, 68]. Strapped sandwich complexes can also be synthesised

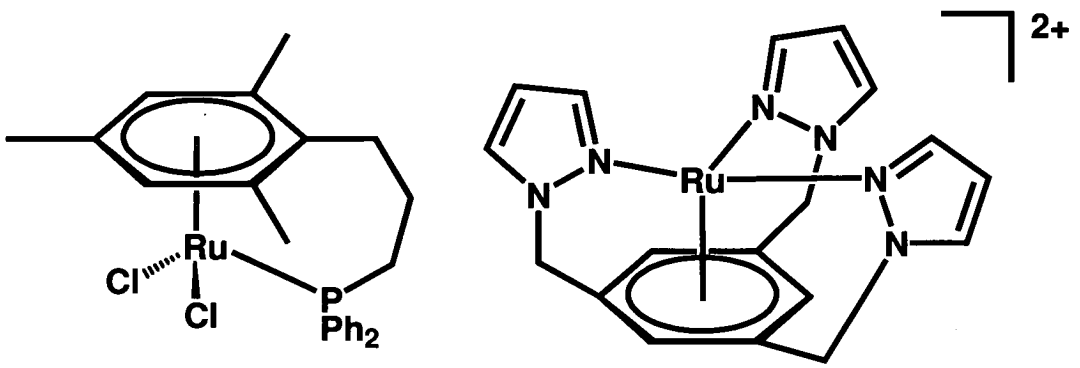

tethered Ru^{II} arene **encapsulated Ru^{II} arene**

Figure 1.7: Examples of tethered and encapsulated Ru^{II} arene complexes.

[69]. Furthermore, it is possible to encapsulate Ru^{II} by an η^6-arene possessing a triple strap (Figure 1.7) [70, 71].

1.4.2 Structure

A typical structure of a half-sandwich "piano-stool" [(η^6-arene)Ru(X)(Y)(Z)] complex is shown in Figure 1.8, where the arene forms the seat of the piano stool and the ligands resemble the legs.

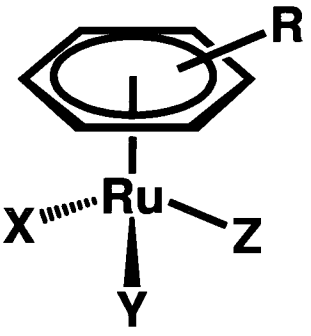

Figure 1.8: Typical structure of a Ru^{II} half-sandwich 'piano-stool' complex. Coordination positions X, Y and Z and arene substituent(s) R provide scope for investigation of anticancer structure-activity relationships.

The X-ray crystal structure [72] of $[(\eta^6\text{-bip})Ru(en)Cl)]^+$, where bip = biphenyl, en = ethylenediamine, is shown in Figure 1.9. The complex exhibits the normal characteristic features of mono-arene Ru^{II} complexes: an alternation of the lengths of the C-C bonds for the coordinated arene and irregular Ru-C bond lengths, with the longest of 2.24 Å (compared to 2.14 Å for the shortest) being for the carbon attached to the phenyl substitutent.

The framework of ruthenium(II) arene complexes provides considerable scope for optimising the design in terms of solubility, reactivity and biological activity [50]. Linking the ligands Y and Z to form a bidentate chelating ligand (L) seems to be advantageous for anticancer activity. The structure of Ru^{II} half-sandwich complexes allows for variations of the three main building blocks, the monodentate ligand X, the bidentate ligand L and the arene, to fine-tune the pharmacological properties of these complexes. The nature of the arene can help to influence cell uptake and interactions with potential targets. The leaving group, which typically is

chloride and occupies the biomolecule binding site on the metal centre, can be of importance to control the timing of activation of these complexes.

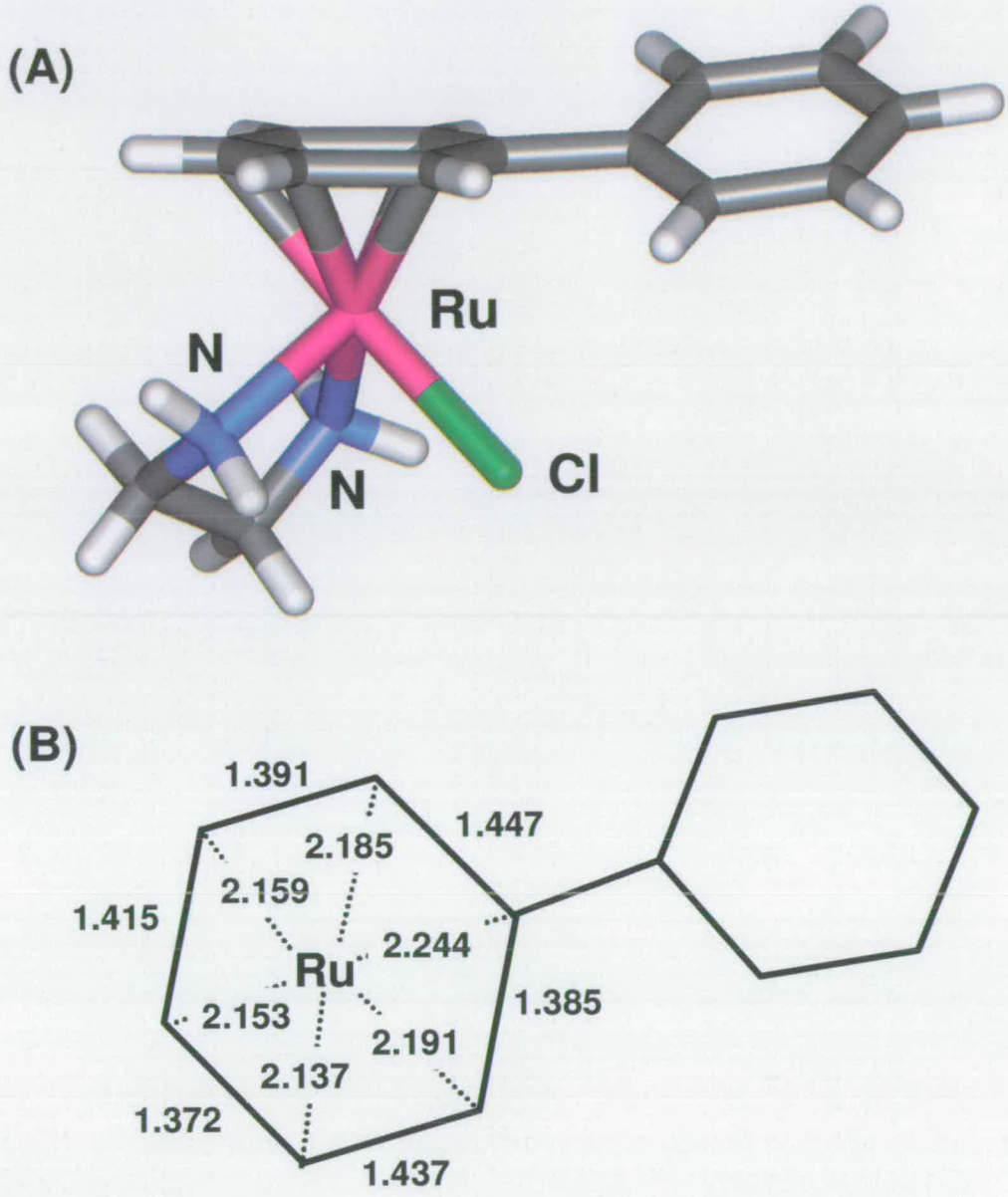

Figure 1.9: X-ray crystal structure of the cation in the cytotoxic complex [(η^6-bip)Ru(en)Cl]PF_6 [72] (A). The complex has the characteristic 'piano-stool' structure with alternation of C-C bond lengths for the coordinated phenyl ring and irregular Ru-C bond lengths as shown diagrammatically in (B).

1.4.3 Biological activity

1.4.3.1 Antibacterial

Some Ru^{II} arene complexes have been reported to exhibit antimicrobial activity. Tocher *et al.* found that in the complex $[(\eta^6\text{-benzene})Ru(metro)Cl_2]$, where metro = 1-$\beta$-hydroxyethyl-2-methyl-5-nitroimidazole (Figure 1.10A), the electron affinity of metro was not altered, but decreased the lifetime of the one-electron reduction product (the nitro radical anion) and increased the differential cytotoxicity towards *E. coli* grown under hypoxic conditions [73].

Çetinkaya *et al.* [74] have reported antibacterial and antifungal activities of complexes of the type $[(\eta^6\text{-arene})Ru(X)Cl_2]$, where arene = *p*-cymene or hexamethylbenzene, and X = nitrogen or carbon donors. The conclusion was that compounds with hydrophobic substituents (Figure 1.10B) displayed significantly more activity because of an increased ability to cross the cellular membrane.

Allardyce *et al.* [29] have noted that some phosphine complexes of the type $[(\eta^6\text{-}p\text{-cymene})Ru(pta)X_2]$ (Figure 1.10C), where X = Cl, NCS, and pta = 1,3,5-triaza-7-phosphatricyclo[3.3.1.1]decane) exhibit antibacterial activity, but no doses were specified. They suggested that proteins rather than DNA may be the target sites.

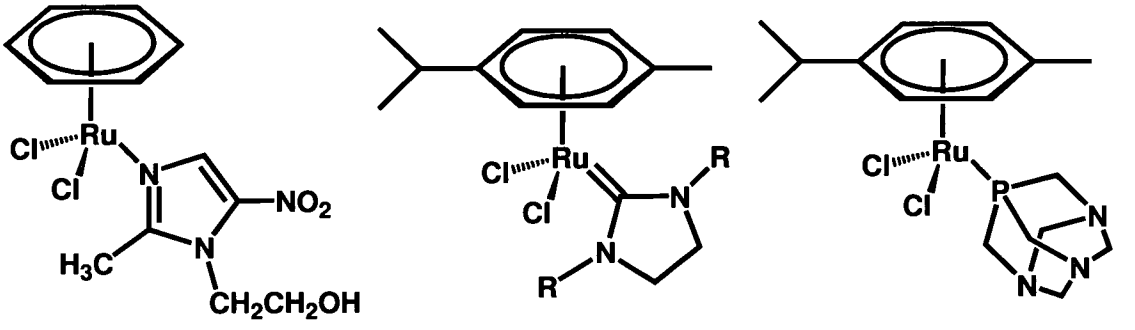

Figure 1.10: Antimicrobial Ru^{II} arene complexes.

1.4.3.2 Anticancer

Sheldrick *et al.* reported the *in vivo* antitumour activity of the complex $[(\eta^6\text{-}C_6H_6)Ru(pro)Cl]$, where pro = proline, towards P388 leukaemia cells [45]. However, no data were given and no further reports appear to have been published.

Reproducible cytotoxicities against A2780 human ovarian cancer cells are exhibited by the complexes $[(\eta^6\text{-arene})Ru(en)Cl]^+$ (Figure 1.11) [72]. Activity appears to increase with the size of the coordinated arene: benzene (bz) < *p*-cymene (*p*-cym) < biphenyl (bip) < dihydroanthracene (DHA) < tetrahydroanthracene (THA), such that, in this cell line, the bip complex has similar cytotoxicity to the anticancer drug carboplatin (IC_{50}, the dose which inhibits growth of 50% of the cells, 6 μM) and the THA complex is as active as cisplatin (IC_{50} 0.6 μM) (Table 1.1) [75]. The complexes $[(\eta^6\text{-}p\text{-cym})Ru(X)_2Y]^{n+}$ (X or Y = halide, acetonitrile or

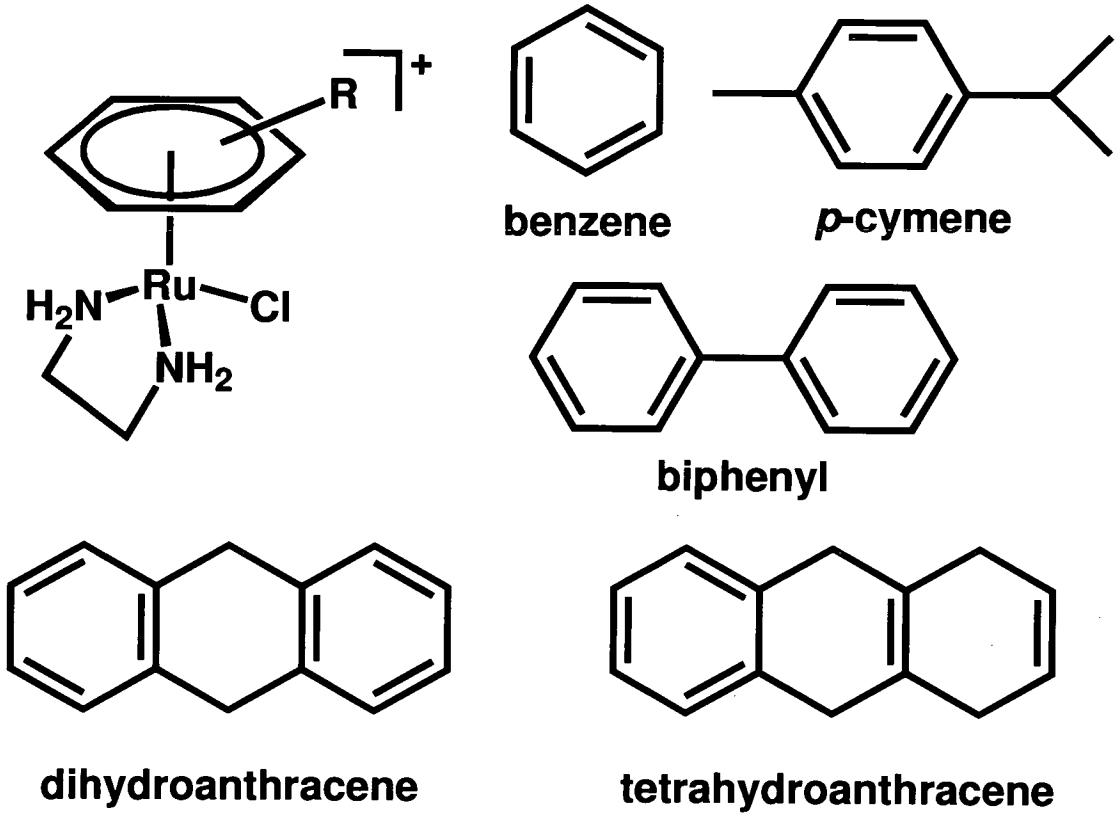

Figure 1.11: Five $[(\eta^6\text{-arene})Ru(en)Cl]^+$ complexes (arenes shown separately) for which activity against A2780 human ovarian cancer cells has been investigated [72].

Table 1.1: IC_{50} values of Ru^{II} arene complexes [(η^6-arene)RuX(Y)Cl]A [A = PF_6^- for positively-charged complexes] in A2780 human ovarian cancer cells after 24 h drug exposure and comparison with carboplatin and cisplatin [75].

Arene/*Pt complex*	X	Y	IC_{50} (μM)
p-Cymene	CH_3CN	CH_3CN	>100
p-Cymene	Cl	isonicotinamide	>100
$C_6H_5CO_2CH_3$	$H_2NCH_2CH_2NH_2$		56
Benzene	$H_2NCH_2CH_2NH_2$		17
p-Cymene	$H_2NCH_2CH_2NH_2$		10
Carboplatin			6
$C_6H_5C_6H_5$	$H_2NCH_2CH_2NH(Et)$		6
$C_6H_5C_6H_5$	$H_2NCH_2CH_2NH_2$		5
Dihydroanthracene	$H_2NCH_2CH_2NH_2$		2
Cisplatin			0.6
Tetrahydroanthracene	$H_2NCH_2CH_2NH_2$		0.5

isonicotinamide), with 3 monodentate ligands, are however inactive (IC_{50} > 100 μM) towards A2780 human ovarian cancer cells *in vitro* [72]. The findings agree with results obtained for other Ru^{II} arene complexes containing three monodentate ligands, for which only poor cytotoxicity has been reported [76, 77, 78]. These complexes may be too reactive with components of the cell culture medium and/or the cells and are deactivated for example by biomolecules before they reach their target sites.

From the above results, it appears that a more hydrophobic arene ligand and a single ligand exchange site (occupation of the other two coordination sites by a stable bidentate chelating ligand) are associated with high cytotoxicity. Recent cytotoxicity tests on a more extensive range of Ru^{II} arene complexes have indicated, however, that the structure-activity relationship is more complex [79]. Replacing en by N, N, N′, N′-tetramethylethylenediamine or 2,2′-bipyridine results in complexes with

insignificant cytotoxicity, whilst complexes with 1,2-diaminobenzene as the chelating ligand show comparable or enhanced cytotoxicity compared to the en analogues.

The leaving group X can also have an influence on the cytotoxicity in complexes of the type $[(\eta^6\text{-arene})Ru(en)X]^{n+}$ [80]. For example, complexes $[(\eta^6\text{-hmb})Ru(en)X]^{n+}$, where hmb = hexamethylbenzene, with X = I^- or pcp, where pcp = 4-cyanopyridine, are very active against the human ovarian cancer cell line A2780. With X = pic, where pic = 3-methylpyridine, only moderate activity was found and with X = py, where py = pyridine, no activity was observed.

Important was the finding that these $[(\eta^6\text{-arene})Ru(N,N)Cl]^+$ complexes are equally potent towards wild-type and cisplatin-resistant cancer cells in culture [75]. This suggested that the mechanism of action was different from cisplatin.

Ruthenium arene complexes appear to have a wide spectrum of cytotoxicity towards cancer cells. For example, the complexes $[(\eta^6\text{-bip})Ru(en)Cl]PF_6$ and $[(\eta^6\text{-DHA})Ru(en)Cl]PF_6$ are active against not only A2780 human ovarian cancer cells, but also HT29 colon, Panc-1 pancreatic and NX02 lung cancer cells with IC_{50} values in the range 1-13 μM [79].

The patterns of activity established *in vitro* for $[(\eta^6\text{-bip})Ru(en)Cl]PF_6$ are mirrored to a large degree *in vivo* [75].

1.4.4 Interaction with biologically-relevant molecules

In biological systems, $[(\eta^6\text{-arene})Ru(L)X]^{n+}$ complexes will encounter an array of biomolecules with which they could potentially react. Such interactions could be relevant in their roles as deactivating pathways, transport mechanisms or targets. Hence it is important to gain a detailed understanding of such interactions with ligands ranging from water and chloride to nucleobases, oligonucleotides, DNA, amino acids and proteins. Reactions in media with low dielectric constants may also

be relevant to the passage of the complexes across membranes. An interesting possibility is that Ru^{II} could become involved in blocking Fe^{II} pathways but this has yet to be studied.

This section will mainly focus on complexes of the type $[(\eta^6\text{-arene})Ru(en)X]^{n+}$ and reports by the Sadler group. Reactions and interactions involving other ruthenium arene complexes, predominantly with three monodentate ligands, have been reviewed recently [51].

1.4.4.1 Aquation

Since it appears [81, 82] that aquation can be the rate-limiting step in the reactions of Ru^{II} arene complexes with both amino acids and nucleotides, detailed studies of the factors which influence the rate and extent of aquation and the pK_a value of the resulting aqua adduct have been undertaken.

Taube *et al.* [83] carried out early studies on the chemistry of aqua adducts of Ru^{II} arene complexes and reported pK_a values of 6.3 for $[(\eta^6\text{-benzene})Ru(NH_3)_2(H_2O)]^{2+}$ and 7.9 for the en analogue. They noted the increase in affinity of Ru^{II} for chloride when three ammonia ligands are replaced by benzene, attributable to the electron-withdrawing power of the η^6-bonded arene. Dadci *et al.* [84] reported that introduction of benzene into the Ru^{II} hexaaqua complex $[Ru(H_2O)_6]^{2+}$ enhances the water exchange rate by a factor of 640, whereas the additional introduction of 2,2'-bipyridine (bpy) into $[(\eta^6\text{-benzene})Ru(H_2O)_3]^{2+}$ to give $[(\eta^6\text{-benzene})Ru(bpy)H_2O]^{2+}$ reduces the rate by 174 and becomes only *ca.* 4x faster than the hexaaqua ion.

The X-ray crystal structures of the aqua complexes $[(\eta^6\text{-arene})Ru(en)X](PF_6)_n$, where arene = biphenyl (bip), X = 0.5 H_2O / 0.5 OH, n = 1.5, arene = tetrahydroanthracene (THA), X = 0.5 H_2O / 0.5 OH, n = 1.5, arene = THA, X = H_2O, n = 2, and arene = dihydroanthracene (DHA), X = H_2O, n = 2, have been

reported [85]. In the bip complex, there is a large propeller twist of 45° of the pendent phenyl ring with respect to the coordinated phenyl ring. The tricyclic THA ligand is relatively flat in these aqua complexes, but the DHA ring system is markedly bent (hinge bend *ca.* 35°) as it is in the chloro complex (41°) (Table 1.2). These finding highlight the structural flexibility of the coordinated arenes.

Table 1.2: Change in hinge-bending and orientation of the arene in [η^6-arene)Ru(en)X]$^+$ complexes (arene = DHA and THA) induced by substitution of Cl^- by water or N7-bound 9-ethylguanine [81, 85].

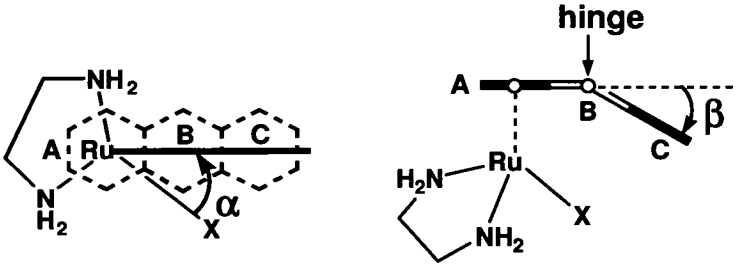

Arene	Orientation angle α (°) X =			Hinge bending angle (°) X =		
	Cl	H_2O	9EtG	Cl	H_2O	9EtG
Dihydroanthracene	64.1	34.0[a]	20.1	40.6	35.1[a]	31.9
Tetrahydroanthracene	45.1	63.7	25.6	-7.5	-1.8	27.8

[a] Average for two independent cations in unit cell

1.4.4.2 Aqueous chemistry

In aqueous media the chloride ligand of [(η^6-arene)Ru(L)Cl]$^+$ complexes can exchange with water to form aqua complexes [(η^6-arene)Ru(L)H_2O]$^{2+}$. For L = en, the chloride-containing complexes generally undergo substitution reactions very much more slowly than the corresponding aqua compounds [81], hence it is important to understand the thermodynamics and kinetics of formation of the aqua complexes (*i.e.* activated form of the ruthenium arene complexes). The rates of aquation of [(η^6-arene)Ru(en)Cl]PF_6 (arene = bip, DHA and THA) at 310 K and

ionic strength (I, $NaClO_4$) of 0.1 M (k_{H_2O} 3.95 – 6.84 × 10^{-3} s^{-1}) are an order of magnitude faster than that of cisplatin [85]. The reverse, anation reactions in the presence of 100 mM NaCl (similar concentration to that in blood plasma) are also very rapid (k_{Cl} 0.435 – 0.722 M^{-1} s^{-1}, 310 K, I = 0.1 M). The aquation and anation reactions are *ca.* 2 times faster for the DHA and THA complexes compared to the bip complex, suggesting that variations in the steric and electronic effects of the arene ligands modulate the ligand exchange reactions. The exchange reactions appear to occur *via* an associative pathway, $\Delta S^{\ddagger}$ being negative [85]. Since the anation reactions are rapid, the equilibrium constants for aquation (k_{H_2O}/k_{Cl}) are small, 9.0 – 11.7 × 10^{-3} M. Hence at physiologically-relevant concentrations of the ruthenium(II) arene complexes (0.5 – 5 μM), the complexes should be present in blood plasma ($[Cl^-]$ = 104 mM) largely as the less reactive chloro complexes (> 89%), whereas in the cell nucleus ($[Cl^-]$ = 4 mM) [86, 87] significant amounts (45 – 65%) of the more reactive aqua species would be formed readily (Figure 1.12), together with smaller amounts of hydroxo complexes (9 – 25%).

The hydrolysis rates of $[(\eta^6\text{-arene})Ru(en)X]^{n+}$ complexes are dependent on the nature of the arene and the leaving group in particular. Half-lives vary from seconds (hmb/Cl^-) to minutes (*e.g.* hmb/N_3^-) to hours (*e.g.* hmb/dcp, bip/N_3), where dcp = 3,5-dichloropyridine, or half-lives which are too slow to be measured (*e.g.* hmb/py) [80].

The coordinated aqua ligand of $[(\eta^6\text{-arene})Ru(en)H_2O]^{2+}$ undergoes acid dissociation to give the hydroxo complex $[(\eta^6\text{-arene})Ru(en)OH]^+$, which is less susceptible to substitution reactions than the aqua complex [81]. Hence knowledge of the pK_a values of aqua adducts could be useful in drug design. The pK_a values range from 7.71 to 7.89 and 8.01 for the bip, DHA and THA aqua complexes, respectively [85]. Since the pK_a values are high, only small amounts of the hydroxo species (<10% of the total Ru arene complex) would be present at biological pH (7.2 – 7.4)

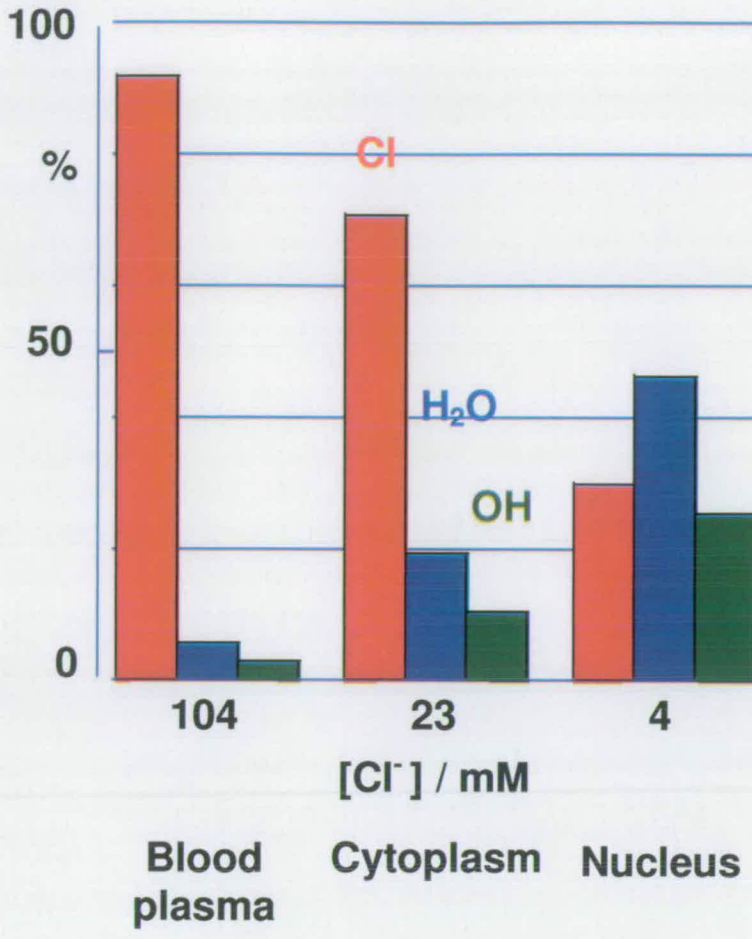

Figure 1.12: Speciation of $[(\eta^6\text{-bip})Ru(en)Cl]^+$ [5 μM] in blood plasma, cytoplasm and nucleus at equilibrium, calculated based on the chloride concentration and pH in these environments and the equilibrium constant of aquation and pK_a of the complex [85].

(Figure 1.12), *cf.* for cisplatin, the dominant species in the cell nucleus are the less reactive hydroxo forms [87].

1.4.4.3 Nucleobase and DNA binding

Binding studies of ruthenium(II) arene complexes with nucleobases are of special interest since DNA is the primary target of the archetypal metal-based drug, cisplatin [88].

Sheldrick *et al.* have provided solid state evidence of the ability of a ruthenium arene fragment to coordinate to two guanine bases in the X-ray crystal structure of $[(\eta^6\text{-}C_6H_6)Ru(H_2O)(9EtG)_2](CF_3SO_3)_2$ [48].

Chelation of $\{(\eta^6\text{-arene})Ru\}^{2+}$ to N7 and deprotonated N6 of adenine derivatives to give a 5-membered ring is facile, giving rise to tri- (or tetra-, when N9 available) nuclear adducts (Figure 1.13) [48]. Reaction of $[(\eta^6\text{-benzene})Ru(D_2O)_3]^{2+}$ with 5'-AMP (adenosine 5'-monophosphate) gives rise to diastereomeric cyclic trimers $[\{(\eta^6\text{-benzene})Ru(5'\text{-AMP})\}_3]$ in which 5'-AMP is coordinated by N1, N7 and deprotonated N6 of 5'-AMP [47].

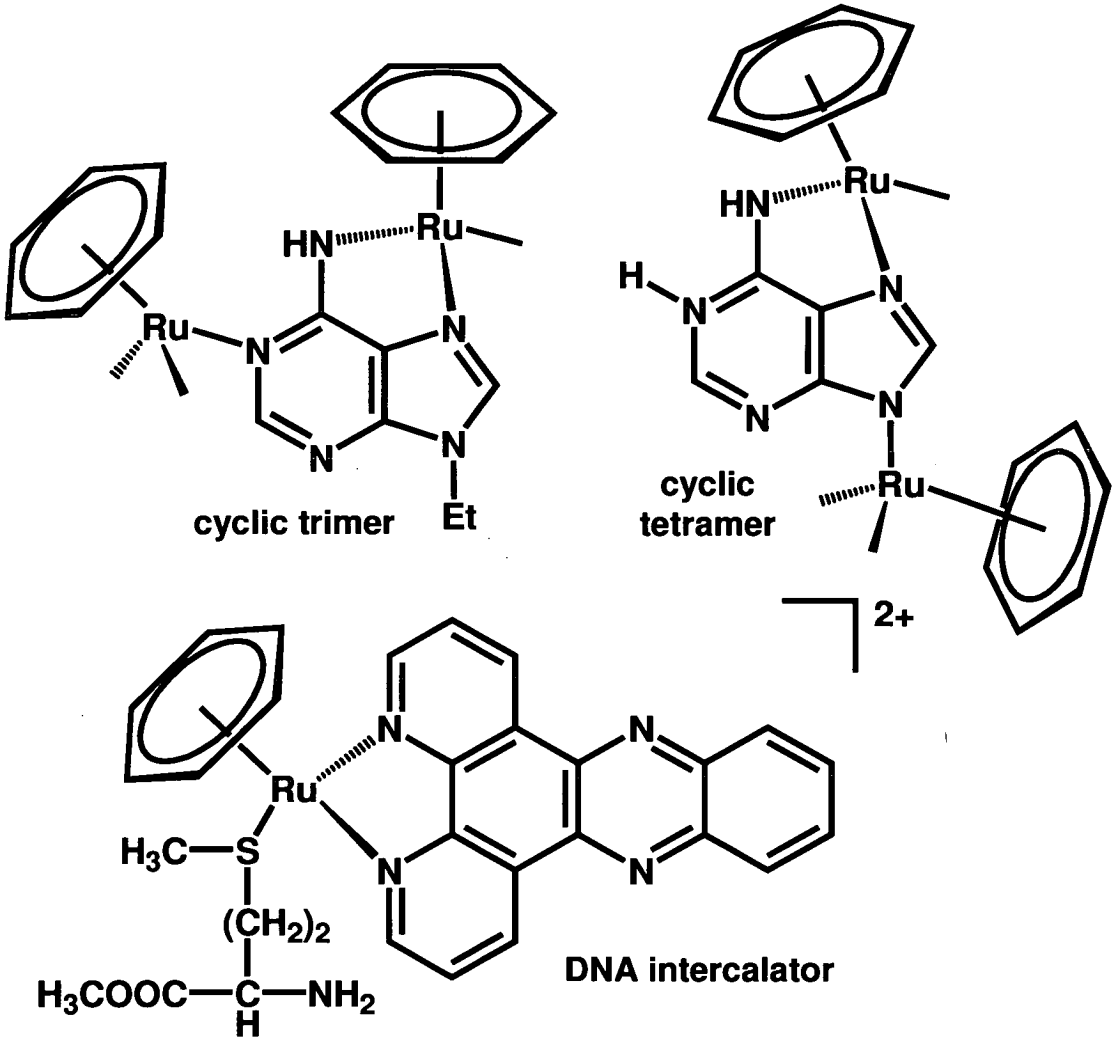

Figure 1.13: Bridging modes of binding for 9-ethyladenine in a cyclic trimer and adenine in a cyclic tetramer. Complex containing a diamine as a DNA intercalator.

Frodl *et al.* [89] have incorporated the DNA intercalator dppz (dipyrido[3,2-*a*:2',3'-*c*]phenazine) as a chelated diamine into $[(\eta^6\text{-arene})Ru(Aa)(dppz)]^{n+}$ (Aa = L-cysteine or L-methionine) complexes (Figure 1.13). Stable intercalative binding was observed with stability constants which increased from *ca.* 10^5 to *ca.* 10^7 as the charge on the complexes increased from +1 to +3.

Reactions of complexes $[(\eta^6\text{-arene})Ru(en)X]^{n+}$, where arene = bip, THA, DHA, p-cym and bz, X = Cl^- or H_2O, with nucleic acid derivatives (Figure 1.14) as models of DNA were investigated [81]. For mononucleosides, $\{(\eta^6\text{-bip})Ru(en)\}^{2+}$ binds only to N7 of guanosine (Guo) and to N3 of thymidine (Thy). Binding to N3 of cytidine (Cyt) is weak, and almost no binding to adenosine (Ado) is observed. The reactivity of the various binding sites of nucleobases towards Ru^{II} at neutral pH decreases in the order Guo(N7) > Thy(N3) > Cyt(N3) > Ado(N7), Ado(N1). Although this parallels the preference of cisplatin for binding with guanine (G) over adenine (A) [90], the diamino Ru^{II} arene complexes are more highly discriminatory between G and A bases than Pt^{II} complexes. This site-selectivity appears to be enhanced by the en NH_2 groups, which H-bond with exocyclic oxygens (*e.g.* C6O of G, Figure 1.15) but are non-bonding and repulsive towards exocyclic amino groups of the nucleobases (*e.g.* $C6NH_2$ of A, Figure 1.15). Strong stereospecific intramolecular H-bonding between an en NH proton oriented away from the arene and the C6O carbonyl of G is present in the crystal structures of these guanine adducts [91] (Figure 1.16; average N···O distance 2.8 Å, N-H···O angle 163°).

For mononucleotides, the same pattern of site selectivity is observed with reactions proceeding *via* aquation of $[(\eta^6\text{-arene})Ru(en)Cl]^+$, followed by rapid binding to the 5′-phosphate group, and then rearrangement to give N7, N1 or N3-bound products [81]. In competitive reactions of $[(\eta^6\text{-bip})Ru(en)Cl]^+$ with mono-phosphates 5′-GMP, 5′-AMP, 5′-CMP and 5′-TMP, the only final adduct is $[(\eta^6\text{-bip})Ru(en)\ GMP\text{-}N7]^{2+}$. In solution, NMR studies provided evidence that en NH

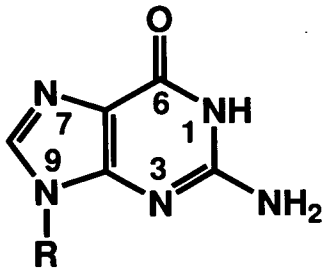

guanosine (R = R^1)
5'-GMP (R = R^2)
cGMP (R = R^3)

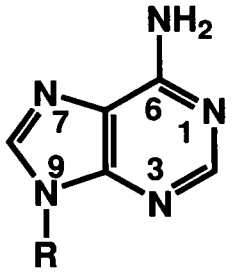

adenosine (R = R^1)
5'-AMP (R = R^2)
cAMP (R = R^3)

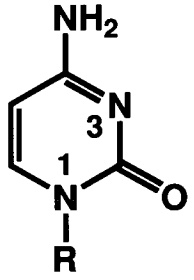

cytidine (R = R^1)
5'-CMP (R = R^2)

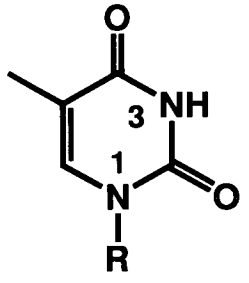

thymidine (R = 2' deoxy-R^1)
5'-TMP (R = 2'deoxy-R^2)

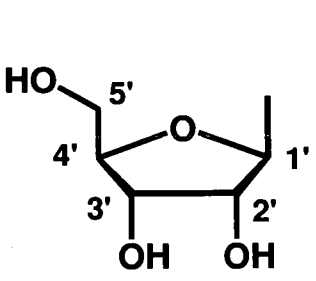

R^1

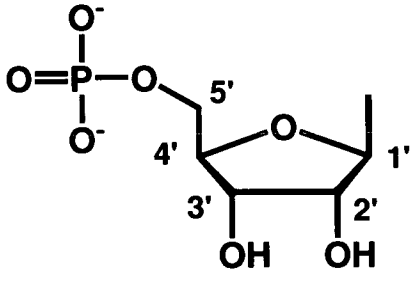

R^2

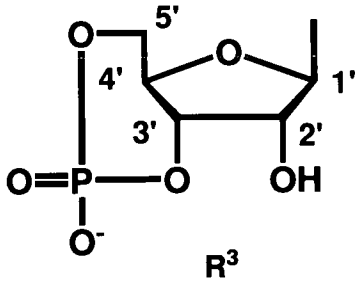

R^3

Figure 1.14: Structures of mononucleosides (guanosine, adenosine, cytidine, thymidine), mononucleotides (5'-GMP, 5'-AMP, 5'-CMP, 5'-TMP), and cyclic nucleotides (cGMP, cAMP).

protons of the 5'-GMP adduct are involved in strong H-bonding with the 5'-phosphate and C6O of 5'-GMP. Significant amounts of the 5'-phosphate-bound species (40-60%) are also present at equilibrium for 5'-TMP, 5'-CMP and 5'-AMP.

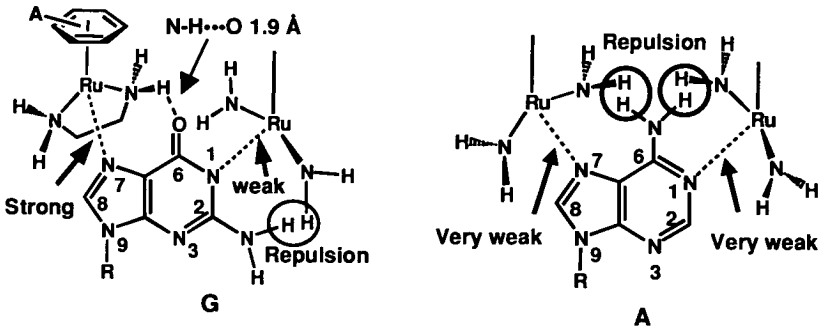

Figure 1.15: H-bonding and steric interactions which give rise to strong binding of $\{(\eta^6\text{-arene})Ru(en)\}^{2+}$ to guanine but very weak binding to adenine [81]. For clarity the arene and en ring are omitted in the right-hand (A) structure.

Binding of $\{(\eta^6\text{-bip})Ru(en)\}^{2+}$ to N7 of 5'-GMP lowers the pK_a of N1H by 1.4 units. Such a lowering is also observed for Pt^{II}-G adducts [92, 93]. Metallation of N7 of G, which is accessible from the major groove of B-DNA, can therefore lead to significant electronic perturbations at N1H which is an H-bond donor in G-C base-pairs in a Watson-Crick double helix. This may influence the stability of the duplex.

No binding to the phosphodiester groups of 3′,5′- cyclic guanosine monophosphate (cGMP) or cAMP (Figure 1.14) is detected, suggesting that Ru^{II} arene complexes do not bind to the phosphodiester groups of the DNA backbone.

There is evidence that N7-binding of guanine is also promoted by favourable arene-purine hydrophobic interactions in the associative transition state [81]. The rates of reaction of 3′,5′- cyclic guanosine monophosphate with $[(\eta^6\text{-arene})Ru(en)X]^{n+}$ (where X = Cl^- or H_2O) (pH 7.0, 298 K, 100 mM $NaClO_4$) decrease in the order THA > bip > DHA >> *p*-cym > bz. Strong arene-nucleobase π-stacking is present in the crystal structures of the 9-ethylguanine (9EtG) complexes $[(\eta^6\text{-DHA})Ru(en)(9EtG\text{-}N7)](PF_6)_2$ (Figure 1.16) and $[(\eta^6\text{-THA})Ru(en)(9EtG\text{-}N7)](PF_6)_2$ [91]. The outer ring of the DHA ligand stacks over the purine base at a distance of 3.45 Å, and for THA at 3.31 Å, with dihedral angles of 3.3° and 3.1°, respectively.

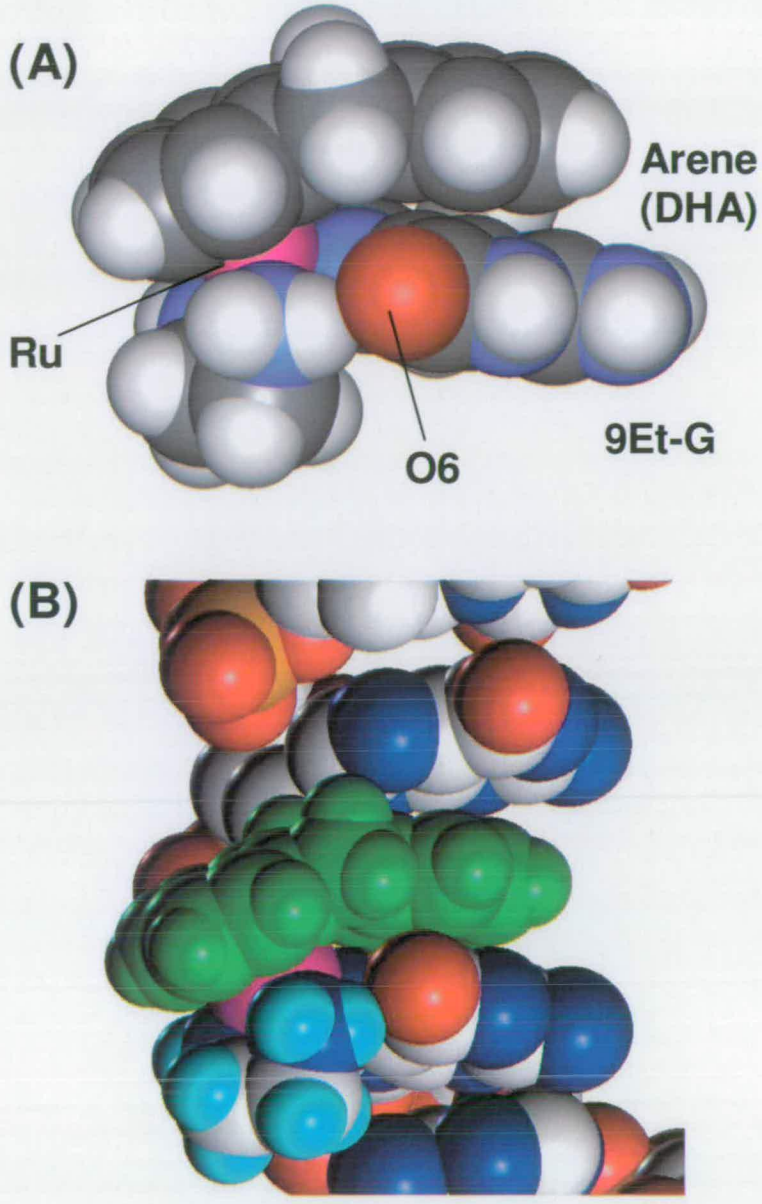

Figure 1.16: Arene-purine $\pi - \pi$ stacking. A: $[(\eta^6\text{-DHA})Ru(en)(9EtG\text{-}N7)]^{2+}$ [91]. Ru^{II} is coordinated to N7 and O6 of 9EtG and is strongly H-bonded to en-NH. B: Model of a strand of B-DNA showing how the coordinated arene could intercalate between a pair of G bases (model built by J.A. Parkinson, see [91]).

In the crystal structure of the guanosine (Guo) adduct $[(\eta^6\text{-bip})Ru(en)(Guo\text{-}N7)](PF_6)_2$ there is intramolecular stacking of the pendent phenyl ring with the purine five-membered ring (3.8 Å, 23.8°). Despite no observed intramolecular stacking between the pendent phenyl ring and the purine six-membered ring, which have an

anti orientation in the structure of $[(\eta^6\text{-bip})Ru(en)(9EtG\text{-}N7)](PF_6)_2$, in solution a *syn* orientation predominates for all the bip adducts as revealed by NMR NOE studies. The predominance of the *syn* orientation can be attributed to hydrophobic interactions between the arene and purine rings. The arene ligands are flexible through rotation around the arene-Ru π-bonds, through twisting about the Ph-Ph bond (for bip), and ring bending (for THA and DHA), so as to maximise intra- or intermolecular stacking with the purine ring (Table 1.2) [91].

While for most studied complexes aquation appears to be the first step in the reaction with guanine bases, the complex $[(\eta^6\text{-hmb})Ru(en)SPh]PF_6$, where SPh = thiophenolate, does not hydrolyse yet it reacts with GMP [80]. The reaction has been proposed to proceed *via* oxidation of S (*vide infra*), which can then undergo direct substitution by GMP.

The strong preference of $\{(\eta^6\text{-arene})Ru(en)\}^{2+}$ complexes for guanine N7 binding is attributable to a combination of the high electron density on G N7, the strong H-bonding between en NH and G C6O and possible arene-purine stacking. Thus direct coordination to the bases, intercalation, and stereospecific H-bonding are useful features to incorporate into the design of Ru^{II} arene complexes to optimise the recognition of DNA. The strong preference for G bases may allow Ru^{II} complexes to target selectively G-rich regions of DNA, such as telomeres which play key roles in cell division. Telomeres occur as guanine-rich overhangs at the 3′ ends of eukaryotic chromosomes and typically contain repeat sequences such as $(TTAGGG)_n$ [94].

The concept of induced-fit recognition of DNA by organometallic Ru^{II} arene complexes containing dynamic stereogenic centers *via* dynamic epimerization, intercalation and cross-linking may be useful in the design of anticancer drugs [95]. For example, highly diastereoselective binding of 9EtG to the $R_{Ru}{}^*R_N{}^*$ and $S_{Ru}{}^*R_N{}^*$ diastereomers of $[(\eta^6\text{-bip})Ru(Et\text{-}en)Cl]^+$ (Et-en = $EtNHCH_2CH_2NH_2$) (Figure 1.17) probably proceeds *via* epimerization of $R_{Ru}{}^*R_N{}^*$ to $S_{Ru}{}^*R_N{}^*$-$[(\eta^6\text{-bip})RuCl(Et\text{-}en)]^+$ to

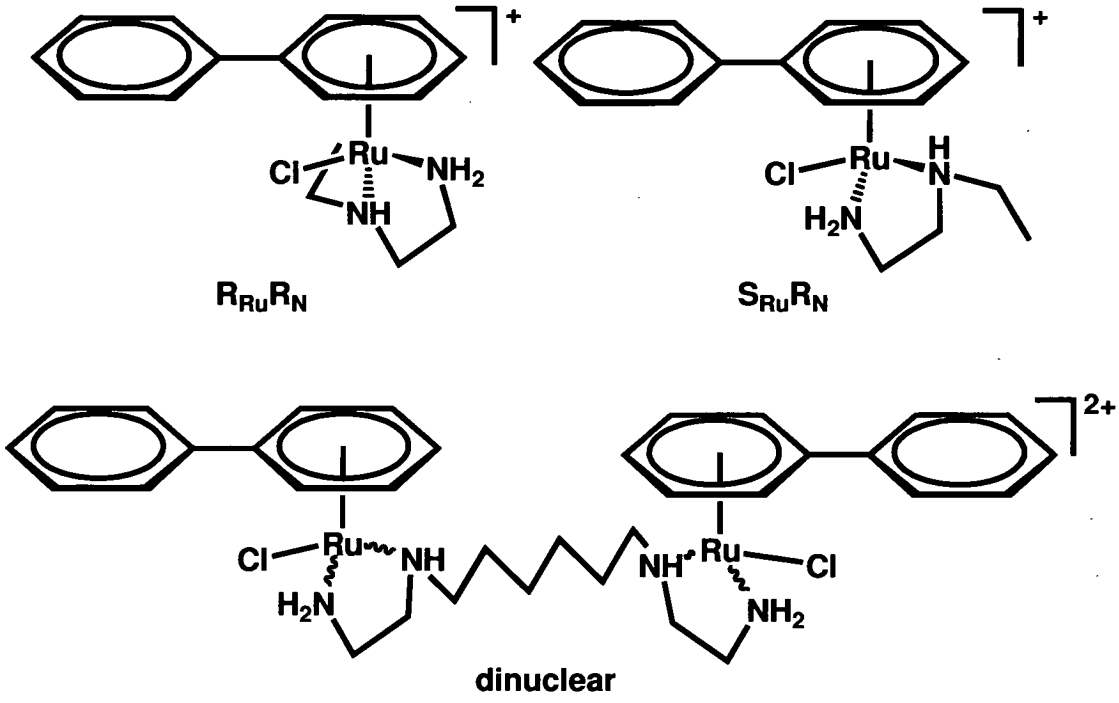

Figure 1.17: Mono- and di-nuclear complexes containing chiral ruthenium and nitrogen centres. There are 10 possible configurations for the dinuclear complex: four racemic pairs, $(R^*R^*R^*R^*)$-(±), $(S^*R^*R^*R^*)$-(±), $(R^*S^*R^*R^*)$-(±) and $(S^*R^*R^*S^*)$-(±), and two meso forms, *SSRR* and *SRSR*. The synthesis of the mononuclear complex gives two diastereomers in the mol ratio $R_{Ru}{}^*R_N{}^*$: $S_{Ru}{}^*R_N{}^*$ = 74:26. Each unit of the dinuclear complex has a similar population of diastereomers [95].

give selectively (95%) the $S_{Ru}{}^*R_N{}^*$ adduct, although for the chloro complex the $R_{Ru}{}^*R_N{}^*$ diastereomer (73%) is more stable than the $S_{Ru}{}^*R_N{}^*$ diastereomer (27%) [95].

The dinuclear complex $[((\eta^6\text{-bip})RuCl(en))_2\text{-}(CH_2)_6]^{2+}$ (Figure 1.17) has similar dynamic characteristics, induces a large unwinding (31°) of plasmid DNA, and effectively inhibits DNA-directed RNA synthesis *in vitro*. This unwinding angle is more than twice that induced by the mononuclear complex $[(\eta^6\text{-bip})Ru(Et\text{-}en)Cl]^+$ (Table 1.3) and is attributable to cross-linking of the DNA and perturbation of the DNA structure by the pendent phenyl rings. It is notable that Ru^{II} complexes containing arenes which cannot intercalate into DNA (*e.g.* $[(\eta^6\text{-}p\text{-cym})Ru(en)Cl]^+$) produce only small unwinding angles similar to the monofunctional Pt^{II} complex $[Pt(dien)Cl]^+$ (6° [96]).

Table 1.3: Unwinding of supercoiled pSP73KB DNA by Ru^{II} arene complexes as determined from electrophoresis studies of the comigration of supercoiled and nicked forms [95, 96, 98].

Complex	Unwinding angle
$[(\eta^6\text{-}p\text{-cymene})Ru(en)Cl]^+$	7°
$[Pt(dien)Cl]^+$	6°
$[(\eta^6\text{-biphenyl})Ru(en)Cl]^+$	14°
$[(\eta^6\text{-tetrahydroanthracene})Ru(en)Cl]^+$	14°
$[(\eta^6\text{-dihydroanthracene})Ru(en)Cl]^+$	14°
$[(\eta^6\text{-biphenyl})Ru(Et\text{-}en)Cl]^+$	14°
$[((\eta^6\text{-biphenyl})Ru(en)Cl)(CH_2)_6]^{2+}$	31°

1.4.4.4 Interactions with oligonucleotides and DNA

The complex $[(\eta^6\text{-}p\text{-cym})Ru(en)Cl]PF_6$ binds selectively to G bases on DNA oligonucleotides, forming Ru-G_7 and Ru-G_8 monoruthenated and G_7(Ru)-G_8(Ru) diruthenated adducts on the 14-mer d(ATACATG$_7$G$_8$TACATA) [72]. The reaction of the complementary strand d(TATG$_4$TACCATG$_{11}$TAT) with $[(\eta^6\text{-bip})Ru(en)Cl]PF_6$ in triethylammonium acetate buffer (pH 7.03) also gives mono- and diruthenated oligonucleotides, as indicated by LC-ESI-MS [97]. At 310 K *ca.* 92% of the latter oligonucleotide is ruthenated, of which *ca.* 52% forms the diruthenated product, further suggesting a high affinity of $[(\eta^6\text{-bip})Ru(en)Cl]PF_6$ for G bases.

Comparative studies have shown that $[(\eta^6\text{-arene})Ru(en)Cl]^+$ complexes (arene = bip, DHA, THA or *p*-cym) bind relatively rapidly to calf thymus (CT) DNA at 310 K, with 50% binding in 3 h for the *p*-cym complex and 10-15 min for the others [98]. Circular dichroism (CD) data suggest that intercalation and/or minor groove binding are involved in the binding of the bip and anthracene derivatives, but not the *p*-cym complex, to CT DNA. Further evidence for partial intercalation of the bip, DHA and

THA complexes into DNA is provided by flow linear dichroism (LD), the induced loss of fluorescence of DNA-ethidium bromide adducts consistent with displacement of the intercalated ethidium cations by the Ru^{II} arenes, as well as by characteristic differences in the melting temperature (t_m, temperature at which transition from duplex to single-stranded DNA occurs) of CT DNA. Overall, the above results provide strong evidence for combined intercalative and coordinative binding modes for the bip and anthracene complexes.

Distortions of DNA duplexes (15 – 20 base pairs) by complexes $[(\eta^6\text{-}p\text{-cym})Ru(en)Cl]^+$ (Ru-*p*-cym, non-intercalating) and $[(\eta^6\text{-THA})Ru(en)Cl]^+$ (Ru-THA, intercalating) were not recognized by the DNA-binding HMGB1 protein [99], which is in contrast to the proposed recognition of cisplatin and its direct analogues [100, 101]. Removal of the above Ru^{II} adducts from DNA (faster for Ru-*p*-cym than for Ru-THA) occurs preferentially by mechanisms other than nucleotide excision repair (a major mechanism contributing to cisplatin resistance) [102, 103, 104]. This provides additional support for a different mechanism for antitumour activity of Ru^{II} arene complexes compared to cisplatin.

1.4.4.5 Reactions with amino acids and proteins

Reactions between the sulfur-containing amino acids cysteine and methionine (Figure 1.18) and ruthenium(II) arene anticancer complexes are of much interest in view of the strong influence of sulfur amino acids on the intracellular chemistry of platinum drugs, in particular, their involvement in detoxification and resistance mechanisms [36]. Protein targets may also play a role in the mechanism of action of Ru^{II} arene complexes, including the possibility that ruthenium can substitute for iron in proteins.

It was found [82] that $[(\eta^6\text{-bip})Ru(en)Cl]PF_6$ reacts slowly, and only to about 50% completion, with the thiol amino acid *L*-cysteine (*L*-Cys) in aqueous solution at

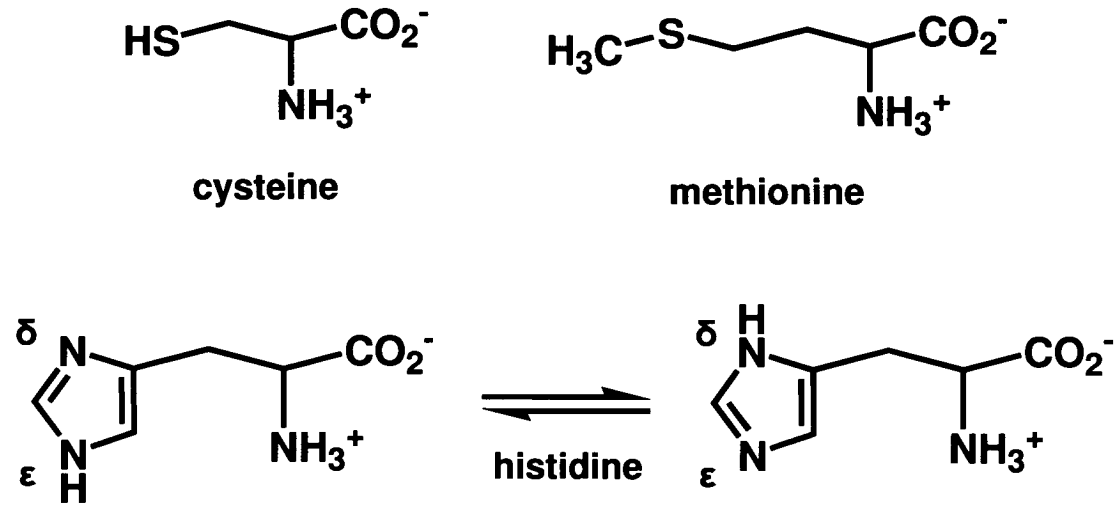

Figure 1.18: Structures of cysteine, methionine and histidine.

310 K, pH 2-5 at a 1:2 mM ratio. Reactions appeared to involve aquation as the first step followed by initial formation of 1:1 adducts *via* substitution of Cl by S-bound or O-bound cysteine. Two dinuclear complexes were also detected as products from the reaction. These arise from the loss of chelated ethylenediamine, and contain one or two bridging cysteines. The unusual cluster species $\{(bip)Ru\}_8$ was also formed especially at higher cysteine concentrations. The reaction was suppressed in 50 mM triethylammonium acetate solution at pH > 5 or in 100 mM NaCl suggesting that thiols may not readily inactivate Ru^{II}-en arene complexes in blood plasma or in cells. Similarly, reactions with the thioether sulfur of methionine appeared to be relatively weak. Only 27% of $[(\eta^6\text{-bip})Ru(en)Cl]PF_6$ reacted with *L*-methionine (*L*-Met) at an initial pH of 5.7 after 48 h at 310 K, and gave rise to only one adduct $[(\eta^6\text{-bip})Ru(en)(L\text{-Met-}S)]^{2+}$.

In recent work the surprisingly facile oxidation of the sulfur of coordinated glutathione (γ-*L*-Glu-*L*-Cys-Gly, GSH) to give sulfenato complexes was detected [105]. Ruthenium-bound sulfenato ligands appear to be readily displaced by guanine. Under physiologically-relevant conditions a competition reaction of $[(\eta^6\text{-bip})Ru(en)Cl]PF_6$ with 250 mol equivalents of GSH and 25 mol equivalents of

cGMP gave rise to the cGMP adduct $[(\eta^6\text{-bip})Ru(en)cGMP\text{-}N7]^+$ as the major adduct (*ca.* 62%). Hence, there may be redox-mediated pathways for the ruthenation of DNA (and RNA) *via* glutathione intermediates. Glutathione is present in cells at millimolar concentrations [106].

Histidine residues are also possible binding sites for ruthenium arene complexes in proteins. Hence, the reaction of $[(\eta^6\text{-bip})Ru(en)Cl]PF_6$ with *L*-histidine (*L*-His, Figure 1.18) was studied in aqueous solution at 310 K [97]. This reaction is also slow, and gives two isomeric imidazole-bound *L*-His adducts, $[(\eta^6\text{-bip})Ru(en)N_\delta\text{-}L\text{-His}]^{2+}$ and $[(\eta^6\text{-bip})Ru(en)N_\varepsilon\text{-}L\text{-His}]^{2+}$. Considering the two isomers together, an equilibrium constant of 0.14 mM^{-1} was determined for the reaction between *L*-His and the aquated species $[(\eta^6\text{-bip})Ru(en)H_2O]^{2+}$. Comparison of this value to those obtained for *L*-cysteine (0.60 mM^{-1}) and *L*-methionine (0.34 mM^{-1}) [82] suggests that the affinity of the $\{(\eta^6\text{-bip})Ru(en)\}^{2+}$ fragment for these amino acids decrease in the order *L*-Cys > *L*-Met > *L*-His.

Reactions between $[(\eta^6\text{-bip})Ru(en)Cl]PF_6$ and the haem protein cytochrome c have also been studied [97]. Cytochrome c has a buried (His26) and an exposed surface histidine residue (His33). Electrospray mass spectrometry indicated that in both water (pH 8.7) and triethylammonium acetate buffer (pH 7.6) only monoruthenated cytochrome c products are formed, even when $[(\eta^6\text{-bip})Ru(en)Cl]PF_6$ is present in ten-fold molar excess. Analysis by ICP-AES revealed that 50% of cytochrome c was ruthenated. Interestingly, 2D [^{1}H, ^{15}N] HSQC NMR data show that the ruthenium complexes are bound to carboxylate groups (*ca.* 30%) and the amino terminus (*ca.* 70%), instead of the histidine residues, of cytochrome c. This is probably due to the steric constraints imposed on the single coordination site of $\{(\eta^6\text{-bip})Ru(en)\}^{2+}$ by the arene and en ligands.

The presence of cytochrome c (1 mol equiv) or *L*-histidine (4 mol equiv), has little effect on the amounts of mono- and diruthenated oligonucleotide products

formed, and no [(η^6-bip)Ru(en)] – histidine or [(η^6-bip)Ru(en)] – cytochrome c adducts are detected [97].

In complexes of the type [(η^6-arene)Ru(en)Cl]$^+$ the en chelate ring remains bound under most tested conditions. Other reactions of ruthenium(II) arene complexes studied could be of relevance to systems where loss of the chelating ligand occurs, as has been observed for some osmium arene complexes [107]. Apart from potential formation of bis-guanine adducts [48] and chelation of adenine bases [47] (*vide supra*), binding of amino acids and peptides in modes different to those found for {(η^6-arene)Ru(en)}$^{2+}$ is possible. Examples include the X-ray crystal structures of the complexes [(η^6-benzene)Ru(Aa)Cl]$^{n+}$, where Aa = penicillamine, histidine methyl ester and triglycine [45]. Penicillamine is chelated *via* the amino group and thiolate S which bridges between two Ru atoms giving a 4-membered Ru-S-Ru-S ring (Figure 1.19). Histidine is chelated *via* amino and imidazole nitrogens, and in the triglycine complex (prepared in water by reaction with the dimer [(η^6-benzene)$RuCl_2$]$_2$), the tripeptide is chelated *via* the amino terminus and a deprotonated peptide N.

Another possibility of coordination for such complexes is illustrated by the arene ruthenium-enzyme complex [(η^6-*p*-cym)Ru(lysozyme)Cl_2]. X-ray crystallography (at 1.6 Å resolution) showed that the ruthenium atom is selectively

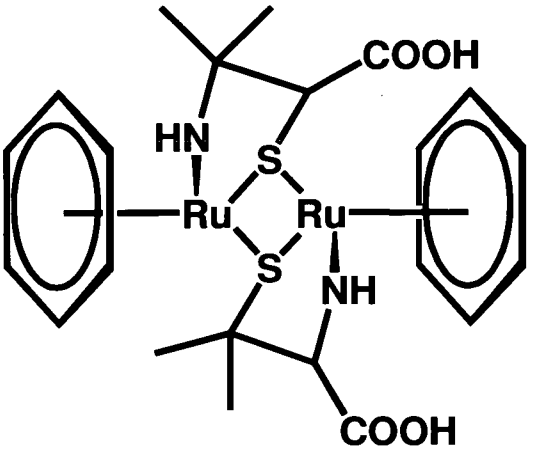

Figure 1.19: Dinuclear complex with bridging penicillamine thiolate sulfurs.

bound to N_ε of the imidazole ring of His15, situated at the surface of the protein (Figure 1.20) [108]. Ruthenation has little effect on the rest of the enzyme structure and the Ru complex is provided with a rather hydrophobic binding pocket. The specificity of the binding of $\{(\eta^6\text{-}p\text{-cym})RuCl_2\}$ to lysozyme and the ability of Ru^{II} arene complexes to catalyse transfer hydrogenation reactions [109] suggest that ruthenium-protein complexes might provide a basis for the design of enantioselective artificial metalloenzymes [110].

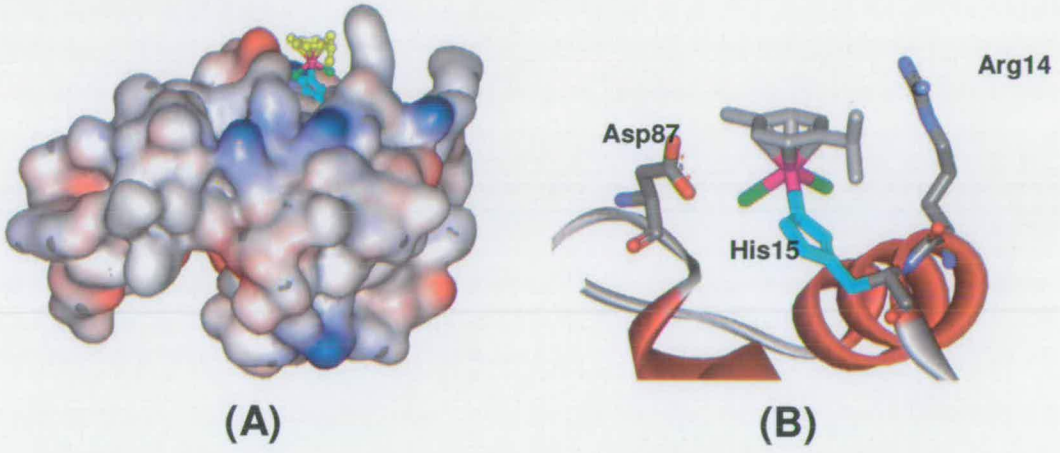

Figure 1.20: Crystal structure of $[(\eta^6\text{-}p\text{-cym})Ru(lysozyme)Cl_2]$. A: space-filling model (with surface colouring to indicate the electrostatic potential: red – negative, blue – positive) showing the position of the Ru complex (ball-and-stick model) in the protein. B: details of the binding pocket showing the side-chains of the His15, Asp87 and Arg14 residues [108].

It is possible that the histidine-bound Ru-lysozyme complex is the kinetic product of the reaction between the enzyme and $[(\eta^6\text{-}p\text{-cym})Ru(H_2O)Cl_2]$, and that slow conversion to a thermodynamically more stable complex, with Ru π-bonded to an aromatic side-chain, could occur. Under some conditions it is possible to form π-complexes between $\{(arene)Ru^{II}\}$ / $\{CpRu^{II}\}$ and aromatic amino acid side-chains (Phe, Trp) [111, 112], although such reactions are often blocked when competitive binding to other side-chain donors (*e.g.* His, Asp, Glu) is possible.

Overall, the observed preference of $[(\eta^6\text{-arene})Ru(en)Cl]^+$ complexes to bind to DNA, also when under competition from amino acids, proteins and GSH, suggests that DNA (or RNA) could be the favoured binding site for this type of complex. The lower reactivity of the latter biomolecules towards ruthenium arene complexes may account for the low toxic side effects of such complexes [75]. On the other hand, the relatively weak binding of amino acids and proteins to these complexes may aid the transport and delivery of the latter to cancer cells, and allow some amino acids, peptides and proteins to serve as drug reservoirs for DNA ruthenation, as has been proposed for cisplatin [36].

1.5 Project Aims

Previous work in the Sadler group on ruthenium(II) arene complexes has focussed on monofunctional, ethylenediamine-containing complexes of the type $[(\eta^6\text{-arene})Ru(en)Cl]^+$. In order to broaden the scope of ruthenium(II) arene complexes as potential anticancer compounds in general it is important to a): investigate different structural features, which could lead to a different spectrum of activity and b): learn more about the associated solution chemistry, including reactions with potential target sites. Therefore this project was concerned with the following topics.

1. Synthesis of ruthenium(II) arene complexes containing monoanionic *O,O*-chelating ligands.
2. Evaluation of their cytotoxic activity and investigations of structure-activity relationships.
3. Studies of the role of the chelating ligand in monofuntional Ru^{II} arene complexes on the rate and extent of hydrolysis.
4. Investigation of possible changes in the binding to DNA bases resulting from changing the H-bond donating amine group in ethylenediamine to an H-bond accepting oxygen in *O,O*-chelating ligands.

5. Establishment of a synthetic route for novel, bifunctional, water-soluble, nitrogen-containing tethered ruthenium(II) arene complexes.
6. Studies of the aqueous chemistry relevant to potential applications as anticancer agents, including stability, hydrolysis and control of reactivity. The possible influence of the amine group in the tether backbone on the formation of bifunctional guanine adducts *via* H-bond donation was of particular interest.
7. Investigation of hydride transfer reactions by cytotoxic, ethylenediamine-containing ruthenium(II) arene complexes and their possible relevance for cytotoxic activity, including the study of a potential target molecule.

1.6 References

[1] P.J. Sadler, *Adv. Inorg. Chem.* **1991**, *36*, 1–48.

[2] M.J. Clarke, *Coord. Chem. Rev.* **2003**, *236*, 209–233.

[3] Z. Guo, P.J. Sadler, *Angew. Chem. Int. Ed.* **1999**, *38*, 1512–1531.

[4] Z. Guo, P.J. Sadler, *Adv. Inorg. Chem.* **2000**, *49*, 183–306.

[5] M.J. Cleare, J.D. Hoeschele, *Bioinorg. Chem.* **1973**, *2*, 187–210.

[6] R.D. Murdoch, J. Pepys, *Int. Arch. Allergy Appl. Immunol.* **1985**, *77*, 456–458.

[7] H.M. Pinedo, J.H. Schornagel (Eds.), *Platinum and Other Metal Coordination Compounds in Cancer Chemotherapy*, Plenum, New York, **1996**.

[8] J. Halpern, *Pure Appl. Chem.* **2001**, *73*, 209–220.

[9] G. Jaouen, W. Beck, M.J. McGlinchey, in *Bioorganometallics: Biomolecules, Labeling, Medicine*, Vol. 1, (Ed. G. Jaouen), Wiley VCH Verlag GmbH & Co. KGaA: Weinheim, **2006**, pp. 1–37.

[10] R.H. Fish, G. Jaouen, *Organometallics* **2003**, *22*, 2166–2177.

[11] C. Elschenbroich, A. Salzer, *Organometallics: a concise introduction*, VCH, Weinheim, 2nd edn., **1992**.

[12] P. Köpf-Maier, H. Köpf, in *Metal Compounds in Cancer Therapy*, S. P. Fricker (Ed.); Chapman & Hall, London, **1994**, pp. 109–146.

[13] G. Jaouen, A. Vessières, I.S. Butler, *Acc. Chem. Res.* **1993**, *26*, 361–369.

[14] R. Alberto, R. Schibli, R. Waibel, U. Abram, A.P. Schubiger, *Coord. Chem. Rev.* **1999**, *190-192*, 901–919.

[15] R.H. Fish, *Coord. Chem. Rev.* **1999**, *185-186*, 569–584.

[16] F. Le Bideau, M. Salmain, S. Top, G. Jaouen, *Chem. Eur. J.* **2001**, *7*, 2289–2294.

[17] B. Rosenberg, L. van Camp, J.E. Trosko, V.H. Mansour, *Nature (London)* **1969**, *222*, 385–386.

[18] E.R. Jamieson, S.J. Lippard, *Chem. Rev.* **1999**, *99*, 2467 – 2498.

[19] M. Guo, Z. Guo, P.J. Sadler, *J. Biol. Inorg. Chem.* **2001**, *6*, 698–707.

[20] K. Mross, P. Robben-Bathe, L. Edler, J. Baumgart, W.E. Berdel, H. Fiebig, C. Unger, *Onkologie* **2000**, *23*, 576–579.

[21] N. Kröger, U.R. Kleeberg, K. Mross, L. Edler, G. Saß, D.K. Hossfeld, *Onkologie* **2000**, *23*, 60–62.

[22] T. Pieper, K. Borsky, B.K. Keppler in *Topics in Biological Inorganic Chemistry*, Vol. 1, M.J. Clarke, P.J. Sadler (Eds.), Springer Verlag, Berlin, **1999**, pp. 171–199.

[23] S. Top, A. Vessieres, C. Cabestaing, I. Laios, G. Leclercq, C. Provot, G. Jaouen, *J. Organomet. Chem.* **2001**, *637-639*, 500–506.

[24] S. Top, A. Vessieres, G. Leclercq, J. Quivy, J. Tang, J. Vaissermann, M. Huche, G. Jaouen, *Chem. Eur. J.* **2003**, *9*, 5223–5236.

[25] C.S. Allardyce, A. Dorcier, C. Scolaro, P.J. Dyson, *Appl. Organometal. Chem.* **2005**, *19*, 1–10.

[26] D.S. Dwyer, K. Gordon, B. Jones, *Int. J. Immunopharm.* **1995**, *17*, 931–940.

[27] M.J. Clarke, V. Bailey, P. Doan, C. Hiller, K.J. LaChance-Galang, H. Daghlian, S. Mandal, C.M. Bastos, D. Lang, *Inorg. Chem.* **1996**, *35*, 4896–4903.

[28] T.W. Hayton, P. Legzdins, W.B. Sharp, *Chem. Rev.* **2002**, *102*, 935–991.

[29] C.S. Allardyce, P.J. Dyson, D.J. Ellis, P.A. Salter, R. Scopelliti, *J. Organomet. Chem.* **2003**, *668*, 35–42.

[30] R.A. Sanchez-Delgado, M. Navarro, H. Perez, J.A. Urbina, *J. Med. Chem.* **1996**, *39*, 1095–1099.

[31] K.C. Reed, F.L. Bygrave, *Biochem. J.* **1974**, *140*, 143–155.

[32] M.J. Clarke, *Met. Ions Biol. Syst.* **1980**, *11*, 231–283.

[33] M.J. Clarke, S. Bitler, D. Rennert, M. Buchbinder, A.D. Kelman, *J. Inorg. Biochem.* **1980**, *12*, 79–87.

[34] G.M. Coleman, J.W. Gesler, E.A. Shirley, J.R. Kuempel, *Inorg. Chem.* **1973**, *12*, 1036–1038.

[35] J.A. Marchant, T. Matsubara, P.C. Ford, *Inorg. Chem.* **1977**, *16*, 2160–2165.

[36] J. Reedijk, *Proc. Natl. Acad. Sci. USA* **2003**, *100*, 3611–3616.

[37] C.G. Kuehn, H. Taube, *J. Am. Chem. Soc.* **1976**, *98*, 689–702.

[38] D. Frasca, M.J. Clarke, *J. Am. Chem. Soc.* **1999**, *121*, 8523–8532.

[39] G. Sava, E. Alessio, A. Bergamo, G. Mestroni in *Topics in Biological Inorganic Chemistry*, Vol. 1, M.J. Clarke, P.J. Sadler (Eds.), Springer Verlag, Berlin, **1999**, pp. 143–169.

[40] M. Galanski, V.B. Arion, M.A. Jakupec, B.K. Keppler, *Curr. Pharm. Des.* **2003**, *9*, 2078–2089.

[41] A.H. Velders, H. Kooijman, A.L. Spek, J.G. Haasnoot, D. de Vos, J. Reedijk, *Inorg. Chem.* **2000**, *39*, 2966–2967.

[42] R.A. Vilaplana, F. González-Vílchez, E. Gutierrez-Puebla, C. Ruiz-Valero, *Inorg. Chim. Acta* **1994**, *224*, 15–18.

[43] Z. Guo, A. Habtemariam, P.J. Sadler, B.R. James, *Inorg. Chim. Acta* **1998**, *273*, 1–7.

[44] W.S. Sheldrick, S. Heeb, *J. Organomet. Chem.* **1989**, *377*, 357–366.

[45] W.S. Sheldrick, S. Heeb, *Inorg. Chim. Acta* **1990**, *168*, 93–100.

[46] W.S. Sheldrick, H.S. Hagen-Eckhard, S. Heeb, *Inorg. Chim. Acta* **1993**, *206*, 15–21.

[47] S. Korn, W.S. Sheldrick, *J. Chem. Soc., Dalton Trans.* **1997**, 2191–2199.

[48] S. Korn, W.S. Sheldrick, *Inorg. Chim. Acta* **1997**, *254*, 85–91.

[49] P. Annen, S. Schildberg, W.S. Sheldrick, *Inorg. Chim. Acta* **2000**, *307*, 115–214.

[50] Y.K. Yan, M. Melchart, A. Habtemariam, P.J. Sadler, *Chem. Commun.* **2005**, 4764–4776.

[51] M. Melchart, P.J. Sadler in *Bioorganometallics: Biomolecules, Labeling, Medicine*, Vol. 1, (Ed. G. Jaouen), Wiley VCH Verlag GmbH & Co. KGaA: Weinheim, **2006**, pp. 39–64.

[52] H. Le Bozec, D. Touchard, P.H. Dixneuf, *Adv. Organomet. Chem.* **1989**, *29*, 163–247.

[53] J. Soleimannejad, A. Sisson, C. White, *Inorg. Chim. Acta* **2003**, *352*, 121–128.

[54] M. Bassetti, F. Centola, D. Sémeril, C. Bruneau, P.H. Dixneuf, *Organometallics* **2003**, *22*, 4459–4466.

[55] D. Jan, L. Delaude, F. Simal, A. Demonceau, A.F. Noels, *J. Organomet. Chem.* **2000**, *606*, 55–64.

[56] S. Ogo, T. Abura, Y. Watanabe, *Organometallics* **2002**, *21*, 2964–2969.

[57] E.O. Fischer, R. Böttcher, *Z. Anorg. Allgem. Chem.* **1957**, *291*, 305–309.

[58] E.O. Fischer, C. Elschenbroich, C.G. Kreiter, *J. Organomet. Chem.* **1967**, *7*, 481–485.

[59] G. Winkhaus, H. Singer, *J. Organomet. Chem.* **1967**, *7*, 487–491.

[60] M.A. Bennett, G.B. Robertson, A.K. Smith, *J. Organomet. Chem.* **1972**, *43*, C41–C43.

[61] R.A. Zelonka, M.C. Baird, *J. Organomet. Chem.* **1972**, *35*, C43–C46.

[62] S. Suravajjala, J.R. Polam, L.C. Porter, *J. Organomet. Chem.* **1993**, *461*, 201–205.

[63] S. Bhambri, D.A. Tocher, *Polyhedron* **1996**, *15*, 2763–2770.

[64] E.L. Muetterties, J.R. Bleeke, E.J. Wucherer, T.A. Albright, *Chem. Rev.* **1982**, *82*, 499–525.

[65] B. Therrien, T.R. Ward, M. Pilkington, C. Hoffmann, F. Gilardoni, J. Weber, *Organometallics* **1998**, *17*, 330–337.

[66] M.A. Bennett, A.J. Edwards, J.R. Harper, T. Khimyak, A.C. Willis, *J. Organomet. Chem.* **2001**, *629*, 7–18.

[67] F. Simal, D. Jan, A. Demonceau, A.F. Noels, *Tetrahedron Lett.* **1999**, *40*, 1653–1656.

[68] Y. Miyaki, T. Onishi, S. Ogoshi, H. Kurosawa, *J. Organomet. Chem.* **2000**, *616*, 135–139.

[69] J.R. Miura, J.B. Davidson, G.C. Hincapié, D.J. Burkey, *Organometallics* **2002**, *21*, 584–586.

[70] C.M. Hartshorn, P.J. Steel, *Angew. Chem. Int. Ed. Engl.* **1996**, *35*, 2655–2657.

[71] W.Y. Sun, J. Xie, T. Okamura, C.K. Huang, N. Ueyama, *Chem. Commun.* **2000**, 1429–1430.

[72] R.E. Morris, R.E. Aird, P. del S. Murdoch, H. Chen, J. Cummings, N.D. Hughes, S. Parsons, A. Parkin, G. Boyd, D.I. Jodrell, P.J. Sadler, *J. Chem. Med.* **2001**, *44*, 3616–3621.

[73] L.D. Dale, J.H. Tocher, T.M. Dyson, D.I. Edwards, D.A. Tocher, *Anti-Cancer Drug Design* **1992**, *7*, 3–14.

[74] B. Çetinkaya, I. Özdemir, B. Binbaşioğlu, R. Durmaz, S. Günal, *Arzneim.-Forsch./Drug Res.* **1999**, *49*, 538–540.

[75] R.E. Aird, J. Cummings, A.A. Ritchie, M. Muir, R.E. Morris, H. Chen, P.J. Sadler, D.I. Jodrell, *Br. J. Cancer* **2002**, *86*, 1652–1657.

[76] Y.N.V. Gopal, D. Jayaraju, A.K. Kondapi, *Biochemistry* **1999**, *38*, 4382–4388.

[77] L.A. Huxham, E.L.S. Cheu, B.O. Patrick, B.R. James, *Inorg. Chim. Acta* **2003**, *352*, 238–246.

[78] C. Scolaro, A. Bergamo, L. Brescacin, R. Delfino, M. Cocchietto, G. Laurenczy, T.J. Geldbach, G. Sava, P.J. Dyson, *J. Med. Chem.* **2005**, *48*, 4161–4171.

[79] A. Habtemariam, M. Melchart, R. Fernández, S. Parsons, I.D.H. Oswald, A. Parkin, F.P.A. Fabbiani, J.E. Davidson, A. Dawson, R.E. Aird, D.I. Jodrell, P.J. Sadler, *J. Med. Chem.*, in press.

[80] F. Wang, A. Habtemariam, E.P.L. van der Geer, R. Fernández, M. Melchart, R.J. Deeth, R. Aird, S. Guichard, F.P.A. Fabbiani, P. Lozano-Casal, I.D.H. Oswald, D.I. Jodrell, S. Parsons, P.J. Sadler, *Proc. Natl. Acad. Sci. USA* **2005**, *102*, 18269–18274.

[81] H. Chen, J.A. Parkinson, R.E. Morris, P.J. Sadler, *J. Am. Chem. Soc.* **2003**, *125*, 173–186.

[82] F. Wang, H. Chen, J.A. Parkinson, P. del S. Murdoch, P.J. Sadler, *Inorg. Chem.* **2002**, *41*, 4509–4523.

[83] Y. Hung, W.J. Kung, H. Taube, *Inorg. Chem.* **1981**, *20*, 457–463.

[84] L. Dadci, H. Elias, U. Frey, A. Hörnig, U. Koelle, A.E. Merbach, H. Paulus, J.S. Schneider, *Inorg. Chem.* **1995**, *34*, 306–315.

[85] F. Wang, H. Chen, S. Parsons, I.D.H. Oswald, J.E. Davidson, P.J. Sadler, *Chem. Eur. J.* **2003**, *9*, 5810–5820.

[86] M. Jennerwein, P.A. Andrews, *Drug Metab. Dispos.* **1995**, *23*, 178–184.

[87] R.B. Martin, in *Cisplatin: Chemistry and Biochemistry of a Leading Anticancer Drug*, B. Lippert (Ed), Wiley-VCH, Zürich, **1999**, pp. 183–205.

[88] S.E. Sherman, S.J. Lippard, *Chem. Rev.* **1987**, *87*, 1153–1181.

[89] A. Frodl, D. Herebian, W.S. Sheldrick, *J. Chem. Soc., Dalton Trans.* **2002**, 3664–3673.

[90] M.H. Baik, R.A. Friesner, S.J. Lippard, *J. Am. Chem. Soc.* **2003**, *125*, 14082–14092.

[91] H. Chen, J.A. Parkinson, S. Parsons, R.A. Coxall, R.O. Gould, P.J. Sadler, *J. Am. Chem. Soc.* **2003**, *125*, 3064–3082.

[92] K. Inagaki, Y. Kidani, *J. Inorg. Biochem.* **1979**, *11*, 39–47.

[93] G. Schröder, B. Lippert, M. Sabat, C.J.L. Lock, R. Faggiani, B. Song, H. Sigel, *J. Chem. Soc., Dalton Trans.* **1995**, 3767–3776.

[94] S. Neidle, *Nucleic Acid Structure and Recognition*, Oxford University Press, Oxford, **2002**, pp. 76–81.

[95] H. Chen, J.A. Parkinson, O. Novakova, J. Bella, F. Wang, A. Dawson, R. Gould, S. Parsons, V. Brabec, P.J. Sadler, *Proc. Natl. Acad. Sci. USA* **2003**, *100*, 14623–14628.

[96] M.V. Keck, S.J. Lippard, *J. Am. Chem. Soc.* **1992**, *114*, 3386–3390.

[97] F. Wang, J. Bella, J.A. Parkinson, P.J. Sadler, *J. Biol. Inorg. Chem.* **2005**, *10*, 147–155.

[98] O. Novakova, H. Chen, O. Vrana, A. Rodger, P.J. Sadler, V. Brabec, *Biochemistry* **2003**, *42*, 11544–11554.

[99] O. Novakova, J. Kasparkova, V. Bursova, C. Hofr, M. Vojtiskova, H. Chen, P.J. Sadler, V. Brabec, *Chem. Biol.* **2005**, *12*, 121–129.

[100] S.M. Cohen, S.J. Lippard, in *Progress in Nucleic Acid Research and Molecular Biology*, vol. 67, K. Moldave (Ed), Academic Press, San Diego, **2001**, pp. 93–130.

[101] V. Brabec, in *Progress in Nucleic Acid Research and Molecular Biology*, vol. 71, K. Moldave (Ed), Academic Press, San Diego, **2002**, pp. 1–68.

[102] T. Furuta, T. Ueda, G. Aune, A. Sarasin, K.H. Kraemer, Y. Pommier, *Cancer Res.* **2002**, *62*, 4899–4902.

[103] D. Wang, R. Hara, G. Singh, A. Sancar, S.J. Lippard, *Biochemistry* **2003**, *42*, 6747–6753.

[104] M. Selvakumaran, D.A. Pisarcik, R. Bao, A.T. Yeung, T.C. Hamilton, *Cancer Res.* **2003**, *63*, 1311–1316.

[105] F. Wang, J. Xu, A. Habtemariam, J. Bella, P.J. Sadler, *J. Am. Chem. Soc.* **2005**, *127*, 17734–17743.

[106] N.S. Kosower, E.M. Kosower, *Int. Rev. Cytol.* **1978**, *54*, 109–160.

[107] A.F.A. Peacock, A. Habtemariam, R. Fernández, V. Walland, F.P.A. Fabbiani, S. Parsons, R.E. Aird, D.I. Jodrell, P.J. Sadler, *J. Am. Chem. Soc.* **2006**, *128*, 1739–1748.

[108] I.W. McNae, K. Fishburne, A. Habtemariam, T.M. Hunter, M. Melchart, F. Wang, M.D. Walkinshaw, P.J. Sadler, *Chem. Commun.* **2004**, 1786–1787.

[109] S. Ogo, T. Abura, Y. Watanabe, *Organometallics* **2002**, *21*, 2964–2969.

[110] C.M. Thomas, T.R. Ward, *Chem. Soc. Rev.* **2005**, *34*, 337–346.

[111] A. Schlüter, K. Bieber, W.S. Sheldrick, *Inorg. Chim. Acta* **2002**, *340*, 35–43.

[112] D.B. Grotjahn, *Coord. Chem. Rev.* **1999**, *190–192*, 1125–1141.

Chapter 2
Materials and Methods

2.1 Chemicals

Most reagents were obtained from Aldrich, including D_2O (99.9%), $CDCl_3$ (99.8%), MeOD-d_4 (99.8%) and DMSO-d_6 (99.9%). Nucleic acid derivatives were acquired from Sigma Aldrich. Sodium acetate, pyridine and potassium carbonate anhydrous was purchased from BDH. Most solvents, as well as silver nitrate, dried magnesium sulphate, sodium hydroxide and sodium chloride, were supplied by Fisher. Methyl sulfoxide, benzoic acid and 4-phenylphenol were obtained from Acros. Nitromethane, lithium aluminium hydride, anhydrous silver tetrafluoroborate and pentamethylbenzaldehyde were purchased from Fluka. Hexane and 1,4-dioxane were supplied by Rathburn. 3,5-Difluoropyridine was obtained from Lancaster and 1,2-dichloroethane from both Prolabo and Aldrich. $RuCl_3.xH_2O$ was acquired from Alfa Aesar.

All chemicals were used as received. Where applicable, solvents were dried using standard methods (THF/Na/benzophenone; diethyl ether/Na; acetone/K_2CO_3; methanol/Mg/I and ethanol/Mg/I).

2.2 NMR Spectroscopy

^1H NMR spectra were acquired in 5mm NMR tubes at 298 K (unless stated otherwise) on either Bruker DMX 500, Bruker DPX 360, Bruker AVA 600, Bruker BIO 600 or a Bruker AVA 800 NMR spectrometers, respectively, using TBI [^1H, ^{13}C, X] or TXI [^1H, ^{13}C, X] probeheads and equipped for *z*-field gradients. All data processing was carried out using XWIN-NMR version 3.6 (Bruker U.K. Ltd.). ^1H NMR chemical shifts were internally referenced to TSP or TMS *via* 1,4-dioxane

(3.75 ppm), $CHCl_3$ (7.27 ppm), MeOH (3.31 ppm) or residual DMSO (2.50 ppm). Juraj Bella, University of Edinburgh, assisted in some of the NMR work.

1D spectra were recorded using standard pulse sequences. Typically, data were acquired with 64 transients into 16 k data points over a spectral width of 14 ppm. 2D spectra were recorded using standard pulse pulse sequences, which were modified by Dr. Dusan Uhrin and Mr. Juraj Bella, University of Edinburgh. Water signals were suppressed using "Presaturation" and "Shaka" [1].

COSY (Correlation SpectroscopY) was used to identify pairs of nuclei which are *J*-coupled to one another [2, 3]. Typically, data were acquired with 2 transients into 1024 data points over a spectral width of 10 ppm using a relaxation delay of 1.5 s and a mixing time of 0.06 s. 2D NOESY (Nuclear Overhauser Effect SpectroscopY) [4, 5] and 2D ROESY (Rotating frame nuclear Overhauser Effect SpectroscopY) [6, 7] were used to establish structural information resulting from through space interactions between protons that are in close spatial proximity. Typically, data were acquired with 16 - 32 transients into 2048 data points over a spectral width of 10 ppm using a relaxation delay of 1.5 s and a mixing time (for NOESY) of 0.4 – 0.6 s.

2.3 X-ray Crystallography

Diffraction data were collected with Mo-Kα radiation on a Bruker Smart APEX CCD diffractometer equipped with an Oxford Cryosystems low-temperature device typically operating at 150 K. Data collection and solution of the structures were carried out by Dr. Simon Parsons and co-workers in the School of Chemistry, University of Edinburgh. Absorption corrections were applied with the multi-scan procedure SADABS [8]. The structures of complexes **3.7**, **3.21a**, **3.22**, **3.24**, **3.26**, **4.4**, **4.16** and **4.20** were solved by Patterson methods (DIRDIF) [9], those of complexes **3.5**, **3.6**, **3.8**, **3.25a**, **4.5**, **4.6**, **4.7**, **4.10**, **4.11b**, **4.14**, **4.18**, **4.31** and **4.32** by

direct methods (SIR92) [10]. All structures were refined by full-matrix least squares against F^2 using SHELXL-97 [11], except for complexes **3.22**, **3.24**, **3.25a**, **3.26**, **4.4**, **4.6**, **4.7**, **4.11b**, **4.31** and **4.32** where CRYSTALS was used [12].

2.4 CHN Analysis

CHN elemental analysis was performed by the CHN service at the University of St Andrews, except for complexes **3.5**, **3.6**, **3.7** and **3.8**, which were analysed at the University of Edinburgh.

2.5 pH Measurements

The pH values of NMR solutions were measured at ambient temperature directly in the NMR tube, before and after recording NMR spectra, using a Corning 145 pH meter equipped with an Aldrich micro combination electrode calibrated with Aldrich buffer solutions at pH 4, 7 and 10. The pH values were adjusted with dilute $HClO_4$ and NaOH. No correction has been applied for the effect of deuterium on the glass electrode. For measurements in D_2O, pH* = pH meter reading of the solution.

The pK_a values were determined by fitting the ^1H NMR pH titration curves to the Henderson – Hasselbalch equation using the program KALEIDAGRAPH [13], with the assumption that the observed chemical shifts are weighted averages according to the population of the protonated and deprotonated species.

2.6 IR Spectroscopy

Infrared spectra were recorded by Mr. Alejandro Sanchez-Perucha, University of Edinburgh, as KBr pellets in the range 4000 – 400 cm^{-1} on a Perkin-Elmer Paragon 1000 Fourier-transform spectrometer.

2.7 Electrospray Ionisation-Mass Spectrometry (MS-ES)

Positive-ion electrospray ionisation mass spectra were obtained on a Platform II mass spectrometer (Micromass, Manchester, UK) with the assistance of Drs. Fabio Zobi and Ana Pizarro, University of Edinburgh. Data were processed using Masslynx (version 3.5) Windows XP PC data systems.

2.8 Pressure Vessel

The pressure vessel was manufactured by Mr. Stuart Johnstone, University of Edinburgh. It is a modified Quickfit round bottom flask equipped with a lid containing a rubber ring, which can be sealed tightly with a metal clamp (Figure 2.1). The reactions were performed in an oil bath at 393 K (boiling point of 1,2-dichloroethane is 357 K). During the reactions, the oil bath with the immersed pressure vessel was covered in Al-foil to prevent potential photochemical decomposition pathways (Figure 2.2).

Caution!!! Despite not having encountered any problems during these syntheses of tethered complexes (Chapter 4), the vessel is under pressure. Blast screens should be placed around the experimental set-up (Figure 2.2) and appropriate precautions taken in case of an explosion. After heating, the pressure vessel was allowed to cool to ambient temperature to reduce the internal pressure inside the vessel.

2.9 Molecular Models

Molecular models were constructed using the program Spartan'02 (Wavefunction Inc., Irvine CA, USA) using molecular mechanics (MMFF forcefield) followed by semi – empirical molecular orbital (PM3) calculations.

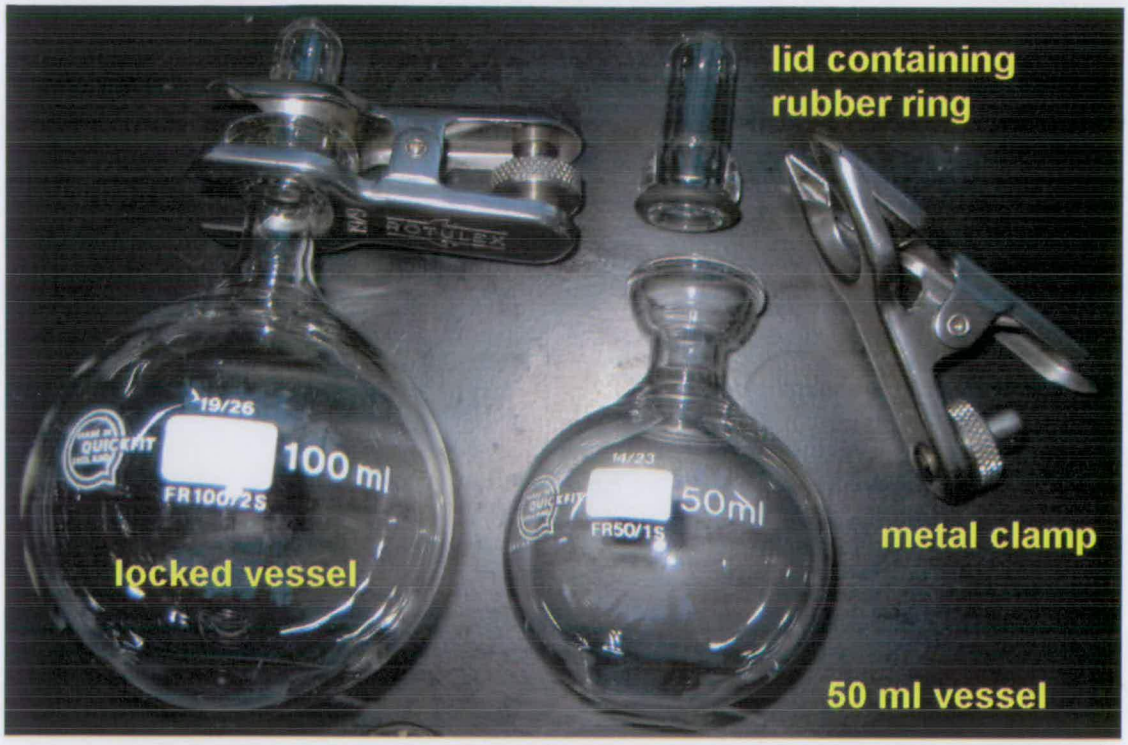

Figure 2.1: The pressure vessel, consisting of a modified Quickfit round bottom flask equipped with a lid containing a rubber ring and a metal clamp (right). The locked vessel is shown on the left.

Figure 2.2: Full experimental set-up for the synthesis of tethered Ru^{II} arene complexes using the pressure vessel. The oil bath with the immersed pressure vessel is covered with Al-foil. For safety reasons, blast screens are placed around the set-up.

2.10 References

[1] T.L. Hwang, A.J. Shaka, *J. Magn. Reson.* **1995**, *Series A 112*, 275–279.

[2] W.P. Aue, E. Bartholdi, R.R. Ernst, *J. Chem. Phys.* **1976**, *64*, 2229–2246.

[3] K. Nagayama, A. Kumar, K. Wüthrich, R.R. Ernst, *J. Magn. Reson.* **1980**, *40*, 321–334.

[4] J. Jeener, B.H. Meier, P. Bachmann, R.R. Ernst, *J. Chem. Phys.* **1979**, *71*, 4546–4553.

[5] A. Kumar, R.R. Ernst, K. Wüthrich, *Biochem. Biophys. Res. Commun.* **1980**, *95*, 1–6.

[6] J.K.M. Sanders, B.K. Hunter, *Modern NMR Spectroscopy*, Oxford University Press, New York, **1997**.

[7] J.B. Lambert, H.F. Shurvell, D.A. Lighter, R.G. Cooks, *Organic Structural Spectroscopy*, Prentice Hall, New Jersey, **1998**.

[8] G.M. Sheldrick, SADABS, University of Göttingen, Germany, **2004**.

[9] P.T. Beurskens, G. Beurskens, W.P. Bosman, R. de Gelder, S. Garcia-Granda, R.O. Gould, R. Israel, J.M.M. Smits, The DIRDIF96 Program System, Technical Report of the Crystallography Laboratory, University of Nijmegen, The Netherlands, **1996**.

[10] A. Altomare, G. Cascarano, C. Giacovazzo, A. Guagliardi, *J. Appl. Crystallogr.* **1993**, *26*, 343–350.

[11] G.M. Sheldrick, SHELXL97, University of Göttingen, Germany, **1997**.

[12] P.W. Betteridge, J.R. Carruthers, R.I. Cooper, K. Prout, D.J. Watkin, *J. Appl. Crystallogr.* **2003**, *36*, 1487.

[13] KALEIDAGRAPH, Version 3.09; Synergy Software: Reading, PA, **1997**.

Chapter 3
Ruthenium(II) Arene Complexes Containing Monoanionic *O,O*-Chelating Ligands

3.1 Introduction

Metal complexes have potential for design as novel therapeutic agents [1, 2]. Some metal complexes are relatively inert, but others are likely to be pro-drugs which undergo ligand substitution and/or redox reactions before they reach their target site. An example is the successful anticancer drug cisplatin which is activated in cells by aquation.

Half-sandwich ruthenium(II) arene complexes of the type $[(\eta^6\text{-arene})Ru(en)Cl]^+$ (Figure 3.1), where en = ethylenediamine, exhibit anticancer activity both *in vitro* [3, 4, 5] and *in vivo* [6], including activity against cisplatin-resistant cancer cells. They bind to DNA oligonucleotides forming monofunctional adducts [4, 7]. For complexes such as $[(\eta^6\text{-biphenyl})Ru(en)Cl]^+$ containing the H-bond donor en, there is exclusive binding to N7 of guanine in competitive nucleobase reactions with a strong H-bond between the carbonyl C6O and en-NH [8]. In the absence of guanine, binding to cytosine or thymine but not to adenine is observed [9]. The reaction proceeds *via* initial aquation of the chloro complex.

For metal complexes in general, the nature of the metal ion, its oxidation state, and the types and number of bound ligands, can all exert a critical influence on the biological activity of a metal complex [1, 2]. With this in mind, it was of interest to explore ways in which to influence and control the chemical reactivity and selectivity towards potential targets of ruthenium(II) arene complexes. Optimization of the design of half-sandwich organometallic Ru^{II} arene complexes as anticancer agents depends on control of ligand exchange reactions. Since aquation appears to be an important activation step for Ru^{II} arene complexes [10, 11], it is desirable to

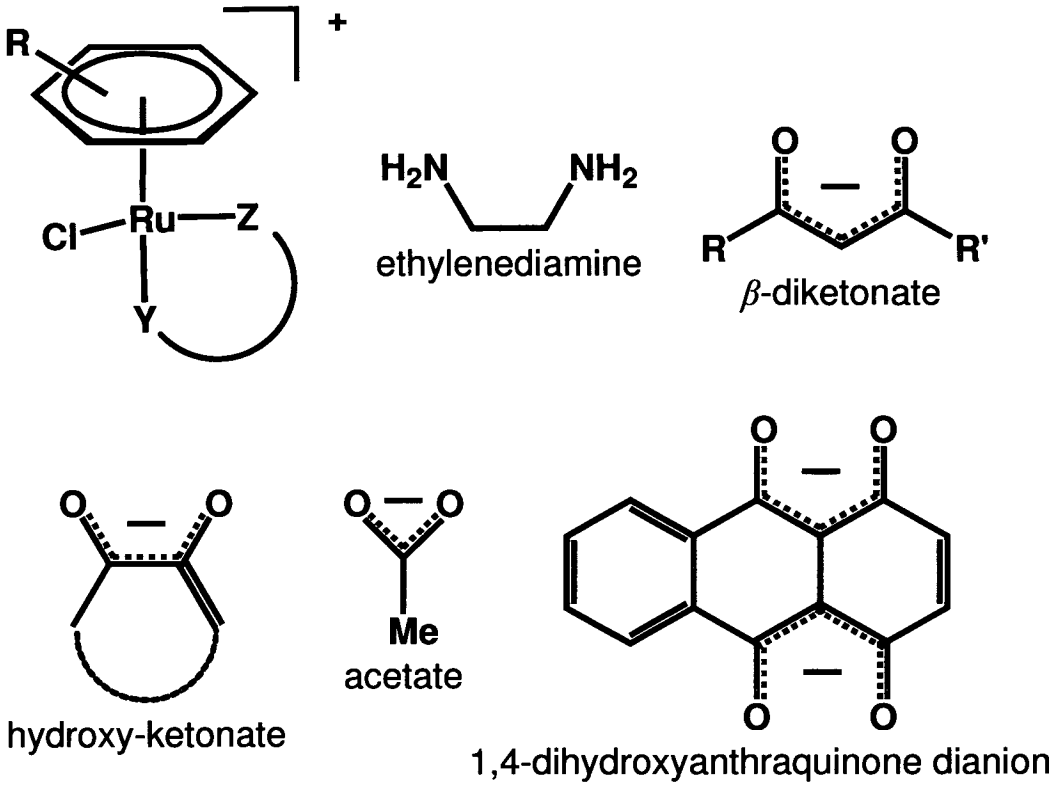

Figure 3.1: The general structures of ruthenium(II) arene complexes containing the neutral chelating ligand ethylenediamine, mono-anionic β-diketonates, hydroxy-ketonates and acetate, and the bridging 1,4-dihydroxyanthraquinone dianion.

control the associated kinetics, both in terms of rate and extent, as well as the stability of aqua adducts. Furthermore, recent results suggest that DNA may be an important target site for complexes of the kind $[(\eta^6\text{-arene})Ru(en)Cl]^+$ [11]. The rational design of new DNA binding agents that recognize specific sequences or structures, and can modify specific DNA functions such as replication and transcription, provides an effective approach for the development of novel chemotherapeutic anticancer drugs [12, 13].

In the present work features in the design of ruthenium(II) arenes, which might allow control of the specificity of binding to nucleobases have been investigated. Ru^{II} arene complexes containing *O,O*-chelating ligands which form six-membered chelate rings with the metal centre (β-diketonates, 1,4-

dihydroxyanthraquinone dianion), five-membered rings (hydroxy-ketonates) and four-membered rings (acetate) were synthesised (Figure 3.1). Their aqueous chemistry, including competitive reactions with nucleobases, was studied. It is demonstrated that incorporation of anionic *O,O*-chelating ligands of the *β*-diketonate and hydroxy-ketonate families into $\{(\eta^6\text{-arene})Ru\}^{2+}$ complexes leads to significant changes in the recognition of DNA bases compared to the neutral *N,N*-chelating ligand ethylenediamine, and also has a major effect on the electronic properties of the (arene)Ru^{II} centre, thus influencing the behaviour of the leaving group (Cl^-/H_2O). In contrast, a comparable acetato complex readily undergoes decomposition in solution. The cytotoxicity of some of the complexes towards the human ovarian cancer cell line A2780 was investigated.

3.2 Experimental Section

3.2.1 Materials

The ruthenium(II) dimer precursors $[(\eta^6\text{-}p\text{-cym})RuCl_2]_2$ (**3.1**), $[(\eta^6\text{-bip})RuCl_2]_2$ (**3.2**), $[(\eta^6\text{-bz})RuCl_2]_2$ (**3.3**) and $[(\eta^6\text{-ind})RuCl_2]_2$ (**3.4**), where *p*-cym = para-cymene, bip = biphenyl, bz = benzene, ind = indan, were synthesised according to a previously published route [14] (Scheme 3.1). The latter three dimers were kindly made available by Dr. Abraha Habtemariam, University of Edinburgh. 4,4,4-Trifluoro-1-phenyl-1,3-butanedione was kindly provided by Chris Baxter, University of Edinburgh.

All reactions were performed at ambient temperature, unless indicated otherwise.

3.2.2. Methods

In general, pH titrations were performed in 90% H_2O/10% D_2O, containing 0.1 M $NaClO_4$ and 8 mM Ru, referenced to 1,4-dioxane, at 298 K. For $[(\eta^6\text{-}p\text{-}$

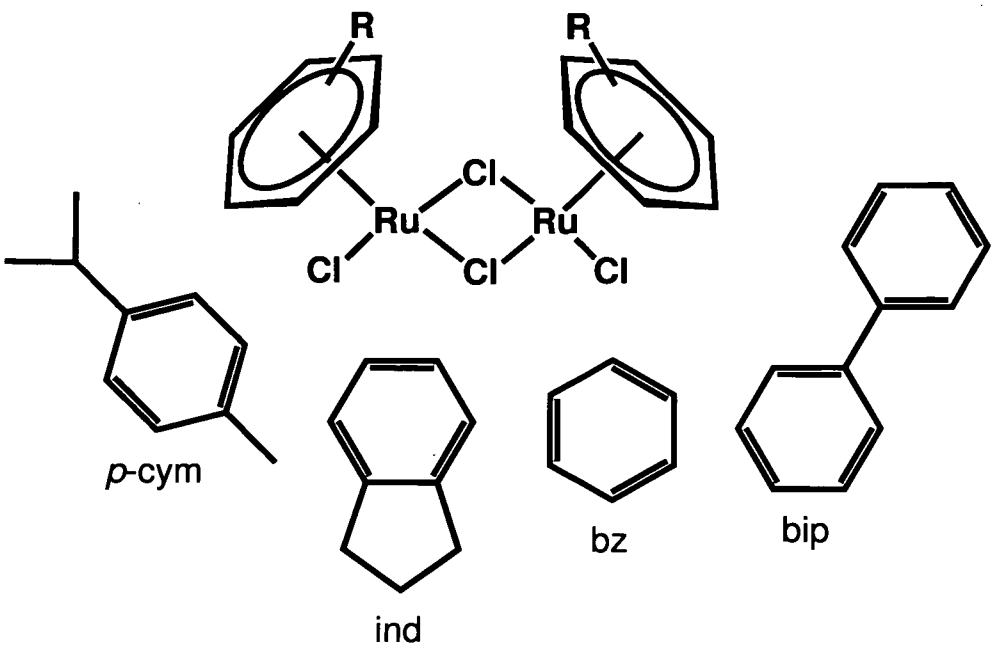

Scheme 3.1: The structures of ruthenium(II) arene dimer precursors $[(\eta^6\text{-}p\text{-cym})RuCl_2]_2$ (**3.1**), $[(\eta^6\text{-bip})RuCl_2]_2$ (**3.2**), $[(\eta^6\text{-bz})RuCl_2]_2$ (**3.3**) and $[(\eta^6\text{-ind})RuCl_2]_2$ (**3.4**).

cym)Ru($H_3CCOCHCOCH_3$ – *O,O*)H_2O]NO_3 (**3.14a**) and [(η^6-*p*-cym)Ru($C_7H_5O_2$ – *O,O*)H_2O]NO_3 (**3.25a**) the synthesised products were used, for [(η^6-*p*-cym)Ru($C_6H_5O_3$ – *O,O*)H_2O]NO_3 (**3.29**) the aqua adduct was made *in situ* by reaction of the chloride-containing complex [(η^6-*p*-cym)Ru($C_6H_5O_3$ – *O,O*)Cl] (**3.24**) with an equimolar amount of $AgNO_3$, followed by filtration. Addition of $NaClO_4$ to nucleobase adducts of $\{(\eta^6\text{-}p\text{-cym})Ru(C_7H_5O_2 - O,O)\}^+$ complexes led to the precipitation of the sample and was not added during titrations. It was also omitted for adducts of $\{(\eta^6\text{-}p\text{-cym})Ru(C_6H_5O_3 - O,O)\}^+$.

3.2.3 Preparation of Ru^{II} arene β-diketonato complexes

3.2.3.1 Neutral, chloride-containing compounds

[(η^6-*p*-cym)Ru($H_3CCOCHCOCH_3$ – *O,O*)Cl] (3.5): 3.1 (665.4 mg, 1.09 mmol) and sodium acetylacetonate monohydrate (402.9 mg, 2.88 mmol) were stirred in acetone (80 ml) for 50 min. The solvent was removed on a rotary evaporator and after

extraction with dichloromethane, followed by filtration, the solvent was removed on a rotary evaporator. The residue was dissolved in acetone and the solution concentrated on a rotary evaporator, then diluted with diethyl ether. A first fraction of red crystals (435.4 mg), suitable for X-ray diffraction, was obtained by filtration after storage at 253 K overnight. The solvents were removed on a rotary evaporator and a second fraction of product (57.9 mg) was obtained from acetone/diethyl ether at 253 K after nine days. The combined product (493.3 mg, 1.33 mmol, 61.2% yield) was dried *in vacuo*. ^{1}H NMR ($CDCl_3$): δ 5.46 (d, 2H, J = 6 Hz), 5.21 (d, 2H, J = 6 Hz), 5.16 (s, 1H), 2.88 (sp, 1H, J = 7 Hz), 2.27 (s, 3H), 2.00 (s, 6H), 1.32 (d, 6H, J = 7Hz). Elemental analysis: calculated for $C_{15}H_{21}RuClO_2$: C, 48.71; H, 5.72. Found: C, 48.73; H, 5.59%.

[(η^6-*p*-cym)Ru($C_6H_5COCHCOC_6H_5$ – *O,O*)Cl] (3.6): 1,3-Diphenyl-1,3-propanedione (277 mg, 1.24 mmol) and sodium methoxide (62 mg, 1.15 mmol) were stirred in methanol (30 ml) for 100 min. The solvent was removed on a rotary evaporator and the residue washed with diethyl ether. The obtained sodium salt (210 mg, 0.85 mmol, 73.9% yield) and **3.1** (240 mg, 0.39 mmol) were stirred in acetone (25 ml) for 40 min. After work-up as for **3.5**, dark red crystals (238 mg, 0.48 mmol, 61.8% yield), suitable for X-ray diffraction, were collected by filtration and dried *in vacuo*. ^{1}H NMR ($CDCl_3$): δ 7.92 (d, 4H, J = 7 Hz), 7.46 (t, 2H, J = 7 Hz), 7.39 (m, 4H, J = 7 Hz), 6.46 (s, 1H), 5.60 (d, 2H, J = 6 Hz), 5.33 (d, 2H, J = 6 Hz), 3.04 (sp, 1H, J = 7 Hz), 2.36 (s, 3H), 1.42 (d, 6H, J = 7 Hz). Elemental analysis: calculated for $C_{25}H_{25}RuClO_2$: C, 60.78; H, 5.10. Found: C, 60.92; H, 5.20%.

[(η^6-*p*-cym)Ru($(CH_3)_3CCOCHCOC(CH_3)_3$ – *O,O*)Cl] (3.7): 2,2,6,6-Tetramethyl-3,5-heptanedione (299 mg, 1.62 mmol) and sodium methoxide (68 mg, 1.26 mmol) were stirred in methanol (40 ml) for 5 h. The solvent and residual starting material were removed on a rotary evaporator. The obtained sodium salt (233 mg, 1.13 mmol, 89.6% yield) and **3.1** (258 mg, 0.42 mmol) were stirred in acetone (25 ml) for 40

min. After work-up as for **3.5**, except for use of diethyl ether/hexane at 253 K, orange needles (215 mg, 0.47 mmol, 56.0% yield), suitable for X-ray diffraction, were collected by filtration and dried *in vacuo*. ^{1}H NMR ($CDCl_3$): δ 5.41 (d, 2H, J = 6 Hz), 5.40 (s, 1H), 5.13 (d, 2H, J = 6 Hz), 2.91 (sp, 1H, J = 7 Hz), 2.24 (s, 3H), 1.36 (d, 6H, J = 7 Hz), 1.13 (s, 18H). Elemental analysis: calculated for $C_{21}H_{33}RuClO_2$: C, 55.56; H, 7.33. Found: C, 55.54; H, 7.15%.

[(η^6-*p*-cym)Ru($F_3CCOCHCOCF_3$ – *O,O*)Cl] (3.8): 3.1 (250 mg, 0.41 mmol) and sodium hexafluoroacetylacetonate (260 mg, 1.13 mmol) were stirred in acetone (25 ml) for 40 min. After work-up as for **3.5**, except for use of diethyl ether/hexane at 253 K, violet-brown crystals (277 mg, 0.58 mmol, 70.7% yield), suitable for X-ray diffraction, were collected by filtration and dried *in vacuo*. ^{1}H NMR ($CDCl_3$): δ 5.89 (s, 1H), 5.66 (d, 2H, J = 6 Hz), 5.39 (d, 2H, J = 6 Hz), 2.91 (sp, 1H, J = 7 Hz), 2.27 (s, 3H), 1.36 (d, 6H, J = 7 Hz). Elemental analysis: calculated for $C_{15}H_{15}RuClO_2F_6$: C, 37.71; H, 3.16. Found: C, 37.83; H, 3.17%.

[(η^6-*p*-cym)Ru($C_6H_5COCHCOCH_3$ – *O,O*)Cl] (3.9): 1-Phenyl-1,3-butanedione (60.8 mg, 0.38 mmol) and sodium methoxide (21.4 mg, 0.40 mmol) were stirred in methanol (7 ml) for 25 min. To this **3.1** (88.2 mg, 0.14 mmol), which had been stirred in methanol (10 ml) for 10 min, was added and the solution stirred for 60 min. After work-up as for **3.5**, except for storage at 253 K for 3 d, the dark orange crystals (93.5 mg, 0.22 mmol, 75.0%) were collected by filtration, washed with little diethyl ether and dried in air. ^{1}H NMR ($CDCl_3$): δ 7.82 (d, 2H, J = 7 Hz), 7.42 (t, 1H, J = 7 Hz), 7.36 (t, 2H, J = 7 Hz), 5.81 (s, 1H), 5.55 (d, 2H, J = 6 Hz), 5.52 (d, 2H, J = 6 Hz), 5.26 (dd, 2H, J = 6), 2.96 (sp, 1H, J = 7 Hz), 2.31 (s, 3H), 2.14 (s, 3H), 1.37 (d, 6H, J = 7 Hz). Elemental analysis: calculated for $C_{20}H_{23}RuClO_2$: C, 55.62; H, 5.37. Found: C, 55.63; H, 5.24%.

[(η^6-*p*-cym)Ru($C_6H_5COCHCOCF_3$ – *O,O*)Cl] (3.10): 4,4,4-Trifluoro-1-phenyl-1,3-butanedione (71.0 mg, 0.33 mmol) and sodium methoxide (18.8 mg, 0.35 mmol)

were stirred in methanol (7 ml) for 40 min. To this **3.1** (78.2 mg, 0.13 mmol), which had been stirred in methanol (10 ml) for 25 min, was added and the solution stirred for 45 min. After work-up as for **3.9,** the dark red crystals (104.7 mg, 0.22 mmol, 84.0%) were collected by filtration, washed with little diethyl ether and dried in air. ^{1}H NMR ($CDCl_3$): δ 7.87 (d, 2H, J = 8 Hz), 7.53 (t, 1H, J = 7 Hz), 7.42 (t, 2H, J = 7 Hz), 6.21 (s, 1H), 5.64 (d, 2H, J = 6 Hz), 5.61 (d, 2H, J = 6 Hz), 5.35 (dd, 2H, J = 6.5), 2.98 (sp, 1H, J = 7 Hz), 2.31 (s, 3H), 1.40 (dd, 6H, J = 6 Hz). Elemental analysis: calculated for $C_{20}H_{20}RuClO_2F_3$: C, 49.44; H, 4.15. Found: C, 49.51; H, 3.95%.

[(η^6-bip)Ru($H_3CCOCHCOCH_3$ – *O,O*)Cl] (3.11): 3.2 (250 mg, 0.38 mmol) was refluxed in water (25 ml) for 2 h. The heat was reduced below boiling point and sodium acetylacetonate monohydrate (141 mg, 1.01 mmol) was added. The solution was stirred for 30 min and hot filtered. After work-up as for **3.5**, except for storage at 253 K for 6 d, a red microcrystalline product (65 mg, 0.16 mmol, 21.3% yield) was collected by filtration and dried *in vacuo*. ^{1}H NMR ($CDCl_3$): δ 7.72 – 7.70 (m, 2H), 7.49 – 7.45 (m, 3H), 5.86 (t, 2H, J = 6 Hz), 5.80 (d, 2H, J = 6 Hz), 5.77 (t, 1H, J = 6 Hz), 5.13 (s, 1H), 1.93 (s, 6H). Elemental analysis: calculated for $C_{17}H_{17}RuClO_2$: C, 52.38; H, 4.40. Found: C, 52.64; H, 4.22%.

[(η^6-bz)Ru($H_3CCOCHCOCH_3$ – *O,O*)Cl] (3.12): 3.3 (150 mg, 0.30 mmol) and sodium acetylacetonate monohydrate (110.1 mg, 0.79 mmol) were stirred in acetone (10 ml) and methanol (30 ml) overnight. After work-up as for **3.5**, except for use of methanol/dichloromethane/diethyl ether at 253 K, an orange product (67.5 mg, 0.22 mmol, 36.7% yield) was collected by filtration and dried *in vacuo*. ^{1}H NMR ($CDCl_3$): δ 5.64 (s, 6H), 5.19 (s, 1H), 2.01 (s, 6H). Elemental analysis: calculated for $C_{11}H_{13}RuClO_2$: C, 42.11; H, 4.18. Found: C, 42.42; H, 3.93%.

[(η^6-ind)Ru($H_3CCOCHCOCH_3$ – *O,O*)Cl] (3.13): 3.4 (100 mg, 0.17 mmol) and sodium acetylacetonate monohydrate (63.1 mg, 0.45 mmol) were stirred in methanol

(25 ml) for 2 h. After work-up as for **3.5**, except for use of methanol/diethyl ether at 253 K, an orange product (31.9 mg, 0.09 mmol, 26.5% yield) was collected by filtration and dried *in vacuo*. ^{1}H NMR ($CDCl_3$): δ 5.52 (s, 4H), 5.16 (s, 1H), 2.89 – 2.84 (m, 2H), 2.58 – 2.50 (m, 2H), 2.18 – 2.06 (m, 2H), 2.00 (s, 6H). Elemental analysis: calculated for $C_{14}H_{17}RuClO_2$: C, 47.53; H, 4.84. Found: C, 47.96; H, 4.20%.

3.2.3.2 Positively-charged compounds

[(η^6-*p*-cym)Ru($H_3CCOCHCOCH_3$ – *O,O*)H_2O]NO_3 (3.14a): Silver nitrate (70.5 mg, 0.42 mmol) and **3.5** (153.5 mg, 0.42 mmol) were stirred in water (25 ml) overnight. After filtration, the solvent was removed on a rotary evaporator. Trituration of the oily residue with diethyl ether gave the final product as an orange powder (170.6 mg, 0.41 mmol, 98% yield), which was collected by filtration and dried in air. ^{1}H NMR ($CDCl_3$): δ 5.59 (d, 2H, J = 5 Hz), 5.32 (d, 2H, J = 5 Hz), 5.10 (s, 1H), 2.88 (sp, 1H, J = 7 Hz), 2.26 (s, 3H), 2.00 (s, 6H), 1.34 (d, 6H, J = 7Hz).

[(η^6-*p*-cym)Ru($H_3CCOCHCOCH_3$ – *O,O*)CH_3CN]BF_4 (3.15): 3.5 (144 mg, 0.39 mmol) and silver tetrafluoroborate (72 mg, 0.37 mmol) were stirred in acetonitrile (20 ml) overnight. After filtration, the solvent was removed on a rotary evaporator. The residue was dissolved in a minimum amount of acetone, and diethyl ether was added until precipitation occurred. Storage of the solution at 253 K for 4 d yielded orange crystals (149 mg, 0.32 mmol, 87.1% yield), which were collected by filtration and dried *in vacuo*. ^{1}H NMR ($CDCl_3$): δ 5.77 (d, 2H, J = 6 Hz), 5.51 (d, 2H, J = 6 Hz), 5.19 (s, 1H), 2.88 (sp, 1H, J = 7 Hz), 2.45 (s, 3H), 2.23 (s, 3H), 2.02 (s, 6H), 1.35 (d, 6H, J = 7 Hz).

[(η^6-*p*-cym)Ru($H_3CCOCHCOCH_3$ – *O,O*)$C_5H_3NCl_2$]PF_6 (3.16): 3,5-Dichloropyridine (300 mg, 2.03 mmol) and **3.14a** (26.7 mg, 0.06 mmol) were dissolved in water (3 ml) and ammonium hexafluorophosphate (300 mg, 1.84 mmol)

was added. The resulting precipitate was dissolved by addition of acetone. The solution was then filtered and allowed to partially evaporate overnight. The yellow-green microcrystalline product (18.2 mg, 0.03 mmol, 45.0% yield) was collected by filtration, washed with cold water, then diethyl ether and dried in air. ^{1}H NMR ($CDCl_3$): δ 8.24 (s, 2H), 7.87 (t, 1H), 5.68 (d, 2H, J = 6 Hz), 5.57 (d, 2H, J = 6 Hz), 5.08 (s, 1H), 2.82 (sp, 1H, J = 7 Hz), 2.16 (s, 3H), 2.00 (s, 6H), 1.34 (d, 6H, J = 7 Hz). Elemental analysis: calculated for $C_{20}H_{24}RuO_2NCl_2PF_6$: C, 38.29; H, 3.86; N 2.23. Found: C, 37.67; H, 3.34; N 2.28%.

[(η^6-*p*-cym)Ru($H_3CCOCHCOCH_3$ – *O,O*)$C_5H_3NF_2$]PF_6 (3.17): 3,5-Difluoropyridine (47.2 mg, 0.41 mmol) and **3.14a** (17.3 mg, 0.04 mmol) were dissolved in water (5 ml) and ammonium hexafluorophosphate (194.2 mg, 1.19 mmol) was added. After work-up as for **3.16**, a bright yellow product (18.4 mg, 0.03 mmol, 74.1% yield) was obtained after 5 d, which was collected by filtration, washed with cold water, then diethyl ether and dried in air. ^{1}H NMR ($CDCl_3$): δ 8.14 (s, 2H), 7.44 (tt, 1H), 5.67 (d, 2H, J = 6 Hz), 5.56 (d, 2H, J = 6 Hz), 5.08 (s, 1H), 2.84 (sp, 1H, J = 7 Hz), 2.17 (s, 3H), 2.00 (s, 6H), 1.35 (d, 6H, J = 7 Hz).

[(η^6-*p*-cym)Ru($H_3CCOCHCOCH_3$ – *O,O*)C_5H_5N]PF_6 (3.18): Pyridine (287 mg, 3.63 mmol) and **3.14a** (26.7 mg, 0.06 mmol) were dissolved in water (7 ml) and ammonium hexafluorophosphate (315 mg, 1.93 mmol) was added. After work-up as for **3.16**, an oil formed and the solvents were decanted. Exposure of the oil to air for 4 d lead to formation of a yellow powder (17.6 mg, 0.03 mmol, 48.9% yield), which was washed with cold water, then diethyl ether and dried in air. ^{1}H NMR ($CDCl_3$): δ 8.40 (d, 2H, J = 6 Hz), 7.87 (t, 1H, J = 8 Hz), 7.49 (t, 2H, J = 6 Hz), 5.61 (d, 2H, J = 6 Hz), 5.44 (d, 2H, J = 6 Hz), 5.02 (s, 1H), 2.79 (sp, 1H, J = 7 Hz), 2.08 (s, 3H), 1.96 (s, 6H), 1.32 (d, 6H, J = 6 Hz).

[(η^6-*p*-cym)Ru($H_3CCOCHCOCH_3$ – *O,O*)C_5H_4NCN]PF_6 (3.19): 4-Cyanopyridine (63.7 mg, 0.61 mmol) and **3.14a** (23.3 mg, 0.06 mmol) were allowed to stand in

water (5 ml) for 1 h and ammonium hexafluorophosphate (256 mg, 1.57 mmol) was added. After work-up as for **3.16**, an orange product (20.1 mg, 0.03 mmol, 61.3% yield) was obtained after 5 d, which was collected by filtration, washed with cold water, then diethyl ether and dried in air. ^{1}H NMR ($CDCl_3$): δ 8.65 (d, 2H, J = 6 Hz), 7.71 (d, 2H, J = 6 Hz), 5.65 (d, 2H, J = 6 Hz), 5.52 (d, 2H, J = 6 Hz), 5.05 (s, 1H), 2.80 (sp, 1H, J = 7 Hz), 2.12 (s, 3H), 1.98 (s, 6H), 1.33 (d, 6H, J = 7 Hz).

[(η^6-*p*-cym)Ru($H_3CCOCHCOCH_3$ – *O,O*)$C_7H_9N_5$]PF_6 (3.20): 9-Ethyladenine (11.5 mg, 0.07 mmol) and **3.5** (52.1 mg, 0.14 mmol) were stirred in water (30 ml) overnight, and the volume was reduced to *ca.* 20 ml on a rotary evaporator. Upon addition of ammonium hexafluorophosphate (46.0 mg, 0.28 mmol) a precipitate formed and the reaction mixture was allowed to stand for 3 d. The solution was centrifuged and the supernatant decanted. The yellow powder (52.5 mg) was dried *in vacuo* and used as obtained.

[(η^6-*p*-cym)Ru($C_6H_5COCHCOC_6H_5$ – *O,O*)H_2O]NO_3 (3.21a): Silver nitrate (134.2 mg, 0.79 mmol) and **3.6** (390.4 mg, 0.79 mmol) were stirred in acetone (25 ml) and water (15 ml) for 5.5 h. After filtration, the solvent was removed on a rotary evaporator. The resulting orange powder was dried in air and used as obtained. ^{1}H NMR ($CDCl_3$): δ 7.91 (d, 4H, J = 7 Hz), 7.48 (t, 2H, J = 7 Hz), 7.42 (t, 4H, J = 7 Hz), 6.43 (s, 1H), 5.69 (d, 2H, J = 6 Hz), 5.45 (d, 2H, J = 6 Hz), 3.05 (sp, 1H, J = 7 Hz), 2.39 (s, 3H), 1.45 (d, 6H, J = 7 Hz).

[(η^6-*p*-cym)Ru($C_6H_5COCHCOC_6H_5$ – *O,O*)$C_7H_9N_5O$]CF_3SO_3 (3.22): 3.21a (40.7 mg, 0.08 mmol) and 9-ethylguanine (13.6 mg, 0.08 mmol) were stirred in methanol (16 ml) and water (4 ml) for 1 h. The solution was concentrated to *ca.* 5 ml on a rotary evaporator, sodium trifluoromethanesulfonate (78.8 mg, 0.46 mmol) was added and the solvent removed on a rotary evaporator. Water was added to the residue followed by ultra sonication. After filtration, the powder was dissolved in acetone, the solvent removed on a rotary evaporator and the oily residue triturated

with diethyl ether. The resulting yellow powder was dried in air and used as obtained. ^{1}H NMR ($CDCl_3$): δ 9.37 (s, 1H), 7.88 (d, 4H, J = 7 Hz), 7.52 (t, 2H, J = 7 Hz), 7.46 (t, 4H, J = 7 Hz), 7.24 (s, 1H), 6.33 (s, 1H), 5.81 (d, 2H, J = 6 Hz), 5.66 (d, 2H, J = 6 Hz), 5.54 (s, 2H), 3.90 (q, 2H, J = 7 Hz), 2.88 (sp, 1H, J = 7 Hz), 2.20 (s, 3H), 1.31 (d, 6H J = 7 Hz), 1.15 (t, 3H, J = 7 Hz).

3.2.4 Preparation of Ru^{II} *p*-cymene hydroxy-ketonato complexes

[(η^6-*p*-cym)Ru($C_7H_5O_2$ – *O,O*)Cl] (3.23): Tropolone (108.5 mg, 0.89 mmol) and sodium methoxide (48.0 mg, 0.89 mmol) were stirred in methanol (10 ml) for 45 min. To this **3.1** (208.7 mg, 0.34 mmol), which had been stirred in methanol (10 ml) for 20 min, was added and the solution stirred for 1 h. After work-up as for **3.5**, the orange product (215 mg, 0.55 mmol, 80.5%) was collected by filtration, washed with minimal diethyl ether and dried in air. ^{1}H NMR ($CDCl_3$): δ 7.23 – 7.17 (m, 4H), 6.78 (tt, 1H, J = 8.5 Hz), 5.55 (d, 2H, J = 6 Hz), 5.33 (d, 2H, J = 6 Hz), 2.92 (sp, 1H, J = 7 Hz), 2.34 (s, 3H), 1.33 (d, 6H, J = 7 Hz). Elemental analysis: calculated for $C_{17}H_{19}RuClO_2$: C, 52.10; H, 4.89. Found: C, 52.66; H, 4.15%.

[(η^6-*p*-cym)Ru($C_6H_5O_3$ – *O,O*)Cl] (3.24): 3.1 (203.7 mg, 0.33 mmol) was stirred in methanol (15 ml) for 1 h. To this a solution containing maltol (109.1 mg, 0.87 mmol) and sodium methoxide (49.0 mg, 0.91 mmol), which had been stirred in methanol (15 ml) for 45 min, was added in portions of 1 ml and the solution stirred for 1 h. After work-up as for **3.5**, except for use of warm acetone to extract the residue and concentration of the solution until onset of precipitation before addition of diethyl ether, the orange product (174.7 mg, 0.44 mmol, 66.3%) was collected by filtration and dried in air. ^{1}H NMR ($CDCl_3$): δ 7.55 (d, 1H, J = 5 Hz), 6.51 (d, 1H, J = 5 Hz), 5.54 (d, 1H, J = 5.5 Hz), 5.51 (d, 1H, J = 5.5 Hz), 5.32 (d, 1H, J = 5.5 Hz), 5.28 (d, 1H, J = 5.5 Hz), 2.92 (sp, 1H, J = 7 Hz), 2.42 (s, 3H), 2.33 (s, 3H), 1.34 (d, 3H, J = 7

Hz), 1.31 (d, 3H, J = 7 Hz). Elemental analysis: calculated for $C_{16}H_{19}RuClO_3$: C, 48.55; H, 4.84. Found: C, 48.61; H, 4.62%.

[(η^6-*p*-cym)Ru($C_7H_5O_2$ – *O,O*)H_2O]NO_3 (3.25a): 3.23 (103.7 mg, 0.26 mmol) and silver nitrate (45.0 mg, 0.26 mmol) were stirred in water (10 ml) for 1 h. After filtration, the solvent was removed on a rotary evaporator and the product was triturated with diethyl ether. The resulting orange powder was dried in air and used as obtained. ^{1}H NMR ($CDCl_3$): δ 7.29 – 7.24 (m, 4H), 6.87 (m, 1H), 5.68 (d, 2H, J = 6 Hz), 5.43 (d, 2H, J = 6 Hz), 2.91 (sp, 1H, J = 7 Hz), 2.34 (s, 3H), 1.36 (d, 6H, J = 7 Hz).

3.2.5 Preparation of a Ru^{II} *p*-cymene acetato complex

[(η^6-*p*-cym)Ru(O_2CCH_3 – *O,O*)Cl] (3.26): 3.1 (250 mg, 0.41 mmol) and sodium acetate (89 mg, 1.08 mmol) were stirred in methanol (25 ml) for 40 min. After extraction (see **3.5**), the residue was dissolved in a minimum of acetone, and hexane was added until the solution became opaque. After filtration, the solvents were removed on a rotary evaporator and the procedure was repeated. The product was then crystallised from acetone/hexane at 253 K overnight. The free-floating crystals (30 mg, 0.09 mmol, 11.0% yield), suitable for X-ray diffraction, were collected by filtration and dried *in air*. ^{1}H NMR ($CDCl_3$): 5.64 (d, 2H, J = 6 Hz), 5.42 (d, 2H, J = 6 Hz), 2.94 (sp, 1H, J = 7 Hz), 2.33 (s, 3H), 1.83 (s, 3H), 1.40 (d, 6H, J = 7 Hz). Elemental analysis: calculated for $C_{12}H_{17}RuClO_2$: C, 43.70; H, 5.20. Found: C, 43.99; H, 5.09%.

3.2.6 Preparation of a Ru^{II} *p*-cymene hydroxo-bridged dimer

[((η^6-*p*-cym)Ru)$_2$(μ-OH)$_3$]$^+$ (3.27): This complex was prepared *in situ* from a solution of **3.26** (3 mM Ru) in water at *ca.* pH 9 (by addition of a 1 M solution of sodium hydroxide). Mass spectrometry (MS-ES): obs. 522.2 m/z, calc for

$[C_{20}H_{31}Ru_2O_3]^+$ 521.6 m/z. ^{1}H NMR (D_2O): 5.38 (d, 2H, J = 6 Hz), 5.17 (d, 2H, J = 6 Hz), 2.67 (sp, 1H, J = 7 Hz), 2.08 (s, 3H), 1.22 (d, 6H, J = 7 Hz).

3.2.7 Preparation of a Ru^{II} *p*-cymene complex bridged by a dianionic *O,O*-chelating ligand

$[(\eta^6$-*p*-cym$)_2Ru_2(C_6H_4(CO)_2C_6H_2O_2$ – $(O,O)_2)Cl_2]$ (3.28): 1,4-Dihydroxyanthraquinone (41.3 mg, 0.17 mmol) and sodium methoxide (20.4 mg, 0.37 mmol) were stirred in methanol (25 ml) for 30 min. To this **3.1** (175 mg, 0.29 mmol) was added and the solution stirred overnight. After extraction (see **3.5**), the residue was washed thoroughly with acetone, and dissolved in methanol. Diethyl ether was added and the solution was stored at 253 K for 3 d. A powder was collected by filtration but still contained **3.1**. It was washed with acetonitrile, then dissolved in acetonitrile. Diethyl ether was added and the solution stored at 253 K for 3d. The dark green product (32.2 mg, 0.04 mmol, 24.0% yield) was collected by filtration and dried *in vacuo*. ^{1}H NMR ($CDCl_3$): δ 8.37 (q, 2H, J = 3 Hz), 7.63 (q, 2H, J = 3 Hz), 7.04 (s, 2H), δ 5.59 (d, 2H, J = 5.5 Hz), 5.55 (d, 2H, J = 5.5 Hz), 5.28 (dd, 4H, J = 5.5 Hz), 2.96 (sp, 2H, J = 7 Hz), 2.28 (s, 6H), 1.38 (d, 12H, J = 7 Hz). Elemental analysis: calculated for $C_{34}H_{34}Ru_2Cl_2O_4$: C, 52.38; H, 4.40. Found: C, 51.79; H, 3.54%.

3.3 Synthesis and Characterisation

3.3.1 Results

3.3.1.1 Ru^{II} arene β-diketonato complexes

The neutral, chloride-containing, ruthenium(II) arene *β*-diketonato complexes $[(\eta^6$-*p*-cym)Ru(acac)Cl] (**3.5**), $[(\eta^6$-*p*-cym)Ru(Ph_2acac)Cl] (**3.6**), $[(\eta^6$-*p*-cym)Ru($^tBu_2$acac)Cl] (**3.7**), $[(\eta^6$-*p*-cym)Ru($(CF_3)_2$acac)Cl] (**3.8**), $[(\eta^6$-*p*-cym)Ru(PhacacMe)Cl] (**3.9**), $[(\eta^6$-*p*-cym)Ru(PhacacCF_3)Cl] (**3.10**), $[(\eta^6$-

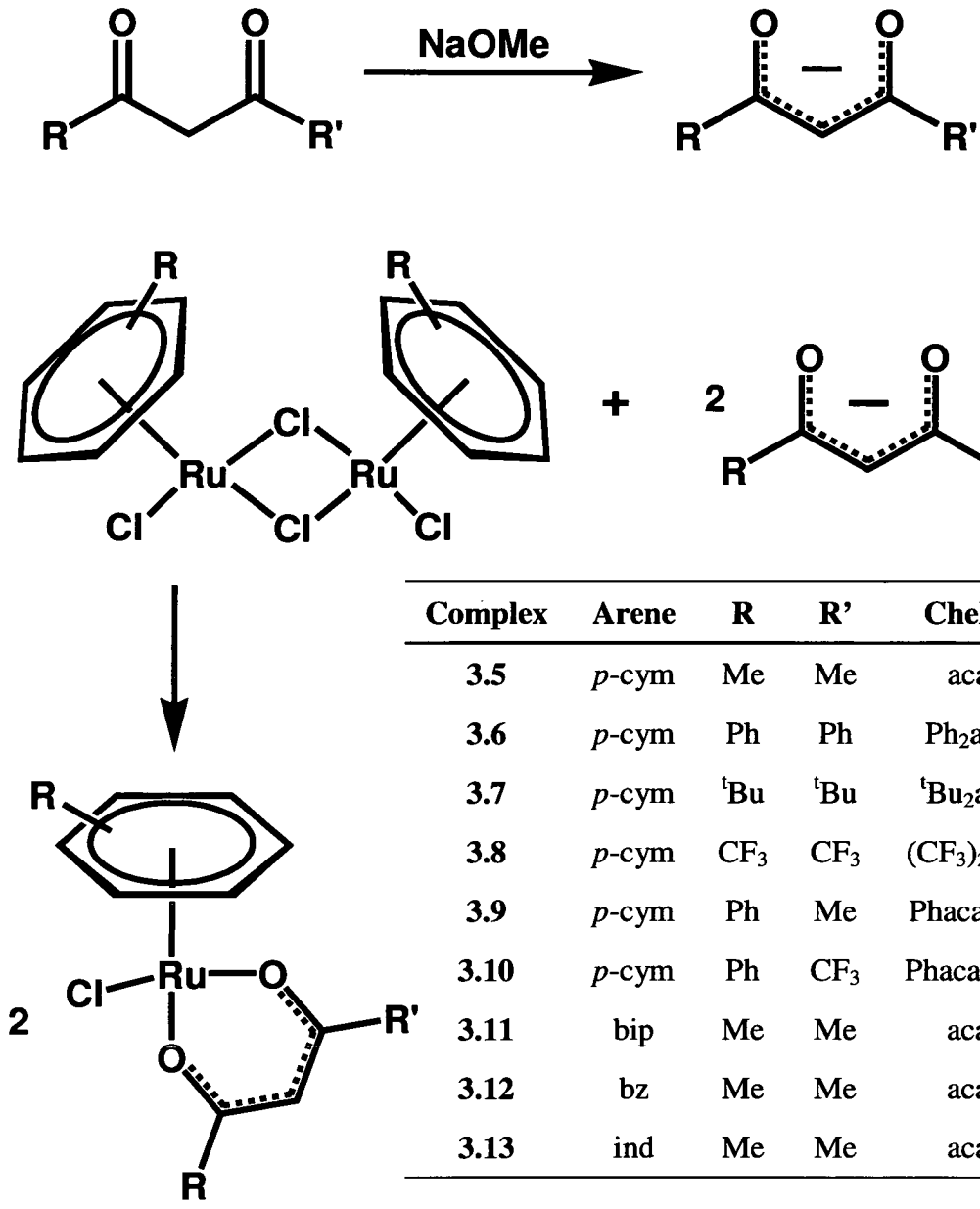

Complex	Arene	R	R'	Chelate
3.5	*p*-cym	Me	Me	acac
3.6	*p*-cym	Ph	Ph	Ph_2acac
3.7	*p*-cym	^{t}Bu	^{t}Bu	$^t Bu_2$acac
3.8	*p*-cym	CF_3	CF_3	$(CF_3)_2$acac
3.9	*p*-cym	Ph	Me	PhacacMe
3.10	*p*-cym	Ph	CF_3	PhacacCF_3
3.11	bip	Me	Me	acac
3.12	bz	Me	Me	acac
3.13	ind	Me	Me	acac

Scheme 3.2: Reaction scheme for the synthesis of neutral, chloride-containing Ru^{II} arene β-diketonato complexes, including numbering and ligand definitions.

bip)Ru(acac)Cl] (**3.11**), [(η^6-bz)Ru(acac)Cl] (**3.12**) and [(η^6-ind)Ru(acac)Cl] (**3.13**) were synthesised in high purity and moderate to good yields as described in Scheme 3.2, which also shows the respective structures, including the ligand definitions. The syntheses were aided by a previously reported route for the synthesis of **3.5** [15]. In

general, no major problems were encountered. However, synthesis of **3.5** led to varying yields (30-60%) and occasional decomposition of the product in solution.

The chloride-bridged ruthenium arene dimers $[(\eta^6\text{-arene})RuCl_2]_2$, which were used as precursors, were produced in high yields by reacting the reduced form of the arene as its cyclic diene with $RuCl_3.xH_2O$ in refluxing ethanol, which leads to the reduction of Ru^{III} to Ru^{II} and the aromatization of the diene. The dimers were then reacted with appropriate β-diketonate ligands. Where no sodium salt of a β-diketone was commercially available, it was produced *in situ* by reaction with sodium methoxide. The presence of the two carbonyl groups in the 1- and 3-positions makes the hydrogen atoms on the central C2 carbon acidic, thus allowing easy abstraction of one hydrogen atom with bases such as sodium methoxide. This creates a negative charge on the C2 carbon atom, which is delocalised over the ligand [16].

All complexes were characterised by ^1H NMR. The most interesting feature is the dependence of the chemical shift of the peak for the central β-diketonate proton on the nature of the side groups. A range of 1.3 ppm has been observed, whereas the nature of the arene has a less pronounced influence (0.06 ppm).

Crystals suitable for X-ray diffraction studies were obtained for $[(\eta^6\text{-}p\text{-cym})Ru(acac)Cl]$ (**3.5**) and $[(\eta^6\text{-}p\text{-cym})Ru(Ph_2acac)Cl]$ (**3.6**) from acetone/diethyl ether, for $[(\eta^6\text{-}p\text{-cym})Ru(^tBu_2acac)Cl]$ (**3.7**) and $[(\eta^6\text{-}p\text{-cym})Ru((CF_3)_2acac)Cl]$ (**3.8**) from diethyl ether/hexane, all at 253 K. Their crystal data are shown in Tables A.3.1 and A.3.2 and the respective structures in Figure 3.2. All four complexes have the characteristic "piano stool" geometry, where the arene forms the seat of the stool and the other two ligands the legs, and appear structurally very similar. The β-diketonate ligands form six-membered chelate rings with the ruthenium centre. Selected bond lengths and angles are shown in Table 3.1. The Ru – O bond lengths in complexes **3.5**, **3.6** and **3.7** are in a range of 2.063(2) – 2.0768(16) Å, which is comparable to that range of other known structures of Ru^{II} arene complexes containing acac-type

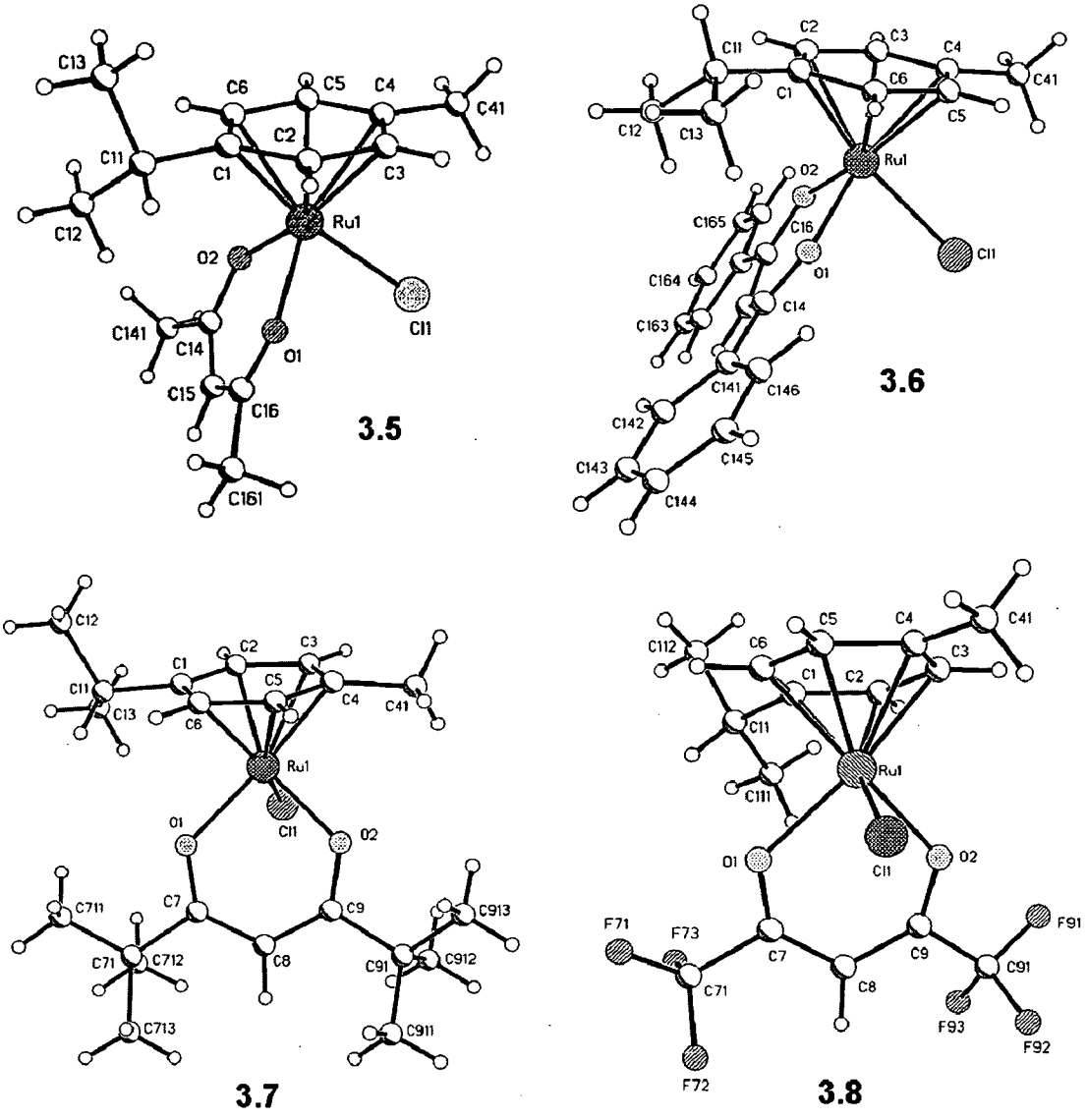

Figure 3.2: The X-ray crystal structures of [(η^6-*p*-cym)Ru(acac)Cl] (**3.5**), [(η^6-*p*-cym)Ru(Ph_2acac)Cl] (**3.6**), [(η^6-*p*-cym)Ru(^{t}Bu_2acac)Cl] (**3.7**) and [(η^6-*p*-cym)Ru((CF_3)$_2$acac)Cl] (**3.8**) and atom numbering scheme.

ligands [17, 18]. The Ru – O bond lengths for **3.8** are significantly longer with 2.097(3) and 2.111(3) Å, respectively. The Ru – Cl bond lengths of 2.4015(11) to 2.4197(6) Å are within the range known for other Ru^{II} arene complexes, with that of **3.8** *ca.* 0.08 Å shorter compared to **3.7**. The Ru – C(arene) bond lengths are between 2.155(2) – 2.199(2) Å, all within the known range for ruthenium arene complexes, but spanning a comparatively narrower range. The Ru – centroid distances are

Table 3.1: Selected bond lengths (Å) and angles (°) for [(η^6-*p*-cym)Ru(acac)Cl] (**3.5**), [(η^6-*p*-cym)Ru(Ph_2acac)Cl] (**3.6**), [(η^6-*p*-cym)Ru($^tBu_2$acac)Cl] (**3.7**) and [(η^6-*p*-cym)Ru($(CF_3)_2$acac)Cl] (**3.8**).

	3.5	**3.6**	**3.7**	**3.8**
Ru-Cl	2.4197(6)	2.4156(5)	2.4102(9)	2.4015(11)
Ru-O1	2.0709(16)	2.0647(13)	2.063(2)	2.111(3)
Ru-O2	2.0768(16)	2.0639(14)	2.0670(19)	2.097(3)
Ru-C1	2.175(2)	2.1968(19)	2.168(4)	2.178(4)
Ru-C2	2.156(2)	2.162(2)	2.169(4)	2.174(4)
Ru-C3	2.175(2)	2.1646(19)	2.168(3)	2.164(4)
Ru-C4	2.199(2)	2.1938(18)	2.183(3)	2.193(4)
Ru-C5	2.178(2)	2.1792(18)	2.182(3)	2.168(4)
Ru-C6	2.155(2)	2.1694(18)	2.168(3)	2.170(4)
Ru-centroid[a]	1.647	1.649	1.647	1.647
O1-Ru-O2	88.01(7)	87.67(5)	88.32(9)	87.12(11)
O1-Ru-Cl	84.94(5)	84.91(4)	84.08(7)	85.94(8)
O2-Ru-Cl	86.78(5)	85.36(4)	85.3(1)	86.5(1)

[a] = measured using Mercury 1.4.

around 1.65 Å. In complex **3.6** the two phenyl side-groups are tilted at an angle of 17.09° from each other.

An interesting feature in the structure for **3.5** is the linking of molecules into dimers about an inversion centre by pairs of strong acac oxygen – *p*-cymene ring CH H-bonds (O···H3 2.29 Å, cf. van der Waals sum 2.72 Å), as shown in Figure 3.3 and Table 3.2. These dimers are linked into a three-dimensional array, principally by Cl1···H6 interactions (2.65 Å, cf. van der Waals sum 2.95 Å).

A number of positively-charged complexes, where chloride was replaced by neutral σ-donors, was synthesised. They are shown and described in Scheme 3.3. The

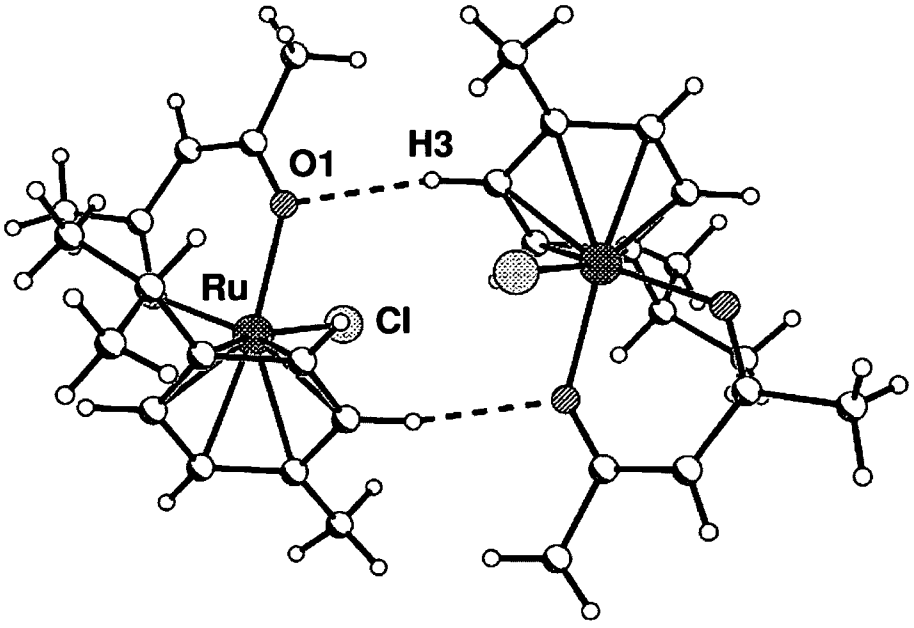

Figure 3.3: Dimer formation in the X-ray crystal structure of [(η^6-*p*-cym)Ru(acac)Cl] (**3.5**) by strong H-bonding between acac oxygen O1 and arene ring H3. The coordinated chloride (Cl1) is involved in H-bonding to H6 of the arene ring of another molecule thus linking the dimers into a 3D array.

Table 3.2: H-bonding in the X-ray crystal structure of [(η^6-*p*-cym)Ru(acac)Cl] (**3.5**). For atom labelling scheme see Figure 3.2.

D	H	A	D-H (Å)	H···A (Å)	D···A (Å)	Angle D-H-A (°)
C(2)	H(2)	Cl(1)[a]	0.98	2.79	3.689(2)	153
C(3)	H(3)	O(1)[a]	0.98	2.29	3.234(3)	161
C(6)	H(6)	Cl(1)[b]	0.98	2.65	3.567(2)	155
C(161)	H(161)	Cl(1)[c]	0.98	2.76	3.679(3)	156
C(41)	H(413)	Cl(1)[d]	0.98	2.72	3.380(3)	125

Equivalent positions: [a] 2-x, -y, 2-z. [b] 3/2-x, 1/2+y, 3/2-z. [c] 1-x, -y, 2-z. [d] intramolecular.

aqua adducts [(η^6-*p*-cym)Ru(acac)H_2O]NO_3 (**3.14a**) and [(η^6-*p*-cym)Ru(Ph_2acac)H_2O]NO_3 (**3.21a**) were synthesised by abstraction of chloride with $AgNO_3$ from the respective chloro-complexes, in water for **3.5** and in acetone/water for **3.6**. Both aqua adducts also were useful precursors in ligand exchange reactions.

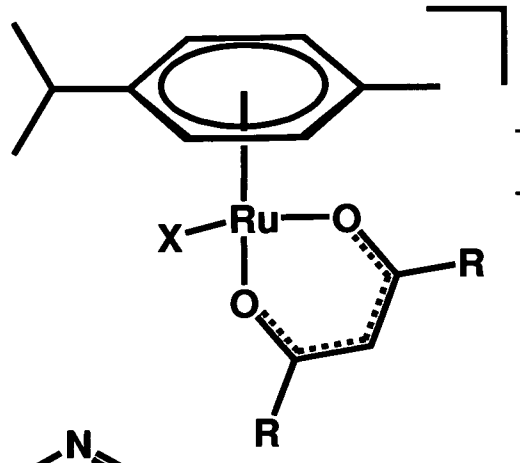

Complex	Chelate	X	A
3.14a	acac	H_2O	NO_3^-
3.15	acac	CH_3CN	BF_4^-
3.16	acac	dcp	PF_6^-
3.17	acac	dfp	PF_6^-
3.18	acac	py	PF_6^-
3.19	acac	pcp	PF_6^-
3.20	acac	9EtA	PF_6^-
3.21a	Ph_2acac	H_2O	NO_3^-
3.22	Ph_2acac	9EtG	$CF_3SO_3^-$

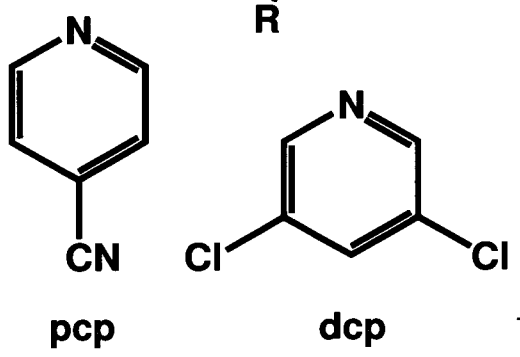

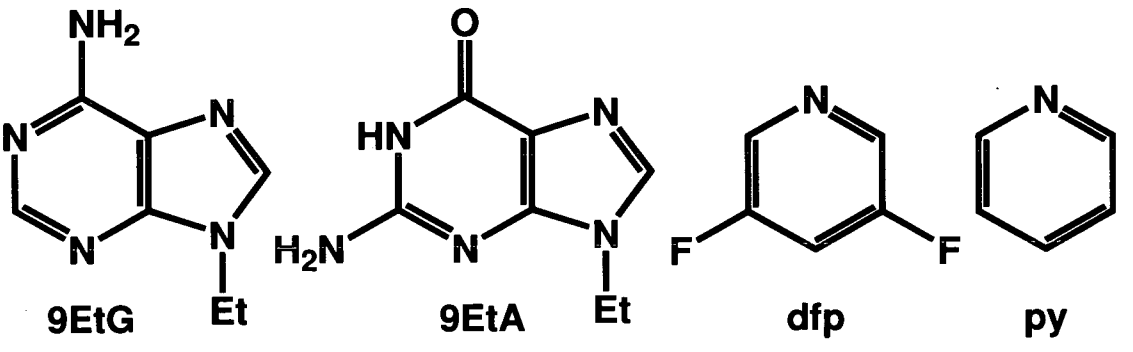

Scheme 3.3: The structures of positively-charged Ru^{II} *p*-cymene *β*-diketonato complexes, including numbering and ligand definitions, where A = counter anion.

$[(\eta^6\text{-}p\text{-cym})Ru(acac)CH_3CN]BF_4$ (**3.15**) was synthesised by chloride abstraction from **3.5** with $AgBF_4$ directly in acetonitrile.

The complexes $[(\eta^6\text{-}p\text{-cym})Ru(acac)dcp]PF_6$ (**3.16**), $[(\eta^6\text{-}p\text{-cym})Ru(acac)dfp]PF_6$ (**3.17**), $[(\eta^6\text{-}p\text{-cym})Ru(acac)py]PF_6$ (**3.18**) and $[(\eta^6\text{-}p\text{-cym})Ru(acac)pcp]PF_6$ (**3.19**), where dcp = 3,5-dichloropyridine, dfp = 3,5-difluoropyridine, py = pyridine, pcp = 4-cyanopyridine, were synthesised by reaction

of the appropriate pyridine-type ligand with **3.14a** and counter anion metathesis. All complexes were characterised using ^{1}H NMR spectroscopy.

Complexes of Ru^{II} *p*-cymene *β*-diketonates with DNA base derivatives were produced under mild conditions. Reaction of 9-ethyladenine (9EtA) with the chloride-containing complex **3.5** in water, followed by counter anion metathesis, resulted in a mixture of complexes, including [(η^6-*p*-cym)Ru(acac)9EtA-*N7*]PF_6 (**3.20**). The aqua adduct **3.21a** was reacted with 9-ethylguanine (9EtG) followed by addition of $NaCF_3SO_3$ in MeOH/water to yield [(η^6-*p*-cym)Ru(Ph_2acac)9EtG-*N7*]CF_3SO_3 (**3.22**).

3.3.1.2 Ru^{II} p-cymene hydroxy-ketonato complexes

The neutral, chloride-containing complexes [(η^6-*p*-cym)Ru(trop)Cl] (**3.23**) and [(η^6-*p*-cym)Ru(ma)Cl] (**3.24**), where trop = tropolonate, ma = maltolate, were

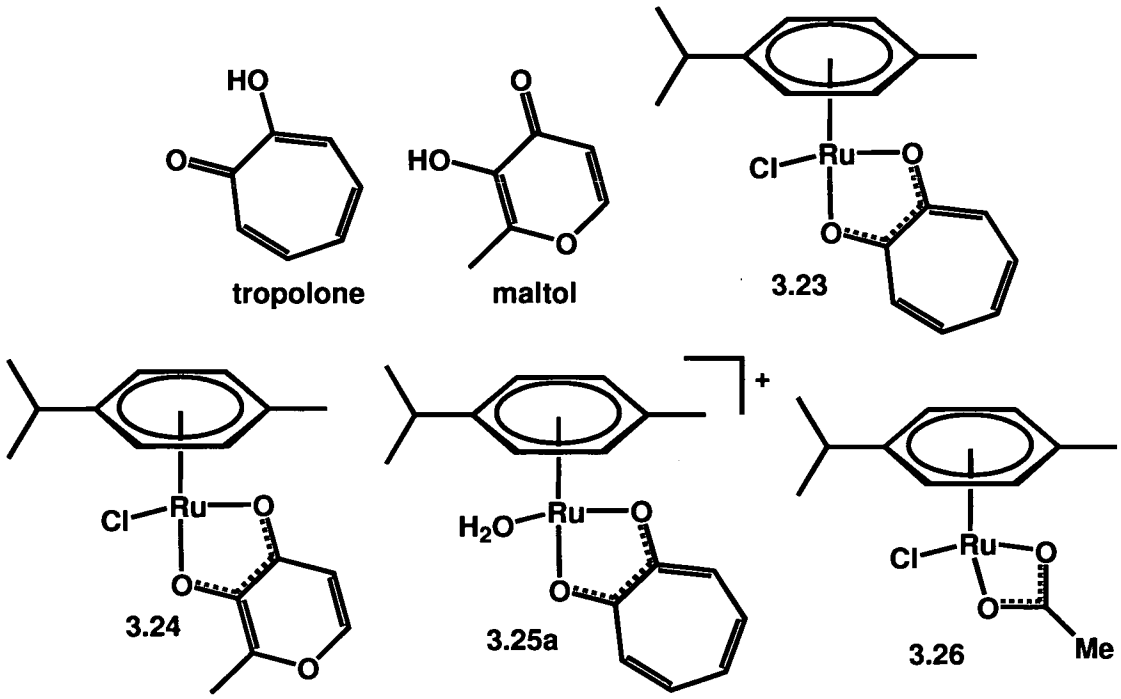

Scheme 3.4: The structures of tropolone, maltol and [(η^6-*p*-cym)Ru(trop)Cl] (**3.23**), [(η^6-*p*-cym)Ru(ma)Cl] (**3.24**), [(η^6-*p*-cym)Ru(trop)H_2O]NO_3 (**3.25a**) and [(η^6-*p*-cym)Ru(AcO)Cl] (**3.26**).

synthesised similarly to the β-diketonato complexes in good yields and purity. The tropolonate and maltolate ligands were synthesised by reaction of the neutral ligands tropolone and maltol, respectively, with sodium methoxide (Scheme 3.4). The syntheses were aided by previously reported routes for the synthesis of [(η^6-*p*-cym)Ru(acac)Cl] (**3.5**) [15] and [(η^6-mes)Ru(ma)Cl], where mes = 1,3,5-trimethylbenzene [19].

The tropolonate ^{1}H NMR peaks for complexes **3.23** and **3.25a** as well as for the free ligand (tropH) are shown in Figure 3.4 and listed in Table 3.3. The splitting patterns are complex, however, using the Hc signal as a marker it is clear that the tropolonate signals in both **3.23** and **3.25a** are shifted upfield compared to free tropolone, by *ca.* 0.3 and 0.2 ppm, respectively. This is in contrast to reports that in

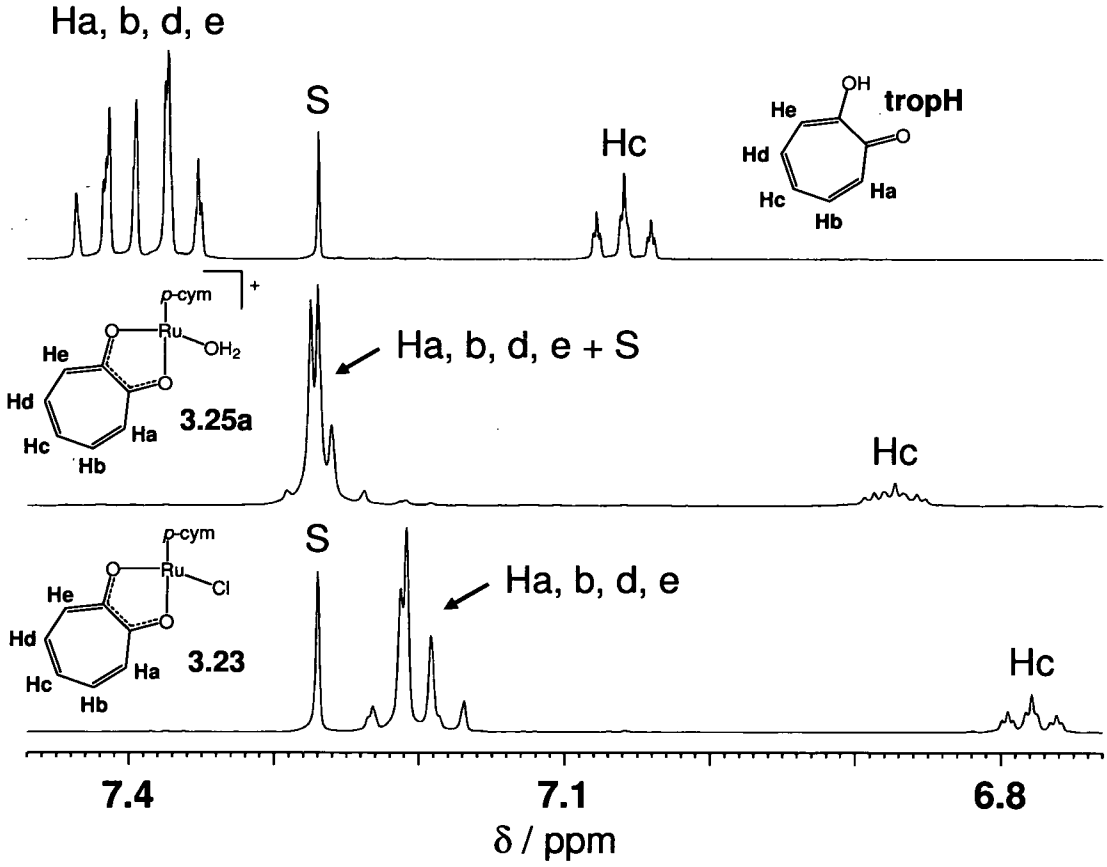

Figure 3.4: Low-field region of ^{1}H NMR spectra at 298 K of free tropolone and tropolonate in complexes [(η^6-*p*-cym)Ru(trop)H_2O]NO_3 (**3.25a**) and [(η^6-*p*-cym)Ru(trop)Cl] (**3.23**), respectively, in $CDCl_3$. S corresponds to $CHCl_3$.

Table 3.3: The ^{1}H NMR chemical shifts (ppm) of free tropolone and bound tropolonate in [(η^6-*p*-cym)Ru(trop)Cl] (**3.23**) and [(η^6-*p*-cym)Ru(trop)H_2O]NO_3 (**3.25a**) in $CDCl_3$ at 298 K.

Compound	δ(^{1}H) Ha, b, d, e	δ(^{1}H) Hc
Tropolone	7.44 – 7.35	7.06
[(η^6-*p*-cym)Ru(trop)H_2O]NO_3 (**3.25a**)	7.29 – 7.24	6.87
[(η^6-*p*-cym)Ru(trop)Cl] (**3.23**)	7.23 – 7.17	6.78

$CDCl_3$ the ^{1}H NMR peaks for coordinated tropolonate in some metal complexes tend to shift downfield compared to free tropolone [20, 21, 22].

X-ray diffraction quality crystals of **3.24** were grown in an NMR tube from water containing the complex and an excess of NaCl over a period of 2 d at ambient temperature. The crystal data are shown in Table A.3.2 and the structure in Figure 3.5. Selected bond lengths and angles are shown in Table 3.4.

The complex crystallised as [(η^6-*p*-cym)Ru(ma)Cl].$2H_2O$ as a racemic mixture and shows the five-membered chelate ring formed between the central ruthenium and the maltolate ligand. The Ru – Cl bond length is 2.4329(5) Å and the Ru – O bond lengths 2.0901(13) Å and 2.0901(13) Å, respectively. Those distances

Table 3.4: Selected bond lengths (Å) and angles (°) for [(η^6-*p*-cym)Ru(ma)Cl].$2H_2O$ (**3.24**).$2H_2O$.

Bond	Length	Bond	Length/angle
Ru-Cl	2.4329(5)	Ru-C51	2.1445(18)
Ru-O12	2.1035(13)	Ru-C61	2.1717(19)
Ru-O22	2.0901(13)	Ru-centroid[a]	1.640
Ru-C11	2.1887(19)	O12-Ru-O22	78.79(5)
Ru-C21	2.1543(19)	O12-Ru-Cl	83.42(4)
Ru-C31	2.1593(19)	O22-Ru-Cl	85.89(4)
Ru-C41	2.1880(18)		

[a] = measured using Mercury 1.4.

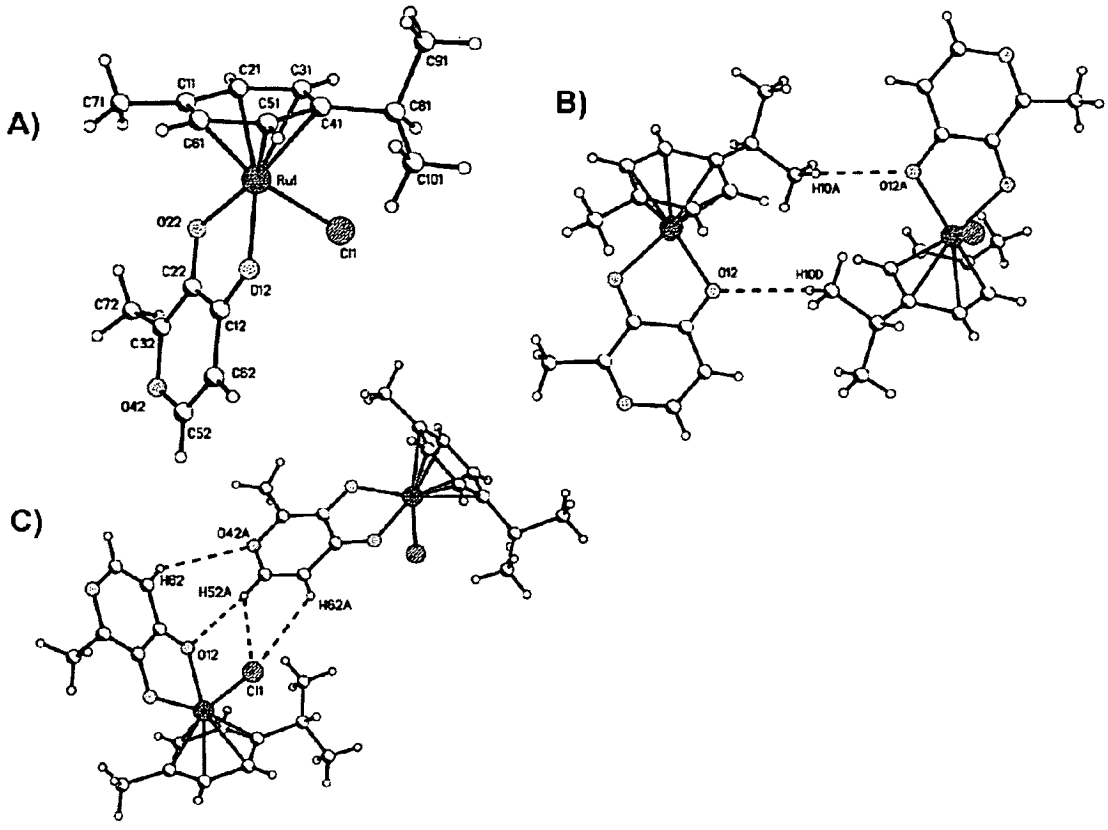

Figure 3.5: The X-ray crystal structure of [(η^6-*p*-cym)Ru(ma)Cl].2H_2O (**3.24**).2H_2O. A: Numbering scheme for [(η^6-*p*-cym)Ru(ma)Cl]. B: Formation of dimers *via* interactions between the ma oxygen O12 with isopropyl proton H10A. C: Interactions between chloride and maltolate.

are close to the range of values reported for related complexes, though marginally longer [19, 23, 24]. The Ru – centroid distance is 1.64 Å.

The water molecules form a chain, which is flanked by the same enantiomers of the ruthenium complex on either side (Figure 3.6). The H_2O(H4W) – Cl interaction distance is 2.52 Å (O2W···Cl 3.240(2) Å), that of H_2O(H1W) – Maltol(O22) is 2.09 Å (O1W···O22 2.805(2) Å) and for the water molecules the O1W···O2W separations are 2.771(3) Å and 2.852(3) Å respectively, which compares well with the values reported for similar interactions in the complex [(η^6-mes)Ru($NC_5H_4CO_2$ – *N,O*)Cl].3H_2O, where mes = 1,3,5-trimethylbenzene [25]. In addition, the maltolate oxygen O12 interacts with the *p*-cymene isopropyl proton

H10A (2.67 Å, O12···C101 3.449(3) Å), linking opposite enantiomers together (Figure 3.5 b). Furthermore a grid is formed by interactions between the same enantiomers of the maltolate chelating oxygen atom O12 and the H52 proton of the maltolate backbone (2.37 Å, O12···C52 3.288(2) Å). The second proton of the backbone (H62) has a weak interaction with a neighbouring chloride at a distance of 2.99 Å (C62···Cl 3.661(2) Å) (Figure 3.5 c).

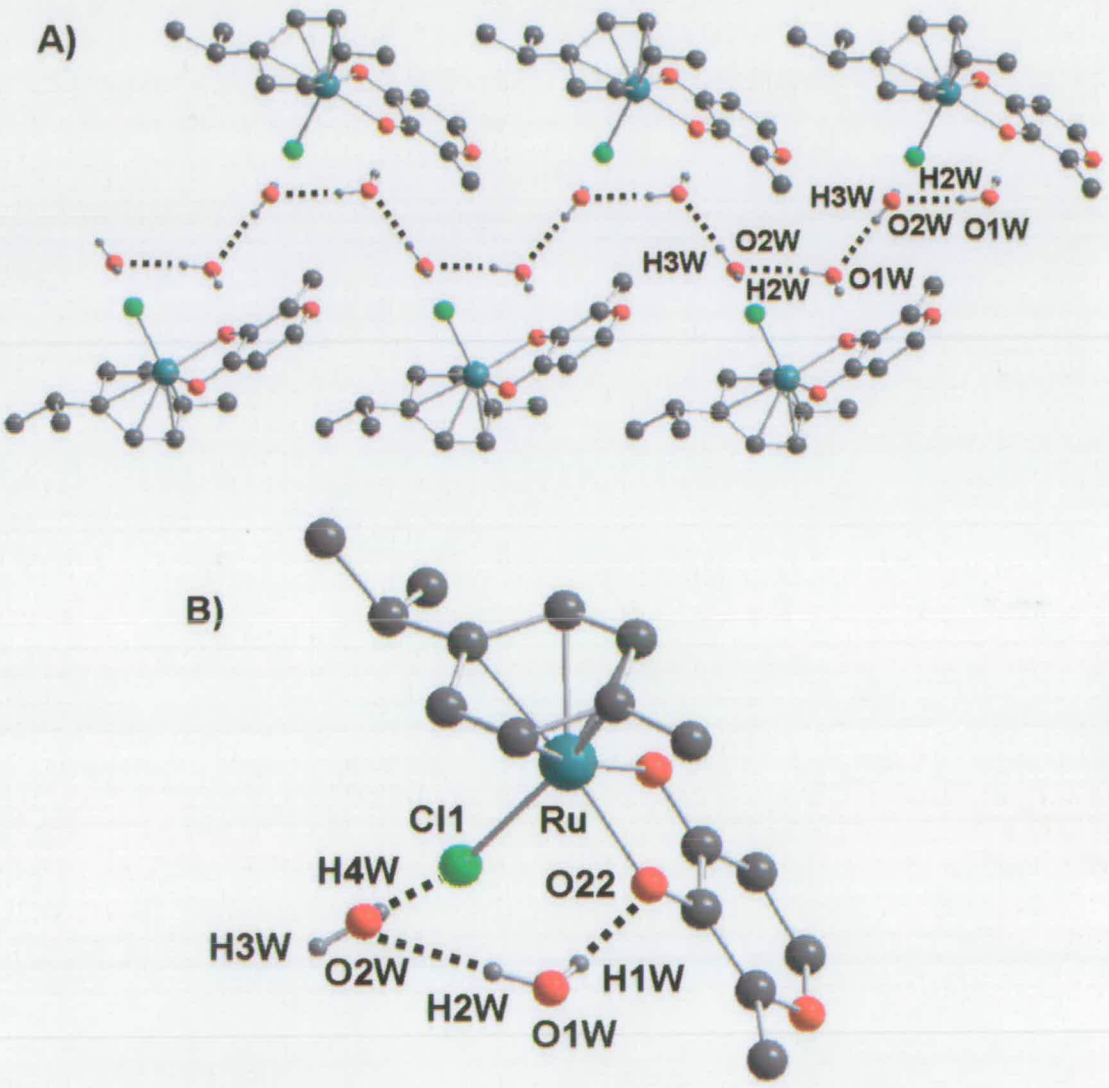

Figure 3.6: The X-ray crystal structure of [(η^6-*p*-cym)Ru(ma)Cl].2H_2O (**3.24**).2H_2O. A: Formation of chains of water molecules, flanked by ruthenium complexes on either side. B: Ring of H-bonds formed between the water molecules and **3.24**.

3.3.1.3 Ru^{II} p-cymene acetato complex

[(η^6-*p*-cym)Ru(AcO)Cl] (**3.26**) (Scheme 3.4), where AcO = acetate, was synthesised by a procedure similar to that used for related *β*-diketonato complexes in poor yield. Its X-ray crystal structure was determined using crystals grown from acetone/hexane at 253 K (Figure 3.7, Tables 3.5 and A.3.2). There are few reported X-ray structures of metal arene complexes containing bidentate carboxylate ligands. The first reported example appears to be that of [(η^6-*p*-cym)Ru(O_2CNEt_2)$_2$] [26] and

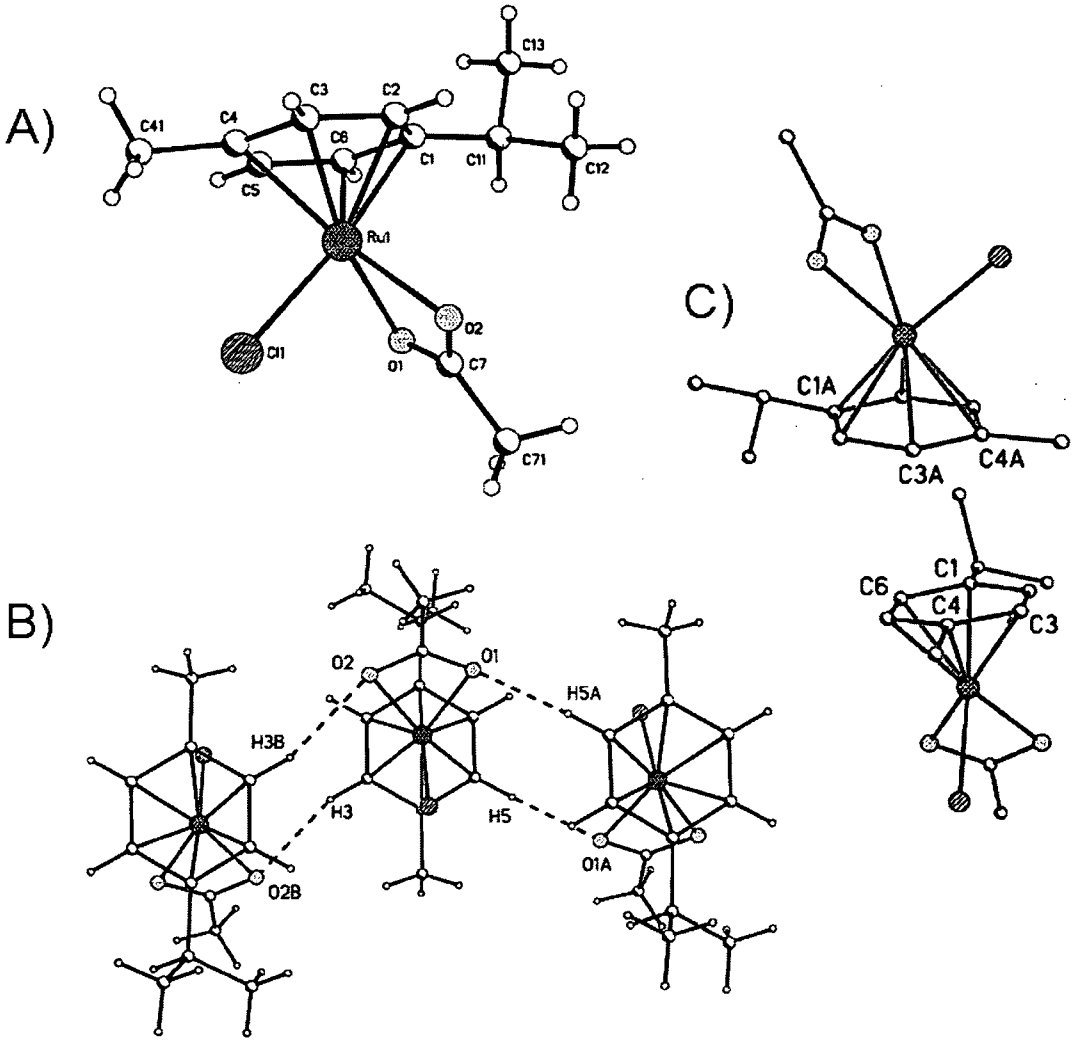

Figure 3.7: X-ray crystal structure of [(η^6-*p*-cym)Ru(AcO)Cl] (**3.26**). A: Numbering scheme. B: Chain formation *via* interactions between the AcO oxygens O1 and O2 with arene protons H5 and H3, respectively. C: Formation of $\pi - \pi$ stacking between neighbouring *p*-cymene rings. The hydrogen atoms have been omitted for clarity.

Table 3.5: Selected bond lengths (Å) and angles (°) for [(η^6-*p*-cym)Ru(AcO)Cl] (**3.26**).

Bond	Length	Bond	Length/angle
Ru-Cl	2.3848(5)	Ru-C5	2.168(2)
Ru-O1	2.1469(14)	Ru-C6	2.128(2)
Ru-O2	2.1659(15)	Ru-centroid[a]	1.638
Ru-C1	2.1741(19)	O1-Ru-O2	60.22(5)
Ru-C2	2.137(2)	O1-Ru-Cl	85.73(4)
Ru-C3	2.167(2)	O2-Ru-Cl	84.81(4)
Ru-C4	2.203(2)		

[a] = measured using Mercury 1.4.

during the course of this study a structure for [(η^6-*p*-cym)Ru(AcO)Cl] (**3.26**) was published [27].

The bond lengths and angles for **3.26** are almost identical to the published values [27], with the two structures related by symmetry. The H-atoms of the acetate methyl group (based on C71) show disorder over two components related by a 60° rotation about C71-C7. The Ru – Cl bond length is 2.3848(5) Å and the Ru – O bond lengths are 2.1469(14) Å and 2.1659(15) Å, respectively. The Ru – centroid distance is 1.64 Å.

As in the case of complexes [(η^6-*p*-cym)Ru(acac)Cl] (**3.5**) and [(η^6-*p*-cym)Ru(trop)H_2O]NO_3 (**3.25a**) (*vide infra*), there are interactions between the arene protons and the oxygen atoms of the chelated ligand. The molecules in **3.26** are arranged in chains, held together by H-bond interactions (d = 2.29 Å, O1···C5 3.198(3) Å and 2.42 Å, O2···C3 3.644(3) Å) involving both the carboxylate oxygen atoms O1 and O2 and arene protons H5 and H3, respectively (Figure 3.7B). There is also evidence for intermolecular $\pi - \pi$ interactions between *p*-cymene ligands. The arene rings are slightly tilted with respect to each other. The shortest distance is between carbons C3 and C4 in neighbouring arene ligands (d = 3.443(3) Å), and the

longest for C6 which interacts with the neighbouring C6 and C1 carbons at distances of 3.933(3) Å and 4.049(3) Å, respectively (Figure 3.7C).

3.3.1.4 Ru^{II} p-cymene complex bridged by a O,O-chelating ligand

Using 1,4-dihydroxyanthraquinone dianion as a chelating ligand, the bridged bi-functional complex $[(\eta^6\text{-}p\text{-cym})_2Ru_2(C_6H_4(CO)_2C_6H_2O_2 - (O,O)_2)Cl_2]$ (**3.28**) was synthesised. The symmetry of the proton signals of the chelating ligand in the ^1H NMR spectrum confirmed binding of two ruthenium atoms.

3.3.2 Discussion

3.3.2.1 X-ray crystal structures

The structures of the solved Ru^{II} *p*-cymene *β*-diketonato complexes do not differ greatly from each other, despite the different nature of the substituents on the chelate rings. Compared to the analogous ethylenediamine complex $[(\eta^6\text{-}p\text{-cym})Ru(en)Cl]PF_6$ [4], the Ru – N bond lengths are *ca.* 0.05 Å longer than the Ru – O bond lengths of compounds $[(\eta^6\text{-}p\text{-cym})Ru(acac)Cl]$ (**3.5**), $[(\eta^6\text{-}p\text{-cym})Ru(Ph_2acac)Cl]$ (**3.6**), $[(\eta^6\text{-}p\text{-cym})Ru(^tBu_2acac)Cl]$ (**3.7**) and $[(\eta^6\text{-}p\text{-cym})Ru((CF_3)_2acac)Cl]$ (**3.8**). The respective Ru – Cl bond lengths are within the range displayed by other compounds of the type $[(\eta^6\text{-arene})Ru(en)Cl]^+$ (2.41 – 2.44 Å) [4, 8]. The Ru – O bond lengths in the *β*-diketonato complexes are comparable with the exception of **3.8**, where that distance is significantly longer (>3σ, with σ defined as $(\sigma_1^2 + \sigma_2^2)^{1/2}$, where σ_1 and σ_2 are the standard deviations of the compared bond lengths). It results in a higher distortion of the ligand and also indicates that the electron-withdrawing ability of the six fluorine atoms leads to weaker binding of the ligand to the ruthenium centre compared to the other ligands, thus making it potentially more labile. Due to the electron withdrawing effect of the ligand the

contribution of the chloride to the electron density on the metal centre is increased, reflected by a significantly shorter Ru – Cl bond length (>3σ).

Compared to the Ru – Cl and Ru – O bond lengths for the *β*-diketonates, the corresponding values for the maltolato complex are longer on average, even though potentially bond elongating effects exerted by interactions with water, which cannot be quantified, could have an influence in that.

For the acetato complex, the bond lengths are significantly different, with a shorter Ru – Cl distance and longer Ru – O bonds compared to the compounds containing five- and six-membered chelate rings. The comparatively long Ru – O bonds in particular indicate relatively weak binding of the acetate chelate to the metal centre.

An interesting feature of some of the above crystal structures is their ability to form intermolecular CH···O bonds. Such interactions have received increasing attention during recent years due to their potentially important role in biological systems [28]. The possibility of formation of H-bonds involving these ruthenium(II) complexes could be relevant to interactions with biomolecules, *e.g.* proteins.

In summary, it appears that the side groups of *β*-diketonate ligands have little influence on the structural appearance of complexes of the type [(η^6-*p*-cym)Ru(*β*-diketonate)Cl]. Differences in bond lengths and angles are generally subtle, with the exception of [(η^6-*p*-cym)Ru($(CF_3)_2$acac)Cl] (**3.8**).

Comparing the influence of the chelate ring size on the bond lengths, neglecting any contribution the nature of substituents on the respective ligands might have on them, the following observations can be made. A decrease in the chelate ring size is reflected by a decrease in the O – Ru – O bite angle. The Ru – O bond lengths appear to increase with decreasing chelate ring size, whereas the Ru – centroid bond lengths decrease. No apparent trend for the Ru – Cl bond lengths is evident.

3.4 Cancer Cell Growth Inhibition

3.4.1 Results

The screening for cancer cell cytotoxicity of compounds **3.5 – 8**, **3.11 – 13**, **3.15**, **3.28** was carried out by Rhona Aird, Western General Hospital (Edinburgh, UK), using the procedure described by Morris *et al.* [4]. A2780 cells (human ovarian cancer cells) were plated on day zero, and Ru^{II} arene complex was added on day 3. The complex was removed on day 4 (*i.e.* 24 h cell exposure), and after growth in fresh medium in the absence of the drug, the cells were counted on day 7 (*i.e.* 72 h incubation). Because it is known that metal coordination complexes can undergo ligand substitution reactions with components of the media in which they are dissolved, freshly-made stock solutions of each compound were used. The

Table 3.6: Table of the IC_{50} values (concentration which causes 50% inhibition of cell growth) of complexes tested against A2780 (human ovarian) and A549 (human lung) cancer cell lines. Cisplatin is used as a standard. RM121 is the ethylenediamine-containing complex $[(\eta^6\text{-}p\text{-cym})Ru(en)Cl]PF_6$ [4].

Complex	A2780 IC_{50} (μM)	Complex	A2780 IC_{50} (μM)	A549 IC_{50} (μM)
cisplatin	0.6	cisplatin	3.3	5.8
3.5	19	**3.9**	39.1	>100
3.6	11	**3.10**	>100	86.4
3.7	14	**3.16**	57.7	>100
3.8	>100	**3.17**	48.4	>100
3.11	21	**3.18**	63.0	>100
3.12	>50	**3.19**	59.1	>100
3.13	>50			
3.15	22			
3.28	53			
RM 121 [4]	9			

complexes were stored in the dark at 277 K as a precaution against photochemical decomposition. The screening for cancer cell cytotoxicity of compounds **3.9 – 10**, **3.16 – 19** was carried out by Emily Jones, Oncosense Ltd., following the same procedure, with a different incubation period of 96 h. The IC_{50} values (the concentration which causes 50% inhibition of cell growth) are listed in Table 3.6. Cytotoxicity towards the A2780 cell line is observed for some complexes containing acac-derivatives. The activity of [(η^6-*p*-cym)Ru(Ph_2acac)Cl] (**3.6**) is comparable to its ethylenediamine-containing analogue. The activity towards the A549 cell line is poor for all complexes.

3.4.2 Discussion

Platinum complexes are the most widely used anticancer drugs in clinics, and cisplatin is used as a standard in the cytotoxicity tests performed for complexes investigated in this study. A number of Ru^{II} arene complexes containing en as the chelating ligand produced in the Sadler group have shown promising activity against the human ovarian cancer cell line A2780, some as potent as carboplatin and cisplatin [6].

It was therefore of great interest to investigate how changing nitrogen-based chelating ligands to oxygen-based ligands would affect the cytotoxic potency of those complexes. A direct comparison of activity, however, is potentially complex, with differences resulting from change of ligand ranging from charge, chelate ring size, structural properties to charge distribution and chemical properties including stability. Possibly different recognition and/or transport mechanisms during testing *in vitro* could also be important. The resulting effects of such differences could be difficult to elucidate.

The neutral complexes in particular showed limited to poor water solubility. Ideally, anticancer agents should have good water solubility in order for them to be

administered *in vivo*. $[(\eta^6\text{-arene})Ru(en)Cl]PF_6$ complexes are positively charged, making them generally fairly soluble in water. The increased hydrophobic character of the neutral Ru^{II} arene complexes, however, could also be an advantage since uptake through the lipophilic cell membrane might be faster and more favourable than for the en complexes.

Interestingly, the cytotoxic activity of some of the *p*-cymene *β*-diketonato complexes approached that of the analogous ethylenediamine containing complex. Complexes which were inactive include those acac-type ligands with CF_3 substituents and those containing five-membered chelate rings. The reason for the inactivity for the latter is not obvious, whereas in the case of the former complex a potential lack of stability might be the reason. As seen in the crystal structure of $[(\eta^6\text{-}p\text{-cym})Ru((CF_3)_2acac)Cl]$ (**3.8**), the chelate ligand appeared to be more weakly bound than the other ligands, possibly as a consequence of the electron withdrawing CF_3 groups. Thus breakage of the relatively weak Ru – O bonds might lead to ring opening of the chelate in solution, which could be a deactivation pathway for these complexes (*e.g.* formation of a hydroxo-bridged dimer (*vide infra*)). Surprisingly, the only complex with an IC_{50} value < 100 μM against the human lung cancer cell line A549 was the CF_3-containing complex $[(\eta^6\text{-}p\text{-cym})Ru(PhacacCF_3)Cl]$ (**3.10**).

For $[(\eta^6\text{-arene})Ru(en)Cl]PF_6$ complexes an increase in the hydrophobicity of the arene tends to increase it cytotoxicity in the order of dihydroanthracene (DHA) > biphenyl > indan > *p*-cymene > benzene [6]. Intriguingly, with acac as the ligand, a different order of *p*-cymene > biphenyl > DHA [5] >> benzene, indan was found.

There does not appear to be a clear structure-activity relationship for the *O,O*-chelated complexes examined here. The apparent strong dependence of activity on the nature of the arene is remarkable. While electronic effects from change in arene could be expected to be marginal, steric effects could be more important. Both *p*-cymene (pendant isopropyl group) and biphenyl (pendant benzene ring) contain

rotating components, which can exert steric hindrance below the plane of the arene towards the reactive site on the ruthenium centre (Figure 3.8). Benzene is unsubstituted and the arenes DHA and indan contain flexible substituents, not necessarily having a strong steric influence below the plane of the arene. Also, sterically demanding substituents on the β-diketonate ligands increase the activity of the tested complexes. Both the five-membered chelate rings in the inactive compounds [(η^6-*p*-cym)Ru(trop)Cl] (**3.23**) and [(η^6-*p*-cym)Ru(ma)Cl] (**3.24**) are planar. The role of bulky substituents, however, could be subtle, since crystallographic data suggest that potential steric hinderances would not occur in close proximity to the metal centre. Possibly, sterically-demanding substituents could slow down deactivation especially by bulky bioligands, *e.g.* proteins, by limiting their access to the metal centre.

The activity of the positively-charged complexes with respect to their neutral, chloride containing analogue is noteworthy. The activities for complexes [(η^6-*p*-

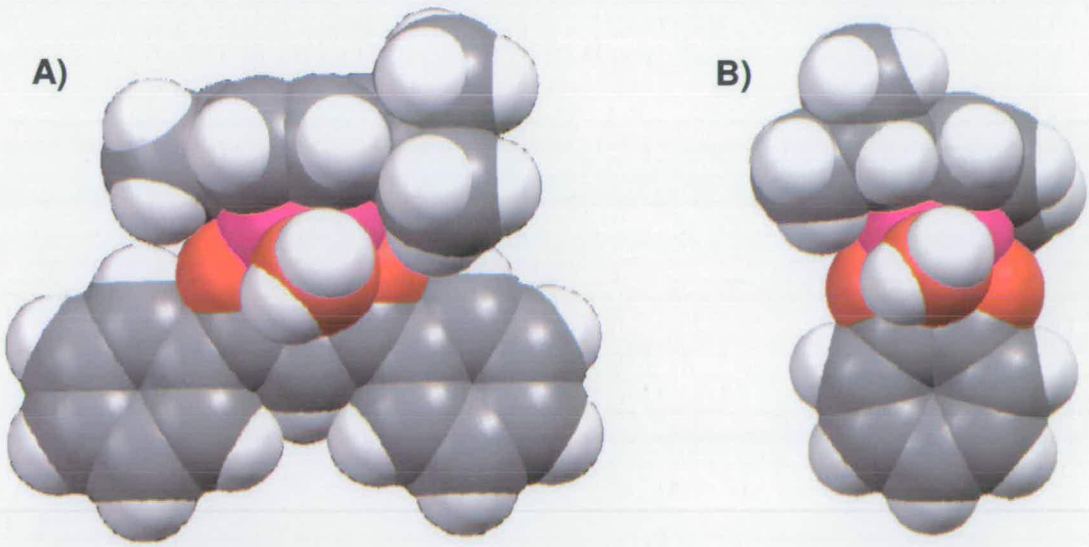

Figure 3.8: Spacefilling models of the X-ray crystal structures of cations in [(η^6-*p*-cym)Ru(Ph_2acac)H_2O]$^+$ (**3.21b**) (A) and [(η^6-*p*-cym)Ru(trop)H_2O]$^+$ (**3.25b**) (B), showing possible steric hindrance at the reactive metal binding site exerted by the pendent isopropyl group.

cym)Ru(acac)Cl] (**3.5**) and [(η^6-*p*-cym)Ru(acac)CH_3CN]BF_4 (**3.15**) are almost identical and under different testing conditions the complexes containing pyridine derivatives (**3.16 – 19**) have comparable values. This points towards a common mode of activation for these compounds, one which could be independent of the leaving group (*vide infra*).

3.5 Solution Chemistry

3.5.1 Results

3.5.1.1 Stability in water

The chloride-containing complexes [(η^6-*p*-cym)Ru(acac)Cl] (**3.5**), [(η^6-*p*-cym)Ru(trop)Cl] (**3.23**), [(η^6-*p*-cym)Ru(ma)Cl] (**3.24**) and [(η^6-*p*-cym)Ru(AcO)Cl] (**3.26**) were all dissolved in D_2O (8 mM Ru) and their ^1H NMR spectra recorded at 298 K and pH* values of 6.95, 7.11, 6.93 and 4.14, respectively, where pH* = pH meter reading of the D_2O solution. The spectra of complexes with 5- and 6-membered chelate rings gave rise to single sets of peaks, whereas that of **3.26** appeared more complex.

The ^1H NMR spectrum of **3.26** was recorded 10 min after dissolution in D_2O and again after 19 h. During this time the pH* value changed from 4.14 to 4.28 at 298 K, and the intensity of the *p*-cymene arene ring proton signals changed. Analysis of the doublets for the p-cymene ring protons suggested that six species were present in solution, one, with peaks at 5.38 and 5.17 ppm, clearly dominating (Figure 3.9). After addition of NaOH, this latter species was the only one present in solution, and was shown by mass spectrometry (MS-ES) to be the hydroxo-bridged dimer [((η^6-*p*-cym)Ru)$_2$(μ-OH)$_3$]$^+$ (**3.27**). This dimer has been reported in the literature, but has not been characterised in water [29]. The chemical shifts of the peaks for the dimer did not change under basic conditions. A singlet, which increased in intensity upon addition of free acetate, shifted from around δ 2.50 (acidic pH) to δ 1.90 (basic pH).

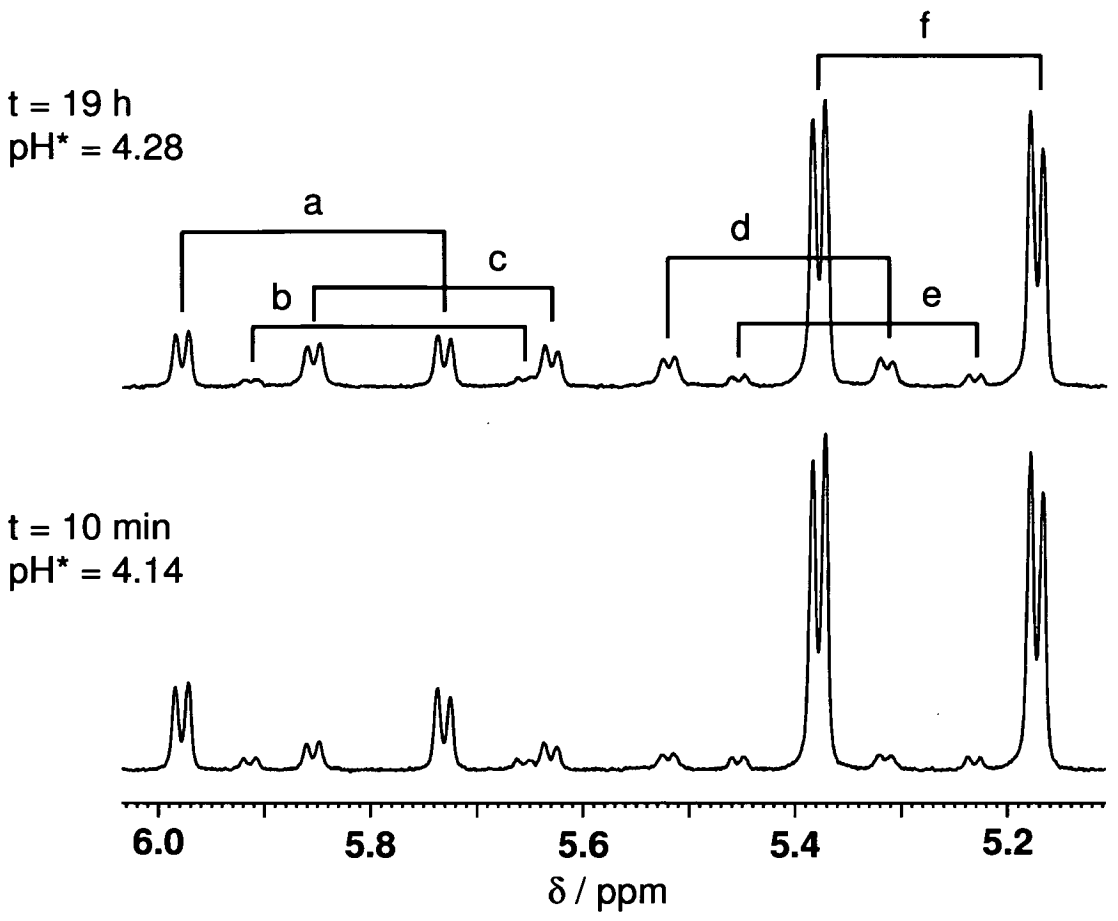

Figure 3.9: The *p*-cymene ring proton region of the ^{1}H NMR spectrum of [(η^6-*p*-cym)Ru(AcO)Cl] (**3.26**) in D_2O at 298 K after 10 min at pH* = 4.14 and after 19 h at pH* = 4.28, respectively. The labels correspond to *p*-cymene ligands in different species present in solution, which have not been further characterized, except for species f, which is [((η^6-*p*-cym)Ru)$_2$(μ-OD)$_3$]$^+$ (**3.27**).

3.5.1.2 Hydrolysis studies

The hydrolysis of [(η^6-*p*-cym)Ru(acac)Cl] (**3.5**) was investigated. UV-vis experiments and conductivity measurements indicated that the hydrolysis of **3.5** is too fast to follow, the latter suggesting the existence of ionic species in solution [30].

A chloride titration was followed by ^{1}H NMR with up to 1.75 M of added chloride. It was found that a change in [Cl^-] resulted in a shift of the peaks for **3.5**. In

a separate experiment, the chemical shifts of complexes **3.5** and [(η^6-*p*-cym)Ru(acac)H_2O]NO_3 (**3.14a**) in water were found to be very similar.

The analytically pure compound [(η^6-*p*-cym)Ru(acac)dcp]PF_6 (**3.16**), where dcp = 3,5-dichloropyridine, was dissolved in D_2O (*ca.* 350 μM, pH* = 7.66, 298 K) and its ^1H NMR spectrum recorded 25 min after dissolution. Three *p*-cymene-containing species were noted at relative intensities of 1 : 3 : 0.2. When the spectrum was re-recorded after 48 h (pH* = 7.08) the intensities had changed to 1 : 3.4: 1.7. A separate solution recorded after 40 min in D_2O (*ca.* 175 μM, pH* = 8.31, 298 K) produced relative intensities of 1 : 5.5 : 0.9. The *p*-cymene ring proton and central acac peaks of one species were broad, whereas the other signals were sharp.

Figure 3.10 shows the spectrum of **3.24** in $CDCl_3$ and D_2O (pH* = 6.95 at

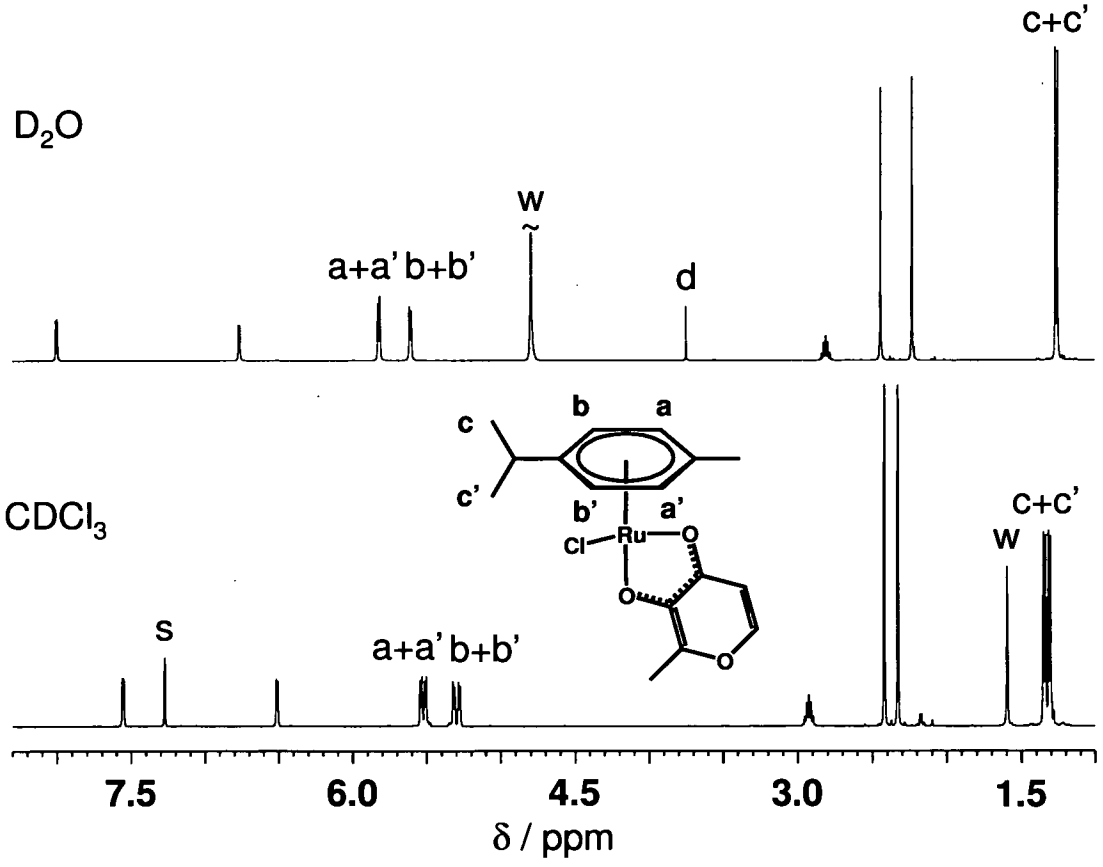

Figure 3.10: The ^1H NMR spectrum of [(η^6-*p*-cym)Ru(ma)Cl] (**3.24**) in $CDCl_3$ and D_2O (pH* 6.95) at 298 K, including partial peak assignment. Assignments: s = $CHCl_3$; w = residual water; d = 1,4-dioxane.

298 K). The spectrum in $CDCl_3$ gives rise to a pattern which suggests chirality at the metal centre, since the *p*-cymene ring protons (four separate peaks) and the isopropyl group (two separate peaks) appear magnetically inequivalent. In contrast, the spectrum in water shows resonances of magnetically equivalent *p*-cymene ring protons, assignable to a non-chiral species.

3.5.1.3 pK_a values of coordinated water

The pK_a values of coordinated water in the aqua adducts [(η^6-*p*-cym)Ru(acac)H_2O]NO_3 (**3.14a**), [(η^6-*p*-cym)Ru(trop)H_2O]NO_3 (**3.25a**) and [(η^6-*p*-cym)Ru(ma)H_2O]NO_3 (**3.29**) were determined by ^1H NMR pH titrations (Figure A.3.1). Figure 3.11 shows a plot of the dependence of the ^1H NMR chemical shift of the acac CH resonance of **3.14a** on pH. Those for the trop and ma systems are shown in Figures A.3.2 and A.3.3. The values were found to be 9.41 (**3.14a**), 9.12 (**3.25a**) and 9.23 (**3.29**) respectively (Table 3.7).

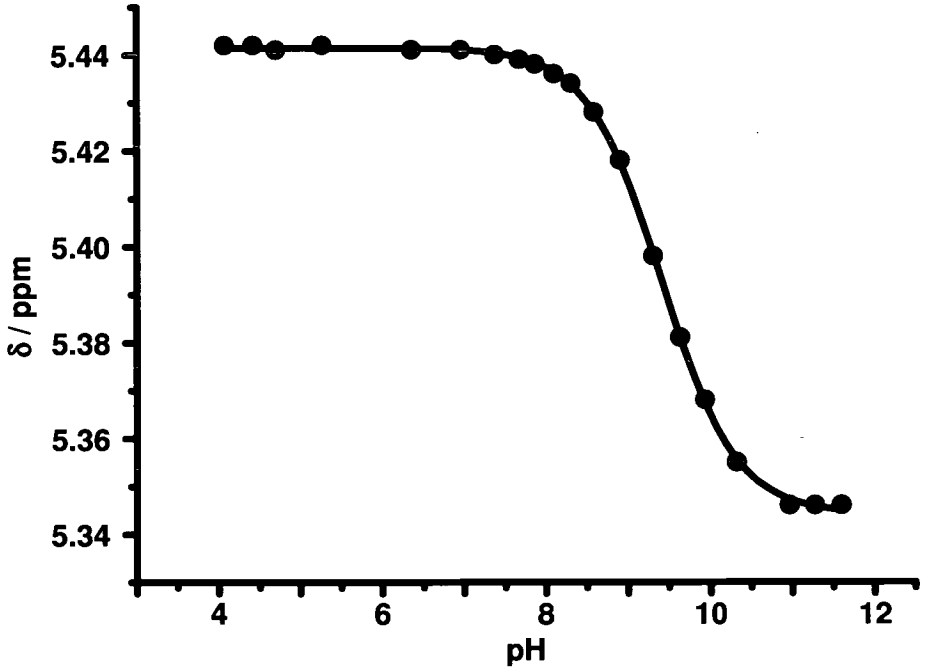

Figure 3.11: Dependence of the ^1H NMR chemical shift of the acac CH resonance of [(η^6-*p*-cym)Ru(acac)H_2O]NO_3 (**3.14a**, 10% D_2O/ 90% H_2O, 0.1 M $NaClO_4$, 298 K) on pH. The line is a computer fit giving pK_a (H_2O) = 9.41 ± 0.01.

Table 3.7: The pK_a values for coordinated water in complexes [(η^6-*p*-cym)Ru(acac)H_2O]NO_3 (**3.14a**), [(η^6-*p*-cym)Ru(trop)H_2O]NO_3 (**3.25a**) and [(η^6-*p*-cym)Ru(ma)H_2O]NO_3 (**3.29**).

Complex	Chelate	pK_a (H_2O)
3.14a	acac	9.41 ± 0.1
3.25a	trop	9.12 ± 0.1
3.29	ma	9.23 ± 0.1

Table 3.8: Selected bond lengths (Å) and angles (°) for [(η^6-*p*-cym)Ru(Ph_2acac)H_2O]CF_3SO_3 (**3.21b**) and [(η^6-*p*-cym)Ru(trop)H_2O]CF_3SO_3 (**3.25b**).

	3.21b X = 1	**3.21b X = 2**		**3.25b**
RuX-O11X	2.0575(17)	2.0627(16)	Ru-O1	2.0488(18)
RuX-O15X	2.0547(16)	2.0454(15)	Ru-O2	2.0641(19)
RuX-OX	2.1334(17)	2.1345(17)	Ru-O3	2.158(2)
RuX-C1X	2.189(2)	2.186(2)	Ru-C1A	2.180(3)
RuX-C2X	2.156(2)	2.162(2)	Ru-C2A	2.149(3)
RuX-C3X	2.176(2)	2.183(2)	Ru-C3A	2.161(3)
RuX-C4X	2.181(2)	2.178(2)	Ru-C4A	2.195(3)
RuX-C5X	2.152(2)	2.146(3)	Ru-C5A	2.165(3)
RuX-C6X	2.157(2)	2.141(3)	Ru-C6A	2.171(3)
RuX-centroidX[a]	1.640	1.645	Ru-centroid[a]	1.645
O11X-RuX-O15X	88.21(6)	87.49(6)	O1-Ru-O2	77.40(8)
O11X-RuX-OX	80.23(7)	81.56(7)	O1-Ru-O3	79.72(8)
O15X-RuX-OX	83.07(7)	80.83(6)	O2-Ru-O3	80.94(8)

[a] = measured using Mercury 1.4.

3.5.1.4 X-ray crystal structures

Counterion metathesis from NO_3^- to $CF_3SO_3^-$ of **3.21a** (solubilised in minimal ethanol) and **3.25a** in water to produce $[(\eta^6\text{-}p\text{-cym})Ru(Ph_2acac)H_2O]CF_3SO_3$ (**3.21b**) and $[(\eta^6\text{-}p\text{-cym})Ru(trop)H_2O]CF_3SO_3$ (**3.25b**), respectively, followed by extraction with diethyl ether and separation, enabled the growth of crystals suitable for X-ray diffraction by slow evaporation of diethyl ether at 253 K. Their X-ray crystal structures are shown in Figures 3.12 and 3.13, respectively, crystallographic data in Table A.3.3, bond lengths and angles are listed in Table 3.8.

The asymmetric unit of the structure of **3.21b** consists of two molecules (molecules 1 and 2) and each molecule forms a dimer with an equivalent molecule. These dimers show interactions between oxygens and hydrogens of bound water with solvent ether (d = 1.94 Å, O1···O36 2.703(3) Å and 1.98 Å, O2···O35 2.739(3) Å) and solvent water (d = 1.88 Å, O1···O7 2.657(3) Å and 1.94 Å, O2···O8 2.622(3) Å), the latter forming strong hydrogen bonds with the $CF_3SO_3^-$ counter anions (d = 2.02 – 2.12 Å) (Figure 3.12B). The Ru – $O(H_2O)$ distances are 2.1334(17) Å and 2.1345(17) Å for the two molecules, which is similar to values reported for other ruthenium arene aqua adducts containing bidentate chelating ligands such as 2,2-bis(2-oxazolinyl)propane [31] and deprotonated (*S*)-(*α*-methylbenzyl)salicylaldimine 32], as well as ethylenediamine-containing complexes (2.09 – 2.16 Å) [33].

The Ru – $O(Ph_2acac)$ distances vary between 2.0454(15) Å and 2.0627(16) Å, the Ru – C(arene) bond lengths are in the range of 2.141(3) Å to 2.189(2) Å and Ru – centroid distances are 1.64 Å and 1.65 Å. There is partial $\pi - \pi$ stacking between neighbouring *p*-cymene rings, where C32···C41 and C42···C31 are 3.420(3) Å and 3.458(3) Å, respectively. The shortest $H(H_2O)$ – $O(Ph_2acac)$ distances are 2.59 Å and 2.64 Å, respectively. The phenyl rings on each molecule are tilted at angles of 18.97° and 32.68°, respectively, from each other. The counter anion shows disorder, as does the isopropyl group of one molecule.

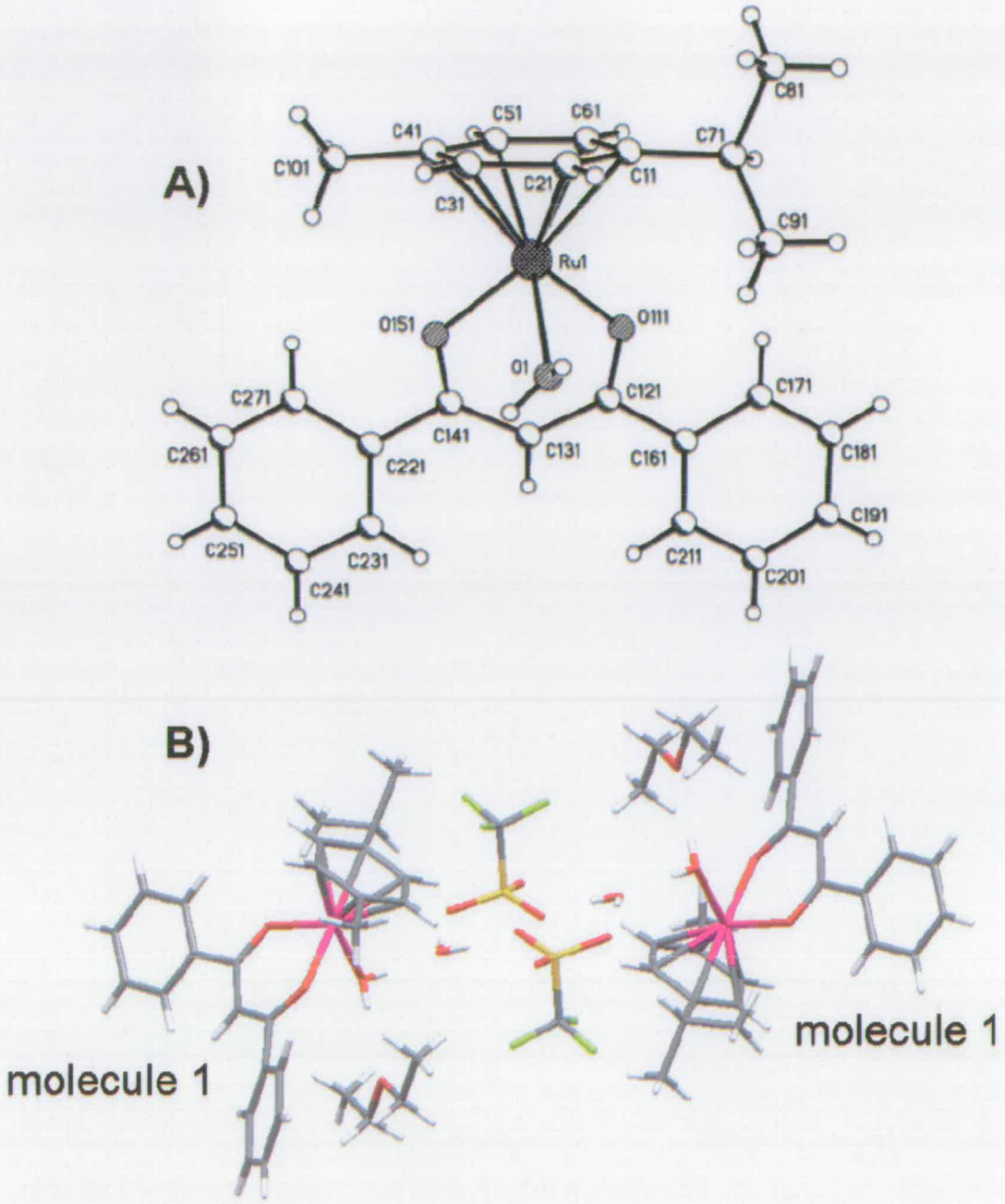

Figure 3.12: X-ray crystal structure of $[(\eta^6\text{-}p\text{-cym})Ru(Ph_2acac)H_2O]CF_3SO_3$ (**3.21b**). The asymmetric unit contains two molecules. A: Numbering scheme (shown for molecule 1, anion omitted). B: Formation of dimers (shown for molecule 1) of **3.21b**, showing interactions of bound water with solvent diethyl ether and water, the latter forming H-bonds with the counter anion.

For $[(\eta^6\text{-}p\text{-cym})Ru(trop)H_2O]CF_3SO_3$ (**3.25b**), the asymmetric unit contains one molecule of **3.25b** which forms dimers, held together by strong hydrogen bond interactions between the protons of coordinated water and oxygen atoms of the $CF_3SO_3^-$ counter anion (d = 1.89 – 1.99 Å), which is distorted (Figure 3.13B). The Ru – $O(H_2O)$ bond distance is 2.158(2) Å, the Ru – O(trop) bond lengths are 2.0488(18) Å and 2.0641(19) Å, and the Ru – C(arene) distances are in the range of 2.149(3) Å to 2.195(3) Å, with Ru – centroid 1.65 Å.

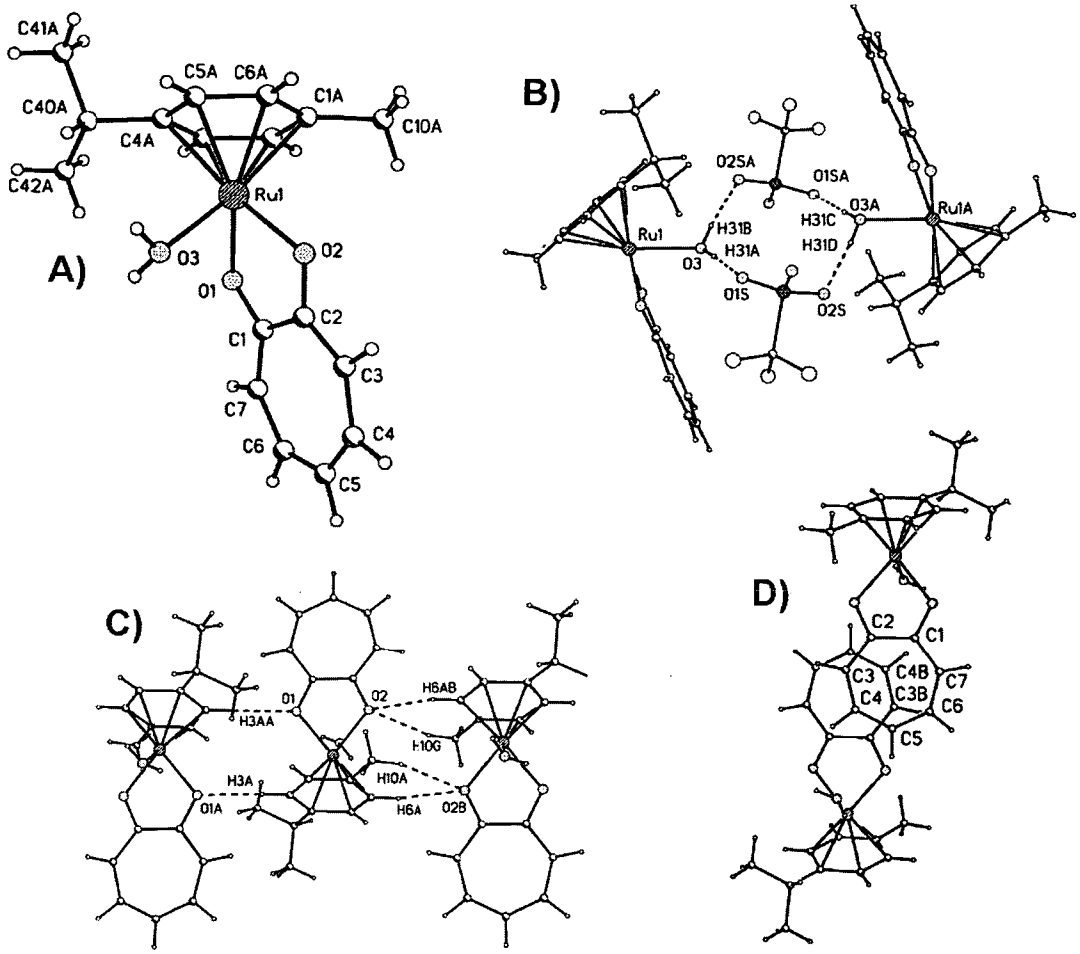

Figure 3.13: X-ray crystal structure of $[(\eta^6\text{-}p\text{-cym})Ru(trop)H_2O]^+$ (**3.25a**). A: Numbering scheme. B: Formation of dimers of **3.25a** *via* H-bond interactions between coordinated water and the counter anion. C: Chain formation *via* the trop oxygens O1 and O2 with *p*-cymene protons H3 and H6 and H10, respectively. D: Formation of π – π stacking between neighbouring tropolonate rings *via* the C3 and C4 carbons and the C3 and C5 carbons, respectively.

Both tropolonate oxygen atoms interact with respective neighbouring arene protons as seen for complexes [(η^6-*p*-cym)Ru(acac)Cl] (**3.5**) and [(η^6-*p*-cym)Ru(AcO)Cl] (**3.26**) (*vide supra*). The oxygen atom O2 has a short contact with the H10A proton of the methyl group of *p*-cymene (d = 2.51 Å, O2···C10A 3.417(4) Å) and the adjacent H6A arene proton (d = 2.55 Å, O2···C6A 3.191(4) Å), whereas oxygen atom O1 interacts with the H3A arene proton at a distance of 2.30 Å (O1···C3A 3.118(4) Å), thus linking the molecules into chains along the z axis (Figure 3.13C). The $\pi - \pi$ stacking of two neighbouring tropolonate ligands *via* the C3 and C4 carbons (d = 3.535(6) Å) and C3 and C5 carbons (d = 3.491(6) Å), respectively, forms a grid parallel to the (210) plane and the H-bonded dimer formation links the layers together (Figure 3.13D).

There are significant differences between the bond lengths of free tropolone [34] and those of coordinated tropolonate, which appears common for metal complexes. The tropolonate ring shows only a slight distortion from planarity, with C – C bond lengths decreasing from ring atoms C1 and C2 towards the C5 position. This phenomenon also seems to be the case for at least two of the three rings in the complex $Ga(trop)_3$ [20], but not for several other reported structures [20, 21, 22, 35]. The shortest $H(H_2O)$ – O(trop) distance is 2.65 Å.

3.5.1.5 Reactions in chloroform

It was noticed that both complexes [(η^6-*p*-cym)Ru(AcO)Cl] (**3.26**) and [(η^6-*p*-cym)Ru(trop)H_2O]NO_3 (**3.25a**) can undergo reactions in $CDCl_3$.

In the ^{1}H NMR spectrum of [(η^6-*p*-cym)Ru(AcO)Cl] (**3.26**) in $CDCl_3$, the *p*-cymene signals in the δ 5.65 – 5.30 region suggest the presence of two *p*-cymene species, one of which is **3.26** as assigned by Tocher *et al.* [36]. The relative concentrations of the two species varied between different ^{1}H NMR spectra. The ^{1}H NMR spectrum of a sample of **3.26** in $CDCl_3$ was recorded 10 min after dissolution.

It was then sealed to prevent evaporation of the solvent, stored away from direct sunlight to prevent photochemical reactions, and recorded again after 2 d 19 h. The ratio of **3.26** : new product changed from 9.6 : 1 to 2.8 : 1 (Figure A.3.4).

A concentrated solution of **3.25a** in $CDCl_3$ (*ca.* 10 mM Ru) was recorded 10 min after dissolution and again after 3 d 22 h. Also, some of that solution recorded after 10 min was taken and diluted by more $CDCl_3$ (*ca.* 20-fold) and the spectrum was recorded both after 10 min and 20 h. For the concentrated sample, *p*-cymene arene signals for a new species were evident, the intensities increasing from initially 36 : 1 to 7 : 1 over a period of 3 d 22 h. For the diluted sample, more species appeared to be present in solution according to *p*-cymene arene signals, including the two found in the concentrated sample, their relative intensities changing from 1 : 3.3 to 1 : 2.1 over a period of 20 h.

3.5.2 Discussion

3.5.2.1 Stability in water

The stable ^1H NMR spectra obtained for complexes [(η^6-*p*-cym)Ru(acac)Cl] (**3.5**), [(η^6-*p*-cym)Ru(trop)Cl] (**3.23**) and [(η^6-*p*-cym)Ru(ma)Cl] (**3.24**) in water makes them suitable candidates for further studies in aqueous media. This is in

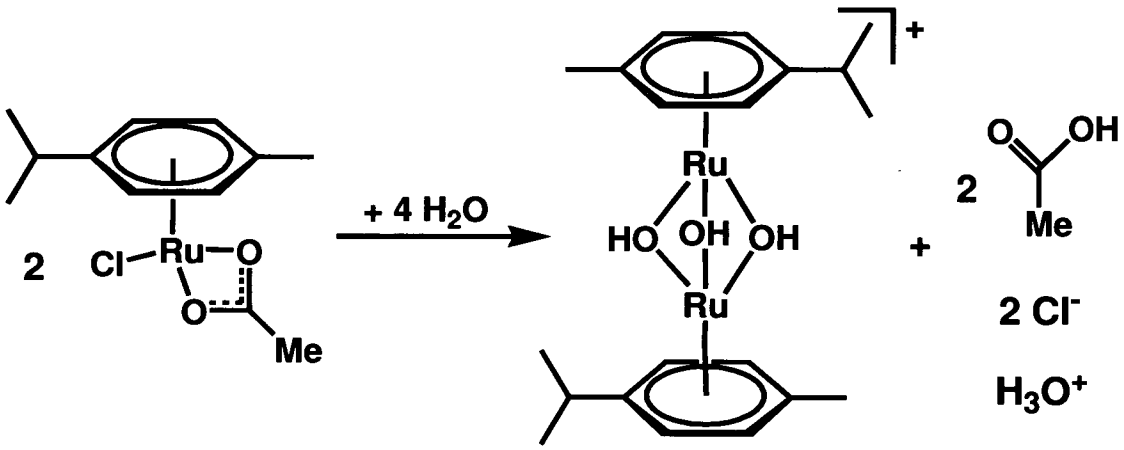

Scheme 3.5: Balanced equation for the formation of [((η^6-*p*-cym)Ru)$_2$(μ-OH)$_3$]$^+$ (**3.27**) from [(η^6-*p*-cym)Ru(AcO)Cl] (**3.26**) in water.

contrast to [(η^6-*p*-cym)Ru(AcO)Cl] (**3.26**), which decomposes rapidly by hydrolysis of both chloride and acetate to form the hydroxo-bridged dimer [((η^6-*p*-cym)Ru)$_2$(μ-OH)$_3$]$^+$ (**3.27**) (Scheme 3.5). Figure 3.14 shows a spectrum of **3.26** in D_2O at different pH* values. The positions of the peaks for **3.27** do not change over a pH range of more than 6 units, which shows its high stability and inertness.

Tocher *et al.* have pointed out previously that dissociation of acetate from such complexes can occur in polar solvents [36]. Acetate has been proposed to act as an intramolecular base in palladium complexes [37] and such a mechanism could facilitate the formation of the hydroxo-bridged dimer at acidic pH* values (*ca.* 4). The proposed use of [(η^6-*p*-cym)Ru(AcO)Cl] (**3.26**) as a precursor for the

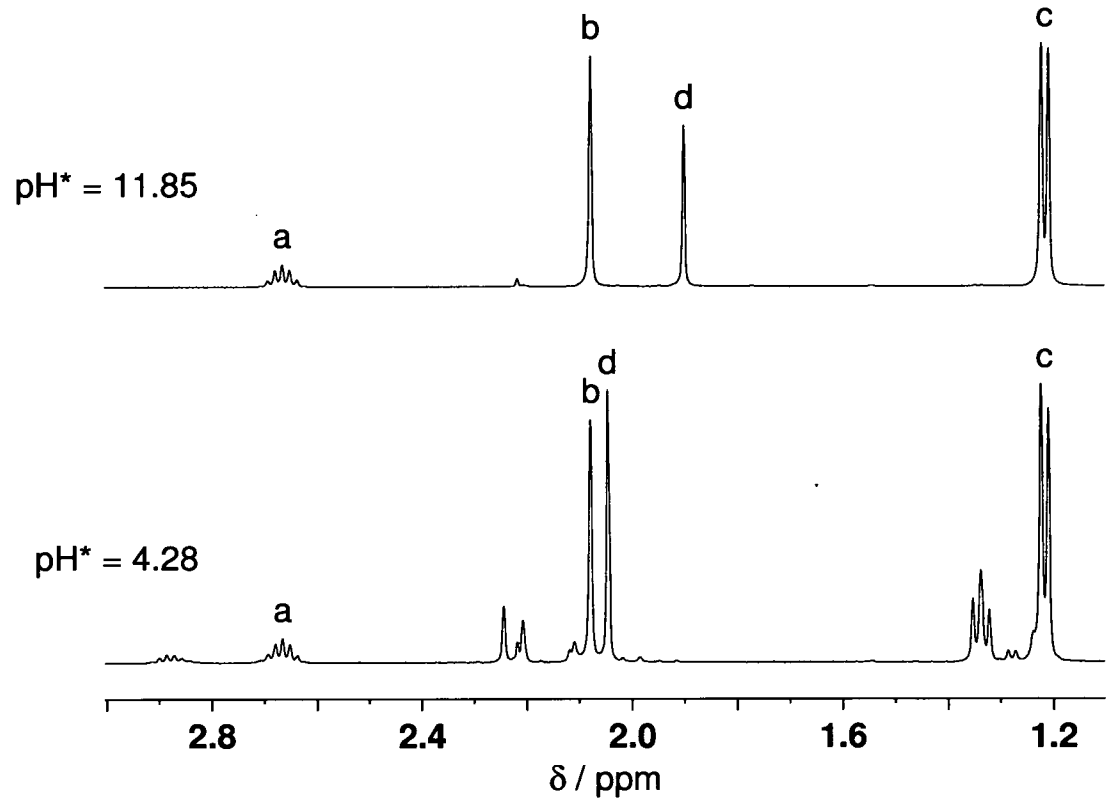

Figure 3.14: The high-field region of the ^{1}H NMR spectrum of [(η^6-*p*-cym)Ru(AcO)Cl] (**3.26**) in D_2O at 298 K and pH* = 4.28 and 11.85, respectively. The main species present is [((η^6-*p*-cym)Ru)$_2$(μ-OH)$_3$]$^+$ (**3.27**). Assignments: a = *p*-cymene isopropyl CH (**3.27**); b = *p*-cymene CH_3 (**3.27**); c = *p*-cymene isopropyl $(CH_3)_2$ (**3.27**); d = free acetate CH_3.

cyclometallation of imines by Davies *et al.* [27] further suggests an inherent lability of the acetate ligand.

These findings also provide evidence for the surprisingly facile formation of the ruthenium arene hydroxo-bridged dimer **3.27**. Recent studies on related osmium complexes have shown the pronounced tendency of those complexes to undergo formation of hydroxo-bridged dimers, even at acidic pH [38].

3.5.2.2 Hydrolysis studies

The ^{1}H NMR spectrum of [(η^6-*p*-cym)Ru(acac)Cl] (**3.5**) in 90% H_2O/10% D_2O contained a single set of peaks, and conductivity measurements indicated the existence of ionic species in aqueous solution, suggesting that hydrolysis occurs [30]. This is consistent with the NMR chemical shifts, which are very similar to those of the aqua complex [(η^6-*p*-cym)Ru(acac)H_2O]NO_3 (**3.14a**). Hydrolysis of **3.5** appeared to be rapid, since equilibrium was reached by the time the first ^{1}H NMR spectrum was recorded (< 5 min).

Figure 3.15 shows a plot of the dependence of the acac Me protons on chloride concentration. Anation of hydrolysed **3.5** was almost complete on addition of *ca.* 1 M NaCl. The curve, however, does not have a good fit to a chloride/aqua equilibrium. The reason for this presumably is that shifts are not only influenced by chloride anation alone, but also by an increase in pH resulting from both addition of increasing amounts of NaCl solution and dissociation of acac at high [Cl^-], as well as a strong influence of ionic strength, especially at high [Cl^-].

During the chloride titration, the ^{1}H NMR spectra showed only a single set of peaks for **3.5**, indicative of relatively fast exchange between water and chloride on the NMR timescale. Davies *et al.* have pointed out the critical role of hydrogen bond interactions for Ru^{II} arene complexes with *O,O*-chelating ligands forming five-membered chelate rings and proposed an equilibrium state between co-ordinated

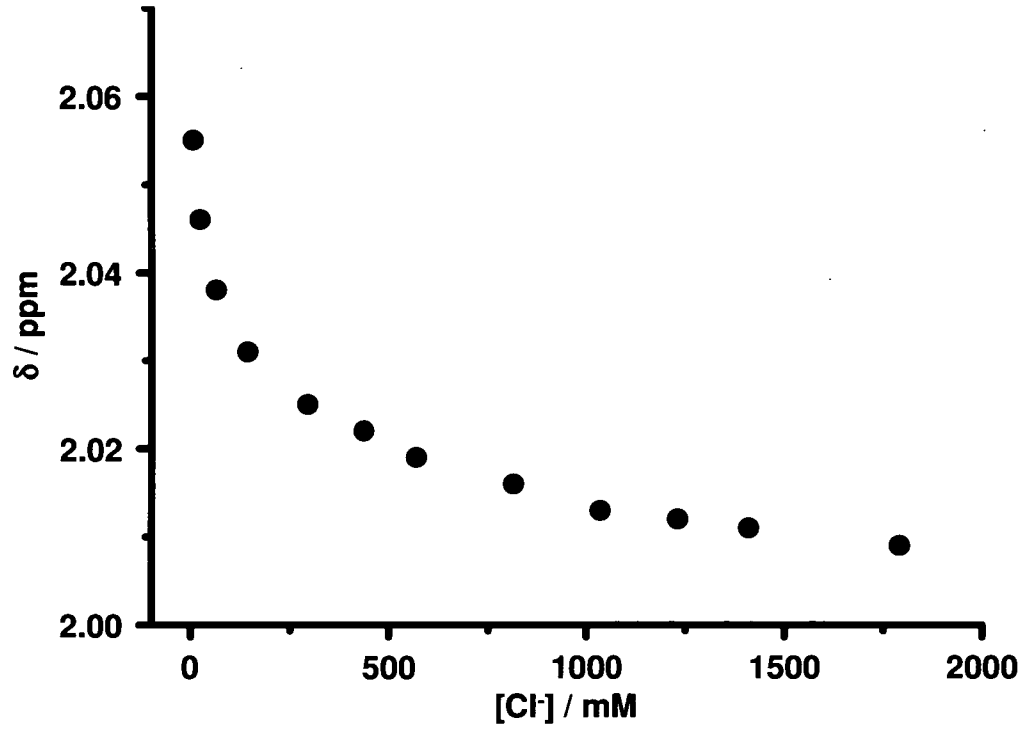

Figure 3.15: Variation of the ^{1}H NMR chemical shift of the acac Me protons of an hydrolyzed sample of [(η^6-*p*-cym)Ru(acac)Cl] (**3.5**) on addition of increasing amounts of NaCl.

water and co-ordinated chloride during hydrolysis [39]. The X-ray crystal structure of [(η^6-*p*-cym)Ru(ma)Cl].2H_2O (**3.24**).2H_2O provides solid state evidence for interactions of water with the chloro complex. The water molecules are apparently pre-organised for hydrolysis of the complex, but may also stabilize coordinated chloride, factors which could contribute to the observed rapid exchange of water and chloride. The arrangement of the water molecules is similar to that found in the calculated transition state for aquation of the related acac complex [(η^6-*p*-cym)Os(acac)Cl] [40]. Hence the solid state structure provides a "snapshot" of the possible hydrolysis pathway.

The ^{1}H NMR spectrum of [(η^6-*p*-cym)Ru(acac)dcp]PF_6 (**3.16**) in water contains the three species **3.16**, [(η^6-*p*-cym)Ru(acac)H_2O]PF_6 (**3.14b**) and [((η^6-*p*-cym)Ru)$_2$(μ-OH)$_3$]$^+$ (**3.27**) (Figure 3.16). The extent of hydrolysis cannot be

determined accurately due to gradual formation of the hydroxo-bridged dimer **3.27** and appears to be concentration dependent, indicated by the significantly higher presence of **3.14b** at lower concentrations of **3.16**.

An exchange mechanism appears to be the reason for the different spectra of **3.24** in $CDCl_3$ and D_2O. Maltolate is an unsymmetrical ligand making the Ru centre chiral, and thus the *p*-cymene ring protons are inequivalent, giving rise to four signals in the non-coordinating solvent chloroform. The signals for the aqueous solution do not indicate inequivalence, which means that the peaks are either

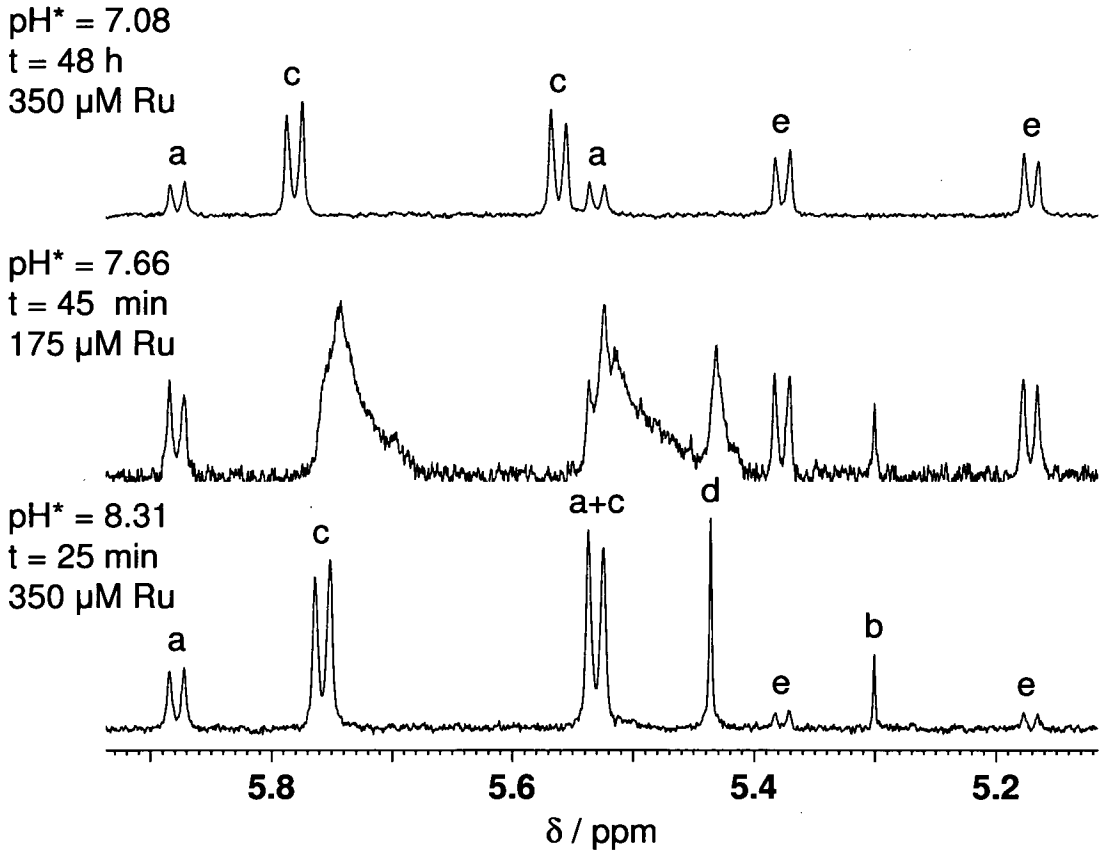

Figure 3.16: The *p*-cymene ring proton and acac CH region of the ^1H NMR spectrum of $[(\eta^6\text{-}p\text{-cym})Ru(acac)dcp]PF_6$ (**3.16**) in D_2O at 298 K. The three species present are (**3.16**), $[(\eta^6\text{-}p\text{-cym})Ru(acac)H_2O]PF_6$ (**3.14b**) and $[((\eta^6\text{-}p\text{-cym})Ru)_2(\mu\text{-}OH)_3]^+$ (**3.27**). Assignments: a = *p*-cymene CH (**3.16**); b = acac CH (**3.16**); c = *p*-cymene CH (**3.14b**); d = acac CH (**3.14b**); e = *p*-cymene CH (**3.27**). Peaks b and d have disappeared after 48 h due to proton exchange in D_2O.

accidentally equivalent or that a fluxional process is occurring, which makes them equivalent on the NMR timescale. Davies *et al.* have put forward an explanation for $[(\eta^5\text{-Cp*})\text{Rh(ema)Cl}]$, where Cp* = pentamethylcyclopentadienyl, ema = ethylmaltolate, which shows the chiral and non-chiral behaviour in chloroform and water, respectively, as does **3.24** [39]. The proposed mechanism is shown in Scheme 3.6. **3.24** can be assumed to hydrolyse rapidly and almost fully in water, similarly to the acac system. This aqua complex can then undergo the proposed water exchange reactions. Further evidence was obtained by Davies *et al.* by low temperature studies in CD_3OD, which showed the splitting of signals into two independent sets of signals. Similar studies on complex $[(\eta^6\text{-}p\text{-cym})\text{Os(ma)Cl}]$, which exhibits the same behaviour as its ruthenium analogue, have also shown this splitting at low temperature [40], and a ring opening mechanism was proposed. The appearance of the broad peaks for **3.14b** at low concentrations points towards an exchange or ring opening mechanism, which is reasonably slow on the NMR timescale.

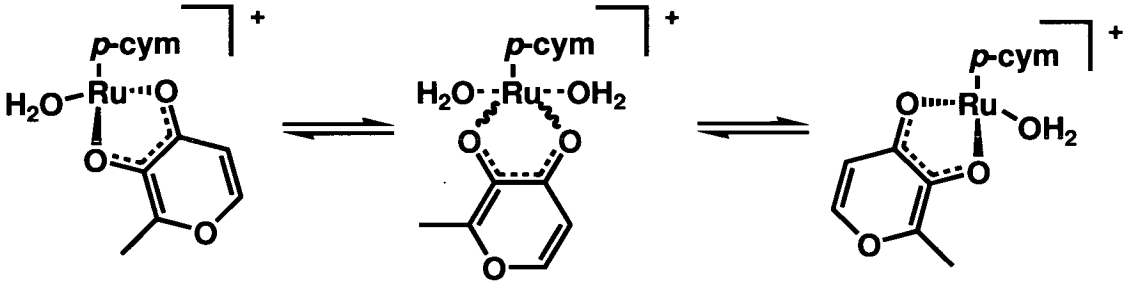

Scheme 3.6: Proposed mechanism of fluxionality for complex $[(\eta^6\text{-}p\text{-cym})\text{Ru(ma)Cl}]$ (**3.24**) after hydrolysis in water, adapted from a report by Davies *et al.* [39].

The hydrolysis studies of complexes **3.5** and **3.16** suggest that at least for the acac system the complexes would be largely present as $[(\eta^6\text{-arene})\text{Ru(acac)}H_2O]^+$ at the micromolar concentrations used in the screening for cancer cell cytotoxicity. The implied independence on the leaving group could be the source of a common mode of activation for all these compounds.

Chloride titrations of $[(\eta^6\text{-arene})Ru(en)Cl]PF_6$ complexes have shown essentially full chlorination at physiological chloride levels (104 mM), *e.g.* > 89% for $[(\eta^6\text{-bip})Ru(en)Cl]PF_6$ [10]. For **3.5**, the titration suggested a chloro : aquo complex ratio of 55 : 45 at that level (104 mM). This could also apply to the positively-charged acac-containing compounds, since results for **3.16** suggest that already at concentrations *ca.* 5 times higher than those employed during cell testing they show a large extent of hydrolysis. These findings imply that for the acac system there might not be as strong a dependence of activity on the nature of the leaving group as was recently found for en-containing complexes [11].

In addition, upon introduction of acac-containing Ru^{II} arene complexes into the cell media, a considerable percentage of these might essentially be immediately present in its more reactive aqua form and could be lost due to deactivation by biomolecules. On the other hand, possible immediate reactivity could also be the reason for activity, either by rapid reaction with a target or by enabling transport mechanisms, whereby the complexes react with a biomolecule and are shuttled to their target site.

These results show that the chelating ligand acac has a pronounced effect on both the rate and extent of hydrolysis in Ru^{II} arenes compared to en. Chloride displacement occurs readily and anation is suppressed, even at elevated $[Cl^-]$. A reason for this might be electronic effects of the acac ligand. Acetylacetonate ligands are known to be strongly electron-donating towards Ru^{II} centres [41], and the high electron density on Ru^{II} in $[(\eta^6\text{-arene})Ru(acac)H_2O]^+$ compared to the analogous en complex makes the substitution of the aqua ligand by negatively-charged Cl^- less favourable [42]. Similar behaviour can also be inferred for trop and ma. *O,O*-Chelating ligands also appear to favour a rapid chloride/water exchange mechanism, possibly due to interactions between chloride, water and the chelate oxygen atoms as seen in the solid structure of **3.24**.$2H_2O$.

In addition, potentially favourable H-bond interactions between a coordinated water molecule and the oxygen atoms of the chelating ligands in solution could lead to added stability of the aqua adduct compared to its chlorinated form as has been suggested to occur in another complex [25].

3.5.2.3 pK_a values of coordinated water

The pK_a values of coordinated water can have an important influence on the reactivity of Ru^{II} arene complexes (Scheme 3.7). Aquo complexes of the type $[(\eta^6\text{-arene})Ru(en)H_2O]^{2+}$ are very reactive towards potential target molecules, whereas their hydroxo analogues are less reactive [9].

The pK_a values of bound water in complexes $[(\eta^6\text{-}p\text{-cym})Ru(acac)H_2O]^+$ (**3.14a**), $[(\eta^6\text{-}p\text{-cym})Ru(trop)H_2O]^+$ (**3.25a**) and $[(\eta^6\text{-}p\text{-cym})Ru(ma)H_2O]^+$ (**3.29**) were found to be in a similar range, all greater than 9. Those values are between 0.9 – 1.2 pK_a units higher than that for the respective en analogue $[(\eta^6\text{-}p\text{-cym})Ru(en)H_2O]^{2+}$ (8.25) [10]. Therefore, at physiological pH (7.4), the *O,O*-chelated complexes **3.14a, 3.25a** and **3.29** would be expected to be mainly present in their reactive aqua forms rather than as the less reactive hydroxo complexes.

The pH titration showed that at pH values < 4, acac dissociated from ruthenium, whereas the maltolato and tropolonato complexes appeared significantly

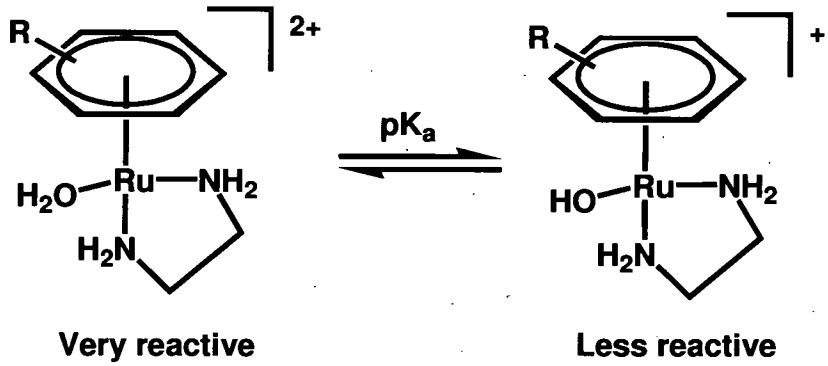

Scheme 3.7: The influence of the pK_a value of water in complexes of the type $[(\eta^6\text{-arene})Ru(en)H_2O]^{2+}$ on reactivity [9].

more stable. In addition, at pH values greater than 9, the hydroxo-bridged dimer $[((\eta^6\text{-}p\text{-cym})Ru)_2(\mu\text{-}OH)_3]^+$ (**3.27**) formed, which was further confirmed by the appearance of signals due to the free chelating ligands. Upon acidification the chelated complexes formed again, indicating a large degree of reversibility of dimer formation in the case of ruthenium. This is in contrast to osmium analogues, where dimer formation appeared to be irreversible [38, 40].

The large increase of *ca.* one unit in the pK_a value of the aqua ligand in the *O,O*-chelated complex **3.14a, 3.25a** and **3.29** compared to the en complex, can be rationalized on the basis of the increased electron density on Ru^{II}. Additional interactions between bound water and the chelating ligand could enhance the stability of the aqua complex further.

These findings show how chelating ligands can be used to fine-tune the stability of coordinated water in ruthenium(II) anticancer complexes over a considerable range. The comparatively low pK_a value of 7.3 in the complex $[(\eta^6\text{-hmb})Ru(bpy)H_2O]^{2+}$, where hmb = hexamethylbenzene, bpy = 2,2'-bipyridine, further emphasises this point [43].

3.5.2.4 X-ray crystal structures

The X-ray crystal structures of $[(\eta^6\text{-}p\text{-cym})Ru(Ph_2acac)H_2O]CF_3SO_3$ (**3.21b**) and $[(\eta^6\text{-}p\text{-cym})Ru(trop)H_2O]CF_3SO_3$ (**3.25b**) show that *O,O*-chelated ruthenium arene complexes can form stable aqua adducts. They also reveal that the key bond-lengths in both complexes are remarkably similar. In addition, there does not appear to be strong intramolecular hydrogen bonding between the chelating ligand and coordinated water in the solid state. It therefore seems likely that the high pK_a values of the *O,O*-chelated complexes compared to the en analogue arise mainly from electronic effects exerted by the ligand on the metal centre. However, stabilising intramolecular interactions could occur in solution.

For **3.25b** there were $\pi - \pi$ stacking interactions between neighbouring tropolonato rings. In the solid state structure of free tropolone, slightly distorted intermolecular $\pi - \pi$ stacking (d = 3.42 – 3.77 Å) is observed for whole rings, also between formally single and double bonds [34]. Once coordinated to a metal, tropolonate tends to be involved in only partial $\pi - \pi$ stacking, with intermolecular distances generally in the range of 3.32 and 3.60 Å [20, 21, 22]. Interestingly, in the structure of [Fe(oep)(η^2-trop)].C_6H_5Me, where oep is the octaethylporphyrinato dianion, reported by Richter-Addo *et al.* [35], there are π-π interactions between the tropolonate ring and residual toluene. Therefore, {(η^6-*p*-cym)Ru(trop)}$^+$ could take part in potential $\pi - \pi$ stacking interactions with aromatic side-chains, *e.g.* tryptophan of proteins.

3.5.2.5 Reactions in chloroform

For [(η^6-*p*-cym)Ru(AcO)Cl] (**3.26**) the observations indicate that the complex decomposes slowly over time in $CDCl_3$. However, neither Tocher *et al.* nor Davies *et al.* reported any side-products for [(η^6-*p*-cym)Ru(AcO)Cl] in deuterated chloroform for their ^{1}H NMR data.

Figure 3.17 shows the 2.4 – 1.2 ppm region of **3.26** in $CDCl_3$ at 298 K. It shows that already after 10 min free acetic acid (confirmed by recording a spectrum of acetic acid in $CDCl_3$ and comparing the chemical shifts) can be detected in solution (peak d). The amount of acetic acid increases over a period of 2 d 19 h and an additional signal (peak b) appears, which could originate from displaced and potentially reacted acetate. An attempt to record a spectrum of acetate showed a peak with the same shift as peak b, however, since acetate has very poor solubility it is not conclusive whether the signal originates from marginally soluble acetate or an impurity. It is clear, however, that **3.26** is losing acetate, which is converted into acetic acid. It can be speculated that residual water protonates acetate and leads to

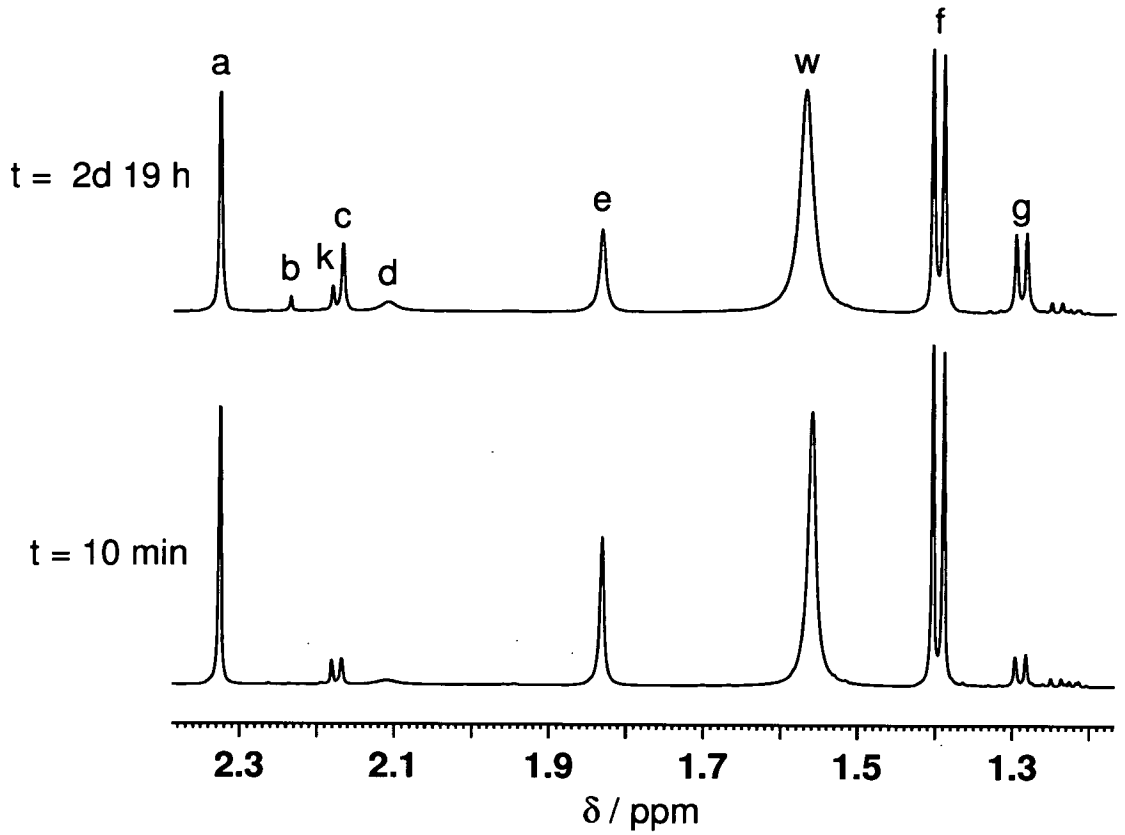

Figure 3.17: The high field region of the ^{1}H NMR spectrum of [(η^6-*p*-cym)Ru(AcO)Cl] (**3.26**) in $CDCl_3$ at 298 K, after 10 min and 2 d 19 h, respectively. The new product could be [(η^6-*p*-cym)$RuCl_2$]$_2$ (**3.1**). Assignments: a = *p*-cymene CH_3 (**3.26**); b = free acetate (?); c = *p*-cymene CH_3 (**3.1**); d = free acetic acid; e = acetate CH_3 (**3.26**); f = *p*-cymene isopropyl $(CH_3)_2$ (**3.26**); g = *p*-cymene isopropyl $(CH_3)_2$ (**3.1**); k = residual acetone, w = residual water.

formation of the hydroxo-bridged dimer [((η^6-*p*-cym)Ru)$_2$(μ-OH)$_3$]$^+$ (**3.27**). This might explain peak b as free acetate in its role as a counter anion. The chemical shifts of the new ruthenium species, however, are identical to those of the *p*-cymene dimer [(η^6-*p*-cym)$RuCl_2$]$_2$ (**3.1**). This strongly suggests that **3.26** is able to obtain chloride from a $CDCl_3$ solution, possibly from residual DCl, which would explain the formation of acetic acid, or even by abstraction reactions from $CDCl_3$ itself, which could lead to an unknown product incorporating acetate, resulting in signal b.

Formation of Ru – Cl bonds is further supported by the findings of experiments with $[(\eta^6\text{-}p\text{-cym})Ru(trop)H_2O]NO_3$ (**3.25a**) in $CDCl_3$ (Figure 3.18). In case of the concentrated sample of the aqua complex **3.25a**, the new signals which appear over time have the same chemical shifts as those of chloro complex **3.23**. The same is indicated for the tropolonato resonances. No signals for either chloride-bridged *p*-cymene dimer or free tropolone were detected, highlighting the strength of a five-membered chelate ring over a four-membered one.

In summary, it was possible to show previously undetected decomposition tendencies of **3.26** in both polar and non-polar solvents. The results also suggest that ruthenium arene complexes may abstract chloride from $CDCl_3$.

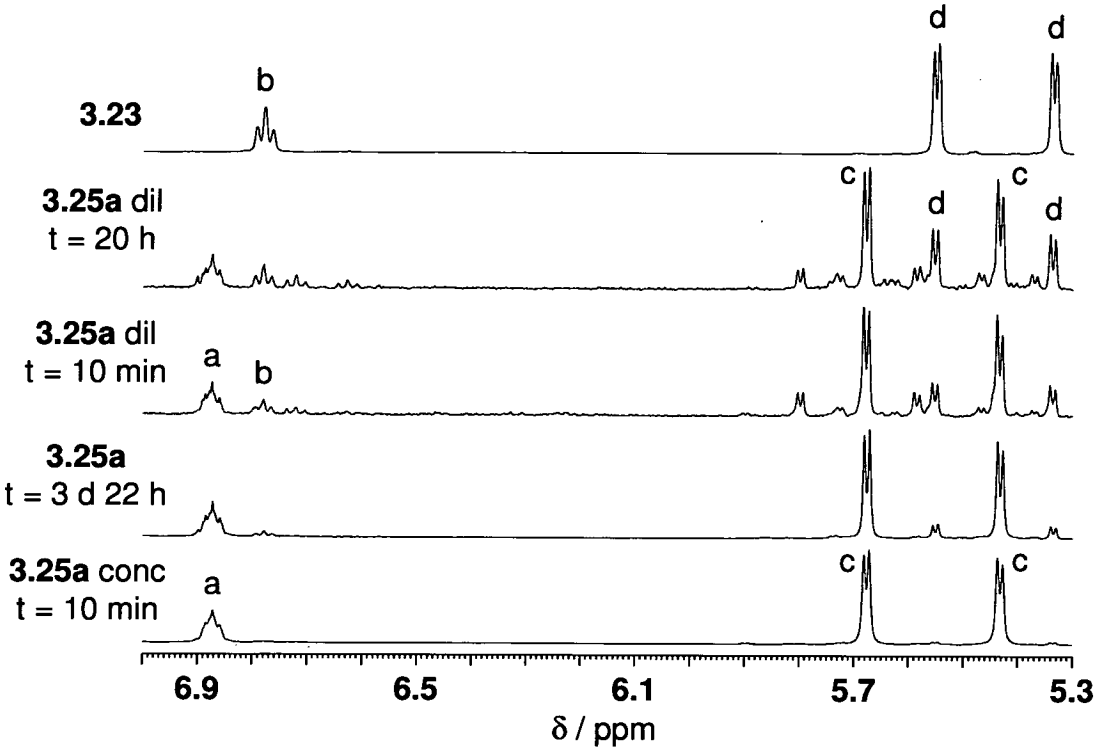

Figure 3.18: The high field region of the ^1H NMR spectra of $[(\eta^6\text{-}p\text{-cym})Ru(trop)Cl]$ (**3.23**) and $[(\eta^6\text{-}p\text{-cym})Ru(trop)H_2O]NO_3$ (**3.25a**) in $CDCl_3$ at 298 K. Spectra of **3.25a** were taken of concentrated (conc, ca. 10 mM Ru) solutions after 10 min and 3 d 22 h and of diluted (dil, ca. 500 μM Ru) solutions after 10 min and 20 h, respectively. Assignments: a = Hc trop (**3.25a**); b = Hc trop (**3.23**); c = *p*-cymene CH (**3.25a**); d = *p*-cymene CH (**3.23**).

3.6 Binding to DNA Bases

3.6.1 Results

Reactions of the *O,O*-chelated complexes [(η^6-*p*-cym)Ru(acac)Cl] (**3.5**), [(η^6-*p*-cym)Ru(trop)Cl] (**3.23**) and [(η^6-*p*-cym)Ru(ma)Cl] (**3.24**) with DNA model bases guanosine, adenosine, cytidine and thymidine (Figure 3.19) and of the hydroxo-bridged dimer [((η^6-*p*-cym)Ru)$_2$(μ-OH)$_3$]$^+$ (**3.27**) with 9-ethylguanine were studied in water by ^{1}H NMR spectroscopy.

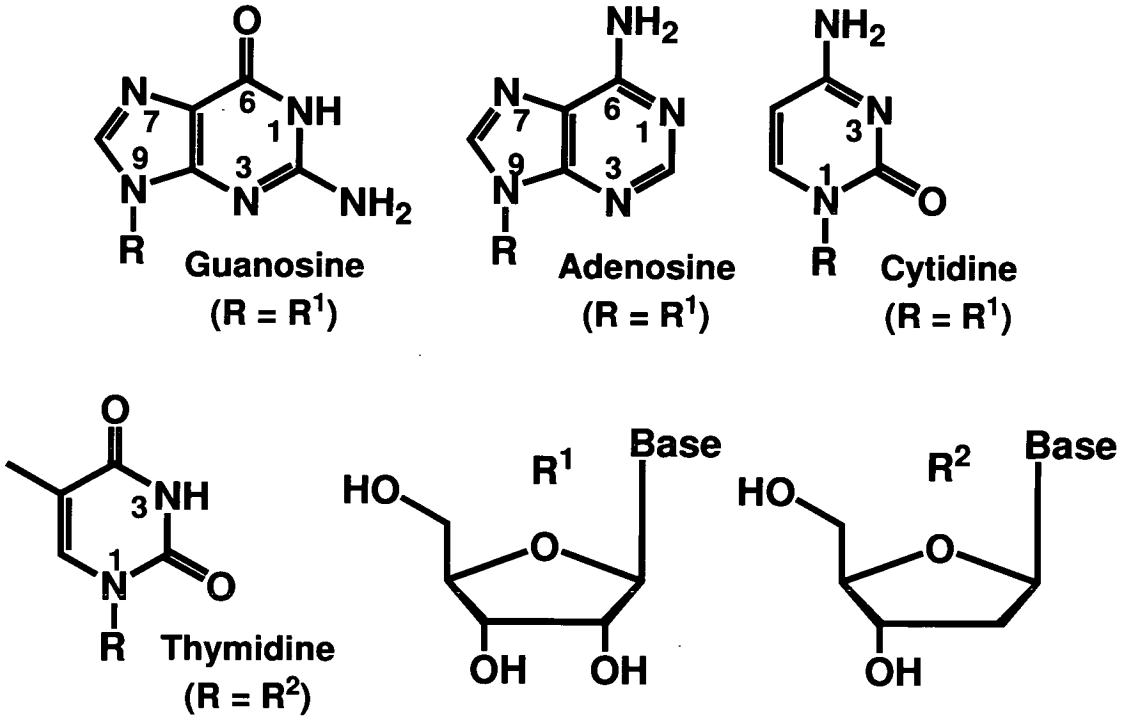

Figure 3.19: The structures of mononucleosides guanosine, adenosine, cytidine and thymidine.

3.6.1.1 Reactions of O,O-chelated complexes with guanosine

The ^{1}H NMR spectrum of a 1:1 mol ratio mixture of guanosine and **3.5** (8 mM Ru, pH 5.33) was recorded. Similarly, the ^{1}H NMR spectra of the reactions of **3.23** (8 mM Ru, pH 6.55) and **3.24** (7 mM Ru, pH 6.12) were recorded. About 80% of **3.5** and **3.23** and about 75% of **3.24** had reacted by the time the first spectra were recorded (*ca.* 10 min).

For each reaction, a new H8 ^{1}H NMR peak was noted at δ 7.92 ppm (**3.5**), and at δ 7.91 ppm (**3.23** and **3.24**), respectively, each with an upfield shift of δ 0.08 ppm compared to free guanosine at δ 8.00 ppm (**3.5**) and 7.99 ppm (**3.23** and **3.24**), respectively. Compared to unreacted starting material, the central acac proton signal of the product had moved upfield by 0.28 ppm (**3.5**) and the trop and ma proton signals of the products had moved upfield by an average of 0.18 ppm (**3.23**) and 0.20 ppm (**3.24**), respectively. The ^{1}H NMR spectrum of the reaction of **3.5** recorded after 24 h was unchanged.

3.6.1.2 Reactions of O,O-chelated complexes with adenosine

The ^{1}H NMR spectrum of a 1:1 mol ratio mixture of adenosine and **3.5** (8 mM Ru, pH 5.80) was recorded. Similarly, the ^{1}H NMR spectra of the reactions of **3.23** (8 mM Ru, pH 7.35) and **3.24** (9 mM Ru, pH 7.22) were recorded. In each reaction about 80% of the starting material had reacted by the time the first spectrum was recorded (*ca.* 10 min).

The region of δ 8.65 – 8.20 showed six peaks for the reaction of **3.5** (overlapped peaks in the cases of **3.23** and **3.24**), indicating that a reaction had taken place. A ^{1}H NMR spectrum of the reaction of **3.5** recorded after > 24 h was unchanged [30].

3.6.1.3 Competition between adenosine and guanosine in reactions with O,O-chelated complexes

To an aqueous solution containing a 1:1 mol ratio mixture of guanosine and adenosine was added one mol equivalent of **3.5** (8 mM Ru, pH 5.78) and the ^{1}H NMR spectrum was recorded. Similarly, the ^{1}H NMR spectra of the reactions of **3.23** (9 mM Ru, pH 6.63) and **3.24** (8 mM Ru, pH 6.22) were recorded.

For the three reactions, the same peaks as were observed in the individual reactions of each Ru complex with either guanosine or adenosine alone were observed in the spectra, along with almost similar proportions of the free nucleosides.

3.6.1.4 Displacement reactions involving adenosine, guanosine and [(η^6-p-cym)Ru(acac)Cl] (3.5)

To a 1:1 mol ratio mixture of **3.5** (8 mM Ru) and adenosine was added one mol equivalent of guanosine and the ^{1}H NMR spectrum was recorded at pH 4.97. Similarly, to a 1:1 mol ratio mixture of **3.5** (8 mM Ru) and guanosine was added one mol equivalent of adenosine and the ^{1}H NMR spectrum was recorded at pH 6.22. The spectra obtained were very similar to what was observed in the reaction of **3.5** in Section 3.6.1.3.

3.6.1.5 Reaction of [(η^6-p-cym)Ru(acac)H_2O]NO_3 (3.14a) with cytidine and thymidine

The ^{1}H NMR spectrum of a 1:1 mol ratio mixture of **3.14a** and cytidine was recorded over a pH range of 2.50 to 10.40. Similarly, the ^{1}H NMR spectrum of a 1:1 mol ratio mixture of **3.14a** and thymidine was recorded over a pH range of 2.46 to 12.38. In each case the spectra showed peaks for the free nucleosides only and the signals of **3.14a** had similar chemical shifts to those observed in the pH titration of the complex.

3.6.1.6 Reaction of [((η^6-p-cym)Ru)$_2$(μ-OD)$_3$]$^+$ (3.27) with 9-ethylguanine

The reaction of the dimer [((η^6-*p*-cym)Ru)$_2$(μ-OD)$_3$]$^+$ (**3.27**) (prepared *in situ* using a solution of [(η^6-*p*-cym)Ru(AcO)Cl] (**3.26**) (8 mM Ru) at pH* = 6.74) with one mol equivalent, with respect to **3.26**, of 9-ethylguanine in D_2O at an initial pH*

of 7.27 gave rise to new peaks in the δ 7.5 – 8.8 ppm region after 21 h, suggesting that a number of adducts had been formed (Figure A.3.5). Integration of the new peaks indicated that < 20% of 9-ethylguanine had reacted.

3.6.1.7 X-ray crystal structures

The growth of X-ray diffraction quality crystals of $[(\eta^6\text{-}p\text{-cym})Ru(acac)9EtA]PF_6$ (**3.20**), where 9EtA = 9-ethyladenine, and $[(\eta^6\text{-}p\text{-cym})Ru(Ph_2acac)9EtG]CF_3SO_3$ (**3.22**), where 9EtG = 9-ethylguanine, occurred by difficulties from formation of powders and oils as well as decomposition.

An attempt to grow crystals of **3.20** from methanol/water at ambient temperature over a period of five months resulted in poor quality crystals of the trimeric complex $[(\eta^6\text{-}p\text{-cym})Ru(9EtAH_{-1})]_3(PF_6)_3$ (**3.30**), which had lost the acac chelate (Figure 3.20). The C6 amino group appeared to have been deprotonated to form a mono-anionic five-membered chelate ring with the N7 nitrogen with N1 bridging to another ruthenium centre. The structure was not fully refined since the R-factor was high (11%) but the parameters are very similar to a previously reported structure (CF_3SO_3 counter anion instead of PF_6) [44].

Good quality crystals of $[(\eta^6\text{-}p\text{-cym})Ru(acac)9EtA]PF_6$ (**3.20**) were eventually obtained from a solution containing water, methanol and diethyl ether stored at 253 K over a period of one and a half years (Figure 3.21). The

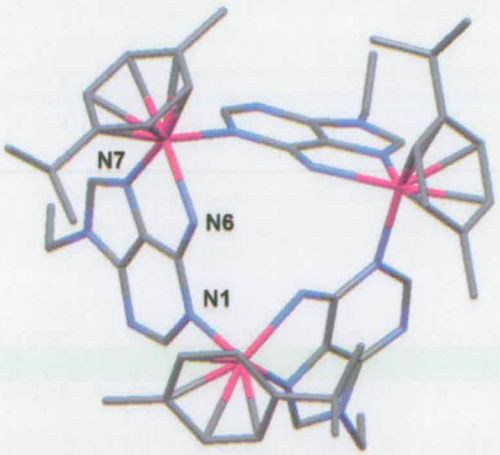

Figure 3.20: The structure of the trinuclear cation in $[(\eta^6\text{-}p\text{-cym})Ru(9EtAH_{-1})]_3(PF_6)_3$ (**3.30**). Nitrogen atoms N7 and N6 are part of a five-membered chelate ring, while N1 is a bridging nitrogen. Hydrogen atoms have been omitted for clarity.

Table 3.9: Selected bond lengths (Å) and angles (°) for [(η^6-*p*-cym)Ru(acac)9EtA]PF_6 (**3.20**).

Bond	Length	Bond	Length/angle
Ru-O1	2.049(7)	Ru-C5	2.157(10)
Ru-O2	2.081(7)	Ru-C6	2.133(11)
Ru-N7A	2.135(9)	Ru-centroid[a]	1.649
Ru-C1	2.179(11)	O1-Ru-O2	88.3(3)
Ru-C2	2.180(11)	O1-Ru-N7A	83.2(3)
Ru-C3	2.155(11)	O2-Ru-N7A	87.3(3)
Ru-C4	2.189(11)		

[a] = measured using Mercury 1.4.

crystallographic data are listed in Table A.3.3, bond lengths and angles are listed in Table 3.9. The structure confirms monodentate binding of 9EtA to ruthenium *via* the N7 nitrogen. The Ru – O(acac) bond lengths are 2.049(7) Å and 2.081(7) Å, respectively. The Ru – N7(9EtA) bond length is 2.135(9) Å. The Ru – C(arene) distances are in the range of 2.133(11) Å to 2.189(11) Å, with Ru – centroid 1.65 Å. There is an H-bond interaction between NH6 and O(acac) with a distance of 2.07 Å (O1···N6A 2.813(11) Å). The structure forms dimers held together by H-bond interactions between NH6 and N1 (d = 2.16 Å, N1A···N6A 3.036(12) Å) (Figure 3.21B). A grid is formed *via* the PF_6 counterions, which have multiple interactions with *p*-cymene ring protons, methyl and isopropyl groups as well as acac methyl and 9EtA ethyl groups all in a range of 2.37 – 2.65 Å.

X-ray diffraction quality crystals of [(η^6-*p*-cym)Ru(Ph_2acac)9EtG]CF_3SO_3 (**3.22**) were obtained by allowing a solution of 1,2-dichloroethane to evaporate to dryness, taking up the residue in warm toluene under sonication and leaving the solution to stand at ambient temperature. Crystals started forming within thirty minutes. The structure is shown in Figure 3.22, the crystallographic data are listed in Table A.3.4 and bond lengths and angles in Table 3.10.

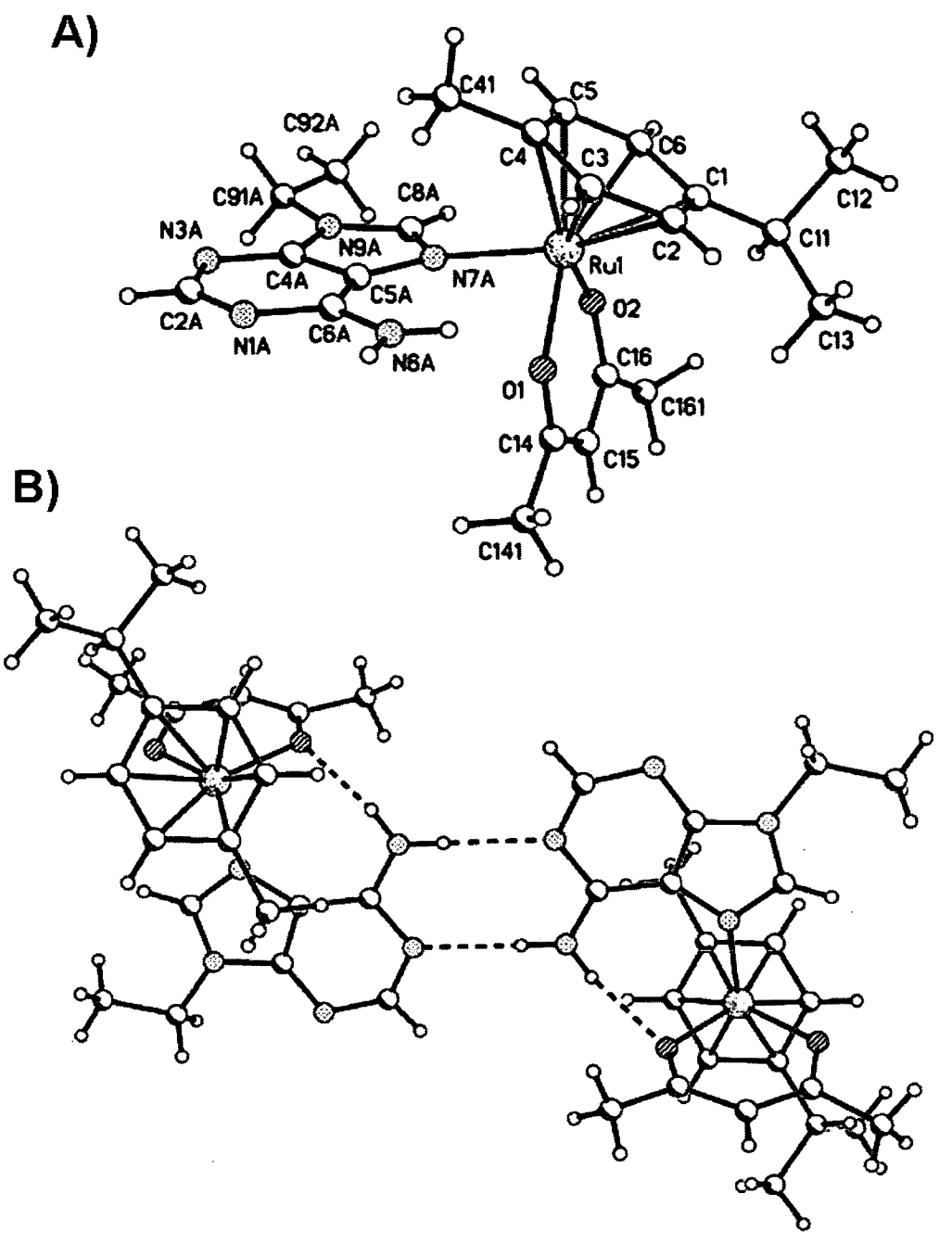

Figure 3.21: X-ray crystal structure of the cation $[(\eta^6\text{-}p\text{-cym})Ru(acac)9EtA]^+$ in complex **3.20**. A: Numbering scheme. B: Formation of dimers *via* hydrogen bonds formed by neighbouring N6H and N1 atoms.

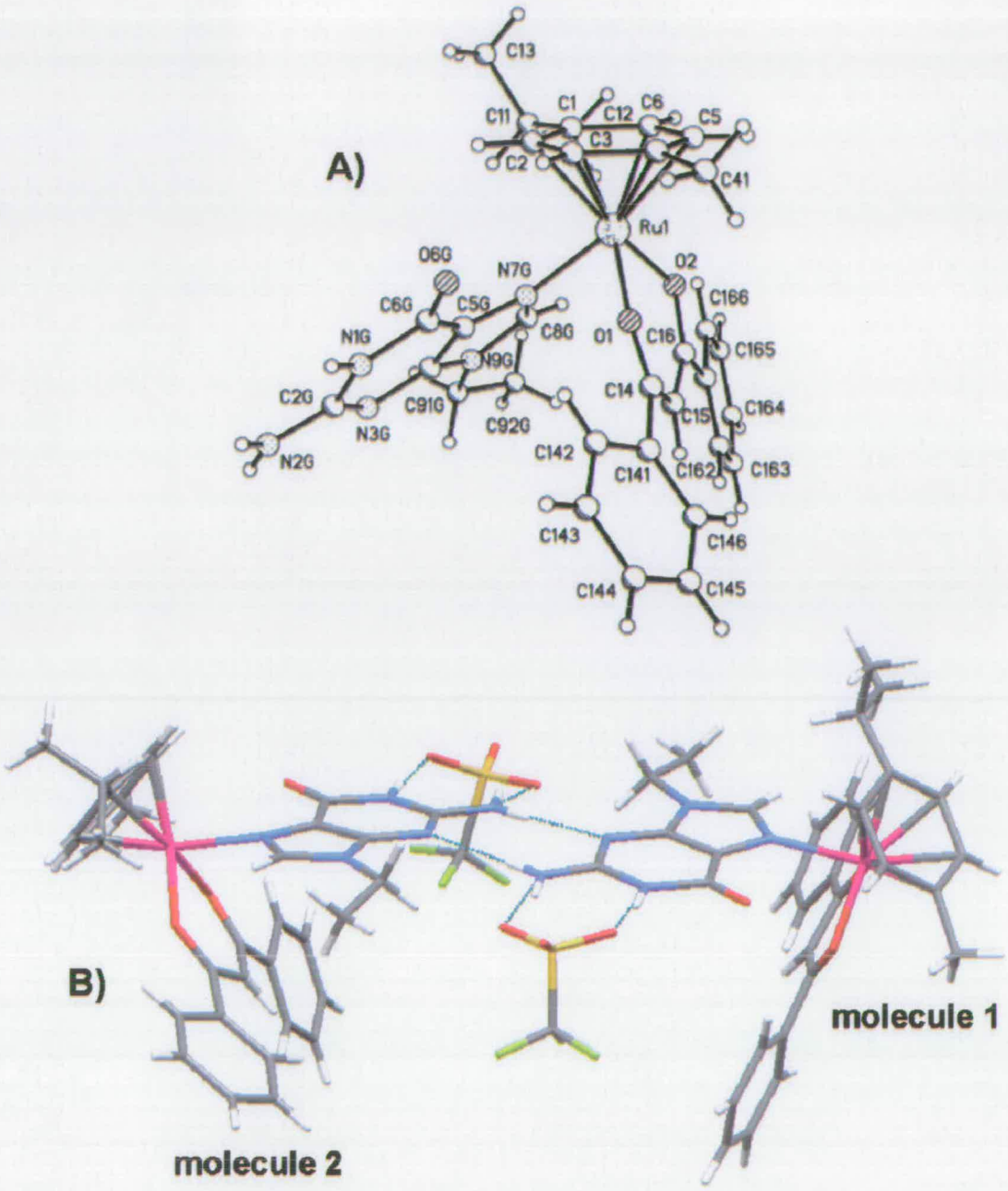

Figure 3.22: X-ray crystal structure of $[(\eta^6\text{-}p\text{-cym})Ru(Ph_2acac)9EtG]CF_3SO_3$ (**3.22**). A: Numbering scheme (anion omitted). B: Formation of dimers between two different molecules *via* hydrogen bonds formed by neighbouring N2H and N3 atoms. The $CF_3SO_3^-$ counter anions show H-bonds with N2H and N1H.

Table 3.10: Selected bond lengths (Å) and angles (°) for [(η^6-*p*-cym)Ru(Ph_2acac)9EtG]CF_3SO_3 (**3.22**).

	X = 1	X = 2
Ru1_X-O1_X	2.060(3)	2.055(3)
Ru1_X-O2_X	2.065(3)	2.080(3)
Ru1_X-N7G_X	2.140(3)	2.126(3)
Ru1_X-C1_X	2.194(3)	2.224(4)
Ru1_X-C2_X	2.148(4)	2.172(4)
Ru1_X-C3_X	2.175(4)	2.172(4)
Ru1_X-C4_X	2.201(3)	2.190(4)
Ru1_X-C5_X	2.182(3)	2.186(4)
Ru1_X-C6_X	2.173(3)	2.171(4)
Ru-centroid[a]	1.651	1.663
O1_X-Ru1_X-O2_X	87.70(11)	86.70(12)
O1_X-Ru1_X-N7G_X	84.10(11)	82.64(12)
O2_X-Ru1_X-N7G_X	82.30(11)	82.59(11)

[a] = measured using Mercury 1.4.

The complex crystallized with two independent molecules in the asymmetric unit (disordered phenyl Ph_2acac ring in molecule 1), which form dimers held together *via* interactions between the N2H and N3 atoms of 9EtG (Figure 3.22B). In addition the $CF_3SO_3^-$ counter anions show H-bonds with N2H and N1H. For the Ph_2acac ligand the Ru – O distances are 2.060(3) Å and 2.065(3) Å for molecule 1 and 2.055(3) Å and 2.080(3) Å for molecule 2, respectively. The Ru – N7(9EtG) distances vary between 2.140(3) Å and 2.126(3) Å for the two structures. The Ru – C(arene) bond distances are in the range of 2.148(4) Å to 2.201(3) Å for molecule 1 and 2.171(4) Å to 2.224(4) Å for molecule 2, with Ru – centroid of 1.65 Å and 1.66 Å, respectively. The packing in the structure is disordered, however, $\pi - \pi$ stacking interactions between neighbouring phenyl rings of Ph_2acac and the *p*-cymene ring are

indicated. Stacking of the arene in molecule 2 is tilted, but involves all atoms, with the shortest distance between C145_1 and C3_2 (3.43 Å) and the longest between C141_1 and carbons C2_2, C1_2 and C6_2, respectively (4.31 – 4.39 Å). The stacking involving the arene in molecule 1 is only partial, where the shortest distances are 3.66 Å (C6_1 – C161_2) and 3.83 Å (C1_1 – C162_2) as well as 3.59 Å (C6_1 – C168_2) and 3.63 Å (C5_1 – C169_2) for the disordered phenyl ring.

3.6.2 Discussion

3.6.2.1 Reactions with guanine bases

With the possibility that the oxygen atoms of the chelating ligands acac, trop and ma might interact unfavourably with the C6O oxygen of guanine (G), it was of interest to study the reactions between complexes [(η^6-*p*-cym)Ru(acac)Cl] (**3.5**), [(η^6-*p*-cym)Ru(trop)Cl] (**3.23**) and [(η^6-*p*-cym)Ru(ma)Cl] (**3.24**) and guanosine (Guo) by ^{1}H NMR spectroscopy.

The rate and extent of these reactions was very similar. By the time the first spectra were recorded (*ca.* 10 min after mixing), *ca.* 75 – 80% of Guo was bound (Figures 3.23, A.3.6, A.3.7). The spectrum for the reaction with **3.5** remained unchanged after 24 h, indicating that equilibrium was reached rapidly.

It is well established that N7 of G is the preferred nucleotide binding site for many transition metals ions [45, 46], and metal-N7 binding has been documented by NMR and Raman spectroscopy and by X-ray structural studies on metal-oligonucleotide complexes [47]. Strong and selective binding to G-N7 on DNA oligomers has been observed for {(η^6-arene)Ru(en)}$^{2+}$ [4, 8], and guanine also binds *via* N7 to {(η^6-arene)Ru(alanine)}$^+$ and {(η^6-arene)$RuCl_2$} complexes [48].

Binding of *O,O*-chelated Ru^{II} *p*-cymene complexes to Guo-N7 was confirmed by ^{1}H NMR pH titrations (Figure A.3.8). No shifts of H8 attributable to protonation

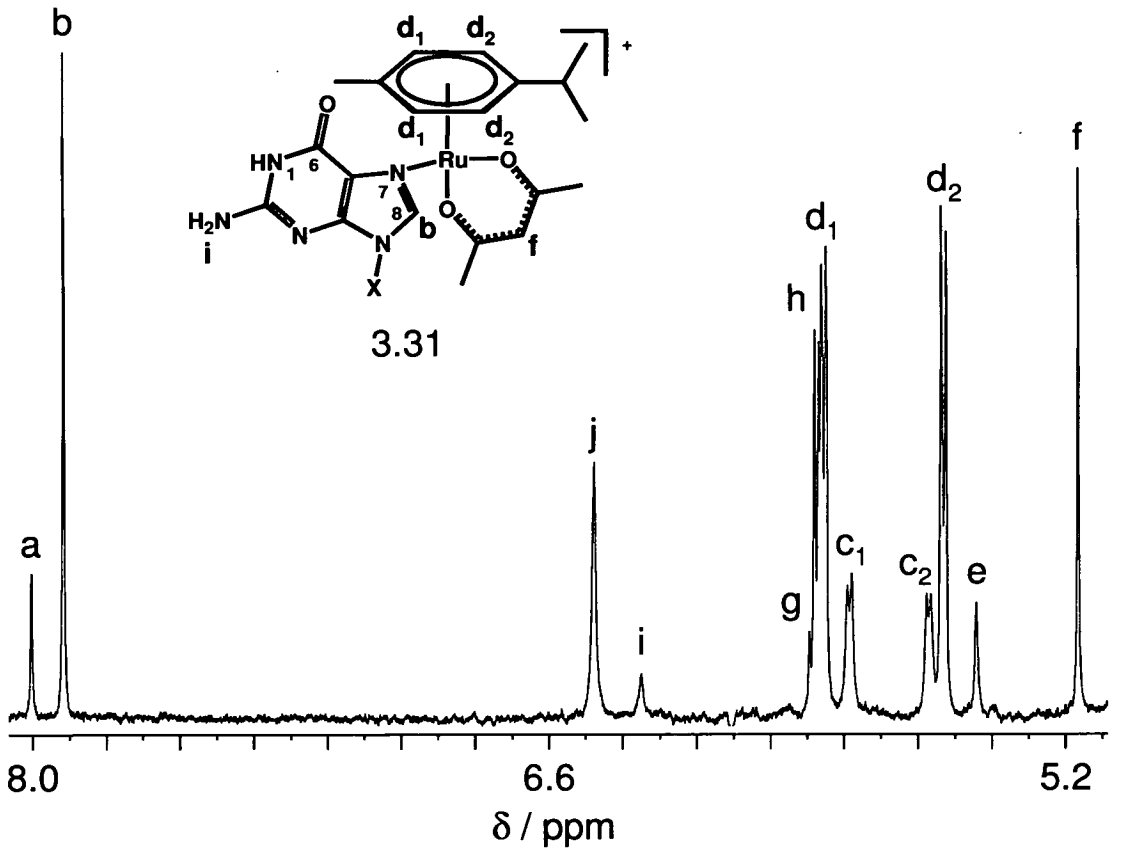

Figure 3.23: Low field region of the ^{1}H NMR spectrum of an equilibrium solution containing guanosine and [(η^6-*p*-cym)Ru(acac)Cl] (**3.5**) in a 1:1 mol ratio in 10% D_2O/ 90% H_2O at pH 5.33 and 298 K. The product is [(η^6-*p*-cym)Ru(acac)Guo-*N7*]$^+$ (**3.31**). Assignments: a = H8 (free Guo); b = H8 (**3.31**); c_1, c_2 = *p*-cymene CH (**3.5**); d_1, d_2 = *p*-cymene CH (**3.31**); e = acac CH (**3.5**); f = acac CH (**3.31**); g = ribose-H1′ (free Guo); h = ribose-H1′ (**3.31**); i = NH_2 (free Guo); j = NH_2 (**3.31**). X corresponds to ribose.

of N7 of Guo were observed above pH 3 (pK_a of N7 of Guo is 2.11 [49]), confirming that the N7 nitrogen is bound to ruthenium and can therefore not be protonated.

Plots of the H8 chemical shifts of adducts [(η^6-*p*-cym)Ru(acac)Guo-*N7*]$^+$ (**3.31**), [(η^6-*p*-cym)Ru(trop)Guo-*N7*]$^+$ (**3.32**) and [(η^6-*p*-cym)Ru(ma)Guo-*N7*]$^+$ (**3.33**) versus pH showed associated pK_a values of 9.25 (**3.31**), 9.07 (**3.32**) and 9.11 (**3.33**), which can be assigned to deprotonation of N1 of coordinated Guo (Figures 3.24, A.3.9 and A.3.10). These pK_a values are comparable and almost identical to the

literature value for free Guo (9.22) [49] and are therefore unexpectedly high for N7-coordinated Guo. The values observed for the respective en complex [8] or for Pt^{II} am(m)ine adducts of guanine derivatives can be *ca.* 1.1 – 1.3 pK_a units lower [50, 51]. These findings are another illustration of the differing electronic effects of the monoanionic *O,O*-chelating ligands studied here compared to am(m)ines.

Another unusual feature of these systems is the observed upfield shift of 0.08 ppm of the H8 signals of coordinated Guo. Metallation at N7 sites of purines by $[(\eta^6\text{-arene})Ru(en)Cl]^+$ complexes [8, 9] and other metal ions usually produces a marked low-field H8 shift of *ca.* 0.3 – 1 ppm [52]. The origin of these shifts is unclear.

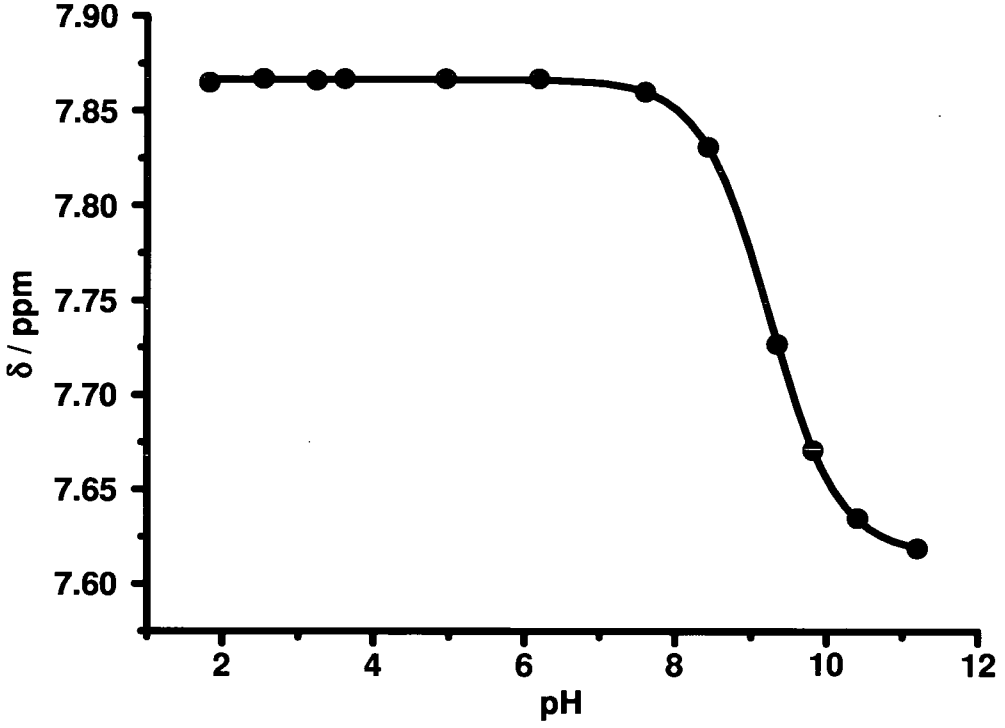

Figure 3.24: Dependence of the ^1H NMR chemical shift of the guanosine H8 resonance of $[(\eta^6\text{-}p\text{-cym})Ru(acac)Guo\text{-}N7]^+$ (**3.31**, 10% D_2O/ 90% H_2O, 298 K) on pH. The line is a computer fit giving pK_a (N1H) = 9.25 ± 0.01.

The X-ray crystal structure of $[(\eta^6\text{-}p\text{-cym})Ru(Ph_2acac)9EtG]CF_3SO_3$ (**3.22**) confirms binding of ruthenium to N7 of 9EtG. The Ru – N7 distances of 2.140(3) Å and 2.126(3) Å are on the higher end of the known range of other Ru^{II} complexes

containing one bound guanine derivative [8, 48, 53, 54, 55]. The C6O – O(acac) distances are 3.267(4) Å and 3.084(4) Å, suggesting that repulsion interactions between these oxygen atoms could be responsible for the decreased affinity of *O,O*-chelated ligands, and acac in particular (*vide infra*), for guanine. In both molecules, the phenyl side-rings are tilted towards the exocyclic C6O oxygen, forming CH···O bonds of 2.93 Å and 2.64 Å, which could help to stabilise the coordination of 9EtG. The formation of $\pi - \pi$ stacking in the structure demonstrates the potential of both the arene- and the phenyl side-rings to be involved in such stabilising interactions.

The reactivity of the hydroxo-bridged dimer $[((\eta^6\text{-}p\text{-cym})\text{Ru})_2(\mu\text{-OD})_3]^+$ (**3.27**) with 9EtG was investigated. Reactions of this dimer with pyrazolate ligands [56] and diphenylphosphine [57] have been reported. However, integration of the new peaks suggested that < 20% of the 9EtG had reacted, illustrating a high stability of the hydroxo-bridged dimer.

Formation of the dimer **3.27** under conditions of biological testing (media at *ca.* pH 7) would be expected to lower the potential activity of **3.26**, decreasing its reactivity towards target sites such as DNA. Therefore incorporation of *O,O*-chelating ligands which form more stable 5- or 6-membered rings provides a strategy for avoiding this reaction pathway.

3.6.2.2 Reactions with adenine bases

The existence of an NH_2 group at the 6 position of adenosine might lead to hydrogen bonding with the oxygen atoms of the *O,O*-chelating ligands, which in turn might lead to stronger binding and a selectivity for adenosine over guanosine.

Reactions between $[(\eta^6\text{-}p\text{-cym})\text{Ru(acac)Cl}]$ (**3.5**), $[(\eta^6\text{-}p\text{-cym})\text{Ru(trop)Cl}]$ (**3.23**) and $[(\eta^6\text{-}p\text{-cym})\text{Ru(ma)Cl}]$ (**3.24**) with adenosine (Ado) all led to the appearance of new signals in the δ 8.65 – 8.2 ppm region, where the H8 and H2

signals of Ado appear (Figures 3.25, A.3.11 and A.3.12). For all three reactions, *ca.* 80% binding of Ado was found at equilibrium after 10 min (unchanged for acac after > 24 h [30]).

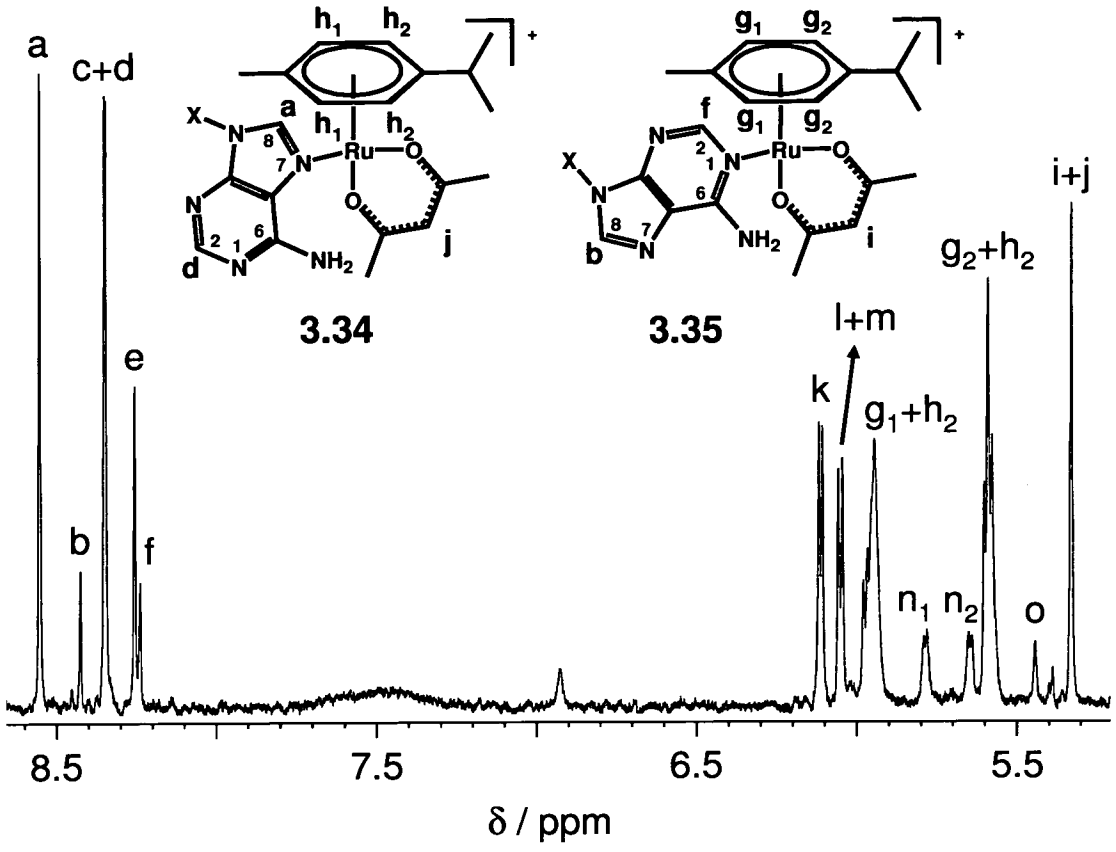

Figure 3.25: Low-field frequency region of the ^{1}H NMR spectrum of a solution containing [(η^6-*p*-cym)Ru(acac)Cl] (**3.5**) and adenosine in a 1:1 mol ratio in 90% H_2O/10% D_2O at pH 5.80 and 298 K. The products are [(η^6-*p*-cym)Ru(acac)Ado-*N7*]$^+$ (**3.34**) and [(η^6-*p*-cym)Ru(acac)Ado-*N1*]$^+$ (**3.35**). Assignments: a = H8 (**3.34**); b = H8 (**3.35**); c = H8, (free Ado); d = H2 (**3.34**); e = H2 (free Ado); f = H2 (**3.35**); g = *p*-cymene CH (**3.35**); h = *p*-cymene CH (**3.34**); i = acac CH (**3.35**); j = acac CH (**3.34**); k = ribose-H1' (**3.34**); l = ribose-H1' (**3.35**); m = ribose-H1' (free Ado); n = *p*-cymene CH (**3.5**); o = acac CH (**3.5**). X corresponds to ribose.

Adenine bases have different binding sites and binding modes. In recent years a number of papers have been published, which deal with binding of Ru^{II} arene complexes to adenine bases [44, 58, 59, 60, 61]. Binding sites identified are N9, N7, N1 and a bidentate chelate involving N1 and N6. The complexes studied were Ru^{II} arenes with 2 or 3 reactive sites and formation of tri- and tetranuclear species appear to be the prevalent binding modes. An example is the structure in Section 3.6.1.7.

The assignment of the products was done using ^1H NMR titrations (Figures 3.26 and 3.27). For adenosine, protonation of N1 occurs at a significantly higher pH (pK_a *ca.* 3.61) than that for N7 (pK_a *ca.* -1.50) [62]. Also, metallation at N7 is known

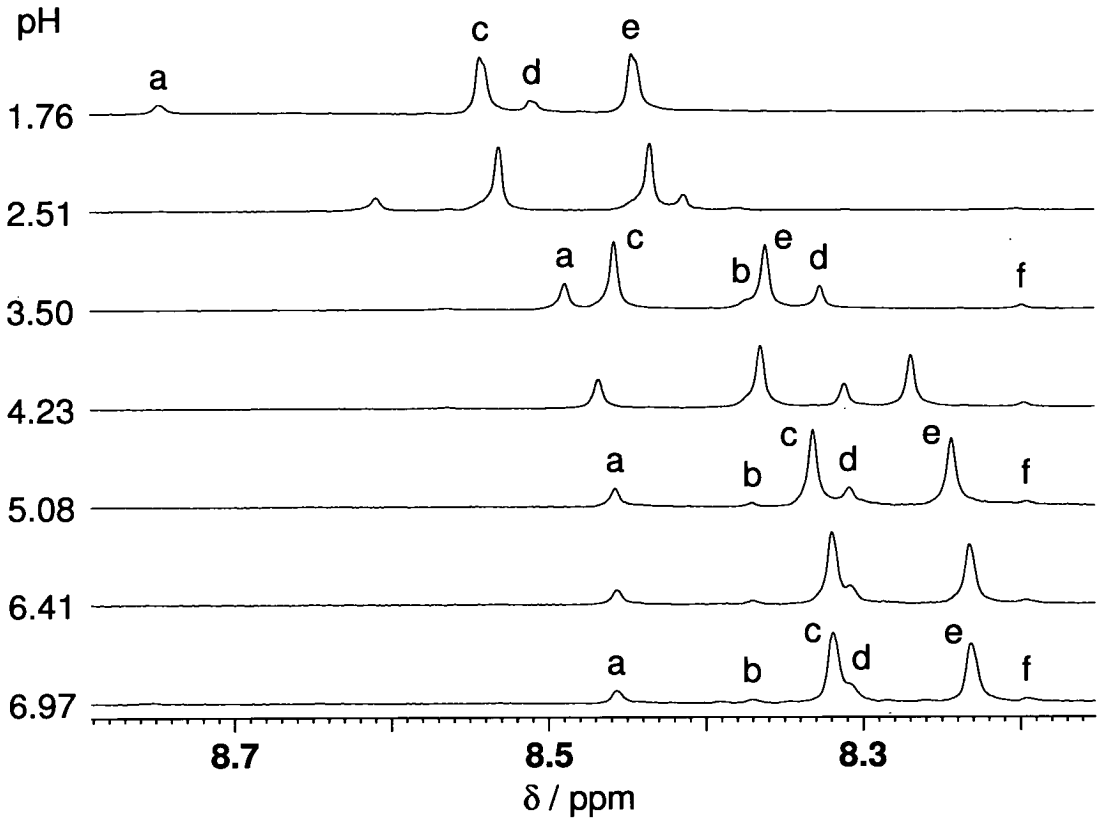

Figure 3.26: Dependence on pH of the low field region of the ^1H NMR spectrum of a solution containing adenosine and [(η^6-*p*-cym)Ru(acac)Cl] (**3.5**) in a 1:1 mol ratio in 10% D_2O/ 90% H_2O at 298 K. The products are [(η^6-*p*-cym)Ru(acac)Ado-*N7*]$^+$ (**3.34**) and [(η^6-*p*-cym)Ru(acac)Ado-*N1*]$^+$ (**3.35**). Assignments: a = H8 (**3.34**); b = H8 (**3.35**); c = H8 (free Ado); d = H2 (**3.34**); e = H2 (free Ado); f = H2 (**3.35**).

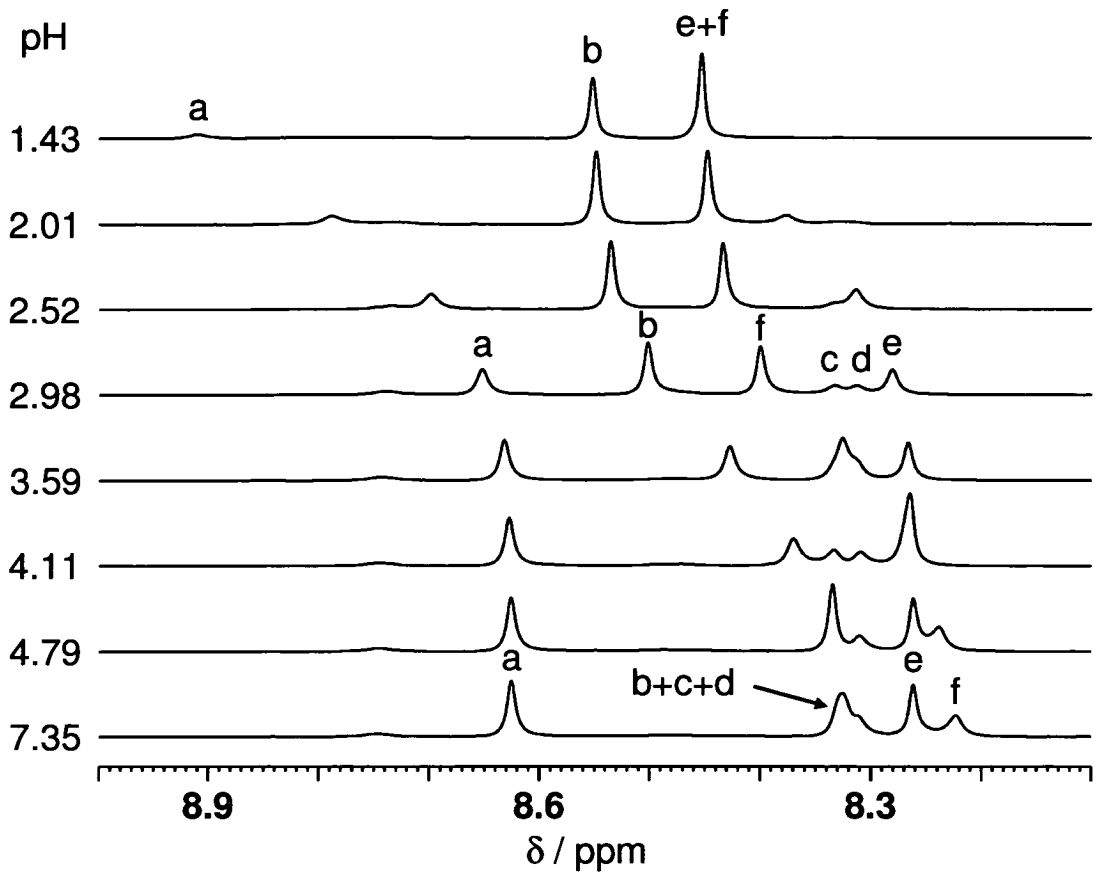

Figure 3.27: Dependence on pH of the low field region of the ^{1}H NMR spectrum of a solution containing adenosine and [(η^6-*p*-cym)Ru(trop)Cl] (**3.23**) in a 1:1 mol ratio in 10% D_2O/ 90% H_2O at 298 K. The products are [(η^6-*p*-cym)Ru(trop)Ado-*N7*]$^+$ (**3.36**) and [(η^6-*p*-cym)Ru(trop)Ado-*N1*]$^+$ (**3.37**). Assignments: a = H8 (**3.36**); b = H8 (free Ado); c = H8 (**3.37**); d = H2 (**3.37**); e = H2 (**3.36**); f = H2 (free Ado).

to acidify the N1 proton, so that the pK_a value for N1 drops [52]. For the acac system, plots of the H8 and H2 ^{1}H NMR chemical shifts for Ado peaks are shown in Figure 3.28. Peaks a and d were assigned to H8 and H2, respectively, of [(η^6-*p*-cym)Ru(acac)Ado-*N7*]$^+$ (**3.34**), since the observed pH-dependent shifts at pH > 4 for peaks within the range 8.46 – 8.74 ppm for H8 and 8.31 – 8.50 ppm for H2 can be attributed to protonation of N1, and peaks b and f were assigned to [(η^6-*p*-cym)Ru(acac)Ado-*N1*]$^+$ (**3.35**). The pK_a value for protonation of N1 in adduct **3.34** was determined to be *ca.* 2.3. That for free adenosine was 3.62, in agreement with

the literature value [62]. For the trop system $\{(\eta^6\text{-}p\text{-cym})Ru(trop)\}^+$, plots of the H8 and H2 ^1H NMR chemical shifts for Ado peaks are shown in Figure 3.29. Similar to the acac system, peaks a and e were assigned to H8 and H2, respectively, of $[(\eta^6\text{-}p\text{-cym})Ru(trop)Ado\text{-}N7]^+$ (**3.36**), and peaks c and d to $[(\eta^6\text{-}p\text{-cym})Ru(trop)Ado\text{-}N1]^+$ (**3.37**). The spectrum for the ma system $\{(\eta^6\text{-}p\text{-cym})Ru(ma)\}^+$ was comparable to that of trop complexes, and pK_a values between 2.1 – 2 were determined for protonation of N1 for the respective adducts (Figure A.3.13).

The H8 and H2 peaks for N7-coordinated Ado, which are sensitive to pH values < 5, were separated by about 0.21 ppm for acac complex (pH = 5.8). For the trop complex this difference increased to *ca.* 0.36 ppm (pH = 7.35) and *ca.* 0.34 ppm (pH = 7.22) for ma. In contrast, the separation of the H8 and H2 peaks of N1-

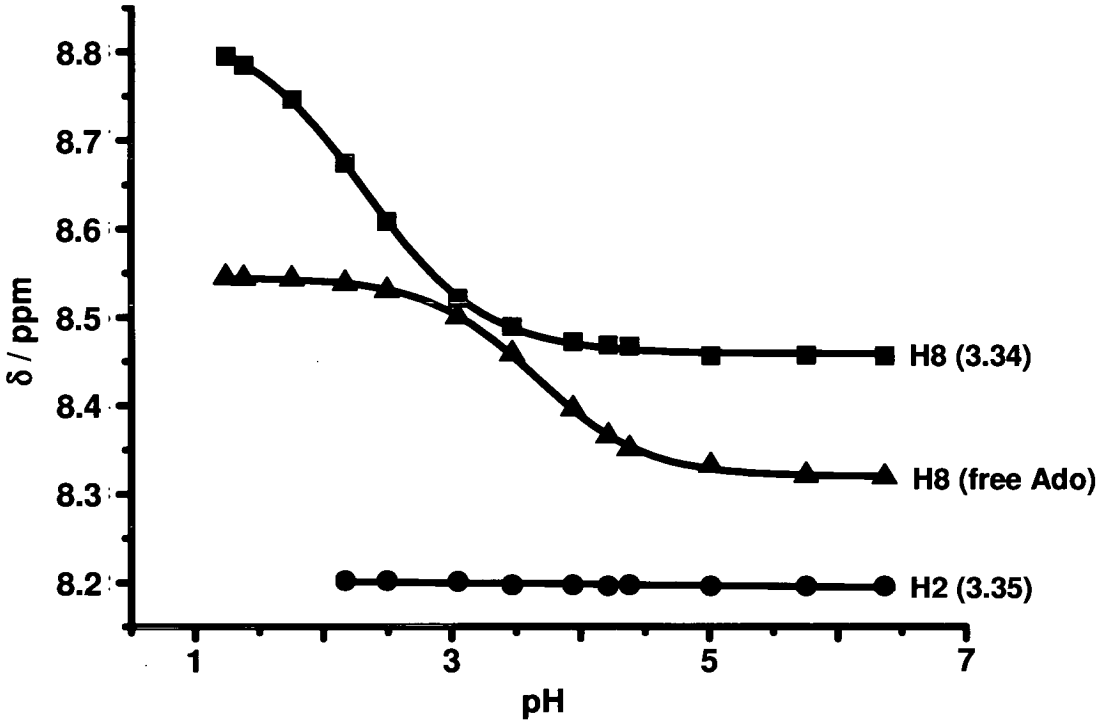

Figure 3.28: Dependence of the H8 and H2 ^1H NMR chemical shifts of adenosine, $[(\eta^6\text{-}p\text{-cym})Ru(acac)Ado\text{-}N7]^+$ (**3.34**) and $[(\eta^6\text{-}p\text{-cym})Ru(trop)Ado\text{-}N1]^+$ (**3.35**) (10% D_2O/ 90% H_2O, 298 K) on pH. The line for H8 (free Ado) is a computer fit giving pK_a (N1H) = 3.62 ± 0.01. For clarity only one plot per species is shown.

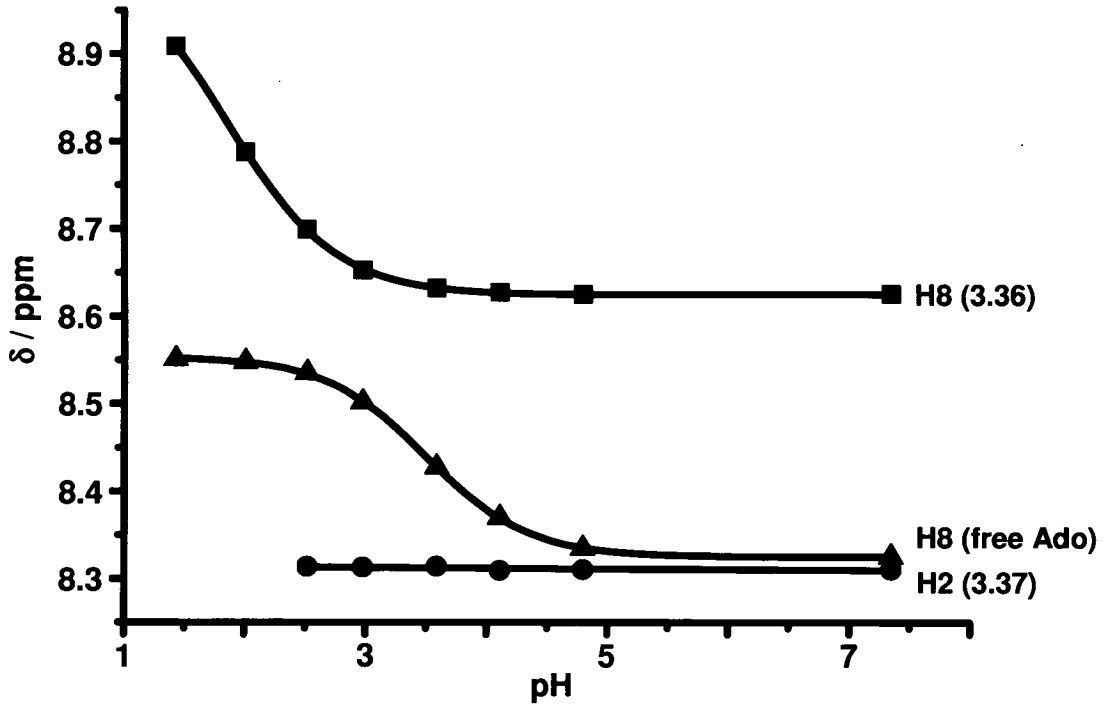

Figure 3.29: Dependence of the H8 and H2 ^{1}H NMR chemical shifts of adenosine, [(η^6-*p*-cym)Ru(trop)Ado-*N7*]$^+$ (**3.36**) and [(η^6-*p*-cym)Ru(trop)Ado-*N1*]$^+$ (**3.37**) (10% D_2O/ 90% H_2O, 298 K) on pH. The line for H8 (free Ado) is a computer fit giving pK_a (N1H) = 3.50 ± 0.01. For clarity only one plot per species is shown.

coordinated Ado for the acac complex is *ca.* 0.18 ppm, which decreased to 0.02 ppm for trop and 0.03 ppm for ma.

In the X-ray crystal structure of [(η^6-*p*-cym)Ru(acac)9EtA]PF_6 (**3.20**), 9EtA is coordinated to the ruthenium *via* the N7 nitrogen, which was suggested to be the predominant binding site in the ^{1}H NMR solution studies. The structure confirms the existence of a strong H-bond between N6H···O(acac) of *ca.* 2.07 Å, which contributes to the stabilisation of this adduct and can account for the significant binding of adenine bases to {(η^6-*p*-cym)Ru(acac)}$^+$. This structure, along with a recently published Ru^{III} structure of *mer, trans*-[$Ru^{III}Cl_3$(Hind)$_2$(made)], where Hind = indazole, made = 9-methyladenine [63], appear to be the only two examples showing mono-dentate coordination of adenine bases to ruthenium. In that Ru^{III} complex, the Ru – N7 bond length is *ca.* 0.04 Å shorter than in the acac structure.

The NH6 – Cl H-bond interactions of 2.386 Å and 2.411 Å, respectively, reported for the ruthenium(III) complex are significantly longer than the H-bond formed between NH6···O(acac).

The nature of the chelate ring appears to have an influence on the N7 : N1 coordination ratios. These were determined from the ^{1}H NMR spectra by integration of the respective Ado H8 and H2 signals as well as the *p*-cymene peaks. For the acac system the ratio N7 : N1 was *ca.* 4.5 : 1 (pH = 5.8), for trop *ca.* 2 : 1 (pH = 7.35) and for ma *ca.* 3 : 1 (pH = 7.22). Consideration of molecular models suggests that N6H···O(acac) H-bonding is more favourable for N7- compared to N1-coordination of 9EtA to {(η^6-*p*-cym)Ru(acac)}$^+$. When acac is replaced by trop (or ma) the N6H-O(trop) distance for binding at N1 is substantially shorter than that for binding at N7, which might contribute to the increased extent of binding to N1. It has been suggested [63] that the involvement of functional groups of adenine in intermolecular hydrogen bond interactions, which lead to self-pairing, can determine the metal-binding site (c.f. Figure 3.21B).

3.6.2.3 Competition between adenosine and guanosine

Having shown that *O,O*-chelated Ru^{II} *p*-cymene complexes can react with both adenosine and guanosine, competition reactions between the two bases in reactions with [(η^6-*p*-cym)Ru(acac)Cl] (**3.5**), [(η^6-*p*-cym)Ru(trop)Cl] (**3.23**) and [(η^6-*p*-cym)Ru(ma)Cl] (**3.24**) were studied (Figures 3.30, A.3.14 and A.3.15).

For all reactions equilibrium was reached by the time the first spectra were recorded (*ca.* 10 min) and separate peaks were observed for free and bound nucleosides indicative of slow exchange on the NMR timescale and strong binding. Table 3.11 shows the relative proportions of the signals observed for Guo-N7, Ado-N7 and Ado-N1 binding, respectively. The data show that binding to both guanosine

and adenosine has been retained under competition. For trop and ma, there is a slight preference for guanosine over the combined Ado-(N7+N1) adducts, whereas for acac binding to adenosine appears to be favoured. The relative binding ratios Ado-N7 :

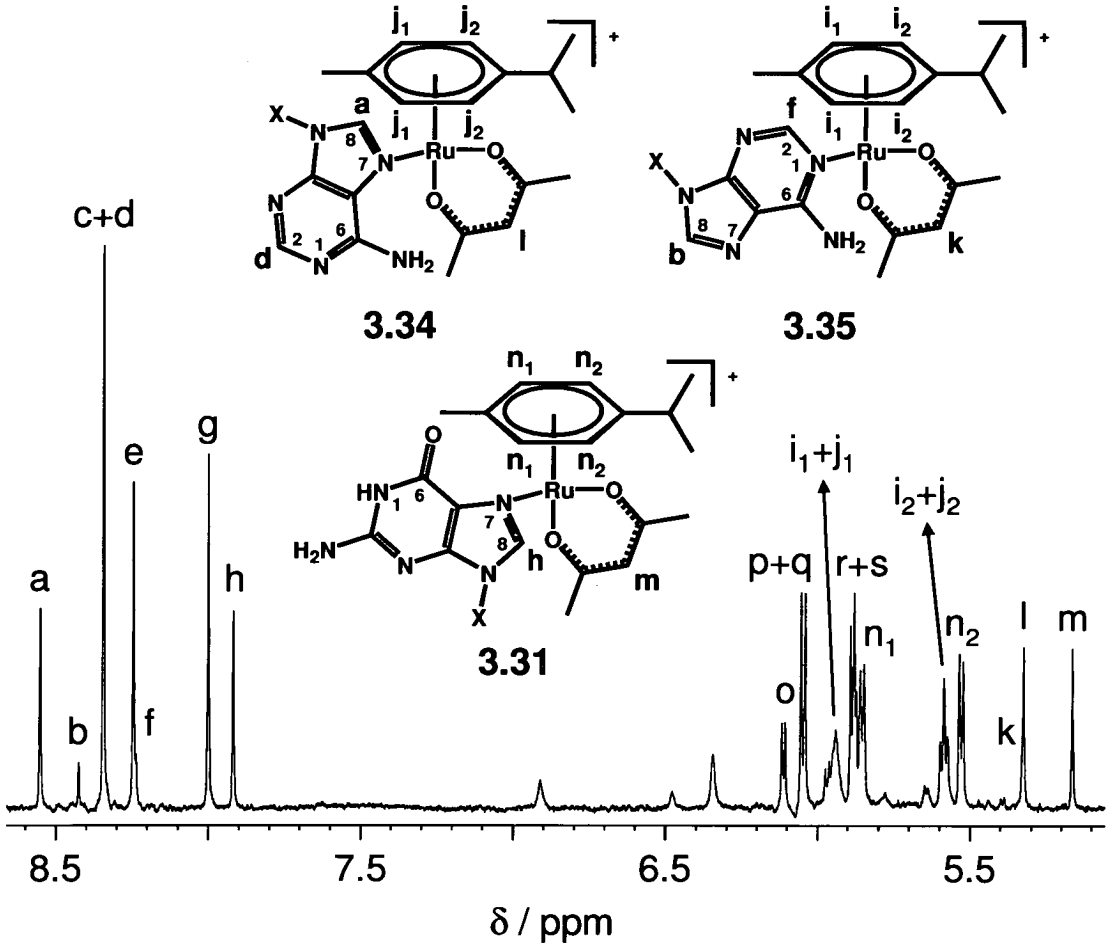

Figure 3.30: Low-field region of the ^{1}H NMR spectrum of a solution containing adenosine, guanosine and [(η^6-*p*-cym)Ru(acac)Cl] (**3.5**) in a 1:1:1 mol ratio in 90% H_2O/10% D_2O at pH 6.63 and 298 K. The products are [(η^6-*p*-cym)Ru(acac)Guo-*N7*]$^+$ (**3.31**), [(η^6-*p*-cym)Ru(acac)Ado-*N7*]$^+$ (**3.34**) and [(η^6-*p*-cym)Ru(acac)Ado-*N1*]$^+$ (**3.35**). Assignments: a = H8 (**3.34**); b = H8 (**3.35**); c = H8 (free Ado); d = H2 (**3.34**); e = H2 (free Ado); f = H2 (**3.35**); g = H8 (free Guo); h = H8 (**3.31**); i = *p*-cymene CH (**3.35**); j = *p*-cymene CH (**3.34**); k = acac CH (**3.35**); l = acac CH (**3.34**); m = acac CH (**3.31**); n = *p*-cymene CH (**3.31**); o = ribose-H1' (**3.34**); p = ribose-H1' (**3.35**); q = ribose-H1' (free Ado); r = ribose-H1' (free Guo); s = ribose-H1' (**3.31**). X corresponds to ribose.

Table 3.11: The relative proportions of adducts formed in a competitive reaction of adenosine and guanosine with complexes [(η^6-*p*-cym)Ru(acac)Cl] (**3.5**), [(η^6-*p*-cym)Ru(trop)Cl] (**3.23**) and [(η^6-*p*-cym)Ru(ma)Cl] (**3.24**) in 90% H_2O/10% D_2O at 298K.

Complex	Chelate	Guo-*N7* : Ado-(*N7*+*N1*)	Ado-*N7* : Ado-*N1*	pH
3.5	acac	1 : 1.25	4 : 1	5.78
3.23	trop	1.3 : 1	2 : 1	6.63
3.24	ma	1.1 : 1	3 : 1	6.22

Ado-N1 were the same as observed for the reactions with adenosine alone. The reason for the preference of Ado by the acac system could be a consequence of the larger bite-angle of the ligand. The result is a wider O – Ru – O angle than for the trop and ma system, which could increase repulsion between the oxygen atom of the ligand and that of the C6O carbonyl of Guo.

However, both Guo and Ado adducts are kinetically labile. Addition of either Ado to a solution of **3.31**, or Guo to a solution of **3.34** and **3.35**, rapidly (*ca.* 10 min) resulted in the same equilibrium mixture of adducts as those obtained when complex **3.5** was reacted directly with Guo or Ado in competition.

3.6.2.4 Reactions with cytidine and thymidine

^{1}H NMR studies of mixtures of **3.5** with the pyrimidine nucleosides cytidine and thymidine showed that no adducts were formed over a pH range of 2.4 – 10.4, in contrast to [(η^6-arene)Ru(en)Cl]$^+$ complexes, for which significant binding to N3 was observed [9]. The lack of binding to the acac complex can be ascribed to unfavourable steric and electronic interactions of the nucleobase carbonyl groups with the acac ligand.

3.7 Conclusions

In conclusion, it was demonstrated that the chelating ligand in cytotoxic complexes of the type $[(\eta^6\text{-arene})Ru(chelate)Cl]^{n+}$ has a major influence on the rate and extent of aquation, on the pK_a of the aqua adduct, and on the rate and selectivity of binding to nucleobases. Replacement of neutral en by anionic *O,O*-chelating ligands increases the rate and extent of hydrolysis, the pK_a of the aqua complex (from 8.25 to over 9 for arene = *p*-cymene), and changes the nucleobase specificity. For complexes containing the H-bond donor en, there is exclusive binding to guanine nucleobases in competitive reactions, and in the absence of guanine there is binding to cytosine or thymidine, but little binding to adenine bases [9]. In contrast, when the chelated ligand is the H-bond acceptor acac, the overall affinity for adenosine can be greater than for guanosine, and there is little binding to cytidine or thymidine. Binding of Ru^{II} arene complexes of acac-type ligands to guanine and adenine was further supported by X-ray crystallographic results.

Furthermore *O,O*-chelating ligands can be used to control the reactivity of Ru^{II} arene complexes. In aqueous solution, $[(\eta^6\text{-}p\text{-cym})Ru(AcO)Cl]$ (**3.26**), which contains a four-membered *O,O*-chelate ring, undergoes hydrolysis with loss of acetate, leading largely to the less reactive hydroxo-bridged dimer $[((\eta^6\text{-}p\text{-cym})Ru)_2(\mu\text{-}OH)_3]^+$ (**3.27**). In contrast, the 5- and 6-membered *O,O*-chelate rings formed by trop, ma and acac in $\{(\eta^6\text{-}p\text{-cym})RuCl\}^+$ complexes are relatively stable in solution.

These findings can now be incorporated into design concepts for organometallic Ru^{II} arene anticancer complexes.

Appendix A.3 contains Tables A.3.1 – 4 and Figures A.3.1 – 15.

3.8 References

[1] Z.Guo, P.J. Sadler, Angew. Chem. Int. Ed. **1999**, *38*, 1512–1531.

[2] Z. Guo, P.J. Sadler, Adv. Inorg. Chem. **2000**, *49*, 183–306.

[3] J. Cummings, R.E. Aird, R. Morris, P. del S. Murdoch, P.J. Sadler, J.F. Smyth, D.I. Jodrell, *Clin. Cancer Res.* **2000**, *6*, 142.

[4] R.E. Morris, R.E. Aird, P. del S. Murdoch, H. Chen, J. Cummings, N.D. Hughes, S. Parsons, A. Parkin, G. Boyd, D.I. Jodrell, P.J. Sadler, *J. Med. Chem.* **2001**, *44*, 3616–3621.

[5] A. Habtemariam, M. Melchart, R. Fernández, S. Parsons, I.D.H. Oswald, A. Parkin, F.P.A. Fabbiani, J.E. Davidson, A. Dawson, R.E. Aird, D.I. Jodrell, P.J. Sadler, *J. Med. Chem.*, in press.

[6] R.E. Aird, J. Cummings, A.A. Ritchie, M. Muir, R.E. Morris, H. Chen, P.J. Sadler, D.I. Jodrell, *Brit. J. Cancer* **2002**, *86*, 1652–1657.

[7] O. Novakova, H. Chen, O. Vrana, A. Rodger, P.J. Sadler, V. Brabec, *Biochemistry* **2003**, *42*, 5497–5500.

[8] H. Chen, J.A. Parkinson, S. Parsons, R.A. Coxall, R.O. Gould, P.J. Sadler, *J. Am. Chem. Soc.* **2002**, *124*, 3064–3082.

[9] H. Chen, J.A. Parkinson, R.E. Morris, P.J. Sadler, *J. Am. Chem. Soc.* **2003**, *125*, 173–186.

[10] F. Wang, H. Chen, S. Parsons, I.D.H. Oswald, J.E. Davidson, P.J. Sadler, *Chem. Eur. J.* **2003**, *9*, 5810–5820.

[11] F. Wang, A. Habtemariam, E.P.L. van der Geer, R. Fernández, M. Melchart, R.J. Deeth, R.E. Aird, S. Guichard, F.P.A. Fabbiani, P. Lozano-Casal, I.D.H. Oswald, D.I. Jodrell, S. Parsons, P.J. Sadler, *Proc. Natl. Acad. Sci. USA* **2005**, *102*, 18269–18274.

[12] J.B. Chaires, *Curr. Opin. Struct. Biol.* **1998**, 314–320.

[13] T.C. Jenkins, *Curr. Med. Chem.* **2000**, *7*, 99–115.

[14] M.A. Bennett, A.K. Smith, *J. Chem. Soc., Dalton Trans.* **1974**, 233–241.

[15] D. Carmona, J. Ferrer, L. A. Oro, M. C. Apreda, C. Foces-Foces, F. H. Cano, J. Elguero and M. L. Jimeno, *J. Chem. Soc., Dalton Trans.*, **1990**, 1463–1476.

[16] J. March, *Advanced Organic Chemistry*, 4th edn., Wiley Interscience, New York, **1992**, 72.

[17] F. Kuhlwein, K. Polborn, W. Beck, *Z. Anorg. Allg. Chem.* **1997**, *623*, 1211–1219.

[18] P. Govindaswamy, S.M. Mobin, C. Thöne, M.R. Kollipara, *J. Organomet. Chem.* **2005**, *690*, 1218–1225.

[19] G. Capper, L.C. Carter, D.L. Davies, J. Fawcett, D.R Russell, *J. Chem. Soc., Dalton Trans.*, **1996**, 1399–1403.

[20] F. Nepveu, F. Jasanada, L. Walz, *Inorg. Chim. Acta* **1993**, *211*, 141–147.

[21] D.C. Ware, H.R. Palmer, P.J. Brothers, C.E.F. Rickard, W.R. Wilson, W.A. Denny, *J. Inorg. Biochem.* **1997**, *68*, 215–224.

[22] M.C. Barret, M.F. Mahon, K.C. Molloy, J.W. Steed, P. Wright, *Inorg. Chem.* **2001**, *40*, 4384–4388.

[23] R. Lang, K. Polborn, T. Severin, K. Severin, *Inorg. Chim. Acta* **1999**, *294*, 62–67.

[24] Z. Grote, R. Scopelliti, K. Severin, *J. Am. Chem. Soc.* **2004**, *126*, 16959–16972.

[25] L. Carter, D.L. Davies, J. Fawcett, D.R. Russell, *Polyhedron* **1993**, *12*, 1599–1602.

[26] D.B. Dell'Amico, F. Calderazzo, L. Labella, F. Marchetti, E. Sbrana, *J. Organomet. Chem.* **2002**, *651*, 52–59.

[27] D.L. Davies, O. Al-Duaij, J. Fawcett, M. Giardiello, S.T. Milton, D.R. Russell, *J. Chem. Soc., Dalton Trans.* **2003**, 4132–4138.

[28] G.R. Desiraju, *Chem. Commun.* **2005**, 2995–3001, and references therein.

[29] T. Arthur, D.R. Robertson, D.A. Tocher, T.A. Stephenson, *J. Organomet Chem.* **1981**, *208*, 389–400.

[30] R. Fernández, M. Melchart, A. Habtemariam, S. Parsons, P.J. Sadler, *Chem. Eur. J.* **2004**, *10*, 5173–5179.

[31] D.L. Davies, J. Fawcett, S.A. Garratt, D.R. Russell, *Organometallics* **2001**, *20*, 3029–3034.

[32] S.K. Mandal, A.R. Chakravarty, *Inorg. Chem.* **1993**, *32*, 3851–3854.

[33] F. Wang, H. Chen, S. Parsons, I.D.H. Oswald, J.E. Davidson, P.J. Sadler, *Chem. Eur. J.* **2003**, *9*, 5810–5820.

[34] H. Shimanouchi, Y. Sasada, *Acta Cryst.* **1973**, *B 29*, 81–90.

[35] L. Cheng, M.A. Khan, D.R. Powell, R.W. Taylor, G.B. Richter-Addo, *Chem. Commun.* **1999**, 1941–1942.

[36] D. A. Tocher, R. O. Gould, T. A. Stephenson, M. A. Bennett, J. P. Ennett, T. W. Matheson, L. Sawyer and V. K. Shah, *J. Chem. Soc., Dalton Trans.* **1983**, 1571–1581.

[37] A.D. Ryabov, *Chem. Rev.* **1990**, *90*, 403–424.

[38] A.F.A. Peacock, A. Habtemariam, R. Fernández, V. Walland, F.P.A. Fabbiani, S. Parsons, R.E. Aird, D.I. Jodrell, P.J. Sadler, *J. Am. Chem. Soc.* **2006**, *128*, 1739–1748.

[39] A.P. Abbott, G. Capper, D.L. Davies, J. Fawcett, D.R. Russell, *J. Chem. Soc., Dalton Trans.* **1995**, 3709–3713.

[40] A.F.A. Peacock, M. Melchart, R.J. Deeth, A. Habtemariam, S. Parsons, P.J. Sadler, unpublished results.

[41] T. Hasegawa, T.C. Lau, H. Taube, W.P. Schaefer, *Inorg. Chem.* **1991**, *30*, 2921–2928.

[42] F. Wang, H. Chen, J. A. Parkinson, P. del S. Murdoch, P. J. Sadler, *Inorg. Chem.* **2002**, *41*, 4509–4523.

[43] L. Dadci, H. Elias, U. Frey, A. Hörnig, U. Koelle, A.E. Merbach, H. Paulus, J.S. Schneider, *Inorg. Chem.* **1995**, *34*, 306–315.

[44] S. Korn, W.S. Sheldrick, *Inorg. Chim. Acta* **1997**, *254*, 85–91.

[45] R.B. Martin, Y.H. Mariam in *Metal Ions Biol. Syst.,* Vol. 8 (Ed.: H. Sigel), Marcel Dekker, New York, **1979**; pp. 57–124.

[46] B. Lippert, *Coord, Chem. Rev.* **2000**, *200-202*, 487–518.

[47] J. Sponer, M. Sabat, L. Gorb, J. Leszczynski, B. Lippert, P. Hobza, *J. Phys. Chem. B* **2000**, *104*, 7535–7544, and references therein.

[48] W.S Sheldrick, S. Heeb, *Inorg. Chim. Acta* **1990**, *168*, 93–100.

[49] H. Sigel, S.S. Massoud, N.A. Corfù, *J. Am. Chem. Soc.* **1994**, *116*, 2958–2971.

[50] K. Inagaki, Y. Kidani, *J. Inorg. Biochem.* **1979**, *11*, 39–47.

[51] G. Schröder, B. Lippert, M. Sabat, C.J.L. Lock, R. Faggiani, B. Song, H. Sigel, *J. Chem. Soc., Dalton Trans.* **1995**, *23*, 3767–3775.

[52] K.H. Scheller, V. Scheller-Krattiger, R.B. Martin, *J. Am. Chem. Soc.* **1981**, *103*, 6833–6839.

[53] P.M. van Vliet, J.G. Haasnoot, J. Reedijk, *Inorg. Chem.* **1994**, *33*, 1934–1939.

[54] H. Chen, J.A. Parkinson, O. Novakova, J. Bella, F. Wang, A. Dawson, R. Gould, S. Parsons, V. Brabec, P.J. Sadler, *Proc. Natl. Acad. Sci. USA*, **2003**, *100*, 14623–14628.

[55] F. Zobi, M. Hohl, I. Zimmermann, R. Alberto, *Inorg. Chem.* **2004**, *43*, 2771–2772.

[56] L.A. Oro, M.P. Garcia, D. Carmona, *Inorg. Chim. Acta* **1985**, *96*, L21–L22.

[57] J.A. Cabeza, F. Mulla, V. Riera, *J. Organomet. Chem.* **1994**, *470*, 173–177.

[58] W.S. Sheldrick, H.S. Hagen-Eckhard, S. Heeb, *Inorg. Chim. Acta* **1993**, *206*, 15–21.

[59] S. Korn, W.S. Sheldrick, *Inorg. Chim. Acta* **1997**, *254*, 85–91.

[60] S. Korn and W.S. Sheldrick, *J. Chem. Soc, Dalton Trans.* **1997**, 2191–2199.

[61] P. Annen, S. Schildberg, W.S. Sheldrick, *Inorg. Chim. Acta* **2000**, *307*, 115–124.

[62] G. Kampf, L.E. Kapinos, R. Griesser, B. Lippert, H. Sigel, *J. Chem. Soc., Perkin Trans. 2* **2002**, 1320–1327.

[63] A. Egger, V.B. Arion, E. Reisner, B. Cebrián-Losantos, S. Soba, G. Trettenhahn, B.K. Keppler, *Inorg. Chem.* **2005**, *44*, 122–132.

Chapter 4
Tethered Ruthenium(II) Arene Complexes

4.1 Introduction

Metal-containing complexes offer potential for applications as anticancer agents [1]. The widely-used platinum-containing anticancer complexes cisplatin and carboplatin are well-known examples. Several ruthenium-containing complexes have been identified as potential antitumour therapeutics [2], and a range of organometallic complexes, metallocenes [3] and more recently ferrocenyl derivatives [4] have shown interesting activity against cancer-cells.

Sadler *et al.* have shown that some organometallic ruthenium(II) arene complexes of the type $[(\eta^6\text{-arene})Ru(en)Cl]^+$, where en is the bidentate chelating ligand ethylenediamine, exhibit promising cytotoxicity, as potent as carboplatin, against various cancer cell lines [5, 6]. These complexes form mono-functional adducts with biomolecules, including DNA bases [7, 8]. In contrast, cytotoxic platinum(II) diam(m)ine complexes, *e.g.* cisplatin, have two reactive sites available and can bind to their target DNA in a bifunctional manner [9]. Recent results suggest that DNA may be an important target site for $\{(\eta^6\text{-arene})Ru(en)\}^{2+}$ complexes [10]. Although some tested bifunctional Ru^{II} arene complexes, containing pyridine and phosphine ligands show poor cytotoxicity against some cancer cell lines [11, 12], it is of interest to investigate ways of introducing bifunctional reactivity into ruthenium(II) arene complexes to increase interactions with potential targets such as DNA, comparable to cisplatin. Other examples of bifunctional cytotoxic compounds include metallocenes, which can also undergo bidentate coordination towards DNA bases [13]. For Ru^{II} arenes, structural differences could lead to a different spectrum of activity and the possibility of coordination to two guanines as has been shown for the fragment $\{(\eta^6\text{-}p\text{-cymene})Ru\}^{2+}$ [14].

The activity of Pt am(m)ine anticancer compounds appears to depend on the presence of hydrogen bond donating NH groups [15]. Similarly, it has been demonstrated that ligands coordinated to Ru^{II} arenes can have a critical role in controlling and promoting interactions with DNA nucleobases [8, 16, 17]. For example, in reactions with such bases, $\{(\eta^6\text{-arene})Ru(en)\}^{2+}$ reacts exclusively with guanine derivatives [8, 11]. This site selectivity appears to be controlled by the NH_2 groups of the en ligand, which can form strong hydrogen bonds with the C6O carbonyl group of guanine bases [18]. It was therefore of interest to incorporate H-bond donors, *e.g. via* an amine group, into bifunctional Ru^{II} arene complexes, since the previously used pyridine and phosphine ligands offer few of these recognition features. However, monodentate NH_2R groups in $[(\eta^6\text{-}p\text{-cymene})Ru(NH_2R)Cl_2]$ and $[(\eta^6\text{-arene})Ru(L\text{-alaMe})Cl_2]$ complexes, where NH_2R = NH_2CMe_3, L-alaMe = L-alanine methyl ester, can undergo substitution reactions [19, 20], and complexes such as $[(\eta^6\text{-mesitylene})Ru(NHR_2)Cl_2]$, where R = Et or Bu, are unstable in solution [21]. For potential anticancer applications, the chemistry of such complexes could be difficult to predict or control. A potential strategy for incorporation of an amine group into a bifunctional ruthenium(II) arene complex, which would be substitutionally inert and add stability to the molecule to prevent decomposition, is to use a tether (Figure 4.1A).

Research on tethered Ru^{II} arene complexes has received increasing attention over the past few years, mainly due to potential applications in catalysis [22 – 27]. Most of the documented examples are bifunctional complexes containing phosphine ligands, which coordinate to ruthenium in a mono-dentate binding mode, and two chloride ligands (Figure 4.1B) [28 – 33]. Tethered Ru^{II} arene complexes containing sulfur [34] and oxygen [35 – 38] are also known. There are examples of tethered Ru^{II} arene compounds in the literature, which chelate *via* two side arms [39, 40] and three [41, 42, 43], so-called coelenterands, which encapsulate the metal centre.

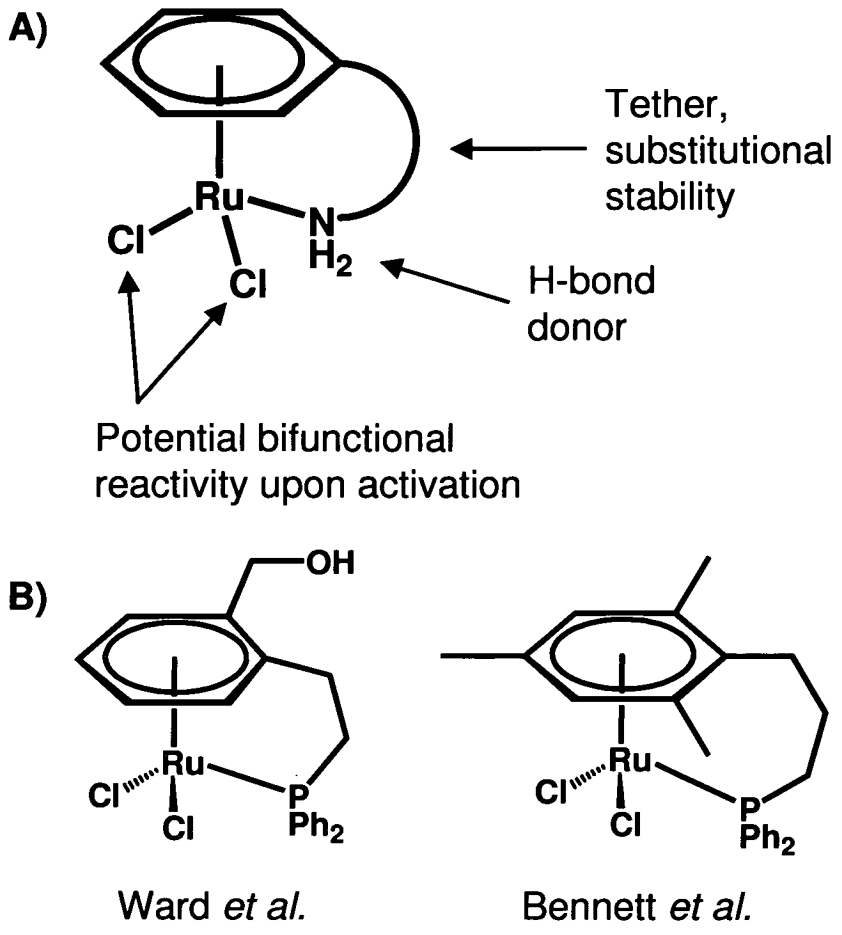

Figure 4.1: Bifunctional tethered ruthenium(II) arene complexes. A: Incorporation of an H-bond donating amine group. B: Tethered complexes synthesised by Ward *et al.* [29] and Bennett *et al.* [30] containing phosphine ligands.

At the start of these studies nitrogen ligands had received very little attention in tethered ruthenium(II) arenes. Reported examples include the above mentioned chelating side-arms [39 – 43], amine tethers, where either one or both remaining binding sites were blocked by phosphorus-containing ligands or 2,2'-bipyridine, respectively [35, 44], and complexes with nitrogen-containing tethered chelating ligands (*e.g.* $[(\eta^6\text{-}C_6H_5(CH_2)_3NH(1S,2S\text{-}CHC_6H_5)_2NSO_2C_6H_4CH_3 - N,N)RuCl]$) for use in catalysis [45, 46].

Here the synthesis and solid state characterisation of novel nitrogen-containing, bifunctional tethered Ru^{II} arene complexes are reported. Aspects of the solution chemistry of these water-soluble molecules and their hydrolysis behaviour have been investigated. Interactions with the DNA base guanine have been studied. Evidence is presented that amine tethered complexes can form bifunctional adducts with guanine, as does cisplatin, both in solution and the solid state.

4.2 Experimental Section

4.2.1 Materials

The ruthenium dimer precursor $[(\eta^6\text{-etb})RuCl_2]_2$ (**4.2**), where etb = ethyl benzoate, was prepared according to a previously published route [29]. 1,3,5-Triaza-7-phosphaadamantane was kindly made available by Anna F. A. Peacock, University of Edinburgh.

All syntheses were performed at ambient temperature, unless indicated otherwise.

4.2.2 Methods

Measurement of pH values was performed as described in Chapter 2.

A description of the pressure vessel and the general experimental set-up can be found in Chapter 2.

In time-course ^1H NMR experiments, the time of dissolution of reactants, or when solutions of all reactants are added together, is taken as t = 0 min. Reactions were then monitored at times t = x min.

In chloride titrations, the concentration of total chloride ($[Cl^-]_t$) is defined as $[Cl^-]_t = 2*[Ru]_t + [Cl^-]_a$, where $[Ru]_t$ = concentration of total Ru, $[Cl^-]_a$ = concentration of added chloride. The amount of free chloride (Cl^-_f) was calculated by integration of the arene proton signals of the di-chloro, the mono-aqua and the diaqua

species. The concentration of free chloride ($[Cl^-]_f$) is defined as $[Cl^-]_f = [Cl^-]_t - [Ru(Cl)H_2O] - [RuCl_2]$.

Hydrolysis equilibrium constants were determined from the following equations. $K_1 = ([Ru(Cl)H_2O] / [RuCl_2]) / [Cl^-]_f$ and $K_2 = ([Ru(H_2O)_2] / ([Ru(Cl)H_2O]) / [Cl^-]_f$.

4.2.3 Preparation of a Ru^{II} ethyl benzoate dimer

[Ethyl-1,4-cyclohexadiene-3-carboxylate] (4.1): Benzoic acid (38.65 g, 0.32 mol) was stirred in dry ethanol (150 ml) at 195 K and liquid ammonia was added (600 ml). Small pieces of sodium (21.7 g, 0.94 mol) were added to the solution over a period of 30 min. Upon decolourisation of the mixture the solution was stirred for a further 1 h, then allowed to reach ambient temperature overnight. The white solid in the vessel was dissolved in chilled water (500 ml), which was then acidified with conc. hydrochloric acid to pH 1-2 and the product extracted three times with diethyl ether. The extractant was dried over anhydrous magnesium sulphate, filtered, and diethyl ether removed on a rotary evaporator. Vacuum distillation of the crude oil gave two products, the first fraction (2.38 g) at 0.10 – 0.08 Torr and 311 – 312 K, the second fraction (33.52 g) at 0.08 Torr and 352 – 355 K. After ^1H NMR, analysis the two fractions were combined and refluxed in dry ethanol (250 ml) and 98% sulfuric acid (17 ml) under argon overnight. The pH was adjusted to *ca.* 8 with sodium hydroxide. Sodium chloride was added for better layer separation and the product extracted with dichloromethane. The organic layer was separated, dried over anhydrous magnesium sulphate, filtered, and the solvents were removed on a rotary evaporator to yield the product (40.73 g). The ^1H NMR spectrum showed that the product still contained ethanol and trace impurities.

$[(\eta^6\text{-etb})RuCl_2]_2$ (4.2): $RuCl_3.xH_2O$ (2.01 g, 9.69 mmol) and **4.1** (7.39 g, 48.56 mmol) were stirred under reflux in dry ethanol (150 ml) under argon for 16 h. The

mixture was allowed to cool, the precipitate filtered and the solid washed with minimal ethanol, then with hexane and diethyl ether. The orange-red solid (2.18 g, 3.38 mmol, 69.8%) was collected by filtration and dried in air. ^{1}H NMR ($CDCl_3$): δ 6.48 (d, 2H, J = 6 Hz), 5.99 (t, 1H, J = 6 Hz), 5.79 (t, 2H, J = 6 Hz), 4.48 (q, 2H, J = 7 Hz), 1.43 (t, 3H, J = 7 Hz).

4.2.4 Preparation of ligands

1-Benzyl-1-*H*-pyrazole (4.3): NaH (60% dispersed in mineral oil) (3.08 g, 77.0 mmol) was dissolved in dry THF (200 ml) and stirred at ambient temperature. Addition of pyrazole (2.56 g, 37.6 mmol) led to gas evolution. The solution was stirred at ambient temperature under argon for 70 h. Drops of EtOH and THF/H_2O were added until gas evolution was quenched. The solvents were removed on a rotary evaporator. The product was dissolved in acetone (40 ml) and benzyl chloride (50 ml) and stirred at ambient temperature for 18 h. The solution was filtered and acetone removed on a rotary evaporator. Excess benzyl chloride was removed by vacuum distillation. Vacuum distillation of the crude product at 0.2 – 0.3 Torr and 342 – 347 K gave the title compound as a colourless liquid (4.17 g, 26.4 mmol, 70.2% yield). ^{1}H NMR (DMSO-d_6): δ 7.81 (d, 1H, J = 2 Hz), 7.46 (d, 1H, J = 2 Hz), 7.33 (t, 2H, J = 7 Hz), 7.27 (t, 1H, J = 7 Hz), 7.20 (d, 2H, J = 7 Hz), 6.27 (t, 1H, J = 2 Hz), 5.33 (s, 2H).

Dipyrido(3,2-*a*:2',3'-*c*)phenazine (4.13): 1,10-Phenanthroline-5,6-dione (0.41 g, 1.96 mmol) and 1,2-diaminobenzene (0.42 g, 3.84 mmol) were dissolved in ethanol (50 ml). The mixture was stirred and heated to reflux for 60 min. The solvent was removed on a rotary evaporator, and the residue was washed with MeOH, then diethyl ether. The light orange solid was dissolved in hot MeOH and the solution stored at 253 K overnight. A fluffy off-white material (243.7 mg, 0.86 mmol, 44.0% yield) was collected by filtration and dried in air. ^{1}H NMR (DMSO-d_6): δ 9.50 (d,

2H, J = 8 Hz), 9.20 (d, 2H, J = 3 Hz), 8.36 (dd, 2H, J = 3.5), 8.05 (dd, 2H, J = 3.5), 7.93 (dd, 2H, J = 4.5 Hz).

2-(2,4,6-Trimethylphenyl)ethylamine (4.24): Mesitylacetonitrile (745.9 mg, 4.68 mmol) in dry diethyl ether (40 ml) was added dropwise over a period of 90 min to a stirred suspension of lithium aluminium hydride (390.8 mg, 10.3 mmol) in dry diethyl ether (30 ml) under argon. The mixture was then refluxed for 240 min and quenched with water. Near-saturation with NaCl of the water layer was followed by acidification with conc hydrochloric acid. The pH was then adjusted to *ca.* 11 with NaOH. The organic layer was separated, the water layer extracted with further diethyl ether, which was then removed on a rotary evaporator. The residue was dissolved in dichloromethane and shaken with water (pH *ca.* 12). The organic layer was separated, dried over anhydrous magnesium sulphate and filtered. The resulting oil was allowed to dry in air, but did not fully solidify. Water, diethyl ether and conc hydrochloric acid were added to form a precipitate, which was filtered and washed with water and diethyl ether. The white solid (384 mg, 1.92 mmol, 41.0%) was dried *in vacuo*. ^{1}H NMR (DMSO-d_6): δ 7.94 (s, 3H), 6.82 (s, 2H), 2.86 – 2.83 (m, 2H), 2.79 – 2.73 (m, 2H), 2.26 (s, 6H), 2.18 (s, 3H). The salt was shaken with diethyl ether and water (pH *ca.* 12) until it dissolved. NaCl was added and the organic layer was separated, then dried over anhydrous magnesium sulphate and filtered. The solvent was removed on a rotary evaporator and the resulting oil was dried in air to form a white solid (289.3 mg, 1.77 mmol, 37.8%), which was collected by filtration and dried in air. ^{1}H NMR ($CDCl_3$): δ 6.85 (s, 2H), δ 2.85 – 2.77 (m, 4H), 2.32 (s, 6H), 2.25 (s, 3H), 1.55 (b, 2H).

(2-Nitroethenyl)-2,3,4,5,6-pentamethylbenzene (4.25): Pentamethylbenzaldehyde (2.00 g, 11.3 mmol), ammonium acetate (2.20 g, 28.5 mmol) and nitromethane (1.53 ml, 28.4 mmol) were added to glacial acetic acid (9.5 ml). The mixture was stirred and heated to 383 K for 300 min under argon. The solvents were removed on a rotary

evaporator. The product was extracted from water with dichloromethane twice, and the organic layer was washed with brine, dried over anhydrous magnesium sulphate and filtered. The solvent was removed on a rotary evaporator. The residue was dissolved in hot ethanol (*ca.* 20 ml) and upon cooling a yellow crystalline material (1.74 g, 7.93 mmol, 70.2% yield) formed in solution, which was collected by filtration and dried in air. ^{1}H NMR ($CDCl_3$): δ 8.28 (d, 1H, J = 14 Hz), 7.06 (d, 1H, J = 14 Hz), 2.29 (s, 3H), 2.27 (s, 6H), 2.25 (s, 6H).

(2,3,4,5,6-Pentamethyl)phenethylamine (4.26): 4.25 (616.4 mg, 2.81 mmol) in dry diethyl ether (40 ml) was added dropwise over a period of 90 min to a stirred suspension of lithium aluminium hydride (392.7 mg, 10.4 mmol) in dry diethyl ether (40 ml) under argon. The mixture was then refluxed for 60 min and quenched with water. The water was acidified with conc hydrochloric acid and the pH then adjusted to *ca.* 12 with NaOH. The organic layer was separated and the solvent removed on a rotary evaporator. The product was dissolved in dichloromethane and shaken with water (pH *ca.* 12). The organic layer was separated, dried over anhydrous magnesium sulphate and filtered. The solvent was removed on a rotary evaporator. The white powder (493.8 mg, 2.58 mmol, 91.1% yield) was collected by filtration and dried in air. ^{1}H NMR ($CDCl_3$): δ 2.90 – 2.81 (m, 4H), 2.29 (s, 6H), 2.24 (s, 3H), 2.23 (s, 6H), 1.41 (b, 2H).

4-(2-Nitroethenyl)-1,1'-biphenyl (4.27): 4-Biphenylcarboxaldehyde (1.39 g, 7.63 mmol), ammonium acetate (1.49 g, 19.3 mmol) and nitromethane (1.03 ml, 19.1 mmol) were added to glacial acetic acid (6.0 ml). The mixture was stirred and heated to 378 K for 180 min. The solvents were removed on a rotary evaporator. The product was extracted from water with dichloromethane twice, and the organic layer washed with brine, dried over anhydrous magnesium sulphate and filtered. The solvent was removed on a rotary evaporator. The residue was dissolved in hot ethanol (*ca.* 70 ml) and water was added until the solution remained opaque. The

solution was heated to dissolve the precipitate and allowed to cool overnight. After removal of a brown residue by filtration, the solvent was removed on a rotary evaporator and the residue dissolved in hot ethanol (*ca.* 20 ml). Upon cooling a yellow-orange precipitate (768 mg, 3.41 mmol, 44.7% yield) precipitated from the solution, which was collected by filtration and dried in air. ^{1}H NMR ($CDCl_3$): δ 8.06 (d, 1H, J = 14 Hz), 7.70 (d, 2H, J = 7.5 Hz), 7.66 – 7.63 (m, 5H), 7.49 (t, 2H, J = 7 Hz), 7.42 (t, 1H, J = 7 Hz).

4-Phenylphenethylamine (4.28): 4.27 (640.5 mg, 2.84 mmol) and lithium aluminium hydride (400.3 mg, 10.6 mmol) were reacted and worked-up as described for **4.26**. After filtering off the magnesium sulphate, the solvent was removed on a rotary evaporator and diethyl ether added. The solution was filtered to remove undissolved material and the solvent removed on a rotary evaporator. The resulting oil was dried in air to form a white powder (270.7 mg, 1.37 mmol, 48.2%), which was collected by filtration and dried in air. ^{1}H NMR ($CDCl_3$): δ 7.59 (d, 2H, J = 7 Hz), 7.55 (d, 2H, J = 8 Hz), 7.46 – 7.42 (m, 2H), 7.34 (t, 1H, J = 7 Hz), 7.29 (d, 2H, J = 8 Hz), 3.03 (t, 2H, J = 7 Hz), 2.81 (t, 2H, J = 7 Hz), 1.52 (b, 2H).

[(1,1'-Biphenyl)-4-yloxy]acetonitrile (4.30): 4-Phenylphenol (3.79 g, 22.3 mmol) and potassium carbonate (2.92 g, 21.1 mmol) were added to dry acetone (40 ml). The mixture was stirred and heated to reflux for 60 min. Bromoacetonitrile (1.71 ml, 24.5 mmol) in dry acetone (30ml) was added over a period of 90 min, and the solution refluxed for a further 60 min and allowed to cool. The solution was filtered, the precipitate rinsed with diethyl ether and the combined solvents were removed on a rotary evaporator. The resulting residue was dissolved in diethyl ether, the solution washed twice with a 5% solution of NaOH in water and once with pure water. The organic layer was dried over anhydrous magnesium sulphate and filtered. The solvent was removed on a rotary evaporator, and the white solid (3.65 g, 17.4 mmol, 82.5% yield) collected by filtration and dried in air. ^{1}H NMR ($CDCl_3$): δ 7.59 (d, 2H,

J = 9 Hz), 7.57 (d, 2H, J = 7.5 Hz), 7.45 (t, 2H, J = 7.5 Hz), 7.36 (t, 1H, J = 7.5 Hz), 7.08 (d, 2H, J = 9 Hz), 4.82 (s, 2H).

4.2.5 Preparation of neutral di-chloro tethered Ru^{II} arene complexes

$[(\eta^6:\eta^1\text{-}C_6H_5(CH_2)_3NH_2)RuCl_2]$ (4.4). *Method A*: **4.2** (372.4 mg, 0.58 mmol) and 3-phenyl-1-propylamine (148.5 mg, 1.10 mmol) were dissolved in 1,2-dichloroethane (50 ml). A few drops of THF were added and the solution stirred for 60 min. The solution was then heated to reflux for 90 h under argon. The solvents were removed on a rotary evaporator and the product extracted with large amounts of methanol, which was concentrated on a rotary evaporator until precipitation of the product occurred. Diethyl ether was added and the solution was stored at 253 K overnight. The yellow-orange microcrystalline solid (129.2 mg, 0.42 mmol, 42.1% yield) was collected by filtration, washed with diethyl ether and dried in air. ^{1}H NMR ($CDCl_3$): δ 5.88 (t, 2H, J = 6 Hz), 5.73 (t, 1H, J = 6 Hz), 5.16 (d, 2H, J = 6 Hz), 3.22 (b, 2H), 2.95 (m, 2H, J = 5.5 Hz), 2.49 (t, 2H, J = 6 Hz), 2.20 (m, 2H).

Method B: **4.2** (514.2 mg, 0.80 mmol) and 3-phenyl-1-propylamine (0.23 ml, 1.60 mmol) were dissolved in 1,2-dichloroethane (20 ml) in the pressure vessel and stirred for 50 min. Additional 1,2-dichloroethane (60 ml) and THF (2 ml) were added and the solution was degassed with argon for 30 min. The vessel was locked and the solution heated to 393 K for 22 h. The solvent was removed on a rotary evaporator, the residue was washed with acetone and the product extracted with hot MeOH. The solvent was concentrated to *ca.* 15 ml on a rotary evaporator and a red microcrystalline solid (327.6 mg) was obtained by filtration. The filtrate and the acetone washing were combined, the solvents removed on a rotary evaporator and the residue washed with diethyl ether, then acetone. The product was extracted using hot MeOH. The solution was concentrated to yield more solid (54.9 mg). The two portions were combined (382.5 mg, 1.25 mmol, 78.1% yield), washed with diethyl

ether and dried in air. Elemental analysis: calculated for $C_9H_{13}NRuCl_2$: C, 35.19; H, 4.27; N, 4.56. Found: C, 35.45; H, 3.85; N, 4.51%.

[(η^6:η^1-$C_6H_5(CH_2)_2NH_2$)$RuCl_2$] (4.5). *Method A*: **4.2** (420.5 mg, 0.65 mmol) and 2-phenethylamine (150.0 mg, 1.24 mmol) were dissolved in 1,2-dichloroethane (50 ml). A few drops of THF were added and the solution stirred for 60 min. The solution was then heated to reflux for 41 h under argon. The solvents were removed on a rotary evaporator and the product extracted with copious amounts of methanol, which was concentrated on a rotary evaporator until precipitation occurred. Diethyl ether was added and the solution stored at 253 K for 2 d. The orange microcrystalline solid (182.8 mg, 0.62 mmol, 50.4% yield) was collected by filtration, washed with diethyl ether and dried in air. ^{1}H NMR ($CDCl_3$): δ 5.94 (t, 2H, J = 5.5 Hz), 5.53 (t, 1H, J = 5.5 Hz), 5.22 (d, 2H, J = 5.5 Hz), 3.90 (m, 2H, J = 5.5 Hz), 3.60 (b, 2H), 2.84 (m, 2H, J = 6.5 Hz).

Method B: **4.2** (146.7 mg, 0.23 mmol) and 2-phenethylamine (57 μl, 0.46 mmol) were dissolved in 1,2-dichloroethane (30 ml) in the pressure vessel and stirred for 40 min. THF (1 ml) was added and the solution was degassed with argon for 30 min. The vessel was locked and the solution heated to 393 K for 15 h. The solvent was removed on a rotary evaporator, the residue was washed with diethyl ether and extracted with hot MeOH. The solvent was removed on a rotary evaporator, the residue washed with acetone to leave a red-brown microcrystalline solid (98.0 mg, 0.33 mmol, 73.4% yield), which was collected by filtration, washed with diethyl ether and dried in air. Elemental analysis: calculated for $C_8H_{11}NRuCl_2$: C, 32.78; H, 3.78; N, 4.78. Found: C, 33.08; H, 3.83; N, 4.76%.

[(η^6:η^1-$C_6H_5O(CH_2)_2NH_2$)$RuCl_2$] (4.6): 4.2 (202.7 mg, 0.32 mmol) and 2-phenoxyethylamine (82 μl, 0.63 mmol) were dissolved in 1,2-dichloroethane (25 ml) in the pressure vessel and stirred for 50 min. More 1,2-dichloroethane (15 ml) and THF (1 ml) were added and the solution was degassed with argon for 30 min. The

vessel was locked and the solution heated to 393 K for 18 h. The solvent was removed on a rotary evaporator, the residue was washed with diethyl ether, then acetone and extracted with hot MeOH. After filtration, the solvent was concentrated to *ca.* 12 ml on a rotary evaporator and a red microcrystalline solid (93.8 mg) was obtained by filtration. The filtrate and the acetone washing were combined, the solvents removed on a rotary evaporator, and the residue washed with diethyl ether, then acetone. The product was extracted using hot MeOH. The solution was concentrated, then heated to dissolve the product and allowed to cool to ambient temperature. After two days, X-ray quality crystals (13.6 mg) had formed, which were collected by filtration. The two portions were combined (107.4 mg, 0.35 mmol, 55.2% yield), washed with diethyl ether and dried in air. ^{1}H NMR ($CDCl_3$): δ 5.93 (t, 2H, J = 6 Hz), 5.62 (t, 1H, J = 5.5 Hz), 5.28 (d, 2H, J = 6 Hz), 4.51 (m, 2H, J = 4 Hz), 3.48 (b, 2H), 3.08 (m, 2H). Elemental analysis: calculated for $C_8H_{11}NORuCl_2$: C, 31.08; H, 3.59; N, 4.53. Found: C, 31.37; H, 3.21; N, 4.51%.

[(η^6:η^1-$C_6H_5(CH_2)C_5H_4N$)$RuCl_2$] (4.7): **4.2** (252.3 mg, 0.39 mmol) and 2-benzylpyridine (0.13 ml, 0.78 mmol) were dissolved in 1,2-dichloroethane (25 ml) in the pressure vessel and stirred for 60 min. More 1,2-dichloroethane (15 ml) and THF (1 ml) were added and the solution was degassed with argon for 30 min. The vessel was locked and the solution heated to 393 K for 18 h. An orange-brown microcrystalline product was isolated by filtration, the solvent was removed on a rotary evaporator, the residue was washed with diethyl ether, then acetone. The two products were combined, washed with acetone, then diethyl ether to leave an orange-brown solid (243.5 mg, 0.71 mmol, 91.2% yield), which was dried in air. ^{1}H NMR ($CDCl_3$): δ 8.18 (d, 1H, J = 6 Hz), 7.79 (t, 1H, J = 8 Hz), 7.31 – 7.25 (t + d, 1H + 1H), 6.11 (t, 2H, J = 6 Hz), 5.54 (t, 1H, J = 5.5 Hz), 5.51 (d, 2H, J = 5.5 Hz), 4.28 (s, 2H). Elemental analysis: calculated for $C_{12}H_{11}NRuCl_2$: C, 42.24; H, 3.25; N, 4.11. Found: C, 42.24; H, 3.03; N, 4.05%.

[(η^6:η^1-$C_6H_5(C_6H_4)NH_2$)$RuCl_2$] (4.8). *Method A*: **4.2** (174.0 mg, 0.27 mmol) and 2-aminobiphenyl (86.3 mg, 0.51 mmol) were dissolved in 1,2-dichloroethane (15 ml) and the solution stirred for 35 min. More 1,2-dichloromethane (35 ml) and a few drops of THF were added and the solution then heated to reflux for 17.5 h under argon. The solution was concentrated on a rotatory evaporator to *ca.* 20 ml and the solution stored at 253 K overnight. A yellow-brown powder (47.8 mg, 0.14 mmol, 27.5% yield) was collected by filtration, washed with acetone and diethyl ether and dried in air. ^{1}H NMR (DMSO-d_6): δ 7.39 (d, 1H, J = 7 Hz), 7.17 (t, 1H, J = 7 Hz), 6.80 (d, 1H, J = 8 Hz), 6.68 (t, 1H, J = 7.5 Hz), 6.23 (d, 2H, J = 5.5 Hz), 6.14 (t, 1H, J = 5 Hz), 5.95 (t, 2H, J = 5.5 Hz), 5.41 (s, 2H).

Method B: **4.2** (426.8 mg, 0.66 mmol) and 2-aminobiphenyl (231.0 mg, 1.37 mmol) were dissolved in 1,2-dichloroethane (60 ml) in the pressure vessel and stirred for 30 min. THF (2 ml) was added and the solution degassed with argon for 40 min. The vessel was locked and the solution heated to 393 K for 17 h. A dark orange-brown microcrystalline product (385.7 mg, 1.13 mmol, 85.3% yield) was collected by filtration, washed with acetone, methanol and diethyl ether and dried in air. Elemental analysis: calculated for $C_{12}H_{11}NRuCl_2$: C, 42.24; H, 3.25; N, 4.11. Found: C, 41.77; H, 2.94; N, 3.96%.

[(η^6:η^1-$C_6H_5(CH_2)C_3H_3N_2$)$RuCl_2$] (4.9): 4.2 (148.1 mg, 0.23 mmol) and **4.3** (73.1 mg, 0.46 mmol) were dissolved in 1,2-dichloroethane (30 ml) in the pressure vessel and stirred for 45 min. THF (1 ml) was added and the solution degassed with argon for 50 min. The vessel was locked and the solution heated to 393 K for 18 h. The solvent was removed on a rotary evaporator, resulting in dark orange-brown microcrystalline and black residues, which were washed with diethyl ether and partially extracted with hot MeOH. Upon filtration, the black material was washed out of the flask, leaving some of the product (54.2 mg, 0.16 mmol, 35.7% yield) behind, which was collected by filtration, washed with acetone, then diethyl ether

and dried in air. Methanol from the extraction was removed on a rotary evaporator, resulting in a yellow-green powder (17.5 mg, 0.05 mmol, 11.5% yield), which was collected by filtration and dried in air. ^{1}H NMR ($CDCl_3$): δ 7.65 (d, 1H, J = 3 Hz), 7.44 (d, 1H, J = 2 Hz), 6.50 (t, 1H), 6.17 (t, 2H, J = 6 Hz), 5.67 (t, 1H, J = 5.5 Hz), 5.54 (d, 2H, J = 6 Hz), 5.06 (s, 2H). Elemental analysis: calculated for $C_{10}H_{10}N_2RuCl_2$: C, 36.38; H, 3.05; N, 8.48. Found: C, 35.99; H, 2.71; N, 8.25%.

[(η^6:η^1-$C_6H_2(CH_3)_3(CH_2)_2NH_2$)$RuCl_2$] (4.29): 4.2 (181.6 mg, 0.28 mmol) and **4.24** (92.0 mg, 0.56 mmol) were dissolved in 1,2-dichloroethane (35 ml) and THF (1 ml) in the pressure vessel and stirred for 45 min. An orange-brown precipitate formed and the solution was degassed with argon for 45 min. The vessel was locked and the solution heated to 393 K for 16 h. The orange solution was filtered and the solvent was removed on a rotary evaporator. The residue was washed with diethyl ether and extracted with hot MeOH, which was then removed on a rotary evaporator to produce an oily residue. Trituration with diethyl ether and removal of it on a rotary evaporator resulted in an orange powder (90.6 mg, 0.27 mmol, 48.0% yield), which was collected by filtration and dried in air. ^{1}H NMR in DMSO-d_6 showed the presence of up to five species containing the {(η^6:η^1-$C_6H_2(CH_3)_3(CH_2)_2NH_2$)Ru}$^{2+}$ fragment (*vide infra*). Elemental analysis: calculated for $C_{11}H_{17}NRuCl_2$: C, 39.41; H, 5.11; N, 4.18. Found: C, 38.58; H, 5.18; N, 3.96%.

4.2.6 Preparation of tethered Ru^{II} arene complexes containing non-chloride monodentate ligands

[(η^6:η^1-$C_6H_5(CH_2)_3NH_2$)$Ru(NO_3)_2$] (4.10): 4.4 (110.3 mg, 0.36 mmol) and silver nitrate (121.9 mg, 0.72 mmol) were dissolved in water (25 ml) and the solution stirred for 150 min. After filtration, the solvent was removed on a rotary evaporator and the product extracted with water. Filtration and removal of the solvent on a rotary evaporator yielded an orange powder (121.5 mg, 0.34 mmol, 93.9% yield),

which was collected by filtration, washed with diethyl ether and dried in air. ^{1}H NMR (90% H_2O/ 10% D_2O, pH 4.10): δ 6.07 – 6.02 (m, 3H), 5.43 (d, 2H, J = 6 Hz), 3.96 (b, 2H), 2.97 (m, 2H), 2.57 (t, 2H, J = 6 Hz), 2.30 (m, 2H).

[(η^6:η^1-$C_6H_5(CH_2)_3NH_2$)Ru(9EtG)$_2$](PF_6)$_2$ (4.11a): 4.10 (43.8 mg, 122 μmol) and 9EtG (47.2 mg, 264 μmol) were dissolved in methanol (15 ml) and the mixture stirred for 20 h. The solution was concentrated to *ca.* 5 ml on a rotary evaporator and heated to dissolve a greenish precipitate. Addition of NH_4PF_6 (177.5 mg, 1.09 mmol) was followed by addition of diethyl ether, which led to the formation of a greenish precipitate and the solution was stored at ambient temperature overnight. The light green powder (98.1 mg) was collected by filtration, washed with diethyl ether and dried in air. ^{1}H NMR (D_2O, pH* 6.56): δ 8.25 (s, 1H), 5.88 (t, 2H, J = 6 Hz), 5.81 (t, 1H, J = 6 Hz), 5.79 (d, 2H, J = 6 Hz), 5.42 (m, 1H), 4.17 – 4.03 (m, 4H), 2.73 (m, 2H), 2.65 (m, 2H), 2.32 (m, 2H), 1.33 (t, 3H, J = 7 Hz). Crystals suitable for X-ray crystallography, which diffracted poorly, were grown by slow evaporation of acetone at ambient temperature. However, they contained 2xNO_3 as the counter anions. Elemental analysis suggested PF_6^- to be the predominant counter anion though. Elemental analysis: calculated for $C_{23}H_{31}N_{11}O_2RuP_2F_{12}$: C, 31.23; H, 3.53; N, 17.42. Found: C, 31.94; H, 3.57; N, 19.55%.

[(η^6:η^1-$C_6H_5(CH_2)_3NH_2$)Ru(9EtG)$_2$](CF_3SO_3)$_2$ (4.11b): This product was made for crystallisation purposes only. **4.4** (37.9 mg, 123 μmol) and 9EtG (51.4 mg, 287 μmol) were dissolved in methanol (25 ml) and the mixture stirred for 22 h. The solution was concentrated to *ca.* 10 ml and $NaCF_3SO_3$ (176.3 mg, 1.02 mmol) was added. The solvent was removed on a rotary evaporator and the product extracted with acetone. The solution was filtered, the solvent removed on a rotary evaporator and a yellow-green powder (228.4 mg) was collected, washed with diethyl ether and dried in air. Before crystallisation, the powder was washed with a minimum of ethanol to dissolve the excess $NaCF_3SO_3$. The solution was filtered and the then

yellow powder washed with diethyl ether. X-ray diffraction quality crystals were grown from diffusion of diethyl ether into an acetone solution containing **4.11b** at ambient temperature.

$[(\eta^6{:}\eta^1\text{-}C_6H_5(CH_2)_3NH_2)Ru(9EtG)NO_3]PF_6$ (4.12): 4.10 (46.7 mg, 130 μmol) and 9EtG (20.0 mg, 112 μmol) were dissolved in methanol (12 ml) and the mixture stirred for 20 h. A yellow precipitate formed and the solution was concentrated to *ca.* 7 ml on a rotary evaporator and heated to dissolve the precipitate. Addition of NH_4PF_6 (187.2 mg, 1.15 mmol) followed by addition of diethyl ether, led to formation of a yellow-brown precipitate, and the solution was stored at ambient temperature for overnight. The precipitate (61.9 mg) was collected by filtration, washed with diethyl ether and dried in air. ^{1}H NMR (D_2O, pH* 5.71): δ 8.17 (s, 1H), 6.17 (t, 1H, J = 6 Hz), 5.79 (m, 1H), 5.62 (d, 1H, J = 6 Hz), 5.48 – 5.46 (m, 2H), 4.72 (m, 1H), 4.16 (q, 2H, J = 7.5 Hz), 3.70 (m, 1H), 3.25 – 3.21 (m, 1H), 2.96 – 2.90 (m, 1H), 2.74 – 2.68 (m, 1H), 2.47 – 2.28 (m, 3H), 1.44 (t, 3H, J = 7 Hz). Elemental analysis: calculated for $C_{16}H_{22}N_7O_4RuPF_6$: C, 30.87; H, 3.56; N, 15.75. Found: C, 30.81; H, 3.58; N, 15.24%.

$[(\eta^6{:}\eta^1\text{-}C_6H_5(CH_2)_3NH_2)Ru(P(C_6H_5)_3)Cl]PF_6$ (4.22): Triphenylphosphine (41.4 mg, 0.16 mmol) in MeOH (5 ml) was added dropwise over a period of 15 min to a stirred solution of **4.4** (50.8 mg, 0.17 mmol) in MeOH (20 ml). The solution was stirred for 24.5 h. NH_4PF_6 (108.9 mg, 0.67 mmol) was added and the solvent removed on a rotary evaporator. The residue was washed with diethyl ether, MeOH (8 ml) was added and the solution was heated to dissolve the material. Upon cooling to ambient temperature a dark orange microcrystalline product (73.6 mg, 0.11 mmol, 68.7% yield) formed, which was collected by filtration, washed with methanol, then diethyl ether and dried in air. ^{1}H NMR (DMSO-d_6): δ 7.62 – 7.58 (m, 3H), 7.56 – 7.52 (m, 4H), 7.49 – 7.45 (m, 4H), 6.28 (t, 1H, J = 6 Hz), 6.21 (d, 1H, J = 6 Hz), 5.81 (t, 1H, J = 5.5 Hz), 5.09 (d, 1H, J = 6 Hz), 4.41 (b, 1H), 4.27 (q, 1H, J = 5 Hz), 2.98

(b, 1H), 2.75 – 2.66 (m, 2H), 2.53 – 2.47 (m, 1H), 2.42 – 2.36 (m, 1H), 2.13 – 2.07 (m, 1H), 2.04 – 1.96 (m, 1H). Elemental analysis: calculated for $C_{27}H_{28}NRuClP_2F_6$: C, 47.76; H, 4.16; N, 2.06. Found: C, 47.94; H, 4.04; N, 2.24%.

$[(\eta^6:\eta^1\text{-}C_6H_5(CH_2)_3NH_2)Ru(PN_3C_6H_{12})Cl]PF_6$ (4.23): 1,3,5-Triaza-7-phosphaadamantane (29.6 mg, 0.20 mmol) in MeOH (5 ml) was added dropwise over a period of 15 min to a stirred solution of **4.4** (64.5 mg, 0.21 mmol) in MeOH (20 ml). The solution was stirred 25 h. NH_4PF_6 (144.4 mg, 0.89 mmol) was added and the solution removed on a rotary evaporator. The residue was washed with diethyl ether, MeOH (10 ml) was added and heated to dissolve the material. Upon cooling to ambient temperature a yellow powder (73.4 mg, 0.13 mmol, 64.0% yield) formed, which was collected by filtration, washed with methanol, then diethyl ether and dried in air. ^{1}H NMR (DMSO-d_6): δ 6.17 (d, 1H, J = 6 Hz), 6.06 (q, 1H, J = 5 Hz), 5.85 (t, 1H, J = 6 Hz), 5.56 (t, 1H, J = 5.5 Hz), 5.16 (d, 1H, J = 5.5 Hz), 4.45 (s, 6H), 4.31 (b, 1H), 4.23 (s, 6H), 4.13 (b, 1H), 2.56 – 2.40 (m, 4H), 2.05 (m, 1H), 1.74 (m, 1H). Elemental analysis: calculated for $C_{15}H_{25}N_4RuClP_2F_6$: C, 31.40; H, 4.39; N, 9.76. Found: C, 31.44; H, 4.07; N, 9.57%.

4.2.7 Preparation of tethered Ru^{II} arene complexes containing bidentate chelating ligands

$[(\eta^6:\eta^1\text{-}C_6H_5(CH_2)_3NH_2)Ru(C_2O_4 - O,O)]$ (4.14): 4.4 (42.4 mg, 0.14 mmol) and silver nitrate (46.4 mg, 0.27 mmol) were dissolved in water (15 ml) and the solution stirred for 45 min. After filtration, disodium oxalate (21.7 mg, 0.16 mmol) was added and the solution stirred for 45 min. The solvent was removed on a rotary evaporator and the product extracted with methanol. After filtration, the solution was concentrated to *ca.* 7 ml on a rotary evaporator. Upon cooling to ambient temperature, a precipitate formed and diethyl ether was added. The yellow powder (38.4 mg, 0.12 mmol, 85.5% yield) was collected by filtration, washed with diethyl

ether and dried in air. ^{1}H NMR (DMSO-d_6): δ 5.80 (t, 2H, J = 6 Hz), 5.61 (t, 1H, J = 5.5 Hz), 5.29 (d, 2H, J = 6 Hz), 3.84 (b, 2H), 2.66 (m, 2H, J = 5.5 Hz), 2.44 (t, 2H, J = 6 Hz), 2.10 – 2.06 (m, 2H).

[(η^6:η^1-$C_6H_5(CH_2)_2NH_2$)Ru(C_2O_4 – *O,O*)] (4.15): 4.5 (42.5 mg, 0.15 mmol) and silver nitrate (48.6 mg, 0.29 mmol) were dissolved in water (20 ml) and the solution stirred for 90 min. After filtration, disodium oxalate (25.3 mg, 0.19 mmol) was added and the solution stirred for 90 min. The solvent was removed on a rotary evaporator and the product extracted with warm methanol. After filtration, the solution was concentrated on a rotary evaporator until a precipitate formed. The yellow powder (34.3 mg, 0.11 mmol, 76.6% yield) was collected by filtration, washed with diethyl ether and dried in air. ^{1}H NMR (DMSO-d_6): δ 5.91 (t, 2H, J = 6 Hz), 5.44 (t, 1H, J = 5.5 Hz), 5.35 (d, 2H, J = 6 Hz), 4.70 (b, 2H), 3.60 (m, 2H, J = 6 Hz), 2.73 (t, 2H, J = 6.5 Hz). IR (KBr, cm^{-1}): 1670 s [υ(C=O)], 1385 m [υ(C-O)].

[(η^6:η^1-$C_6H_5(C_6H_4)NH_2$)Ru(C_2O_4 – *O,O*)] (4.16): 4.8 (31.5 mg, 0.92 mmol) and silver nitrate (31.2 mg, 0.18 mmol) were dissolved in water (20 ml) and the solution stirred for 180 min. After filtration, disodium oxalate (16.4 mg, 0.12 mmol) was added and the solution stirred for 90 min. The solvent was removed on a rotary evaporator and the product was extracted with warm methanol. After filtration, the solution was concentrated on a rotary evaporator until a precipitate formed and diethyl ether was added. The yellow-brown powder (14.9 mg, 0.41 mmol, 34.1% yield) was collected by filtration, washed with diethyl ether and dried in air. ^{1}H NMR (D_2O, pH* 5.67): δ 7.64 (d, 1H, J = 7 Hz), 7.54 – 7.47 (m, 2H), 6.11 (t, 2H, J = 6 Hz), 5.71 (t, 1H, J = 6 Hz), 5.50 (d, 2H, J = 6 Hz).

[(η^6:η^1-$(C_6H_5)CH_2(C_5H_4N)$)Ru(C_2O_4 – *O,O*)] (4.17): 4.7 (44.4 mg, 0.13 mmol) and silver nitrate (43.9 mg, 0.26 mmol) were dissolved in water (15 ml) and the solution stirred for 30 min. After filtration, disodium oxalate (22.6 mg, 0.17 mmol) was added and the solution stirred for 45 min. The solvent was removed on a rotary evaporator

and the product extracted with methanol. After filtration, the solution was concentrated on a rotary evaporator until a precipitate formed and diethyl ether was added. The solution was stored at 253 K overnight and the black powder (41.3 mg, 0.12 mmol, 88.5% yield) was collected by filtration, washed with diethyl ether and dried in air. ^{1}H NMR (DMSO-d_6): δ 8.08 (t, 1H, J = 8 Hz), 7.68 (d, 1H, J = 8 Hz), 7.47 (t, 1H, J = 6.5 Hz), 6.56 (d, 1H, J = 6 Hz), 6.15 (t, 2H, J = 6 Hz), 5.87 (d, 2H, J = 6 Hz), 5.62 (t, 1H, J = 5.5 Hz), 4.55 (s, 2H).

[(η^6:η^1-$C_6H_5(CH_2)_3NH_2$)Ru($C_5H_7O_2$ – *O,O*)]PF_6 (4.18): 4.4 (39.9 mg, 0.13 mmol) and sodium acetylacetonate monohydrate (25.0 mg, 178 μmol) were dissolved in water (5 ml) and the solution stirred for 90 min. Addition of NH_4PF_6 (106.7 mg, 0.66 mmol) led to the formation of a precipitate and the solution was stored at 277 K for 3 d. The dark yellow powder (43.8 mg, 0.88 mmol, 67.6% yield) was collected by filtration, washed with isopropanol, then diethyl ether and dried in air. ^{1}H NMR ($CDCl_3$): δ 5.72 (t, 2H, J = 6 Hz), 5.48 (t, 1H, J = 6 Hz), 5.27 (s + d, 1H + 2H), 3.00 (m, 2H), 2.65 (b, 2H), 2.57 (t, 2H, J = 6 Hz), 2.35 (m, 2H), 2.02 (s, 6H). Elemental analysis: calculated for $C_{14}H_{20}NO_2RuPF_6$: C, 35.01; H, 4.20; N, 2.92. Found: C, 35.09; H, 4.01; N, 2.94%.

[(η^6:η^1-$C_6H_5(CH_2)C_5H_4N$)Ru($C_5H_7O_2$ – *O,O*)]PF_6 (4.19): 4.7 (37.3 mg, 0.11 mmol) and sodium acetylacetonate monohydrate (21.5 mg, 0.15 mmol) were dissolved in water (15 ml) and the solution stirred for 240 min. After filtration, addition of NH_4PF_6 (99.4 mg, 0.61 mmol) led to the formation of a precipitate and the solution was allowed to settle at ambient temperature, protected by Al-foil. The green powder (27.0 mg, 0.05 mmol, 46.5% yield) was collected by filtration, washed with isopropanol, then diethyl ether and dried in air. ^{1}H NMR ($CDCl_3$): δ 7.93 (t, 1H, J = 8 Hz), 7.63 (t, 1H, J = 8 Hz), 7.25 (t, 1H, J = 6 Hz), 6.59 (d, 1H, J = 6 Hz), 5.92 (t, 2H, J = 6 Hz), 5.67 (d, 2H, J = 6 Hz), 5.47 (s, 1H), 5.42 (t, 1H, J = 6 Hz), 4.66 (s,

2H), 2.09 (s, 6H). Elemental analysis: calculated for $C_{17}H_{18}NO_2RuPF_6$: C, 39.70; H, 3.53; N, 2.72. Found: C, 39.69; H, 3.22; N, 2.66%.

$[(\eta^6{:}\eta^1\text{-}C_6H_5(CH_2)_3NH_2)Ru(C_9H_{10}NO_2$ – *N,O*)$]PF_6$ (4.20): 4.4 (39.1 mg, 0.13 mmol) and silver nitrate (43.2 mg, 0.25 mmol) were dissolved in water (5 ml) and the solution stirred for 60 min. After filtration, the solvent was removed on a rotary evaporator. *L*-Phenylalanine (27.1 mg, 0.16 mmol) and sodium methoxide (8.93 mg, 0.17 mmol) were dissolved in methanol (5 ml) and the mixture stirred for 90 min. The solution was added to the ruthenium compound in methanol (7 ml). After stirring at 318 K for 45 min, the solvent was concentrated to *ca.* 5 ml on a rotary evaporator. NH_4PF_6 (91.4 mg, 0.56 mmol) in methanol (1 ml) was added and the solution concentrated on a rotary evaporator until a precipitate formed. Diethyl ether was added and the solution was stored at ambient temperature overnight. The light yellow powder (33.5 mg, 0.61 mmol, 48.2% yield) was collected by filtration, washed with diethyl ether and dried in air. ^{1}H NMR (DMSO-d_6): δ 7.38 – 7.26 (m, 5H), 6.02 – 5.98 (m, 1H), 5.94 (t, 1H, J = 5.5 Hz), 5.85 (t, 1H, J = 5.5 Hz), 5.60 (d, 1H, J = 5.5 Hz), 5.39 (t, 1H, J = 5.5 Hz), 5.02 (d, 1H, J = 5.5 Hz), 4.58 – 4.54 (m, 1H), 4.09 – 4.05 (m, 1H), 3.97 – 3.93 (m, 1H), 3.11 – 3.07 (m, 1H), 2.97 – 2.92 (m, 1H), 2.81 – 2.76 (m, 1H), 2.68 – 2.63 (m, 2H), 2.48 – 2.43 (m, 1H), 2.38 – 2.33 (m, 1H), 2.10 – 2.03 (m, 1H), 1.92 – 1.85 (m, 1H).

$[(\eta^6{:}\eta^1\text{-}C_6H_5(CH_2)_3NH_2)Ru(C_{18}H_{10}N_4$ – *N,N*$)](PF_6)_2$ (4.21): 4.4 (32.6 mg, 0.11 mmol) and silver nitrate (35.8 mg, 0.21 mmol) were dissolved in water (20 ml) and the solution stirred for 60 min. After filtration, the solvent was removed on a rotary evaporator. The residue and **4.13** (30.8 mg, 0.11 mmol) were dissolved in methanol (25 ml) and the solution stirred for 60 min. After filtration, the solution was concentrated to *ca.* 20 ml on a rotary evaporator and heated to dissolve the precipitate. Addition of NH_4PF_6 (180.7 mg, 1.11 mmol) led to the formation of a precipitate and the solution was stored at 253 K overnight. The yellow powder (65.2

mg, 0.81 mmol, 76.0% yield) was collected by filtration, washed with diethyl ether and dried in air. ^{1}H NMR (DMSO-d_6): δ 9.87 (d, 2H, J = 6 Hz), 9.83 (d, 2H, J = 8 Hz), 8.55 (dd, 2H, J = 3.5 Hz), 8.35 (dd, 2H, J = 5 Hz), 8.24 (dd, 2H, J = 3.5 Hz), 6.58 (t, 2H, J = 6 Hz), 6.17 (d, 2H, J = 6 Hz), 5.81 (t, 1H, J = 6 Hz), 4.49 (s, 2H), 2.81 (t, 2H, J = 5.5 Hz), 2.56 (m, 2H), 2.20 (m, 2H).

4.2.8 Preparation of a tethered Ru^{II} arene precursor complex

[(η^6-etb)Ru($C_{12}H_{12}N_2$)Cl_2] (4.31): 4.2 (187.2 mg, 0.29 mmol) and 2-benzylaminopyridine (133.4 mg, 0.72 mmol) were stirred in dichloromethane (30 ml) for 120 min. The solution was concentrated to *ca.* 7 ml on a rotary evaporator and slow addition of diethyl ether (*ca.* 10 ml) led to the precipitation of an orange powder (254.0 mg, 0.50 mmol, 86.3% yield), which was collected by filtration, washed with diethyl ether and dried in air. ^{1}H NMR ($CDCl_3$): δ 8.54 (d, 1H, J = 6 Hz), δ 7.96 (t, 1H, J = 6 Hz), 7.45 – 7.28 (m, 6H), 6.59 (t, 1H, J = 6.5 Hz), 6.44 – 6.41 (m, 3H), 6.02 (t, 1H, J = 6 Hz), 5.81 (t, 2H, J = 6 Hz), 4.42 (d, 2H, J = 6 Hz), 4.31 (q, 2H, J = 7 Hz), 1.36 (t, 3H, J = 7 Hz).

4.2.9 Preparation of a tether-opened Ru^{II} arene complex

[(η^6:η^1-$C_6H_5(C_6H_4)NH_3$)$RuCl_3$] (4.32): 4.8 (144.2 mg, 0.42 mmol) was dissolved in conc. hydrochloric acid (37%, 35 ml) and the solution stirred at 348 K for 180 min. The solvent was removed on a rotary evaporator. Ethanol was added to wash the residue and removed on a rotary evaporator. The dark red microcrystalline solid (150.8 mg, 0.40 mmol, 94.4% yield) was collected by filtration, washed with diethyl ether and dried in air. ^{1}H NMR (DMSO-d_6): δ 7.56 (d, 1H, J = 7 Hz), 7.28 (t, 1H, J = 7 Hz), 7.01 (d, 1H, J = 7 Hz), 6.91 (t, 1H, J = 7 Hz), 6.26 (d, 2H, J = 6 Hz), 6.19 (t, 1H, J = 5.5 Hz), 5.97 (t, 2H, J = 5.5 Hz).

4.3 Bifunctional Tethered Ru^{II} Arene (Mono-substituted) Complexes

4.3.1 Results

4.3.1.1 Synthesis

The precursor diene ethyl-1,4-cyclohexadiene-3-carboxylate (**4.1**) for the synthesis of the ruthenium dimer $[(\eta^6\text{-etb})RuCl_2]_2$ (**4.2**), where etb = ethyl benzoate, was synthesised *via* the Birch reduction of benzoic acid, since direct reduction of ethyl benzoate [47] only returned benzoic acid, followed by esterification (Scheme 4.1). 1-Benzyl-1-*H*-pyrazole (**4.3**) was synthesised by proton abstraction of pyrazole, followed by reaction with benzyl chloride.

The synthesis of complexes $[(\eta^6{:}\eta^1\text{-}C_6H_5(CH_2)_3NH_2)RuCl_2]$ (**4.4**), $[(\eta^6{:}\eta^1\text{-}C_6H_5(CH_2)_2NH_2)RuCl_2]$ (**4.5**), $[(\eta^6{:}\eta^1\text{-}C_6H_5O(CH_2)_2NH_2)RuCl_2]$ (**4.6**), $[(\eta^6{:}\eta^1\text{-}C_6H_5(CH_2)C_5H_4N)RuCl_2]$ (**4.7**), $[(\eta^6{:}\eta^1\text{-}C_6H_5(C_6H_4)NH_2)RuCl_2]$ (**4.8**) and $[(\eta^6{:}\eta^1\text{-}C_6H_5(CH_2)C_3H_3N_2)RuCl_2]$ (**4.9**) (Figure 4.2) was inspired by the route pioneered by Ward *et al.* [29], which involves the thermal displacement of ethyl benzoate (etb) in $[(\eta^6\text{-etb})RuCl_2]_2$ from the appropriate N-donor derivatives (Scheme 4.2). The advantage is that synthetically challenging or poor yielding Birch reductions for each compound can be avoided. Furthermore, optimisation of this methodology towards synthesis of nitrogen-based tethered molecules provides easy and fast access to a potentially vast number of complexes.

Thermal displacement reactions for phosphine-containing tethered ruthenium

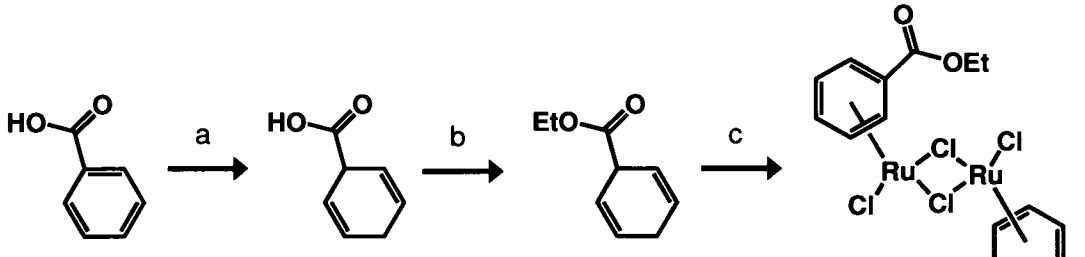

a: sodium metal, liquid ammonia at 195 K
b: dry ethanol (250 ml), 98% H_2SO_4 (17 ml), argon, overnight, reflux
c: $RuCl_3.xH_2O$, dry ethanol (150 ml), argon, overnight, reflux

Scheme 4.1: General synthetic route for the preparation of the ruthenium starting dimer $[(\eta^6\text{-etb})RuCl_2]_2$ (**4.2**).

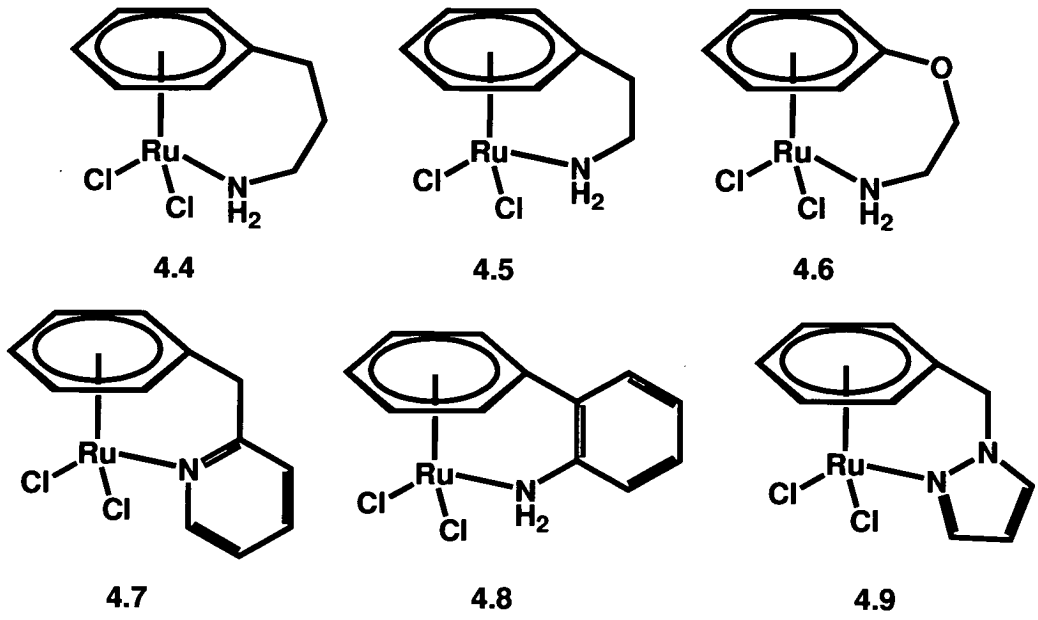

Figure 4.2: The structures of $[(\eta^6{:}\eta^1\text{-}C_6H_5(CH_2)_3NH_2)RuCl_2]$ (**4.4**), $[(\eta^6{:}\eta^1\text{-}C_6H_5(CH_2)_2NH_2)RuCl_2]$ (**4.5**), $[(\eta^6{:}\eta^1\text{-}C_6H_5O(CH_2)_2NH_2)RuCl_2]$ (**4.6**), $[(\eta^6{:}\eta^1\text{-}C_6H_5(CH_2)C_5H_4N)RuCl_2]$ (**4.7**), $[(\eta^6{:}\eta^1\text{-}C_6H_5(C_6H_4)NH_2)RuCl_2]$ (**4.8**) and $[(\eta^6{:}\eta^1\text{-}C_6H_5(CH_2)C_3H_3N_2)RuCl_2]$ (**4.9**).

arene complexes have also been described by Wright *et al.* [33], who used $[(\eta^6\text{-}p\text{-cym})RuCl_2]_2$, where *p*-cym = *p*-cymene, as the starting material. This method was adapted by others [28, 31, 48] but has also been reported to have failed [29, 30]. Only ruthenium dimers containing ethyl benzoate or methyl *o*-toluate appear to have been used as starting materials for the synthesis of phosphine-containing tethered complexes under forcing conditions (dichloromethane at 393 K) [29, 30]. Bennett *et al.* have found that addition of small amounts of THF to the reaction mixture can improve yields and shorten reaction times in these syntheses [30]. Alternative methods have also been reported [35, 49, 50].

Initially, it was found that reactions of $[(\eta^6\text{-etb})RuCl_2]_2$ (**4.2**) with either 3-phenyl-1-propylamine or 2-phenethylamine in 1,2-dichloroethane under reflux and argon produced complexes $[(\eta^6{:}\eta^1\text{-}C_6H_5(CH_2)_3NH_2)RuCl_2]$ (**4.4**) and $[(\eta^6{:}\eta^1\text{-}C_6H_5(CH_2)_2NH_2)RuCl_2]$ (**4.5**), respectively, in satisfactory yield and purity. The

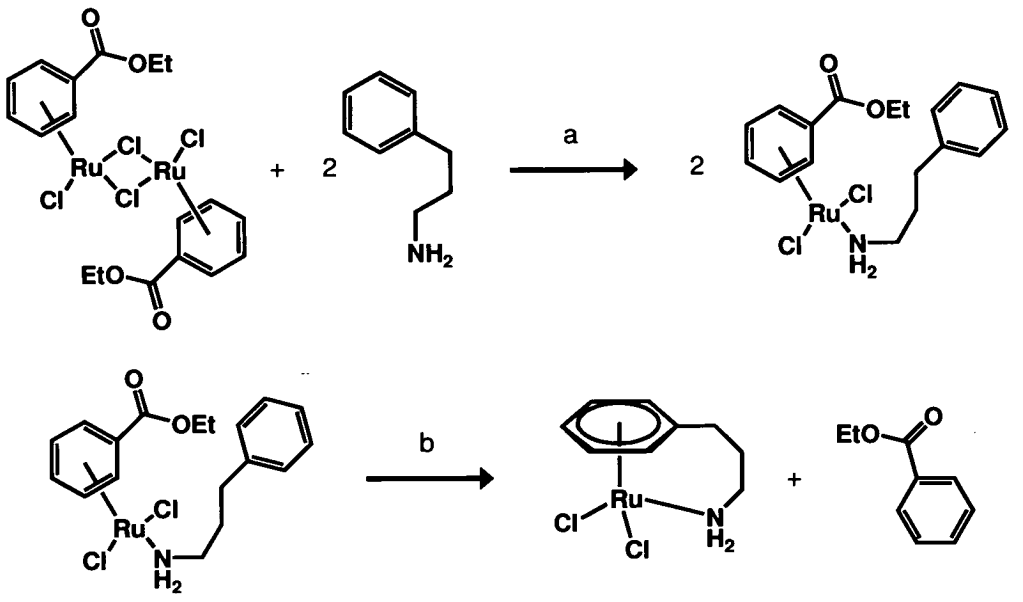

a: 1,2-dichloroethane (20 ml), 50 min at ambient temperature
b: 1,2-dichloroethane (80 ml), THF (2 ml), argon, pressure vessel, 22 h at 393 K

Scheme 4.2: General synthetic route for tethered complexes, illustrated for $[(\eta^6{:}\eta^1\text{-}C_6H_5(CH_2)_3NH_2)RuCl_2]$ (**4.4**).

experimental set-up was not sufficiently stable, however, since on occasions the condenser was lifted from the vessel, leading to loss of almost all solvent. Reflux under reduced temperature resulted in poor yields for other ligands, such as 2-aminobiphenyl and 1-benzyl-1-*H*-pyrazole (Table 4.1).

Using the synthesis of **4.4** as a model, different reaction conditions were investigated with a view to improving the yield (Table 4.1). Use of the high-boiling solvent 1,2,3-trichloropropane generally resulted in no isolatable complex, except in poor yield under reflux conditions using an oil bath. The presence of THF in millilitre quantities during the reactions appeared to increase the yields. Use of a pressure vessel increased the yields dramatically. This allows reactions to be carried out in an oil bath at 393 K (boiling point of 1,2-dichloroethane is 357 K) without loss of solvent. The complexes described in this section were synthesised in the pressure vessel with yields ranging from 55% (**4.7**) to 91% (**4.6**). Complexes **4.7**, **4.8** and **4.9** were obtained as microcrystalline, analytically pure precipitates at the bottom of the pressure vessel after the reaction.

Table 4.1: Synthetic conditions for the syntheses of tethered complexes. In set-up dce = 1,2-dichloroethane, tcp = 1,2,3-trichloropropane. Unless indicated by hm (heating mantle), all reactions were performed in an oil bath.

Product	**4.2** / mg	Set-up	V / ml	THF / ml	T / K	t / h	Yield / %
4.5	420.5	condenser dce	50	Few drops	Reflux (hm)	41	50.4
4.5	146.7	pressure dce	30	1	393	15	73.4
4.4	372.4	condenser dce	50	Few drops	Reflux (hm)	90	42.1
4.4	109.9	condenser tcp	50	none	393	17.5	0
4.4	119.4	condenser tcp	25	15 drops	393	21.3	0
4.4	348.8	condenser tcp	50	1	Reflux	14	11.9
4.4	349.1	condenser tcp	50	30 drops	Reflux (hm)	18	0
4.4	232.4	pressure dce	50	15 drops	393	18.6	50.9
4.4	514.2	pressure dce	80	2	393	22	78.1
4.4	526.2	pressure dce	70	3	393	18	75.5
4.6	202.7	pressure dce	40	1	393	18	55.2
4.7	198.8	pressure dce	60	20 drops	393	16.6	78.5
4.7	252.3	pressure dce	40	1	393	18	91.2
4.8	174.0	condenser dce	50	Few drops	363	17.5	27.5
4.8	184.4	pressure dce	40	1	393	20.3	70.8
4.8	426.8	pressure dce	60	2	393	17	85.3
4.9	226.7	condenser dce	50	Ten drops	363	19	0
4.9	148.1	pressure dce	30	1	393	18	47.2
4.29	181.6	pressure dce	35	1	393	16	48.0

4.3.1.2 Characterisation

Crystals, suitable for X-ray diffraction, were grown from water, after addition of NaCl, at ambient temperature for $[(\eta^6:\eta^1\text{-}C_6H_5(CH_2)_2NH_2)RuCl_2]$ (**4.5**) and $[(\eta^6:\eta^1\text{-}C_6H_5(CH_2)C_5H_4N)RuCl_2]$ (**4.7**). For $[(\eta^6:\eta^1\text{-}C_6H_5O(CH_2)_2NH_2)RuCl_2]$ (**4.6**) they were obtained from methanol at ambient temperature, and for $[(\eta^6:\eta^1\text{-}C_6H_5(CH_2)_3NH_2)RuCl_2]$ (**4.4**) from MeOH at 253 K. Their X-ray crystal structures are the first examples of di-chloro, tethered Ru^{II} arene complexes containing a nitrogen linker. Thus far comparable neutral and bifunctional structures have mainly contained phosphorus as the metal-coordinating atom of a tether [28 – 33].

Complex $[(\eta^6:\eta^1\text{-}C_6H_5(CH_2)_3NH_2)RuCl_2]$ (**4.4**) crystallized with the tether disordered over two positions (Figure 4.3). The crystal data are shown in Table A.4.1 and bond angles and lengths in Table 4.2. The Ru – Cl, Ru – N and the Ru – C(arene) bond lengths are independent of the orientation of the tether. The C – C and the N –C bond lengths within the tether, however, show slight variations. The Ru –

Table 4.2: Selected bond lengths (Å) and angles (°) for $[(\eta^6:\eta^1\text{-}C_6H_5(CH_2)_3NH_2)RuCl_2]$ (**4.4**).

Bond	Length	Bond	Length/angle
Ru-N10	2.129(5)	Ru-centroid[a]	1.653
Ru-Cl1	2.425(3)	N10-Ru-Cl1	83.7(2)
Ru-Cl2	2.437(3)	N10-Ru-Cl2	81.8(2)
Ru-C1	2.169(9)	Cl1-Ru-Cl2	89.39(8)
Ru-C2	2.161(9)	Ru-N10-C9	118.0(5)
Ru-C3	2.196(7)	Ru-N10-C91	118.7(7)
Ru-C4	2.172(10)	Ru-C6-C7	127.1(3)
Ru-C5	2.175(9)	N10-Ru-C6	90.55(19)
Ru-C6	2.179(6)		

[a] = measured using Mercury 1.4.

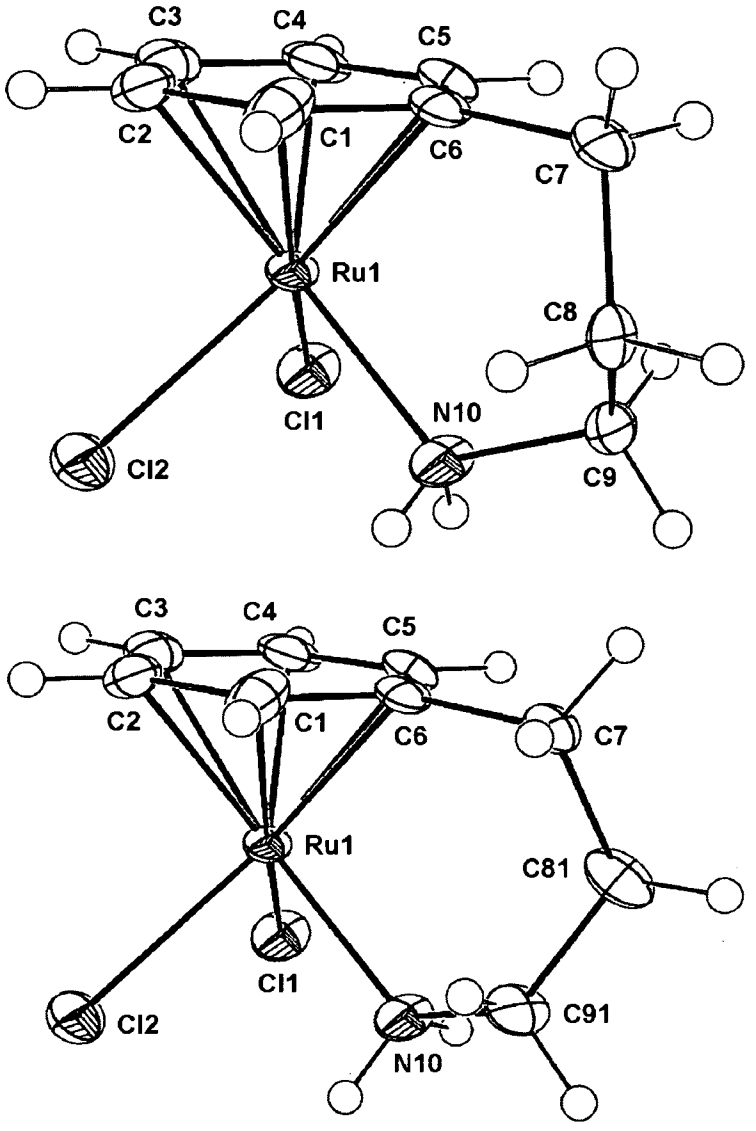

Figure 4.3: Ortep diagram (50% probability ellipsoids) and atom numbering scheme for the X-ray crystal structure of $[(\eta^6{:}\eta^1\text{-}C_6H_5(CH_2)_3NH_2)RuCl_2]$ (**4.4**), showing the two conformations of the tether.

Cl bond lengths are 2.425(3) Å and 2.437(3) Å respectively, with Ru – N of 2.129(5) Å. The Ru – centroid distance is 1.65 Å, which is between 0.04 – 0.05 Å shorter than other three carbon tethered phosphorus-containing complexes [22, 30, 33, 49, 51]. The Ru – C(arene) bond lengths of those phosphorus tethered complexes are in the range of 2.16 – 2.27 Å, whereas those in **4.4** are within the comparatively narrow range of 2.161(9) – 2.196(7) Å. The Ru – C6 – C7 angle, where C6 is the arene

carbon where the tether is connected and C7 the first carbon atom of the tether, is 127.17(3)°. The C6 – Ru – N angle is 90.55(19)°. The angle between the plane defined by all arene carbons and that of C6, Ru and N is 88.77°.

Similar to **4.4**, complex $[(\eta^6:\eta^1\text{-}C_6H_5(CH_2)_2NH_2)RuCl_2]$ (**4.5**) crystallized with the tether disordered over two positions (Figure 4.4) and contains a mirror plane through C4, C1, C5, Ru and N1. The crystal data are shown in Table A.4.1 and bond

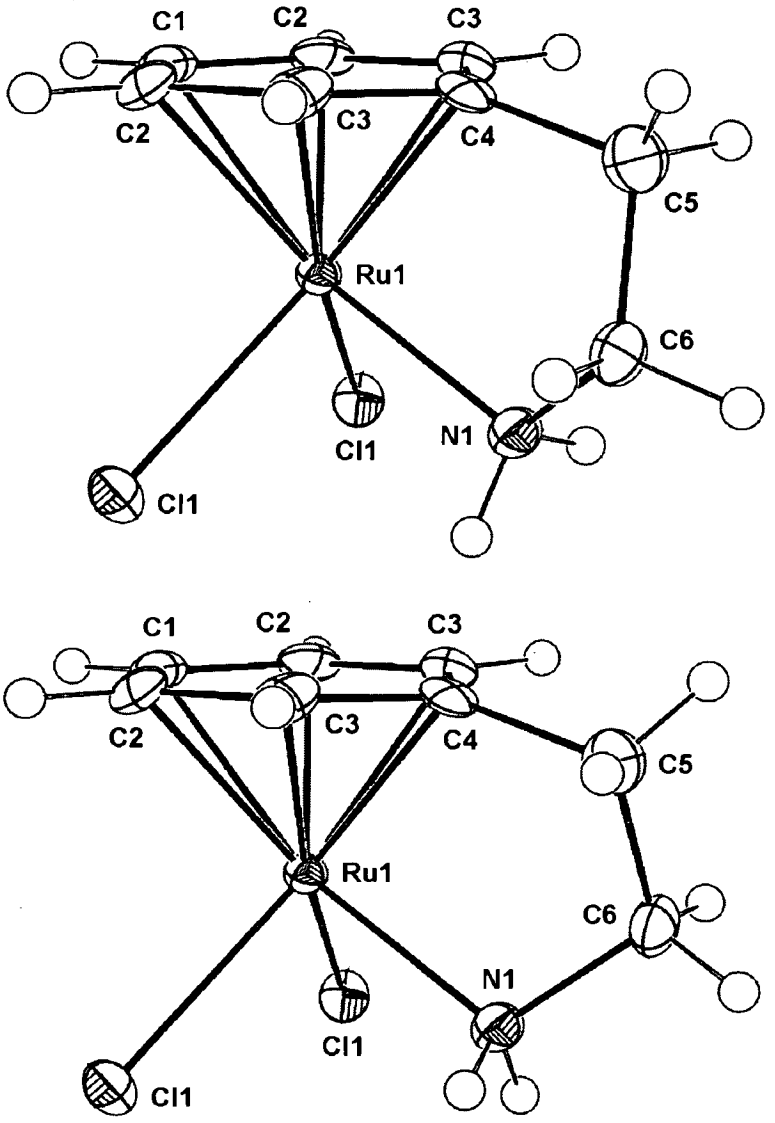

Figure 4.4: Ortep diagram (50% probability ellipsoids) and atom numbering scheme for the X-ray crystal structure of $[(\eta^6:\eta^1\text{-}C_6H_5(CH_2)_2NH_2)RuCl_2]$ (**4.5**), showing the two conformations of the tether.

angles and lengths in Table 4.3. The Ru – C(arene) bond lengths are in the range of 2.095(3) – 2.199(4) Å, shorter than in phosphorus containing two-carbon tethers and a phosphorus ligand-containing analogue of **4.5**, for which ranges of 2.15 – 2.28 Å [28, 29, 39] and 2.16 – 2.26 Å [44], respectively, have been reported. The Ru – centroid distances in those complexes are 0.06 – 0.08 Å [28, 29, 39, 44] shorter than for **4.5**, which is 1.63 Å, comparable to the three carbon tether **4.4**. The arene carbon C4 (where the tether is connected) is pulled towards the ruthenium centre, whereas the opposite carbon C1 is furthest away from the metal resulting in buckling of the arene. The Ru – Cl bond lengths are 2.4133(7) Å, and Ru – N 2.117(3) Å. The angle defined by N – Ru – C4 is 80.04(13)°, which is very similar to the analogous angle in phosphorus-containing complexes. The Ru – N – C6 angle, where C6 is the tether-carbon connected to the nitrogen, is 110.00(2)° and therefore *ca.* 10° wider than two carbon phosphorus-tethered complexes. The angle between the plane defined by all arene carbons and that of C6, Ru and N is 90.00(3)°.

Table 4.3: Selected bond lengths (Å) and angles (°) for [(η^6:η^1-$C_6H_5(CH_2)_2NH_2$)$RuCl_2$] (**4.5**) (mirror plane through C4, C1, C5, Ru and N1).

Bond	Length	Bond	Length/angle
Ru-N1	2.117(3)	Ru-centroid[a]	1.631
Ru-Cl1	2.4133(7)	N1-Ru-Cl1	86.28(6)
Ru-Cl1#1	2.4133(7)	N1-Ru-Cl1#1	86.28(6)
Ru-C1	2.199(4)	Cl1-Ru-Cl1#1	90.00(3)
Ru-C2	2.164(2)	Ru-N1-C6	110.0(2)
Ru-C2#1	2.164(2)	Ru-N1-C6#1	110.0(2)
Ru-C3	2.158(2)	Ru-C4-C5	114.7(2)
Ru-C3#1	2.158(2)	N1-Ru-C4	80.04(13)
Ru-C4	2.095(3)		

[a] = measured using Mercury 1.4.

The complex $[(\eta^6:\eta^1\text{-}C_6H_5O(CH_2)_2NH_2)RuCl_2]$ (**4.6**) contains a three atom tether, which incorporates a heteroatom (Figure 4.5). The crystal data are shown in Table A.4.1 and bond angles and lengths in Table 4.4. The Ru – Cl bond lengths are 2.4217(6) Å and 2.4247(6) Å, respectively, with Ru – N1 of 2.1419(19) Å. The range of Ru – C(arene) bond lengths, 2.158(2) – 2.202(2) Å, is comparable to **4.4** and the

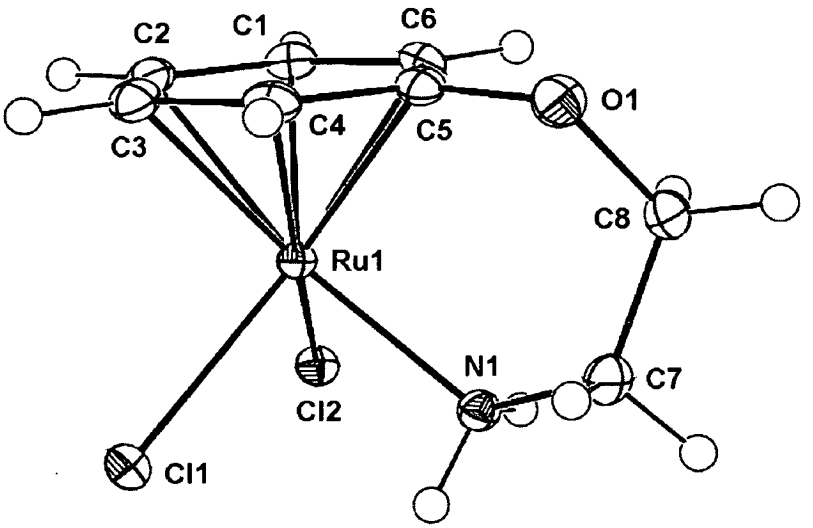

Figure 4.5: Ortep diagram (50% probability ellipsoids) and atom numbering scheme for the X-ray crystal structure of $[(\eta^6:\eta^1\text{-}C_6H_5O(CH_2)_2NH_2)RuCl_2]$ (**4.6**).

Table 4.4: Selected bond lengths (Å) and angles (°) for $[(\eta^6:\eta^1\text{-}C_6H_5O(CH_2)_2NH_2)RuCl_2]$ (**4.6**).

Bond	Length	Bond	Length/angle
Ru-N1	2.1419(19)	Ru-C6	2.183(2)
Ru-Cl1	2.4217(6)	Ru-centroid[a]	1.658
Ru-Cl2	2.4247(6)	N1-Ru-Cl1	85.64(6)
Ru-C1	2.166(2)	N1-Ru-Cl2	81.14(5)
Ru-C2	2.202(2)	Cl1-Ru-Cl2	87.81(2)
Ru-C3	2.187(2)	Ru-N1-C7	121.17(15)
Ru-C4	2.196(2)	Ru-C5-O1	126.52(16)
Ru-C5	2.158(2)	N1-Ru-C5	88.38(8)

[a] = measured using Mercury 1.4.

Ru – centroid distance is 1.66 Å. The Ru – C5 – O1 angle, where C5 is the arene carbon where the tether is connected and O1 the first carbon atom of the tether, is 126.52(16)°. The C5 – Ru – N1 angle is 88.38(8)°. The angle between the plane defined by all arene carbons and that of C5, Ru and N1 is 85.58°. In contrast to the above structures, the amine protons are involved in short contact interactions with chloride atoms of 2.50 Å (Cl2···N1 3.337(2) Å) and 2.52 Å (Cl1···N1 3.446(2) Å), respectively. Interactions involving O1···H2 (2.67 Å, O1···C2 3.580(3) Å) and Cl2···H82 (2.70 Å, Cl2···C8 3.507(3) Å) link the molecules into chains, and those molecules show $\pi - \pi$ interactions with neighbouring arenes with C5···C6 3.227(3) Å. Proton···chloride interactions, including those with amine protons, link one molecule with two others, where Cl2···H6 2.74 Å (Cl2···C6 3.729(2) Å) and Cl2···H81 2.76 Å (Cl2···C8 3.687(3) Å).

The complex $[(\eta^6{:}\eta^1\text{-}C_6H_5(CH_2)C_5H_4N)RuCl_2]$ (**4.7**) contains a pyridine derivative as the tether (Figure 4.6). The crystal data are shown in Table A.4.2 and bond angles and lengths in Table 4.5. The Ru – Cl bond lengths are 2.4039(7) Å and 2.4218(7) Å, respectively, with Ru – N of 2.119(2) Å. The Ru – centroid distance is

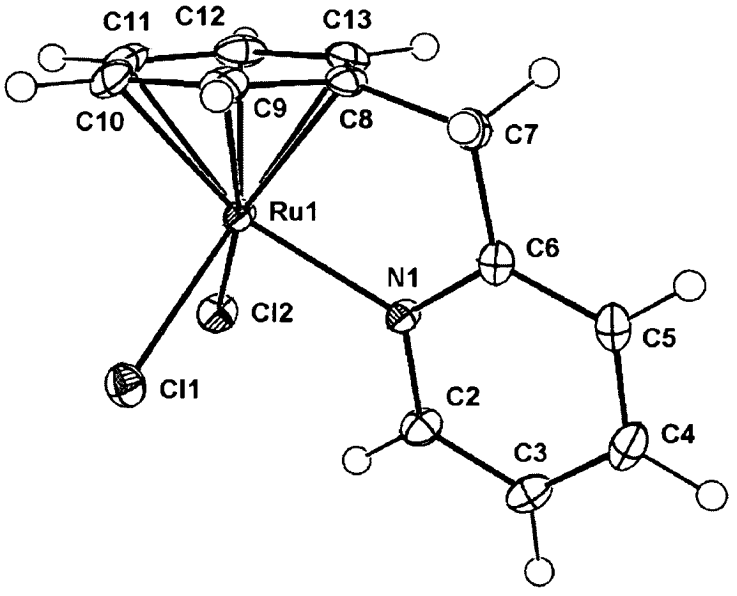

Figure 4.6: Ortep diagram (50% probability ellipsoids) and atom numbering scheme for the X-ray crystal structure of $[(\eta^6{:}\eta^1\text{-}C_6H_5(CH_2)C_5H_4N)RuCl_2]$ (**4.7**).

Table 4.5: Selected bond lengths (Å) and angles (°) for [(η^6:η^1-$C_6H_5(CH_2)C_5H_4N$)$RuCl_2$] (**4.7**).

Bond	Length	Bond	Length/angle
Ru-N	2.119(2)	Ru-C13	2.165(3)
Ru-Cl1	2.4039(7)	Ru-centroid[a]	1.629
Ru-Cl2	2.4218(7)	N1-Ru-Cl1	85.75(6)
Ru-C8	2.099(2)	N1-Ru-Cl2	91.02(6)
Ru-C9	2.145(3)	Cl1-Ru-Cl2	88.19(3)
Ru-C10	2.167(3)	Ru-N-C6	116.79(16)
Ru-C11	2.197(3)	Ru-C8-C7	114.73(17)
Ru-C12	2.181(3)	N1-Ru-C8	78.93(9)

[a] = measured using Mercury 1.4.

1.63 Å and the Ru – C(arene) bond lengths are in the range of 2.099(2) – 2.197(3) Å. Similarly to **4.5**, the arene is buckled and arene carbon C8 (where the tether is connected) is pulled towards the ruthenium centre, whereas the opposite carbon C11 is furthest away from the metal. The pyridine rings in the structure are involved in π – π stacking. One face of a pyridine ring interacts strongly with another ring with distances of N1···C4 3.485(3) Å, C2···C5 3.492(4) Å and C3···C6 3.511(4) Å, respectively. The other face shows weaker interactions with distances of N1···C4 4.130(3) Å, C2···C5 4.117(4) Å and C3···C6 4.138(4) Å, respectively (Figure A.4.1). The angle defined by N – Ru – C8 is 78.93(9)°. The Ru – N – C6 angle, where C6 is the pyridine-carbon which the tether is connected to, is 116.79(16)°. The angle between the plane defined by all arene carbons and that of C8, Ru and N is 83.07°.

Most of the complexes were characterized by ^{1}H NMR in $CDCl_3$, solubilised at concentrations between *ca.* 1 – 5 mM by *ca.* 30 min of ultrasonication. For complex **4.7**, two of the pyridine signals were masked by the chloroform peak, whereas **4.8** was highly insoluble in most solvents and decomposed in DMSO (*vide infra*).

The arene proton signals for the tethered amine complexes $[(\eta^6{:}\eta^1\text{-}C_6H_5(CH_2)_3NH_2)RuCl_2]$ (**4.4**), $[(\eta^6{:}\eta^1\text{-}C_6H_5(CH_2)_2NH_2)RuCl_2]$ (**4.5**) and $[(\eta^6{:}\eta^1\text{-}C_6H_5O(CH_2)_2NH_2)RuCl_2]$ (**4.6**) are shifted upfield by *ca.* 1.4 – 2 ppm compared to those of the respective free ligands. Furthermore, three peaks (triplet, triplet, doublet) in a 2 : 1 : 2 ratio are associated with these protons. The signals for the bound NH_2 groups are shifted downfield by 2.2 – 1.9 ppm compared to the free ligand.

The assignment of the tether protons was confirmed by recording a 2D NOESY spectrum. Complex **4.4** is given as an example in Figure 4.7. The arene

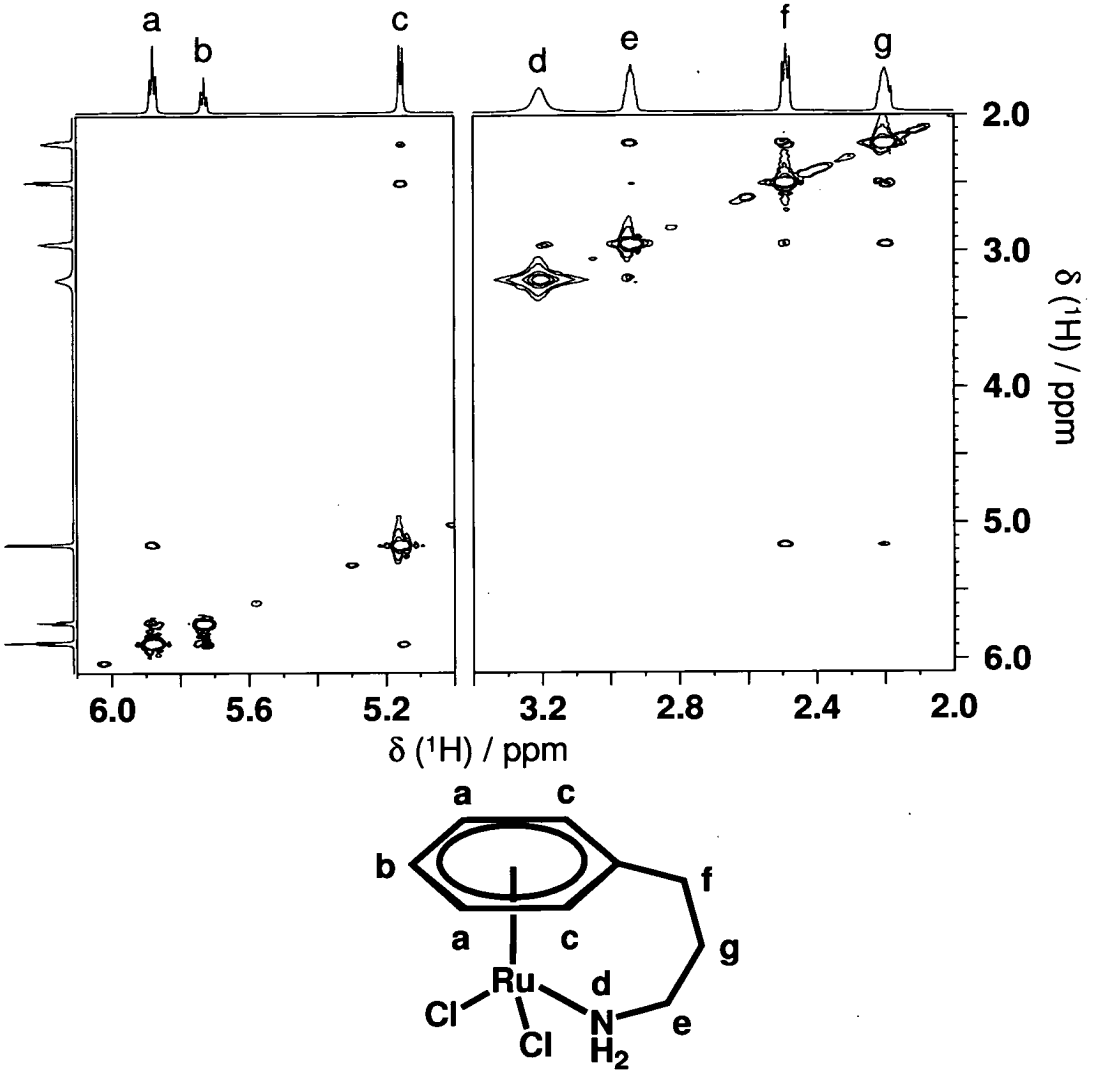

Figure 4.7: The 2D NOESY ^1H NMR spectrum of $[(\eta^6{:}\eta^1\text{-}C_6H_5(CH_2)_3NH_2)RuCl_2]$ (**4.4**) in $CDCl_3$ at 298 K and the peak assignment.

protons at 5.16 ppm show weak and strong cross-peaks to the protons at 2.20 and 2.49 ppm, respectively. The signal at 2.20 ppm shows cross-peaks of comparable intensity to both signals at 2.20 and 2.95 ppm and the NH_2 group shows a cross-peak with the protons at 2.95 ppm.

The protons of the heterocyclic tether backbones in complexes [(η^6:η^1-$C_6H_5(CH_2)C_5H_4N$)$RuCl_2$] (**4.7**) and [(η^6:η^1-$C_6H_5(CH_2)C_3H_3N_2$)$RuCl_2$] (**4.9**) generally showed an upfield shift with respect to the free ligands. In the case of the pyridine derivative, this shift was in the range of 0.2 – 0.3 ppm, except for the proton next to the nitrogen, which shifted downfield by *ca.* 0.35 ppm. For the pyrazole derivative, the upfield shifts are less pronounced with 0.2 – 0.04 ppm. The benzylic CH_2 protons in **4.7** shift downfield by *ca.* 0.15 ppm and upfield by *ca.* 0.3 ppm in **4.9** upon complexation. The coordinated arene protons are shifted upfield by *ca.* 1.1 – 1.7 ppm compared to the free ligands.

4.3.1.3 Aqueous chemistry

All the synthesised di-chloro tethered complexes have reasonable water solubility. Solutions of [(η^6:η^1-$C_6H_5(CH_2)_3NH_2$)$RuCl_2$] (**4.4**) (7.2 mM, pH* = 5.66), [(η^6:η^1-$C_6H_5(CH_2)_2NH_2$)$RuCl_2$] (**4.5**) (7.0 mM Ru, pH* = 5.60), [(η^6:η^1-$C_6H_5O(CH_2)_2NH_2$)$RuCl_2$] (**4.6**) (8.5 mM Ru, pH* = 5.49), [(η^6:η^1-$C_6H_5(CH_2)C_5H_4N$)$RuCl_2$] (**4.7**) (4.0 mM, pH* = 6.24) and [(η^6:η^1-$C_6H_5(C_6H_4)NH_2$)$RuCl_2$] (**4.8**) (2.0 mM Ru, pH* = 5.46), where pH* = pH meter reading of the solution, at 298 K showed no evidence of decomposition over a period of 24 h by ^1H NMR spectroscopy. In the case of [(η^6:η^1-$C_6H_5(CH_2)C_3H_3N_2$)$RuCl_2$] (**4.9**) (6.0 mM Ru, pH* = 5.38, 298 K) a multiplet of negligible intensity at 7.40 – 7.25 ppm appeared after 24 h. Each spectrum indicated the presence of more than one species in solution.

Upon dissolution of **4.5** in D_2O, eleven peaks were observed in the arene-proton region of the ^1H NMR spectrum. Integration suggested that they belong to three species, two with three signals in a 2 : 1 : 2 ratio and one with five signals in a 1 : 1 : 1 : 1 : 1 ratio. A similar scenario was also observed for **4.4**, with some signals overlapping.

Chloride titrations for complexes **4.5** (6.8 mM Ru at start, 6.2 mM Ru at finish) and **4.4** (6.5 mM Ru at start, 5.9 mM Ru at finish) were followed by ^1H NMR in D_2O at 298 K. The relative intensities of the three species changed depending on the concentration of added chloride ($[Cl^-]_a$) (Figures 4.8, A.4.2 and A.4.3). The pH* values increased as the concentration of total chloride ($[Cl^-]_t$) was increased from *ca.* 13 mM to *ca.* 273 mM. Control experiments of solutions of **4.5** with $[Cl^-]_t$ = 13.6 mM ([Ru] = 6.8 mM) and 273.6 mM ([Ru] = 6.2 mM), respectively, were re-

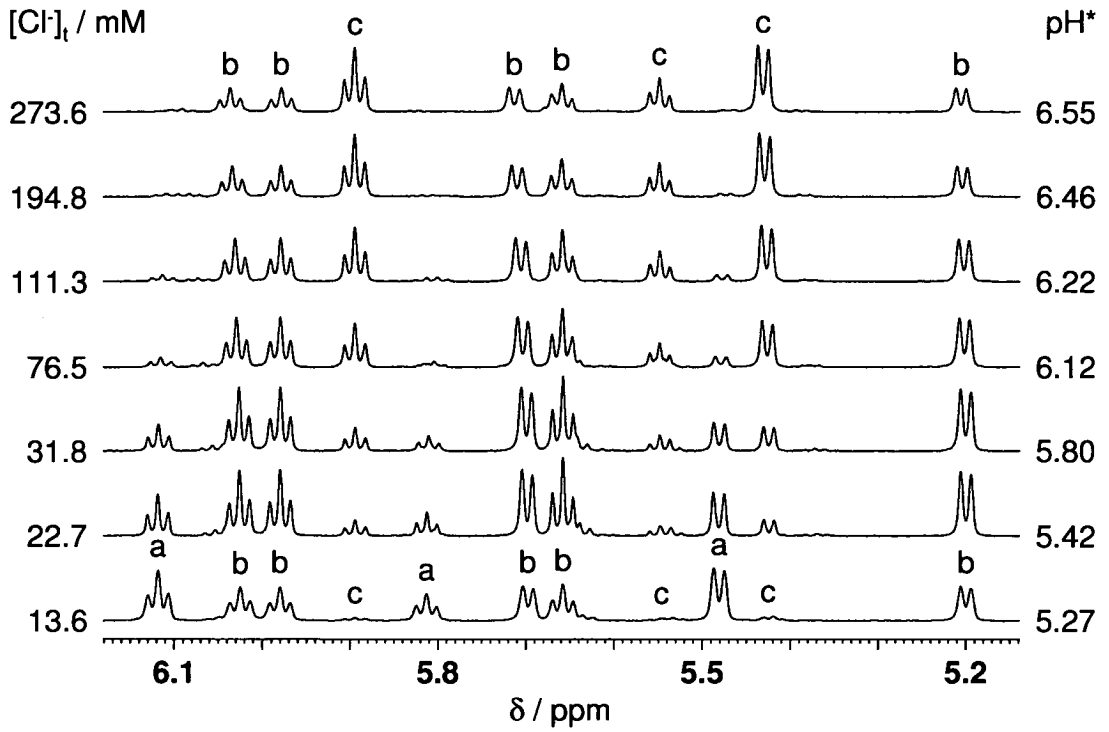

Figure 4.8: The arene proton region of the ^1H NMR spectrum for a chloride titration of $[(\eta^6{:}\eta^1\text{-}C_6H_5(CH_2)_2NH_2)RuCl_2]$ (**4.5**) (6.8 mM) in D_2O at 298 K. Assignments: a = $[(\eta^6{:}\eta^1\text{-}C_6H_5(CH_2)_2NH_2)Ru(H_2O)_2]^{2+}$; b = $[(\eta^6{:}\eta^1\text{-}C_6H_5(CH_2)_2NH_2)Ru(H_2O)Cl]^+$; c = $[(\eta^6{:}\eta^1\text{-}C_6H_5(CH_2)_2NH_2)RuCl_2]$.

recorded after 22 h and showed little change from the original spectra. The same was true for spectra of **4.4** with $[Cl^-]_t$ = 12.9 mM ([Ru] = 6.5 mM) and 273.1 mM ([Ru] = 5.9mM).

The synthesis of the di-aqua complex $[(\eta^6{:}\eta^1\text{-}C_6H_5(CH_2)_3NH_2)Ru(H_2O)_2](NO_3)_2$ was attempted by abstraction of chloride with silver nitrate from $[(\eta^6{:}\eta^1\text{-}C_6H_5(CH_2)_3NH_2)RuCl_2]$ (**4.4**) in water. Nitrate generally is a weak ligand for Ru^{II}. The complex, however, crystallised as $[(\eta^1{:}\eta^6\text{-}C_6H_5(CH_2)_3NH_2)Ru(NO_3)_2]$ (**4.10**) from slow diffusion of diethyl ether into an acetone solution at ambient temperature. The structure is shown in Figure 4.9, the crystal data in Table A.4.2 and bond angles and lengths in Table 4.6. The Ru – O bond lengths are 2.11172(10) Å and 2.1250(10) Å respectively, with Ru – N10 of 2.1241(13) Å. The Ru – C(arene) bond lengths of 2.1707(15) – 2.1986(17) Å are slightly longer on average than for **4.4**. The Ru – centroid distance is 1.66 Å. Strong H-bonds between the amine protons and oxygen atoms of the nitrate ligands result in the formation of dimers between molecules in the structure, where O22···H10A 2.25

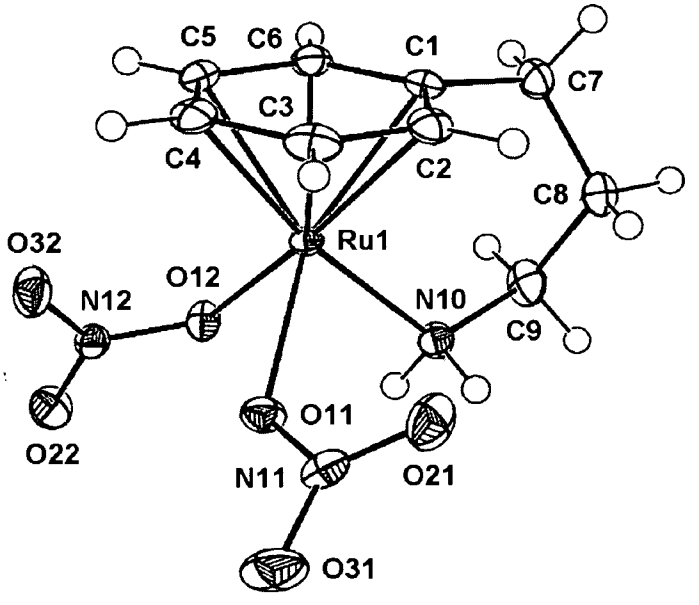

Figure 4.9: Ortep diagram (50% probability ellipsoids) and atom numbering scheme for the X-ray crystal structure of $[(\eta^6{:}\eta^1\text{-}C_6H_5(CH_2)_3NH_2)Ru(NO_3)_2]$ (**4.10**).

Table 4.6: Selected bond lengths (Å) and angles (°) for [(η^6:η^1-$C_6H_5(CH_2)_3NH_2$)$Ru(NO_3)_2$] (**4.10**).

Bond	Length	Bond	Length/angle
Ru-N10	2.1241(13)	Ru-C6	2.1762(14)
Ru-O11	2.1172(10)	Ru-centroid[a]	1.656
Ru-O12	2.1250(10)	N10-Ru-O11	82.20(5)
Ru-C1	2.1766(14)	N10-Ru-O12	79.34(4)
Ru-C2	2.1707(15)	O11-Ru-O12	76.86(4)
Ru-C3	2.1697(15)	Ru-N10-C9	121.52(11)
Ru-C4	2.1986(17)	Ru-C1-C7	125.85(11)
Ru-C5	2.1799(15)	N10-Ru-C1	90.49(5)

[a] = measured using Mercury 1.4.

Å (O22···N10 3.0671(18) Å) and O11···H10B 2.23 Å (O11···N10 3.0935(16) Å), respectively (Figure A.4.4). The Ru – C1 – C7 angle, where C1 is the arene carbon where the tether is connected and C7 the first carbon atom of the tether, is 125.85(11)°. The C1 – Ru – N10 angle is 90.49(5)°. The angle between the plane defined by all arene carbons and that of C1, Ru and N is 83.96°. There appears to be no previous report of a Ru^{II} arene complex containing two mono-dentate nitrate molecules. One Ru^{II} (α-[$Ru(azpy)_2(NO_3)_2$], where azpy = 2-(phenylazo)pyridine) and one Ru^{III} (*cis*-[$RuCl(NO_3)_2$(pdma)NO], where pdma = 1,2-phenylenebis(dimethylarsine)) di-nitrate adduct are documented [52, 53], which both have shorter Ru – O bond lengths than **4.10**, as well as two ruthenium complexes ([(η^5-Cp)$Ru(CO)(AsPh_3)NO_3$], where Cp = cyclopentadienyl, and [(η^6-*p*-cym)$_2Ru_2$(6,6'-Me_2dppz)$(NO_3)_2]^+$, where 6,6'-Me_2dppzH = 2,2'-(1*H*-pyrazole-3,5-diyl)-bis(6-methylpyridine)) containing one monodentate nitrate [54, 55], also with shorter Ru – O bond lengths.

A solution of **4.10** in water gave rise to one species only in the ^{1}H NMR spectrum at pH = 4.1. Raising the pH by stepwise addition of NaOH led to precipitation of an unknown product at pH values as low as 4.8. At pH 7.7 a significant portion of the sample appeared to have precipitated and the colour of the solution was pale yellow. The ^{1}H NMR spectrum showed that the peaks due to the initially present species 'a' started shifting to high-field above pH 5.4. However, they had almost disappeared at pH 6.6, thus preventing determination of the associated pK_a value (Figure 4.10). During each experiment, the pH values measured before

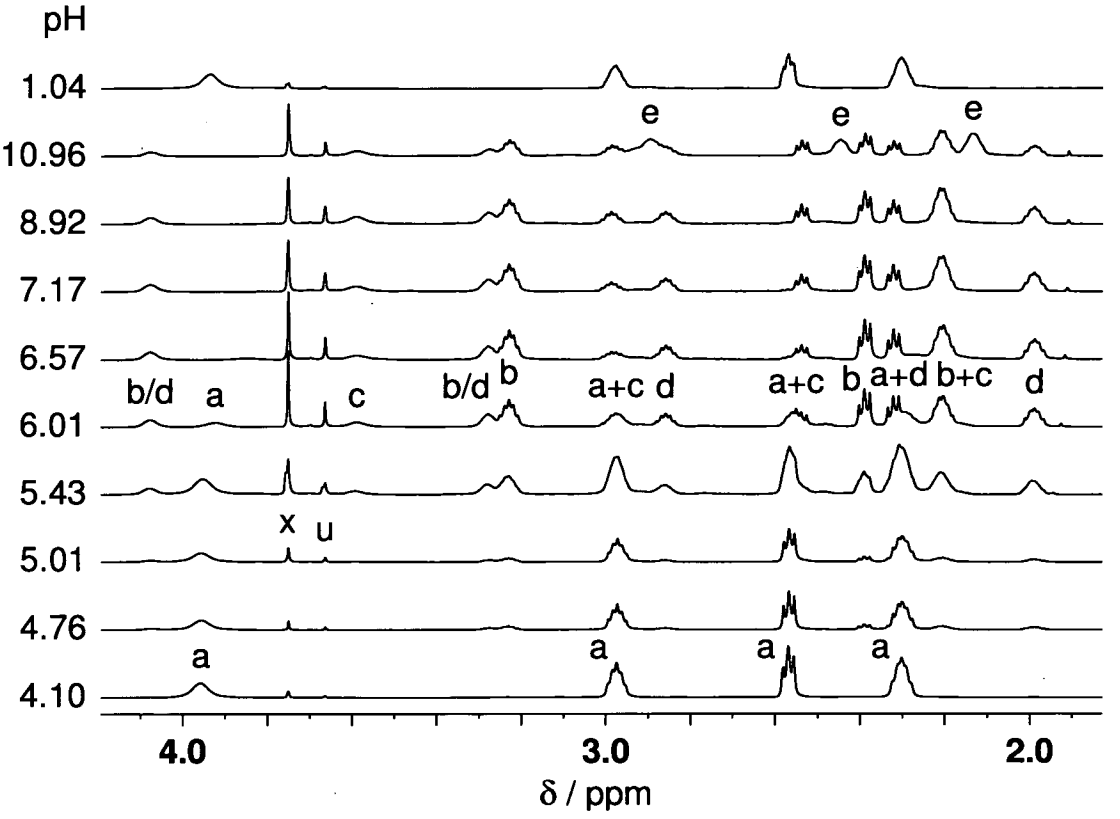

Figure 4.10: The ^{1}H NMR spectra for a pH titration of $[(\eta^6{:}\eta^1\text{-}C_6H_5(CH_2)_3NH_2)Ru(NO_3)_2]$ (**4.10**) in 90% H_2O/ 10 % D_2O at 298 K. With increasing pH a precipitate formed, the initial fully aquated species $[(\eta^1{:}\eta^6\text{-}C_6H_5(CH_2)_3NH_2)Ru(H_2O)_2]^{2+}$ (a) disappears and up to four unknown species (b – e) are present in solution. Upon acidification to pH 1, formation of species (b – e) is reversed, and only species (a) is present in solution. Assignments: x = 1,4-dioxane; u = unknown impurity.

recording the spectrum were always higher by on average 0.2 pH units than those measured after. Three new species were present in solution and the position of their signals did not shift between pH 5.0 to 11.0. When the pH was raised from 8.9 to 11.0, a fourth species appeared. Formation of these species was reversible, since on lowering the pH to 1.0 only 'a' was present in solution. In addition, the precipitate had dissolved.

When the pH of an acidic solution of **4.10** was raised directly to pH 10.1, the presence of the same four main species was detected, however, in different proportions.

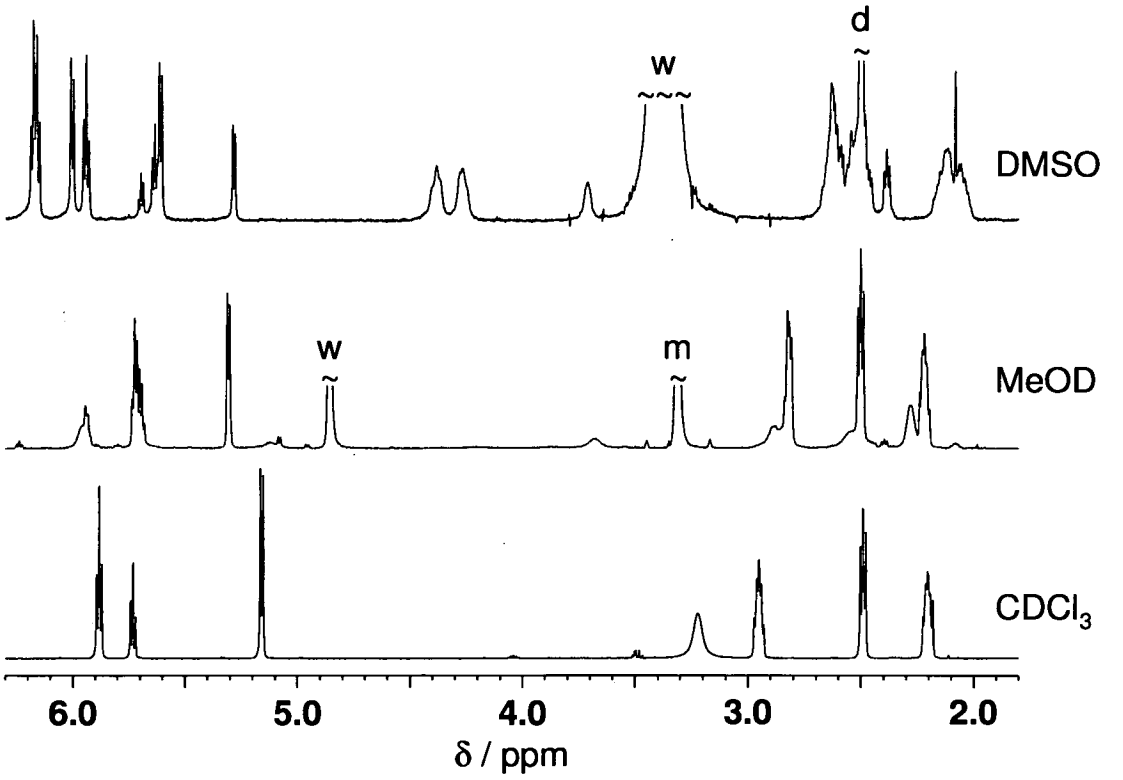

Figure 4.11: The ^{1}H NMR spectra of $[(\eta^6{:}\eta^1\text{-}C_6H_5(CH_2)_3NH_2)RuCl_2]$ (**4.4**) in $CDCl_3$, MeOD-d_4 and DMSO-d_6 at 298 K. One species is present in $CDCl_3$, whereas in MeOD-d_4 and DMSO-d_6 there are two species. Solvent peaks: w = water, m = methanol, d = dimethylsulfoxide.

4.3.1.4 Stability in organic solvents

Figure 4.11 shows a comparison of the ^{1}H NMR spectra of [(η^6:η^1-$C_6H_5(CH_2)_3NH_2$)$RuCl_2$] (**4.4**) in $CDCl_3$, MeOD-d_4 and DMSO-d_6 at 298 K. In contrast to $CDCl_3$, which indicated the presence of only one complex in solution, solutions in MeOD-d_4 and DMSO-d_6 showed the presence of more than one species.

A 2D NOESY spectrum of **4.4** in DMSO-d_6 at 298 K (Figure 4.12) confirmed the presence of two species in solution, one species with three arene and three tether backbone proton signals and one NH_2 proton signal. The other species had five arene, six tether backbone and two NH_2 proton signals.

A spectrum of [(η^6:η^1-$C_6H_5(CH_2)_2NH_2$)$RuCl_2$] (**4.5**) in DMSO-d_6 was recorded at intervals over a period of 450 min at 298 K. During this time the

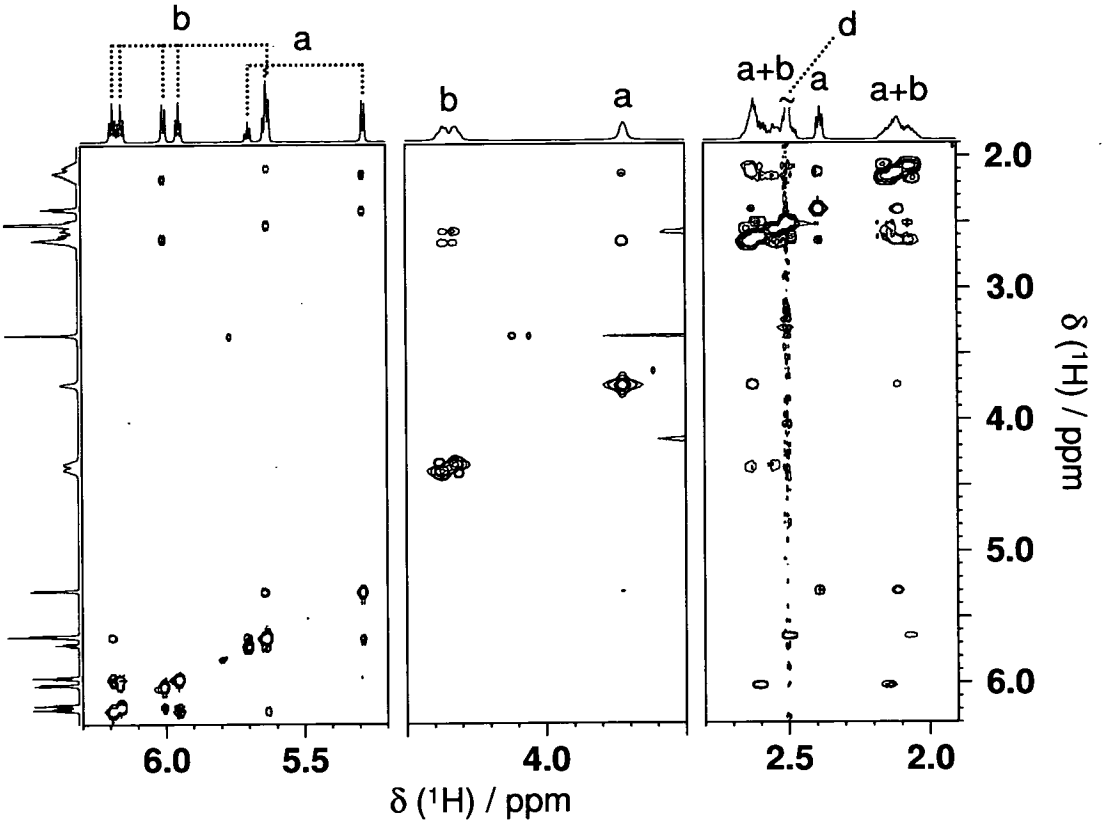

Figure 4.12: The 2D NOESY ^{1}H NMR spectrum of [(η^6:η^1-$C_6H_5(CH_2)_3NH_2$)$RuCl_2$] (**4.4**) in DMSO-d_6 at 298 K. Peaks **a** correspond to [(η^6:η^1-$C_6H_5(CH_2)_3NH_2$)$RuCl_2$] and peaks **b** most likely to [(η^6:η^1-$C_6H_5(CH_2)_3NH_2$)Ru(DMSO)Cl]$^+$.

spectrum changed (Figure 4.13). The eight arene proton- and associated NH_2 peaks disappeared, whereas a complex multiplet at around 7.3 ppm increased in intensity. Figure 4.13 also shows the arene proton region of free 2-phenethylamine. Similar experiments with complexes $[(\eta^6{:}\eta^1\text{-}C_6H_5(CH_2)C_5H_4N)RuCl_2]$ (**4.7**) and $[(\eta^6{:}\eta^1\text{-}C_6H_5(C_6H_4)NH_2)RuCl_2]$ (**4.8**) also showed the appearance of signals with similar chemical shifts to free 2-benzylpyridine and 2-aminobiphenyl, albeit not as rapidly. In contrast, a spectrum of **4.4** monitored over the same period showed no changes in its spectrum in DMSO-d_6.

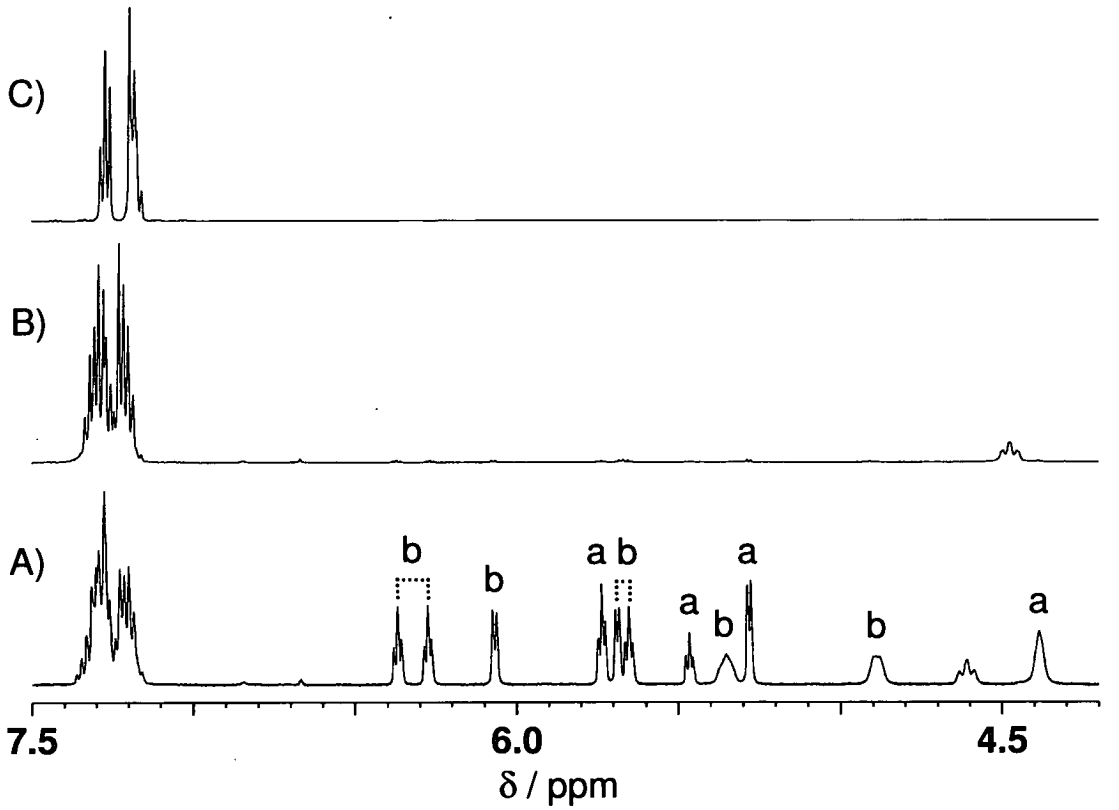

Figure 4.13: The ^1H NMR spectrum of $[(\eta^6{:}\eta^1\text{-}C_6H_5(CH_2)_2NH_2)RuCl_2]$ (**4.5**) in DMSO-d_6 at 298 K. A: After 80 minutes. The solution contains $[(\eta^6{:}\eta^1\text{-}C_6H_5(CH_2)_2NH_2)RuCl_2]$ (**a**) and most likely $[(\eta^6{:}\eta^1\text{-}C_6H_5(CH_2)_2NH_2)Ru(DMSO)Cl]^+$ (**b**). B: After 450 minutes. C: Free 2-phenethylamine.

4.3.1.5 Reactions with nucleobases in solution

Time-course for reaction of $[(\eta^6:\eta^1\text{-}C_6H_5(CH_2)_3NH_2)Ru(NO_3)_2]$ (4.10) with 9EtG: 600 µl of a 2.2 mM solution of 9EtG in 90% H_2O/ 10% D_2O and 5 µl of a 1% solution of 1,4-dioxane in 90% H_2O/ 10% D_2O were added to a 5 mm NMR tube. To this, 58.4 µl of a 12.9 mM solution of **4.10** in 90% H_2O/ 10% D_2O was added and the pH of the solution was measured (5.19). The spectrum was recorded at t = 24 min, t = 46 min and every 20 min for a period of 16.5 h. The starting material appeared to have been consumed by the time the first spectrum was recorded. Two new 9EtG peaks were observed in addition to free 9EtG. With increasing time a different set of arene proton signals was noted, which did not appear to be assignable to 9EtG. The pH of the solution after 16.5 h was 6.22.

Time-course for reaction of $[(\eta^6:\eta^1\text{-}C_6H_5(CH_2)_3NH_2)RuCl_2]$ (4.4) with 9EtG in the presence of chloride ($[Cl^-]_t$ = 21.7 mM): 600 µl of a 2.2 mM solution of 9EtG in 90% H_2O/ 10% D_2O, 5 µl of a 1% solution of 1,4-dioxane in 90% H_2O/ 10% D_2O and 4.4 µl of a 3 M solution of NaCl in 90% H_2O/ 10% D_2O were added to a 5 mm NMR tube. To this, 58.4 µl of a 11.3 mM solution of **4.4** in 90% H_2O/ 10% D_2O was added and the pH of the solution was measured (6.08). The spectrum was recorded at t = 45 min, and another 5 times between t = 45 – 134 min, and then every 30 min from t = 134 min for a period of 18 h. Three new 9EtG peaks, of which two were overlapping each other, were observed in addition to free 9EtG. The pH of the solution after 18 h was 6.53.

Time-course for reaction of $[(\eta^6:\eta^1\text{-}C_6H_5(CH_2)_2NH_2)RuCl_2]$ (4.5) with 9EtG in the presence of chloride ($[Cl^-]_t$ = 21.7 mM): 600 µl of a 2.2 mM solution of 9EtG in 90% H_2O/ 10% D_2O, 5 µl of a 1% solution of 1,4-dioxane in 90% H_2O/ 10% D_2O and 4.4 µl of a 3 M solution of NaCl in 90% H_2O/ 10% D_2O were added to a 5 mm NMR tube. To this, 58.4 µl of a 11.3 mM solution of **4.5** in 90% H_2O/ 10% D_2O was added and the pH of the solution was measured (6.08). The spectrum was

recorded at t = 32 min, t = 53 min, and then every 30 min from t = 123 min for a period of 41 h. The starting material, $[(\eta^6{:}\eta^1\text{-}C_6H_5(CH_2)_2NH_2)RuCl_2]$, appeared to have all reacted within 53 min, and $[(\eta^6{:}\eta^1\text{-}C_6H_5(CH_2)_2NH_2)Ru(H_2O)Cl]^+$ within 183 min. No $[(\eta^6{:}\eta^1\text{-}C_6H_5(CH_2)_2NH_2)Ru(H_2O)_2]^{2+}$ was detected by the time the first spectrum was recorded. Three new 9EtG peaks were observed in addition to free 9EtG. The pH of the solution after 41 h was 6.23.

Hydrolysis of 9EtG adducts of $\{(\eta^6{:}\eta^1\text{-}C_6H_5(CH_2)_3NH_2)Ru\}^{2+}$: The ^1H NMR spectra of three solutions of $[(\eta^6{:}\eta^1\text{-}C_6H_5(CH_2)_3NH_2)Ru(9EtG)_2](PF_6)_2$ (**4.11a**), (a) 4.3 mM Ru, pH* = 6.47, (b) 1.95 mM Ru, pH* = 3.95 and (c) 0.96 mM Ru, pH* = 7.66, were recorded in D_2O at 298 K. The spectra showed the presence of one species in solution, which was assigned to the title compound (Figure 4.14). The product 9EtG H8 peaks appeared at *ca.* 8.25 ppm, an upfield shift of 0.43 ppm compared to free 9EtG. The tether NH_2 signal had shifted from 3.92 ppm (pH = 6.22) for the fully aquated complex, to 5.41 ppm (pH* = 6.47) and 5.57 ppm (pH* = 7.66). Each solution also contained traces (<3%) of $[(\eta^6{:}\eta^1\text{-}C_6H_5(CH_2)_3NH_2)Ru(9EtG)(H_2O)]^{2+}$ and free 9EtG. The spectra were re-recorded after 22.5 h (17 h for solution (b)), with pH* = 6.31 for solution (a), pH* = 4.40 for solution (b) and pH* = 6.74 for solution (c), and additional signals were noted.

The ^1H NMR spectrum of a solution of **4.11a** (3.0 mM Ru) in D_2O at pH* = 6.67 and 298 K was recorded at t = 10 min, t = 19 min and then every 20 min starting at t = 42 for a period of 20 h. A singlet at 8.25 ppm decreased in intensity and two new signals at 8.14 and 7.82 ppm increased in intensity. The pH* of the solution after 20 h was 6.02.

The ^1H NMR spectrum of a solution containing $[(\eta^6{:}\eta^1\text{-}C_6H_5(CH_2)_3NH_2)Ru(9EtG)NO_3]PF_6$ (**4.12**) (*ca.* 4.0 mM) was recorded at pH* = 5.71 and 298 K. The spectrum showed the presence of mainly $[(\eta^6{:}\eta^1\text{-}C_6H_5(CH_2)_3NH_2)Ru(9EtG)]^+$ as well as the di-9EtG adduct. The ratio of the di- to the

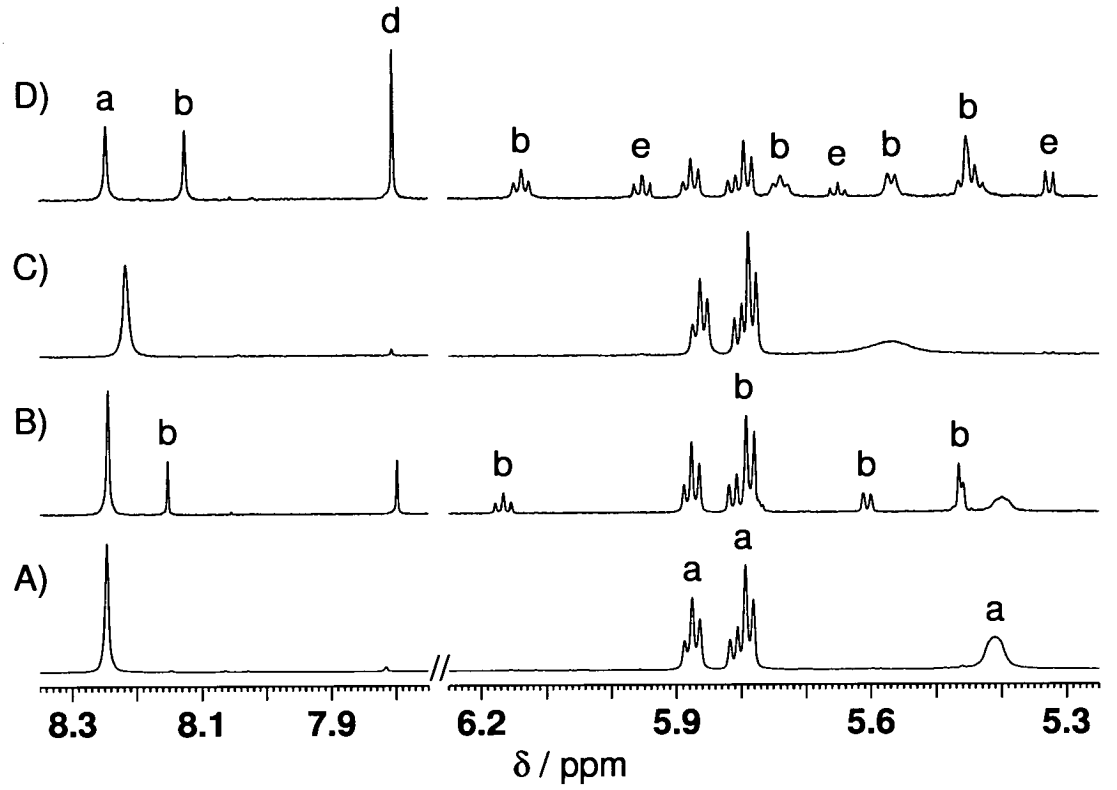

Figure 4.14: The 9EtG H8 proton and arene proton region of the ^{1}H NMR spectrum of $[(\eta^6{:}\eta^1\text{-}C_6H_5(CH_2)_3NH_2)Ru(9EtG)_2]^{2+}$ (**4.11a**) in D_2O at 298 K. A: 4.3 mM Ru after dissolution at pH* = 6.47. B: 4.3 mM Ru after 22.5 h at pH* = 6.31. C: 0.96 mM Ru after dissolution at pH* = 7.66. D: 0.96 mM Ru after 22.5 h at pH* = 6.74. Assignments: a = $[(\eta^6{:}\eta^1\text{-}C_6H_5(CH_2)_3NH_2)Ru(9EtG)_2]^{2+}$; b = $[(\eta^6{:}\eta^1\text{-}C_6H_5(CH_2)_3NH_2)Ru(9EtG)(H_2O/OH)]^{n+}$ n = 2/1; d = free 9EtG; e = hydroxo-bridged species?

mono-9EtG adduct changed from an initial *ca.* 0.09 : 1 to *ca.* 0.16 : 1 after 22 h (pH* = 5.57). In addition an increase in the presence of the diaqua complex $[(\eta^6{:}\eta^1\text{-}C_6H_5(CH_2)_3NH_2)Ru(H_2O)_2]^{2+}$ was detected.

Reaction of $[(\eta^6{:}\eta^1\text{-}C_6H_5(CH_2)_3NH_2)Ru(NO_3)_2]$ (4.10) with guanosine: The addition of guanosine to a solution of $[(\eta^6{:}\eta^1\text{-}C_6H_5(CH_2)_3NH_2)Ru(NO_3)_2]$ (**4.10**) (7.4 mM Ru) in 90% H_2O/ 10% D_2O was monitored by ^{1}H NMR at t = 20 min (Figure 4.15). Two singlets, at 8.40 and 8.39 ppm, appeared in the Guo H8 region after addition of 0.75 equiv of Guo at 298 K and pH 4.86. Addition of a total of 1.5

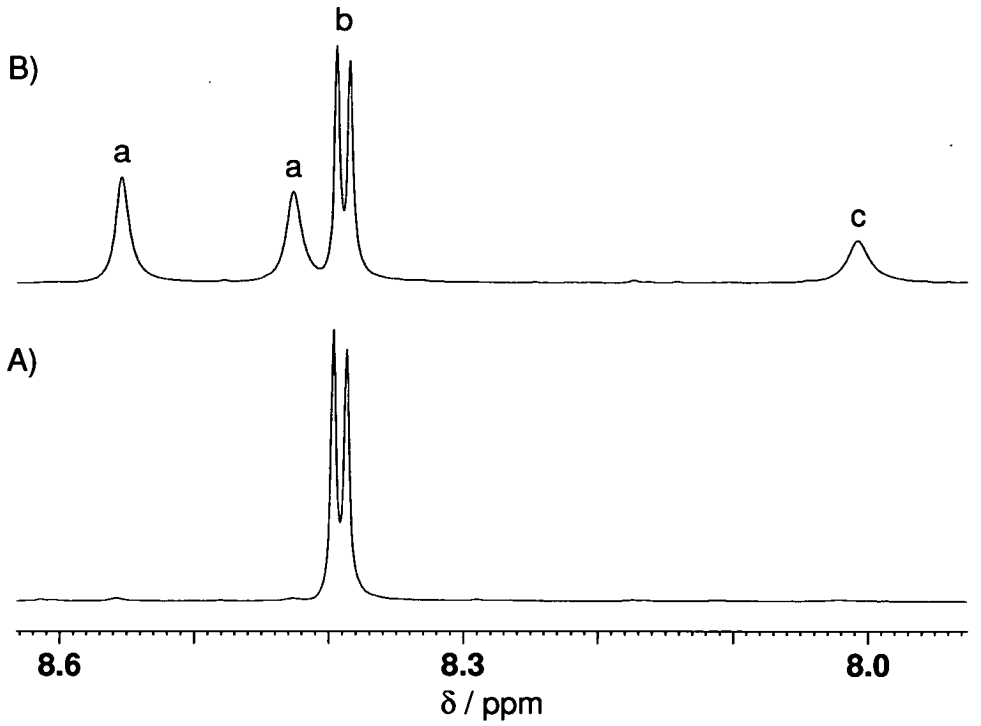

Figure 4.15: The Guo H8 proton region of the ^{1}H NMR spectrum of a solution containing Guo and $[(\eta^1{:}\eta^6\text{-}C_6H_5(CH_2)_3NH_2)Ru(NO_3)_2]$ (**4.10**) in 90% H_2O / 10% D_2O. A: 0.75 mol equiv Guo at pH = 4.86 and 298 K after 30 min. B: 1.5 mol equiv of Guo after incubation at 310 K for 10 h at pH = 5.39. Assignments: a = $[(\eta^6{:}\eta^1\text{-}C_6H_5(CH_2)_3NH_2)Ru^*(Guo^*)_2]^{2+}$; b = $[(\eta^6{:}\eta^1\text{-}C_6H_5(CH_2)_3NH_2)Ru^*(Guo^*)H_2O]^+$; c = free Guo.

mol equiv of Guo and incubation of the solution at 310 K for 10 h (pH = 5.39) resulted in two other new peaks at 8.55 and 8.43 ppm.

4.3.1.6 X-ray crystal structure of $[(\eta^6{:}\eta^1\text{-}C_6H_5(CH_2)_3NH_2)Ru(9EtG)_2](CF_3SO_3)_2$ (4.11b)

Slow evaporation of an acetone solution containing $[(\eta^6{:}\eta^1\text{-}C_6H_5(CH_2)_3NH_2)Ru(9EtG)_2](PF_6)_2$ (**4.11a**) was the technique used in an attempt to grow crystals of **4.11a**. However, the structure obtained was that of $[(\eta^6{:}\eta^1\text{-}C_6H_5(CH_2)_3NH_2)Ru(9EtG)_2](NO_3)_2$ (Figure A.4.5). Thus X-ray crystallography showed that counterion metathesis from NO_3^- to PF_6^- had not gone to completion,

possibly due to apparent ability of nitrate to participate in H-bond interactions with N1H and N2H. The structure was not fully refined though since the crystals were of poor quality.

Crystals of X-ray diffraction quality were obtained for $[(\eta^6{:}\eta^1\text{-}C_6H_5(CH_2)_3NH_2)Ru(9EtG)_2](CF_3SO_3)_2$ (**4.11b**) by slow diffusion of diethyl ether into an acetone solution containing **4.11b** at ambient temperature. The structure is shown in Figure 4.16, the crystal data in Table A.4.2 and bond angles and lengths in Table 4.7. The Ru – N(tether) bond length is 2.121(2) Å, the Ru – N(9EtG) distances are 2.101(2) Å and 2.1588(18) Å, respectively. The Ru – C(arene) bond lengths of 2.165(2) – 2.22(3) Å are longer on average than for **4.4**. The Ru – centroid distance is 1.67 Å. The Ru – C5 – C4 angle, where C5 is the arene carbon where the tether is

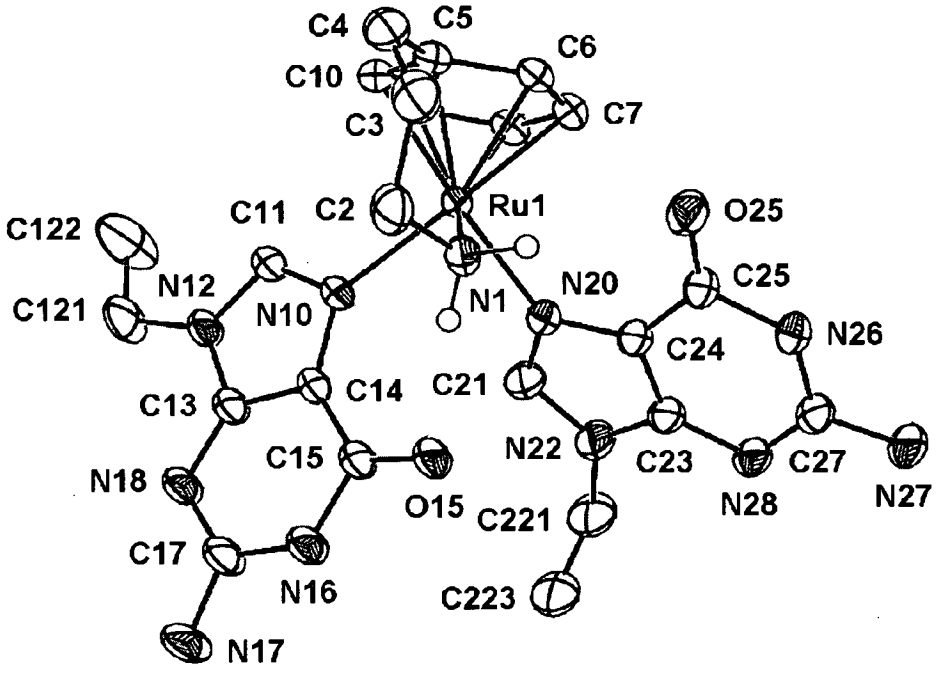

Figure 4.16: Ortep diagram (50% probability ellipsoids) and atom numbering scheme for the cation in the X-ray crystal structure of $[(\eta^6{:}\eta^1\text{-}C_6H_5(CH_2)_3NH_2)Ru(9EtG)_2](CF_3SO_3)_2$ (**4.11b**). The hydrogen atoms, with the exception of the tether NH_2 protons, which are H-bonded to O15 and O25, have been omitted for clarity.

Table 4.7: Selected bond lengths (Å) and angles (°) for $[(\eta^6:\eta^1\text{-}C_6H_5(CH_2)_3NH_2)Ru(9EtG)_2](CF_3SO_3)_2$ (**4.11b**).

Bond	Length	Bond	Length/angle
Ru-N1	2.121(2)	Ru-C10	2.191(2)
Ru-N10	2.1588(18)	Ru-centroid[a]	1.672
Ru-N20	2.101(2)	N1-Ru-N10	86.94(8)
Ru-C5	2.178(2)	N1-Ru-N20	82.96(8)
Ru-C6	2.172(2)	N10-Ru-N20	87.49(8)
Ru-C7	2.165(2)	Ru-N1-C2	117.26(17)
Ru-C8	2.210(3)	Ru-C5-C4	123.85(19)
Ru-C9	2.232(3)	N1-Ru-C5	89.94(10)

[a] = measured using Mercury 1.4.

connected and C4 the first carbon atom of the tether, is 123.85(19)°. The C5 – Ru – N(tether) angle is 89.94(10)°. The angle between the plane defined by all arene carbons and that of C5, Ru and N(tether) is 72.77°. The coordinated 9EtG molecules show a number of H-bond interactions with the tether amine, residual water, the CF_3SO_3 counter anion as well as neighbouring 9EtG ligands. The tether amine protons both show hydrogen bonds with the carbonyl groups of 9EtG, where H11···O15 1.98 Å (N1···O15 2.869(3) Å) and H12···O25 2.32 Å (N1···O25 3.085(3) Å), with the latter carbonyl also interacting with residual water (H2···O25 2.14 Å, O1···O25 2.881(3) Å). Interactions between neighbouring N2H and N3 atoms, with H171···N18 2.11 Å (N17···N18 3.004(4) Å) and H271···N28 2.14 Å (N27···N28 3.017(3) Å), are complemented by H-bonds between some oxygen atoms of CF_3SO_3 and the N1H and N2H protons, with H272···O12 2.11 Å (N27···O12 2.972(4) Å) and H261···O11 2.13 Å (N26···O11 3.028(4) Å) as well as H172···O22 2.01 Å (N17···O22 2.871(4) Å) and H161···O23 1.96 Å (N16···O23 2.856(3) Å).

4.3.2 Discussion

4.3.2.1 Synthesis

The synthesis of tethered Ru^{II} arene complexes involved the thermal displacement of ethyl benzoate by a pendent arene. Arene exchange reactions are believed to proceed *via* progressive removal of the arene ligand from η^6 to η^4 and η^2 [56]. An increased presence of THF in the reaction mixture appeared to lead to higher yields, in agreement with Bennett *et al.* [30], possibly because this weakly coordinating solvent could stabilise the transition state.

Increasing the reaction temperature from 363 K (near the boiling point of 1,2-dichloroethane) to 393 K increased the yields in some reactions (see Table 4.1). However, this increase in yield was most likely not simply a consequence of the higher temperature. Keeping the temperature at 393 K, but changing the solvent to 1,2,3-trichloropropane (boiling point of 429 K) generally did not yield a product. The product formed only under reflux conditions, however, in poor yield. Since a product was obtained from comparatively mild heating from an oil bath, but not from stronger heating with a heating mantel, it seems reasonable that too high temperature led to the decomposition of the product. The finding that product formation in 1,2-dichloroethane appears to be strongly favoured under reflux conditions but not in 1,2,3-trichloropropane at similar temperature led to the development of the pressure vessel. Standard reflux reaction set-ups were not stabile enough to cope with temperatures of 393 K without loss of solvent. With the pressure vessel, no solvent was lost and in addition an internal pressure was generated in the vessel. This pressure appeared to be of significant importance with respect to increasing the yields of these reactions, which in turn reduced the amount of impurities from decomposition.

The mechanism by which pressure influences the yield is not clear. However, it could assist in overcoming reaction barriers between the tether arene and the

ruthenium centre. In the case of aliphatic tethers, most impurities could be separated by filtration, whereas for aromatic tethers the precipitate was analytically pure, only requiring filtration.

The pressure vessel provides a very convenient route for preparation of nitrogen-based tethered ruthenium(II) arene complexes for the following reasons.

- Dry solvents not necessarily needed, all were used as received
- Comparatively short, overnight reactions
- Good-to-high yields
- Separation of impurities by filtration, chromatography not required

There could be further scope for improvement of the experimental procedure, by detailed studies of the effect of time and temperature on the reactions. Furthermore, dry solvents might increase the yield.

4.3.2.2 Characterisation

X-ray crystallography confirmed the presence of the tether in all four molecules investigated. Overall, the tether in complex [(η^6:η^1-$C_6H_5(CH_2)_2NH_2$)$RuCl_2$] (**4.5**) appears more strained than comparable phosphorus analogues, since Ru – C(arene) and Ru – N distances tend to be shorter. This strain imposed by the difference in bond lengths is accommodated by a change in angles, most notably the Ru – C4 – C5 angle (114.74° for **4.5**), where C4 is the arene carbon where the tether is connected and C5 the first carbon atom of the tether, which is 5 – 7° more narrow than in phosphorus analogues together with differences of *ca.* 10° in the Ru – N/P – C(tether) angle. Similarly for [(η^6:η^1-$C_6H_5(CH_2)_3NH_2$)$RuCl_2$] (**4.4**), the angles within the tether tend to be slightly wider for phosphorus analogues compared to the three carbon nitrogen tether.

The two-carbon tethered complexes **4.5** and [(η^6:η^1-$C_6H_5(CH_2)C_5H_4N$)$RuCl_2$] (**4.7**) show pronounced buckling of the coordinated arene. This seemingly is a

consequence of the arene accommodating the strain exerted by the chelating tether. The added flexibility offered by the three atom tethered molecules **4.4** and [(η^6:η^1-$C_6H_5O(CH_2)_2NH_2$)$RuCl_2$] (**4.6**) results in the arene adopting a more planar conformation.

For all complexes, the dramatic change in the shifts of the arene upon coordination to ruthenium and the associated 2 : 1 : 2 proton signal intensity pattern (multiplet for uncoordinated arene), due to equivalence of the *ortho* and *meta* protons, are the most significant signs of coordination [57]. For the aliphatic systems, the pronounced shift of the NH_2 signals confirms coordination. The chemical shifts of the CH_2 of the tether are also affected by coordination to ruthenium. The most dramatic example is [(η^6:η^1-$C_6H_5(CH_2)_2NH_2$)$RuCl_2$] (**4.5**), where the signal of the CH_2 group next to the amine is shifted downfield by 0.9 ppm. The resonance for the CH_2 group next to the arene moved upfield by 0.1 ppm with respect to the free ligand. For complex [(η^6:η^1-$C_6H_5(CH_2)_3NH_2$)$RuCl_2$] (**4.4**), the CH_2 shifts of the tether are in the range of 0.15 – 0.4 ppm, those for [(η^6:η^1-$C_6H_5O(CH_2)_2NH_2$)$RuCl_2$] (**4.6**) are 0.1 – 0.5 ppm, all upfield. Assignment of the signals to the CH_2 protons was aided by the coupling of the CH_2 protons to the amine protons. This is not observed in the free ligands, where *e.g.* for 2-phenethylamine two triplets are observed. Upon coordination in **4.5**, they appear as a triplet for the CH_2 group next to the amine and one multiplet, which stems from the CH_2 group next to the amine, which shows coupling to the neighbouring NH_2 and CH_2 groups. The 2D NOESY ^1H NMR spectrum of **4.4** in $CDCl_3$ confirmed the assignment of the signals.

Those tethered complexes containing a heterocyclic backbone showed less pronounced changes of proton shifts between the free and the coordinated ligands.

4.3.2.3 Aqueous chemistry

An important feature of the tethered molecules studied in this work is their water solubility at millimolar concentrations, allowing their aqueous chemistry to be studied by ^{1}H NMR spectroscopy. In the case of $[(\eta^6{:}\eta^1\text{-}C_6H_5(C_6H_4)NH_2)RuCl_2]$ (**4.8**), poor water solubility of the di-chloro species was observed.

In the context of hydrolysis, the following signal pattern for arene ^{1}H NMR peaks can be expected. For the fully chlorinated complex, the molecule possesses an axis of symmetry along the plane including the Ru centre and the tether (Scheme 4.3). The protons in the *ortho* and *meta* positions with respect to the tether are equivalent resulting in three arene proton signals, a doublet and two triplets, with

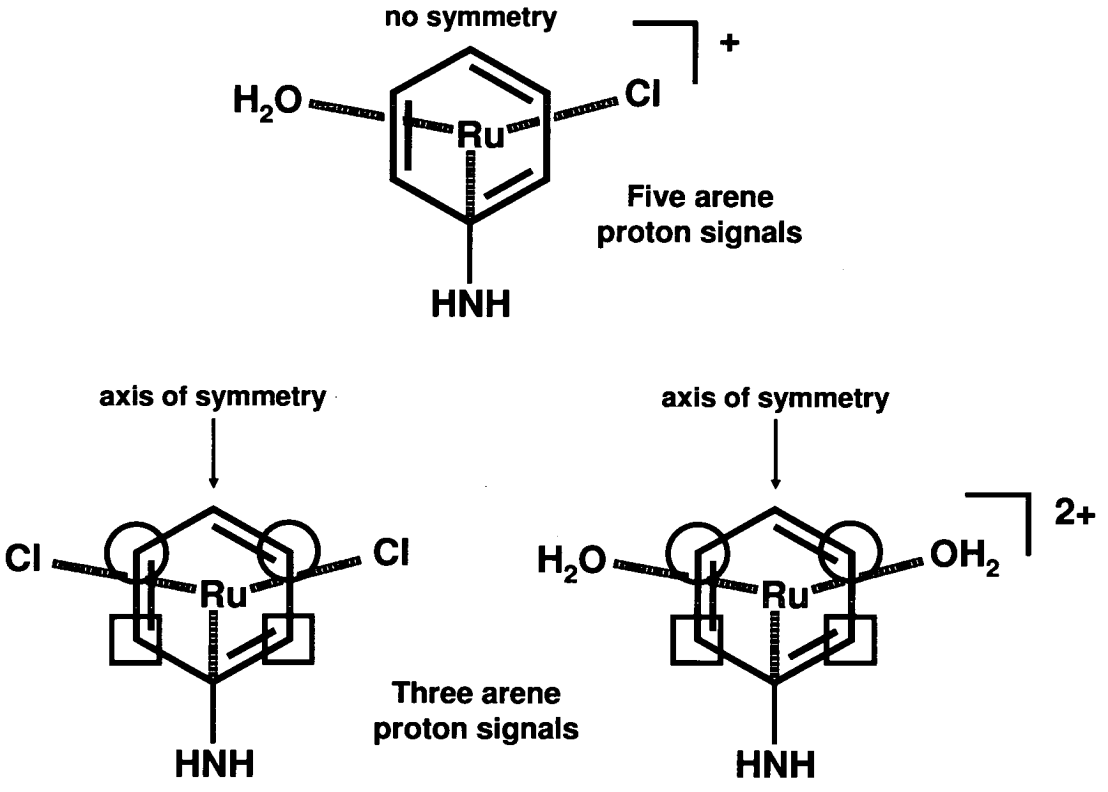

Scheme 4.3: For $[(\eta^6{:}\eta^1\text{-}C_6H_5(CH_2)_3NH_2)Ru(H_2O)Cl]^+$ all arene protons are inequivalent resulting in five arene proton signals in the ^{1}H NMR spectrum. $[(\eta^6{:}\eta^1\text{-}C_6H_5(CH_2)_3NH_2)RuCl_2]$ and $[(\eta^6{:}\eta^1\text{-}C_6H_5(CH_2)_3NH_2)Ru(H_2O)_2]^{2+}$ possess an axis of symmetry, giving rise to magnetically equivalent arene protons (□ and ○), which results in three arene proton signals in the ^{1}H NMR spectra.

relative intensities 2 : 1 : 2. Mono-aquation leads to chirality at the ruthenium centre. The five arene protons are magnetically inequivalent and produce five signals, two doublets and three triplets, all with relative intensities of 1H. Full aquation of the complex restores symmetry and leads to three signals as for the di-chloro adduct.

The chloride titration of $[(\eta^6:\eta^1\text{-}C_6H_5(CH_2)_2NH_2)RuCl_2]$ (**4.5**) illustrates this behaviour (see Figure 4.8). Integration of the area of the arene proton peaks indicates the relative proportions of the three species present in solution. Figure 4.17 shows a plot of the concentration of Ru species versus concentration of free chloride ($[Cl^-]_f$) for **4.5**. The concentration of the diaqua complex $[(\eta^6:\eta^1\text{-}C_6H_5(CH_2)_2NH_2)Ru(H_2O)_2]^{2+}$ (symmetrical, three arene proton signals in the ^1H NMR spectrum) approaches zero with increasing chloride concentration. The

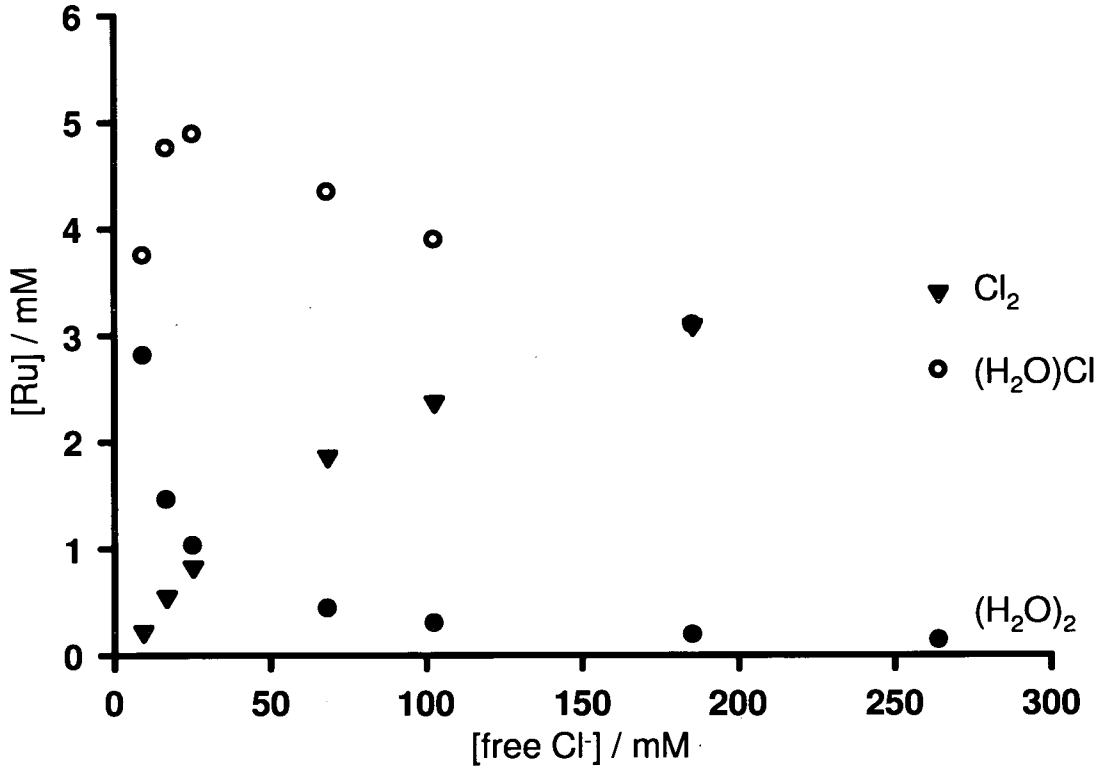

Figure 4.17: Plot of the concentration of Ru species versus concentration of free chloride for $[(\eta^6:\eta^1\text{-}C_6H_5(CH_2)_2NH_2)RuCl_2]$ (**4.5**) (6.8 mM Ru at start of titration). Symbols: (●) = $[(\eta^6:\eta^1\text{-}C_6H_5(CH_2)_2NH_2)Ru(H_2O)_2]^{2+}$; (○) = $[(\eta^6:\eta^1\text{-}C_6H_5(CH_2)_2NH_2)Ru(H_2O)Cl]^+$; (▼) = $[(\eta^6:\eta^1\text{-}C_6H_5(CH_2)_2NH_2)RuCl_2]$.

concentration of the mono-aqua species $[(\eta^6:\eta^1\text{-}C_6H_5(CH_2)_2NH_2)Ru(H_2O)Cl]^+$ (asymmetric, five arene proton signals in the ^1H NMR spectrum), appears to reach a maximum around 40 mM of free chloride and decreases in the presence of further added chloride. The initially increasing presence of the mono-aqua adduct in solution arises from conversion of the diaqua- to the mono-aqua species, the latter being depleted by conversion into the fully chlorinated species upon further addition of chloride. The concentration of $[(\eta^6:\eta^1\text{-}C_6H_5(CH_2)_2NH_2)RuCl_2]$ (symmetrical, three arene proton signals in the ^1H NMR spectrum) increases in intensity as the concentration of chloride increases.

Figure 4.18 shows a plot of the variation in concentration of Ru species present in aqueous solution of $[(\eta^6:\eta^1\text{-}C_6H_5(CH_2)_3NH_2)RuCl_2]$ (**4.4**) in the presence

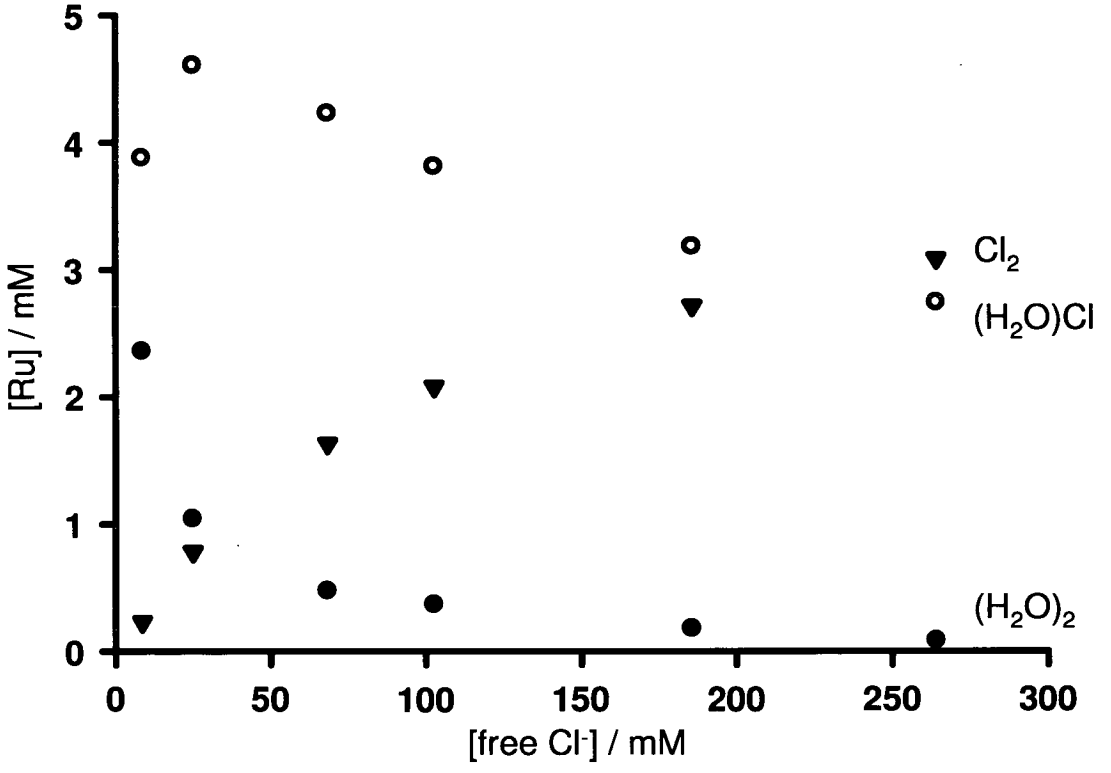

Figure 4.18: Plot of the concentration of Ru species versus concentration of free chloride for $[(\eta^6:\eta^1\text{-}C_6H_5(CH_2)_3NH_2)RuCl_2]$ (**4.4**) (6.5 mM Ru at start of titration). Symbols: (●) = $[(\eta^6:\eta^1\text{-}C_6H_5(CH_2)_3NH_2)Ru(H_2O)_2]^{2+}$; (○) = $[(\eta^6:\eta^1\text{-}C_6H_5(CH_2)_3NH_2)Ru(H_2O)Cl]^+$; (▼) = $[(\eta^6:\eta^1\text{-}C_6H_5(CH_2)_3NH_2)RuCl_2]$.

of increasing concentration of free chloride. The variations in concentration of the di-chloro, mono- and di-aqua complexes are very similar to those for **4.5**.

During the titrations, each spectrum was recorded 20 min after dissolution or after addition of chloride. The observed equilibria were reached within 20 min. For solutions containing **4.5** with $[Cl^-]_t$ 13.6 mM and 273.6 mM as well as for **4.4** with $[Cl^-]_t$ 12.9 mM and 273.1 mM, the spectra were re-recorded after 22 h and showed no significant changes in the proportions of the signals.

This allowed the equilibrium constants to be determined, based on the dependence shown in Scheme 4.4.

For **4.4**, the calculated equilibrium constants (best fit) are K_1 = 139 mM (R^2 = 0.9998) and K_2 = 5.0 mM (R^2 = 0.9968) (Figure 4.19). The values for **4.5** are K_1 = 153 mM (R^2 = 0.9979) and K_2 = 6.5 mM (R^2 = 0.9652) (Figure A.4.6).

The results show that both coordinated chloride ligands can undergo hydrolysis. At $[Cl^-]$ levels comparable to those inside cells (4 – 25 mM), less than 10% of the complexes **4.4** and **4.5** would be present in the fully chlorinated form, with *ca.* 20% in the diaqua- and *ca.* 70% in the mono-aqua form. At physiological $[Cl^-]$ (*ca.* 104 mM), around 60% of the complexes could be present as the mono-aqua adduct, with *ca.* 35% as the di-chloro adduct and negligible amounts of the diaqua complex. It thus appears that in the present tethered systems loss of one chloride ligand is strongly favoured, illustrated by the presence of *ca.* 40% of the mono-hydrolysed species at $[Cl^-]$ as high as 275 mM.

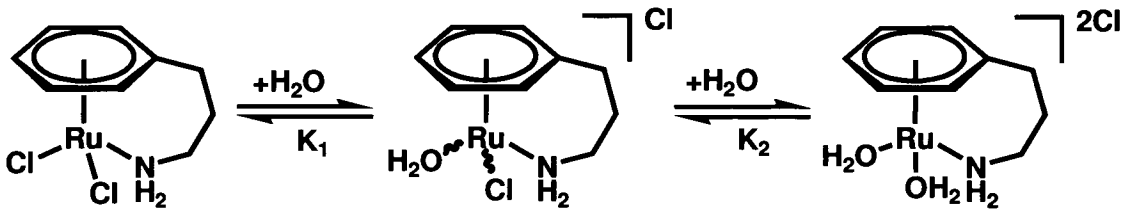

Scheme 4.4: The hydrolysis of $[(\eta^6{:}\eta^1\text{-}C_6H_5(CH_2)_3NH_2)RuCl_2]$ (**4.4**) and the associated equilibrium constants K_1 and K_2.

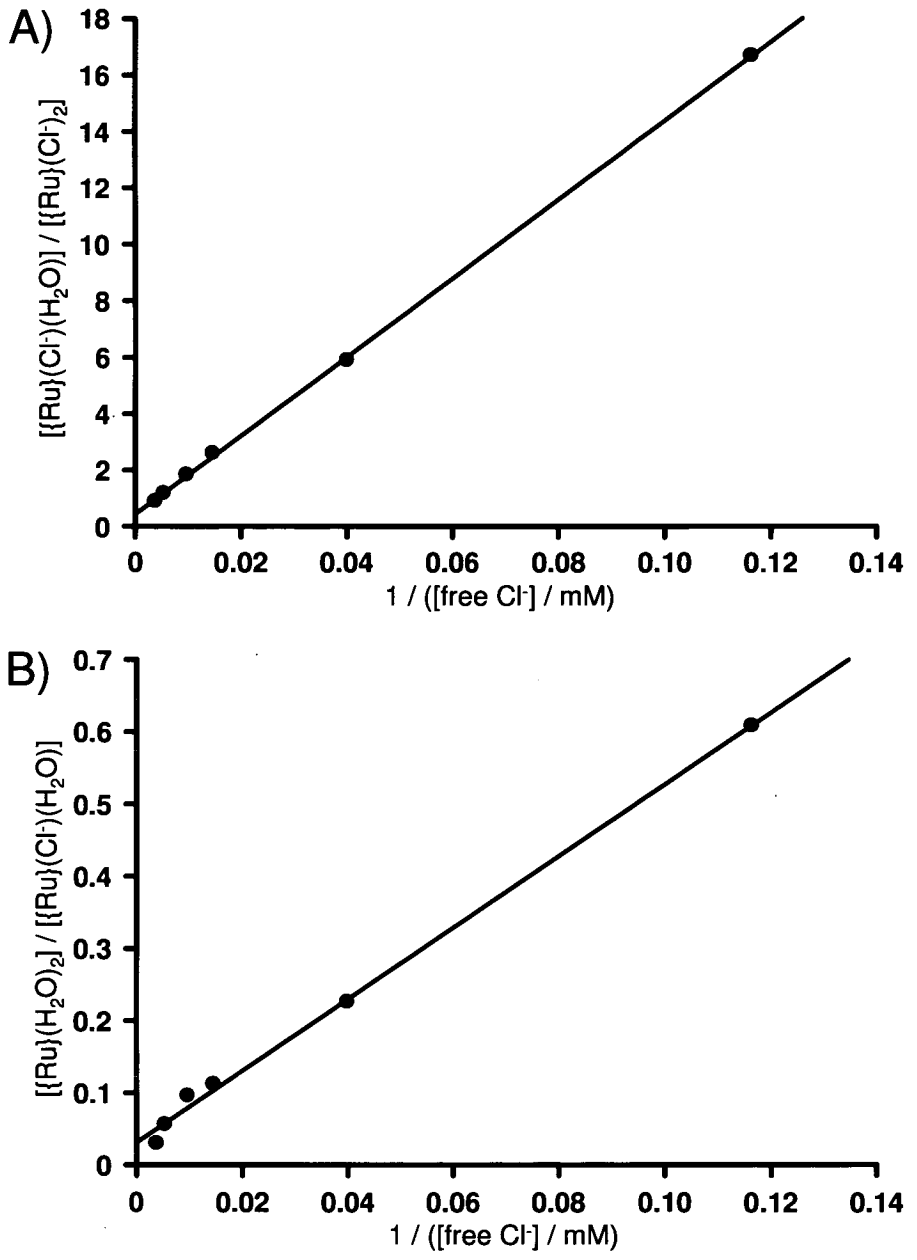

Figure 4.19: Plot of the ratio of the concentrations of the fully aquated over the mono-aquated ruthenium species (A) and the ratio of the concentrations of the mono-aquated over the fully chlorinated (B) ruthenium species versus the concentration of free chloride for a chloride titration of $[(\eta^6{:}\eta^1\text{-}C_6H_5(CH_2)_3NH_2)RuCl_2]$ (**4.4**) (ca. 6.5 mM at start of titration) in D_2O at 298 K. The slopes give the equilibrium constants K_1 = 139 mM (A) and K_2 = 5.0 mM (B), respectively. With the resulting graph lines set to go through the origin K_1 = 145 mM, K_2 = 5.4 mM (**4.4**) are obtained.

The equilibrium constants K_1 and K_2 determined for complexes **4.4** and **4.5** are considerably higher than those of cisplatin for example, for which values for K_1 = 3.3 – 3.9 mM and K_2 = 0.2 – 0.4 mM (0.3 M ionic strength, 298 – 308 K) [58], K_1 = 6.4 mM and K_2 = 0.3 mM (0.1 M ionic strength, 298 K) [59], K_1 = 2.52 mM and K_2 = 0.03 mM (10 mM ionic strength, 310 K) [60] have been reported. The value for K_2, however, is comparable to that found for the aquation of some mono-functional ruthenium(II) arene complexes of the type $\{(\eta^6\text{-arene})Ru(en)\}^{2+}$ [61]. Loss of a negatively-charged chloride ligand from a positively charged complex (*i.e.* complete hydrolysis in the present case) would be expected to be less favourable than from a neutral complex (*i.e.* mono-aquation). Curiously, the hydrolysis equilibrium constants reported by Scolaro *et al.* for $[(\eta^6\text{-}p\text{-cymene})Ru(pta)Cl_2]$, where pta = 1,3,5-triaza-7-phosphaadamantane, of K_1 = 0.03 mM and K_2 = 107 mM at 298 K (*i.e.* $K_1 > K_2$) [12] follow the reverse order of those for platinum diam(m)ine complexes and those for the tethered Ru^{II} arene complexes. The values were determined from a chloride titration with a maximum documented concentration of free chloride of 4 mM. However, no details of the data analysis were given.

The above results for the tethered complexes suggest that under cell-testing conditions, the tethered complexes would be expected to be present mainly as the mono-hydrolysed complex in the extra-cellular medium ($[Cl^-]$ *ca.* 104 mM). Thus the complexes would be able to react with components of the cell medium, potentially giving rise to deactivating pathways.

Dissolution of $[(\eta^6{:}\eta^1\text{-}C_6H_5(CH_2)_3NH_2)Ru(NO_3)_2]$ (**4.10**) in water produces signals for one species only. These are presumably due to the fully hydrolysed complex. Similar complete hydrolysis of the nitrato complex α-$[Ru(azpy)_2(NO_3)_2]$ has been reported [52]. In addition, the observed ^1H NMR peaks have the same chemical shifts as those of the proposed diaqua adduct in aqueous solution of the

chloride complex $[(\eta^6:\eta^1\text{-}C_6H_5(CH_2)_3NH_2)RuCl_2]$ (**4.4**). A ^1H NMR pH titration of **4.10** in water over the range pH 4.1 to 11.0 gave complicated spectra. The presence of up to four species, the signals of which showed no shifts over a pH range from 4.8 to 11.0 was detected. Their reversible degradation to form the initially present **4.10** upon acidification, suggested the involvement of hydroxides as bridging ligands, comparable to complexes $[((\eta^6\text{-}C_6H_6)Ru(\mu\text{-}OH))_4]^{4+}$ and $[(\eta^6\text{-}C_6H_6)Ru(\mu\text{-}OH)_3]^+$, for which solid state structures have been reported [62, 63]. The observed fast hydrolysis of tethered complexes and possible formation of such bridged species already well below physiological pH is expected to deactivate these complexes significantly.

Interestingly, facile formation of a precipitate at comparatively low pH values, has been observed in metallocene chemistry. Kuo *et al.* have shown the existence of monomer – dimer equilibria for molybdocenes in water at pD = 3.5 [64]. In addition, Marks *et al.* showed that titanocene can form an insoluble poly-oxo- and hydroxo-bridged species in water [65]. Similarly, the formation of poly-oxo bridged species has been shown for the ruthenium containing complex NAMI-A to occur in water at low pH values [66]. The exact nature of the precipitate and the species in solution at elevated pH of **4.10** still needs to be determined.

4.3.2.4 Stability in organic solvents

The ^1H NMR spectrum of $[(\eta^6:\eta^1\text{-}C_6H_5(CH_2)_3NH_2)RuCl_2]$ (**4.4**) in chloroform shows a set of peaks for one symmetrical complex assignable to **4.4** itself. In DMSO-d_6 and MeOD-d_4 a second, chiral species is present in solution. No evidence for tether opening was found; therefore chirality must arise from the substitution of chloride. In the case of DMSO-d_6 more residual water appears to increase the formation of that latter product. This suggests that also in the polar solvents MeOD-d_4 and DMSO-d_6 loss of one chloride occurs readily, further supporting the findings of the chloride titration in water, which indicated the

increased lability of the first chloride. Loss of chloride appears to be favoured by an increased presence of water in solution and due to an excess of solvent, either MeOD/MeO^- or DMSO are the likely coordinating molecules.

The 2D NOESY ^1H NMR spectrum of **4.4** in DMSO-d_4 illustrates the effect of metal-based chirality has not only on the arene protons, but also on the tether backbone. Each proton of the tether chain is in a different magnetic environment, giving rise to separate signals.

Complex $[(\eta^6:\eta^1\text{-}C_6H_5(CH_2)_2NH_2)RuCl_2]$ (**4.5**) decomposed in DMSO *via* loss of the arene (see Figure 4.13). The complexity of the free arene signal upon decomposition compared to the simpler one of the free ligand suggests a number of complexes that the amine group could be involved in. However, apart from the signal at 4.47 ppm (which moves to 4.61 ppm), which could be a signal of coordinated amine, no other amine signal could be detected in solution. Loss of the arene has also been documented for a related two carbon amine tether, which contains a phosphine ligand [44]. The apparent rapid decomposition of **4.5** in DMSO is in contrast to the observed stability of this complex in water. However, since cell-testing routinely involves dissolution of complexes in DMSO, this presents another stability problem for this complex. Strongly coordinating solvents such as acetonitrile or DMSO are known to be able to displace arenes from Ru^{II} arene complexes [67]. In the case of the two atom tethered complexes studied here, this decomposition is possibly further accelerated by the strain imposed on the arene by the tether.

Similar, although less rapid, decomposition *via* loss of arene coordination was also noticed for the two atom tethered complexes $[(\eta^6:\eta^1\text{-}C_6H_5(CH_2)C_5H_4N)RuCl_2]$ (**4.7**), $[(\eta^6:\eta^1\text{-}C_6H_5(C_6H_4)NH_2)RuCl_2]$ (**4.8**) and $[(\eta^6:\eta^1\text{-}C_6H_5(CH_2)C_3H_3N_2)RuCl_2]$ (**4.9**), which contain a more rigid tether backbone than $[(\eta^6:\eta^1\text{-}C_6H_5(CH_2)_2NH_2)RuCl_2]$ (**4.5**).

Noteworthy is the appearance of two species in the case of **4.5**, before they both decompose. As for $[(\eta^6{:}\eta^1\text{-}C_6H_5(CH_2)_3NH_2)RuCl_2]$ (**4.4**) these two species presumably are the intact di-chloro complex and the mono-DMSO adduct.

4.3.2.5 Adducts with nucleobases

The products formed from a reaction of $[(\eta^6{:}\eta^1\text{-}C_6H_5(CH_2)_3NH_2)Ru(NO_3)_2]$ (**4.10**) with 9EtG were assigned to $[(\eta^6{:}\eta^1\text{-}C_6H_5(CH_2)_3NH_2)Ru(9EtG)H_2O]^{2+}$ and $[(\eta^6{:}\eta^1\text{-}C_6H_5(CH_2)_3NH_2)Ru(9EtG)_2]^{2+}$, for which the chemical shifts in ^1H NMR spectra recorded in water were similar compared to the synthesised mono- and di-9EtG adducts $[(\eta^6{:}\eta^1\text{-}C_6H_5(CH_2)_3NH_2)Ru(9EtG)NO_3]PF_6$ (**4.12**) and $[(\eta^6{:}\eta^1\text{-}C_6H_5(CH_2)_3NH_2)Ru(9EtG)_2](PF_6)_2$ (**4.11a**), respectively. Figure 4.20 shows a plot of the concentration of 9EtG in the adducts formed in the reaction of **4.10** with 1.75 mol

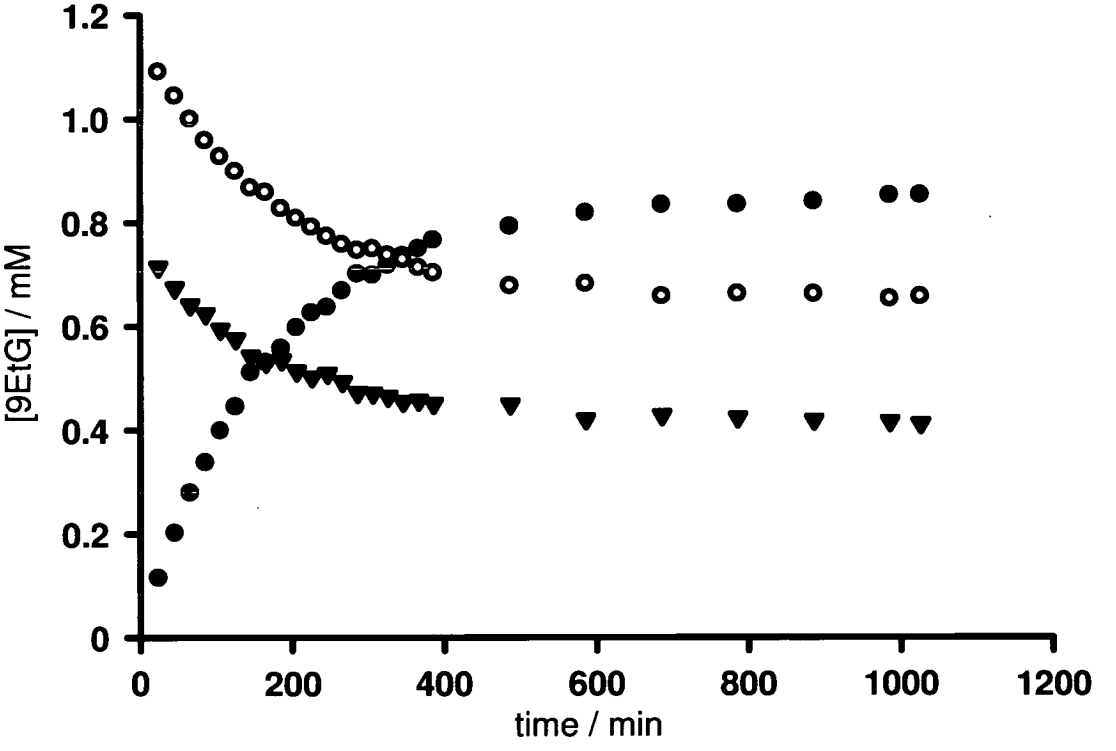

Figure 4.20: Plot of the concentration of 9EtG species versus time for a reaction of **4.10** (1.1 mM Ru) with 1.75 mol equiv of 9EtG at 298 K and pH = 5.19 (start) – 6.22 (finish). Symbols: (○) = $[(\eta^6{:}\eta^1\text{-}C_6H_5(CH_2)_3NH_2)Ru(9EtG)H_2O]^{2+}$; (●) = $[(\eta^6{:}\eta^1\text{-}C_6H_5(CH_2)_3NH_2)Ru(9EtG)_2]^{2+}$; (▼) = free 9EtG.

equiv of 9EtG versus time. Formation of the di-9EtG adduct appeared to have reached equilibrium after *ca.* 700 min at 298 K, in contrast to the rapid (< 20 min) formation of the mono-9EtG adduct. These results suggest that the rate of formation of the mono-9EtG adduct is rapid and formation of the di-9EtG adduct firstly does not go to completion but reaches an equilibrium and secondly is a comparatively slow step, in which 9EtG reacts with $[(\eta^6:\eta^1\text{-}C_6H_5(CH_2)_3NH_2)Ru(9EtG)H_2O]^{2+}$. Formation of increasing amounts of $[(\eta^6:\eta^1\text{-}C_6H_5(CH_2)_3NH_2)Ru(9EtG)_2]^{2+}$ is not correlated to equal consumption of the mono-9EtG adduct and free 9EtG. This appears to be a consequence of an unknown species appearing in the arene proton region which does not contain 9EtG. This side-product could be an unreactive hydroxo-/oxo-bridged species, which leads to the preferential build-up of free 9EtG over the mono-9EtG adduct in solution (*c.f.* species (e) in Figure 4.14).

It was of interest to study the reactivity of both $[(\eta^6:\eta^1\text{-}C_6H_5(CH_2)_3NH_2)RuCl_2]$ (**4.4**) and $[(\eta^6:\eta^1\text{-}C_6H_5(CH_2)_2NH_2)RuCl_2]$ (**4.5**) with 9EtG in the presence of *ca.* 22 mM chloride, comparable to cytoplasmic [Cl^-] [68]. Figure 4.21 shows a plot of the concentration of 9EtG in the species formed during the reaction versus time. As found for the reaction of $[(\eta^6:\eta^1\text{-}C_6H_5(CH_2)_3NH_2)Ru(NO_3)_2]$ (**4.10**), formation of the di-9EtG adduct is time-dependent and the solution appeared to reach equilibrium after *ca.* 22 h. In addition, there were two more species present in solution. Their chemical shifts were compared to those observed in a separate experiment, where abstraction of chloride from **4.5** by silver nitrate in water was followed by reaction with *ca.* 0.8 mol equiv 9EtG. This suggested assignment of one of the two species as $[(\eta^6:\eta^1\text{-}C_6H_5(CH_2)_2NH_2)Ru(9EtG)H_2O]^{2+}$. Addition of NaCl and comparison of the chemical shifts of the new signals suggested assignment of the other species as $[(\eta^6:\eta^1\text{-}C_6H_5(CH_2)_2NH_2)Ru(9EtG)Cl]^+$. As seen in the chloride titration of **4.5** at [Cl^-] *ca.* 20 mM, the majority of the complex would be expected to

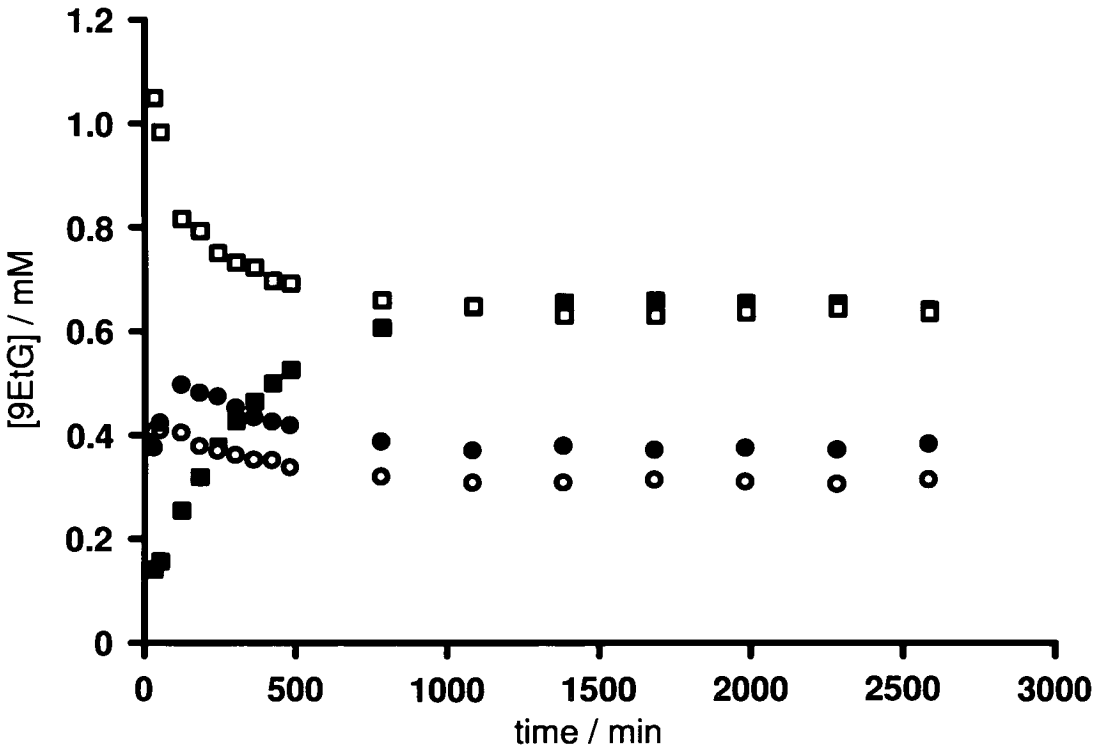

Figure 4.21: Plot of the concentration of 9EtG species versus time for a reaction of $[(\eta^6{:}\eta^1\text{-}C_6H_5(CH_2)_2NH_2)RuCl_2]$ (**4.5**) (0.99 mM Ru) with 2.0 mol equiv of 9EtG at 298 K and pH = 6.08 (start) – 6.23 (finish) in the presence of 21.7 mM chloride. Symbols: (○) = $[(\eta^6{:}\eta^1\text{-}C_6H_5(CH_2)_3NH_2)Ru(9EtG)H_2O]^{2+}$; (●) = $[(\eta^6{:}\eta^1\text{-}C_6H_5(CH_2)_3NH_2)Ru(9EtG)Cl]^{+}$; (■) = $[(\eta^6{:}\eta^1\text{-}C_6H_5(CH_2)_3NH_2)Ru(9EtG)_2]^{2+}$; (□) = free 9EtG.

be present as the mono-aqua adduct. For a reaction with 9EtG this would suggest initial formation of $[(\eta^6{:}\eta^1\text{-}C_6H_5(CH_2)_2NH_2)Ru(9EtG)Cl]^{+}$ *via* displacement of water. Hydrolysis of chloride would be expected to result in an increase in the presence of $[(\eta^6{:}\eta^1\text{-}C_6H_5(CH_2)_2NH_2)Ru(9EtG)H_2O]^{2+}$, which can then further react with another molecule of 9EtG. As shown in Figure 4.22, the presence of $[(\eta^6{:}\eta^1\text{-}C_6H_5(CH_2)_2NH_2)Ru(9EtG)Cl]^{+}$ initially increases, presumably due to the unreacted ruthenium complex, which was still detected at t = 153 min, reacting. At equilibrium, the presence of both the Cl^- and H_2O mono-9EtG adducts decreases to a similar extent, with the chloro-adduct showing a somewhat stronger decrease. This suggests that formation of the di-9EtG adduct predominantly occurs *via* displacement of H_2O

rather than chloride and that consumption of $[(\eta^6:\eta^1\text{-}C_6H_5(CH_2)_2NH_2)Ru(9EtG)H_2O]^{2+}$ is followed by hydrolysis of chloride from $[(\eta^6:\eta^1\text{-}C_6H_5(CH_2)_2NH_2)Ru(9EtG)Cl]^{+}$ to reform the aqua adduct.

In a similar binding experiment with **4.4**, the peaks for $[(\eta^6:\eta^1\text{-}C_6H_5(CH_2)_3NH_2)Ru(9EtG)Cl]^{+}$ and $[(\eta^6:\eta^1\text{-}C_6H_5(CH_2)_3NH_2)Ru(9EtG)H_2O]^{2+}$ appeared to overlap. This prevented determination of the relative proportions of those two adducts. However, the concentrations of free 9EtG, the mono-9EtG adducts (both with H_2O and Cl^-) and the di-9EtG adduct at equilibrium (based on integration of the respective H8 signals after 1034 min, pH between 6.08 – 6.53) were 0.67 mM, 0.83 mM and 0.48 mM, respectively. The concentrations in the

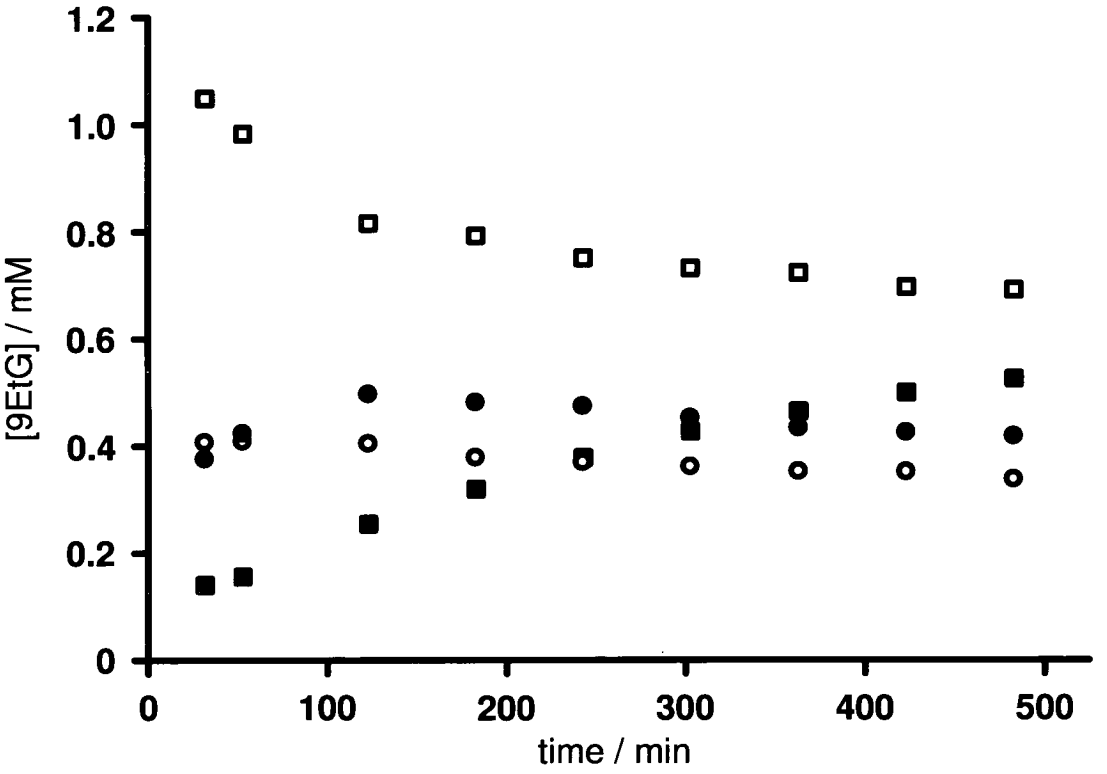

Figure 4.22: Selected region of the plot of the concentration of 9EtG versus time for a reaction of **4.5** (0.99 mM Ru) with 2.0 mol equiv of 9EtG at 298 K and pH = 6.08 (start) – 6.23 (finish) in the presence of 21.7 mM chloride. Symbols: (○) = $[(\eta^6:\eta^1\text{-}C_6H_5(CH_2)_3NH_2)Ru(9EtG)H_2O]^{2+}$; (●) = $[(\eta^6:\eta^1\text{-}C_6H_5(CH_2)_3NH_2)Ru(9EtG)Cl]^{+}$; (■) = $[(\eta^6:\eta^1\text{-}C_6H_5(CH_2)_3NH_2)Ru(9EtG)_2]^{2+}$; (□) = free 9EtG.

reaction of $[(\eta^6{:}\eta^1\text{-}C_6H_5(CH_2)_3NH_2)Ru(NO_3)_2]$ (**4.10**) with 1.75 mol equiv of 9EtG were 0.43 mM, 0.68 mM and 0.88 mM, respectively. Despite a possible influence of pH on the extent of the reaction and the use of only 1.75 equiv of 9EtG for **4.10** (use of two equiv would be expected to result in a further increase in the di-9EtG adduct), these values indicate that chloride can inhibit the formation of di-9EtG adducts of $\{(\eta^6{:}\eta^1\text{-}C_6H_5(CH_2)_3NH_2)Ru\}^{2+}$ (Figure 4.23).

Having shown the time-dependent formation of $[(\eta^6{:}\eta^1\text{-}C_6H_5(CH_2)_3NH_2)Ru(9EtG)_2]^{2+}$ and the associated equilibrium, the displacement of 9EtG by water in this adduct was studied. Figure 4.24 shows the plot of the concentration of 9EtG versus time for the hydrolysis of 9EtG from $[(\eta^6{:}\eta^1\text{-}C_6H_5(CH_2)_3NH_2)Ru(9EtG)_2](PF_6)_2$ (**4.11a**) (3.0 mM Ru) at 298 K and pH = 6.67 (start) – 6.02 (finish). Equilibrium appeared to be reached after *ca.* 700 min. The extent of hydrolysis, however, also appears to be dependent on concentration and pH.

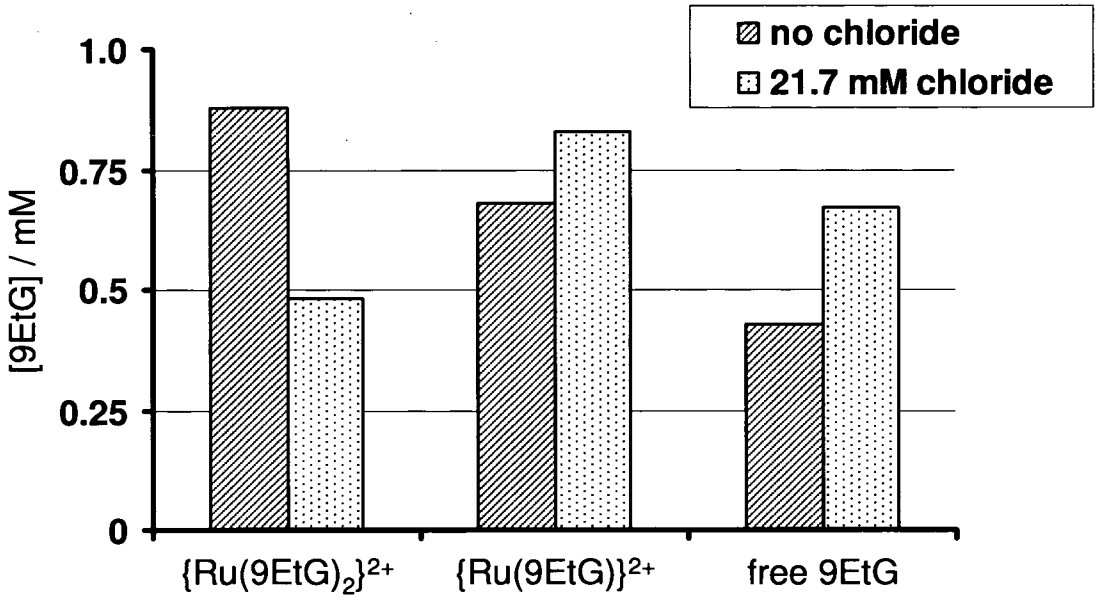

Figure 4.23: Species distribution in reactions of $\{(\eta^6{:}\eta^1\text{-}C_6H_5(CH_2)_3NH_2)Ru\}^{2+}$ with 9EtG in 90% H_2O/ 10% D_2O at 298 K in the presence of no chloride (1.1 mM Ru, 1.75 mol equiv 9EtG, pH = 5.19 (start) – 6.22 (finish)) and 21.7 mM of total chloride (0.99 mM Ru, 2 mol equiv 9EtG, pH = 6.08 (start) – 6.53 (finish)), respectively.

Table 4.8 shows the relative distribution of 9EtG in the hydrolysis products of **4.11a** in D_2O at 298 K after 22.5 h (17 h for [Ru] 1.95 mM) at varying concentrations and pH. The values suggest that loss of coordination of 9EtG increases at lower concentrations of the di-9EtG adduct in solution. In addition, for the solution containing 0.96 mM Ru (*i.e.* 1.92 mM 9EtG), the ^{1}H NMR spectrum shows that there is more free 9EtG than mono-9EtG adduct present in solution, suggesting that a further hydrolysis step has taken place. Indeed, peaks in the arene proton region, which do not appear to be connected to any H8 signal of 9EtG, are detected. These signals have very similar shifts to some signals noted previously at high pH in the pH titration of **4.10**. This, in connection with the significant drop in the pH* value of the solution after 22.5 h, suggests the formation of a hydroxo-bridged species.

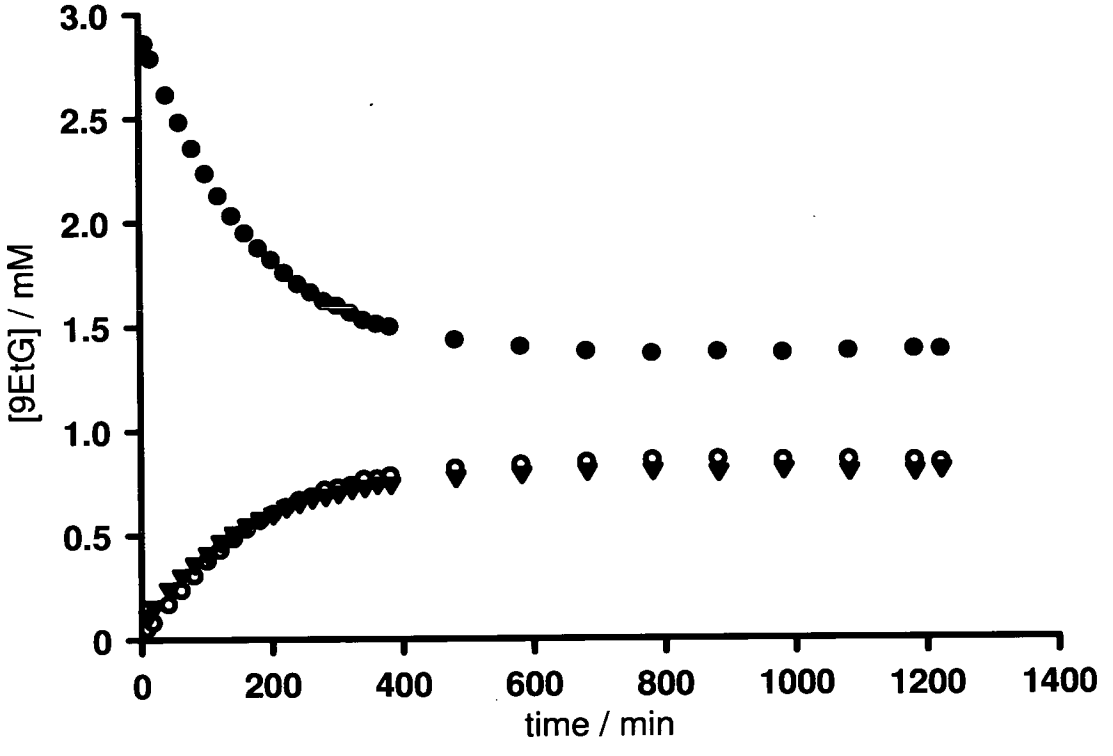

Figure 4.24: Plot of the concentration of 9EtG versus time for the hydrolysis of 9EtG from **4.11a** (3.0 mM Ru) at 298 K and pH = 6.67 (start) – 6.02 (finish). Symbols: (●) = $[(\eta^6{:}\eta^1\text{-}C_6H_5(CH_2)_3NH_2)Ru(9EtG)_2]^{2+}$; (○) = $[(\eta^6{:}\eta^1\text{-}C_6H_5(CH_2)_3NH_2)Ru(9EtG)H_2O]^{2+}$; (▼) = free 9EtG.

Integration of the H8 signals in a solution of $[(\eta^6:\eta^1\text{-}C_6H_5(CH_2)_3NH_2)Ru(9EtG)NO_3]PF_6$ (**4.12**) (*ca.* 4.0 mM) in D_2O indicated an increase in the amount of di-9EtG adduct over the mono-9EtG adduct accompanied by an increase of the signals for the diaqua species over a period of 22 h. This result suggests that further complications of studying the dynamics of reactions between nucleobases and these bifunctional tethered complexes could arise from the possibility of conversion of mono-adducts into di-adducts with formation of the di-aqua species.

Based on the results of the above binding experiments, a scheme for the reaction of tethered Ru^{II} arene complexes with 9EtG in the presence of chloride is shown in Scheme 4.5.

Table 4.8: The relative distribution of 9EtG in the hydrolysis products of $[(\eta^6:\eta^1\text{-}C_6H_5(CH_2)_3NH_2)Ru(9EtG)_2](PF_6)_2$ (**4.11a**) in D_2O at 298 K after 22.5 h (17.5 h for [Ru] 1.95 mM) at varying concentrations and pH*.

[Ru] (mM)	$\{Ru(9EtG)_2\}^{2+}$: 9EtG (%)	$\{Ru(9EtG)H_2O\}^{2+}$: 9EtG (%)	Free 9EtG (%)	pH* (start)	pH* (finish)
4.3	69	15	16	6.47	6.31
1.95	53	23	24	3.95	4.40
0.96	36	27	37	7.66	6.74

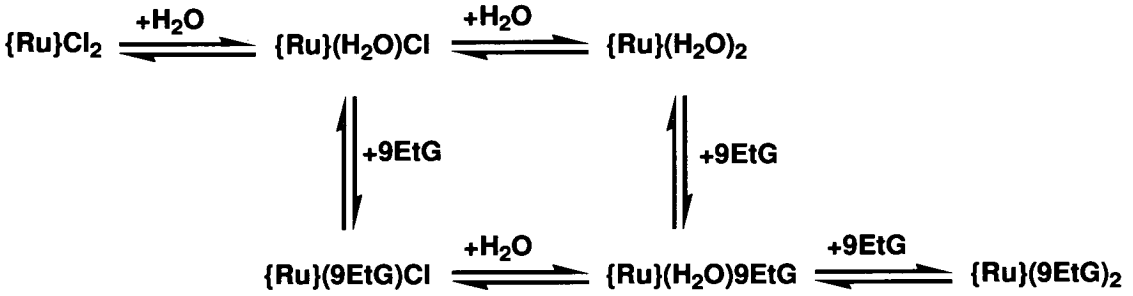

Scheme 4.5: Scheme for the reaction of tethered Ru^{II} arene complexes with 9EtG in the presence of chloride, where {Ru} represents the fragment *e.g.* $\{(\eta^6:\eta^1\text{-}C_6H_5(CH_2)_2NH_2)Ru\}^{2+}$.

The X-ray crystal structure of $[(\eta^6{:}\eta^1\text{-}C_6H_5(CH_2)_3NH_2)Ru(9EtG)_2](CF_3SO_3)_2$ (**4.11b**) shows the involvement of the tether amine group in H-bond interactions with the carbonyl group of 9EtG. The carbonyl groups of both 9EtG ligands point towards the NH_2 group. This is a different orientation from that seen in the structure of $[(\eta^6\text{-}C_6H_6)Ru(H_2O)(9EtG)_2](CF_3SO_3)_2$, where the carbonyl groups are orientated away from each other [69]. Particularly noteworthy is the significant difference between the two Ru – N7(9EtG) bond lengths of *ca.* 0.06 Å. The three reported Ru^{II} di-guanine structures, $[(\eta^6\text{-}C_6H_6)Ru(H_2O)(9EtG)_2](CF_3SO_3)_2$, $[Ru_2(O_2CMe)_{2\text{-}0.18}(O_2CCF_3)_{0.18}(9EtG)_2]^{2+}$ and *cis*-$[Ru(bpy)_2(9\text{-}MeG)_2]^{2+}$, where bpy = 2,2'-bipyridine and 9MeG = 9-methylguanine, have more similar bond lengths (max difference of 0.015 Å) for the two coordinated molecules [69, 70, 71]. Comparing the bond lengths to those Ru – N7(9EtG) distances of other reported examples, ruthenium(II) as well as (III) and both in mono- and di-9EtG adducts, 2.10 Å in the present case appears to be one of the shortest bond lengths. Equal or shorter bond lengths have been found in the Ru^{II} mono-9EtG adduct $[(\eta^6\text{-}C_6H_6)Ru(9EtG)Cl_2]$ (2.10 Å [19]) and in the bridged dinuclear Ru^{II} complex $[Ru_2(O_2CMe)_{2\text{-}0.18}(O_2CCF_3)_{0.18}(9EtG)_2]^{2+}$, where 9EtG coordinates in a bidentate fashion (2.06 Å and 2.08 Å [70]). In contrast, the other Ru – N7(9EtG) bond length of 2.16 Å appears to be the longest documented example. At present no explanation for this difference can be given. The Ru – N7(9EtG/Guo) bond lengths in the Ru^{II} arene complexes $[(\eta^6\text{-bip})Ru(en)9EtG]^{2+}$, $[(\eta^6\text{-bip})Ru(en)Guo]^{2+}$, $[(\eta^6\text{-DHA})Ru(en)9EtG]^{2+}$ and $[(\eta^6\text{-THA})Ru(en)9EtG]^{2+}$ are in the range of 2.12 – 2.13 Å.

The formation of di-guanine adducts at metal centres have been particularly well studied for Pt^{II} complexes, mainly for cisplatin. For these systems the relative orientation of the bases has received much attention [72]. They have been classified as *head-to-head* (HH) and *head-to-tail* (HT) orientations, with HH being energetically more favourable. In square-planar platinum systems, HH describes an

orientation, where the guanine bases are orientated in the same direction (*i.e.* the carbonyl groups are pointing in the same direction) and for HT the bases are orientated in the opposite direction (*i.e.* the carbonyl groups point away from each other) (Scheme 4.6).

In the three reported ruthenium di-guanine adducts, the orientation of the 9EtG ligands is *head-to-tail* [69, 70, 71]. Interestingly, in the structure of $[(\eta^6{:}\eta^1\text{-}C_6H_5(CH_2)_3NH_2)Ru(9EtG)_2](CF_3SO_3)_2$ (**4.11b**) the two 9EtG ligands are orientated towards each other, they adopt a *head-to-head* orientation (see Figure 4.16). The influence of the amine group on this conformation could be crucial as is indicated by the angle between the plane defined by all arene carbons and that of C5 (where the tether is connected), Ru and N(tether). This angle is a measure for the 'outward-swing' of the tether. For the structures of the three atom tethered complexes $[(\eta^6{:}\eta^1\text{-}C_6H_5(CH_2)_3NH_2)RuCl_2]$ (**4.4**), $[(\eta^6{:}\eta^1\text{-}C_6H_5O(CH_2)_2NH_2)RuCl_2]$ (**4.6**) and $[(\eta^6{:}\eta^1\text{-}C_6H_5(CH_2)_3NH_2)Ru(NO_3)_2]$ (**4.10**) this angle is around 90°, whereas for **4.11b** it is 72.77°. This presumably is a consequence of the flexibility of the three carbon tether. The amine group can position itself so as to increase the H-bond interactions with both the carbonyl groups. The carbonyl group with the strongest H-bond to the tether amine protons belongs to the 9EtG ligand, which has the longest Ru – N7(9EtG) bond length.

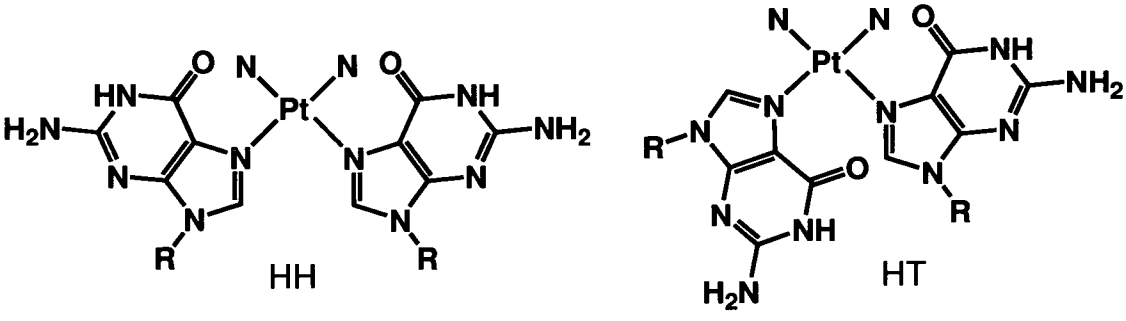

Scheme 4.6: Schematic representation of *head-to-head* (HH) and *head-to-tail* (HT) orientations for a di-guanine adduct of a platinum diam(m)ine. In the HH form the guanine bases are orientated in the same direction whereas in the HT form the bases are orientated in the opposite direction.

Evidence that steric hindrance might not be the cause of the significantly different Ru – N7(9EtG) distances is provided by the ^{1}H NMR studies of $[(\eta^6:\eta^1\text{-}C_6H_5(CH_2)_3NH_2)Ru(9EtG)_2](PF_6)_2$ (**4.11a**) in water. Steric hindrance, resulting in hindered rotation of guanine in the complex *cis*-$[Ru(bpy)_2(9\text{-}MeG)_2]^{2+}$, gives rise to two distinctly different peaks of the H8 protons for each coordinated 9MeG [71]. The CH_2 protons from the ethyl group of 9EtG in complex **4.11a** give rise to two separate peaks, which could be a consequence of rotational hindrance or slow exchange between HH and HT conformations (Figure A.4.7). However, the H8 signal for the two coordinated 9EtG ligands in **4.11a** is a singlet integrating for 2H, and the broadening of some of the tether CH_2 signals suggest that a dynamic exchange process is occurring.

The two peaks observed for the mono-Guo adduct $[(\eta^6:\eta^1\text{-}C_6H_5(CH_2)_3NH_2)Ru(Guo)H_2O]^{2+}$ result from the formation of diastereomers, since guanosine is chiral as is the mono-Guo adduct.

The appearance of two peaks for $[(\eta^6:\eta^1\text{-}C_6H_5(CH_2)_3NH_2)Ru(Guo)_2]^{2+}$ seems to point towards different conformational orientations of bound guanosine (Guo), as has been observed in di-guanosine adducts of Pt^{II} [73, 74]. HH and HT orientations for guanosine in reactions with cisplatin can be studied in solution due to the well-resolved base and H1' regions of the spectra [72]. The comparatively large separation of the H8 peaks of the di-Guo adduct ($\Delta\delta$ = 0.13 ppm) suggest different spatial arrangements in the respective enantiomers.

4.4 Tethered Ru^{II} Arene Complexes Containing Bidentate Chelating Ligands

Some platinum-containing anticancer-active agents, in which both chloride ligands of cisplatin are replaced by a bidentate chelating ligand, show increased solubility and stability of the compounds (Scheme 4.7). More importantly, it has

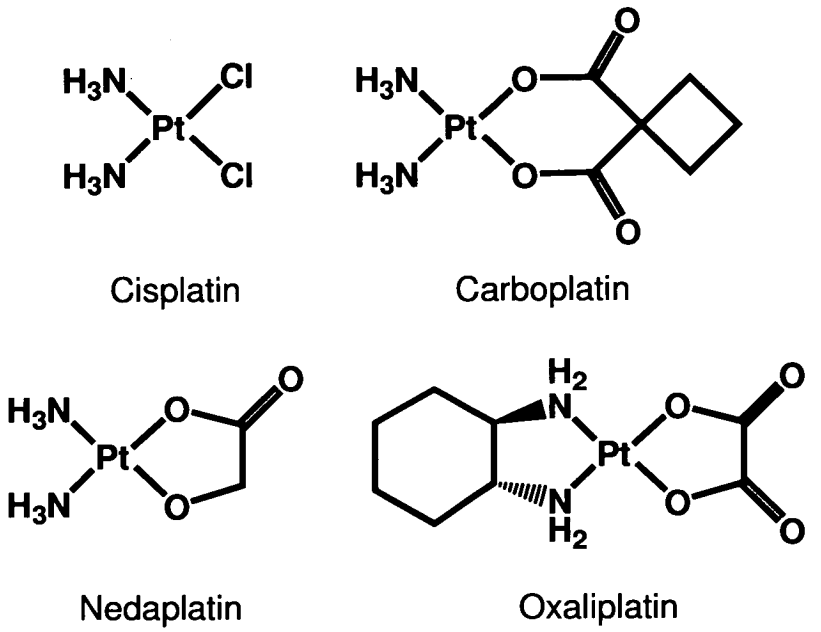

Scheme 4.7: Cisplatin and other anticancer-active platinum complexes, where the two chloride ligands have been replaced by a bidentate chelating ligand.

been shown that such complexes not only retain activity, but also have reduced side-effects [75, 76].

Having demonstrated above that the fast hydrolysis and reactivity of tethered Ru^{II} arene complexes produced in this work could be limiting factors for cytotoxic activity, it was of interest to explore ways in which to employ similar strategies for these compounds. This approach could provide means of slowing down and controlling the rate and extent of hydrolysis. In addition, use of a chelating ligand could significantly slow down the formation of insoluble hydroxo-bridged species, or even fully prevent it in case of stepwise chelate ring opening.

Furthermore, there is potential for incorporating a DNA intercalator [77, 78]. The resulting complexes would be unreactive towards most biomolecules and could possibly be made target-specific.

An alternative route of influencing the chemistry of tethered Ru^{II} arene complexes in solution is to replace one chloride ligand by a strongly coordinating mono-dentate ligand. Such complexes would be expected to be less susceptible to

formation of hydroxo-bridged species. However, they would not offer bifunctional reactivity and also possess metal-based chirality, which for drug design might not be ideal.

4.4.1 Results

4.4.1.1 Synthesis and characterisation

Replacement of the chloride ligands in the neutral tethered Ru^{II} arenes by bidentate chelating ligands, usually *via* abstraction of chloride with silver nitrate, produced complexes $[(\eta^6:\eta^1\text{-}C_6H_5(CH_2)_3NH_2)Ru(ox)]$ (**4.14**), $[(\eta^6:\eta^1\text{-}C_6H_5(CH_2)_2NH_2)Ru(ox)]$ (**4.15**), $[(\eta^6:\eta^1\text{-}C_6H_5(C_6H_4)NH_2)Ru(ox)]$ (**4.16**), $[(\eta^6:\eta^1\text{-}C_6H_5(CH_2)C_5H_4N)Ru(ox)]$ (**4.17**), $[(\eta^6:\eta^1\text{-}C_6H_5(CH_2)_3NH_2)Ru(acac)]PF_6$ (**4.18**), $[(\eta^6:\eta^1\text{-}C_6H_5(CH_2)C_5H_4N)Ru(acac)]PF_6$ (**4.19**), $[(\eta^6:\eta^1\text{-}C_6H_5(CH_2)_3NH_2)Ru(L\text{-pal})]PF_6$ (**4.20**) and $[(\eta^6:\eta^1\text{-}C_6H_5(CH_2)_3NH_2)Ru(dppz)](PF_6)_2$ (**4.21**), where ox = oxalate, acac = acetylacetonate, *L*-pal = *L*-phenylalanine and dppz = dipyrido[3,2-*a*:2',3'-*c*]phenazine (Figure 4.25). In addition, reactions with phosphorus-containing ligands resulted in the mono-functional complexes $[(\eta^6:\eta^1\text{-}C_6H_5(CH_2)_3NH_2)Ru(tpp)Cl]PF_6$ (**4.22**) and $[(\eta^6:\eta^1\text{-}C_6H_5(CH_2)_3NH_2)Ru(pta)Cl]PF_6$ (**4.23**), where tpp = triphenylphosphine and pta = 1,3,5-triaza-7-phosphaadamantane (Figure 4.26).

The syntheses usually were straight-forward, except that adducts of $\{(\eta^6:\eta^1\text{-}C_6H_5(CH_2)C_5H_4N)Ru\}^{2+}$ with mono-anionic or neutral chelating ligands, *e.g.* acac or dppz, appeared to undergo marked decomposition in solution.

X-ray diffraction quality crystals of $[(\eta^6:\eta^1\text{-}C_6H_5(CH_2)_3NH_2)Ru(ox)]$ (**4.14**), $[(\eta^6:\eta^1\text{-}C_6H_5(C_6H_4)NH_2)Ru(ox)]$ (**4.16**), $[(\eta^6:\eta^1\text{-}C_6H_5(CH_2)_3NH_2)Ru(acac)]PF_6$ (**4.18**) and $[(\eta^6:\eta^1\text{-}C_6H_5(CH_2)_3NH_2)Ru(L\text{-pal})]$ (**4.20**) were all grown from diffusion of diethyl ether into a methanol solution of the respective complexes at ambient temperature.

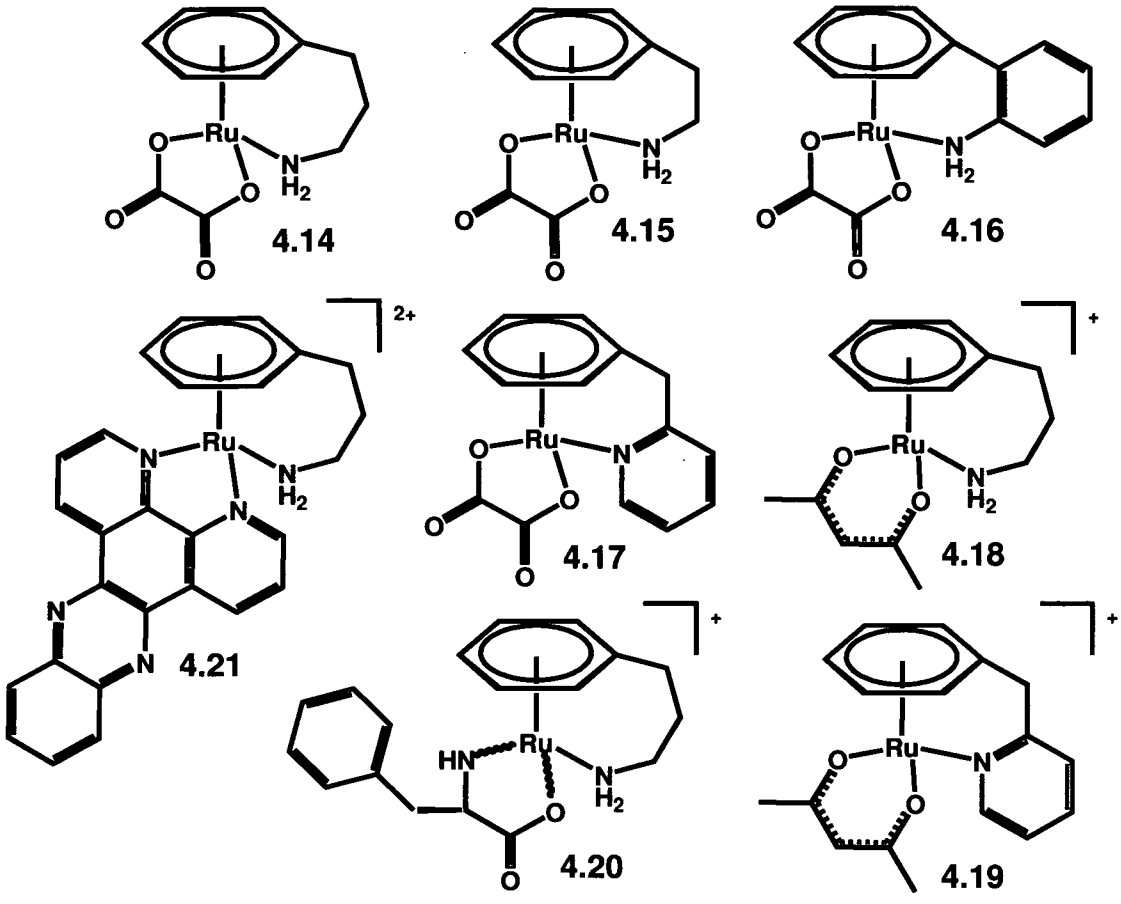

Figure 4.25: The structures of $[(\eta^6{:}\eta^1\text{-}C_6H_5(CH_2)_3NH_2)Ru(ox)]$ (**4.14**), $[(\eta^6{:}\eta^1\text{-}C_6H_5(CH_2)_2NH_2)Ru(ox)]$ (**4.15**), $[(\eta^6{:}\eta^1\text{-}C_6H_5(C_6H_4)NH_2)Ru(ox)]$ (**4.16**), $[(\eta^6{:}\eta^1\text{-}C_6H_5(CH_2)C_5H_4N)Ru(ox)]$ (**4.17**), $[(\eta^6{:}\eta^1\text{-}C_6H_5(CH_2)_3NH_2)Ru(acac)]^+$ (**4.18**), $[(\eta^6{:}\eta^1\text{-}C_6H_5(CH_2)C_5H_4N)Ru(acac)]^+$ (**4.19**), $[(\eta^6{:}\eta^1\text{-}C_6H_5(CH_2)_3NH_2)Ru(L\text{-pal})]^+$ (**4.20**) and $[(\eta^6{:}\eta^1\text{-}C_6H_5(CH_2)_3NH_2)Ru(dppz)]^{2+}$ (**4.21**), where **4.18 – 21** were synthesised as their hexafluorophosphate salts.

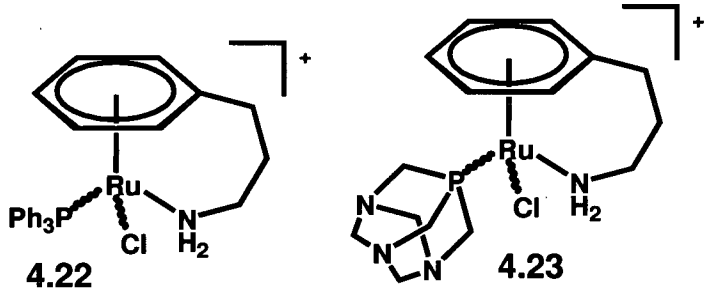

Figure 4.26: The structures of $[(\eta^6{:}\eta^1\text{-}C_6H_5(CH_2)_3NH_2)Ru(tpp)Cl]^+$ (**4.22**) and $[(\eta^6{:}\eta^1\text{-}C_6H_5(CH_2)_3NH_2)Ru(pta)Cl]^+$ (**4.23**), which were synthesised as their hexafluorophosphate salts.

The structure of complex [(η^6:η^1-$C_6H_5(CH_2)_3NH_2$)Ru(ox)] (**4.14**) is shown in Figure 4.27, the crystal data in Table A.4.3 and bond angles and lengths in Table 4.9. The structure shows dimer formation *via* H-bond interactions between the carbonyl oxygen atoms of oxalate and an amine proton with O1A···H1B 2.31 Å (O1A···N1 3.031(4) Å) and O2A···H1B 2.51 Å (O2A···N1 3.309(4) Å) (Figure A.4.8A). H-bond

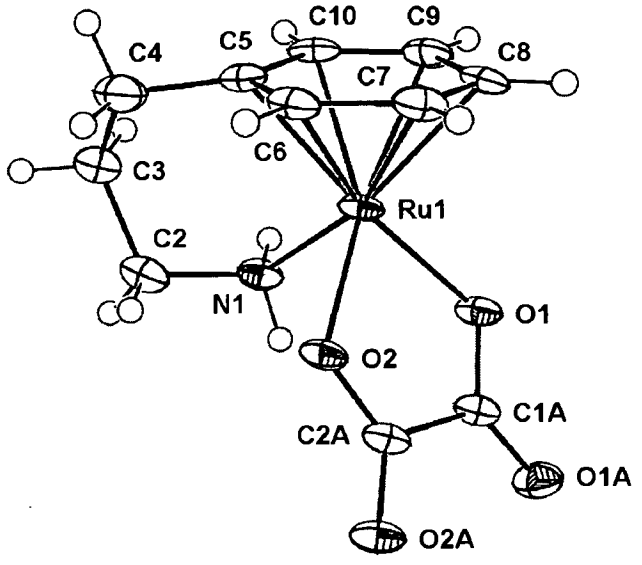

Figure 4.27: Ortep diagram (50% probability ellipsoids) and atom numbering scheme for the X-ray crystal structure of [(η^6:η^1-$C_6H_5(CH_2)_3NH_2$)Ru(ox)] (**4.14**).

Table 4.9: Selected bond lengths (Å) and angles (°) [(η^6:η^1-$C_6H_5(CH_2)_3NH_2$)Ru(ox)] (**4.14**).

Bond	Length	Bond	Length/angle
Ru-N1	2.118(3)	Ru-C10	2.180(3)
Ru-O1	2.099(2)	Ru-centroid[a]	1.651
Ru-O2	2.077(2)	N1-Ru-O1	85.33(12)
Ru-C5	2.157(3)	N1-Ru-O2	82.77(10)
Ru-C6	2.142(3)	O1-Ru-O2	78.86(9)
Ru-C7	2.198(4)	Ru-N-C2	113.6(2)
Ru-C8	2.193(3)	Ru-C5-C4	122.5(2)
Ru-C9	2.186(4)	N1-Ru-C5	91.54(13)

[a] = measured using Mercury 1.4.

formation between the chelating oxygen O1 and amine proton H1A (2.21 Å, O1···N1 3.096(4) Å) links molecules into zig-zag chains (Figure A.4.8B). Another dimer is formed by interactions between arene protons and an oxalate chelating oxygen, where O2···H6 2.58 Å (O2···C6 3.185(4) Å) and O2···H7 2.68 Å (O2···C7 3.227(5) Å) (Figure A.4.8C). Other oxygen-proton short contacts include O2A···H8 2.39 Å (O2A···C8 3.215(3) Å), O2A···H10 2.60 Å (O2A···C10 3.440(4) Å) and O2A···H3B 2.50 Å (O2A···C3 3.308(5) Å). The intramolecular (amine)NH···O(ox) distances are H1B···O1 2.65 Å (N1···O1 2.858(4) Å) and H1B···O2 2.70 Å (N1···O2 2.774(4) Å). The Ru – O distances are 2.077(2) Å and 2.099(2) Å, with Ru – N 2.118(3) Å, and Ru – centroid 1.65 Å. The angle between the plane defined by all arene carbons and that of N1, Ru and C5 (arene carbon to which the tether is connected) is 72.05°.

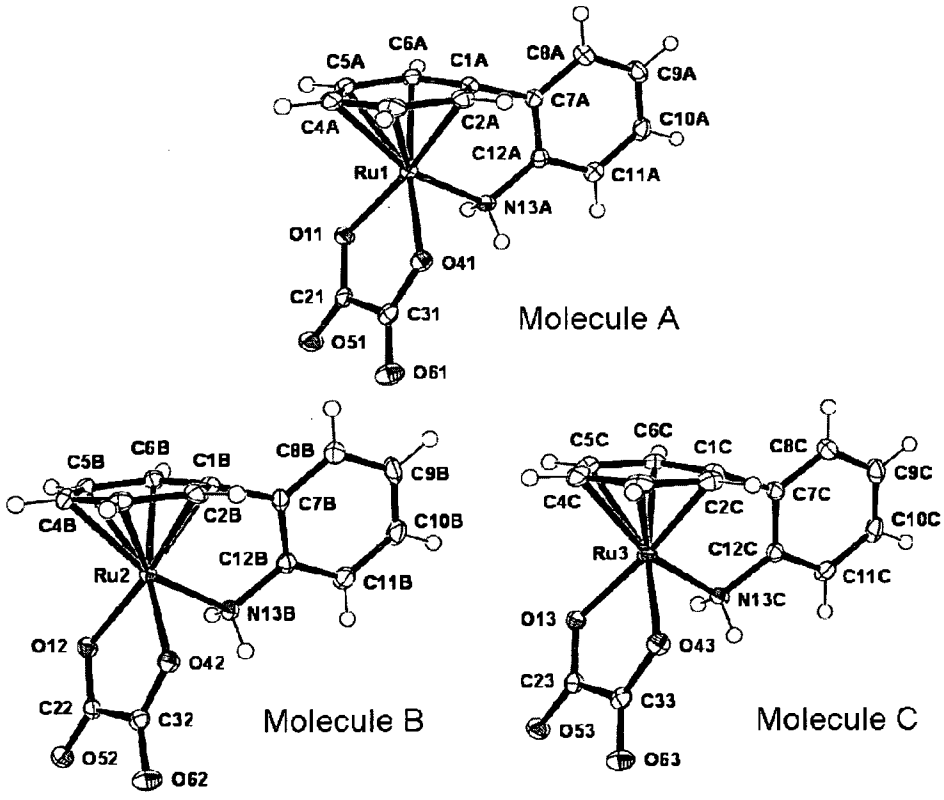

Figure 4.28: Ortep diagram (50% probability ellipsoids) and atom numbering scheme for the X-ray crystal structure of $[(\eta^6{:}\eta^1\text{-}C_6H_5(C_6H_4)NH_2)Ru(ox)]$ (**4.16**), showing the three independent molecules in the asymmetric unit.

Table 4.10: Selected bond lengths (Å) and angles (°) [(η^6:η^1-$C_6H_5(C_6H_4)NH_2$)Ru(ox)] (**4.16**).

Bond	X = 1, Y = A	X = 2, Y = B	X = 3, Y = C
RuX-N13Y	2.1314(18)	2.1446(18)	2.1251(19)
RuX-O1X	2.0807(15)	2.0789(15)	2.0784(15)
RuX-O4X	2.0762(16)	2.0737(16)	2.0788(16)
RuX-C1Y	2.104(2)	2.094(2)	2.101(2)
RuX-C2Y	2.159(2)	2.150(2)	2.154(2)
RuX-C3Y	2.192(2)	2.195(2)	2.189(2)
RuX-C4Y	2.214(2)	2.217(2)	2.212(2)
RuX-C5Y	2.174(2)	2.181(2)	2.179(2)
RuX-C6Y	2.160(2)	2.159(2)	2.160(2)
Ru-centroid[a]	1.638	1.635	1.635
O1X-RuX-O4X	78.42(6)	78.46(6)	78.48(6)
O1X-RuX-N13Y	86.19(6)	86.79(6)	85.47(6)
O4X-RuX-N13Y	86.62(7)	86.93(7)	86.27(7)
RuX-N13Y-C12Y	111.84(14)	110.96(14)	111.89(13)
RuX-C1Y-C7Y	112.49(15)	112.36(15)	112.19(15)
N13Y-RuX-C1Y	80.50(8)	80.52(8)	80.77(8)

[a] = measured using Mercury 1.4.

The structure of [(η^6:η^1-$C_6H_5(C_6H_4)NH_2$)Ru(ox)] (**4.16**) contains three independent molecules (molecules A, B and C) in the asymmetric unit (Figure 4.28). The crystal data are shown in Table A.4.3 and bond angles and lengths in Table 4.10. Molecule A forms chains with itself *via* H-bond interactions between the carbonyl oxygen atoms of oxalate and the amine protons with O51···H13A 2.00 Å (O51···N13A 2.863(3) Å) and O61···H13B 1.97 Å (O61···N13A 2.883(3) Å) (Figure A.4.9A). Similarly, such interactions link the chains together, which are formed between molecules B and C, with O53···H13C 2.06 Å (O53···N13B 2.884(3) Å), O63···H13D 2.01 Å (O63···N13B 2.916(3) Å), O52···H13E 2.09 Å (O52···N13C

2.919(3) Å) and O62···H13F 1.98 Å (O62···N13C 2.901(3) Å) (Figure A.4.9B). Molecules A and B form chains *via* arene proton and oxalate oxygen atom interactions, where O61···H3B 2.39 Å (O61···C3B 3.119(3) Å), O62···H3A 2.37 Å (O62···C3A 3.295(3) Å), O41···H4B 2.63 Å (O41···C4B 3.497(3) Å) and O11···H3B 2.72 Å (O11···C3B 3.404(3) Å) (Figure A.4.9C). Similarly, molecule C forms chains with itself, with O63···H3C 2.29 Å (O63···C3C 3.195(3) Å) and O43···H5C 2.41 Å (O43···C5C 3.340(3) Å) (Figure A.4.9D). The Ru – O bond lengths in the range of 2.0737(16) Å to 2.0807(15) Å are slightly shorter than those in **4.14**. The Ru – centroid bond distances of 1.64 Å are slightly longer than those of the chloride-containing two-atom tethered complexes $[(\eta^6{:}\eta^1\text{-}C_6H_5(CH_2)_2NH_2)RuCl_2]$ (**4.5**) and $[(\eta^6{:}\eta^1\text{-}C_6H_5(CH_2)C_5H_4N)RuCl_2]$ (**4.7**). As was observed for those complexes, there is significant buckling of the arene with Ru – C(arene) bond lengths in the range of 2.094(2) Å to 2.217(2) Å. The angles between the planes defined by all arene carbons and that of N13Y, Ru and C1Y (arene carbon to which the tether is connected), are 83.30°, 79.41° and 83.14° for molecules A, B and C, respectively.

The X-ray crystal structure of $[(\eta^6{:}\eta^1\text{-}C_6H_5(CH_2)_3NH_2)Ru(acac)]PF_6$ (**4.18**) is shown in Figure 4.29, the crystal data in Table A.4.3 and bond angles and lengths in Table 4.11. The molecules form chains held together by interactions of acac oxygen atoms with arene and CH_3(acac) protons with O5···H10 2.53 Å (O5···C10 3.248(3) Å) and O1···H1A1 2.53 Å (O5···C1A 3.332(3) Å) (Figure A.4.10). The amine protons are involved in H-bond interactions with the PF_6 anion with H1A···F2 2.31 Å (N1···F2 3.199(2) Å) and H1B···F5 2.35 Å (N1···F5 3.124(2) Å). 3 PF_6···CH_3(acac) interactions (2.53 – 2.57 Å), 3 PF_6···arene H interactions (2.37 – 2.53 Å) and one PF_6···tether H interaction (2.63 Å) are involved in the formation of a grid. The Ru – O bond lengths are 2.0567(16) Å and 2.0619(13) Å, the Ru – N distance is 2.1334(16) Å and Ru – centroid 1.66 Å. The intramolecular (amine)NH···O(acac) distances are H1A···O1 2.44 Å and H1B···O5 2.49 Å. The angle between the plane

defined by all arene carbons and that of N1, Ru and C5 (arene carbon to which the tether is connected) is 87.51°.

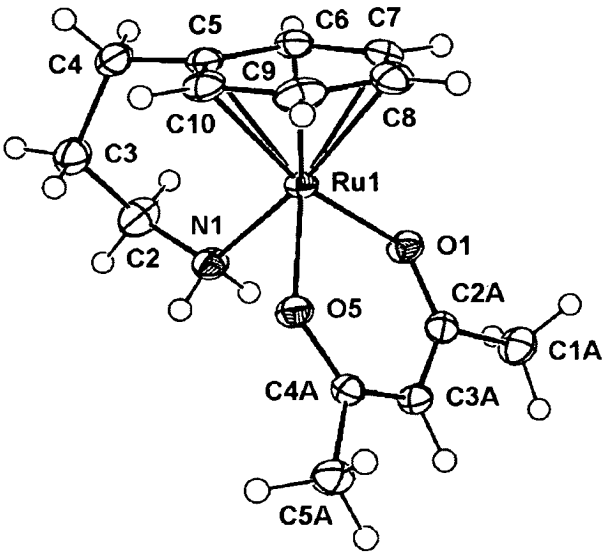

Figure 4.29: Ortep diagram (50% probability ellipsoids) and atom numbering scheme for the cation in the X-ray crystal structure of $[(\eta^6:\eta^1\text{-}C_6H_5(CH_2)_3NH_2)Ru(acac)]PF_6$ (**4.18**).

Table 4.11: Selected bond lengths (Å) and angles (°) for $[(\eta^6:\eta^1\text{-}C_6H_5(CH_2)_3NH_2)Ru(acac)]PF_6$ (**4.18**).

Bond	Length	Bond	Length/angle
Ru-N1	2.1334(16)	Ru-C10	2.1871(18)
Ru-O1	2.0567(13)	Ru-centroid[a]	1.659
Ru-O5	2.0619(13)	N1-Ru-O1	82.80(6)
Ru-C5	2.1855(18)	N1-Ru-O5	82.60(6)
Ru-C6	2.1870(18)	O1-Ru-O5	88.86(5)
Ru-C7	2.1661(19)	Ru-N-C2	120.58(13)
Ru-C8	2.1904(19)	Ru-C5-C4	126.49(12)
Ru-C9	2.1712(19)	N1-Ru-C5	90.83(7)

[a] = measured using Mercury 1.4.

Crystals of $[(\eta^6{:}\eta^1\text{-}C_6H_5(CH_2)_3NH_2)Ru(L\text{-pal})]PF_6$ (**4.20**) contain two independent molecules (molecules A and B) in the asymmetric unit, both with the tether in two conformations due to disorder (Figure 4.30). The crystal data are shown in Table A.4.4 and bond angles and lengths in Table 4.12. Molecules A and B form chains with each other, which show a number of strong hydrogen-bond interactions. Both the oxygen atoms of the chelating *L*-pal H-bond to NH_2 groups of the chelate and the tether with O22···H10C 2.05 Å (O22···N103 2.949(5) Å), H10A···O24 2.08 Å (N101···O24 2.969(5) Å), O22···H44A 2.15 Å (O22···N44 3.038(5) Å), H42A···O14 2.17 Å (N42···O14 3.061(5) Å) and H44A···O12 2.54 Å (N44···O12 3.325(5) Å) (Figure A.4.11). The *L*-pal NH_2 group H-bonds to a PF_6 counter anion and a neighbouring *L*-pal oxygen atom with H42B···F122 2.34 Å (N42···F122 2.989(19) Å) and H42B···O14 2.17 Å (N42···O14 3.061(5) Å). In addition, two molecules of solvent methanol show strong H-bonds with the carbonyl oxygen of *L*-pal with

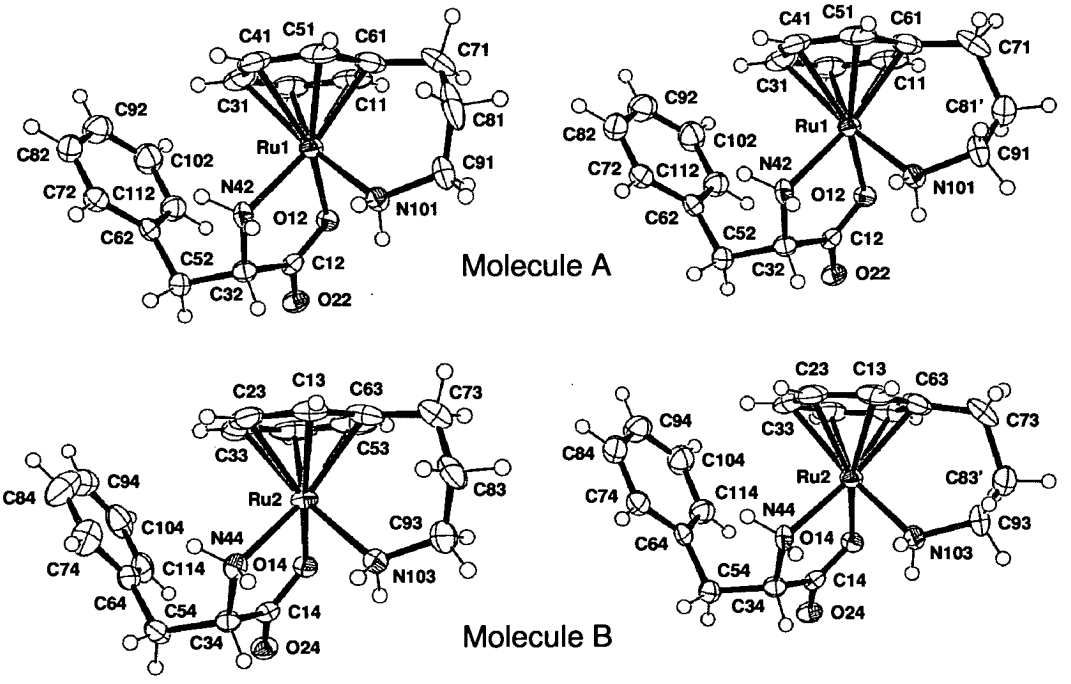

Figure 4.30: Ortep diagram (50% probability ellipsoids) and atom numbering scheme for the cation in the X-ray crystal structure of $[(\eta^6{:}\eta^1\text{-}C_6H_5(CH_2)_3NH_2)Ru(L\text{-pal})]PF_6$ (**4.20**), showing the two independent molecules in the asymmetric unit, each with their respective tether conformations.

Table 4.12: Selected bond lengths (Å) and angles (°) for [(η^6:η^1-$C_6H_5(CH_2)_3NH_2$)Ru(*L*-pal)]PF_6 (**4.20**).

Bond	X = 1, Y = 1, Z = 2	X = 2, Y = 3, Z = 4
RuX-N10Y	2.132(3)	2.133(3)
RuX-O1Z	2.078(3)	2.075(3)
RuX-N4Z	2.130(3)	2.118(3)
RuX-C1Y	2.177(5)	2.184(4)
RuX-C2Y	2.174(5)	2.158(5)
RuX-C3Y	2.188(5)	2.175(5)
RuX-C4Y	2.168(5)	2.160(5)
RuX-C5Y	2.171(4)	2.186(5)
RuX-C6Y	2.192(4)	2.198(5)
RuX-centroidX[a]	1.659	1.666
N10Y-RuX-O1Z	83.48(12)	83.74(12)
N10Y-RuX-N4Z	83.84(13)	83.61(13)
O1Z-RuX-N4Z	78.93(11)	78.93(12)
Ru-N10Y-C9Y	119.4(3)	120.9(3)
Ru-C6Y-C7Y	123.7(4)	125.9(4)
N10Y-Ru-C6Y	91.47(17)	90.45(17)

[a] = measured using Mercury 1.4.

O22···H15 1.98 Å (O22···O15 2.814(4) Å) and O24···H25 2.00 Å (O24···O25 2.824(5) Å) (Figure A.4.11). The Ru – O bond lengths are 2.075(3) Å and 2.078(3) Å, those of Ru – N(*L*-pal) are 2.118(3) Å and 2.130(3) Å and those of Ru – N(tether) are 2.133(3) Å and 2.132(3) Å. The Ru – centroid bond distances (1.66 – 1.67 Å) are slightly longer than those of most of the other three-atom tethered complexes studied in this chapter. The angles between the planes defined by all arene carbons and that of N10Y, Ru and C6Y (arene carbon to which the tether is connected) are 78.63° and 85.56° for molecules A and B, respectively.

4.4.1.2 Stability in solution

The ^{1}H NMR spectra of complexes [(η^6:η^1-$C_6H_5(CH_2)_3NH_2$)Ru(ox)] (**4.14**) and [(η^6:η^1-$C_6H_5(CH_2)_2NH_2$)Ru(ox)] (**4.15**) were recorded in DMSO-d_6 at 298 K and again after storage at ambient temperature for 24 h. In the case of **4.14**, a single species was detected, and no decomposition was observed after 24 h. For **4.15**, the spectrum initially contained one set of signals but additional signals appeared after 24 h.

Solutions of **4.14** (6.7 mM Ru, pH* = 7.12) and **4.15** (6.6 mM Ru, pH* = 7.12) were stable in D_2O at 298 K over the monitored period of 22.5 h and 24.5 h, respectively. Their ^{1}H NMR spectra showed only one set of signals.

4.4.2 Discussion

4.4.2.1 Synthesis and characterisation

The tethered Ru^{II} arene complexes containing bidentate chelating ligands were synthesised generally in good yields and high purity. Crystallographic evidence suggests that for neutral tethered complexes (*i.e.* containing two negatively charged ligands or a di-anionic chelating ligand), the Ru – centroid distances are shorter than for those with an overall +1 or +2 charge. Due to the buckling of the arene observed for [(η^6:η^1-$C_6H_5(CH_2)C_5H_4N$)$RuCl_2$] (**4.7**), it appears that replacement of the chloride ligands by oxalate can stabilise the coordination of the arene, whereas mono-anionic or neutral chelating ligands could lead to an increase in the Ru – centroid distance and a resulting destabilisation of the Ru – C(arene) bonds.

Similar to the structure of [(η^6:η^1-$C_6H_5(CH_2)_3NH_2$)Ru(9EtG)$_2$](CF_3SO_3)$_2$ (**4.11b**), the involvement of the tether amine group of three carbon tethered molecules in marked H-bond interactions is accompanied by a narrowing in the angle between the plane defined by all arene carbons and that N, Ru and the arene carbon to which the tether is connected. For [(η^6:η^1-$C_6H_5(CH_2)_3NH_2$)Ru(acac)]PF_6 (**4.18**),

where no significant H-bonds are observed, this angle is 87.51°, whereas for [(η^6:η^1-$C_6H_5(CH_2)_3NH_2$)Ru(ox)] (**4.14**) and [(η^6:η^1-$C_6H_5(CH_2)_3NH_2$)Ru(*L*-pal)]PF_6 (**4.20**), both with strong H-bonds in the structure, these angles are 72.05°, 78.63° and 85.56°, respectively. This again highlights the orientational freedom of the amine group to form H-bond interactions resulting from the flexibility within the three carbon tether.

The structure of [(η^6:η^1-$C_6H_5(C_6H_4)NH_2$)Ru(ox)] (**4.16**) confirms the ability of 2-aminobiphenyl to act as a tethering ligand in Ru^{II} arene complexes and shows pronounced buckling of the coordinated arene ring. The differences between the two most extreme Ru – C(arene) bond lengths in the molecules of **4.16** in the X-ray crystal structure are in the range of 0.11 – 0.12 Å, comparable to the other two carbon systems [(η^6:η^1-$C_6H_5(CH_2)_2NH_2$)$RuCl_2$] (**4.5**) and [(η^6:η^1-$C_6H_5(CH_2)C_5H_4N$)$RuCl_2$] (**4.7**) with values of *ca.* 0.10 Å. This points towards substantial strain of the arene imposed by the rigidity of the tether backbone in **4.16**.

Complex [(η^6:η^1-$C_6H_5(CH_2)_3NH_2$)Ru(dppz)]$(PF_6)_2$ (**4.21**) is an example of a tethered Ru^{II} arene complex acting as a carrier ligand for a DNA intercalator, in this case dppz [79]. Such a molecule would not be expected to be reactive in a biological medium, since it does not possess any readily available binding sites. This could minimise deactivating side-reactions, and cytotoxic activity might arise from intercalation of the ligand into DNA.

4.4.2.2 Stability in solution

A solution of [(η^6:η^1-$C_6H_5(CH_2)_3NH_2$)Ru(ox)] (**4.14**) in DMSO showed no decomposition after 24 h of storage at ambient temperature, thus further confirming the stability of the three-carbon tethered complexes. In contrast, a solution of [(η^6:η^1-$C_6H_5(CH_2)_2NH_2$)Ru(ox)] (**4.15**) showed decomposition under the same conditions. In addition to a set of signals belonging to **4.15**, new sets of multiplets appeared in the 7.33 – 7.15 ppm region, assignable to 2-phenethylamine with an uncoordinated arene

ring. Integration of the arene proton resonances suggested that decomposition of *ca.* 16% of **4.15** had occurred. This is a significant stabilisation of arene coordination with respect to $[(\eta^6:\eta^1\text{-}C_6H_5(CH_2)_2NH_2)RuCl_2]$ (**4.5**), which instead of oxalate contained two chloride ligands and had fully decomposed within 7.5 h.

Since the ^1H NMR spectra of **4.14** and **4.15** in D_2O gave rise to one set of signals only, in contrast to three for the chloride containing analogues, it appears that oxalate can enhance the aqueous stability of these complexes.

A possible strategy of preventing the formation of hydroxo-bridged species of tethered Ru^{II} arene complexes, is to create a system containing a chelate ring, which can open stepwise. One hydroxide ligand would not be expected to be as good a bridging ligand as two hydroxides coordinated to ruthenium. In addition the pK_a value of a coordinated water molecule might be higher than 7.4 (physiological pH), as has been shown for some Ru^{II} arene mono-aqua complexes [8, 16, 17]. Ideally, upon ring opening the Ru centre could react with its target, *e.g.* DNA, and the open chelate ring would undergo hydrolysis to create a second binding site. This provided the stimulus for the synthesis of complex $[(\eta^6:\eta^1\text{-}C_6H_5(CH_2)_3NH_2)Ru(L\text{-pal})]PF_6$ (**4.20**), which contains *L*-phenylalanine as the chelating ligand. Carmona *et al.* have shown that ruthenium arene complexes containing amino acidates can epimerize in chloroform [80]. It was proposed that epimerization could involve opening of the chelate ring. Investigation of chelate ring opening reactions and their control could be crucial, since such a mechanism could also lead to deactivating pathways. Further solution studies on **4.20** would be needed to investigate this possibility.

Spectra of $[(\eta^6:\eta^1\text{-}C_6H_5(CH_2)_3NH_2)Ru(9EtG)_2](PF_6)_2$ (**4.11a**) in D_2O still contain residual NH_2 signals after 22.5 h (see Figure 4.14), whereas these signals for the di-chloro and oxalato analogues rapidly disappear, *ca.* 30 min for the oxalato complexes $[(\eta^6:\eta^1\text{-}C_6H_5(CH_2)_3NH_2)Ru(ox)]$ (**4.14**) and $[(\eta^6:\eta^1\text{-}$

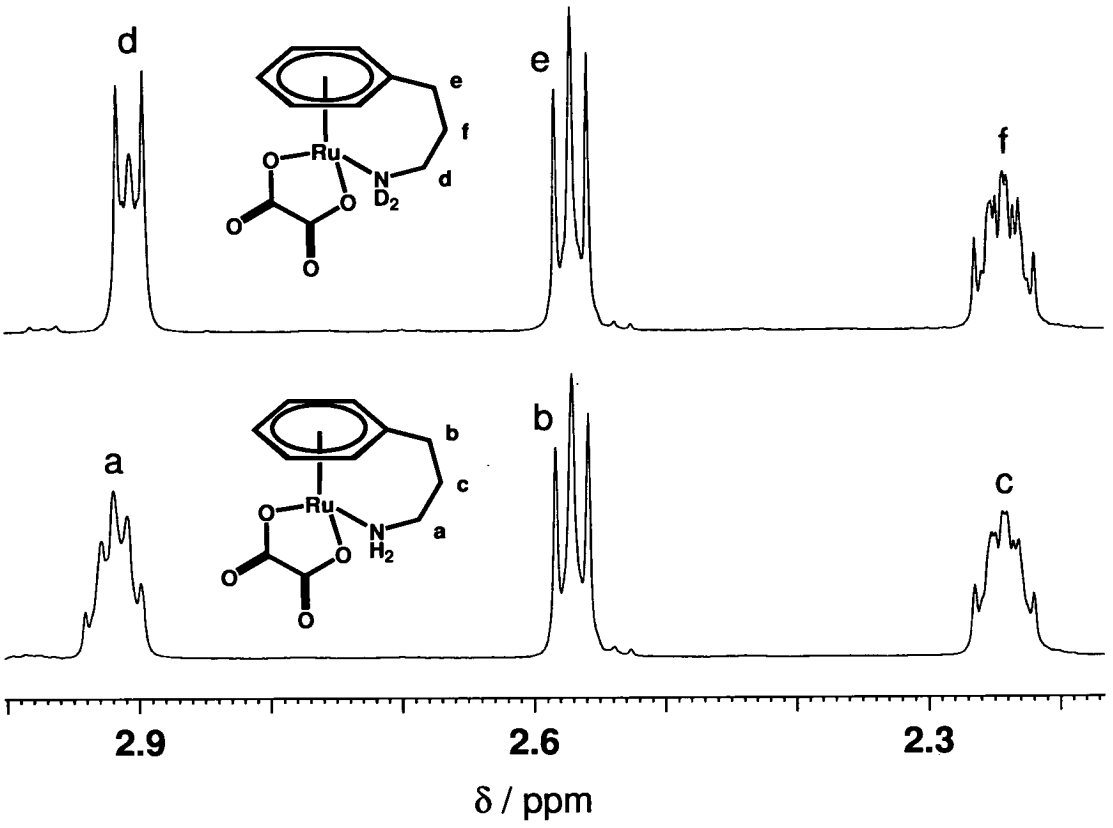

Figure 4.31: The influence of amine H/D exchange of [(η^6:η^1-$C_6H_5(CH_2)_3NH_2$)Ru(ox)] (**4.14**) on the signals for the adjacent CH_2 group.

$C_6H_5(CH_2)_2NH_2$)Ru(ox)] (**4.15**). Upon H/D proton exchange of the NH_2 group, the splitting pattern of the signal for the CH_2 group adjacent to the amine group changes. This is illustrated clearly for the oxalato complexes **4.14** and **4.15**, since their respective aqueous solutions contain one species only and there are no overlapping signals. Figure 4.31 shows the influence of amine NH_2 H/D exchange for **4.14** on the signal of the adjacent CH_2 group (Figure A.4.12 for **4.15**).

4.5 Neutral, Di-chloride Tethered Ru^{II} Arene Complexes: Towards Multi-substituted Arenes

4.5.1 Results

Substituents on the arene ring, particularly by alkyl groups, can increase the stability of coordination of the arene in Ru^{II} arene complexes. It was therefore of

interest to explore ways of incorporating multi substituted arenes into tethered Ru^{II} arene complexes. Similar complexes have been synthesised with phosphorus-containing tethering ligands [23, 30, 40, 49, 50], but in low yields [30].

In addition, substituents on the arene can also play a role in stabilising secondary interactions (*e.g.* H-bonds, $\pi - \pi$ stacking and intercalation) with possible target sites.

4.5.1.1 Synthesis and characterisation

For the synthesis of nitrogen-containing tethered Ru^{II} arene complexes with multi-substituted arene rings, only a limited amount of ligands are commercially

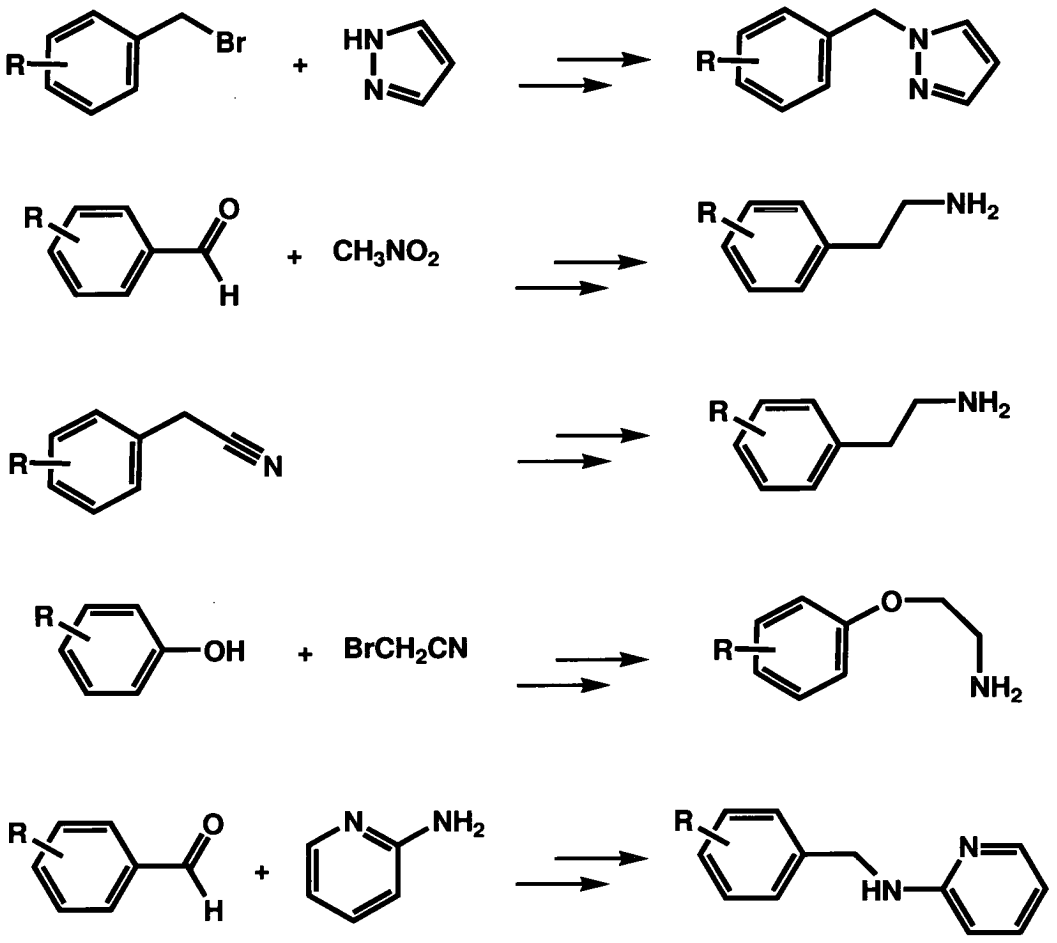

Scheme 4.8: General transformations for the syntheses of precursor ligands for potential use in tethered Ru^{II} arene complexes.

available. However, there a number of synthetic routes towards such ligands, which can be proposed, particularly for two carbon tethers (Scheme 4.8). One of these involves the condensation of pyrazole with benzylchloride. The resulting ligand 1-benzyl-1-*H*-pyrazole (**4.3**) (Figure 4.32) was used to synthesise complex $[(\eta^6{:}\eta^1\text{-}C_6H_5(CH_2)C_3H_3N_2)RuCl_2]$ (**4.9**) successfully (*vide supra*).

Amine-containing ligands were synthesised *via* reduction of mesitylacetonitrile and (2-nitroethenyl)-aryls. The latter were obtained *via* condensation of arylaldehydes with nitromethane [81], using lithium aluminium hydride under conditions described for related systems [82, 83, 84] to yield the ligands 2-(2,4,6-trimethylphenyl)ethylamine (**4.24**), (2,3,4,5,6-pentamethyl)phenethylamine (**4.26**) and 4-phenylphenethylamine (**4.28**). Of these

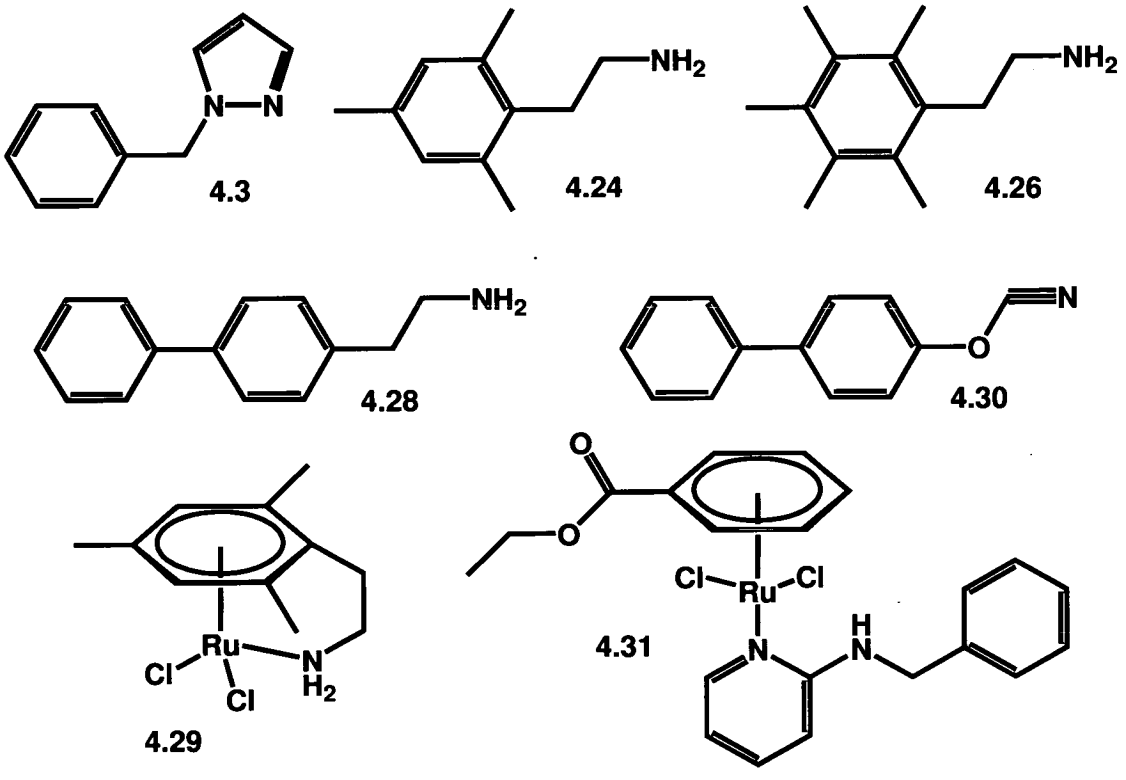

4.3 4.24 4.26 4.28 4.30 4.29 4.31

Figure 4.32: The structures of benzyl-1-*H*-pyrazole (**4.3**), 2-(2,4,6-trimethylphenyl)ethylamine (**4.24**), (2,3,4,5,6-pentamethyl)phenethylamine (**4.26**), and 4-phenylphenethylamine (**4.28**), $[(\eta^6{:}\eta^1\text{-}C_6H_2(CH_3)_3(CH_2)_2NH_2)RuCl_2]$ (**4.29**), [(1,1'-biphenyl)-4-yloxy]acetonitrile (**4.30**) and $[(\eta^6\text{-etb})Ru(bap)Cl_2]$ (**4.31**).

ligands, **4.24** was used to make the tethered complex $[(\eta^6:\eta^1\text{-}C_6H_2(CH_3)_3(CH_2)_2NH_2)RuCl_2]$ (**4.29**) (Figure 4.32).

Three-carbon tether precursors are less readily accessible than their two-carbon analogues, since their synthesis involves a number of steps. However, one convenient route is *via* the condensation of bromoacetonitrile with phenols [85]. The ligand [(1,1'-biphenyl)-4-yloxy]acetonitrile (**4.30**) (Figure 4.32) was synthesised in this way, but the reduction with $LiAlH_4$ failed to yield the desired end product 4-phenylphenoxyethylamine and the reaction mixture turned orange.

In a project with Melanie Brown (undergraduate, 2005, University of Edinburgh) the synthesis of 2-arylaminopyridine compounds was explored *via* condensation of arylaldehydes with 2-aminopyridine [86]. It was shown that such substituted compounds can be synthesised *via* immine formation followed by reduction with $NaBH_4$ to include *e.g.* a pentamethylbenzyl ring [87].

Attempts to synthesise a complex with a tethered pyridine ligand, $[(\eta^6:\eta^1\text{-}C_6H_5(CH_2NH)C_5H_4N)RuCl_2]$, failed. The X-ray crystal structure of the intermediate

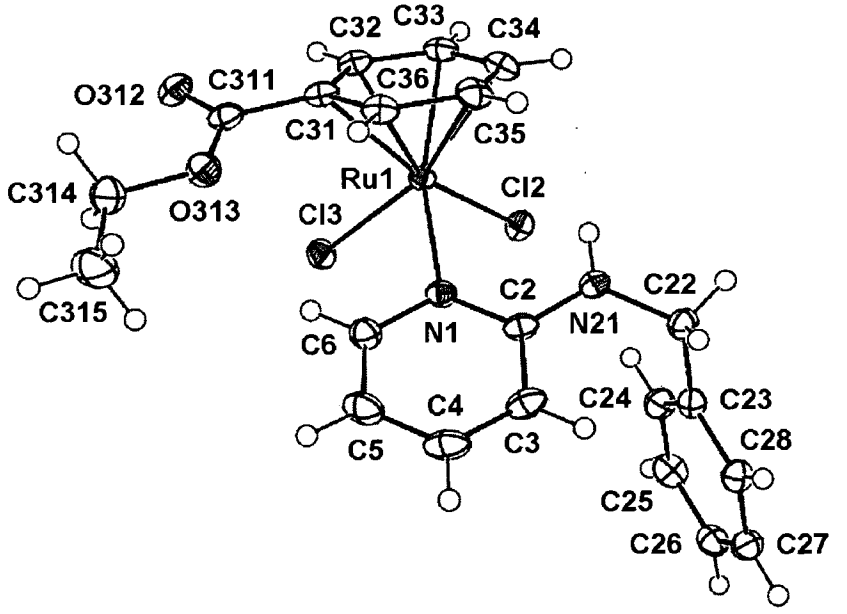

Figure 4.33: Ortep diagram (50% probability ellipsoids) and atom numbering scheme for the X-ray crystal structure of $[(\eta^6\text{-etb})Ru(bap)Cl_2]$ (**4.31**).

Table 4.13: Selected bond lengths (Å) and angles (°) for [(η^6-etb)Ru(bap)Cl_2] (**4.31**).

Bond	Length	Bond	Length/angle
Ru-N	2.1708(13)	Ru-C35	2.1893(17)
Ru-Cl2	2.4074(4)	Ru-C36	2.1646(17)
Ru-Cl3	2.3914(4)	Ru-centroid[a]	1.657
Ru-C31	2.1545(17)	N-Ru-Cl2	90.63(4)
Ru-C32	2.1914(17)	N-Ru-Cl3	86.60(4)
Ru-C33	2.2027(16)	Cl2-Ru-Cl3	85.796(15)
Ru-C34	2.1839(17)		

[a] = measured using Mercury 1.4.

product [(η^6-etb)Ru(bap)Cl_2] (**4.31**), where bap = 2-benzylaminopyridine, was determined from crystals grown by slow diffusion of diethyl ether into a methanol solution at ambient temperature (Figure 4.33). The crystal data are shown in Table A.4.4 and bond angles and lengths in Table 4.13. The structure shows the coordination of bap through the pyridine nitrogen as well as the pendant arene, which could coordinate to ruthenium upon displacement of ethyl benzoate. A chloride ligand and the NH proton of 2-benzylaminopyridine show weak a hydrogen bond (H211···Cl2 2.65 Å, N21···Cl2 3.1466(15) Å). The carbonyl oxygen of ethyl benzoate is involved in a number of short interactions with arene protons, O312···H361 2.47 Å (O312···C36 3.092(2) Å) and O312···H351 2.59 Å (O312···C35 3.156(2) Å), as well as a proton of the pendant benzyl ring (O312···H281 2.59 Å, O312···C28 3.490(2) Å). The Ru – Cl bond lengths are 2.3914(4) Å and 2.4074(4) Å. The Ru – N distance is 2.1708(13) Å, with Ru – centroid 1.66 Å.

4.5.1.2 Stability in solution

[(η^6-etb)Ru(bap)Cl_2] (**4.31**) (Figure 4.32) appeared to undergo decomposition reactions in chloroform. Solutions turned from orange to a green-grey in colour over

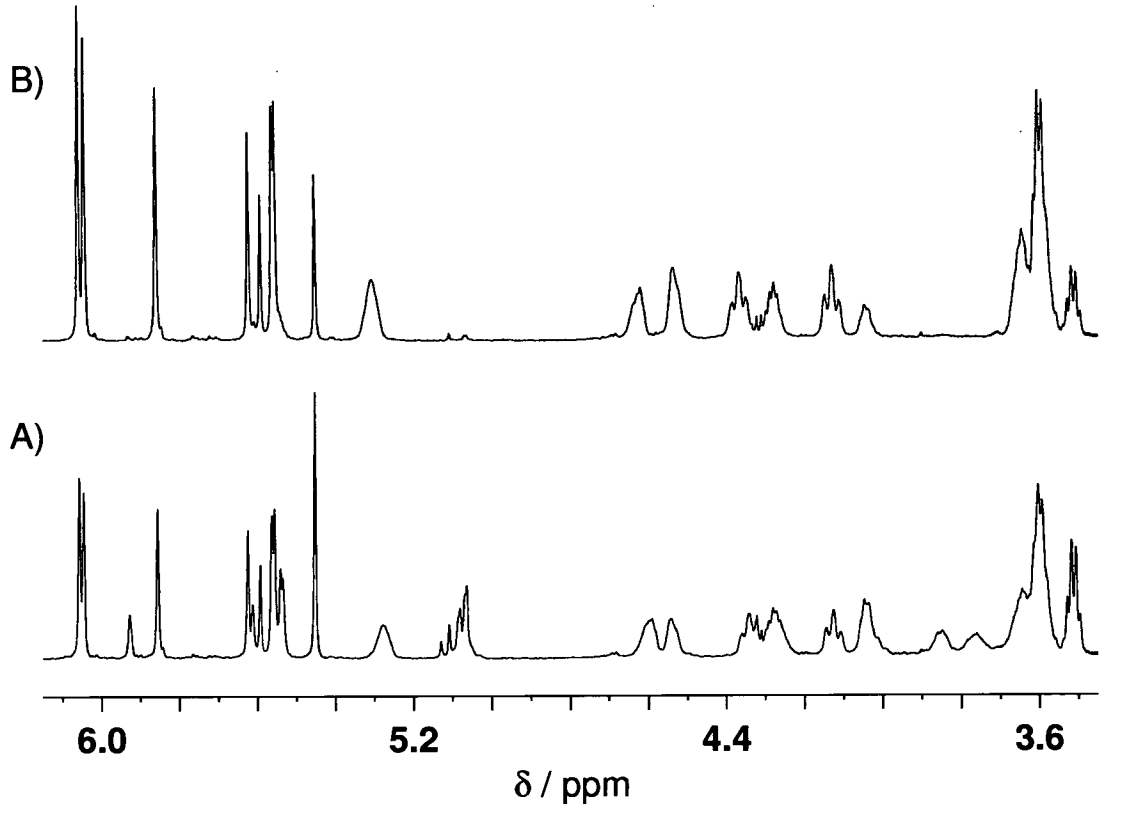

Figure 4.34: Selected region of the ^{1}H NMR spectrum of [(η^6:η^1-$C_6H_2(CH_3)_3(CH_2)_2NH_2$)$RuCl_2$] (**4.29**) in DMSO-$d_6$ at 298 K. A: 10 min after dissolution using ultrasonication. B: 30 min after dissolution using ultrasonication. Previously present peaks have disappeared.

varying time intervals (30 min – 10 h) and the appearance of new signals in the ^{1}H NMR spectrum was noted.

The ^{1}H NMR spectrum of a solution of [(η^6:η^1-$C_6H_2(CH_3)_3(CH_2)_2NH_2$)$RuCl_2$] (**4.29**) in DMSO-$d_6$ at 298 K showed several sets of peaks. Ultrasonication of a different solution gave rise to more peaks in the spectrum (Figure 4.34), which decayed within *ca.* 30 min to produce a spectrum similar to that observed in the spectrum of the former solution. Two new peaks at 6.81 ppm and 6.79 ppm gradually increased in intensity over a monitored period of 17 h, together with two minor peaks at 6.82 ppm and 6.77 ppm. 2D COSY (Figure A.4.13) and ROESY spectra were recorded to assign the peaks (Figure 4.35).

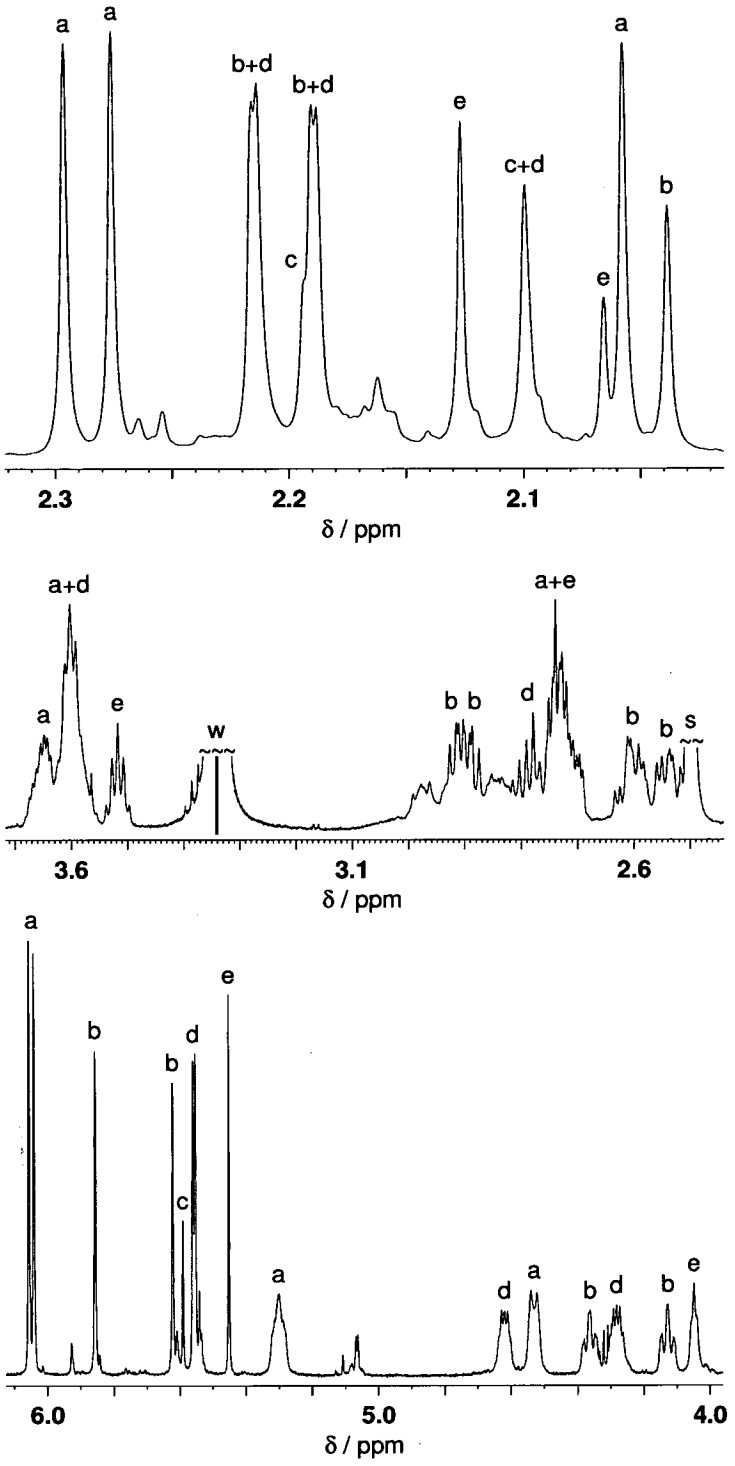

Figure 4.35: The ^{1}H NMR spectrum of $[(\eta^6{:}\eta^1\text{-}C_6H_2(CH_3)_3(CH_2)_2NH_2)RuCl_2]$ (**4.29**) in DMSO-d_6 at 298 K. Only peaks, which can be unambiguously assigned to the respective set of signals of species present in solution, are labelled.

4.5.2 Discussion

4.5.2.1 Synthesis and characterisation

Condensation of pyrazole with chloro- (or bromo-) benzyl derivatives can provide a general route towards pyrazole-containing ligands for the synthesis of tethered ruthenium arene complexes. While $[(\eta^6{:}\eta^1\text{-}C_6H_5(CH_2)C_3H_3N_2)RuCl_2]$ (**4.9**) was synthesised successfully, the yield was the lowest of all the di-chloro tethered complexes. This possibly is due to a more pronounced strain exerted on the arene by the backbone.

Aryl aldehydes are particularly attractive starting materials for the synthesis of tether precursor ligands containing multi-substituted arene rings, since a large number are commercially available which contain a variety of benzene ring substitutions. Of the synthesised two carbon tether ligands, only 2-(2,4,6-trimethylphenyl)ethylamine (**4.24**) was used to attempt the synthesis of the respective tethered Ru^{II} arene complex $[(\eta^6{:}\eta^1\text{-}C_6H_2(CH_3)_3(CH_2)_2NH_2)RuCl_2]$ (**4.29**). Due to the complex behaviour of this compound in solution, no attempts were made to form complexes with ligands (2,3,4,5,6-pentamethyl)phenethylamine (**4.26**) and 4-phenylphenethylamine (**4.28**).

Failure to reduce [(1,1'-biphenyl)-4-yloxy]acetonitrile (**4.30**) appears to be due to cleavage of the ether linkage. The intense orange colour of the solution suggested that the biphenylhydroxy anion was formed.

2-Arylaminopyridine compounds can be produced conveniently in high yields and purity [87]. The coordination of such ligands to $\{(\eta^6\text{-etb})RuCl_2\}$ was confirmed in solution and in the solid state for $[(\eta^6\text{-etb})Ru(bap)Cl_2]$ (**4.31**).

4.5.2.2 Stability in solution

The apparent decomposition of $[(\eta^6\text{-etb})Ru(bap)Cl_2]$ (**4.31**) into unknown species in chloroform might be the reason as to why formation of the tether failed.

The solution of the analytically pure adduct of 2-pentamethylbenzylaminopyridine with $\{(\eta^6\text{-etb})RuCl_2\}$ showed a similar change of colour in chloroform to the benzyl analogue. In addition, crystals grown from a reaction mixture thought to contain this adduct turned out to be those of the ethyl benzoate ruthenium dimer $[(\eta^6\text{-etb})RuCl_2]_2$ (**4.2**) [87], thus suggesting that ligand dissociation can occur, which might be responsible for the failure of tether formation.

The behaviour of $[(\eta^6{:}\eta^1\text{-}C_6H_2(CH_3)_3(CH_2)_2NH_2)RuCl_2]$ (**4.29**) in DMSO-d_6 is complex. According to 2D ^{1}H NMR spectra, there are at least five species present in solution, even more after ultrasonication of the sample. All appear to confer to (2,4,6-trimethylphenyl)ethylamine (**4.24**) with the arene ring coordinated to ruthenium. The new peaks appearing at around 6.8 ppm have a similar chemical shift to free **4.24**, suggesting that loss of arene coordination occurs. This is similar to $[(\eta^6{:}\eta^1\text{-}C_6H_5(CH_2)_2NH_2)RuCl_2]$ (**4.5**). In contrast to **4.5**, the introduction of arene substituents has significantly slowed down decomposition. Whereas **4.5** in DMSO-d_6 was fully decomposed after 7.5 h, *ca.* 40% of **4.29** was still intact after 17 h.

As was observed for the two carbon tether **4.5**, the coordination of the arene ring has a pronounced effect on the chemical shifts of the protons of the tether backbone. A similar separation of these signals was also observed for **4.29**. However, the tether backbone signals for species (b) are significantly closer together than for the other species, and are in similar positions to those of free **4.24** (*ca.* 2.8 – 2.7 ppm). This seems to indicate the presence of at least one species, which has a coordinated arene, but an open tether, possibly with the amine group coordinating to another Ru centre. Tether opening could also help to explain the amount of species present. For the tethered complex, a maximum of three species could be expected, namely the di-chloride-, the mono-DMSO- and the di-DMSO adducts. However, in spectra of other di-chloride tethered complexes a maximum of two species only was noted (*vide supra*). Tether-opening reactions could facilitate the formation of more

species, most likely polymers. Thermal energy derived from ultrasonication, in the form of localised hotspots, could promote the formation of more of such species as observed in the ^{1}H NMR spectrum. A return to equilibrium at 298 K might explain the disappearance of some of the signals. However, the involvement of different coordination modes of DMSO, *i.e.* S *vs.* O coordination, cannot be ruled out [88].

4.6 Tether-opening Reactions

The rate and extent of hydrolysis of bifunctional tethered Ru^{II} arene complexes might not make them suitable for tolerating physiological reaction conditions in terms of anti-cancer applications. Even for complexes of the type $[(\eta^6$-arene)Ru(en)Cl$]^+$ in the presence of 104 mM chloride, the complex is not present entirely as its chloride adduct. About 10% of the complex could exist as the more reactive aqua-adduct [61], which might present a pathway of deactivation of the complex before it enters the cell. It would therefore be desirable to synthesise a complex, which can be activated under controlled conditions, ideally such, which are specific to cancer cells. Such activation techniques could be based on pH, since cancer cells are believed to have a slightly more acidic environment than healthy cells or also activation by light, as has been shown to be possible for some Pt^{IV} complexes [89, 90]. Tethered Ru^{II} arene complexes containing a bidentate chelating ligand, *e.g.* ethylenediamine, would be expected to be unreactive since all binding sites are blocked. Reactions, in which the tether would be irreversibly opened, could lead to complexes similar to those previously found to have good activity against the human ovarian cancer cell line A2780 [5, 6]. In addition, the ethylenediamine-containing, tether-opened complex $[(\eta^6$-$C_6H_5(C_6H_4NH_2))$Ru(en)Cl$]^+$ could have the potential to stabilise binding of guanine for example by formation of two hydrogen bonds with the C6O carbonyl group as shown in the molecular model in Figure 4.36. This could lead to stronger binding and potentially an increase in cytotoxic activity,

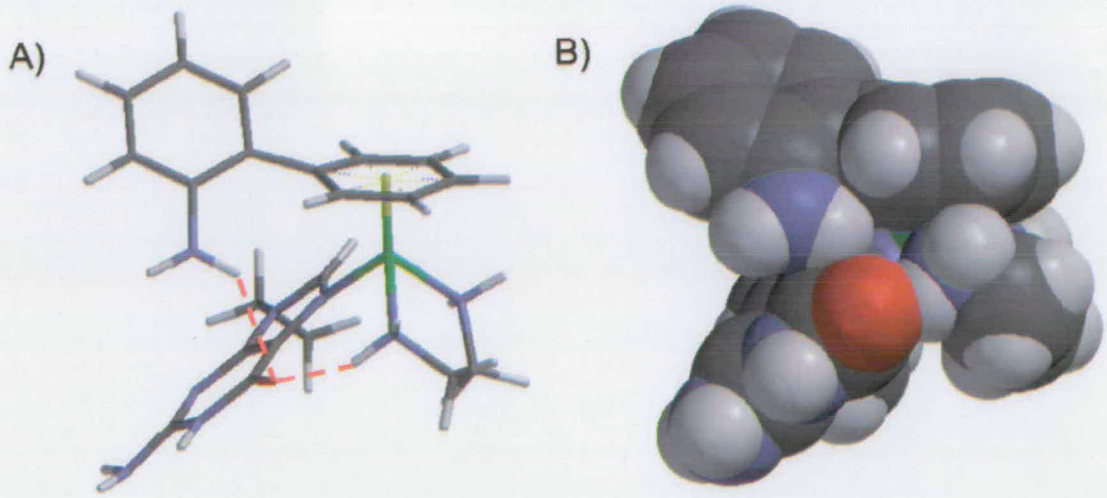

Figure 4.36: Molecular model of the 9EtG adduct $[(\eta^6\text{-}C_6H_5(C_6H_4NH_2))Ru(en)9EtG]^{2+}$. A: Lines showing possible formation of two hydrogen bonds with the C6O carbonyl group. B: Spacefilling model.

especially if activation could be controlled and deactivating side-reactions minimised.

4.6.1 Results

Crystals of X-ray diffraction quality of the tether-opened complex $[(\eta^6{:}\eta^1\text{-}C_6H_5(C_6H_4)NH_3)RuCl_3]$ (**4.32**) were grown by dissolving the tether-closed precursor $[(\eta^6{:}\eta^1\text{-}C_6H_5(C_6H_4)NH_2)RuCl_2]$ (**4.8**) in warm conc. hydrochloric acid (12 M), followed by slow evaporation at ambient temperature over a period of five days. The structure clearly shows that the tether has been opened (Figure 4.37). The crystal data are shown in Table A.4.4 and bond angles and lengths in Table 4.14. Coordination of three chloride ligands to a Ru^{II} arene fragment has mainly been documented for chloride-bridged complexes [91, 92, 93, 94], although recently details of a non-bridged molecule were published [95]. In this respect, the present structure is unusual and can be classed as a zwitterionic molecule. The Ru – Cl bond lengths are 2.41 Å, 2.42 Å and 2.44 Å. The Ru – centroid distance is 1.65 Å and the angle between the coordinated arene and the free aminobenzene ring is 53.5°. The intramolecular Ru···N

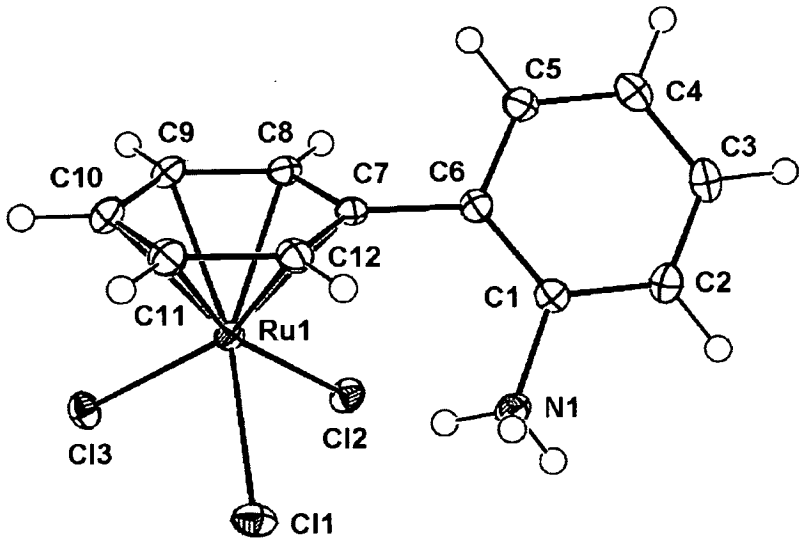

Figure 4.37: Ortep diagram (50% probability ellipsoids) and atom numbering scheme for the X-ray crystal structure of $[(\eta^6{:}\eta^1\text{-}C_6H_5(C_6H_4)NH_3)RuCl_3]$ (**4.32**), showing that the tether has been opened.

Table 4.14: Selected bond lengths (Å) and angles (°) for $[(\eta^6{:}\eta^1\text{-}C_6H_5(C_6H_4)NH_3)RuCl_3]$ (**4.32**).

Bond	Length	Bond	Length/angle
Ru-Cl1	2.4175(5)	Ru-C11	2.1707(18)
Ru-Cl2	2.4367(4)	Ru-centroid[a]	1.647
Ru-Cl3	2.4053(5)	Ru-C12	2.1721(19)
Ru-C7	2.1970(18)	Cl1-Ru-Cl2	86.288(17)
Ru-C8	2.1798(18)	Cl1-Ru-Cl3	87.532(17)
Ru-C9	2.1799(18)	Cl2-Ru-Cl3	87.049(16)
Ru-C10	2.1591(18)	Ru-C7-C6	132.05(12)

[a] = measured using Mercury 1.4.

distance is 3.5723(15) Å. There are intramolecular hydrogen bonds between two chloride ligands and an amine proton with H13···Cl1 2.53 Å (N1···Cl1 3.2804(16) Å) and H13···Cl2 2.66 Å (N1···Cl2 3.3195(15) Å). Intermolecular H-bonds are formed between neighbouring molecules, linking them into chains, with H11···Cl3 2.25 Å (N1···Cl3 3.1075(16) Å) and H12···Cl2 2.31 Å (N1···Cl2 3.6174(15) Å) (Figure

A.4.14A). The aminobenzene rings show π – π stacking for the whole ring with C1···C4 3.657(3) Å, C2···C5 3.629(3) Å and C3···C6 3.652(3) Å (Figure A.4.14B). In addition, there are a number of interactions between chloride and arene protons, with H121···Cl3 2.70 Å (C12···Cl3 3.645(2) Å), H111···Cl1 2.78 Å (C11···Cl1 3.342(2) Å), H101···Cl3 2.82 Å (C10···Cl3 3.476(2) Å) and H111···Cl3 2.88 Å (C11···Cl3 3.499(2) Å), as well as protons of aminobenzene, where H51···Cl1 2.82 Å (C5···Cl1 3.692(2) Å) and H31···Cl2 2.89 Å (C3···Cl2 3.630(2) Å).

4.6.2 Discussion

The X-ray structure of $[(\eta^6{:}\eta^1\text{-}C_6H_5(C_6H_4)NH_3)RuCl_3]$ (**4.32**) confirmed tether opening for this complex in strongly acidic solution. While $[(\eta^6{:}\eta^1\text{-}C_6H_5(CH_2)_3NH_2)RuCl_2]$ (**4.4**) was stable in water at pH 1, the more strained two-carbon systems might be useful candidates for more detailed studies into tether opening mechanisms. Potential might arise from these complexes as orally administered drugs, which could be activated by stomach acid.

4.7 Conclusions

The novel di-chloro, nitrogen-tethered Ru^{II} arene complexes $[(\eta^6{:}\eta^1\text{-}C_6H_5(CH_2)_3NH_2)RuCl_2]$ (**4.4**), $[(\eta^6{:}\eta^1\text{-}C_6H_5(CH_2)_2NH_2)RuCl_2]$ (**4.5**), $[(\eta^6{:}\eta^1\text{-}C_6H_5O(CH_2)_2NH_2)RuCl_2]$ (**4.6**), $[(\eta^6{:}\eta^1\text{-}C_6H_5(CH_2)C_5H_4N)RuCl_2]$ (**4.7**), $[(\eta^6{:}\eta^1\text{-}C_6H_5(C_6H_4)NH_2)RuCl_2]$ (**4.8**) and $[(\eta^6{:}\eta^1\text{-}C_6H_5(CH_2)C_3H_3N_2)RuCl_2]$ (**4.9**) were synthesised. Use of the pressure vessel improved the yields compared to reflux conditions and complexes were obtained in good-to-high yields and high purity. These complexes are water soluble and undergo rapid hydrolysis of bound chloride, to form mono- and di-aqua adducts. The associated equilibrium constants were calculated for two representative complexes. Loss of one chloride appears strongly favourable and anation is only *ca.* 40% complete in the presence of excess chloride

(*ca.* 275 mM). Formation of an insoluble precipitate, probably involving hydroxo- and oxo-bridges, was observed for the diaqua adduct over a range of pH 5.4 – 11.0. Thus in aqueous biological media these complexes may be deactivated by reactions with biomolecules or by precipitation.

The reactivity of these bifunctional tethered Ru^{II} arene complexes towards guanine (9EtG, Guo) was investigated. Rapid binding of one G (< 20 min) was observed followed by slow formation of the di-adduct over a period of *ca.* 10 h. Formation of di-adducts also appears to be suppressed by the presence of chloride and possibly by the formation of hydroxo-bridged species. The X-ray crystal structure of the di-9EtG adduct $[(\eta^6{:}\eta^1\text{-}C_6H_5(CH_2)_3NH_2)Ru(9EtG)_2](CF_3SO_3)_2$ (**4.11b**) reveals an unusual *head-to-head* orientation of the two bases, with formation of H-bonds (1.98 Å and 2.32 Å) between the tether NH_2 group and C6O(9EtG). It also suggests strong binding of one 9EtG ligand and weak binding of the other. In addition, displacement of 9-EtG from the di-9EtG adduct $[(\eta^6{:}\eta^1\text{-}C_6H_5(CH_2)_3NH_2)Ru(9EtG)_2](PF_6)_2$ (**4.11a**) was observed in water.

A number of complexes containing bidentate chelating ligands, such as $[(\eta^6{:}\eta^1\text{-}C_6H_5(CH_2)_3NH_2)Ru(ox)]$ (**4.14**), $[(\eta^6{:}\eta^1\text{-}C_6H_5(CH_2)_2NH_2)Ru(ox)]$ (**4.15**), $[(\eta^6{:}\eta^1\text{-}C_6H_5(C_6H_4)NH_2)Ru(ox)]$ (**4.16**), $[(\eta^6{:}\eta^1\text{-}C_6H_5(CH_2)C_5H_4N)Ru(ox)]$ (**4.17**), $[(\eta^6{:}\eta^1\text{-}C_6H_5(CH_2)_3NH_2)Ru(acac)]PF_6$ (**4.18**), $[(\eta^6{:}\eta^1\text{-}C_6H_5(CH_2)C_5H_4N)Ru(acac)]PF_6$ (**4.19**), $[(\eta^6{:}\eta^1\text{-}C_6H_5(CH_2)_3NH_2)Ru(L\text{-pal})]PF_6$ (**4.20**) and $[(\eta^6{:}\eta^1\text{-}C_6H_5(CH_2)_3NH_2)Ru(dppz)](PF_6)_2$ (**4.21**), were synthesised. They possess the expected higher aqueous stability and could also act as carrier ligands for *e.g.* intercalators.

The possibility of coordination of multi-substituted arene rings in tethered Ru^{II} arene complexes was investigated. A number of suitable synthetic routes towards the synthesis of potentially useful precursors were identified. However, the 2-benzylaminopyridine-containing complex $[(\eta^6\text{-etb})Ru(bap)Cl_2]$ (**4.31**) failed to

yield the corresponding tethered complex. For $[(\eta^6:\eta^1\text{-}C_6H_2(CH_3)_3(CH_2)_2NH_2)RuCl_2]$ (**4.29**) the behaviour in DMSO resulted in formation of at least five species, one which appeared to be tethere-opened.

Finally, tether-opening has been confirmed for $[(\eta^6:\eta^1\text{-}C_6H_5(C_6H_4)NH_3)RuCl_3]$ (**4.32**) in the solid state. Such breakage of the Ru – N bond could warrant potential for tethered complexes as prodrugs, ideally with controllable activation.

Appendix A.4 contains Tables A.4.1 – 4 and Figures A.4.1 – 14.

4.8 References

[1] Z. Guo, P.J. Sadler, *Angew. Chem. Int. Ed.* **1999**, *38*, 1512–1531.

[2] M.J. Clarke, *Coord. Chem. Rev.* **2003**, *236*, 209–233.

[3] M.M. Harding, G. Mokdsi, *Curr. Med. Chem.* **2000**, *7*, 1289–1303.

[4] S. Top, A. Vessières, G. Leclercq, J. Quivy, J. Tang, J. Vaissermann, M. Huché, G. Jaouen, *Chem. Eur. J.* **2003**, *9*, 5223–5236.

[5] R.E. Aird, J. Cummings, A.A. Ritchie, M. Muir, R.E. Morris, H. Chen, P.J. Sadler, D.I. Jodrell, *Brit. J. Cancer* **2002**, *86*, 1652–1657.

[6] A. Habtemariam, M. Melchart, R. Fernández, S. Parsons, I.D.H. Oswald, A. Parkin, F.P.A. Fabbiani, J.E. Davidson, A. Dawson, R.E. Aird, D.I. Jodrell, P.J. Sadler, *J. Med. Chem.*, in press.

[7] F. Wang, J. Bella, J.A. Parkinson, P.J. Sadler, *J. Biol. Inorg. Chem.* **2005**, *10*, 147 – 155.

[8] H. Chen, J.A. Parkinson, R.E. Morris, P.J. Sadler, *J. Am. Chem. Soc.* **2003**, *125*, 173–186.

[9] E.R. Jamieson, S.J. Lippard, *Chem. Rev.* **1999**, *99*, 2467–2498.

[10] F. Wang, A. Habtemariam, E.P.L. van der Geer, R. Fernández, M. Melchart, R.J. Deeth, R. Aird, S. Guichard, F.P.A. Fabbiani, P. Lozano-Casal, I.D.H. Oswald, D.I. Jodrell, S. Parsons, P.J. Sadler, *Proc. Natl. Acad. Sci. USA* **2005**, *102*, 18269–18274.

[11] R.E. Morris, R.E. Aird, P. del S. Murdoch, H. Chen, J. Cummings, N.D. Hughes, S. Parsons, A. Parkin, G. Boyd, D.I. Jodrell, P.J. Sadler, *J. Med. Chem.* **2001**, *44*, 3616–3621.

[12] C. Scolaro, A. Bergamo, L. Brescacin, R. Delfino, M. Cocchietto, G. Laurenczy, T.J. Geldbach, G. Sava, P.J. Dyson, *J. Med. Chem.* **2005**, *48*, 4161–4171.

[13] L.Y. Kuo, A.H. Liu, T.J. Marks in *Metal Ions Biol Syst, Vol. 33* (Eds.: A. Sigel, H. Sigel), Marcel Dekker, New York, **1996**, pp. 53–85.

[14] S. Korn, W.S. Sheldrick, *J. Chem. Soc., Dalton Trans.* **1997**, 2191–2199.

[15] J. Reedijk, *Chem. Rev.* **1999**, *99*, 2499–2510.

[16] R. Fernández, M. Melchart, A. Habtemariam, S. Parsons, P.J. Sadler, *Chem. Eur. J.* **2004**, *10*, 5173–5179.

[17] M. Melchart, A. Habtemariam, S. Parsons, S.A. Moggach, P.J. Sadler, *Inorg. Chim. Acta* **2006**, *359*, 3020–3028.

[18] H. Chen, J.A. Parkinson, S. Parsons, R.A. Coxall, R.O. Gould, P.J. Sadler, *J. Am. Chem. Soc.* **2002**, *124*, 3064–3082.

[19] W.S. Sheldrick, S. Heeb, *Inorg. Chim. Acta* **1990**, *168*, 93–100.

[20] R.S. Bates, M.J. Begley, A.H. Wright, *Polyhedron* **1990**, *9*, 1113–1118.

[21] L. Carter, D.L. Davies, J. Fawcett, D.R. Russell, *Polyhedron* **1993**, *12*, 1123–1128.

[22] A. Fürstner, M. Liebl, C.W. Lehmann, M. Picquet, R. Kunz, C. Bruneau, D. Touchard, P.H. Dixneuf, *Chem. Eur. J.* **2000**, *6*, 1847–1857.

[23] D. Jan, L. Delaude, F. Simal, A. Demonceau, A.F. Noels, *J. Organomet. Chem.* **2000**, *606*, 55–64.

[24] B. Çetinkaya, S. Demir, I. Özdemir, L. Toupet, D. Esmeril, C. Bruneau, P.H. Dixneuf, *Chem. Eur. J.* **2003**, *9*, 2323–2330.

[25] F. Simal, D. Jan, A. Demonceau, A.F. Noels, *Tetrahedron Lett.* **1999**, *40*, 1653–1656.

[26] K. Umezawa-Vizzini, T.R. Lee, *Organometallics* **2003**, *22*, 3066–3076.

[27] Y. Miyaki, T. Onishi, S. Ogoshi, H. Kurosawa, *J. Organomet. Chem.* **2000**, *616*, 135–139.

[28] K. Umezawa-Vizzini, I.Y. Guzman-Jimenez, K.H. Whitmire, T.R. Lee, *Organometallics* **2003**, *22*, 3059–3065.

[29] B. Therrien, T.R. Ward, M. Pilkington, C. Hoffmann, F. Gilardoni, J. Weber, *Organometallics* **1998**, *17*, 330–337.

[30] M.A. Bennett, A.J. Edwards, J.R. Harper, T. Khimyak, A.C. Willis, *J. Organomet. Chem.* **2001**, *629*, 7–18.

[31] S. Jung, K. Ilg, C.D. Brandt, J. Wolf, H. Werner, *J. Chem. Soc., Dalton Trans.* **2002**, 318–327.

[32] J.H. Nelson, K.Y. Ghebreyessus, V.C. Cook, *Organometallics* **2002**, *21*, 1727–1733.

[33] P.D. Smith, A.H. Wright, *J. Organomet. Chem.* **1998**, *559*, 141–147.

[34] M.A. Bennett, L.Y. Goh, A.C. Willis, *J. Am. Chem. Soc.* **1996**, *118*, 4984–4992.

[35] Y. Miyaki, T. Onishi, H. Kurosawa, *Inorg. Chim. Acta* **2000**, *300 – 302*, 369–377.

[36] J. Soleimannejad, A. Sisson, C. White, *Inorg. Chim. Acta* **2003**, *352*, 121–128.

[37] R. Kitaura, Y. Miyaki, T. Onishi, H. Kurosawa, *Inorg. Chim. Acta* **2002**, *334*, 142–148.

[38] J. Čubrilo, I. Hartenbach, T. Schleid, R.F. Winter, *Z. Anorg. Allg. Chem.* **2006**, *632*, 400–408.

[39] B. Therrien, T.R. Ward, *Angew. Chem. Int. Ed.* **1999**, *38*, 405–408.

[40] B. Therrien, A. König, T.R. Ward, *Organometallics* **1999**, *18*, 1565–1568.

[41] C.M. Hartshorn, P.J. Steel, *Aust. J. Chem.* **1995**, *48*, 1587–1599.

[42] C.M. Hartshorn, P.J. Steel, *Angew. Chem. Int. Ed. Engl.* **1996**, *35*, 2655–2657.

[43] W.Y. Sun, J. Xie, T. Okamura, C.K. Huang, N. Ueyama, *Chem. Commun.* **2000**, 1429–1430.

[44] C. Scolaro, T.J. Geldbach, S. Rochat, A. Dorcier, C. Gossens, A. Bergamo, M. Cocchietto, I. Tavernelli, G. Sava, U. Rothlisberger, P.J. Dyson, *Organometallics* **2006**, *25*, 756–765.

[45] F.K. Cheung, A.M. Hayes, J. Hannedouche, A.S.Y. Yim, M. Wills, *J. Org. Chem.* **2005**, *70*, 3188–3197.

[46] A.M. Hayes, D.J. Morris, G.J. Clarkson, M. Wills, *J. Am. Chem. Soc.* **2005**, *127*, 7318–7319.

[47] P.W. Rabideau, D.L. Huser, S.J. Nyikos, *Tetrahedron Lett.* **1980**, *21*, 1401–1404.

[48] A. Abele, R. Wursche, M. Klinga, B. Rieger, *J. Mol. Cat. A: Chemical* **2000**, *160*, 23–33.

[49] K.Y. Ghebreyessus, J.H. Nelson, *Organometallics* **2000**, *19*, 3387–3392.

[50] J.W. Faller, D.G.D'Alliessi, *Organometallics* **2003**, *22*, 2749–2757.

[51] P. Pinto, G. Marconi, F.W. Heinemann, U. Zenneck, *Organometallics* **2004**, *23*, 374–380.

[52] A.C.G. Hotze, A.H. Velders, F. Ugozzoli, M. Biagini-Cingi, A.M. Manotti-Lanfredi, J.G. Haasnoot, J. Reedijk, *Inorg. Chem.* **2000**, *39*, 3838–3844.

[53] B.J. Coe, C.I. McDonald, R.L. Beddoes, *Polyhedron* **1998**, *17*, 1997–2007.

[54] M. Cao, L.V. Do, N.W. Hoffman, M.L. Kwan, J.K. Little, J.M. McGilvray, C.B. Morris, B.C. Söderberg, A. Wierzbicki, T.R. Cundari, C.H. Lake, E.J. Valente, *Organometallics* **2001**, *20*, 2270–2279.

[55] V.J. Catalano, T.J. Craig, *Polyhedron* **2000**, *19*, 475–485.

[56] J.A.S. Howell, N.F. Ashford, D.T. Dixon, J.C. Kola, *Organometallics* **1991**, *10*, 1852–1864.

[57] P.D. Smith, T. Gelbrich, M.B. Hursthouse, *J. Organomet. Chem.* **2002**, *659*, 1–9.

[58] J.W. Reishus, D.S. Martin, *J. Am. Chem. Soc.* **1961**, *83*, 2457–2462.

[59] K. Hindmarsh, D.A. House, M.M. Turnbull, *Inorg. Chim. Acta* **1997**, *257*, 11–18.

[60] B. Kankia, T. Funck, L.A. Marky, *J. Solution Chem.* **1999**, *28*, 1249–1261.

[61] F. Wang, H. Chen, S. Parsons, I.D.H. Oswald, J.E. Davidson, P.J. Sadler, *Chem. Eur. J.* **2003**, *9*, 5810–5820.

[62] R.O. Gould, C.L. Jones, D.R. Robertson, T.A. Stephenson, *J.C.S. Chem. Comm.* **1977**, 222–223.

[63] T. Arthur, D.R. Robertson, D.A. Tocher, T.A. Stephenson, *J. Organomet. Chem.* **1981**, *208*, 389–400.

[64] C. Balzarek, T.J.R. Weakley, L.Y. Kuo, D.R. Tyler, *Organometallics* **2000**, *19*, 2927–2931.

[65] J.H. Toney, T.J. Marks, *J. Am. Chem. Soc.* **1985**, *107*, 947–953.

[66] M. Bouma, B. Nuijen, M.T. Jansen, G. Sava, A. Flaibani, A. Bult, J.H. Beijnen, *Int. J. Pharm.* **2000**, *248*, 239–246.

[67] P. Valerga, M.C. Puerta, D.S. Pandey, *J. Organomet. Chem.* **2002**, *648*, 27–32.

[68] M. Jennerwein, P.A. Andrews, *Drug Metab. Dispos.* **1995**, *23*, 178–184.

[69] S. Korn, W.S. Sheldrick, *Inorg. Chim. Acta* **1997**, *254*, 85–91.

[70] C.A. Crawford, E.F. Day, V.P. Saharan, K. Folting, J.C. Huffman, K.R. Dunbar, G. Christou, *Chem. Commun.* **1996**, 1113–1114.

[71] F. Zobi, M. Hohl, I. Zimmermann, R. Alberto, *Inorg. Chem.* **2004**, *43*, 2771–2772.

[72] S.O. Ano, Z. Kuklenyik, L.G. Marzilli in *Cisplatin* (Ed.: B. Lippert), Verlag Helvetica Chimica Acta, Zürich, **1999**; pp. 247–291.

[73] R.E. Cramer, P.L. Dahlstrom, *J. Am. Chem. Soc.* **1979**, *101*, 3679–3681.

[74] R. Cramer, P. Dahlstrom, *Inorg. Chem.* **1985**, *24*, 3420–3424.

[75] K.R. Harrap, *Cancer Res.* **1995**, *55*, 2761–2768.

[76] S.G. Chaney, *Int. J. Oncol.* **1995**, *6*, 1291–1305.

[77] J.W. Corcoran, F.E. Hahn (Eds.), *Mechanism of Action of Antimicrobial and Antitumor Agents*, Vol. III, Springer-Verlag, New York, **1975**.

[78] S. Neidle, M.J. Waring (Eds.), *Molecular Aspects of Anti-Cancer Drug Action*, MacMillan, London, **1983**.

[79] A. Frodl, D. Herebian, W.S. Sheldrick, *J. Chem. Soc., Dalton Trans.* **2002**, 3664–3673.

[80] D. Carmona, C. Vega, F.J. Lahoz, R. Atencio, L.A. Oro, M.P. Lamata, F. Viguri, E.S. José, *Organometallics* **2000**, *19*, 2273–2280.

[81] R.G. Andrew, R.A. Raphael, *Tetrahedron* **1987**, *43*, 4803–4816.

[82] W.E. Parham, F.L. Ramp, *J. Am. Chem. Soc.* **1951**, *73*, 1293–1295.

[83] F. Benington, R.D. Morin, L.C. Clark, R.P. Fox, *J. Org. Chem.* **1958**, *23*, 1979–1984.

[84] E.Z. Khafagy, J.P. Lambooy, *J. Med. Chem.* **1966**, *9*, 936–940.

[85] C. Djerassi, C.R. Scholz, *J. Am. Chem. Soc.* **1947**, *69*, 1688–1692.

[86] V. Derdau, V. Snieckus, *J. Org. Chem.* **2001**, *66*, 1992–1998.

[87] M.R.H. Brown, M. Melchart, A. Habtemariam, P.J. Sadler, unpublished results.

[88] M. Calligaris, O. Carugo, *Coord. Chem. Rev.* **1996**, *153*, 83–154.

[89] P. Müller, B. Schröder. J.A. Parkinson, N.A. Kratochwil, R.A. Coxall, A. Parkin, S. Parsons, P.J. Sadler, *Angew. Chem. Int. Ed.* **2003**, *42*, 335–339.

[90] F.S. Mackay, J.A. Woods, H. Moseley, J. Ferguson, A. Dawson, S. Parsons, P.J. Sadler, *Chem. Eur. J.* **2006**, *12*, 3155–3161.

[91] D.S. Pandey, A.N Sahay, O.S. Sisodia, N.K. Jha, P. Sharma, H.E. Klaus, A. Cabrera, *J. Organomet. Chem.* **1999**, *592*, 278–282.

[92] A.C. da Silva, H. Piotrowski, P. Mayer, K. Polborn, K. Severin, *Eur. J. Inorg. Chem.* **2001**, 685–691.

[93] R. Baldwin, M.A. Bennett, D.C.R. Hockless, P. Pertici, A. Verrazzani, G. Uccello Barretta, F. Marchetti, P. Salvadori, *J. Chem. Soc., Dalton Trans.* **2002**, *23*, 4488–4496.

[94] S. Gauthier, L. Quebatte, R. Scopelliti, K. Severin, *Chem. Eur. J.* **2004**, *10*, 2811–2821.

[95] J.A. Cabeza, I. da Silva, I. del Rio, S. Garcia-Granda, *Appl. Organomet. Chem.* **2005**, *19*, 209–210.

Chapter 5
Hydride-transfer Catalysed by Cytotoxic Ruthenium(II) Arene Complexes

5.1 Introduction

Interest in the catalytic properties of Ru^{II} mono-arene complexes ranges from alkene- and aromatic-hydrogenation, to Diels-Alder reactions, alkene metathesis, and asymmetric hydrogen transfer reductions of ketones and imines [1]. Catalytic activity usually requires the presence of a labile coordination site on Ru^{II} and/or arene displacement [2, 3]. The nature of the coordinated ligands can have a pronounced effect on the catalytic properties of Ru^{II} arene complexes and interest in their design as catalyst precursors has led to the exploration of a wide range of synthetic routes to complexes containing various substituted arenas, together with other ligands such as hydride, phosphines, alkyl and aryl groups [4].

Such catalysts are likely to be easily poisoned in biological media by the strongly coordinating ligands available, but it is intriguing to speculate that catalytic activity could exist in certain biological compartments to which access of deactivating molecules might be restricted, *e.g.* membranes [5].

With this in mind, a recent report by Ogo *et al.* was of particular interest [6]. The ability of Ru^{II} arene complexes to form stable hydride adducts in aqueous solution with formate as the hydride donor was demonstrated. Furthermore, the system $\{(\eta^6\text{-}C_6Me_6)Ru(bpy)\}^{2+}$, where bpy = 2,2'-bipyridine, was shown to catalyse the transfer hydrogenation of some ketones in water (Scheme 5.1). The studies revealed a marked dependence of the catalytic activity on pH and temperature. Overall, the conditions for optimum turnover were found to be at pH 4 and 343 K, which is not biologically compatible. In addition, the studies were conducted in the presence of *ca.* 6000 mol equivalents of formate with respect to ruthenium.

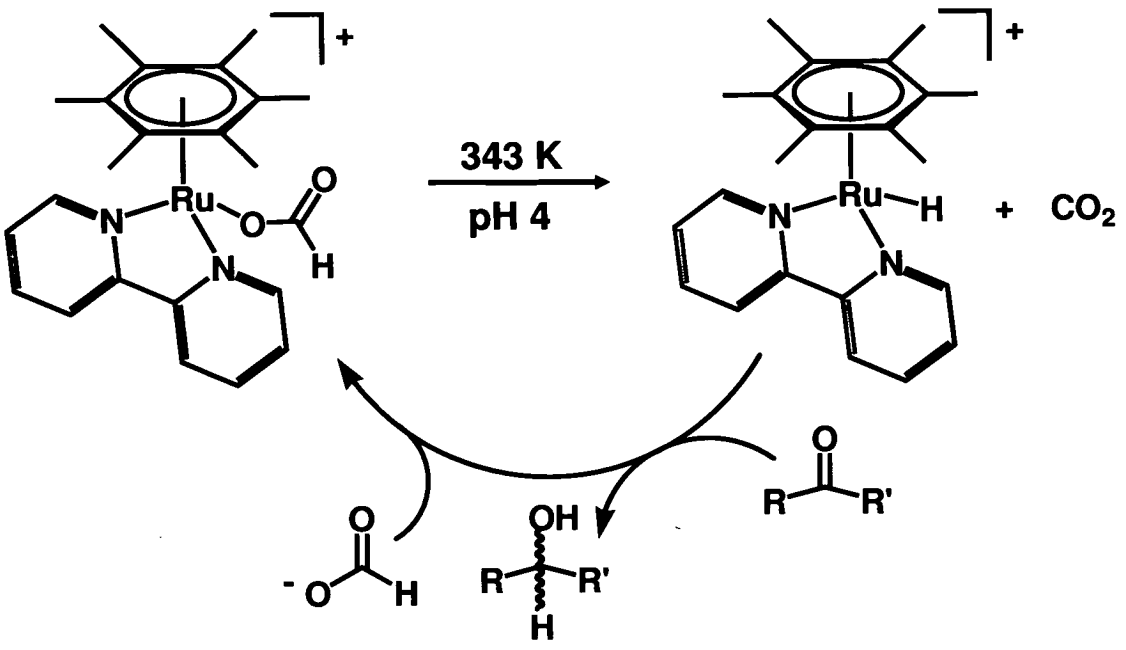

Scheme 5.1: Catalytic cycle for the transfer hydrogenation of ketones with formate by $\{(\eta^6\text{-}C_6Me_6)Ru(bpy)\}^{2+}$ in water. Optimum turnover conditions are 343 K and pH 4.0 [6].

It was thus of interest to explore the potential of Ru^{II} arene complexes from the following view points.

- Some complexes of the type $[(\eta^6\text{-arene})Ru(bpy)Cl]^+$ are non-cytotoxic towards the A2780 human ovarian cancer cell line [7]. Therefore, could transfer hydrogenation also be demonstrated for cytotoxic complexes of the type $[(\eta^6\text{-arene})Ru(en)Cl]^+$, where en = ethylenediamine?
- Would these complexes catalyse the transfer hydrogenation of ketones with biologically-tolerable formate concentrations, *i.e.* significantly less than 6000 mol equivalents of formate?
- Could catalysis be achieved at biologically compatible reaction conditions, *i.e.* pH 7.4 and 310 K?

These questions will be addressed in this Chapter. Furthermore, studies of the regioselective reduction of NAD^+ by ruthenium(II) arene complexes under biologically relevant conditions will be presented.

In the field of biocatalysis, the coenzyme 1,4-NADH is required for many enzymatic reduction reactions which are useful for the stereoselective synthesis of organic compounds [8, 9]. The coenzyme is too expensive to be used in stoichiometric amounts and hence there has been continued interest in finding efficient ways for the *in situ* regeneration of NADH under biologically-compatible conditions [10, 11]. In recent years, significant attention has been focused on transition metal complexes as catalysts for the regioselective reduction of NAD^+ and models for NAD^+ to their corresponding 1,4-NADH derivatives [11, 12].

Steckhan *et al.* [13] and Fish *et al.* [14] have shown that Rh^{III} pentamethylcyclopentadienyl (Cp*) complexes can catalyse the reduction of NAD^+ in the presence of formate (Scheme 5.2). This reduction is regioselective, giving the

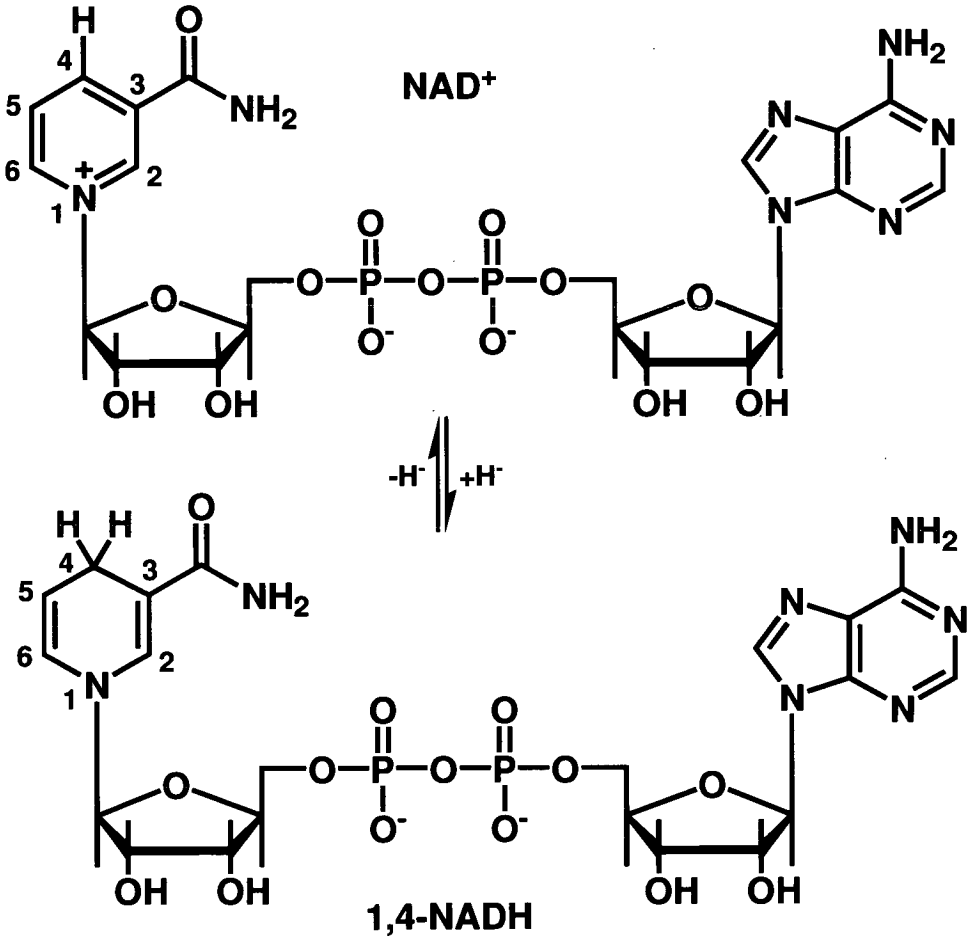

Scheme 5.2: The conversion of NAD^+ into 1,4-NADH *via* hydride transfer.

biologically relevant 1,4-NADH isomer, and can drive enzymatic reactions relying on NADH as cofactor (*e.g.* stereoselective reduction of $PhCH_2CH_2COMe$ catalyzed by alcohol dehydrogenase [15]). Further interest in these studies is generated by the observation by Torabi *et al.* that in cancer cells the NAD^+ content is equal or higher than in normal cells [16]. An interference with this distribution could lead to cell death or also undesirable, stimulated cell growth.

5.2 Experimental Section

5.2.1 Materials

Figure 5.1 shows the molecules studied in this Chapter. The complexes [(η^6-ind)Ru(en)Cl]PF_6 (**5.1**) and [(η^6-hmb)Ru(en)Cl]PF_6 (**5.2**), where ind = indan, hmb = hexamethylbenzene, en = ethylenediamine, were kindly made available by Dr. Abraha Habtemariam, University of Edinburgh. Their syntheses were based on literature methods [17]. The bifunctional complex [(η^6:η^1-$C_6H_5(CH_2)_3NH_2$)Ru(NO_3)$_2$] (**5.3**) was synthesised as outlined in Chapter 4.

All reactions were performed in air and under ambient temperatures, unless indicated otherwise.

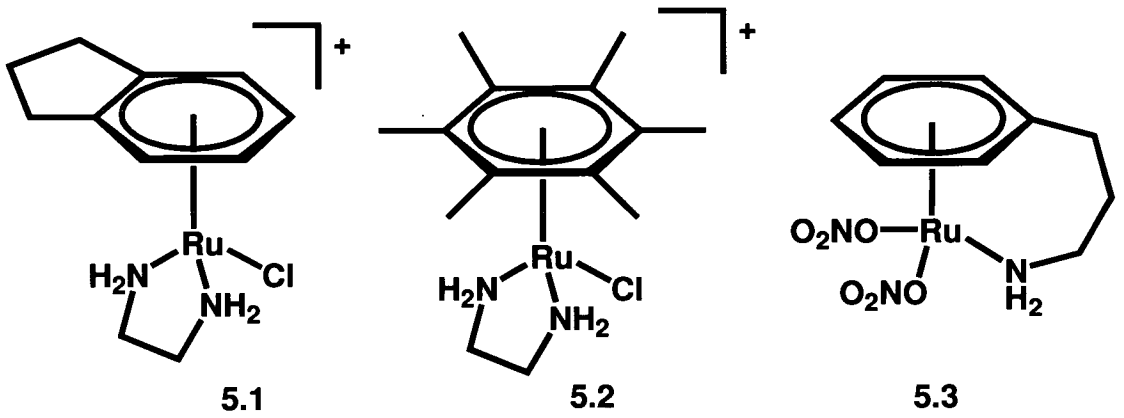

5.1 **5.2** **5.3**

Figure 5.1: Structures of [(η^6-ind)Ru(en)Cl]$^+$ (**5.1**), [(η^6-hmb)Ru(en)Cl]$^+$ (**5.2**) and [(η^6:η^1-$C_6H_5(CH_2)_3NH_2$)Ru(NO_3)$_2$] (**5.3**). Complexes **5.1** and **5.2** were prepared as their hexafluorophosphate salts.

5.2.2. Methods

The chemical shifts of the signals in the ^{1}H NMR spectra recorded in D_2O are quoted in ppm downfield of the methyl signal of sodium 3-(trimethylsilyl)propanesulfonate (TMP); using the residual HDO peak as a secondary internal reference, (δ 4.64 ppm) at 310 K [18]. The pD values were obtained using the relationship pD = 0.4 + (pH meter reading) [19].

5.3 Transfer Hydrogenation of Ketones by Cytotoxic Ru^{II} Arene Complexes

5.3.1 Results

5.3.1.1 Mono-functional complexes

The ^{1}H NMR spectrum of [(η^6-ind)Ru(en)Cl]PF_6 (**5.1**) in the presence of sodium formate (*ca.* 20 mol equiv) in 90% H_2O/ 10% D_2O was recorded 1 h after mixing at pH = 9.61 (Figure A.5.1) and then after incubation (18 h at 338 K) at 298 K. The spectrum showed some alterations in the splitting patterns of the main peaks plus some shifts, but most significantly a new singlet at -6.92 ppm appeared (Figure 5.2).

The ^{1}H NMR spectrum of [(η^6-hmb)Ru(en)Cl]PF_6 (**5.2**) (3.5 mM Ru), acetone (*ca.* 200 mol equiv) and sodium formate (*ca.* 3000 mol equiv) in 90% H_2O/ 10% D_2O was recorded within ten min of mixing and then after incubation (4 h at 343 K) at 298 K. The spectrum showed the presence of acetone (δ 2.36 ppm) as well as two new peaks at 4.12 ppm (multiplet) and 1.29 ppm (doublet) corresponding to 2-propanol (Figure 5.3). Integration of the peak at 1.29 ppm and that for free acetone indicated a ratio of 1 : 1.25.

The ^{1}H NMR spectrum of **5.2** (2.8 mM Ru), pyruvic acid (*ca.* 200 mol equiv) and sodium formate (*ca.* 3500 mol equiv) in 90% H_2O/ 10% D_2O was recorded within ten min of mixing and then after incubation (4 h at 343 K) at 298 K. The peak

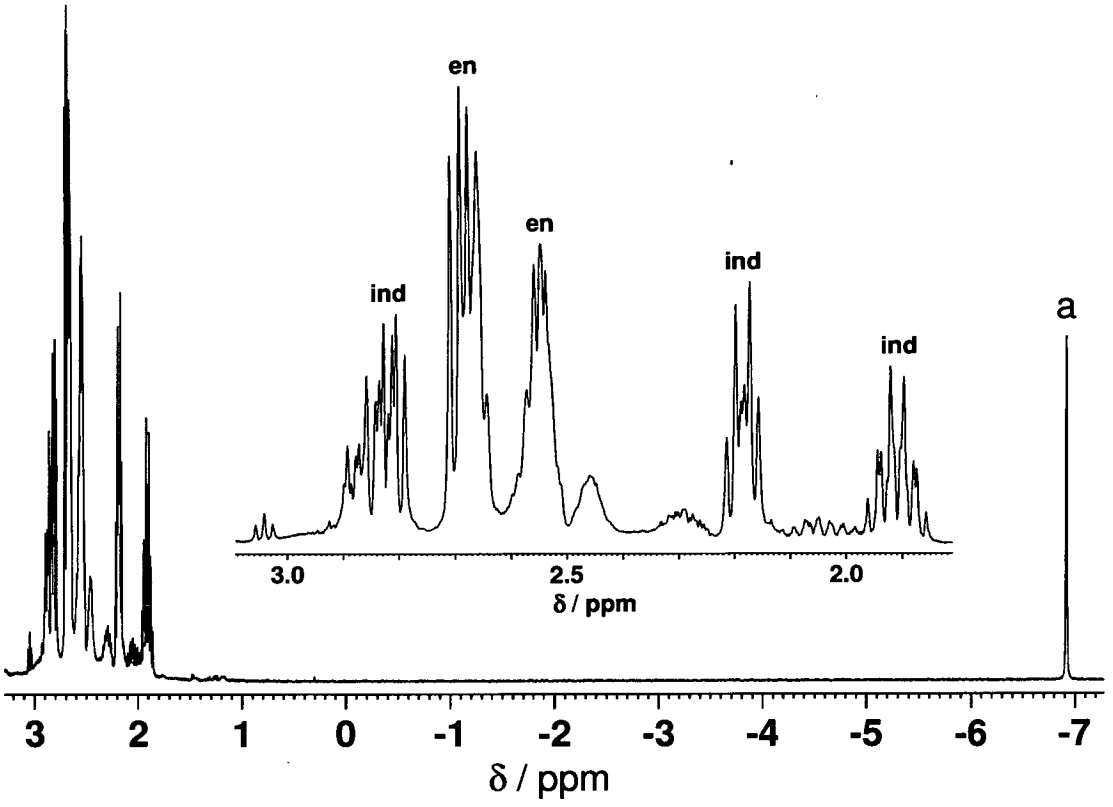

Figure 5.2: The high-field region of the ^{1}H NMR spectrum of [(η^6-ind)Ru(en)Cl]PF_6 (**5.1**) in the presence of sodium formate (*ca.* 20 mol equiv) in 90% H_2O/ 10% D_2O at 298 K. The solution had an initial pH of 9.61 and was incubated for 18 h at 338 K. The major product is [(η^6-ind)Ru(en)H]$^+$. Assignments: ind = CH_2 groups (ind); en = CH_2 groups (en); a = Ru-H.

for free pyruvate (pK_a *ca.* 2.65) at 2.41 ppm had disappeared and two new peaks at 4.27 ppm (multiplet) and 1.47 ppm (doublet) corresponding to 2-hydroxypropanoate (pK_a *ca.* 3.90) appeared.

5.3.1.2 Bifunctional complexes

Addition of $NaBH_4$ (*ca.* 2.5 mol equiv) to a solution of [(η^6:η^1-$C_6H_5(CH_2)_3NH_2$)$Ru(NO_3)_2$] (**5.3**) in 90% H_2O/ 10% D_2O caused a colour change from orange to reddish-brown. The ^{1}H NMR spectrum recorded after 20 min at 298 K indicated two products, giving rise to two singlets in the high-field region at -9.04

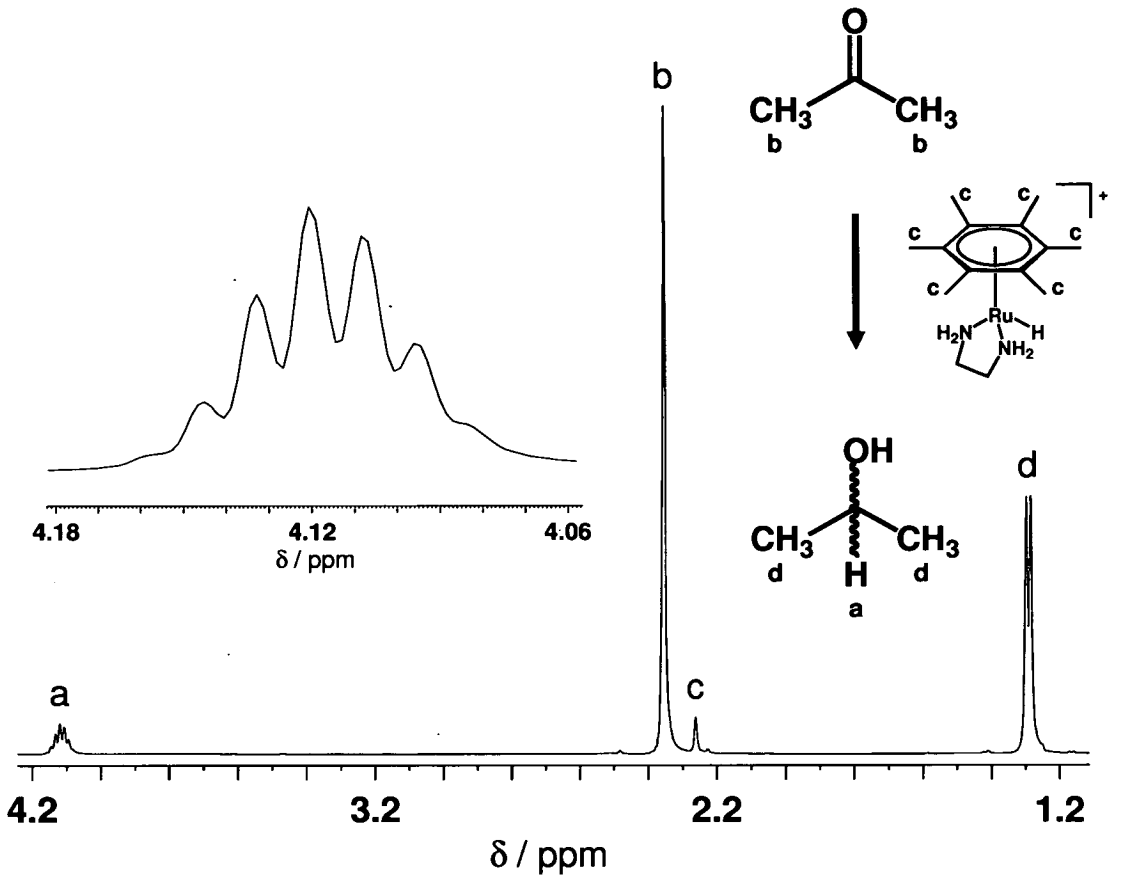

Figure 5.3: The 2-propanol region of the ^{1}H NMR spectrum of a solution containing [(η^6-hmb)Ru(en)Cl]PF_6 (**5.2**) (3.5 mM Ru), acetone (*ca.* 200 mol equiv) and sodium formate (*ca.* 3000 mol equiv) in 90% H_2O/ 10% D_2O at 298 K, including the peak assignments. The solution had been incubated for 4 h at 343 K.

ppm and -15.34 ppm, respectively. The spectrum recorded after 1 h suggested the presence of a number of species as indicated by more than ten peaks in the high-field region of the spectrum (Figure 5.4). In addition, signals with similar shifts to those for free 3-phenyl-1-propylamine were detected in the arene proton region.

A solution of **5.3** (7.1 mM Ru) and sodium formate (100 mol equiv) in 90% H_2O/ 10% D_2O was incubated for 150 min at 310 K and the ^{1}H NMR spectrum recorded at 310 K. The spectrum showed several new singlets in the high-field region (Figure A.5.2). In addition, signals with similar shifts to those for free 3-phenyl-1-propylamine were detected in the arene proton region.

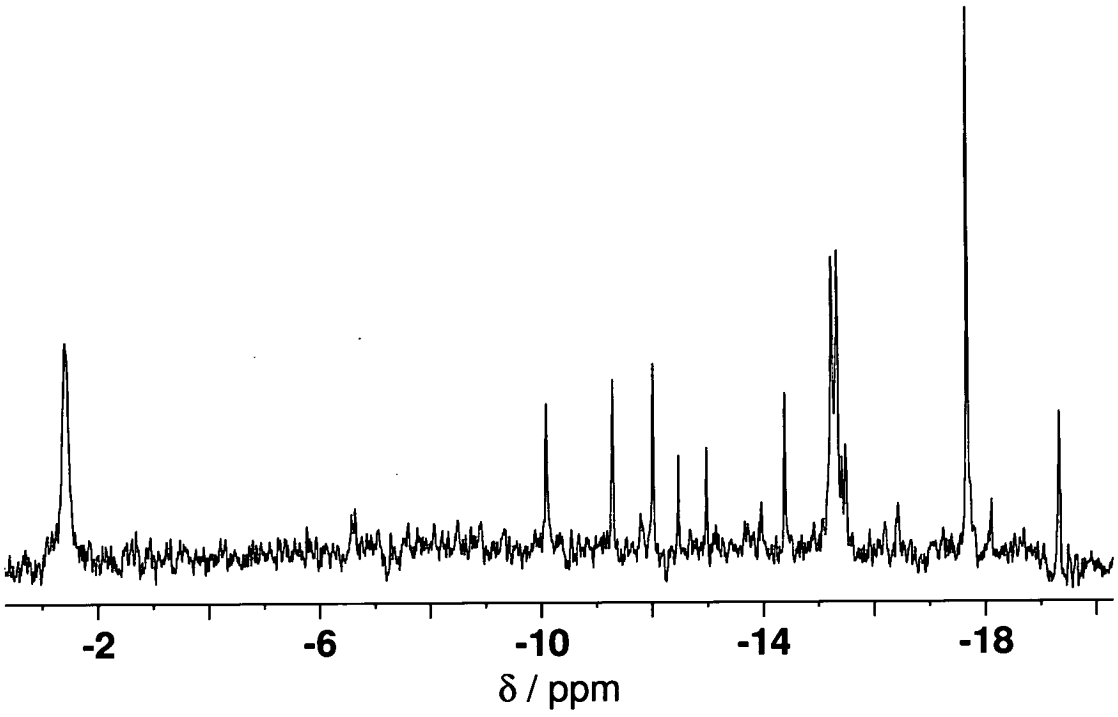

Figure 5.4: The high-field region of the ^{1}H NMR spectrum of a solution containing $NaBH_4$ (*ca.* 2.5 mol equiv) and $[(\eta^6{:}\eta^1\text{-}C_6H_5(CH_2)_3NH_2)Ru(NO_3)_2]$ (**5.3**) in 90% H_2O/ 10% D_2O at 298 K after 1 h, suggesting the presence of a number of hydride-containing species in solution.

A solution of **5.3** (9.3 mM Ru), acetone (*ca.* 100 mol equiv) and sodium formate (*ca.* 100 mol equiv) in 90% H_2O/ 10% D_2O was incubated for 23 h at 310 K and the ^{1}H NMR spectrum recorded 310 K. The spectrum showed two new peaks at 4.14 ppm (multiplet) and 1.31 ppm (doublet) corresponding to 2-propanol. Integration of the peak at 1.31 ppm and that for free acetone indicated a ratio of 1 : 21. In addition, signals with similar shifts to those for free 3-phenyl-1-propylamine were detected in the arene proton region.

5.3.2 Discussion

5.3.2.1 Mono-functional complexes

In the catalytic reactions of the Ru^{II} arene complex $[(\eta^6\text{-hmb})Ru(bpy)H_2O]^{2+}$, where hmb = hexamethylbenzene, bpy = 2,2'-bipyridine, studied by Ogo *et al.* [6], as

well as reactions of the Rh^{III} complex $[(\eta^5\text{-}Cp^*)Rh(bpy)H_2O]^{2+}$, where Cp* = pentamethylcyclopentadienyl, studied by Steckhan *et al.* [13] and Fish *et al.* [14], the metal compounds contained the ligand 2,2'-bipyridine. Systems of the type $[(\eta^5\text{-}Cp^*)M(bpy)H_2O]^{2+}$ (M = Rh, Ir) have been studied electrochemically and spectroscopically and resonance hybrids for coordinatively unsaturated $[(\eta^5\text{-}Cp^*)M(bpy)]$ with a formally oxidation state +I metal centre were proposed (Scheme 5.3) [20].

$$(\eta^5\text{-}Cp^*)M^n(bpy) \longleftrightarrow (\eta^5\text{-}Cp^*)M^{n+1}(bpy^{-1})$$

A **B**

Scheme 5.3: Resonance hybrids for coordinatively unsaturated $[(\eta^5\text{-}Cp^*)M(bpy)]$ with a formally oxidation state +I metal centre [20].

Subsequently it was proposed that these resonance structures are also found for ruthenium arene complexes [20]. While all available data point to a sizeable contribution from resonance structure **B** [20], its role in hydride transfer reactions does not appear to be firmly established.

Despite a likely less favourable electron transfer mechanism between en and Ru^{II}, the spectrum in Figure 5.2 shows that a mixture of $[(\eta^6\text{-ind})Ru(en)Cl]PF_6$ (**5.1**) and formate in water, incubated at 338 K for 18 h, can be converted, to a large extent and cleanly, into the hydrido complex $[(\eta^6\text{-ind})Ru(en)H]^+$. The hydride signal at -6.92 ppm has a comparable chemical shift to that of $[(\eta^6\text{-hmb})Ru(bpy)H]^+$ at -7.45 ppm [6]. This shows that Ru^{II} arene complexes containing an ethylenediamine chelating ligand can form hydrido adducts *via* β-hydrogen elimination reactions with formate.

Transfer hydrogenation of the ketones acetone and pyruvic acid (pyruvate in solution) by $[(\eta^6\text{-hmb})Ru(en)Cl]PF_6$ (**5.2**) converted the substrates into 2-propanol and 2-hydroxypropanoate, respectively. After incubation for 4 h at 343 K *ca.* 44 % of acetone, *i.e. ca.* 90 mol equiv with respect to Ru, had been converted into 2-

propanol, thus indicating a catalytic process. In the case of pyruvate, all of the substrate had been converted into 2-hydroxypropanoic acid during the 4 h incubation period. A scheme for hydride transfer by $\{(\eta^6\text{-arene})Ru(en)\}^{2+}$ complexes is shown in Section 5.4.2 in the context of the reduction of NAD^+ (*vide infra*).

5.3.2.2 Bifunctional complexes

The ^1H NMR signals of the arene protons as well as those of the tether backbone (Figure 5.5) show that two species, one with a non-chiral- (three arene proton plus three tether backbone proton signals) and one with a chiral- (five arene proton plus six tether backbone proton signals) ruthenium centre, formed in the reaction between $NaBH_4$ and the tethered complex $[(\eta^6:\eta^1\text{-}C_6H_5(CH_2)_3NH_2)Ru(NO_3)_2]$ (**5.3**) in water. The chiral species could be $[(\eta^6:\eta^1\text{-}C_6H_5(CH_2)_3NH_2)Ru(OH)H]$ and the other $[((\eta^6:\eta^1\text{-}C_6H_5(CH_2)_3NH_2)Ru)_2(\mu\text{-}H)_2]^{2+}$, since hydride ligands in ruthenium(II) arene complexes are known to be able to act as bridging ligands [21, 22]. However, these species are not very stable and decay to give a number of new hydride-containing species (see Figure 5.4), which could include ruthenium clusters [23, 24, 25]. Similarly, in reactions with formate, the complexes tended to decompose and new hydride signals were noted in the ^1H NMR spectrum, possibly also indicating the formation of clusters.

Due to the multiple decomposition pathways of **5.3**, which also include loss of arene coordination, in the presence of formate, it is not clear which species is responsible for the conversion of acetone into 2-propanol. If it involves the $\{(\eta^6:\eta^1\text{-}C_6H_5(CH_2)_3NH_2)Ru\}^{2+}$ fragment, then with only *ca.* 5% conversion of acetone this system does not posses significant catalytic activity. In contrast, catalytic activity has recently been demonstrated for some amine-tethered complexes, which contain a chelate ring thus resulting in mono-functional compounds (*e.g.* $[(\eta^6\text{-}C_6H_5(CH_2)_3NH(1S,2S\text{-}CHC_6H_5)_2NSO_2C_6H_4CH_3 - N,N)RuCl]$) [26, 27].

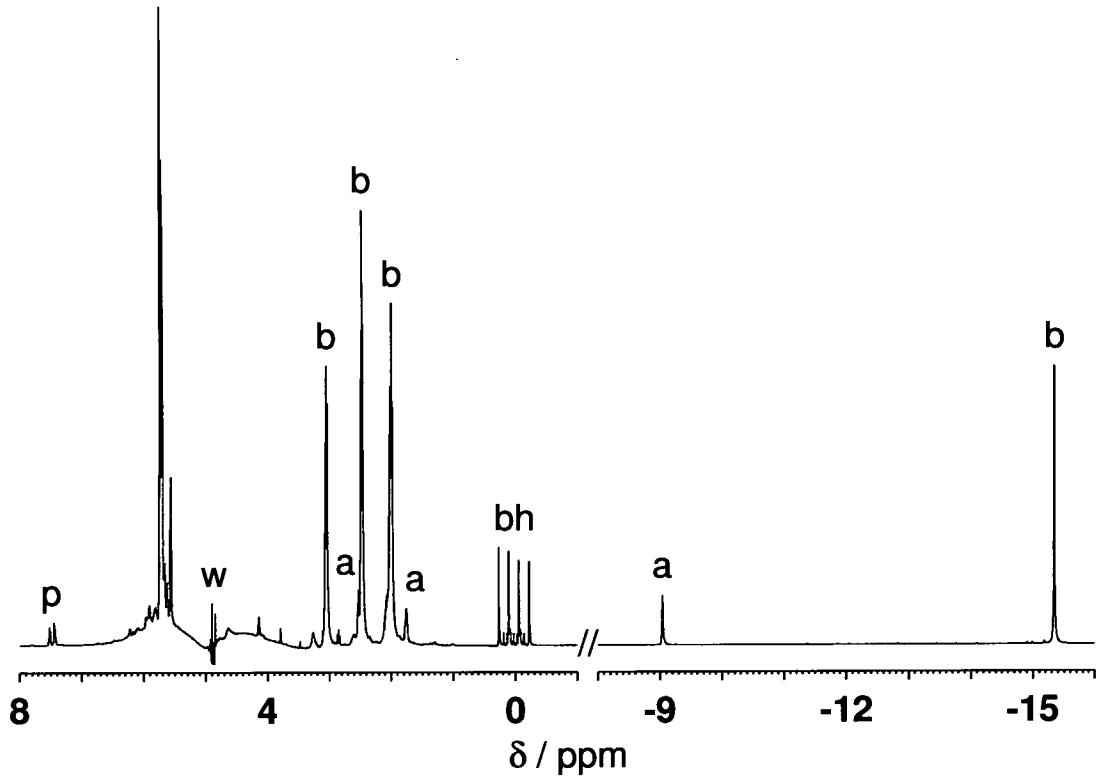

Figure 5.5: The ^{1}H NMR spectrum of a solution containing $NaBH_4$ (*ca.* 2.5 mol equiv) and $[(\eta^6{:}\eta^1\text{-}C_6H_5(CH_2)_3NH_2)Ru(NO_3)_2]$ (**5.3**) in 90% H_2O/ 10% D_2O at 298 K after 20 min. Peaks of species (a) and (b) are only partially labeled. Assignments: p = unbound arene of 3-phenyl-1-propylamine; w = suppressed water; bh = BH_4^-; a = chiral species containing the $\{(\eta^6{:}\eta^1\text{-}C_6H_5(CH_2)_3NH_2)RuH\}^+$ moiety producing five arene proton and six tether backbone proton signals; b = species containing $\{(\eta^6{:}\eta^1\text{-}C_6H_5(CH_2)_3NH_2)RuH_2\}^+$ producing three arene proton and three tether backbone proton signals.

5.4 Catalysis of Regioselective Reduction of NAD^+ by Ru^{II} Arene Complexes

5.4.1 Results

Figure 5.6 shows the ^{1}H NMR spectra of the NAD^+ and 1,4-NADH in D_2O at 310 K and pD 7.0 together with a partial assignment, based on a report by Sarma *et al.* [28].

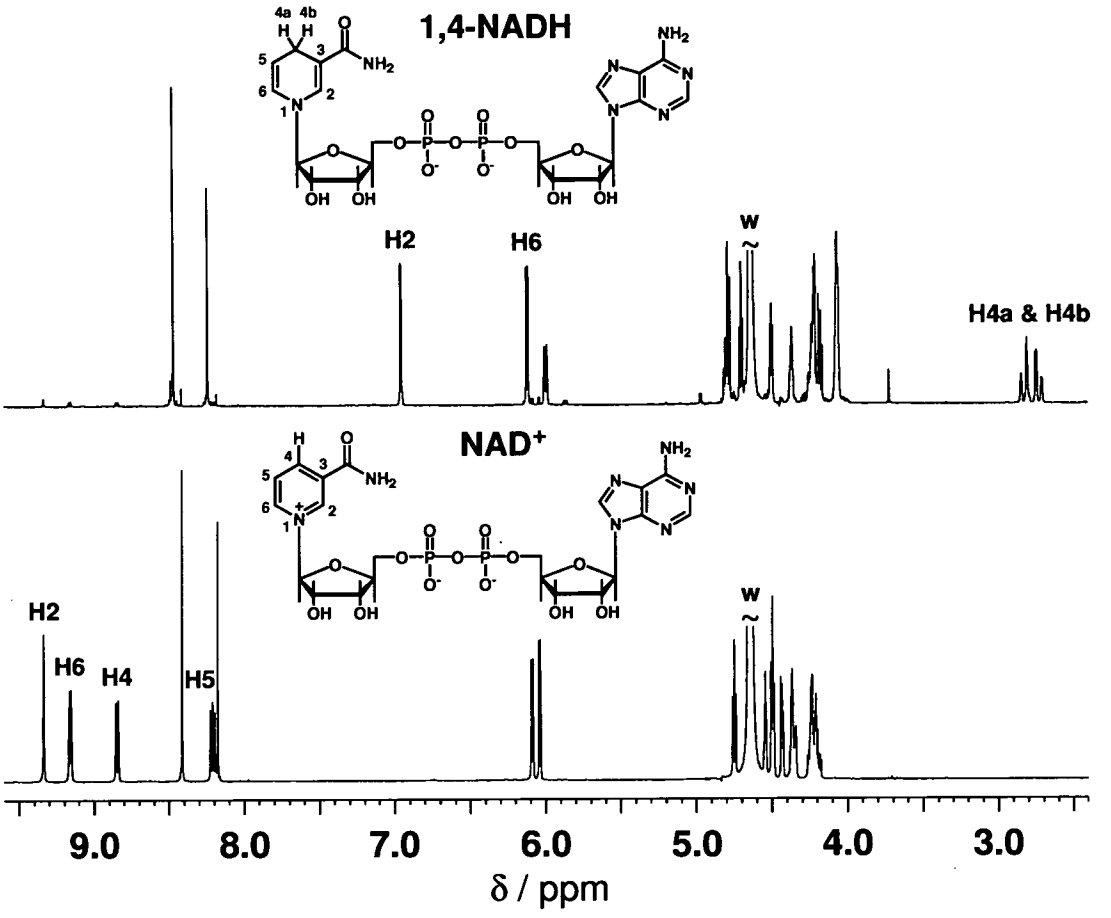

Figure 5.6: The ^{1}H NMR spectra of NAD^+ and 1,4-NADH in D_2O at pD 7.0 and 310 K. Assignment: w = residual water.

A reaction of $[(\eta^6\text{-hmb})Ru(en)Cl]PF_6$ (**5.2**) (1.7 mM Ru) with NAD^+ (2 mol equiv) in the presence of sodium formate (25 mol equiv) was monitored by ^{1}H NMR in D_2O at 310 K and pD 7.2. Over a period of about 3 h the peaks for free NAD^+ disappeared and new peaks assignable to NADH appeared (Figure 5.7).

5.4.2 Discussion

The observed conversion of NAD^+ into 1,4-NADH shows that hydride transfer reactions can be catalysed by cytotoxic Ru^{II} arene complexes under biologically relevant conditions (310 K and pD 7.2). A scheme for the hydride transfer is shown in Scheme 5.4. Hydrolysis of the chloride ligand is followed by

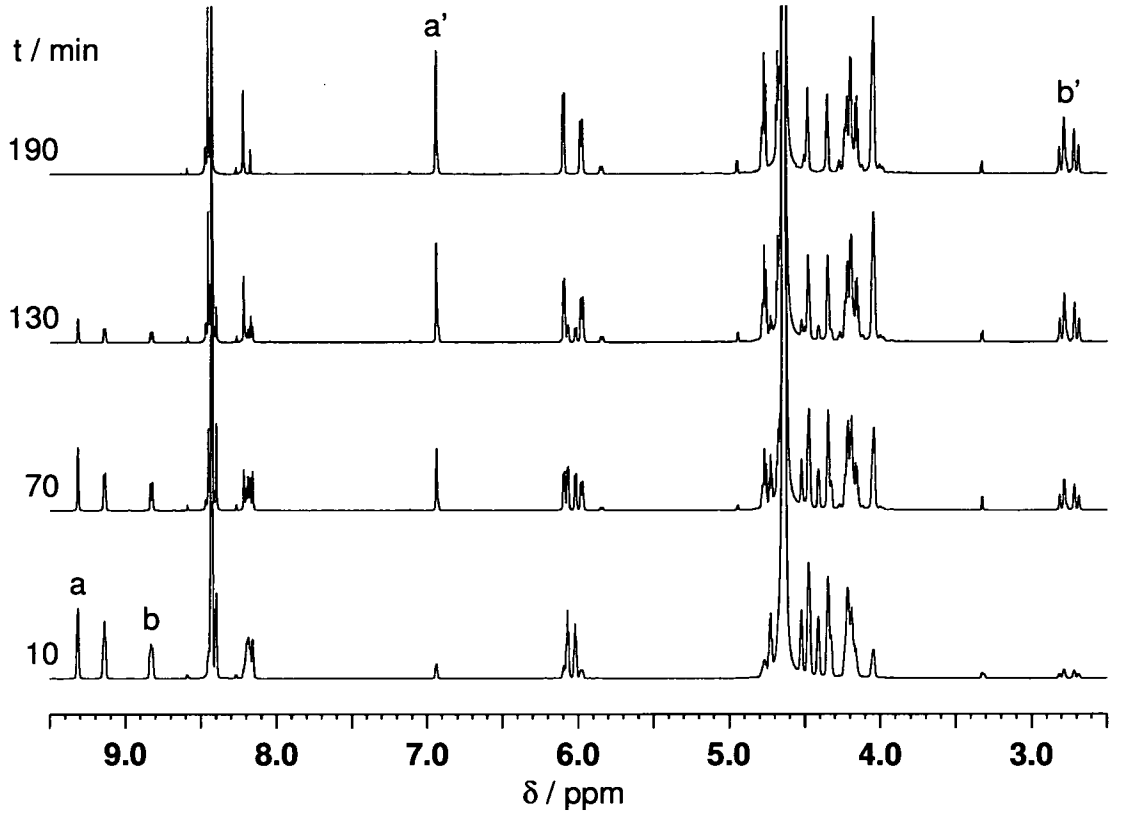

Figure 5.7: The NAD^+/NADH region of the ^1H NMR spectrum for a reaction of $[(\eta^6\text{-hmb})Ru(en)Cl]PF_6$ (**5.2**), NAD^+ and HCO_2^- in mol ratios 1 : 2 : 25, respectively, in D_2O at 37C° after 10, 70, 130 and 190 min. Assignments: a = H2 (NAD^+); a' = H2 (1,4-NADH); b = H4 (NAD^+); b' = H4 (1,4-NADH). A minor product is also evident at long reaction times giving peaks at e.g. 4.95, 5.84 and 8.17 ppm. This may arise from 1,6-NADH, but was not seen at higher equivalents of formate (e.g. 1000) [29].

binding of formate. The next step is *β*-hydrogen elimination, which is thought to proceed *via* ring slippage of the arene, *i.e.* a change of η^6- to η^4-coordination (Figure 5.8) [6]. Hydride transfer to NAD^+ presumably also proceeds *via* ring slippage [14].

These findings led to more detailed studies in collaboration with Dr. Yaw Kai Yan, Nanyang Technological University, regarding the mechanism and the kinetics of hydride transfer [29]. It was demonstrated that the reactions are zero-order with respect to NAD^+, paralleling the observations of Steckhan *et al.* [13] and Fish *et al.* [14] that the $[Cp^*Rh(bpy)H_2O]^{2+}$-catalysed reduction of NAD^+ by formate is zero-

$$[(\eta^6\text{-arene})Ru(en)Cl]^+ \xrightleftharpoons{H_2O} [(\eta^6\text{-arene})Ru(en)H_2O]^{2+} + Cl^- \xrightleftharpoons{+ HCO_2^-}$$

$$[(\eta^6\text{-arene})Ru(en)HCOO]^+ + H_2O \xrightleftharpoons{slow} [(\eta^6\text{-arene})Ru(en)H]^+ + CO_2 \xrightleftharpoons{+ NAD^+}$$

$$[(\eta^6\text{-arene})Ru(en)H_2O]^{2+} + NADH$$

Scheme 5.4: Scheme for hydride transfer between formate and NAD^+ catalysed by Ru^{II} arene complexes containing an ethylenediamine chelating ligand.

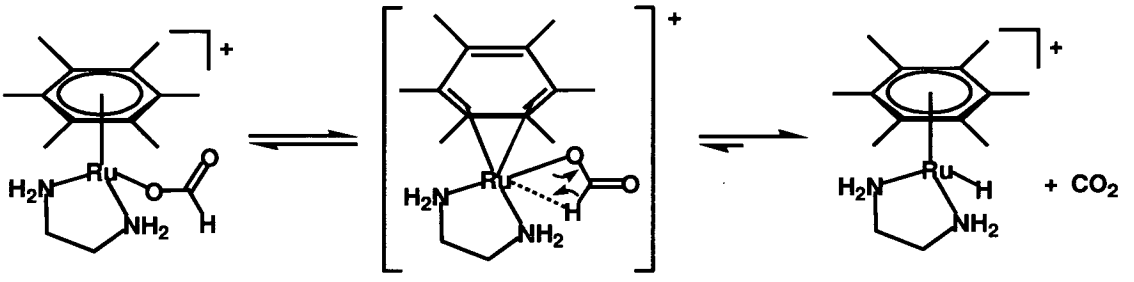

Figure 5.8: Possible ring slippage of the arene ring during the formation of $[(\eta^6\text{-hmb})Ru(en)H]^+$ *via* β-hydrogen elimination from $[(\eta^6\text{-hmb})Ru(en)HCO_2]^+$.

order with respect to NAD^+. Hydride transfer to NAD^+ was also ruled out as the rate-determining step in the reduction of NAD^+ by formate catalysed by complex **5.2**. When $NaHCO_2$ was replaced by $NaDCO_2$, a pronounced kinetic isotope effect was observed suggesting that hydride transfer from formate to Ru is the rate-determining step. The nature of the arene has been shown to influence the turnover frequency of $[(\eta^6\text{-arene})Ru(en)Cl]^+$ complexes, decreasing in the order hmb > indan, *p*-cymene. Removal of chloride resulted in a 20% increase in catalytic activity, suggesting that chloride does compete to a significant extent with formate for the catalytic binding site. A similar further increase in TOF was achieved by performing the reaction under argon, suggesting that one of the reaction intermediates (probably a ruthenium hydride complex) is somewhat oxygen-sensitive.

5.5 Conclusions

The formation of hydrido-complexes by cytotoxic Ru^{II} arene complexes *via* β-hydrogen elimination from the formate-adduct has been demonstrated. The $\{(\eta^6$-hmb)Ru(en)$\}^{2+}$ moiety has been shown to catalyse the transfer hydrogenation of the ketones acetone and pyruvic acid. This system can also catalyse the regioselective reduction of NAD^+ under biologically relevant conditions (pD 7.2, 37°C, in water and air). The bifunctional, tethered ruthenium arene complex $[(\eta^6{:}\eta^1$-$C_6H_5(CH_2)_3NH_2)Ru(NO_3)_2]$ (**5.3**) appeared to undergo initially clean formation of hydride species, but these transformed readily into a number of other hydride-containing species, possibly clusters, in solution.

Appendix A.5 contains Figures A.4.1 – 2.

5.6 References

[1] J. Soleimannejad, A. Sisson, C. White, *Inorg. Chim. Acta* **2003**, *352*, 121–128, and references therein.

[2] M. Bassetti, F. Centola, D. Sémeril, C. Bruneau, P.H. Dixneuf, *Organometallics* **2003**, *22*, 4459–4466.

[3] D. Jan, L. Delaude, F. Simal, A. Demonceau, A.F. Noels, *J. Organomet. Chem.* **2000**, *606*, 55–64.

[4] H. Le Bozec, D. Touchard, P.H. Dixneuf, *Adv. Organomet. Chem.* **1989**, *29*, 163–247.

[5] M. Melchart, P.J. Sadler in *Bioorganometallics: Biomolecules, Labeling, Medicine*, Vol. 1, (Ed. G. Jaouen), Wiley VCH Verlag GmbH & Co. KGaA: Weinheim, **2006**, pp. 39–64.

[6] S. Ogo, T. Abura, Y. Watanabe, *Organometallics* **2002**, *21*, 2964–2969.

[7] A. Habtemariam, R.E. Aird, D.I. Jodrell, P.J. Sadler, unpublished results.

[8] D. Westerhausen, S. Herrmann, W. Hummel, E. Steckhan, *Angew. Chem.* **1992**, *104*, 1496–1498.

[9] C. Wong, D.G. Drueckhammer, H.M. Sweers, *J. Am. Chem. Soc.* **1985**, *107*, 4028–4031.

[10] U. Kragl, D. Vasic-Racki, C. Wandrey, *Bioproc. Eng.* **1996**, *14*, 291–297.

[11] P.S. Wagenknecht, E.J. Sambriski, *Recent Res. Dev. Inorg. Chem.* **2003**, *3*, 35–50.

[12] H.C. Lo, O. Buriez, J.B. Kerr, R.H. Fish, *Angew. Chem., Int. Ed.* **1999**, *38*, 1429–1432.

[13] E. Steckhan, S. Herrmann, R. Ruppert, E. Dietz, M. Frede, E. Spika, *Organometallics* **1991**, *10*, 1568–1577.

[14] H.C. Lo, C. Leiva, O. Buriez, J.B. Kerr, M.M. Olmstead, R.H. Fish, *Inorg. Chem.* **2001**, *40*, 6705–6716.

[15] D. Westerhausen, S. Herrmann, W. Hummel, E. Steckhan, *Angew. Chem., Ed. Engl.* **1992**, *31*, 1529–1531.

[16] F. Torabi, K. Ramanathan, P.O. Larsson, L. Gorton, K. Svanberg, Y. Okamoto, B. Danielsson, M. Khayyami, *Talanta* **1999**, *50*, 787–797.

[17] F. Wang, A. Habtemariam, E.P.L. van der Geer, R. Fernández, M. Melchart, R.J. Deeth, R. Aird, S. Guichard, F.P.A. Fabbiani, P. Lozano-Casal, I.D.H. Oswald, D.I. Jodrell, S. Parsons, P.J. Sadler, *Proc. Natl. Acad. Sci. USA* **2005**, *102*, 18269–18274.

[18] H.E. Gottlieb, V. Kotlyar, A. Nudelman, *J. Org. Chem.* **1997**, *62*, 7512–7515.

[19] P.K. Glasoe, F.A. Long, *J. Phys. Chem.* **1960**, *64*, 188–190.

[20] W. Kaim, R. Reinhardt, M. Sieger, *Inorg. Chem.* **1994**, *33*, 4453–4459, and references therein.

[21] M. Jahncke, A. Neels, H. Stoeckli-Evans, G. Süss-Fink, *J. Organomet. Chem.* **1998**, *565*, 97–103.

[22] G. Süss-Fink, M. Faure, T.R. Ward, *Angew. Chem. Int. Ed.* **2002**, *41*, 99–101.

[23] V. Moberg, P. Homanen, S. Selva, R. Persson, M. Haukka, T.A. Pakkanen, M. Monari, E. Nordlander, *Dalton Trans.* **2006**, 279–288.

[24] Y. Ohki; N. Uehara; H. Suzuki; *Angew. Chem., Int. Ed.* **2002**, *41*, 4085–4087.

[25] F. Cherioux; A. Maisse-Francois; A. Neels; H. Stoeckli-Evans; G. Süss-Fink; *J. Chem. Soc., Dalton Trans.* **2001**, 2184–2187.

[26] F.K. Cheung, A.M. Hayes, J. Hannedouche, A.S.Y. Yim, M. Wills, *J. Org. Chem.* **2005**, *70*, 3188–3197.

[27] A.M. Hayes, D.J. Morris, G.J. Clarkson, M. Wills, *J. Am. Chem. Soc.* **2005**, *127*, 7318–7319.

[28] R.H. Sarma, R.J. Mynott, *J. Am. Chem. Soc.* **1973**, 95, 7470–7480.

[29] Y.K. Yan, M. Melchart, A. Habtemariam, A.F.A. Peacock, P.J. Sadler, *J. Biol. Inorg. Chem.* **2006**, 483–488.

Chapter 6
Future Directions

6.1 Introduction

The ultimate goal in research into metal-based anticancer agents is to find a drug, which is tumour-specific, has predictable and controllable chemistry with no unwanted side-reactions, and can be activated "on demand" by a process from outside the body for additional flexibility in the treatment.

For half-sandwich Ru^{II} arene complexes, optimisation of the design as anticancer agents depends on control of ligand exchange reactions [1]. The framework of these complexes allows a number of variations of the building blocks to fine-tune their pharmacological properties [2]. Aspects of design and reactivity of Ru^{II} arene complexes were investigated in this thesis.

6.2 Ru^{II} Arene Complexes Containing *O,O*-Chelating Ligands

In Chapter 3 the effect of the chelating ligand in Ru^{II} arene complexes on the rate and extent of hydrolysis as well as the nucleobase selectivity was described. The aqueous chemistry of complexes containing acetylacetonate, maltolate and tropolonate were comparable, with similar pK_a values obtained for coordinated water and similar reactivity towards nucleobases, both in terms of extent of reaction and selectivity. Intriguingly, despite the apparent chemical similarities, only complexes containing acetylacetonate and some derivatives were found to be cytotoxic towards the A 2780 human ovarian cancer cell line. The observed dependence of cytotoxicity on steric bulk around the metal centre is also worth noting. An understanding of the factors responsible for activity is of particular interest.

- Studies into the reactivity of complexes, varying steric bulk, hydrophobicity and concentration, with biomolecules including histidines and sulfur-containing molecules might provide clues.
- Investigations into partition coefficients of complexes might help to gain insights into possible ease or difficulty of cell uptake.

Experiments, which address some of these aspects, are currently underway in the Sadler laboratories.

6.3 Tethered Ru^{II} Arene Complexes

Chapter 4 described the synthesis and characterisation of nitrogen-containing tethered Ru^{II} arene complexes. The observed hydrolysis and reactivity with nucleobases, in principle, makes this class of complex suitable for potential anticancer applications. However, the apparent high reactivity and the strong possibility of deactivation, not only by biomolecules, but also from insoluble precipitates need to be overcome. One strategy might involve controlled and especially stepwise activation of tethered ruthenium arene complexes. Recent results showed the pronounced effect of the leaving group (X) on the rate of hydrolysis of complexes of the type $[(\eta^6\text{-arene})Ru(en)X]^{n+}$ [3]. Similar studies on tethered Ru^{II} arene seem worthwhile and would involve the following aspects.

- Synthesis of tethered complexes containing more strongly coordinating ligands than chloride, such as pyridines, phosphines or mixed-atom chelating ligands (which might be susceptible to stepwise ring opening).
- Studies of their aqueous chemistry. Particular emphasis should be placed on the rate and extent of hydrolysis and the stability at physiological pH.
- Thus a suitable choice of ligands could enable activation from pH, light or hydrolysis.

Tethered Ru^{II} arene complexes could also be used as carrier ligands for DNA intercalators or other molecules, which have been used as ligands in other cytotoxic complexes, *e.g.* azopyridines [4].

- Synthesis and investigation into potential cytotoxicity of tethered Ru^{II} arene complexes containing DNA intercalators or azopyridines.

Tethered complexes might be activated by blocking the reactive sites by a bidentate chelate ring and opening of the tether. Ideally such reactions would not have a high degree of reversibility, since tether closure would produce an unreactive species. Such complexes could be useful prodrugs, especially if activation by means of pH control or light could be achieved. Strained, two-atom tethered complexes would appear to be the most suitable complexes, since breakage of the Ru – N(tether) bond was demonstrated in Chapter 4 for such compounds.

- Solution studies of tethered complexes containing bidentate chelating ligands with a view towards tether-opening reactions, initiated by pH, light or strongly coordinating biomolecules, *e.g.* histidine or glutathione.

Tethered Ru^{II} arenes could function as charge carriers, similar to platinum-containing complexes synthesised by Farrell *et al.* [5]. Such complexes could be synthesised by incorporation of a ligand, which could bind/chelate to both the tether-fragment and another metal. This could increase solubility of complexes and be utilised as a bridge between other metal-containing complexes. In addition, such positively-charged complexes could seek out DNA as a target by initial interaction with the negatively-charged phosphate backbone.

- Synthesis of di- or tri-nuclear metal complexes, including tethered Ru^{II} arene fragments as bridging molecules or to increase solubility.

6.4 Hydride Transfer Catalysed by Cytotoxic Ru^{II} Arene Complexes

With the finding that A549 lung cancer cells were tolerant to formate up to 2.5 mM, the possibility of using organometallic complexes as catalytic agents in biological systems arises [6]. This could lead to *in vivo* biocatalysis by organometallic complexes, although it would probably require more active catalysts than those investigated in Chapter 5.

- Bifunctional complexes, such as the tethered Ru^{II} arenes, could be useful as catalysts when bound mono-functionally to proteins or DNA. However, it was shown in Chapter 4 that mono-guanine adducts can undergo hydrolysis, which could lead to deactivation of such catalysts. Therefore optimisation in the binding properties of tethered Ru^{II} arene complexes to DNA bases is required.
- Studies of the stability constants of adducts of tethered complexes with ligands such as 9-ethylguanine or histidine need to be carried out.
- Investigations into transfer hydrogenation of ketones with formate as hydride donor by such adducts as potential biocatalysts.

6.5 References

[1] M. Melchart, A. Habtemariam, S. Parsons, S.A. Moggach, P.J. Sadler, *Inorg. Chim. Acta* **2006**, *359*, 3020–3028.

[2] Y.K. Yan, M. Melchart, A. Habtemariam, P.J. Sadler, *Chem. Commun.* **2005**, 4764–4776.

[3] F. Wang, A. Habtemariam, E.P.L. van der Geer, R. Fernández, M. Melchart, R.J. Deeth, R. Aird, S. Guichard, F.P.A. Fabbiani, P. Lozano-Casal, I.D.H. Oswald, D.I. Jodrell, S. Parsons, P.J. Sadler, *Proc. Natl. Acad. Sci. USA* **2005**, *102*, 18269–18274.

[4] A.C.G. Hotze, E.P.L. van der Geer, H. Kooijman, A.L. Spek, J.G. Haasnoot, J. Reedijk, *Eur. J. Inorg. Chem.* **2005**, 2648–2657.

[5] N. Farrell, Y. Qu, U. Bierbach, M. Valsecchi, E. Menta in *Cisplatin* (Ed.: B. Lippert), Verlag Helvetica Chimica Acta, Zürich, **1999**; pp. 479–496.

[6] Y.K. Yan, M. Melchart, A. Habtemariam, A.F.A. Peacock, P.J. Sadler, *J. Biol. Inorg. Chem.* **2006**, 483–488.

Table A.3.1: X-ray crystallographic data and refinement parameters for [(η^6-*p*-cym)Ru(acac)Cl] (**3.5**), [(η^6-*p*-cym)Ru(Ph$_2$acac)Cl] (**3.6**) and [(η^6-*p*-cym)Ru(^{t}Bu$_2$acac)Cl] (**3.7**).

	3.5	**3.6**	**3.7**
Structure code	Rumm56	Rum513	Rum514
Formula	$C_{15}H_{21}ClO_2Ru$	$C_{25}H_{25}ClO_2Ru$	$C_{21}H_{33}ClO_2Ru$
Molar mass	369.85	493.99	454.01
Crystal system	monoclinic	monoclinic	orthorhombic
Crystal size /mm	0.40 x 0.31 x 0.25	0.78 x 0.24 x 0.12	1.12 x 0.10 x 0.10
Space group	P 1 21/n 1	P 1 21/c 1	P n a 21
Crystal	red / block	red / lath	red / needle
a / Å	9.6398(13)	16.254(2)	11.851(3)
b / Å	13.9993(19)	7.6483(9)	16.854(5)
c / Å	11.5499(16)	17.060(2)	10.668(3)
α / deg	90	90	90
β / deg	96.619(2)	102.909(2)	90
γ / deg	90	90	90
T / K	150	150	150
Z	4	4	4
R [F > 4σ (F)][a]	0.0298	0.0307	0.0280
R_w[b]	0.0346	0.0353	0.0280
GOF[c]	1.0436	1.0654	1.0896
Δρ max and min, / eÅ^{-3}	1.09, -0.48	1.06, -0.48	0.94, -0.94

[a] $R = \Sigma||F_o| - |F_c||/\Sigma|F_o|$. [b] $R_w = [\Sigma w(F_o^2 - F_c^2)^2/\Sigma wF_o^2)]^{1/2}$.

[c] $GOF = [\Sigma w(F_o^2 - F_c^2)^2/(n-p)]^{1/2}$, where n = number of reflections and p = number of parameters.

Table A.3.2: X-ray crystallographic data and refinement parameters for [(η^6-*p*-cym)Ru((CF$_3$)$_2$acac)Cl] (**3.8**), [(η^6-*p*-cym)Ru(ma)Cl].2H$_2$O (**3.24**).2H$_2$O and [(η^6-*p*-cym)Ru(AcO)Cl] (**3.26**).

	3.8	**3.24.2H$_2$O**	**3.26**
Structure code	Mm0512	Rumm45	Rmms18
Formula	$C_{15}H_{15}ClF_6O_2Ru$	$C_{16}H_{23}ClO_5Ru$	$C_{12}H_{17}ClO_2Ru$
Molar mass	477.79	431.86	329.78
Crystal system	monoclinic	monoclinic	monoclinic
Crystal size /mm	0.19 x 0.14 x 0.07	0.96 x 0.30 x 0.17	0.51 x 0.20 x 0.20
Space group	P 1 21/n 1	P21/c	C2/c
Crystal	brown / block	red / lath	red / needle
a / Å	10.6824(15)	13.6816(4)	15.1119(16)
b / Å	13.0258(18)	8.9244(2)	12.5412(13)
c / Å	12.2250(18)	14.4691(4)	14.5525(16)
α / deg	90	90	90
β / deg	91.012(3)	96.783(2)	109.182(2)
γ / deg	90	90	90
T / K	150	150(2)	150(2)
Z	4	4	8
R [F > 4σ (F)][a]	0.0459	0.0252	0.0241
R_w[b]	0.0475	0.0620	0.0609
GOF[c]	1.0417	1.079	1.032
Δρ max and min, / eÅ^{-3}	1.49, -1.23	0.586, -0.387	0.720, -0.394

[a] $R = \sum||F_o| - |F_c||/\sum|F_o|$. [b] $R_w = [\sum w(F_o^2 - F_c^2)^2/\sum wF_o^2)]^{1/2}$.

[c] GOF = $[\sum w(F_o^2 - F_c^2)^2/(n-p)]^{1/2}$, where n = number of reflections and p = number of parameters.

Table A.3.3: X-ray crystallographic data and refinement parameters for [(η^6-*p*-cym)Ru(Ph$_2$acac)H$_2$O]CF$_3$SO$_3$ (**3.21b**), [(η^6-*p*-cym)Ru(trop)H$_2$O]CF$_3$SO$_3$ (**3.25b**) and [(η^6-*p*-cym)Ru(acac)9EtA]PF$_6$ (**3.20**).

	3.21b	**3.25b**	**3.20**
Structure code	Rumm44	Rutrcy	Mm56ad
Formula	$C_{30}H_{39}F_3O_8RuS$	$C_{18}H_{20}F_3O_6RuS$	$C_{22}H_{30}F_6N_5O_2PRu$
Molar mass	717.76	522.47	642.55
Crystal system	triclinic	triclinic	triclinic
Crystal size /mm	0.71 x 0.39 x 0.38	0.25 x 0.17 x 0.14	0.19 x 0.15 x 0.15
Space group	P-1	P-1	P-1
Crystal	orange / block	red / block	orange / aggregate
a / Å	12.6051(3)	9.4405(2)	8.4979(15)
b / Å	16.3880(3)	11.0375(2)	10.6334(17)
c / Å	16.6201(4)	11.6642(3)	14.694(2)
α / deg	80.3290(10)	109.8670(10)	89.838(9)
β / deg	76.2160(10)	109.5840(10)	78.998(9)
γ / deg	79.1430(10)	102.5830(10)	85.403(9)
T / K	150	150(2)	150(2)
Z	4	2	2
R [F > 4σ (F)][a]	0.0368	0.0335	0.0601
R_w[b]	0.0963	0.0840	0.1609
GOF[c]	0.9965	1.110	1.044
Δρ max and min, / eÅ^{-3}	1.48, -1.70	0.749, -0.561	0.736, -0.519

[a] $R = \sum||F_o| - |F_c||/\sum|F_o|$. [b] $R_w = [\sum w(F_o^2 - F_c^2)^2/\sum wF_o^2)]^{1/2}$.

[c] GOF = $[\sum w(F_o^2 - F_c^2)^2/(n-p)]^{1/2}$, where n = number of reflections and p = number of parameters.

Table A.3.4: X-ray crystallographic data and refinement parameters for [(η^6-*p*-cym)Ru(Ph_2acac)9EtG]CF_3SO_3 (**3.22**).

	3.22
Structure code	Rumm6a
Formula	$C_{47}H_{50}F_3N_5O_6RuS$
Molar mass	971.05
Crystal system	monoclinic
Crystal size /mm	0.61 x 0.24 x 0.20
Space group	C 2/c
Crystal	orange / block
a / Å	33.3763(6)
b / Å	21.7362(5)
c / Å	27.4616(5)
α / deg	90
β / deg	104.9664(11)
γ / deg	90
T / K	150(2)
Z	16
R [F > 4σ (F)][a]	0.0703
R_w[b]	0.2131
GOF[c]	1.092
Δρ max and min, / eÅ^{-3}	1.95, -0.95

[a] $R = \sum||F_o| - |F_c||/\sum|F_o|$. [b] $R_w = [\sum w(F_o^2 - F_c^2)^2/\sum wF_o^2)]^{1/2}$.

[c] GOF = $[\sum w(F_o^2 - F_c^2)^2/(n-p)]^{1/2}$, where n = number of reflections and p = number of parameters.

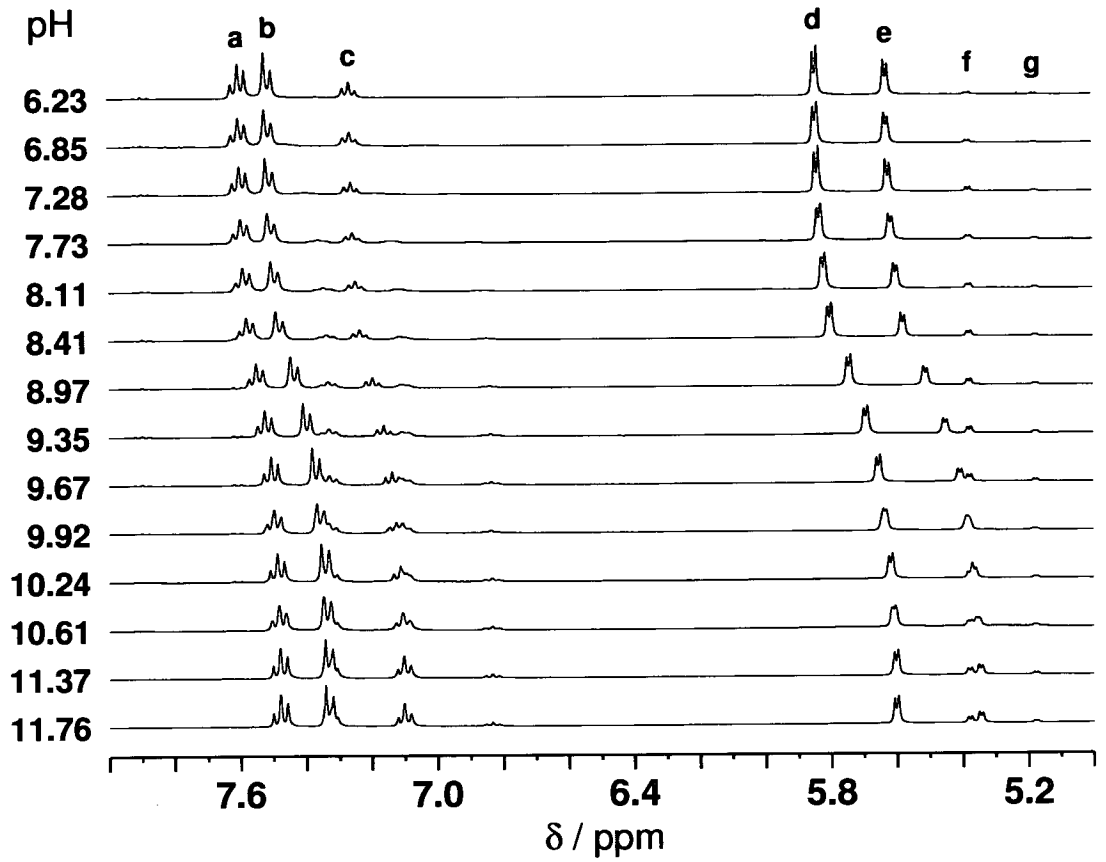

Figure A.3.1: Dependence on pH of the low field region of the ^{1}H NMR spectrum of Ru^{II} *p*-cymene *O,O*-chelated complexes as shown for a solution of $[(\eta^6$-*p*-cym)Ru(trop)$H_2O]NO_3$ (**3.25a**, 10% D_2O/ 90% H_2O, 0.1 M $NaClO_4$, 298 K). Assignments: a = Hb, Hd; b = Ha, He; c = Hc; d+e = *p*-cymene ring H. Signals due to formation of $[((\eta^6$-*p*-cym)$Ru)_2(\mu$-$OH)_3]^+$ (**3.27**): f+g = *p*-cymene ring H.

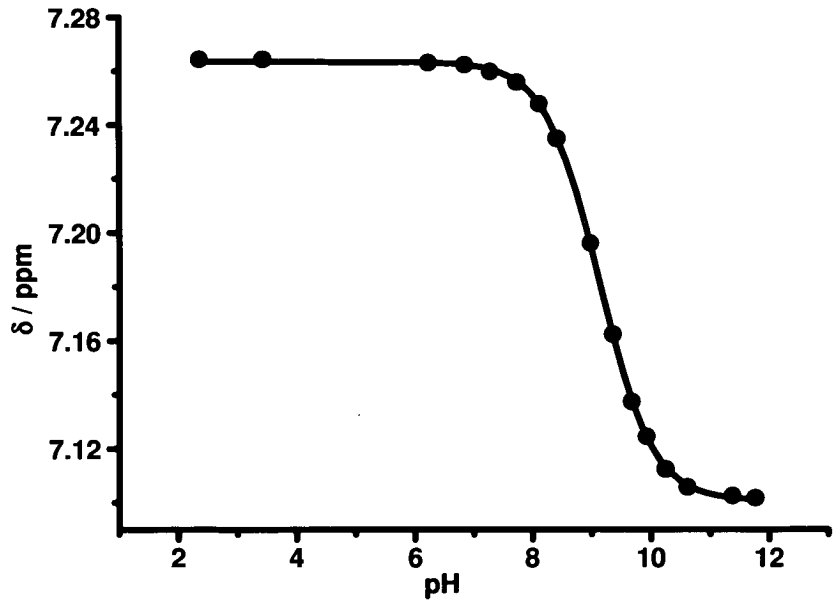

Figure A.3.2: Dependence of the ^{1}H NMR chemical shift of the tropolonate Hc resonance of $[(\eta^6\text{-}p\text{-cym})Ru(trop)H_2O]NO_3$ (**3.25a**, 10% D_2O/ 90% H_2O, 0.1 M $NaClO_4$, 298 K) on pH. The line is a computer fit giving pK_a (H_2O) = 9.12 ± 0.01.

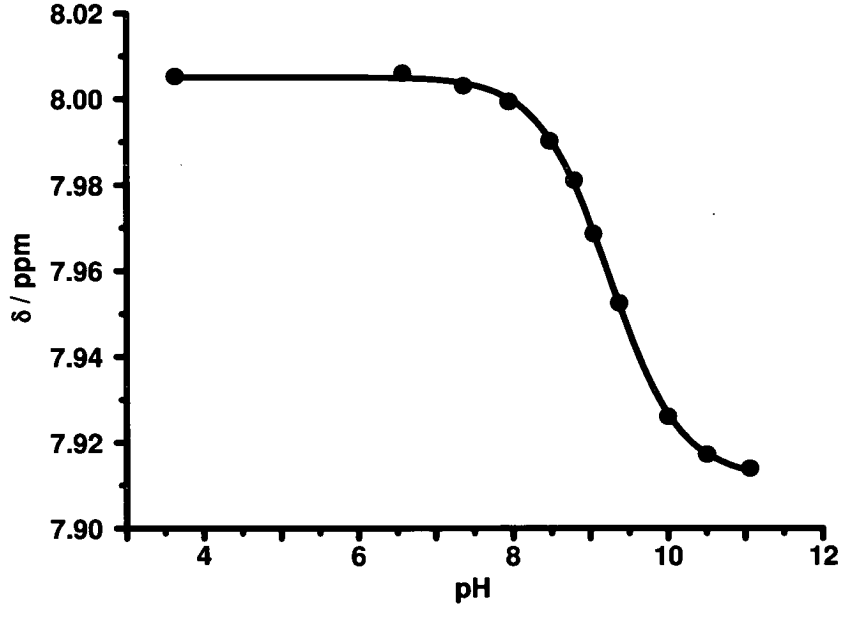

Figure A.3.3: Dependence of the ^{1}H NMR chemical shift of the maltolate H (adjacent to the heterocyclic oxygen) resonance of $[(\eta^6\text{-}p\text{-cym})Ru(ma)H_2O]NO_3$ (**3.29**, 10% D_2O/ 90% H_2O, 0.1 M $NaClO_4$, 298 K) on pH. The line is a computer fit giving pK_a (H_2O) = 9.23 ± 0.01.

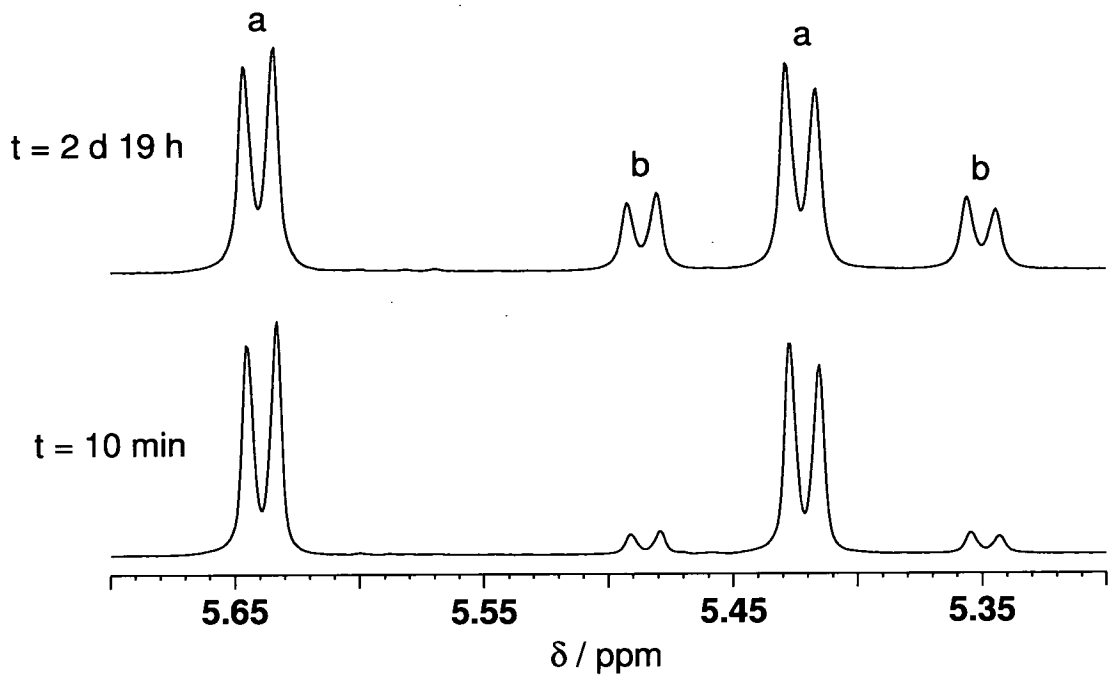

Figure A.3.4: The *p*-cymene ring proton region of the ^{1}H NMR spectrum of [(η^6-*p*-cym)Ru(AcO)Cl] (**3.26**) in $CDCl_3$ at 298 K, after 10 min and 2 d 19h, respectively. The new product could be [(η^6-*p*-cym)$RuCl_2$]$_2$ (**3.1**). Assignments: a = *p*-cymene CH (**3.26**); b = *p*-cymene CH (**3.1**).

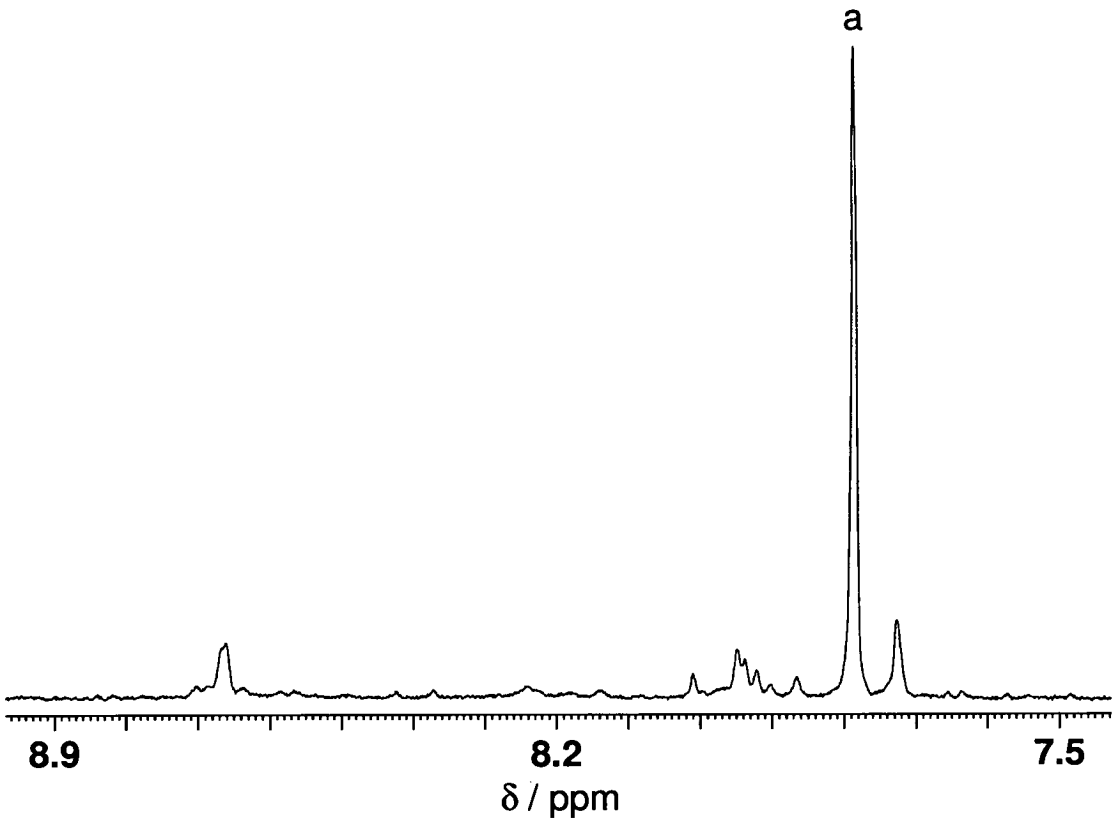

Figure A.3.5: The 9EtG H8 proton region of the ^{1}H NMR spectrum of a reaction between the dimer $[((\eta^6\text{-}p\text{-cym})Ru)_2(\mu\text{-OD})_3]^+$ (**3.27**) with 9-ethylguanine in D_2O at an initial pH* of 7.27 after 21 h. The mol ratio Ru : 9EtG is 1 : 1. Assignment: a = free 9EtG.

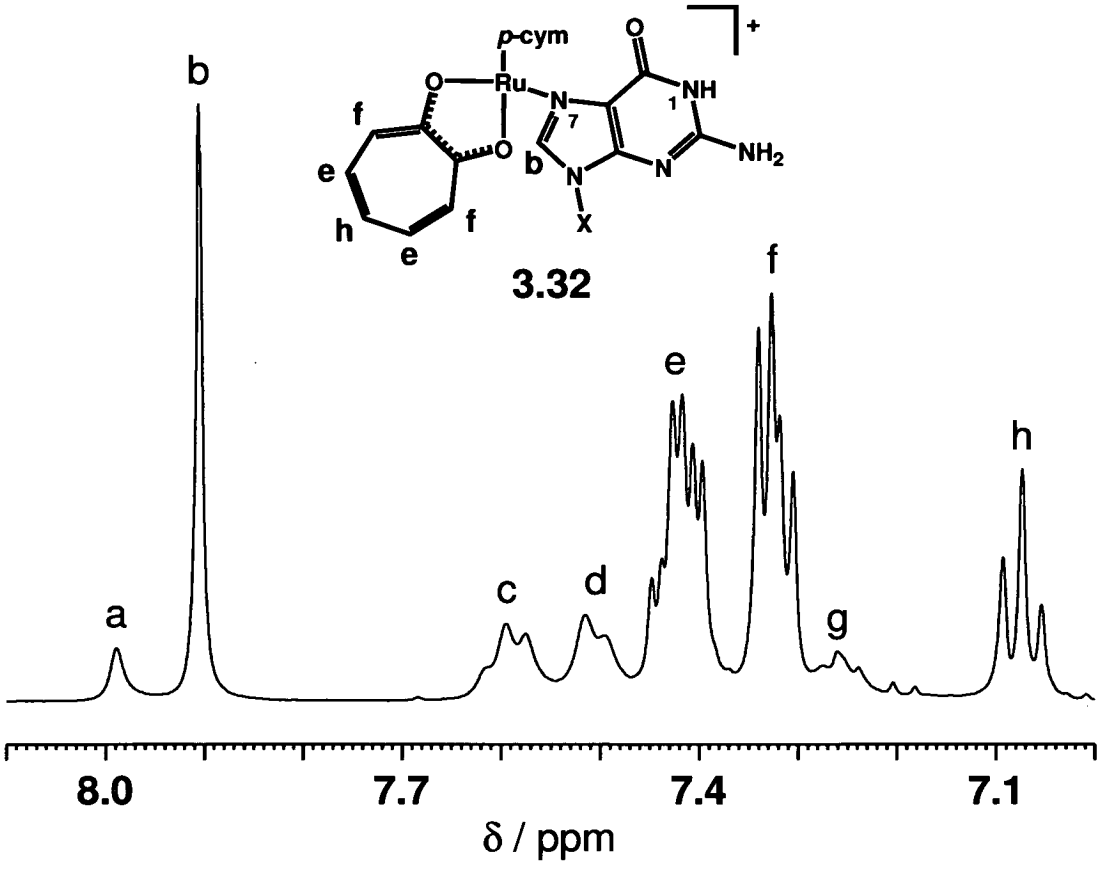

Figure A 3.6: Low field region of the ^{1}H NMR spectrum of an equilibrium solution containing guanosine and [(η^6-*p*-cym)Ru(trop)Cl] (**3.23**) in a 1:1 mol ratio in 10% D_2O/ 90% H_2O at pH 6.55 and 298 K. The product is [(η^6-*p*-cym)Ru(trop)Guo-*N7*]$^+$ (**3.32**). Assignments: a = H8 (free Guo); b = H8 (**3.32**); c = Hb, Hd (**3.23**); d = Ha, He (**3.23**); e = Hb, Hd (**3.32**); f = Ha, He (**3.32**); g = Hc (**3.23**); h = Hc (**3.32**). X corresponds to ribose.

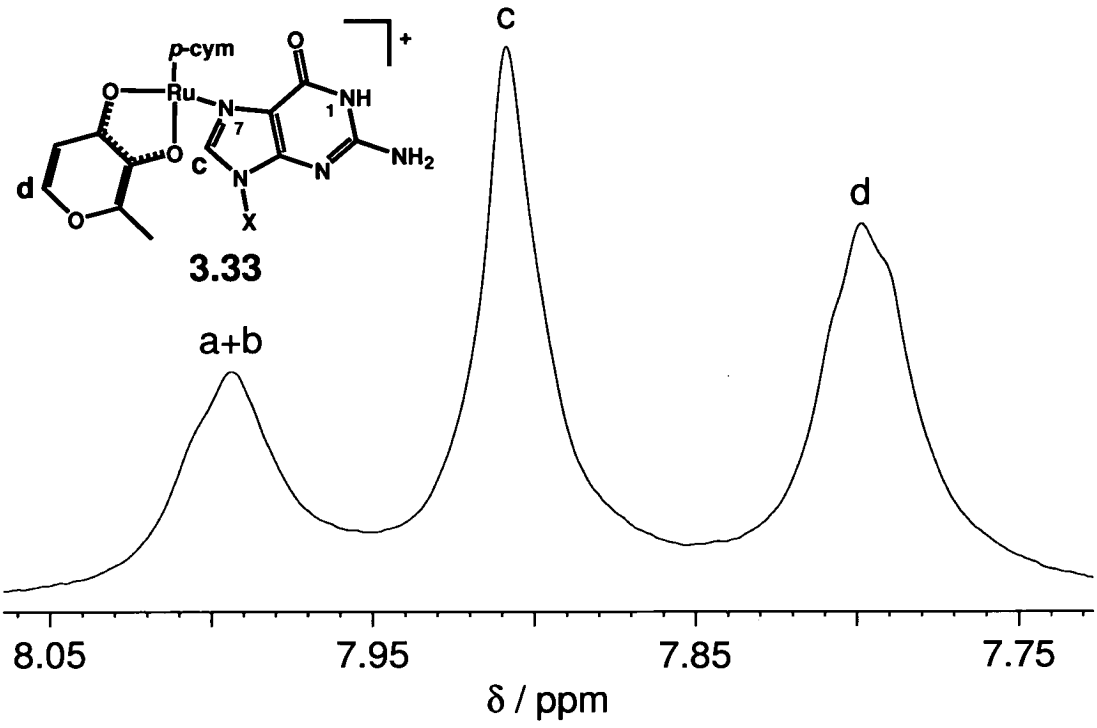

Figure A 3.7: Low field region of the ^{1}H NMR spectrum of an equilibrium solution containing guanosine and [(η^6-*p*-cym)Ru(ma)Cl] (**3.24**) in a 1:1 mol ratio in 10% D_2O/ 90% H_2O at pH 6.12 and 298 K. The product is [(η^6-*p*-cym)Ru(ma)Guo-*N7*]$^+$ (**3.33**). Assignments: a = H8 (free Guo); b = H ma (**3.24**); c = H8 (**3.33**); d = H ma (**3.33**). X corresponds to ribose.

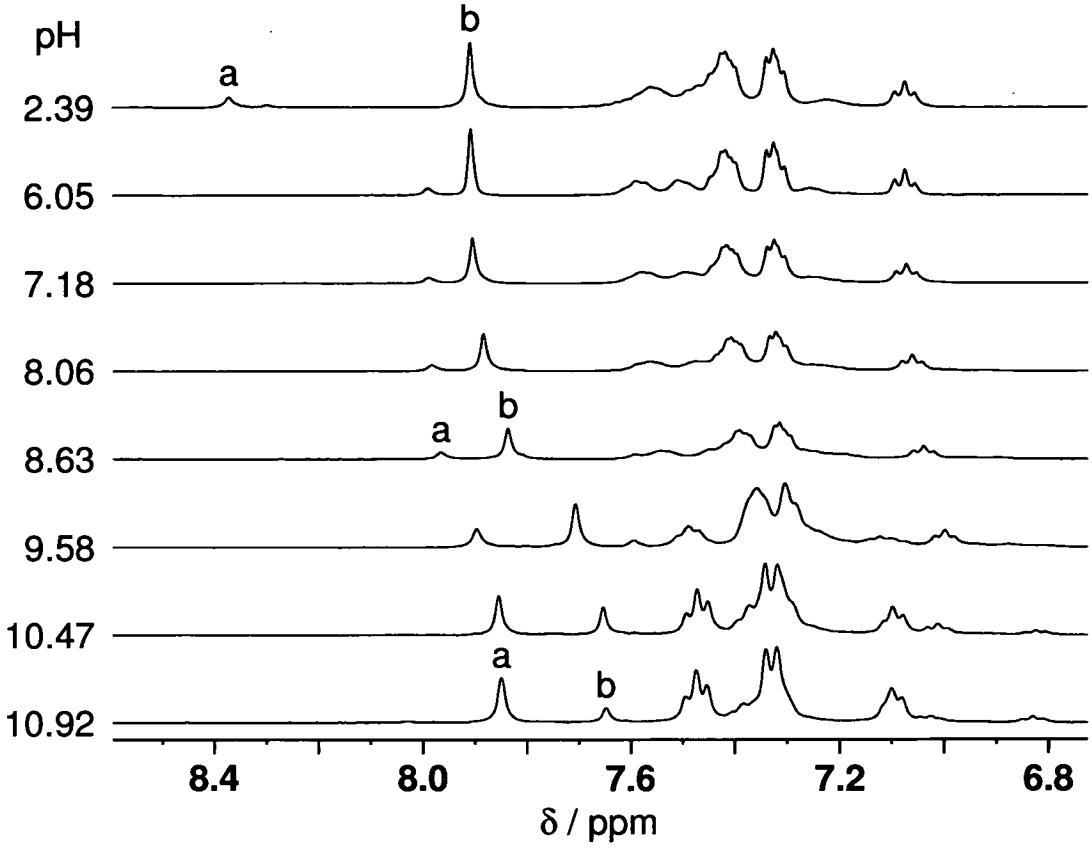

Figure A.3.8: Dependence on pH of the low field region of the ^{1}H NMR spectrum of a solution containing guanosine and [(η^6-*p*-cym)Ru(trop)Cl] (**3.23**) in 10% D_2O/ 90% H_2O at 298 K. The product is [(η^6-*p*-cym)Ru(trop)Guo-*N7*]$^+$ (**3.32**). Assignments: a = H8 (free Guo); b = H8 (**3.32**).

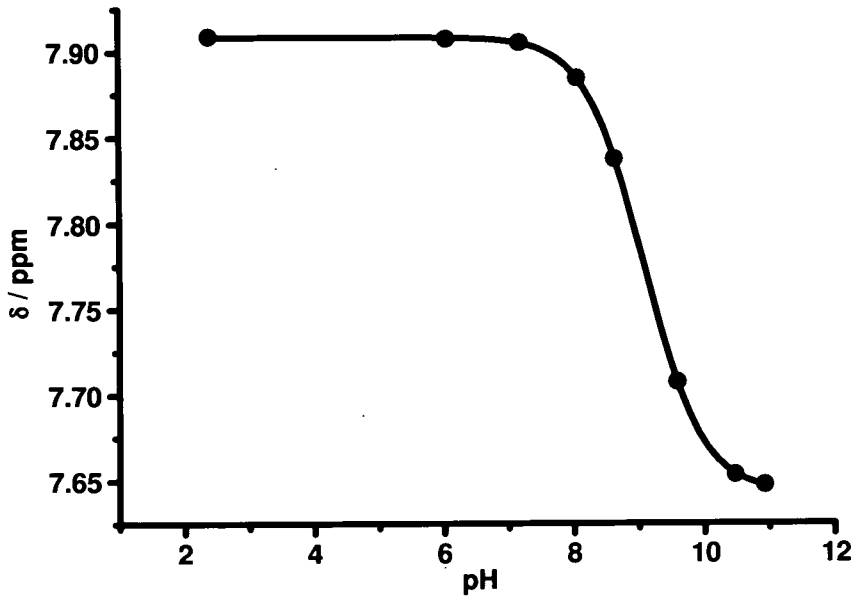

Figure A.3.9: Dependence of the ^{1}H NMR chemical shift of the guanosine H8 resonance of [(η^6-*p*-cym)Ru(trop)Guo-*N7*]$^+$ (**3.32**, 10% D_2O/ 90% H_2O, 298 K) on pH. The line is a computer fit giving pK_a (N1H) = 9.07 ± 0.01.

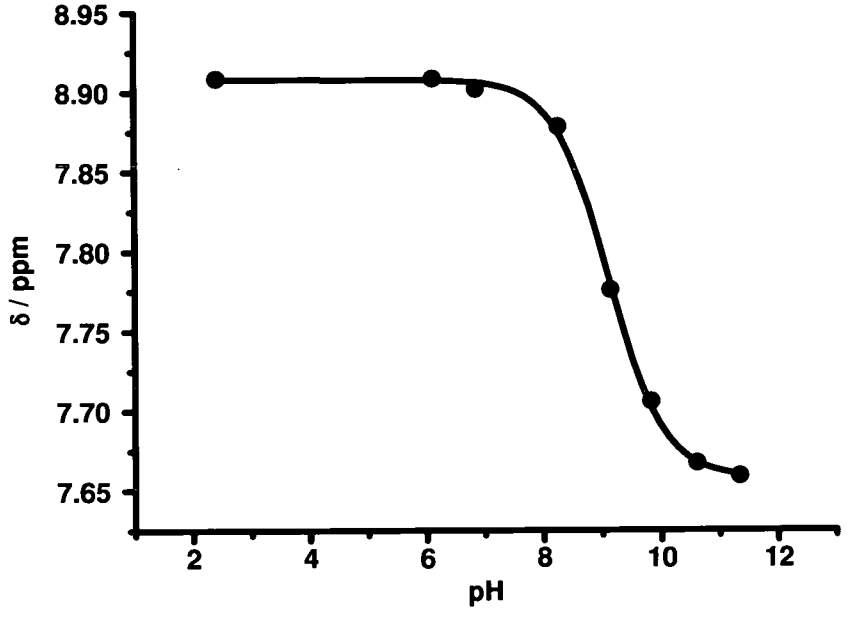

Figure A.3.10: Dependence of the ^{1}H NMR chemical shift of the guanosine H8 resonance of [(η^6-*p*-cym)Ru(ma)Guo-*N7*]$^+$ (**3.33**, 10% D_2O/ 90% H_2O, 298 K) on pH. The line is a computer fit giving pK_a (N1H) = 9.11 ± 0.01.

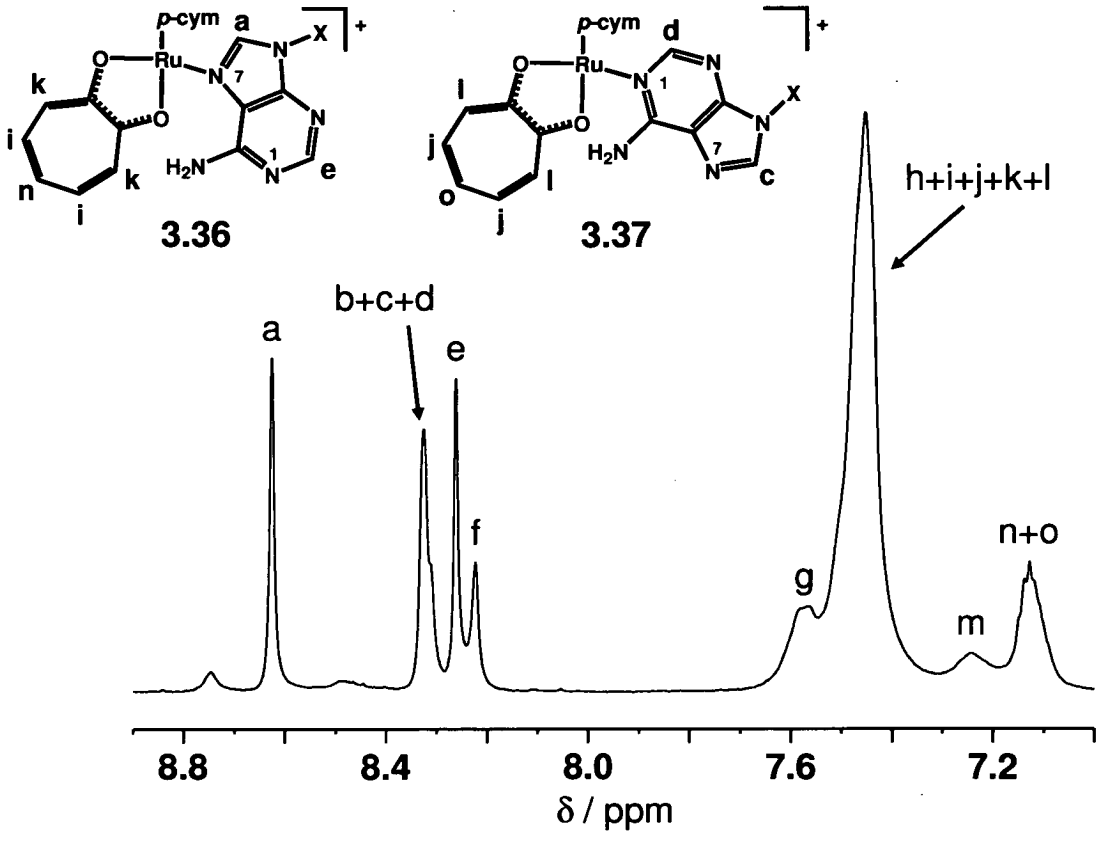

Figure A.3.11: Low field region of the ^{1}H NMR spectrum of a solution containing adenosine and [(η^6-*p*-cym)Ru(trop)Cl] (**3.23**) in a 1:1 mol ratio in 10% D_2O/ 90% H_2O at pH 7.35 and 298 K. The products are [(η^6-*p*-cym)Ru(trop)Ado-*N7*]$^+$ (**3.36**) and [(η^6-*p*-cym)Ru(trop)Ado-*N1*]$^+$ (**3.37**). Assignments: a = H8 (**3.36**); b = H8 (free Ado); c = H8 (**3.37**); d = H2 (**3.37**); e = H2 (**3.36**); f = H2 (free Ado); g = Hb, Hd (**3.23**); h = Ha, He (**3.23**); i = Hb, Hd (**3.36**); j = Hb, Hd (**3.37**); k = Ha, He (**3.36**); l = Ha, He (**3.37**); m = Hc (**3.23**); n = Hc (**3.36**); o = Hc (**3.37**). X corresponds to ribose.

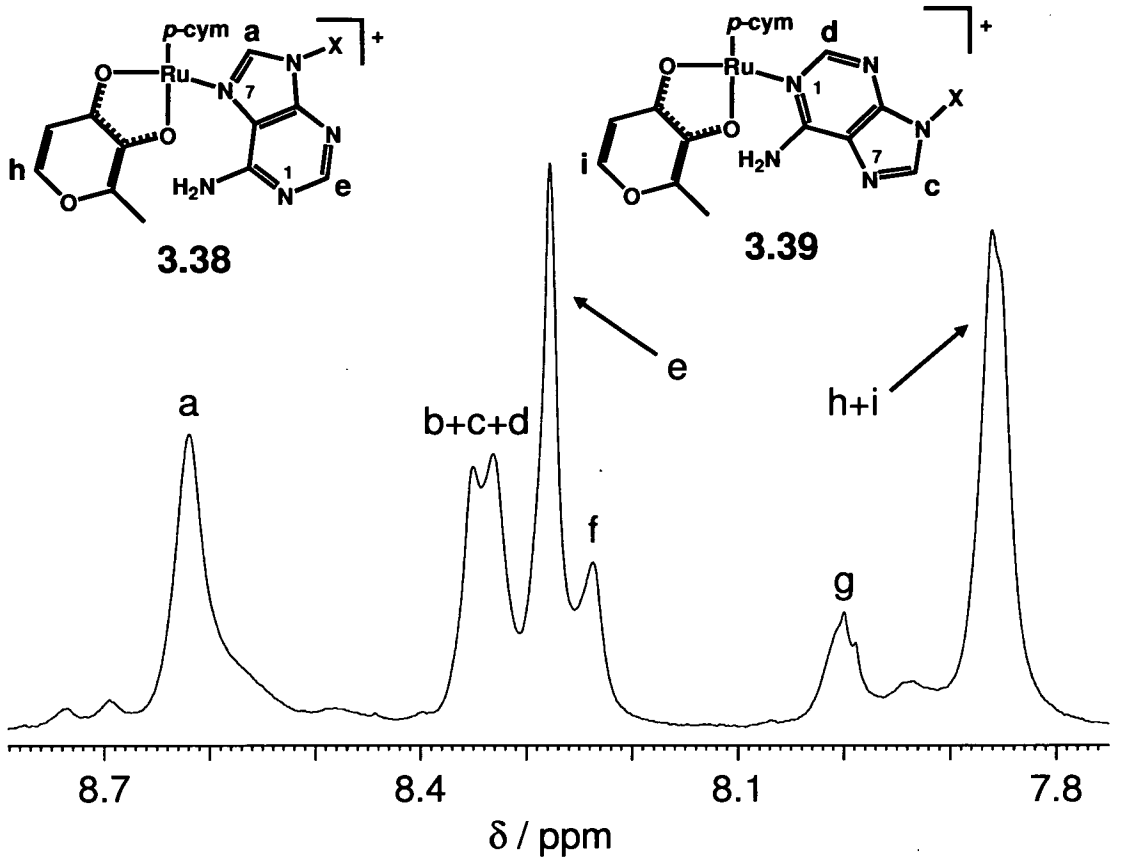

Figure A.3.12: Low field region of the ^{1}H NMR spectrum of a solution containing adenosine and [(η^6-*p*-cym)Ru(ma)Cl] (**3.24**) in a 1:1 mol ratio in 10% D_2O/ 90% H_2O at pH 7.22 and 298 K. The products are [(η^6-*p*-cym)Ru(ma)Ado-*N7*]$^+$ (**3.38**) and [(η^6-*p*-cym)Ru(ma)Ado-*N1*]$^+$ (**3.39**). Assignments: a = H8 (**3.38**); b = H8 (free Ado); c = H8 (**3.39**); d = H2 (**3.39**); e = H2 (**3.38**); f = H2 (free Ado); g = H ma (**3.24**); h = H ma (**3.38**); i = H ma (**3.39**). X corresponds to ribose.

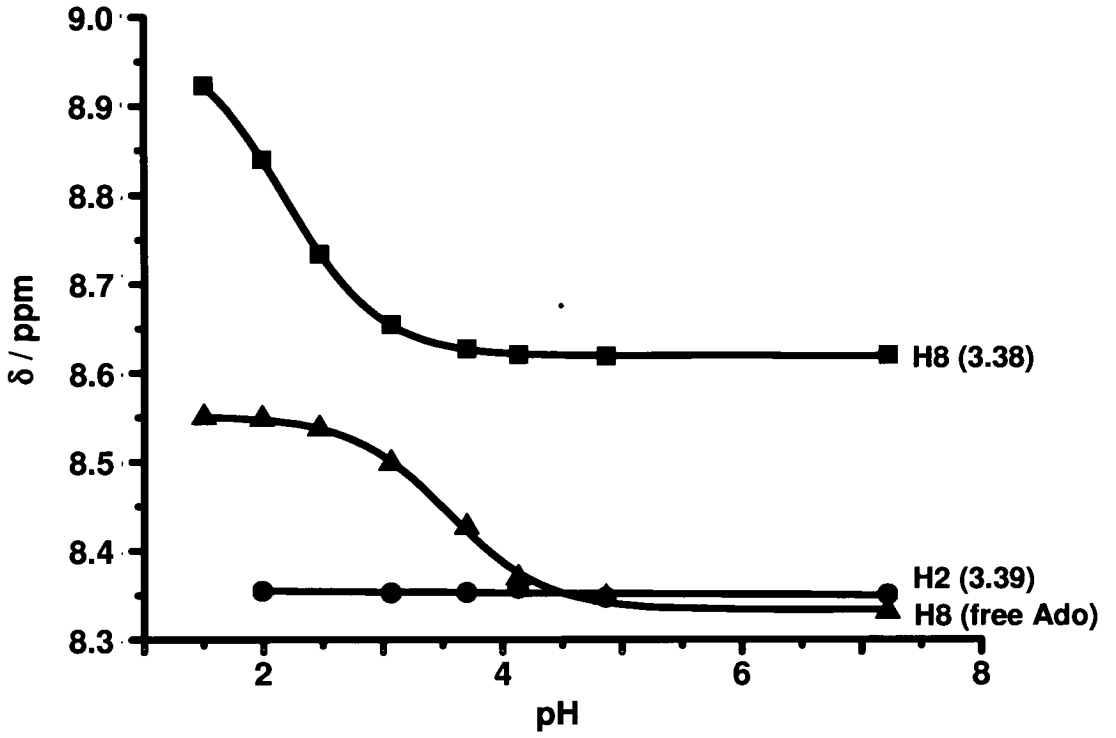

Figure A.3.13: Dependence of the H8 and H2 ^{1}H NMR chemical shifts of adenosine, [(η^6-*p*-cym)Ru(ma)Ado-*N7*]$^+$ (**3.38**) and [(η^6-*p*-cym)Ru(ma)Ado-*N1*]$^+$ (**3.39**) (10% D_2O/ 90% H_2O, 298 K) on pH. The line for H8 (free Ado) is a computer fit giving pK_a (N1H) = 3.54 ± 0.01. For clarity only one plot per species is shown.

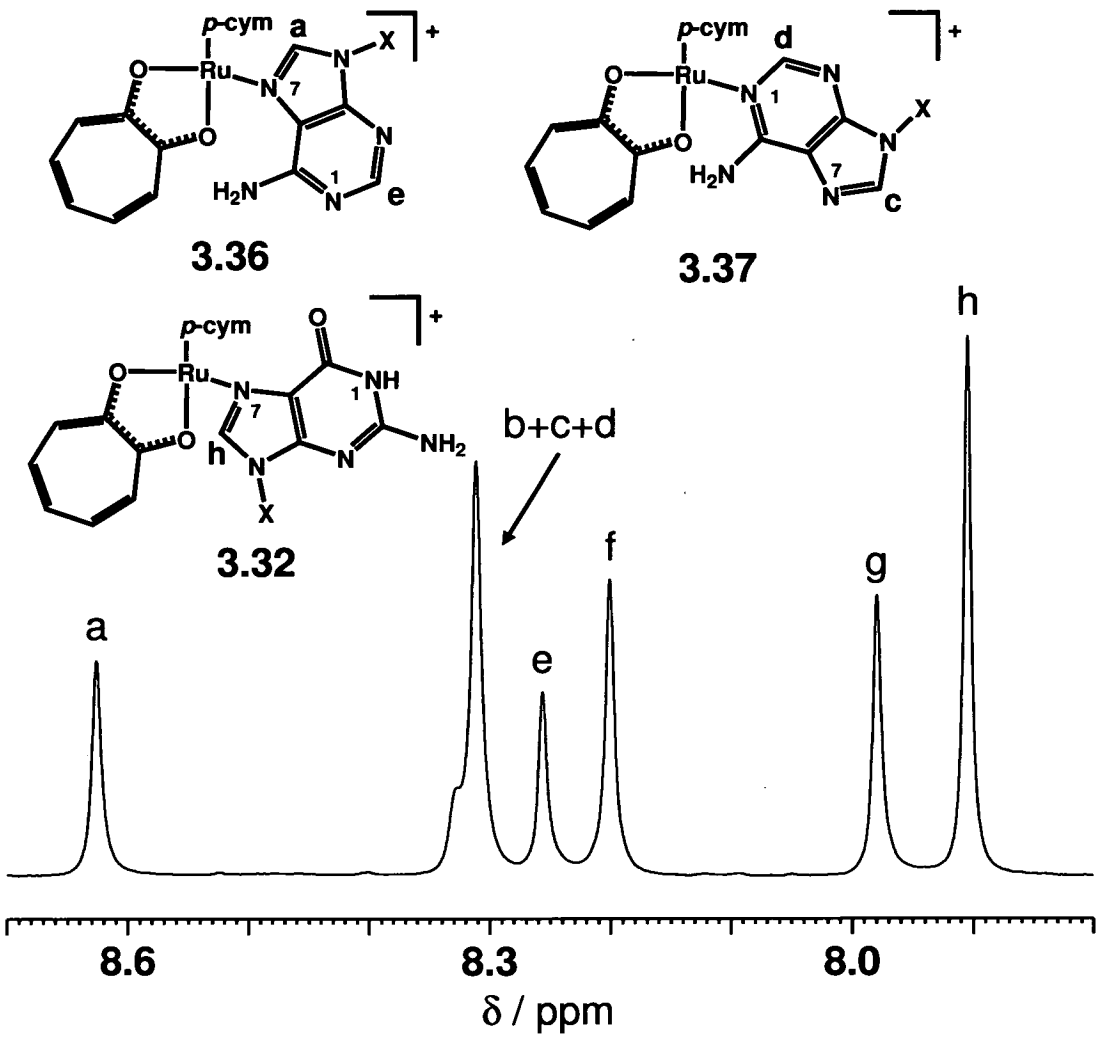

Figure A.3.14: The ^{1}H NMR spectrum of an equilibrium solution containing guanosine, adenosine and [(η^6-*p*-cym)Ru(trop)Cl] (**3.23**) in a *ca.* 1:1:1 mol ratio in 90% H_2O/ 10% D_2O at pH 6.63 and 298 K. The products are [(η^6-*p*-cym)Ru(trop)Guo-*N7*]$^+$ (**3.32**), [(η^6-*p*-cym)Ru(trop)Ado-*N7*]$^+$ (**3.36**) and [(η^6-*p*-cym)Ru(trop)Ado-*N1*]$^+$ (**3.37**). Assignments: a = H8 (**3.36**); b = H8 (free Ado); c = H8 (**3.37**); d = H2 (**3.37**); e = H2 (**3.36**); f = H2 (free Ado); g = H8 (free Guo); h = H8 (**3.32**). X corresponds to ribose.

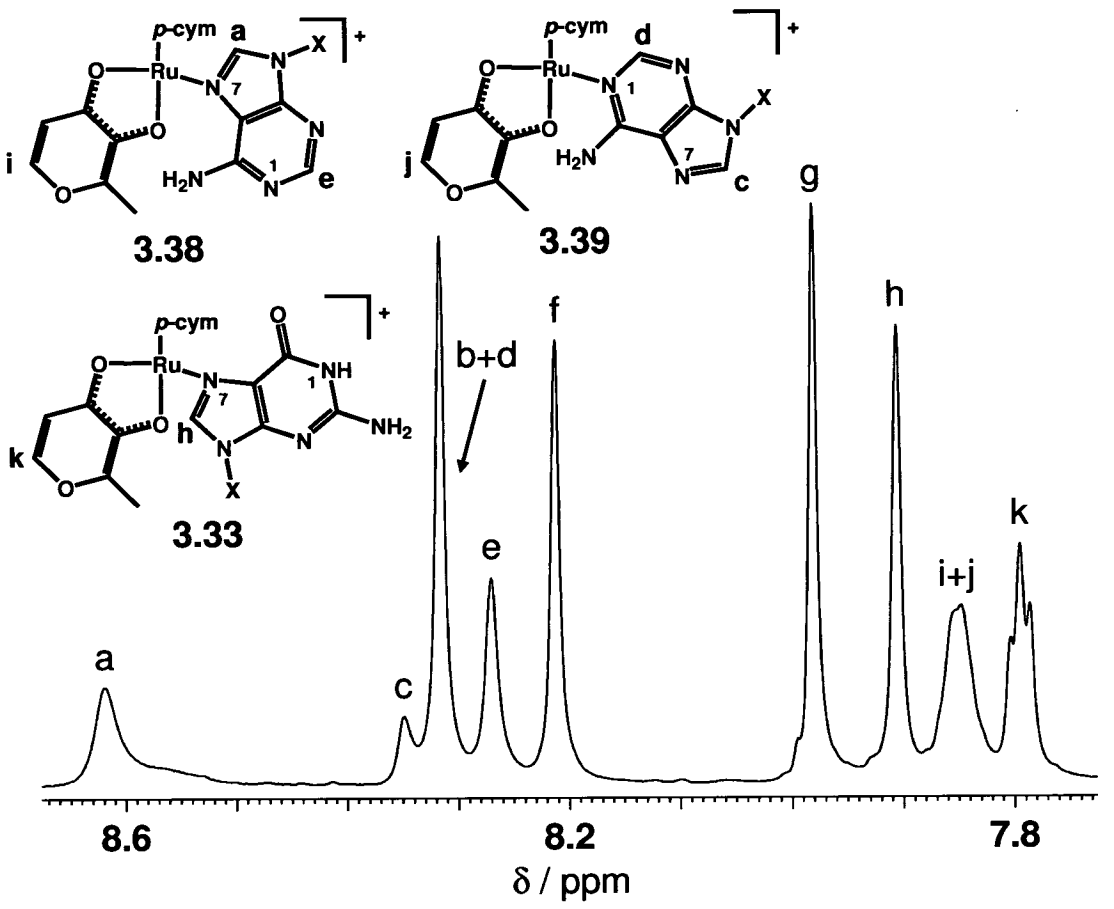

Figure A.3.15: The ^{1}H NMR spectrum of an equilibrium solution containing guanosine, adenosine and [(η^6-*p*-cym)Ru(ma)Cl] (**3.24**) in a *ca.* 1:1:1 mol ratio in 90% H_2O/ 10% D_2O at pH 6.22 and 298 K. The products are [(η^6-*p*-cym)Ru(ma)Guo-*N7*]$^+$ (**3.33**), [(η^6-*p*-cym)Ru(ma)Ado-*N7*]$^+$ (**3.38**) and [(η^6-*p*-cym)Ru(ma)Ado-*N1*]$^+$ (**3.39**). Assignments: a = H8 (**3.38**); b = H8 (free Ado); c = H8 (**3.39**); d = H2 (**3.39**); e = H2 (**3.38**); f = H2 (free Ado); g = H8 (free Guo); h = H8 (**3.33**); i = H ma (**3.38**); j = H ma (**3.39**); k = H ma (**3.33**). X corresponds to ribose.

Table A.4.1: X-ray crystallographic data and refinement parameters for $[(\eta^6:\eta^1\text{-}C_6H_5(CH_2)_3NH_2)RuCl_2]$ (**4.4**), $[(\eta^6:\eta^1\text{-}C_6H_5(CH_2)_2NH_2)RuCl_2]$ (**4.5**) and $[(\eta^6:\eta^1\text{-}C_6H_5O(CH_2)_2NH_2)RuCl_2]$ (**4.6**).

	4.4	**4.5**	**4.6**
Structure code	Mm29ru	Mm24ru	Mm30a1
Formula	$C_9H_{13}Cl_2NRu$	$C_8H_{11}Cl_2NRu$	$C_8H_{11}Cl_2NORu$
Molar mass	307.18	293.15	309.16
Crystal system	Monoclinic twined via 2[100]	Orthorhombic	Monoclinic
Crystal size /mm	0.26 x 0.20 x 0.18	0.13 x 0.12 x 0.093	0.39 x 0.38 x 0.34
Space group	P 1 21/c 1	Pnma	P 1 21/n 1
Crystal	red / block	orange / block	orange / block
a / Å	10.857(3)	8.8880(11)	7.6443(2)
b / Å	10.604(3)	10.8145(13)	8.0013(2)
c / Å	8.992(3)	9.9414(12)	16.0889(4)
α / deg	90	90	90
β / deg	90.438(6)	90	99.4630(10)
γ / deg	90	90	90
T / K	150	150	150
Z	4	4	4
R [F > 4σ (F)][a]	0.0612	0.0251	0.0232
R_w[b]	0.1707	0.0536	0.0613
GOF[c]	0.9901	1.030	1.0816
Δρ max and min, / eÅ^{-3}	2.63, -1.16	0.580, -0.407	0.65, -0.50

[a] $R = \sum||F_o| - |F_c||/\sum|F_o|$; [b] $R_w = [\sum w(F_o^2 - F_c^2)^2/\sum wF_o^2)]^{1/2}$;

[c] $GOF = [\sum w(F_o^2 - F_c^2)^2/(n-p)]^{1/2}$, where n = number of reflections and p = number of parameters.

Table A.4.2: X-ray crystallographic data and refinement parameters for $[(\eta^6:\eta^1\text{-}C_6H_5(CH_2)C_5H_4N)RuCl_2]$ (**4.7**), $[(\eta^6:\eta^1\text{-}C_6H_5(CH_2)_3NH_2)Ru(NO_3)_2]$ (**4.10**) and $[(\eta^6:\eta^1\text{-}C_6H_5(CH_2)_3NH_2)Ru(9EtG)_2](CF_3SO_3)_2$ (**4.11b**).

	4.7	**4.10**	**4.11b**
Structure code	Mm31ru	Ps0502	Ps0514
Formula	$C_{12}H_{11}Cl_2NRu$	$C_9H_{13}N_3O_6Ru$	$C_{25}H_{32}F_6N_{11}O_9RuS_2$
Molar mass	341.20	360.29	909.79
Crystal system	monoclinic	monoclinic	monoclinic
Crystal size /mm	0.45 x 0.23 x 0.15	0.38 x 0.14 x 0.12	0.55 x 0.53 x 0.39
Space group	P 1 21/n 1	P 21/n	P 1 21/c 1
Crystal	orange / plate	orange / block	yellow / block
a / Å	6.7289(8)	8.02280(10)	21.4440(10)
b / Å	13.4867(17)	11.8160(2)	12.2790(6)
c / Å	12.3368(15)	12.6372(2)	15.9360(8)
α / deg	90	90	90
β / deg	93.050(2)	100.7630(10)	111.240(3)
γ / deg	90	90	90
T / K	150	150(2)	293
Z	4	4	4
R [F > 4σ (F)][a]	0.0260	0.0213	0.0446
R_w[b]	0.0627	0.0576	0.0539
GOF[c]	0.9292	1.051	1.0058
Δρ max and min, / eÅ^{-3}	0.61, -0.52	0.584, -0.564	2.08, -0.80

[a] $R = \sum||F_o| - |F_c||/\sum|F_o|$; [b] $R_w = [\sum w(F_o^2 - F_c^2)^2/\sum wF_o^2)]^{1/2}$;

[c] $GOF = [\sum w(F_o^2 - F_c^2)^2/(n-p)]^{1/2}$, where n = number of reflections and p = number of parameters.

Table A.4.3: X-ray crystallographic data and refinement parameters for [(η^6:η^1-$C_6H_5(CH_2)_3NH_2$)Ru(ox)] (**4.14**), [(η^6:η^1-$C_6H_5(C_6H_4)NH_2$)Ru(ox)] (**4.16**) and [(η^6:η^1-$C_6H_5(CH_2)_3NH_2$)Ru(acac)]PF_6 (**4.18**).

	4.14	**4.16**	**4.18**
Structure code	Rumm49	Ps0508	Rumm57
Formula	$C_{11}H_{13}NO_4Ru$	$C_{14}H_{11}NO_4Ru$	$C_{14}H_{20}NO_2RuPF_6$
Molar mass	324.29	358.31	480.35
Crystal system	monoclinic	monoclinic	triclinic
Crystal size /mm	0.26 x 0.19 x 0.16	0.54 x 0.16 x 0.10	0.53 x 0.38 x 0.37
Space group	P 21/c	P 21/c	P-1
Crystal	yellow / block	yellow / needle	yellow / block
a / Å	10.1000(5)	18.1891(4)	8.3030(2)
b / Å	7.9721(4)	6.5799(2)	9.4955(2)
c / Å	13.9070(6)	31.3440(7)	11.8786(2)
α/ deg	90	90	93.8300(10)
β/ deg	106.716(2)	93.598(2)	107.3820(10)
γ/ deg	90	90	104.1680(10)
T / K	293(2)	150(2)	150(2)
Z	4	12	2
R [F > 4σ (F)][a]	0.0379	0.0337	0.0263
R_w[b]	0.0982	0.0768	0.0671
GOF[c]	1.041	1.037	1.051
Δρ max and min, / eÅ^{-3}	2.286, -1.131	1.050, -0.550	0.634, -0.929

[a] $R = \sum||F_o| - |F_c||/\sum|F_o|$; [b] $R_w = [\sum w(F_o^2 - F_c^2)^2/\sum wF_o^2)]^{1/2}$;

[c] $GOF = [\sum w(F_o^2 - F_c^2)^2/(n-p)]^{1/2}$, where n = number of reflections and p = number of parameters.

Table A.4.4: X-ray crystallographic data and refinement parameters for [(η^6:η^1-$C_6H_5(CH_2)_3NH_2$)Ru(*L*-pal)]PF_6 (**4.20**), [(η^6-etb)Ru(bap)Cl_2] (**4.31**) and [(η^6:η^1-$C_6H_5(C_6H_4)NH_3$)$RuCl_3$] (**4.32**).

	4.20	**4.31**	**4.32**
Structure code	Ps0526	Ps0501	Rumm34
Formula	$C_{19}H_{27}F_6N_2O_3PRu$	$C_{21}H_{22}Cl_2N_2O_2Ru$	$C_{12}H_{12}Cl_3NRu$
Molar mass	577.47	506.39	377.66
Crystal system	monoclinic	Orthorhombic	monoclinic
Crystal size /mm	1.70 x 0.19 x 0.19	0.41 x 0.28 x 0.21	0.61 x 0.49 x 0.24
Space group	P21	P b c a	P 1 21/n 1
Crystal	orange / needle	dark red / block	red / block
a / Å	10.0626(4)	14.5555(3)	13.1377(4)
b / Å	21.0481(9)	11.1869(3)	6.8928(2)
c / Å	11.3014(5)	25.3222(5)	15.0526(5)
α / deg	90	90	90
β / deg	113.391(2)	90	110.648(2)
γ / deg	90	90	90
T / K	150(2)	150	150
Z	4	8	4
R [F > 4σ (F)][a]	0.0405	0.0254	0.0235
R_w[b]	0.0970	0.0605	0.0603
GOF[c]	1.010	0.9082	1.0634
Δρ max and min, / eÅ^{-3}	0.747, -0.477	0.70, -0.59	0.61, -0.65

[a] $R = \sum||F_o| - |F_c||/\sum|F_o|$; [b] $R_w = [\sum w(F_o^2 - F_c^2)^2/\sum wF_o^2)]^{1/2}$;

[c] $GOF = [\sum w(F_o^2 - F_c^2)^2/(n-p)]^{1/2}$, where n = number of reflections and p = number of parameters.

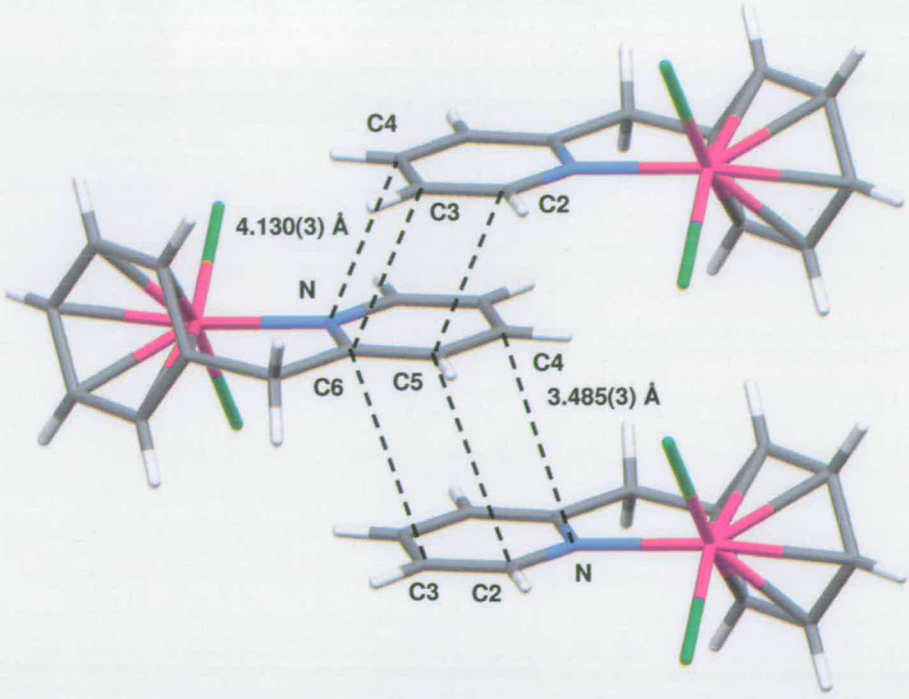

Figure A.4.1: $\pi - \pi$ Stacking interactions between neighbouring pyridine rings in the X-ray crystal structure of $[(\eta^6{:}\eta^1\text{-}C_6H_5(CH_2)C_5H_4N)RuCl_2]$ (**4.7**).

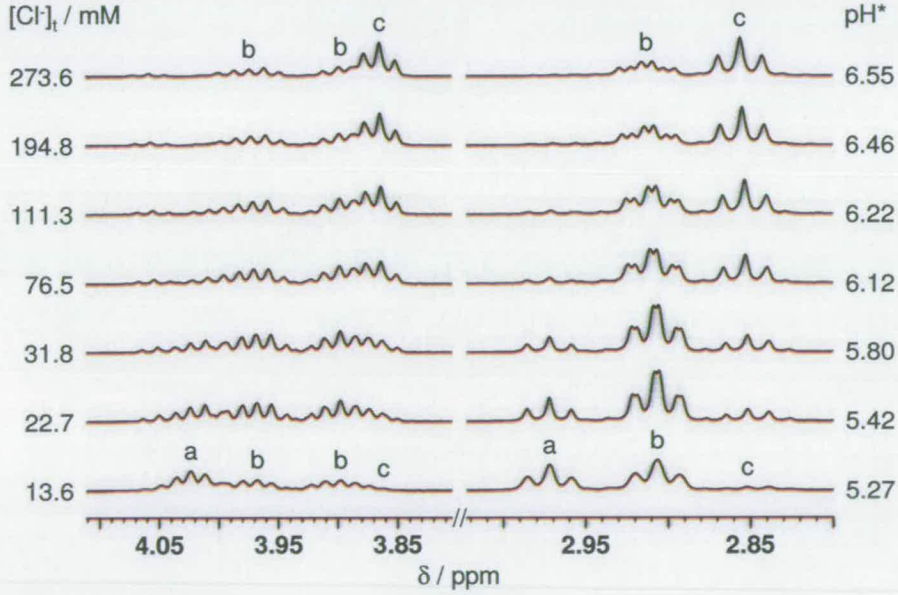

Figure A.4.2: The tether backbone proton region of the ^{1}H NMR spectrum for a chloride titration of $[(\eta^6{:}\eta^1\text{-}C_6H_5(CH_2)_2NH_2)RuCl_2]$ (**4.5**) (6.8 mM Ru) in D_2O at 298 K. Assignments: a = $[(\eta^6{:}\eta^1\text{-}C_6H_5(CH_2)_2NH_2)Ru(H_2O)_2]^{2+}$; b = $[(\eta^6{:}\eta^1\text{-}C_6H_5(CH_2)_2NH_2)Ru(H_2O)Cl]^+$; c = $[(\eta^6{:}\eta^1\text{-}C_6H_5(CH_2)_2NH_2)RuCl_2]$.

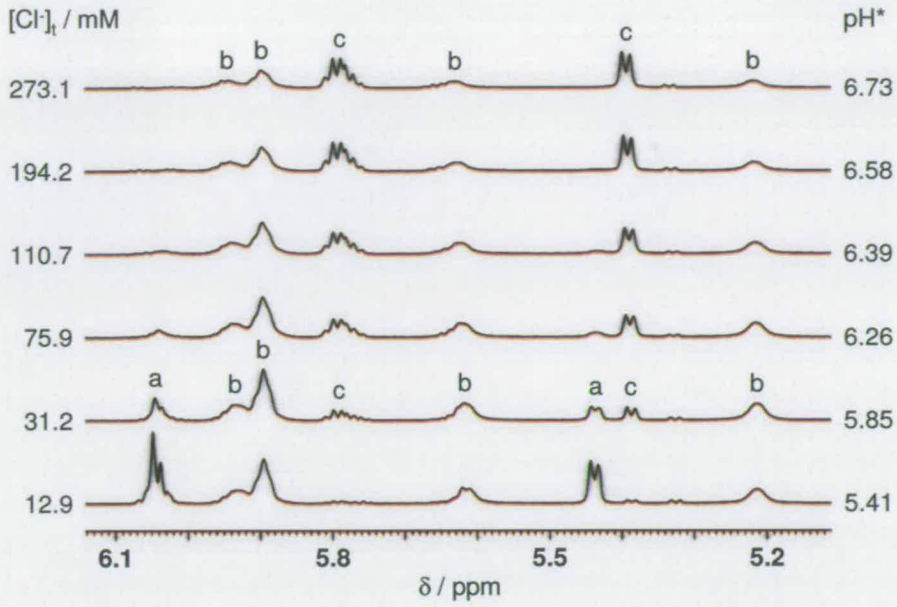

Figure A.4.3: The arene proton region of the ^{1}H NMR spectrum for a chloride titration of $[(\eta^6{:}\eta^1\text{-}C_6H_5(CH_2)_3NH_2)RuCl_2]$ (**4.4**) (6.5 mM Ru) in D_2O at 298 K. Assignments: a = $[(\eta^6{:}\eta^1\text{-}C_6H_5(CH_2)_3NH_2)Ru(H_2O)_2]^{2+}$; b = $[(\eta^6{:}\eta^1\text{-}C_6H_5(CH_2)_3NH_2)Ru(H_2O)Cl]^{+}$; c = $[(\eta^6{:}\eta^1\text{-}C_6H_5(CH_2)_3NH_2)RuCl_2]$.

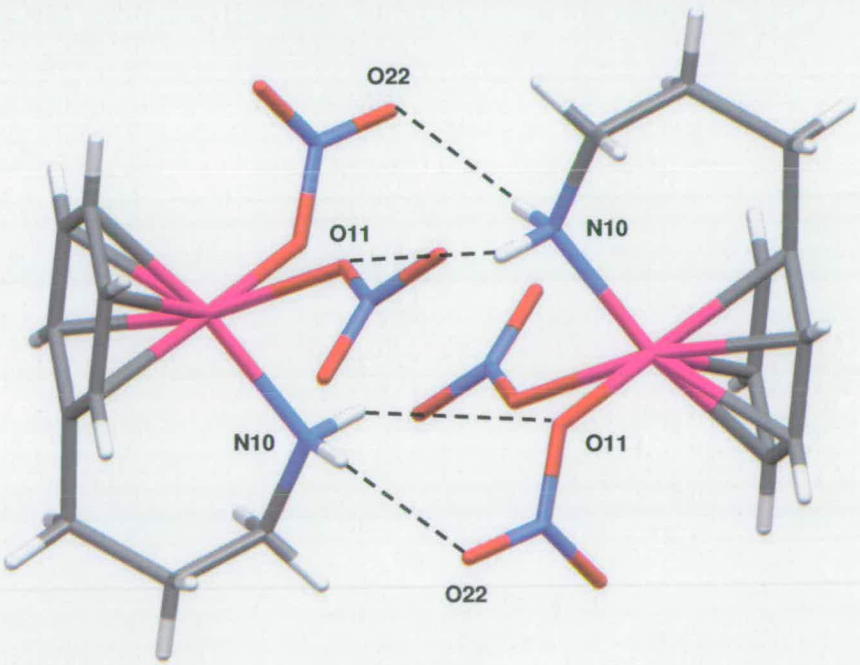

Figure A.4.4: Dimer formation *via* H-bonds between the NH_2 and nitrate oxygen atoms O11 and O22 in the crystal structure of $[(\eta^1{:}\eta^6\text{-}C_6H_5(CH_2)_3NH_2)Ru(NO_3)_2]$ (**4.10**).

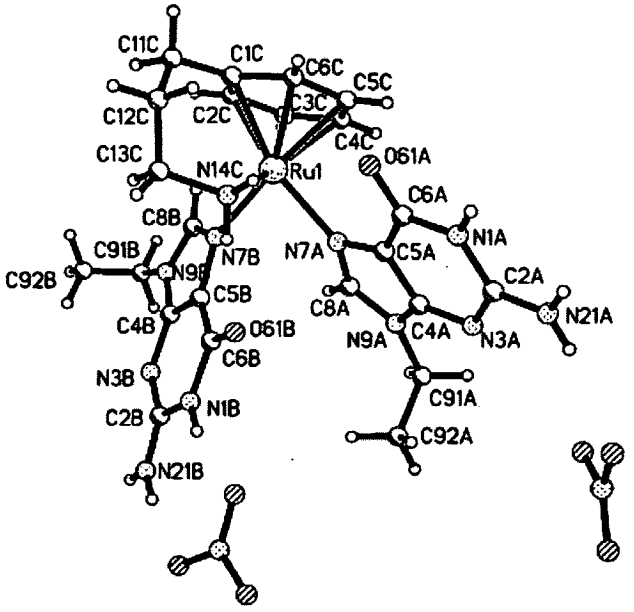

Figure A.4.5: The unrefined X-ray crystal structure of $[(\eta^6{:}\eta^1\text{-}C_6H_5(CH_2)_3NH_2)Ru(9EtG)_2](NO_3)_2$ and atom numbering scheme.

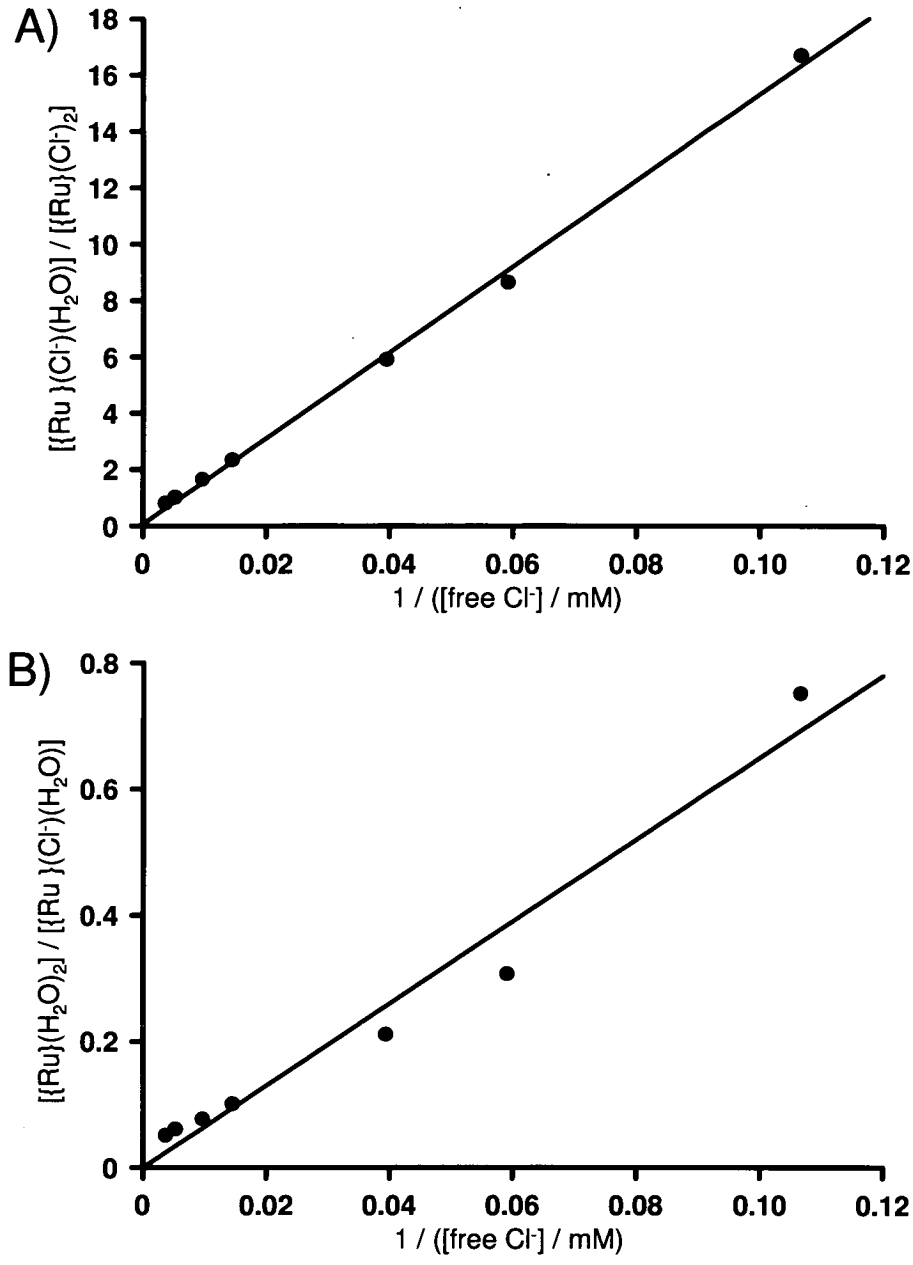

Figure A.4.6: Plot of the ratio of the concentrations of the fully aquated over the mono-aquated ruthenium species (A) and the ratio of the concentrations of the mono-aquated over the fully chlorinated (B) ruthenium species versus the concentration of free chloride for a chloride titration of $[(\eta^6{:}\eta^1\text{-}C_6H_5(CH_2)_2NH_2)RuCl_2]$ **4.5** (ca. 6.5 mM at start of titration) in D_2O at 298 K. The slopes give the equilibrium constants K_1 = 153 mM (A) and K_2 = 6.5 mM (B), respectively. With the resulting graph lines set to go through the origin K_1 = 154 mM, K_2 = 6.5 mM are obtained.

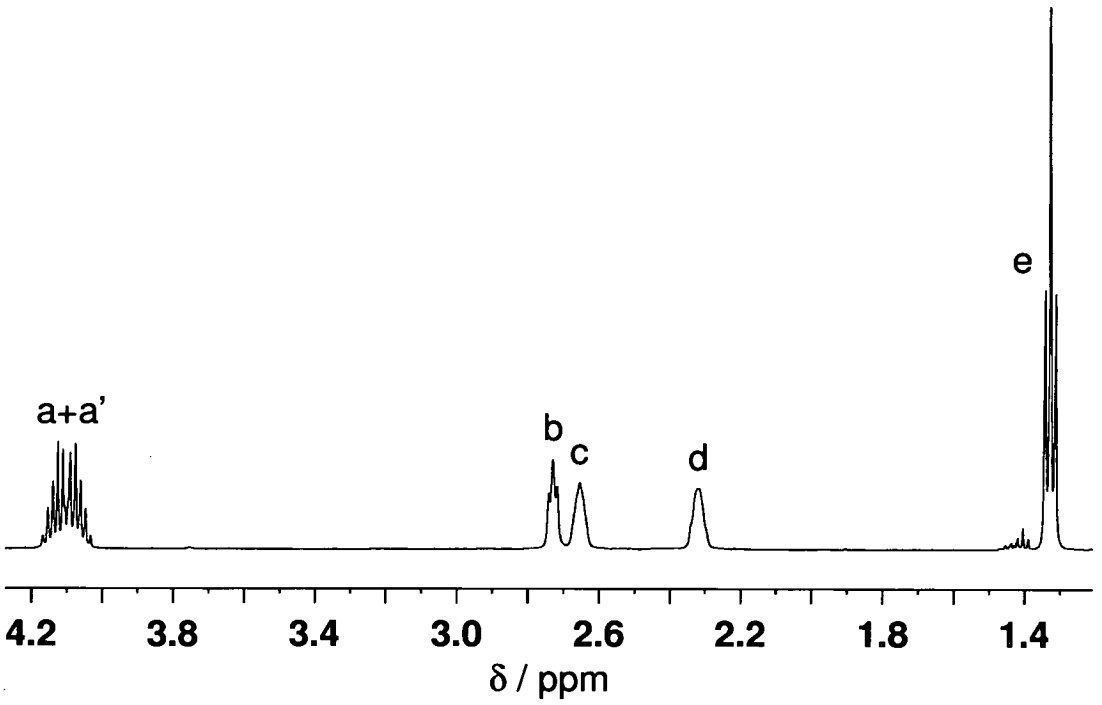

Figure A.4.7: The high-field region of the ^{1}H NMR spectrum of $[(\eta^6{:}\eta^1\text{-}C_6H_5(CH_2)_3NH_2)Ru(9EtG)_2]^{2+}$ (**4.11a**) in D_2O, 4.3 mM Ru, at pH* = 6.47 and 298 K. Assignments: a+a' = CH_2 (9EtG); b, c, d = $(CH_2)_3$ (tether); e = CH_3 (9EtG).

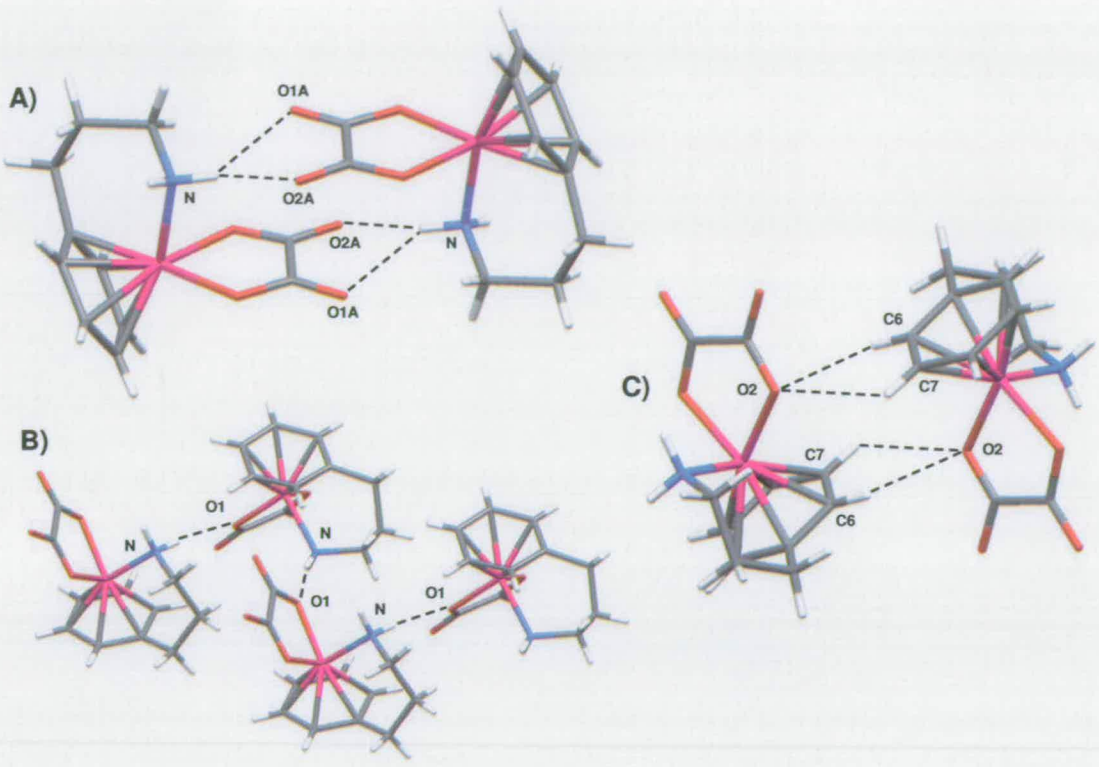

Figure A.4.8: Interactions in the X-ray crystal structure of $[(\eta^6{:}\eta^1\text{-}C_6H_5(CH_2)_3NH_2)Ru(ox)]$ (**4.14**). A: Formation of dimers *via* H-bonds between an amine proton and oxalate oxygens O1A and O2A. B: H-bonds between an amine proton and oxygen O1 resulting in the formation of zig-zag chains. C: Dimer formation *via* short contacts between oxalate oxygen O2 and arene protons.

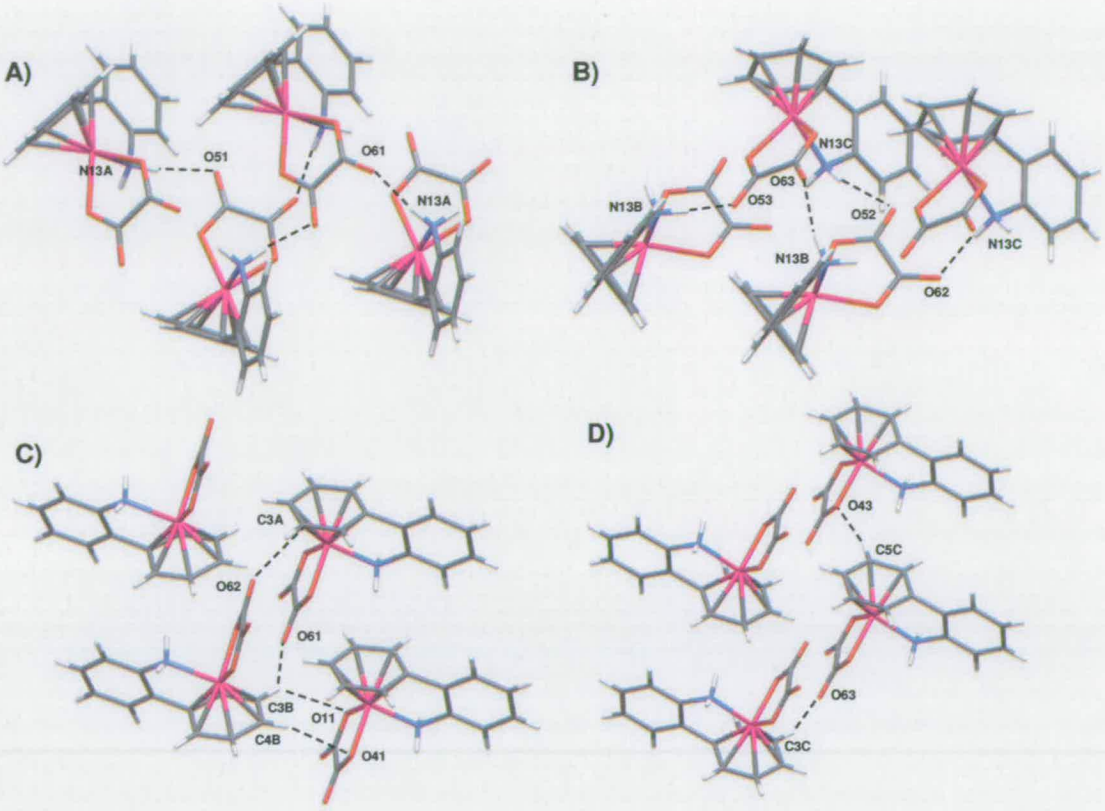

Figure A.4.9: Interactions in the X-ray crystal structure of [(η^6:η^1-$C_6H_5(C_6H_4)NH_2$)Ru(ox)] (**4.16**). A: Chain formation *via* H-bonds between amine protons and oxalate oxygens O51 and O61. B: H-bonds between an amine protons and oxygens O52, O53, O62 and O63 resulting in the formation of chains. C: Chain formation between molecules A and B *via* short contacts between oxalate oxygens and arene protons. D: Chain formation of molecule C *via* short contacts between oxalate oxygens and arene protons.

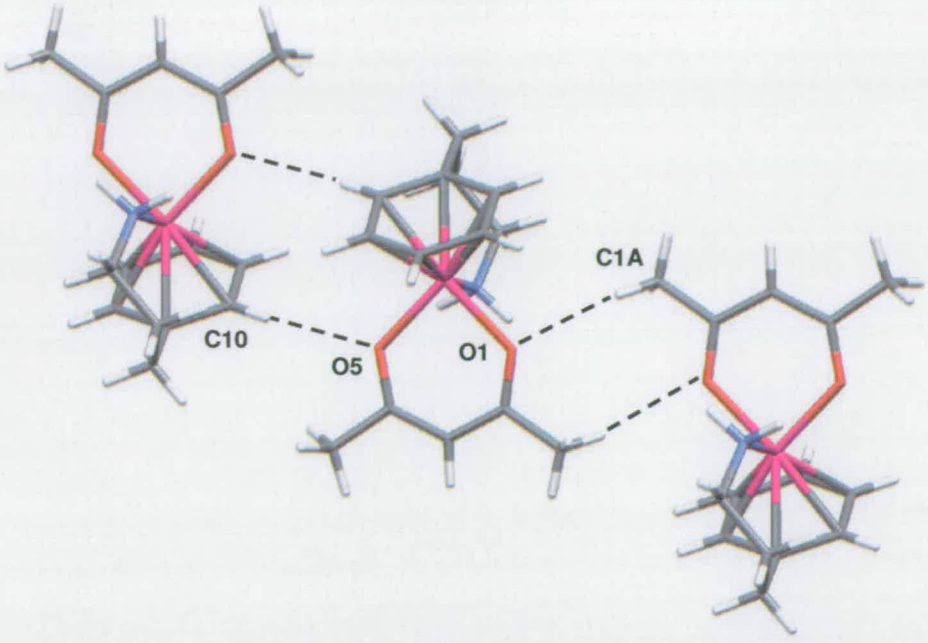

Figure A.4.10: Chain formation *via* H-bonds between acac oxygens with an arene proton and an (CH_3)acac proton, respectively, in the X-ray crystal structure of $[(\eta^6{:}\eta^1\text{-}C_6H_5(CH_2)_3NH_2)Ru(acac)]PF_6$ (**4.18**).

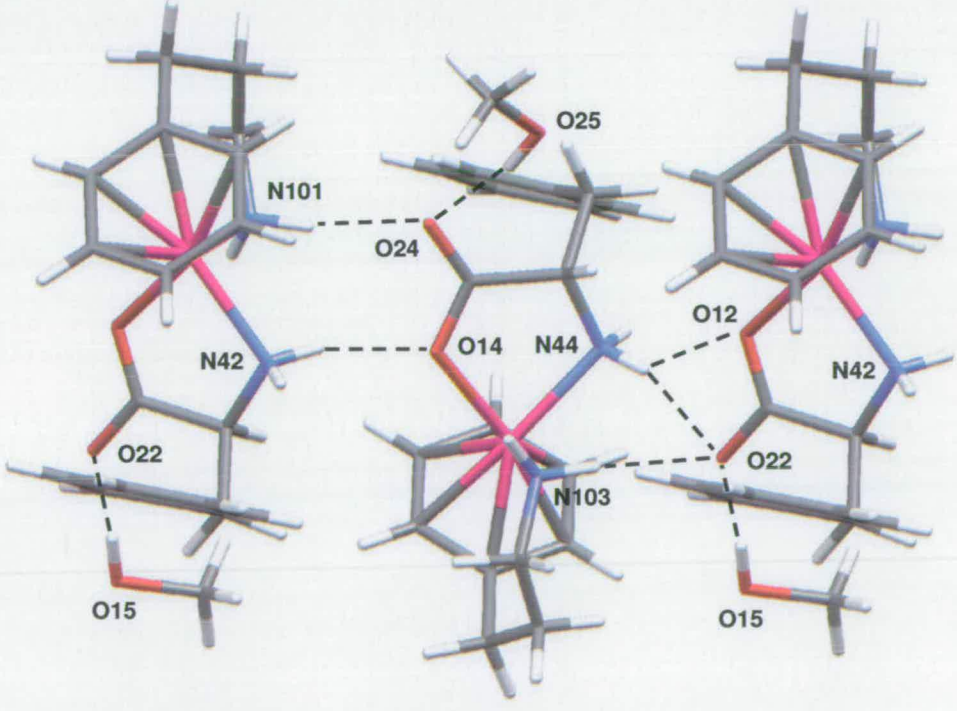

Figure A.4.11: Network of H-bonds in the X-ray crystal structure of $[(\eta^6{:}\eta^1\text{-}C_6H_5(CH_2)_3NH_2)Ru(L\text{-pal})]PF_6$ (**4.20**).

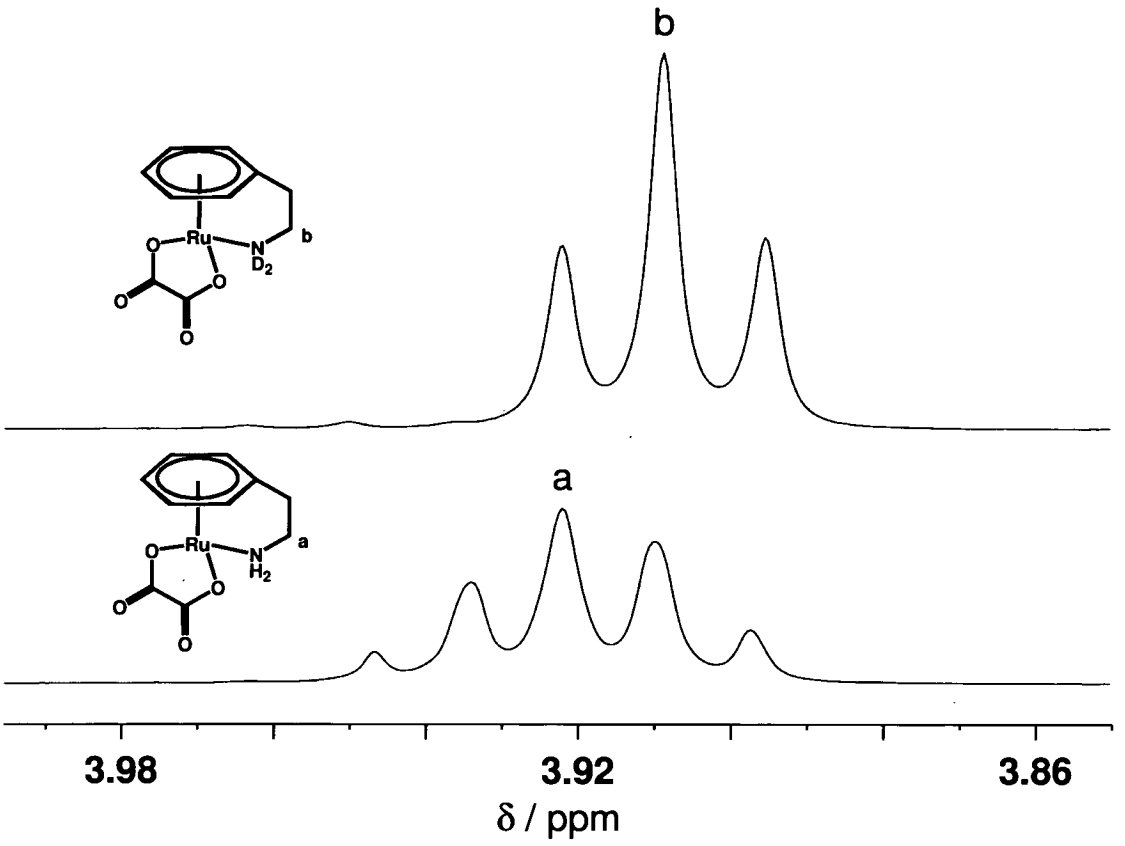

Figure A.4.12: The influence of amine H/D exchange of [(η^6:η^1-$C_6H_5(CH_2)_2NH_2$)Ru(ox)] (**4.15**) on the signals for the adjacent CH_2 group.

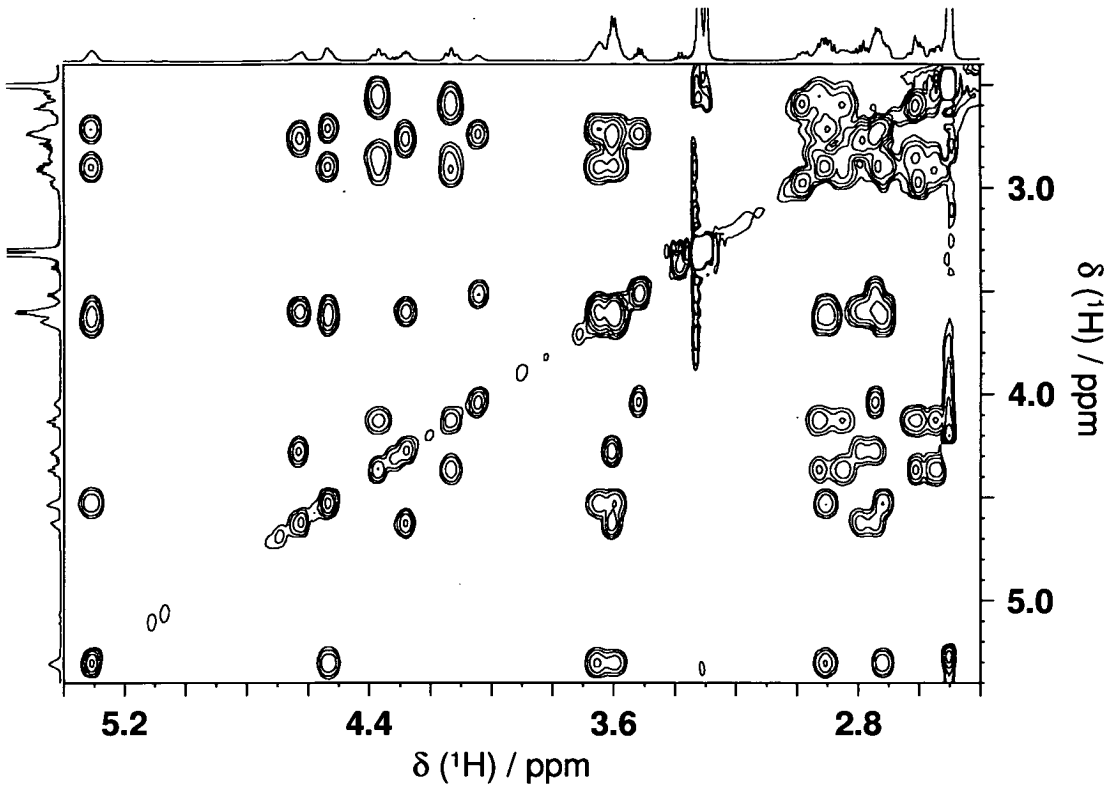

Figure A.4.13: The 2D NOESY ^{1}H NMR spectrum of $[(\eta^{6}:\eta^{1}\text{-}C_{6}H_{2}(CH_{3})_{3}(CH_{2})_{2}NH_{2})RuCl_{2}]$ (**4.29**) in DMSO-d_6 at 298 K. The NH_2 proton signals appear in the region of 5.4 – 4.0 ppm and the protons of the tether backbone in the regions of 3.7 – 3.4 ppm and 3.1 – 2.5 ppm, respectively.

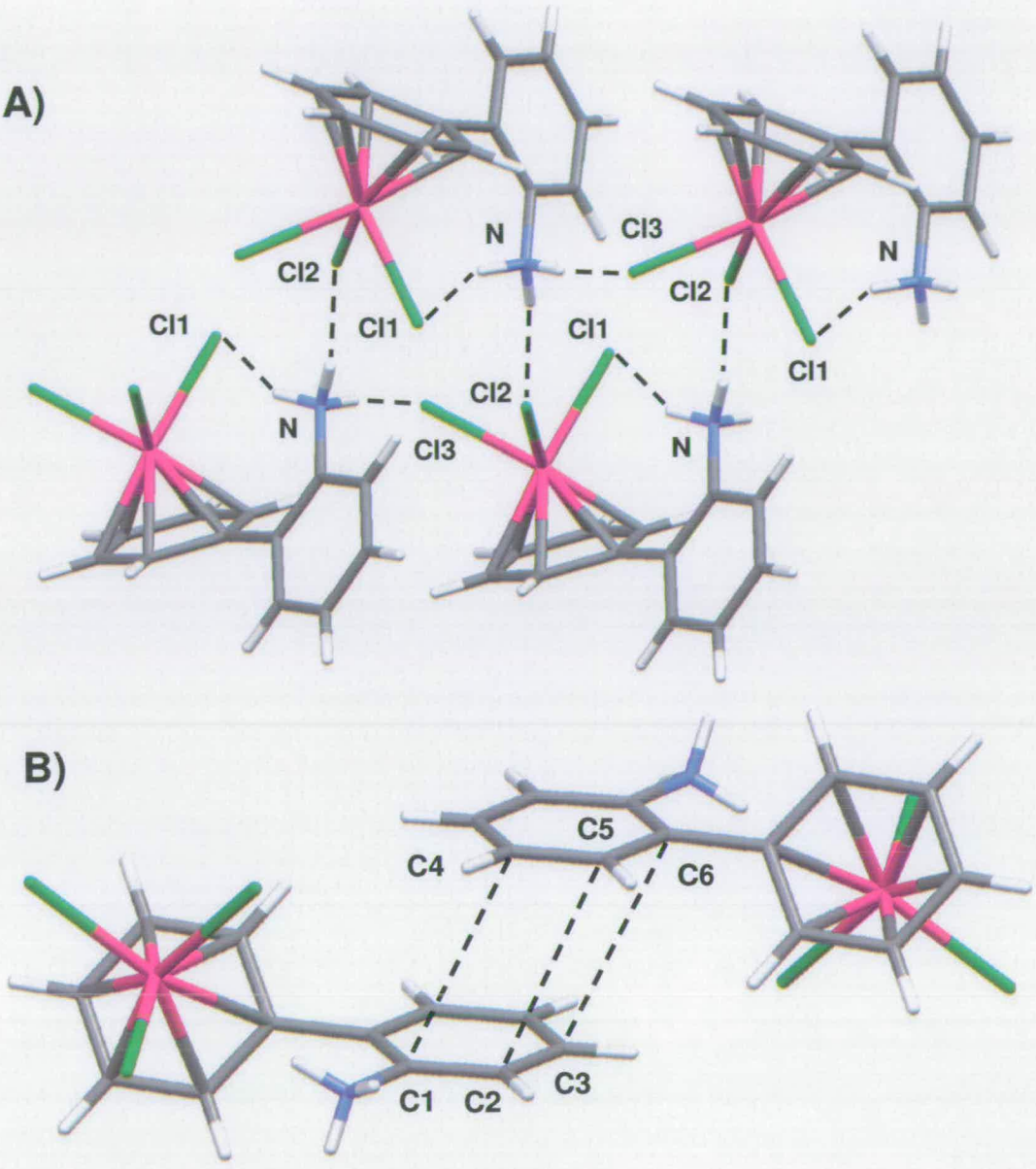

Figure A.4.14: Interactions in the X-ray crystal structure of $[(\eta^6{:}\eta^1\text{-}C_6H_5(C_6H_4)NH_3)RuCl_3]$ (**4.32**). A: Chain formation *via* intermolecular H-bonds between amine protons and chloride ligands. The intramolecular Cl1···NH H-bond is also shown. B: $\pi - \pi$ Stacking interactions between neighbouring aminobenzene rings.

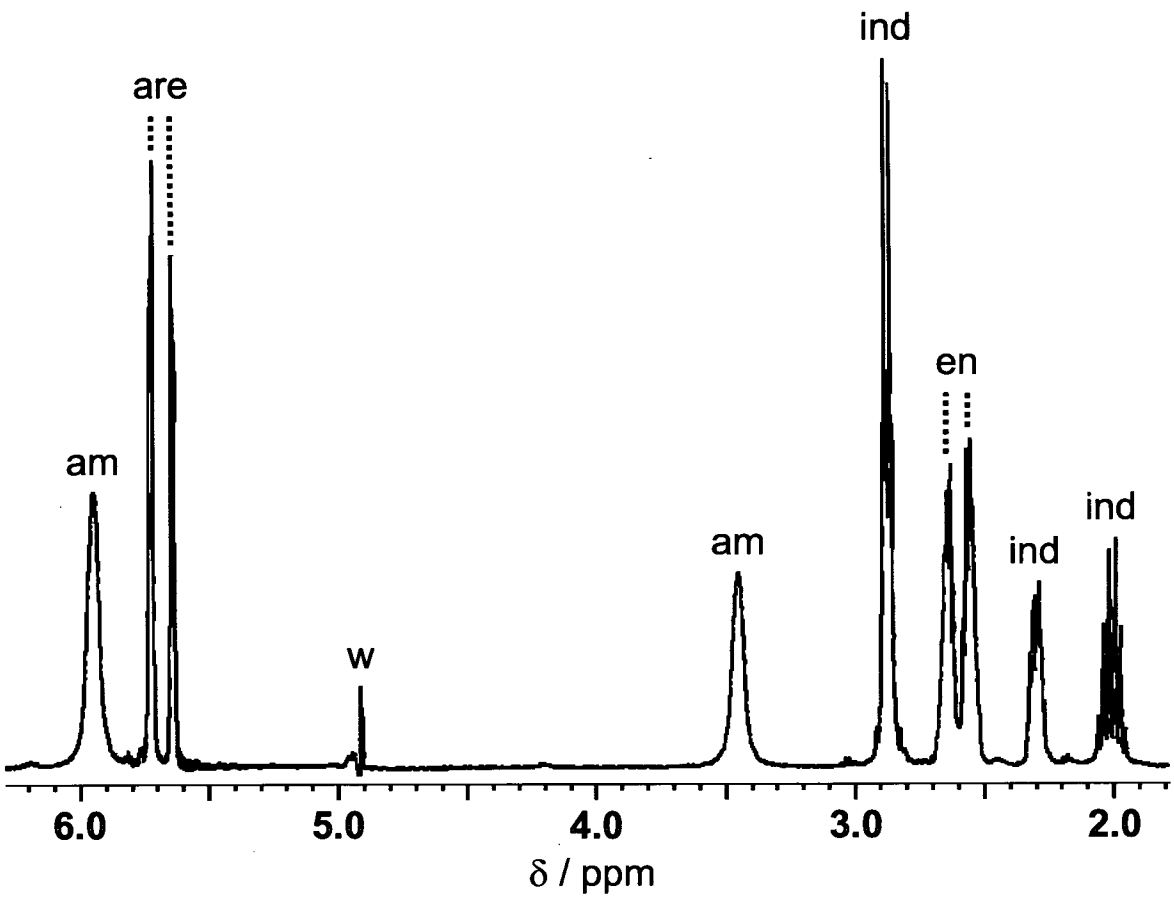

Figure A.5.1: Part of the ^{1}H NMR spectrum of $[(\eta^{6}\text{-ind})Ru(en)Cl]PF_6$ (**5.1**) in the presence of sodium formate (ca. 20 mol equiv) in 90% H_2O/ 10% D_2O at 298 K and pH = 9.61. Assignments: am = NH_2 (en); are = arene protons; w = suppressed water; ind = CH_2 groups (ind); en = CH_2 groups (en).

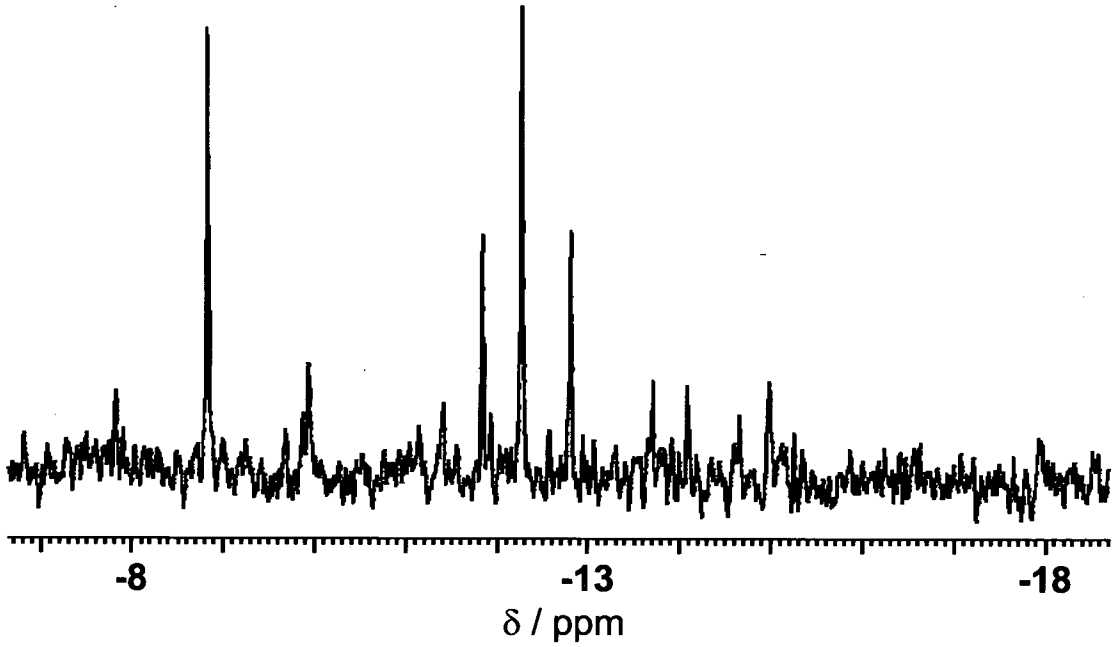

Figure A.5.2: The ^{1}H NMR spectrum of $[(\eta^{6}:\eta^{1}\text{-}C_6H_5(CH_2)_3NH_2)Ru(NO_3)_2]$ (**5.3**) (7.1 mM Ru) and sodium formate (100 mol equiv) in 90% H_2O/ 10% D_2O at 310 K, after incubation for 150 min at 310 K, suggesting the presence of a number of hydride-containing species in solution.

Conferences Attended

37th USIC conference, University of Strathclyde, UK, September 2003 (poster presentation).

2nd International Symposium on Bioorganometallic Chemistry, Zurich, Switzerland, July 2004 (poster presentation).

39th USIC conference, University of Glasgow, UK, September 2005 (oral presentation).

1st European Conference on Chemistry for Life Sciences, Rimini, Italy, October 2005 (poster presentation).

Publications

Structure-Activity Relationship for Cytotoxic Ruthenium(II) Arene Complexes Containing N,N-, N,O- and O,O-Chelating Ligands

A. Habtemariam, M. Melchart, R. Fernández, S. Parsons, I.D.H. Oswald, A. Parkin, F.P.A. Fabbiani, J.E. Davidson, A. Dawson, R.E. Aird, D.I. Jodrell, P.J. Sadler, *J. Med. Chem.* **2006**, in press.

Ruthenium(II) arene complexes containing four- and five-membered monoanionic *O,O*-chelate rings

M. Melchart, A. Habtemariam, S. Parsons, S.A. Moggach, P.J. Sadler, *Inorg. Chim. Acta* **2006**, *359*, 3020–3028.

Catalysis of regioselective reduction of NAD^+ by ruthenium(II) arene complexes under biologically relevant conditions

Y.K. Yan, M. Melchart, A. Habtemariam, A.F.A. Peacock, P.J. Sadler, *J. Biol. Inorg. Chem.* **2006**, 483–488.

Ruthenium arene anticancer complexes

M. Melchart, P.J. Sadler in *Bioorganometallics: Biomolecules, Labeling, Medicine*, Vol. 1, (Ed. G. Jaouen), Wiley VCH Verlag GmbH & Co. KGaA: Weinheim, **2006**, pp. 39–64.

Controlling ligand substitution reactions of organometallic complexes: Tuning cancer cell cytotoxicity

F. Wang, A. Habtemariam, E.P.L. van der Geer, R. Fernández, M. Melchart, R.J. Deeth, R. Aird, S. Guichard, F.P.A. Fabbiani, P. Lozano-Casal, I.D.H. Oswald, D.I. Jodrell, S. Parsons, P.J. Sadler, *Proc. Natl. Acad. Sci. USA* **2005**, *102*, 18269–18274.

Organometallic chemistry, biology and medicine: ruthenium arene anticancer complexes

Y.K. Yan, M. Melchart, A. Habtemariam, P.J. Sadler, *Chem. Commun.* **2005**, 4764–4776.

Use of chelating ligands to tune the reactive site of half-sandwich ruthenium(II)-arene anticancer complexes

R. Fernández, M. Melchart, A. Habtemariam, S. Parsons, P.J. Sadler, *Chem. Eur. J.* **2004**, *10*, 5173–5179.

Half-sandwich arene ruthenium(II)-enzyme complex

I.W. McNae, K. Fishburne, A. Habtemariam, T.M. Hunter, M. Melchart, F. Wang, M.D. Walkinshaw, P.J. Sadler, *Chem. Commun.* **2004**, 1786–1787.

Preparation of half-sandwich ruthenium anticancer complexes

P.J. Sadler, R. Fernández Lainez, A. Habtemariam, M. Melchart, D.I. Jodrell, *PCT Int. Appl.* **2004**, pp. 46.

Ruthenium(II) arene anticancer complexes: selective recognition of nucleobases and control of hydrolysis rates

R. Fernández, M. Melchart, E. van der Geer, F. Wang, A. Habtemariam, P.J. Sadler, *J. Inorg. Biochem.* **2003**, *96*, 130.